Novel Approaches to Functional Polymers for Powder Bed Fusion

By: Eduards Krumins



Supervisors: Steven Howdle and Christopher Tuck

Internal Assessor: Andrei Khlobystov

Department of Engineering

Thesis submitted to the University of Nottingham for the degree of Doctor of Philosophy

August 2022

Abstract

Powder Bed Fusion (PBF) otherwise known as Selective Laser Sintering (SLS) is an additive manufacturing technique, that exploits laser sintering of polymeric particles to achieve rapid prototyping of three-dimensional objects. However, the vast majority (~95%) of the parts are printed with nylon-12 (PA-12); effectively the industry standard polymer. This necessarily restricts the functionality of the items produced; they are usually white or grey and their surface properties are limited; for example, printed PA-12 objects tend to form biofilms and undergo biofouling in wet, food or medical applications. The challenge then is to find an inexpensive, viable alternative that will also work with the vast range of commercial apparatus that the world currently uses. Here we report a simple approach to allow modification of commercially available PA-12 via a facile, clean, and scalable process and to introduce the required versatility, which we demonstrate with coloured printing, colour mixing, and the preparation of PA-12 printed articles that clearly demonstrate anti-attachment properties. Our process exploits supercritical carbon dioxide ($scCO_2$) and simple free radical polymerisation, and we have demonstrated its utility by preparing 10 unique coatings on commercial PA-12 particles that are then sintered and printed into 3-D objects. We have also modified SLS printers in a variety of ways in order to achieve multimaterial printing and attempt to increase the resolution of SLS printing.

Acknowledgements:

In the course of my PhD project, I have received a lot of crucial help, which allowed me to finish this project. First, I would like to thank my family for always being supportive. I would also like to thank my supervisors Christopher Tuck and Steve Howdle for providing invaluable guidance, mentorship, and support. I would like to thank Vincenzo Taresco for all his amazing help, without it, the process would have been much harder. And lastly, I would like to thank all my friends and everybody in B10 and CfAM that has helped me during the last four years.

Declaration:

Except where specific reference has been made to other sources the work presented in this thesis is the original work of the author. It has not been submitted, in whole, or in part, for any other degree or professional qualification.

Signed:……. Date:…….

Eduards Krumins

Publications:

1. Englezou, G. *et al.* 2-Methyltetrahydrofuran (2-MeTHF) as a versatile green solvent for the synthesis of amphiphilic copolymers via ROP, FRP, and RAFT tandem polymerizations. *J. Polym. Sci.* **58**, (2020).
2. O'Brien, D. *et al.* A 'greener' one-pot synthesis of monoterpene-functionalised lactide oligomers. *Eur. Polym. J.* **125**, (2020).
3. Syachina, M., Minaeva, S., Krumins, E., Howdle, S. & Popov, V. Novel materials for high-resolution three-dimensional printing using surface-selective laser sintering. *{IOP} Conf. Ser. Mater. Sci. Eng.* **848**, 12086 (2020).
4. Phan, H. *et al.* Role of self-assembly conditions and amphiphilic balance on nanoparticle formation of PEG-PDLLA copolymers in aqueous environments. *J. Polym. Sci. Part A Polym. Chem.* **57**, (2019).
5. Minaev, N. V *et al.* An Apparatus for Research on Processes of Selective Laser Sintering of Powder Materials with High Spatial Resolution. *Instruments Exp. Tech.* **63**, 288–290 (2020).
6. Larder, R. R. *et al.* Antimicrobial 'inks' for 3D printing: block copolymer-silver nanoparticle composites synthesised using supercritical CO_2. *Polym. Chem.* **13**, 3768 – 3779 (2022).
7. Kortsen, K. *et al.* Exploiting the tuneable density of $scCO_2$ to improve particle size control for dispersion polymerisations in the presence of poly(dimethyl siloxane) stabilisers. *Eur. Polym. J.* **168**, (2022).
8. Krumins, E. *et al.* Development of an innovative 'green', versatile, and industrially viable process for the synthesis of novel and functional materials for SLS. *Nature Materials* (In submission)
9. Krumins, E. *et al.* Polymeric Particulate Materials. Application number: GB21122373.2 Lodged date: 31 August 2021
10. Lentz, J. *et al.* N-hydroxyethyl acrylamide as a functional eROP initiator for the preparation of nanoparticles in 'greener' reaction conditions. Polymer Chemistry (In submission)
11. Monaghan, O. *et al.* A Self-crosslinking monomer, α-pinene Methacrylate. Understanding and Exploiting Hydrogen Abstraction. Polymer Chemistry (Accepted minor revisions)

List of Abbreviations:

PBF – Powder Bed Fusion
SLS – Selective Laser Sintering
PA-12 – Nylon-12 or Polyamide 12
$scCO_2$ – Supercritical carbon dioxide
STL – Stereolithography or Standard Tessellation Language
AM – Additive Manufacturing
CMC – Ceramic matric composites
DARPA – Defense Advanced Research Projects Agency
FDM – Fused Deposition Modelling
CO_2 – Carbon dioxide
IR – Infrared
UV – Ultraviolet
T_m – melting point
T_c – crystallization point
T_g – glass transition temperature
PA-11 – Nylon 11 or Polyamide 11
PEBA – Poly(ether block amide)
PEEK – Poly(ether ether ketone)
TP – Thermoplastic
ND-YAG – Neodymium-doped yttrium aluminium garnet
PMMA – Poly methyl methacrylate
PS – Poly styrene
FRP – Free radical polymerisation
FRDP – Free radical dispersion polymerisation
AIBN – Azobisisobutyronitrile
PDMS-MA – Poly(dimethylsiloxane) methacrylate
TDDFT – Time dependent density functional theory
λ_{max} – Lambda max
CMYK – Cyan, Magenta, Yellow, Black
IBMA – Isobornyl methacrylate
HRSLS – High resolution selective laser sintering
DR1MA – Disperse Red 1 methacrylate
DB3MA – Disperse Blue 3 methacrylate
Y1MA – Yellow 1 methacrylate
QSPR – Quantitative structure property relationship
B3LYP – Becke three parameter Lee-Yang-Parr correlation functional
CAM-B3LYP – Coulomb attenuated B3LYP functional
LC-BLYP – Long range corrected BYLP
BH and HLYP – Becke-half and half LYP
PBEO – Perder-Burke-Ernzerhof exchange correlation functional
PCM – Polarizable continuum method

I-PCM – Implicit PCM
SCI-PCM – Self-consistent isodensity PCM
IEF-PCM – Integral equation formalism PCM
TEA – Triethyl amine
TBAB – Tetrabutylammonium bromide
BuOH – Butyl alcohol
p-TOS – p-Toluene sulfonic acid
MEK – Methyl ether ketone
DCM – Dichloromethane
MMA- Methyl methacrylate
MA – Methacrylic acid
THF – Tetrahydrofuran
HCl – Hydrochloric acid
CAS-PT2 – Complete active space perturbation theory 2
MRCI – Multi reference configuration interaction
CNDO/S – Complete neglect of differential overlap/S
INDO/S – Intermediate neglect of differential overlap/S
DFT – Density Functional theory
UV/vis – ultraviolet and visual region
^{1}H NMR – Hydrogen nuclear magnetic resonance
$CDCl_3$ – Deuterated Chloroform
Y1 – Solvent yellow 7 or 4-phenyl azophenol or 4-phenyldiazenylphenol
DR1 – Disperse red 1
DB3 – Disperse blue 3
CPDT – 2-cyano-2-propyl dodecyl trithiocarbonate
AUCP – Area under the curve of the polymer when compared to the are under the curve of the monomer peak
z-direction/axis – vertical axis
PEKK – Poly(ether ketone ketone)
GPC – Gel permeation chromatography
DSC – Differential scanning calorimetry
SEM – Scanning electron microscopy
LDS – Laser diffraction spectrometry
VdWs – Van der Waals
DLS – Dynamic light scattering
dRI- Differential refractive index
LS – Light scattering
$Đ$ – dispersity
AFM – Atomic force microscopy
etc. – Etcetera
e.g. – For example
et al. – And others
ROP – Ring opening polymerisation

AMA – allyl methacrylate
GMA – Glycidyl methacrylate
HEMA – 2-hydroxy ethyl methacrylate
HEX – Hexadecimal colour
sRGB – Standard Red, Blue, and Green
CIELAB – Colour space defined by the international commission on illumination
LCH – Lightness, chroma, and hue
LRV – Light reflectance value
LAB – Lightness, channel a, and channel b
PBT – Powder bed temperature
CT – Chamber temperature
HS – Hatching Speed
LP – Laser power
HLP – Hatching laser power
CLP – Contour laser power
HD – Hatching distance
PSO – Particle swarm optimisation
GA – Genetic algorithm
P. aeruginosa – Pseudomonas aeruginosa
E. coli – Escherichia coli
C. glabrata – Candida glabrata
C. globosum – Chaetomium globosum
C. albicans – Candida albicans
C. gloeosporioides – Colletotrichum gloeosporioides
eDNA- Environmental deoxyribonucleic acid
VOCs – Volatile organic compounds
RAFT – Reversible addition-fragmentation chain transfer
DP – Degree of Polymerisation
N – Newton
wt % - weight percentage
KDa – Kilo Dalton
Da – Dalton
µm – Micron
nm – Nanometre
mm – Millimetre
g – Gram
mol – Mole
^{o}C – Degrees Celsius
M_w - Weight average molecular weight
M_n – Number average molecular weight
mV – Millivolt
V - Volt
mW – Milliwatt

W – Watt
mmol – Millimole
psi – Pounds per square inch
Pa – Pascal
MPa – Mega Pascal
MHz – Mega Hertz
rpm – Revolutions per minute
hr – Hour
min – Minute
mA – Milliamp
mL – Millilitre
L - Litre
Tof-Sims – Time-of-flight Secondary ion mass spectrometry
XTT- Cell proliferation kit II
YPD – Yeast growth media
PBS – Phosphate buffered saline

Table of Contents:

Introduction 11-46
Introduction to Selective Laser Sintering (SLS).....16-24
Disadvantages to Selective Laser Sintering (SLS).....24-27
Introduction to Polymers.....28-37
Project aims and methodology.....38-46
Chapter 1: Dye monomer synthesis.....47-90
Introduction 47-73
Results and Discussion.....74-84
Conclusion 84-85
Materials and Methods.....85-90
Chapter 2: In situ polymerisation/coating and scale up.....91-134
Introduction 91-98
Results and Discussion.....98-128
Conclusion 128-129
Future work.....129-130
Materials and Methods.....130-134
Chapter 3: Coloured PBF printing.....135-173
Introduction 135-139
Results and Discussion.....139-169
Conclusions 169-170
Future work.....171
Materials and Methods.....171-173
Chapter 4: Developing a colour mixing system for PBF.....174-218
Introduction 174-187
Results and discussion.....187-209
Conclusions 209-211
Future work.....211
Materials and methods.....211-218
Chapter 5: Further Developments for SLS.....219-285
Materials which prevent the formation of biofilm for SLS.....219-245
Materials for improved mechanical properties.....245-270
Multimaterial PBF printing.....270-280
Materials and methods.....280-285
Conclusions 286-295
Appendix 1: Development of a novel High Resolution SLS process..296-345
Introduction 296-308
Results and Discussion.....309-336
Conclusion 336-337
Future work.....337-341
Materials and Methods.....341-345
Appendix 2: Mechanical properties of coloured printed parts.....345-354
References 355-392
Supporting Information.....393-431

Introduction

The polymer industry has grown rapidly and steadily over the last 70 years.[1,2] This is due to two main factors: a rise in demand for plastic materials, and an increasingly varied selection of polymeric materials that have a multitude of functions.[1,2] In parallel the use of additive manufacturing has increased rapidly in the last years. In fact from 2012-2016 sales related to additive manufacturing increased by 12.5% on average per year.[1,2] The industry is growing more rapidly at the moment as it currently produces 21 billion dollars, and is expected to grow to at least 35.6 billion dollars by 2024, with an average annual growth of 24-29% per year.[3–5] This rise in sales is mainly due to the increasing functionality of 3D printers such as speed, accuracy, and capacity of these machines has increased. However, the range of polymeric materials used for 3D printing has not grown and diversified significantly, especially for 3D printing techniques such as Powder Bed Fusion (PBF) otherwise known as Selective Laser Sintering (SLS). The increase in the range of materials available for 3D printing will lead to innovative products, with enhanced and custom-made properties.

The concept of 3D printing was born in 1971 when Johannes F. Gottwald patented the liquid metal recorder.[6,7] This printer was a precursor of an inkjet printer, which was able to print with a conductive metal alloy as the ink.[6,7] This patent states that the aim of this machine was to be able to print structures and patterns.[6,7] The machine would thereby be able to minimize the amount of material used to make a part.[6,7] However, this machine was not very reliable in terms of consistent printing of layers and the process was very expensive, but it “planted the seed”, for what would become the 3d printing industry.

In April 1980, Hideo Kodama invented a type of 3D printing in which a UV beam is shone onto a vat of photopolymer, which hardens the material. In this process the structure of the part being built is produced layer-by-layer, however it was not patented.[8,9] Charles Hull filled a patent in 1984 for a similar system; a stereolithography fabrication system, in which layers are built by curing photopolymers with a UV laser.[10,11] Hull described his system as a "system for generating 3D objects by creating a cross-sectional pattern of the object to be formed" in fact Hull created the STL (stereolithography or standard tessellation language) file format and the digital slicing and infill strategies that are used in the majority of additive manufacturing techniques today.[10,11]

In the late 1980s - 1990's several key printing techniques were invented: Selective laser sintering, direct metal laser sintering, and selective laser melting.[12–14] This era saw the expansion of the powder bed fusion (PBF) techniques as the polymeric printing techniques were advanced, and metal PBF was possible after new material deposition techniques were invented.[15–17]

In the last 20 years additive manufacturing has seen a boom, due to the development of printing techniques as well as a strong intercorrelation and advancement on the synthesis of new materials adoptable as inks.[18] To date, 3D printing technology is used in a variety of industries to create finished parts, instead of the models and prototypes that 3D printing was used for in the past.

This has led the 3D printing field to broaden exponentially its range of applications spanning from automotive to biomedical and from fashion to electronics. In the medical industry 3D printing had been used for a multitude of purposes. The first

prototypes of synthetic organs have been printed, in fact in 2003 a fully functional kidney was printed at Wake Forest University. Since then 3D printing has been used to print livers, heart valves, tissues, blood borne networks, and bone implants.[19–26] Popular clothing brands such as Nike, Adidas, and New Balance have 3D printed sports shoes including football boots. Additive manufacturing (AM) has been used to produce frames for glasses and dresses.[27–29]

The automotive industry has started to utilize this technology as Koenigsegg, Rolls Royce, BMW, Ford, etc. have printed parts for their cars from gearboxes to car frames, door handles, windows, etc.[30,31] In fact, Ford bought the third 3D printer ever created and has been developing prototypes for cars since the 1980s. Ford estimates that in the past decade, the company has saved millions of dollars through the use of AM. A prime example of this saving; is that the design of an engine block through traditional methods costs 500,000 dollars and takes 4 months, while the latest development of an engine block via AM by Ford took just 4 days and cost 3000 dollars.[30] A vast array of parts have been or will soon be manufactured via AM for automobiles (figure 1). However, currently the majority of the parts are for the exterior and are metal based, but through enhancements of SLS technology more polymer-based parts could be produced for an automobile's interior.

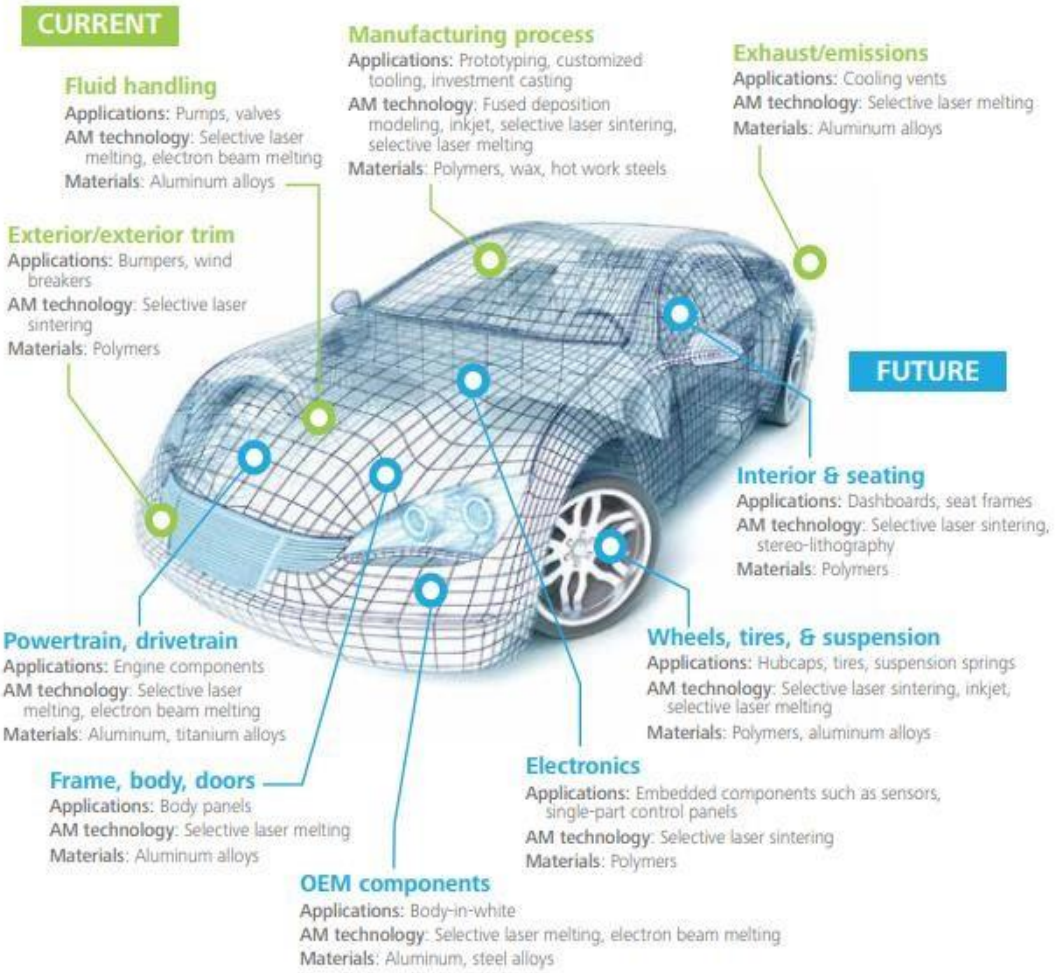


Figure 1 – Current and future parts being produced for the automobile industry via Additive Manufacturing. Showing which additive manufacturing techniques are used to print parts for the automotive industry.[30]

The aircraft and defence industry much like the automotive industry has used AM to streamline their manufacturing process. Research has shown that aircraft and defence companies could experience time savings on prototyping between 43-75%, if they started to use AM.[30] Several companies have taken advantage of this, and Rolls Royce has used additive manufacturing in their aircraft design, specifically their engines.[32–34] The Advance3 engine used in aircrafts produced by Rolls Royce has over 20000 parts built via additive manufacturing out of ceramic matrix composites

(CMCs). In fact this engine is 25% more fuel efficient than its rivals, because the CMC parts built via AM allow the engine to operate at higher temperatures making them more efficient thereby reducing operating costs.[32] Airbus started to use AM for the production of their planes with the Airbus A350 XWB having about 1000 printed parts.[34] The British Royal, the American, and Israeli Air Forces use fighter jets with printed parts. In 2017 GE aviation used AM to simplify the production of their helicopter engine thanks to AM, as the engine is now composed of only 16 parts, whereas with traditional manufacturing techniques the engine had over 9000 parts. Boeing used AM design to build a fully functional vertical take-off and landing aircraft under the direction from the Defense Advanced Research Projects Agency (DARPA) in just 30 days, and with traditional techniques the duration of this project was estimated to be several months.[34] However, the majority of these parts are made via a small number of additive manufacturing techniques.[34]

Fused deposition modelling (FDM) is the most commonly used type of 3D printing, in 2018 46% of all additive manufacturing was done via FDM.[35] At this moment FDM is more popular than other techniques such as SLS/PBF, because it is more inexpensive and has a broader range of materials that can printed with.[35] However, FDM has two main disadvantages, one is that the parts have a lack of detail due to the limited resolution of the technique. Also parts built via FDM commonly have weak points in between layers, thereby making said parts weaker and unsuitable for certain applications.[35] In the past 50 years the 3D printing industry has grown tremendously from an idea into a potentially game-changing industry. However, in order to become truly ubiquitous worldwide and more appealing in different sectors many

improvements have to be made. This project aims to address several of the shortfalls that Selective Laser Sintering (SLS) currently has:

1. The inability to print in colours other than white and black.
2. The maximum resolution that a SLS printer can reach is 60-100 µm
3. The inability to print multimaterial parts with sharp interfaces.
4. PA-12 based parts made via SLS readily undergo biofilm formation and biofouling.
5. PA-12 based parts made via SLS do not have the mechanical properties to be used for 'high-performance' applications

Introduction to Selective Laser Sintering (SLS)

Selective laser sintering (SLS) is a form of additive manufacturing (3D printing), which utilizes a laser to sinter a predetermined pattern (eg. STL file) on successive layers of polymeric particles. The process starts by creating a model of the desired structure on software (such as Magics) which is then inputted into the machine. A roller deposits a layer of particulate material on a powder bed, which is moved by a piston. At this point the sintering process begins. Once the first layer is deposited the laser, frequently a CO_2 laser (in the IR region), rasters a pattern on the material. Where the laser comes into contact with the material, part of the material will melt causing the particles to fuse together (Figure 2). Then the piston lowers the powder bed, and the roller deposits another layer of material on top of the first layer, and the laser rasters the predetermined pattern onto the new layer. To enable the fusion of the particles the powder bed is heated slightly below the melting point (T_m) or glass transition temperature (T_g) of the material. This leads to the laser expending less power in order

to melt the material, and it also keeps the material at a temperature which allows the different layers to fuse to each other and prevents the material from warping. This process of additive manufacturing has many benefits.

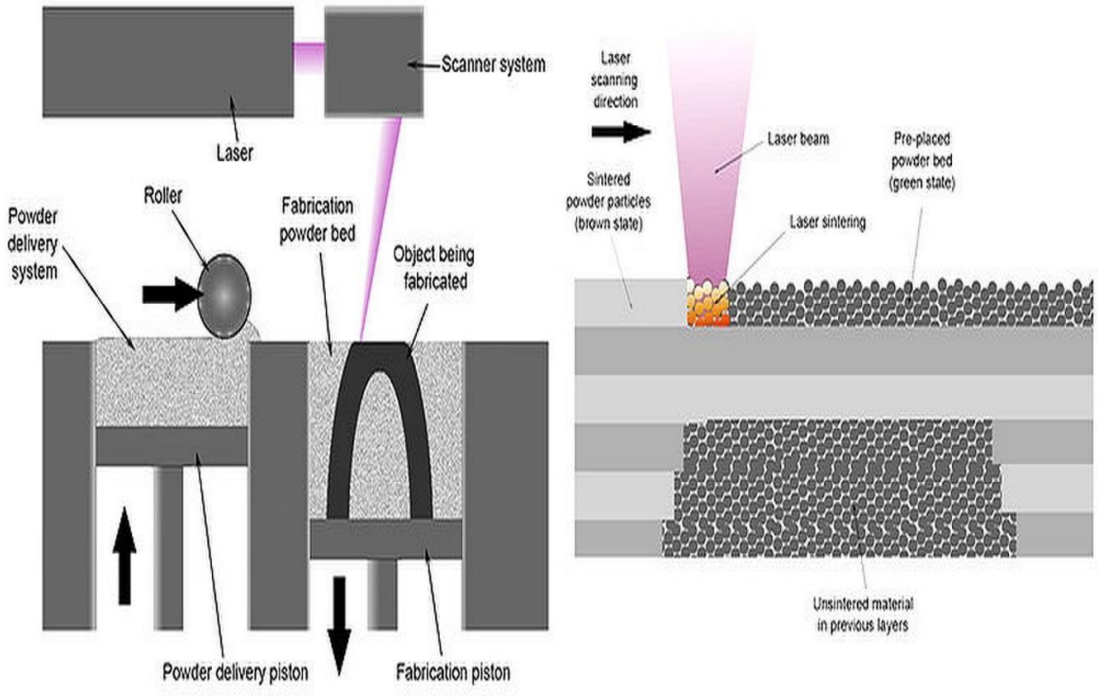


Figure 2 – Mechanism for Selective Laser Sintering. On the right is a schematic of the powder deposition method used in SLS printers. On the left the effect of laser sintering can be seen as the printed particles become solid, whilst the unsintered remain in particulate form.[36]

One of the key advantages of this technique is that the self-supporting nature of the particulate powder allows for production of previously unattainable geometries.[37] Some of these include the production of parts with high overhanging angles and complex geometries embedded deep inside.[37] It is also possible to build several different parts on the powder bed during the same print job.[38] This makes the

technique ideal for rapid prototyping and batch production of complex parts. When compared to subtractive manufacturing methods, SLS can save a considerable amount of material since the part is being built up, instead of being cast from a larger block.[39] SLS could be more economical and environmentally friendly as well, because the non-sintered powder material can be recycled and reused in subsequent prints.[40] A key benefit of SLS is that printing of parts can be achieved in a short amount of time when compared to other additive manufacturing techniques such as stereolithography.[38] The resolution of the built parts in comparison to other additive manufacturing methods such as extrusion printing is quite good as the resolution is often of 100 - 200 µm.[41] The products can also possess high tensile strength and other mechanical properties depending on which materials are used.[42] Even though it is clear that SLS has many advantages, it suffers from several and significant drawbacks.

One of the drawbacks of SLS is that the powder bed causes one constraint on the design of builds, as hollow fully enclosed builds cannot be manufactured.[43] This is not possible because the unsintered material would be inside the build, hence it would not be hollow.[43]

Up to this point colour printing and colour mixing for SLS printing has not been possible, and colour is only added in post-processing.[41] This technical deficiency has limited a wider employment of the SLS technique and it is one of the main consequences related to the narrow range of applicable polymers for this process. In fact approximately 90% of all polymeric SLS printed manufacts are prepared from polyamide-12 (PA-12)-based inks.[44] The other 10% is made up of polyamide 11 (PA-

11) and specialty polymers such as Poly(ether block amide) (PEBA), Poly(ether ether ketone) (PEEK), and thermoplastics (TPs).[44] There have been numerous attempts to use other polymers, but many of these have failed, because for a polymer to function in SLS it has to have fairly specific intrinsic and extrinsic properties.[44]

For a polymer powder to be suitable for SLS, it has to have the appropriate thermal, optical, and rheological (intrinsic) and particle and powder (extrinsic) properties. Intrinsic properties are normally caused by the molecular structure of the polymer; hence, they are not easily altered. In stark contrast the extrinsic properties are routinely altered through postprocessing of the polymeric material.

One of the key factors in a SLS applicable material is its thermal properties. Polymers currently used for SLS printing are semi-crystalline, hence, they possess a crystallisation temperature (T_c) and a melting temperature (T_m).[45] For SLS, the polymeric material needs to have a gap (>10°C) between the T_C and the T_m, this is called the SLS sintering window and is given by equation 1 (figure 3).[45,46]

$$Sintering\ Window = (Tm - Tc)onset$$

Equation 1 – Sintering window

A large sintering window is desired, because if the gap is too small and the temperature dips, then an undesirable crystallization process can be induced, ruining the part (causes reduction in resolution and brittle segments).[45] If the temperature is controlled and remains within the sintering window then crystallization can be inhibited for several sintered layers at a time, making it possible to print a build.

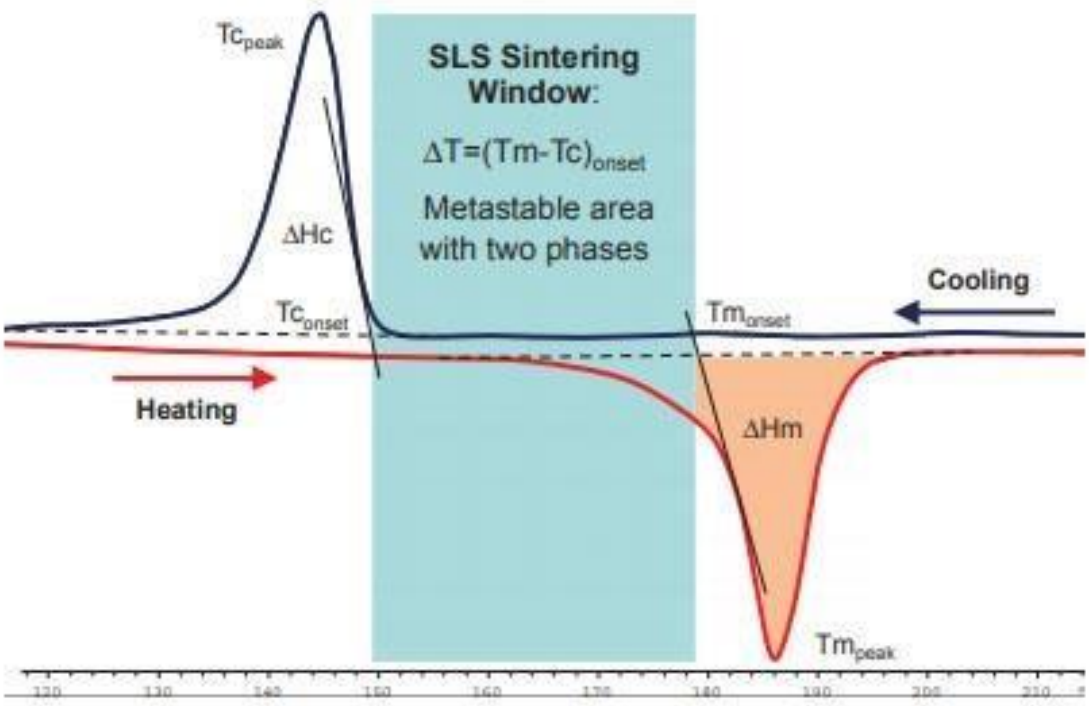


Figure 3 – DSC of PA-12 with sintering window. The sintering window is the area between the T_m and the T_c of the polymer determined by equation 1.[44]

Amorphous polymers have not been frequently used for SLS printing, but they would also have to meet several thermal requirements.[47] One of these is that the transition glass temperature (T_g) has to be relatively high (>60 ^oC). This is because the powder has to be stable at room temperature, and also in the pre-heated powder bed. Since amorphous polymers have no T_m or T_C, there is no conventional sintering window.[47] What, instead, must occur when the laser comes into contact with the particles is that they turn to a very rubbery state, so that the particles can fuse together. It is important that the polymer is not too viscous, because if it is, then there will be not sufficient movement of the polymer chains to cause particle fusion.[47]

The optical requirement of the polymer is that it must absorb radiation at the wavelength of the laser.[41,44] Most SLS printers utilize CO_2 lasers with a wavelength of

10.6 µm. This is suitable for many polymers as the aliphatic C-H bonds in the compounds can absorb radiation at this wavelength. However a consequence of using this laser is that it is not possible to have a higher print resolution than 10.6 µm.[48] Also, the more efficiently a polymer absorbs the radiation, less power needs to be used to sinter the material. Therefore, by altering your polymer, so that it absorbs the lasers radiation, better particle fusion can be achieved. If polymers were made, which can absorb in the UV-region, then theoretically using a UV laser would allow for higher resolutions.[49] This is because a UV laser has a wavelength of 405 nm compared to the frequently used CO_2 lasers which have a wavelength of 10.6 µm, therefore the smallest possible spot size for a UV laser is 405 nm whilst that of a CO_2 laser is 10.6 µm, and the smaller the spot size the higher the theoretical resolution.

The shape and size of the particles is a significant factor for SLS printing, as they affect how the powder will flow and pack on the powder bed. The particle shape that is desired is spherical, as spherical particles have good flow behaviour as the powder is rolled onto the powder bed. The powder has to be free-flowing so that the particles can be placed onto the powder bed evenly.[44] Even distribution of the particles is essential, because gaps in the powder can lead to weak points in the sintered material, which cause the structure to have a weaker tensile strength and sometimes even collapse. PA-12 particles in most cases are free-flowing, but a small amount of flow agents (eg. fumed silica) can be added to improve the flow behaviour of the material.[50,51] The majority of commercial systems use particles ranging from 40- 80 µm, with a narrow size distribution.[44] These properties encourage an even packing and distribution of the polymeric particles. At the current stage, SLS printers usually

do not reach resolution below about 100 µm, but by altering the particle size, shape, laser, and the build platform movement control it could be possible to print at a higher resolution (up to 10 -30 µm).

The laser that is used is essential to SLS. There are several types of lasers that have been used for SLS, but the most common is a CO_2 laser, which has a theoretical spot size of 10.6, however is more frequently in the 100 µm range as the laser passes through a mirror array which can increase the spot size of the laser.[44,52] Neodymium-doped yttrium aluminium garnet lasers (ND-YAG laser) and other high powered lasers can used, but these generate more power, so they can sinter materials more easily, and possibly burn them.[44,52] The type of laser used has to be suitable for the material and vice versa (absorption of laser radiation). If the material can absorb the laser's radiation, the right amount of power has to be used, because if it is too low particle fusion cannot occur, but if it is too high then the material can be degraded. Once the laser is chosen, both scanning speed and spot size can be altered to suit the printing job.

The scanning rate is the speed at which the laser rasters the pattern on the powder bed. The scanning rate has to be slow enough so that the laser can impart sufficient radiation for the melting of each particle in the pattern. However if it is too slow then the amount of time required to build a structure becomes unsuitable, as the time needed for the prints would be too long.[53,54] If the polymer can absorb a significant amount of the laser's radiation or the laser is very powerful, the scanning rate can be quite fast, without damaging the build quality.[53,54] The spot size for the laser influences the resolution of the build, as the resolution cannot be lower than the spot

size. For this reason, the maximum resolution with a CO_2 laser is 10.6 µm, however it is often about 200 µm once it passes through the mirror array . The spot size can affect the power applied onto each particle, as a smaller spot size will focus the energy into smaller segments. By changing the scanning rate and spot size it is possible to alter the resolution and duration time of the build.

In similarity to the laser, the powder bed has several variables that can affect the build quality. One of these is the control over movement of the powder bed in the vertical plane (z-direction). The powder bed moves down before each new layer is deposited, thus the thickness of each layer depends on the distance that the bed is lowered.[55,56] The piston dictates how accurately the powder bed can move, and the more accurately it can lower the bed, the better the resolution can be (figure 4).

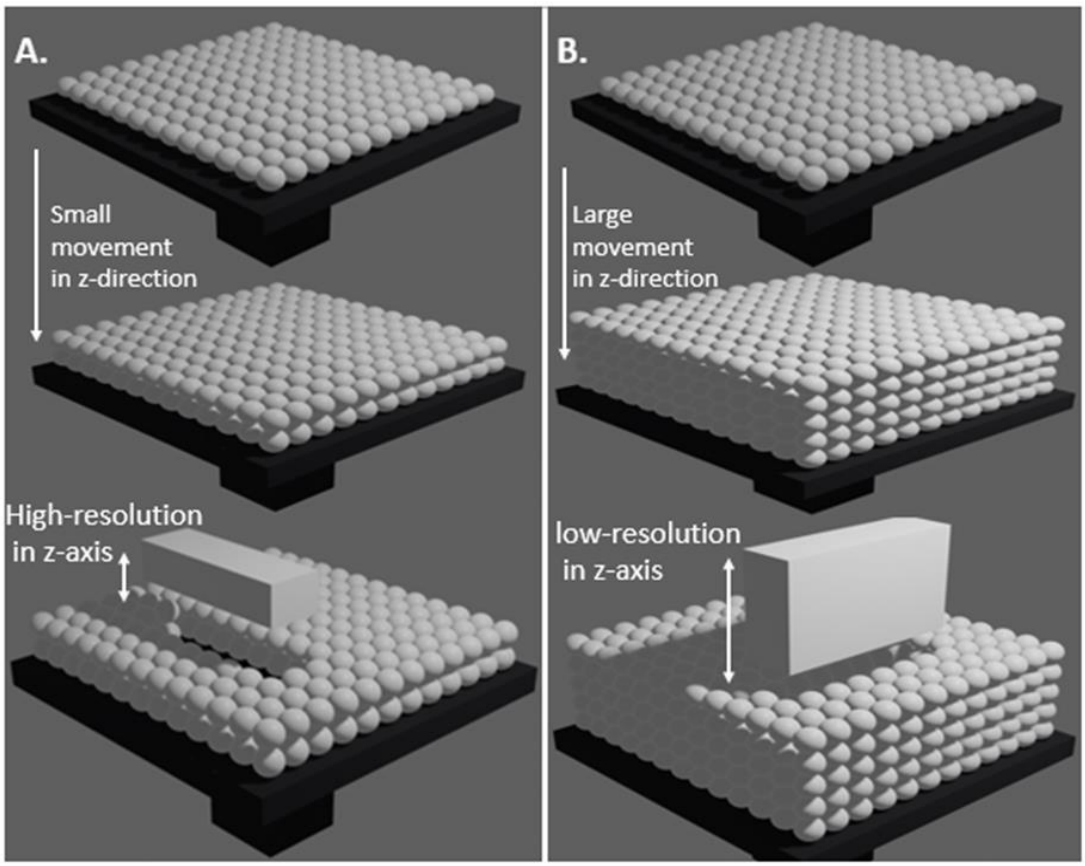


Figure 4 - The effect of the build platform on the resolution of a part. A.) Schematic of higher controller over movement of the build platform in the z-direction leading to higher resolution. B.) Schematic of lower controller over movement of the build platform in the z-direction leading to lower-resolution.

Temperature control over the powder bed is necessary for successful printing, because the powder has to remain in the sintering window while the build is ongoing.[44,45] If one part of the bed is colder than the rest, this can induce crystallization of the material in that area of the powder bed. The method of powder deposition is usually a roller, which feeds powder from a reservoir onto the bed. If classic deposition does not work well, then other methods (pressure gradient deposition and ultrasonic deposition) can be used.[44] As stated previously, one of the largest issues with SLS printing is the lack of different and functionalised materials available for this technique. This project aims to address several of the key issues with SLS and PA-12 based parts produced via SLS.

Disadvantages of Selective Laser Sintering (SLS)

Selective laser sintering has several key disadvantages that keep this technique from being ubiquitous. The first, among others, is that parts can only be printed in white or black. White parts are produced from PA-12 particles and black/grey parts are made with PA-12 and a small percentage of carbon black. In fact, dyeing and/or spray painting the printed parts are currently the only ways to add colour to produced printed parts.[57] The dyeing process can be varied, but the underlying method for most dyeing techniques is similar, they involve submerging the part in a vat of dye at a high

temperature for an extended period of time (≥1hour). The spray-painting process, usually involves applying 4-5 thin coats of paint onto the part, with a wait time (drying period) in between each coat.[57] These processes lead to brightly coloured parts, but they have considerable negative consequences:

1. Lack of colour penetration for the part (≤0.5mm)
2. Added cost
3. Added production time for the part
4. The coatings can influence the dimensions of the parts
5. Labour intensive process for the spray painting[57]

To the authors knowledge the only research conducted into coloured SLS printing was conducted by Powell et. Al. and Hupfeld *et al.* by utilizing silicon coated gold and silver nanoparticles respectively of different sizes along with fabric dyes to add colour to the polymeric powders before printing.[58,59] However, this approach needs fine-tuned conditions in order to print in colour, such as not to damage the gold nanoparticles, and much like in the aforementioned colouring techniques the dye is not chemically bound to the polymer. Even though this process managed to print in colour, it has several disadvantages.[58,59] Firstly, the use of gold and silver nanoparticles adds a significant cost to the process, secondly there is no indication that colour mixing could be possible with this technique.[58,59]

The inability to print parts composed of different materials with sharp interfaces, thereby having portions of the built part with different physical and/or chemical properties, has not been possible. This is a drawback, because the whole part is

composed of the same material, hence the part has the same physical properties throughout. However, novel and innovative applications could be developed if the user could print a part composed of different materials with sharp interfaces. This is largely due to two factors, the deposition methods currently being used do not allow for the deposition of different materials without the materials mixing.

The materials are bound to mix because the roller spreads the material evenly across the whole build platform. The second limitation is material-based, because as aforementioned most used material is PA-12, and two or more different materials are needed, which have similar thermal properties. As long as the materials have similar thermal properties, they should be able to be printed together, thereby yielding a part that has different properties based on the layer of the part.

In selective laser sintering it has not been possible to print at resolutions higher than 60-100 µm. The resolution limit of the SLS process is imposed by a variety of factors as previously mentioned.

1.) Size of polymeric particles.

2.) Size of laser spot size.

3.) Control in z-direction of the build platform[60, 44, 50, 51]

By addressing these three limitations it should be possible to build a SLS system which can print at a higher resolution. Research has been conducted into developing a high resolution SLS system, however this work has been predominately conducted with metal particles instead of polymeric particles. Recently, Roy *et. al.* built an SLS printer with several notable changes, which increased the maximum resolution of metal SLS

printing to ~10 µm. The high resolution was achieved by using a particulate slurry composed of sub-micron metal particles and a surfactant to deposit a polymeric polymer layer, as well as a digital micromirror array in order to get a small laser sport size (~10 µm).[60] However, this like other studies have been conducted with metal particles, instead of polymeric particles.[61,62]

PA-12 based parts also tend to bio-foul quite rapidly. PA-12 membranes are one of the most widely used membranes for water purification, however the membranes degrade rapidly in water as they undergo bio-fouling.[63,64] This occurs with any PA-12 part that spends a significant amount of continuous time in an aqueous environment or in the presence of biofilm forming microorganisms. A material could be synthesized which has anti-fouling properties and similar thermal properties to PA-12, by coating PA-12 particles with an antifouling outer shell, which would enable users to print parts, which do not bio-foul.

Because PA-12 is the most frequently used material for SLS, there is a shortfall in terms of the mechanical strength of the parts built via SLS. Even though PA-12 has favourable mechanical properties when compared to other polymers such as poly methyl methacrylate (PMMA) and poly styrene (PS), it has considerably lower mechanical properties than 'high-performance' materials such as carbon fibre and steel. If these issues are addressed SLS could become a ubiquitous printing technique.

Introduction to Polymers

In order to address some of the problems previously mentioned related with the final performances of the SLS technique, novel polymers must be designed and synthesized. Polymers are large macromolecules that are composed of small repeating units known as monomers. There is a large variety of polymers, as they can be found in nature and be produced synthetically and be used for a wide range of applications. Polymers are often classified into homopolymers, copolymers, block copolymers, and random copolymers. Polymers which are entirely composed of the same repeating unit (monomer) are known as homopolymers. A polymer that is composed of more than one monomer is a copolymer. A random copolymer is a polymer, which is composed of more than one monomer, and the different monomers are randomly located throughout the polymer. A block copolymer is a polymer made up of a sequence of monomers which are arranged in linear blocks; with a block being defined as a portion of polymer molecule where the monomeric units have at least one constitutional or configurational feature absent from the adjacent positions.

Through the modification of a variety of features the properties of a polymer can be significantly changed. One way to alter the properties of homo or copolymers is to change the architecture and chain length of the polymers and/or polymer blocks. The properties of a polymer can be affected through the chemical alteration to the molecular structure of the monomer. Through the advancement of polymer

chemistry a range of polymer architectures have been created showing the versatility of this type of material (figure 5).

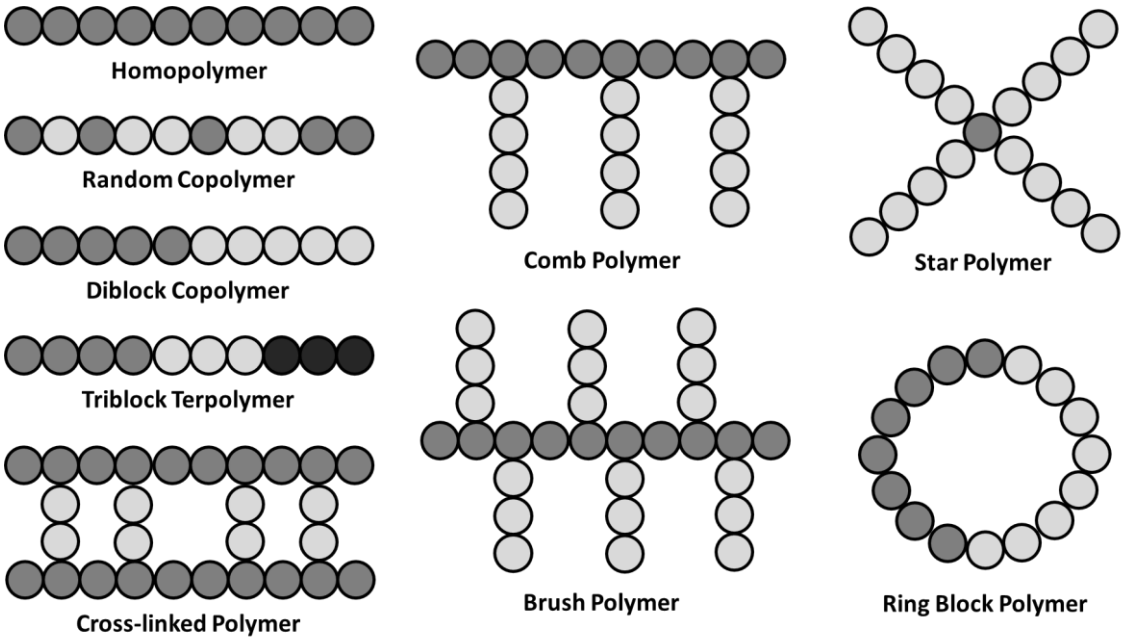


Figure 5 – Basic polymer and copolymer architectures: Homopolymer, Random copolymer, Diblock copolymer, Triblock copolymer, crosslinked polymer, comb polymer, brush polymer, star polymer, and ring block polymer.

Polymers can be synthesized through several methods, all of which belong to two main mechanistic classes. One of which is chain growth, an example of this is free radical polymerisation (FRP). The second class is step-growth polymerisation, an example of this is polycondensation. This project utilized different types of free radical polymerisation.

Free radical polymerisation (FRP)

Free radical polymerisation is a method of polymerisation, which forms a polymer through the successive addition of free-radical building blocks (monomers). The

reaction commences by the activation of an initiator. Initiators decompose into molecules which contain free radicals. Decomposition occurs under the presence of an external stimuli such as light or heat. Once the initiator such as AIBN has homolytically decomposed into two free radicals, they react with a monomer becoming a monomer radical. The monomer radical can then react with other monomers, starting the propagation of the polymer chain. This continues until the chains are terminated and/or the monomer is consumed (figure 6).

$I_2 \rightarrow 2I^{\bullet}$	*(Initiator Decomposition)*
$I^{\bullet} + M \rightarrow IM^{\bullet}$	*(Initiation)*
$IM\bullet + nM \rightarrow Pn+1\bullet$	*(Propagation)*
$Pn\bullet + Pm\bullet \rightarrow Pn+m$	*(Combination)*
$P_n^{\bullet} + P_m^{\bullet} \rightarrow P_n + P_m$	*(Disproportionation)*

Figure 6 – Free Radical polymerisation reaction mechanism, in which “I” stands for the initiator, “M” for monomer, and “P” for polymer chain.

FRP is one of the most common types of polymerisations due to several reasons:

1. The technique can be conducted with a broad range of monomers as it has robust tolerance towards chemical functionality.
2. It can be conducted in a range of solvents or in bulk.
3. It is less sensitive to air or impurities than other polymerisation techniques.
4. It is scalable.

Free radical dispersion polymerisation (FRDP)

A subset of FRP is free radical dispersion polymerisation (FRDP). FRDP is often used to produce particles. FRDP is a type of heterogenous polymerisation in which all the reagents are soluble in the solvent at the start of the reaction. The key reagents in an FRDP reaction are the stabilizer, monomer, initiator, and solvent. In this reaction all the constituents are soluble, but the resulting polymer is not and precipitates out of the reaction medium in particulate form.

To start the reaction an initiator (eg. AIBN) is needed. The initiator decomposes into free radicals, which subsequently react with the monomer, to produce monomer radical species (step 1, figure 7). At this stage the monomer starts to propagate, and until the polymer chains reach a critical molecular weight they remain in the solution (step 2, figure 7). After the threshold of the critical point is crossed, the polymer chains precipitate out (step 3, figure 7) and coagulate until stabilized particles are formed (step 4, figure 7). Stabilisation happens, because the stabilizer (eg. PDMS-MA) is bonded to the polymer particle either through covalent bonds or Van der Waals interactions. The growth of the polymer continues as the monomers add onto stabilized particles. Then the polymerisation ends as the monomer has been depleted.

The stabilizer is essential to the reaction as one end has an affinity toward the solvent and the other to the polymer, hence the stabilizer keeps the polymer particles in the solvent, so that monomer addition can continue.[65] The stabilizer also forms a layer around the particles that prevents particle coagulation.[66,67] This reaction has been utilized in the past to produce particles of PMMA of varying sizes.[66,67]

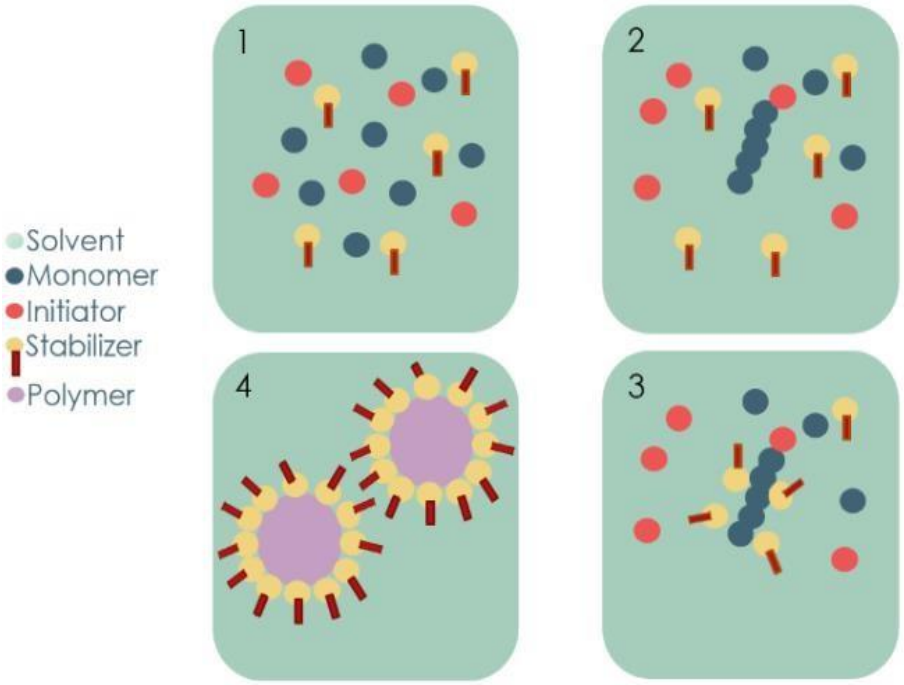


Figure 7 – Reaction scheme of dispersion polymerisation. In step one the reagents are dissolved in the reaction, (e.g. $scCO_2$). In step two the initiators have decomposed into free radical species and have reacted with the monomers, starting the propagation stage of polymerisation. In the third step the polymer chain has reached a critical mass, due to which it interacts with the stabilizer (e.g. poly(dimethylsiloxane)-methacrylate (PDMS-MA)) and starts to form particles. In step 4 the particles have formed, and the reaction finishes inside said particles as the remaining monomer is consumed.

This technique is carried out in traditional organic solvents to make polymeric particles. However, FRDP can also be carried out in supercritical CO_2 ($scCO_2$) , which enables the user to make particles of sizes ranging from 0.5 µm to 10 µm.

Polymerisations and Coatings in Supercritical CO_2 ($scCO_2$)

Through FRDP polymerisation in $scCO_2$, particles with sizes ranging from 0.5 µm to 10 µm can be synthesized, it is possible to coat larger particles as well, and a wide variety of polymer and particle architectures can be obtained.[68–70] This can be done in other reaction media, however CO_2 has several key benefits that make it the preferred reaction media. One of the main benefits for this application is that at the end of the reaction, the CO_2 is simply vented, yielding dry and pure polymer particles. This is important for SLS as the particle powder needs to be very dry, and when conventional methods are used the energy intensive drying steps are required.

$ScCO_2$ is a supercritical fluid which occurs when CO_2 is heated and pressurized past a criticial point, which in the case of CO_2 occurs once a temperature of 31.1 ^oC and a pressure of 7.4 MPa has been exceeded. This supercritical fluid has different properties than its gaseous or liquid states and can be used to tailor the solubility of reagents to suit a particular reaction, as by changing the temperature and pressure of a reaction the solubility of the reagents can change. To use supercritical CO_2 an autoclave must be used (figure 8). The autoclave is composed of 316L Steel, and it is built to withstand the pressures and temperatures used for polymerisations in $scCO_2$ (~2000-4000 psi and 30-100^oC). This range of pressure and temperature in $scCO_2$ allows for the solvation of many monomers such as methyl methacrylate (MMA), styrene, isobornyl methacrylate, etc. and the subsequent formation of polymers with transition glass temperatures and melting temperatures from above 31.1 ^oC to >200 ^oC, allowing for the creation of polymers suitable for PBF.

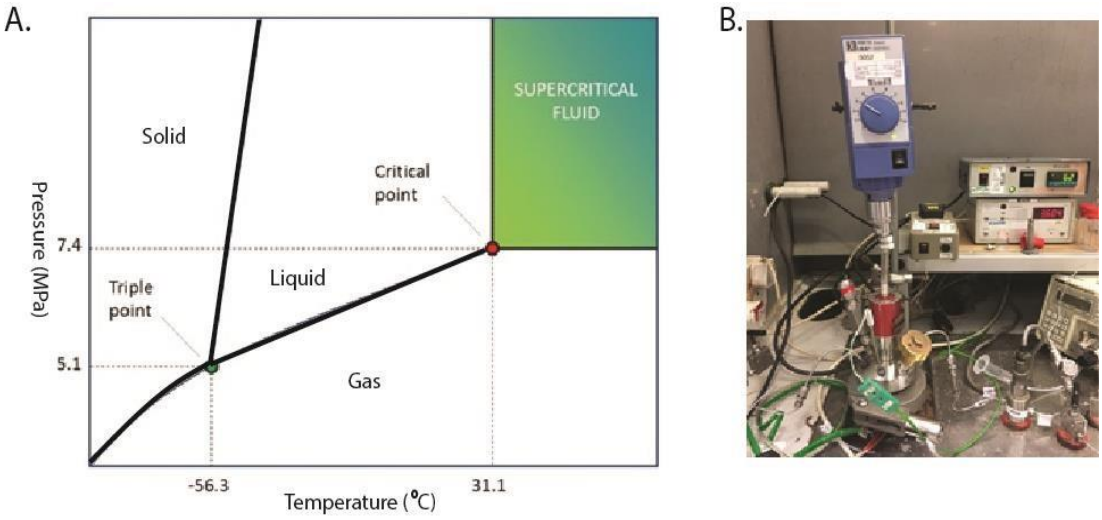


Figure 8 – A). Phase diagram of CO_2 showing that the critical point of CO_2 is at 31.1°C and 7.4 MPa B). Image of autoclave setup showing the autoclave, overhead stirrer, and safety devices such as the pressure and temperature monitors and trip systems.

When $scCO_2$ is used the benefits can be significant in both monetary and environmental costs as $scCO_2$ is cheap, can be recycled, and is a green solvent as it is non-toxic non-flammable, and avoids the energy intensive drying and purification steps.[68–73] The main advantages of this type of polymerisation are:

1. It is a greener polymerisation process as it is performed in $scCO_2$.
2. The dispersion aspect of the reaction allows the polymer to be composed of discrete monodisperse particles.
3. By using FRDP several new polymeric particles can be made, which could be suitable for SLS printing.

It is not only possible to create polymeric particles through dispersion polymerisation in $scCO_2$, but it is also possible to coat already existing particles in $scCO_2$, with an outer shell (figure 9). In the past polymeric particles and polymers of different shapes have been coated and impregnated with a range of substances through the use of $scCO_2$.

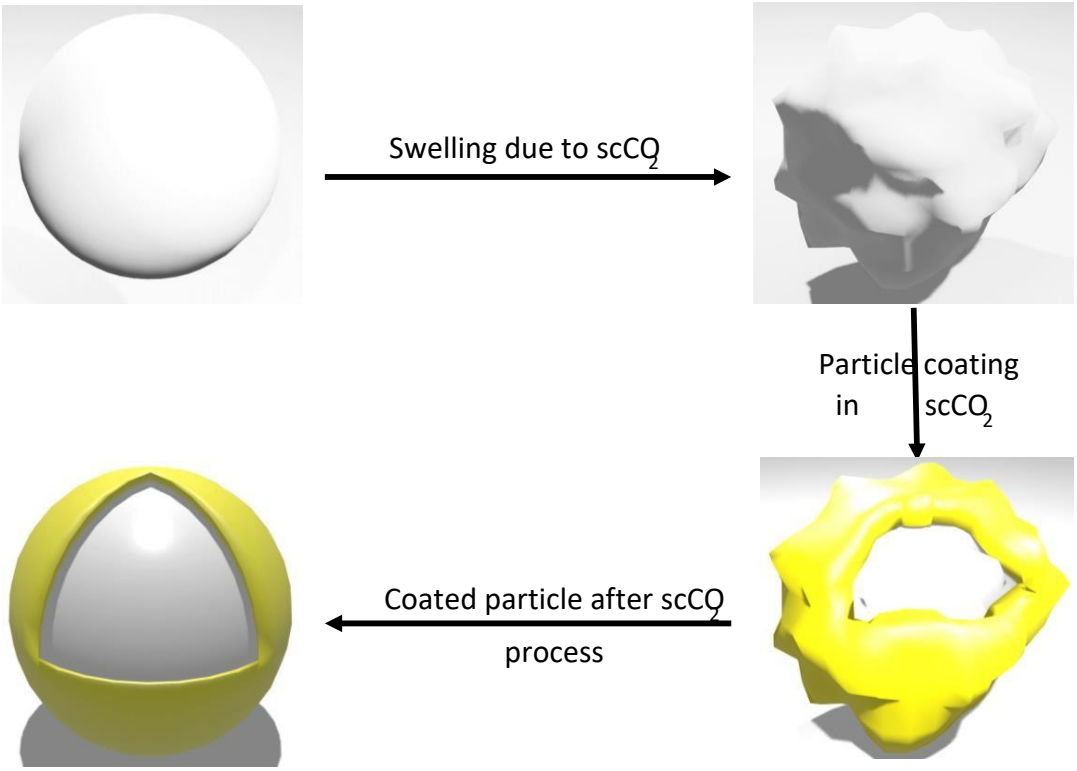


Figure 9 – Schematic of polymeric particle coating through free radical dispersion polymerisation in $scCO_2$. When in $scCO_2$ a polymeric particle will have its amorphous regions swollen by $scCO_2$, the swelling occurs due to CO_2 penetrating between the polymer chains, (swelling refers to the enlargement in size of the amorphous areas of the polymer particle, leading to a marginal growth of the particle, causing gaps in the surface of the polymeric particle). Then by introducing a dopant or a polymer the surface of the polymeric particle can be coated and slightly impregnated. Whilst the pressured is lowered the CO_2 is vacated from its position between the polymer chains

and the particles should return to their previous shape albeit with increased size, as the swelling of the amorphous regions is reversed.

Polymers that are amorphous or semicrystalline can be efficiently coated via $scCO_2$ as the amorphous regions in the polymer particles swell/deform allowing for partial impregnation of the coating species into the core polymeric particle. The swelling occurs due to CO_2 penetrating between the polymer chains and interacting potentially through hydrogen bonding. This creates larger gaps between chains thereby causing the particle as a whole to swell. Literature has shown that polyethylene, polytetrafluoroethylene, polyvinyl acetate, poly methyl methacrylate, etc. can be swollen with $scCO_2$ at varying conditions.[74–77] More specifically and pertaining to this work $scCO_2$ has been shown to swell polyamide materials in different forms from thin films to membranes.[78–81] This aspect has been used to dope a variety of polymers with varying substances as the porosity of the polymers is increased and the rigidity is decreased.[82–88] Polyamide materials have been impregnated with substances such as dyes and pharmaceutical agents, as the $scCO_2$ can swell the amorphous regions of the polymer.[78–81] This feature should allow for the physical formation of shells on particles, thereby allowing for the synthesis of core shelled particles without the need of chemical bonding. The formation of the polymeric outer shells on top of PA-12 particles should work, as the PA-12 particles acts as the reaction locus for the polymerisation. At first in the reaction the monomer and initiator are soluble in $scCO_2$, as is characteristic of dispersion polymerisations in $scCO_2$, and initiation and initial propagation stages of the polymerisation occur in the $scCO_2$ phase and at this point the polymer chains can go into the swollen parts of the polymeric core shell (eg. PA-

12), then when a certain chain length of polymer is reached the polymer chains are no longer soluble in $scCO_2$ and the reaction finishes on the outer shell of each particle. This is analogous to normal dispersion polymerisations in $scCO_2$ in which the polymerisation finishes in the formed particles as the rest of the monomer is consumed. Then once the pressure is lowered by venting the $scCO_2$ out of the reactor that particles will revert to their normal shape, along with their new coating (figure 9). With this method the user should be able to adequately and reliably coat PA-12 particles with a variety of polymeric outer shells, as long as they are initially soluble in $scCO_2$.

Project Aims and Methodology

The aim of this project is to address the aforementioned issues with SLS. The first goal is to synthesize materials and develop a process which would enable users to print in colour. These coloured polymeric particles could be used to develop a colour mixing system for SLS, allowing a user to print in any colour. Novel materials and a powder deposition system will be designed in order to facilitate the production of multimaterial parts with sharp interfaces. This project aims at the development of new polymeric particles along with a new SLS rig to print with resolutions of 10-20 µm. Polymeric parts will be built via SLS that have anti-fouling properties. Lastly polymers will be synthesized that can crosslink in situ during SLS in the hopes of creating materials that have improved physical properties. Accomplishing these aims, will allow for the production of parts, which could have varied applications across different industries.

Development of coloured SLS printing

In order to print parts via SLS in colour, coloured polymeric particles must be produced. The first step to synthesizing said particles is to create monomer dyes. This process is based on well-known methacrylation reactions.[89–92] These reactions add a methacrylate moiety to an alcohol group, either by a reaction utilizing methacryloyl chloride or an enzyme (Novozym 435) when methyl methacrylate is adopted.[89–92] However, to begin, commercial dyes must be chosen that have the correct functionality; an alcohol group and preferably no other functional which react preferentially with methacryloyl chloride. The commercial dyes that have the appropriate functionality need to be screened in terms of their colour "retention" before and after the methacrylation reaction. This is because the addition of the methacrylate moiety may cause a shift of the lambda max of a molecule hypso or bathochromically.[93,94] The colour of the prospective dye monomers can be predicted computationally using time-dependent density-functional- theory (TDDFT) approaches, which are commonly used to predict the colour of a broad range of pigments and dyes[95–97] These computational methods have been used to predict the λ_{max} of dyes within an accuracy of 5 nm.[95–97] Once a dye-monomer is made, it can be homo-polymerised or co-polymerised with other methacrylates. This allows for a wide variety of polymers to be made with a broad range of properties, because in theory these dye monomers could be polymerised, ideally, with any methacrylate that does not provide excessive steric hindrance to the pendant groups of the dye monomers. By exploiting this method cyan, magenta, and yellow dyes can be made, thereby allowing for the creation of a CMYK colour mixing system for SLS. To

introduce colour to SLS, the strategy is to produce coloured PA-12 particles. The coloured PA-12 based particles will be produced by coating commercial PA-12 particles in $scCO_2$. The coated PA-12 particles should have the intrinsic and extrinsic properties needed for SLS printing (figure 10).

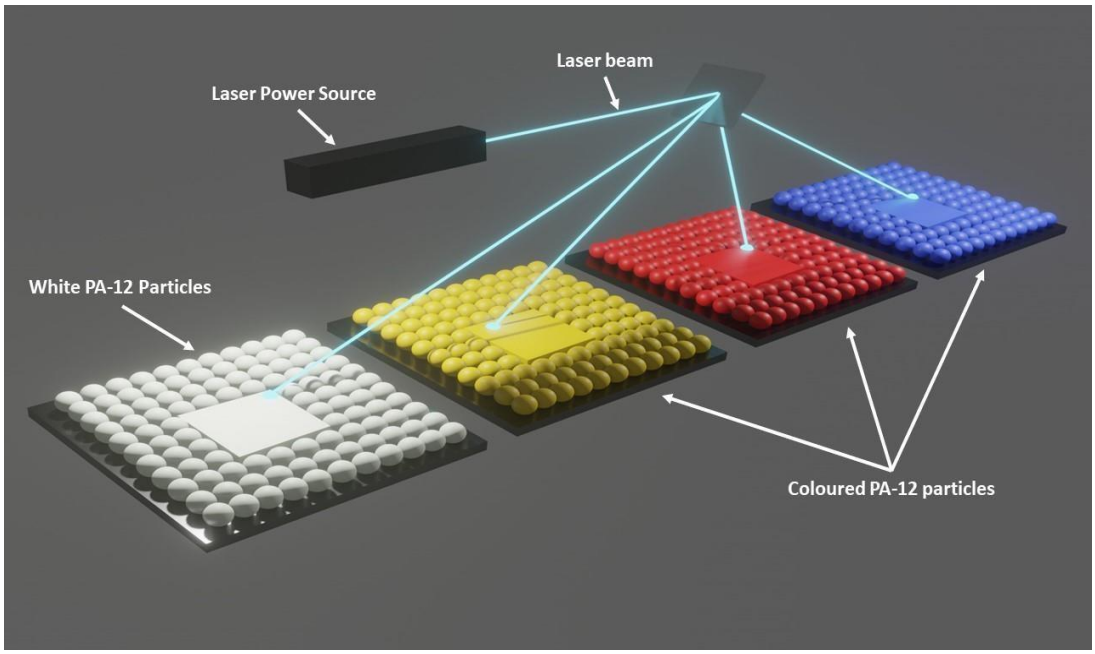


Figure 10 – Selective laser sintering of coloured particles. Commercial PA-12 particles coated with P(IBMA – dye monomer), specifically with yellow, red, and blue dye monomers.

Development of a CMYK colour mixing system for SLS

Through the use of the red, blue, and yellow coated PA-12 particles, a CMYK colour mixing system can in theory be developed for SLS printing. CMYK colour mixing is a form of subtractive colour mixing used for colour inkjet printing. These four colours (Cyan, Yellow, Magenta, and Black) are used as they complement different colours, enabling the production of a wide array of colours by mixing them together in the precise ratios.[100] CMYK functions by partially or entirely masking colours on a light

(white) background, and the ink reduces the light that would be otherwise reflected, thereby creating another colour. Cyan, Yellow, and Magenta are used to make the desired colours on the material, while black is used for only deeply dark areas.[100] In theory only Cyan, Yellow, and Magenta are needed for this colour mixing system to operate, and some inkjet printers work with these three colours, because the mixture of all three can also create black.[100]

Coloured polymeric parts built via SLS could be used for a variety of applications. SLS is used in the automotive, airline, and fashion industry to create parts which are subsequently painted.[30,34] In the automotive industry this technology could be used to print ready to use parts that are coloured such as glove box lids, cup-holders, knobs, switches, etc. In the fashion industry the use of these coloured materials could be extensive as SLS has been used to produce dresses, shirts, and shoes.[27–29] Companies like Puma, Nike, and New Balance have printed customized shoes and shoe soles for athletes.[29] For aircrafts SLS would be able to print lightweight parts for the interior such as belts, armrests, food trays, by being able to print these parts in colour the companies could save time and money.[34]

Development of High Resolution SLS

We propose to achieve High-resolution (10 – 20 μm) SLS combining the synthesis of novel polymeric particles, and the use of an innovative printing rig (figure 11). In particular, via free radical dispersion polymerisations in $scCO_2$ polymer particles can be produced with sizes ranging from 0.5 μm – 10 μm, and narrow dispersities.[70]

The particles produced for this project present a particle size ranging from 1 µm – 3 µm. A variety of co-polymeric particles based on PMMA can be synthesized in order to compare its printability with that of PMMA particles. PMMA particles were processed via ball milling and cryogenic milling in order to improve the particles' SLS pertaining properties. The other two issues: laser spot size and build platform control in the z-direction, were addressed through the use of a SLS printer jointly developed with the institute of photonics and crystallography in Moscow, Russia.

There could be multiple applications for high-resolution SLS printing. This technology could potentially be utilized in the biomedical field and electrical engineering, as this would be a high enough resolution to print detailed biomedical devices and high resolution sensors and circuits.[101,102,103,104]

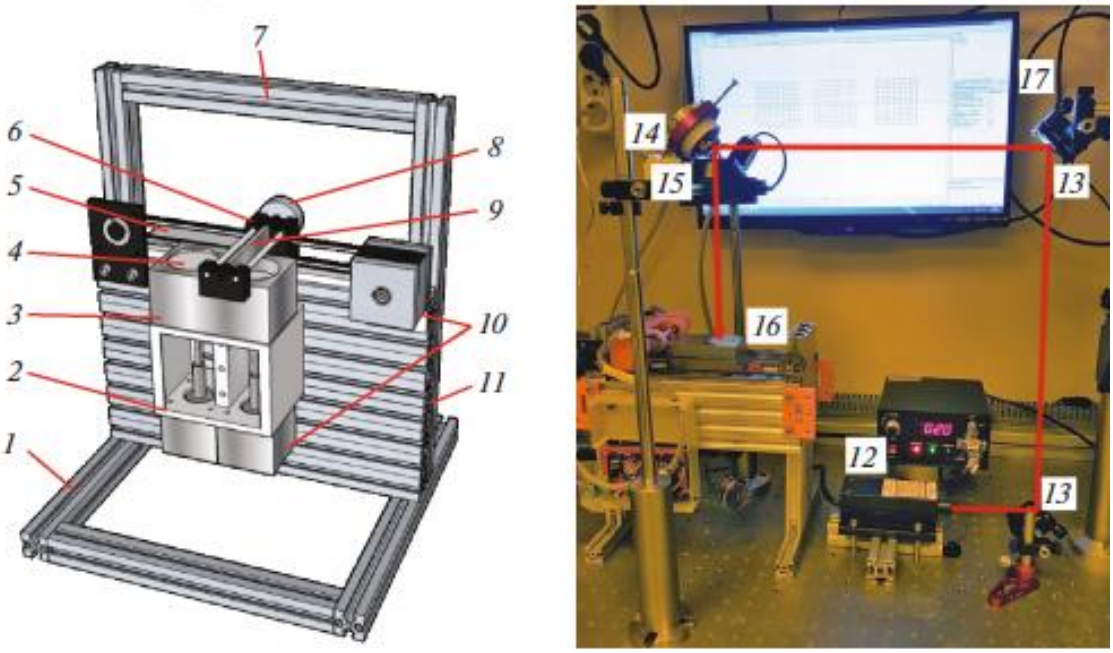


Figure 11 – High resolution Selective laser sintering (HRSLS) A.) Schematic of highly controlled powder deposition for SLS B.) image of HRSLS printer.[105] 1, Frame; 2, piston drive housing; 3, block of working chambers; 4, pistons; 5, unit power supply; 6,

levelling device housing; 7, fastening of the laser scanning module (galvanic scanner); 8, mechanical or piezoelectric levelling device activator; 9, the working element of the levelling device; 10, step drives; 11, microcontroller; 12, laser; 13, mirrors; 14, galvanoscanner; 15, lens; 16, the working layer of powder; and 17, control computer. The powder deposition piston has an accuracy of 5 μm this allows for the creation of layers with a thickness of 5 μm. The laser array (Parts 11-16) operates with a UV laser (405 nm) instead of a CO_2 laser bringing the theoretical resolution from 10.6 μm to 405 nm, thereby enabling high-resolution SLS as long as the correct polymeric particles are utilized.

Production of multi-material objects via SLS

One of the other problems with SLS that will be addressed in this project is the production of parts via SLS that are composed of different materials with sharp interfaces. As previously mentioned, this issue is caused, by two different factors. One being the powder deposition method and the other is the lack of a large variety of materials used for SLS. The powder deposition problem will be solved, by producing an attachment to sit upon the powder spreader. This attachment will only deposit powder in select layers, and not into the powder reservoirs, thereby preventing the mixing of the materials between layers. This should, in theory, provide a mechanism by which to deposit a 2nd material on top of another with a sharp interface. The material issue will be solved by developing materials with different chemical or physical properties that have similar thermal properties. By using materials with similar thermal properties, parts can be printed that are composed of 2 or more materials, with different and/or alternating physical properties based on the location

of the part. Through these two developments printing parts composed of different materials with sharp interfaces should be possible (figure 12).

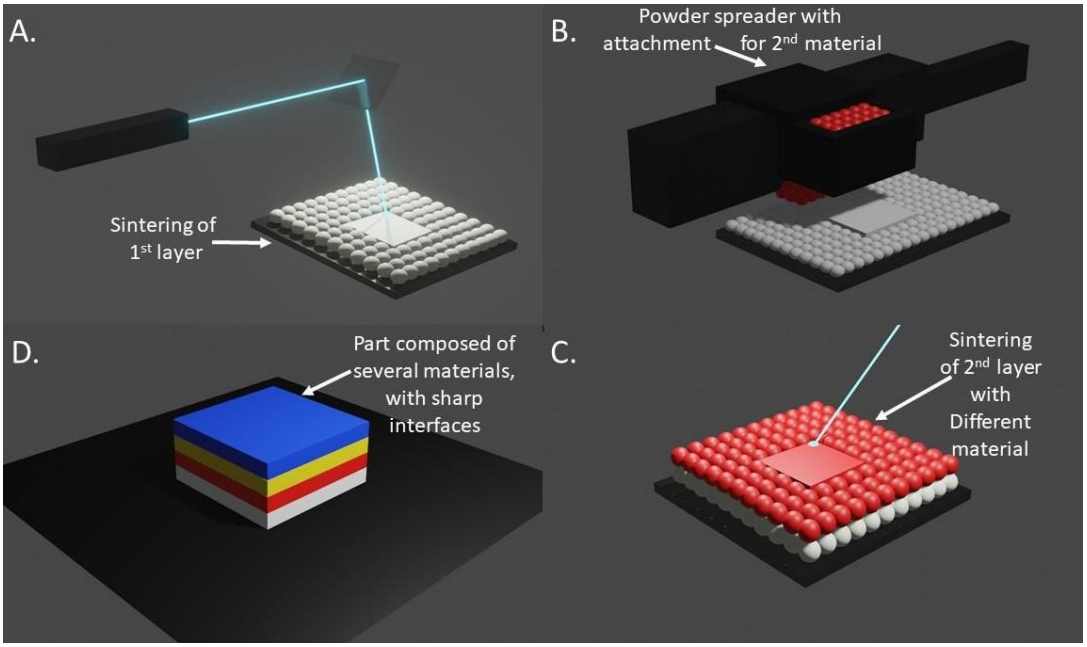


Figure 12 – Production of parts printed via SLS composed of different materials. A.) Printing of the first segment of the part. B.) Deposition of second material aided by the attachment for the dual hopper powder spreader. C.) Sintering of the second segment of the part. D.) Finished part composed of different materials with sharp interfaces.

Synthesis of anti-attachment materials for SLS

PA-12 particles are prone to biofilm formation and subsequent bio-fouling when in an aqueous environment and/or in the presence of microorganisms which cause biofilm formation.[106,107] This has been shown as even though PA-12 membranes have many beneficial properties, they form biofilm rapidly, which significantly decreases their life-time. Biofouling is the accumulation of microorganisms, plants, algae, or small animals on wetted surfaces that have a mechanical function, causing structural or

other functional deficiencies.[106,107] In this project, a coating will be developed, which has anti attachment/ biofilm preventing properties (figure 13). The coatings will be made in $scCO_2$, through FRP. Producing such a coating, will allow for the production of PA-12 parts with longer lifetimes.

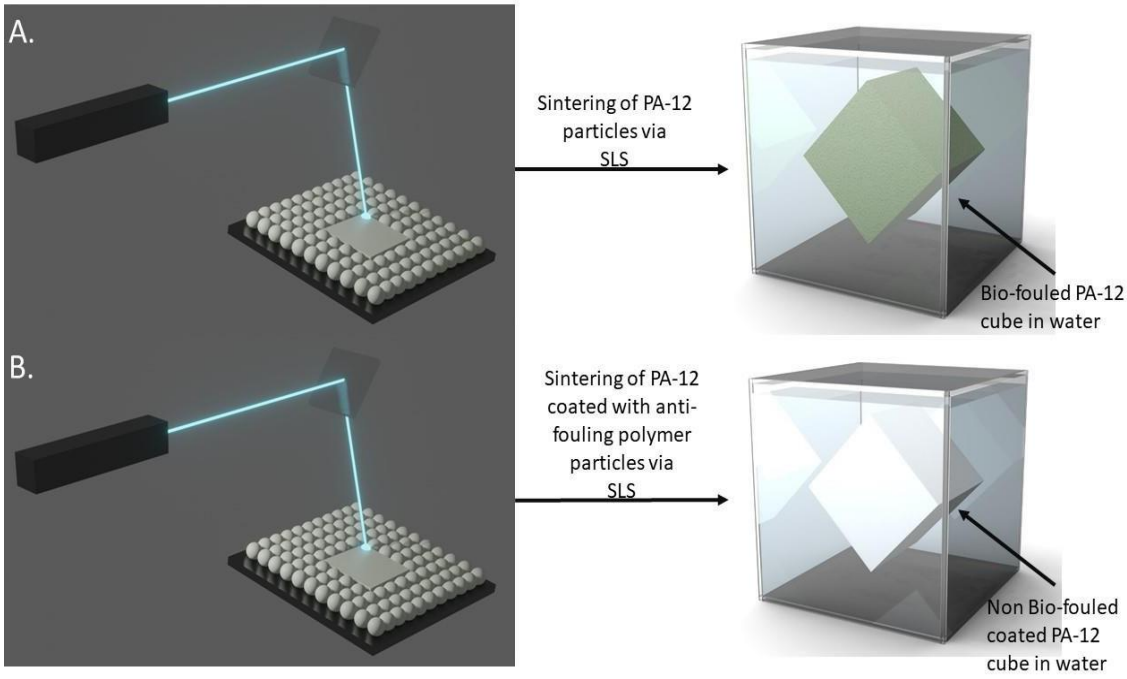


Figure 13 – Schematic of biofouled vs non-fouled PA-12 based parts built via SLS A.) Bio-fouled PA-12 part made via SLS B.) Non-biofouled PA-12 part made via SLS coated with P(IBMA terpene or modified acid (meth)acrylate).

The anti-attachment polymeric particles would have several industrial applications. One possibility comes from the maritime industry, as SLS and other 3D printing technologies are used on land and in the air to quickly produce spare parts for planes and automobiles.[30,34] However, the propensity towards bio-fouling of the PA-12 built parts has inhibited the use of SLS for repairs on boats and other aquatic vehicles. Through the use of this material, parts could be printed, which would withstand

aquatic environments for longer periods of time, therefore it could be used to produce spare parts for boats. Membranes for water filtration could be printed, and would have enhanced properties, as currently PA-12 membranes are used for water filtration because they have excellent properties, with their main downside being a short life-time due to biofouling, and this material would alleviate said issue. These anti-attachment materials could also be used to print household products and biomedical devices which are prone to contacts with microorganisms which can cause biofilm formation and biofouling.

Development of parts with increased tensile strength

The last issue that will be addressed in the project is the production of parts with improved tensile strength for SLS. In order to produce parts with improved tensile strength particles will be functionalised by creating a polymeric shell on the outside of each sphere containing active minor monomers that could undergo crosslinking. The purpose of the of these active monomers was to provide a means of producing in-situ or post printing chemical bonding, to increase the mechanical properties of the parts. Studies show that crosslinking can increase the tensile strength of part (figure 14).[110]

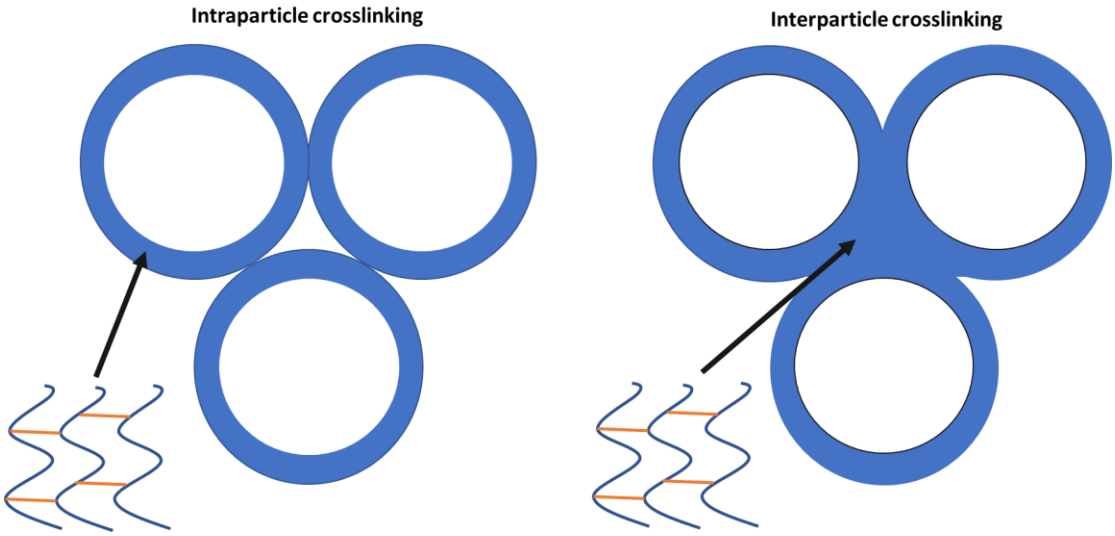


Figure 14 – Difference between intra and inter particle crosslinking. Particles whose outershell is crosslinked pre-sintering, will not result in a crosslinked network, what will occur is a part composed of individually crosslinked particles. Particles which can crosslink in-situ during sintering will result in parts with interparticle crosslinking, thereby having a crosslinked network throughout the part, resulting in improved mechanical properties.

Chapter 1: Dye monomer synthesis

Introduction:

In this part of the project dye monomers were synthesized. The aim of the production of such dye monomers is to use them to coat commercial PA-12 particles, in order to produce polymeric particles that are coloured and can be used for SLS printing. To begin the process of synthesizing the dye monomers, commercial dyes were screened to find dyes that could be functionalized in such a way as to convert them into monomers. The dyes were screened via six search parameters:

1.) The molecule needs to have an alcohol group, preferably a primary alcohol.
2.) The dye cannot be very expensive.
3.) The dye molecule cannot be too large.
4.) Preferably the dye should not have other reactive functional groups.
5.) The dye must have the correct colour.
6.) The dye should not contain halogens.

The type of monomer functionality chosen was a methacrylate moiety, for a variety of reasons: good mechanical, thermal, and optical properties.[1–6] The selected dyes were investigated through TDDFT calculations to ascertain whether or not they would have the desired colour after methacrylation, as changing the molecular structure of a dye can greatly influence its colour. A screening of methacrylate synthesis routes was performed, so that scalable, high conversion, low step (fast), and 'green' reaction routes could be utilized to produce the dye monomers. Suitable reaction routes were used to synthesize three dye monomers: Disperse Red 1 Methacrylate, Yellow 1

Methacrylate, and Disperse Blue 3 Methacrylate, which can readily co-polymerize with a wide range of commercial and in-house methacrylate-based monomers, yielding polymers with varying properties.

Selective laser sintering has many key advantages compared to other additive manufacturing techniques, however one of its drawbacks is that it cannot print in colour.[7] This is because, the polymers used for SLS are white.[7] Black and grey parts have been produced via SLS, but this is because carbon black was added to the polymeric particulate powders. The purpose of carbon black is often not to add colour, but rather to increase the laser absorption of the polymeric powder to encourage better sintering resulting in improved mechanical strength.[8,9]

In order to impart colour, the parts are usually dyed/painted as a post-processing step.[10] The painting process is done by two methods. The first is a dyeing technique that can vary slightly between commercial processes, but the underlying method involves submerging the part in dye at high temperature for an extended period of time (≥ 1 hr). The second is spray painting, which involves applying four to five thin coats of paint onto the part. There is also a drying period after each coat is applied. These processes lead to brightly coloured parts, but they have considerable drawbacks:

1.) Lack of colour penetration (max 0.5 mm)
2.) Added cost
3.) Added production time
4.) The coatings can influence the dimensions of the parts

5.) Labour intensive process for the spray painting.[10]

To the authors knowledge, the only research into coloured SLS printing was conducted by Powell et. al. in which silicon coated gold nanoparticles of different sizes were utilized along with fabric dyes to add colour to the polymeric powders before printing.[11] However, this approach needs fine-tuned conditions to print in colour, so as not to damage the gold nanoparticles, and much like the aforementioned techniques the dye is not chemically bound to the polymer.[11] Even though this process managed to print in colour, it has several disadvantages. Firstly, the use of gold nanoparticles adds a significant cost to this process, secondly there is no indication that colour mixing could be possible with this technique, thirdly this process seems to be only applicable to PA-12 particles, as it was only conducted on PA-12 and for the colour to work the process needed fine-tuned conditions which were optimized for PA-12.

In this project we propose a solution to the aforementioned issue concerning printing via SLS (figure 1). The proposed process starts with the chemical addition or coupling of methacrylate functionality to commercial dyes in order to synthesize red (magenta), blue (cyan), and yellow dye monomers. The methacrylate functionality was chosen as there are many methacrylate-based polymers with a range of thermal, mechanical, and optical properties.[1–6] Through the implementation of a methacrylate moiety, the dye monomers could be copolymerised with a wide range of other monomers. This is advantageous as methacrylate polymers can have a variety of glass transition temperatures (T_g) such as poly(lauryl methacrylate) (-65°C) and poly(isobornyl methacrylate) (165°C).[12,13] This means that one can tune the T_g of the

copolymer to match the T_m or T_g of the material used as the core, so that both the outer shell and core sinter at the same time, which is essential for SLS printing (figure 1).[14–16]

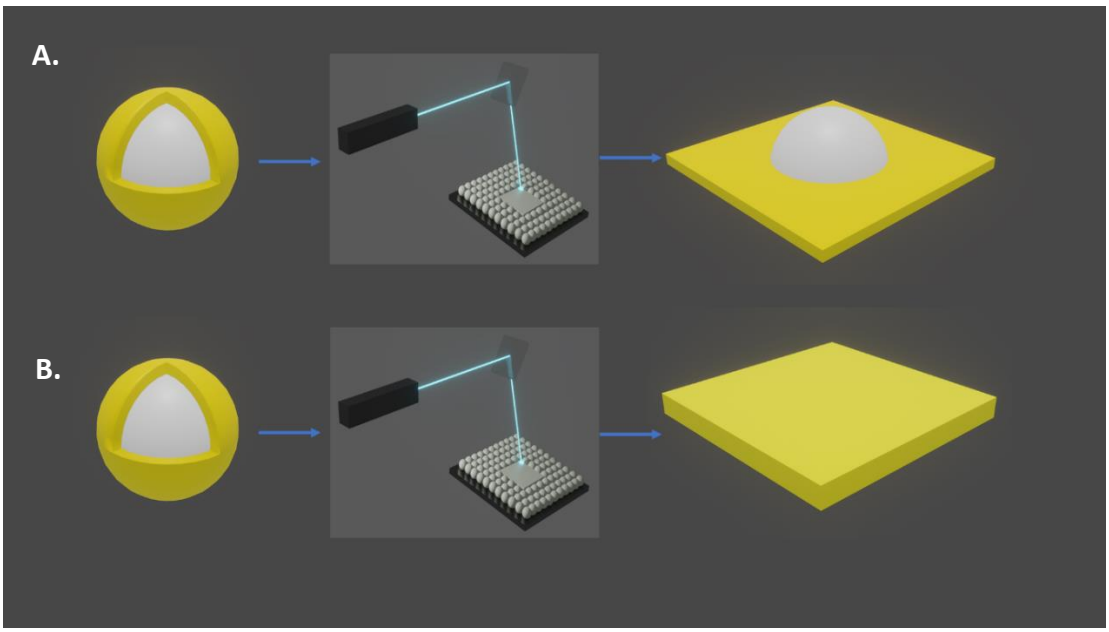


Figure 1 – Differences in sintering depending on the thermal properties of the core and outer shells A.) Undesirable sintering resulting from the core and outer shells having different thermal properties (core does not melt while outer shell melts) B.) Desired sintering occurring as a result of matching thermal properties from the outer and core shells (both core and shell melt at the same time).

The physical properties of many methacrylates are desirable as their mechanical strength is high, an example of such a material is Poly(methyl methacrylate), which is used commonly for trademarked materials such as Plexiglas©. The optical properties of methacrylate-based polymers are suitable for the project as most absorb radiation in the mid-infrared region, hence the polymers could absorb the radiation from the SLS printers, which most often utilize CO_2 lasers with a wavelength of 10.6 µm.[17,18]

Lastly the process by which the polymers will be made uses supercritical CO_2 ($scCO_2$) as a solvent and literature and past work shows that methacrylate monomers readily solubilize in $scCO_2$ and can be polymerized in such a solvent system (Chapter 2 and Appendix 1).[19–22] These factors make the addition of a methacrylate moiety to the commercial dyes enticing. By incorporating a methacrylate moiety onto commercial dyes, we could open a door to a wide variety of possible copolymers.

The three colours that were chosen were red (magenta), blue (cyan), and yellow. These colours make up the basis for an often-used colour mixing technique: CMYK colour mixing (cyan, magenta, yellow, and black).[23–25] This colour mixing technique is a subtractive colour mixing system, in which each layer of colour absorbs some wavelengths of light from the illumination spectrum whilst letting others pass through, resulting in a coloured appearance. This system is used most commonly in the mixing of dyes and inks for coloured printing and photography.[23–25] With CMYK colour mixing a manufacturer can use the red (magenta), blue (cyan), and yellow dyes to create any other colour by mixing them in the appropriate ratios. A black dye monomer is not needed as it is possible to make a black colour by mixing the other three dyes together.[23–25] Red was chosen as one of the three colours, as magenta is an extra spectral colour, hence it is not associated with monochromatic visible light.[26] Magenta is often described as a variety of colours depending on the use/application and/or observation.[26] Often being described as red and/or purple, for this reason red was chosen. Blue was selected as cyan is a subset of blue, with wide ranging definitions as it can sometimes be interpreted to be bluer or greener. The final colour that was selected was yellow as it is the final component needed to develop a CMYK

colour mixing system. Picking red and blue allowed for a more rapid and thorough screening of commercial dyes, which led to the selection of dyes, which had the desired functionalities, cost, colour, and suitability with the reaction vessels (figure 2). In chapter 4 it can be seen that the synthesis of these dye monomers allowed for the creation of the first CMYK colour mixing system for SLS.

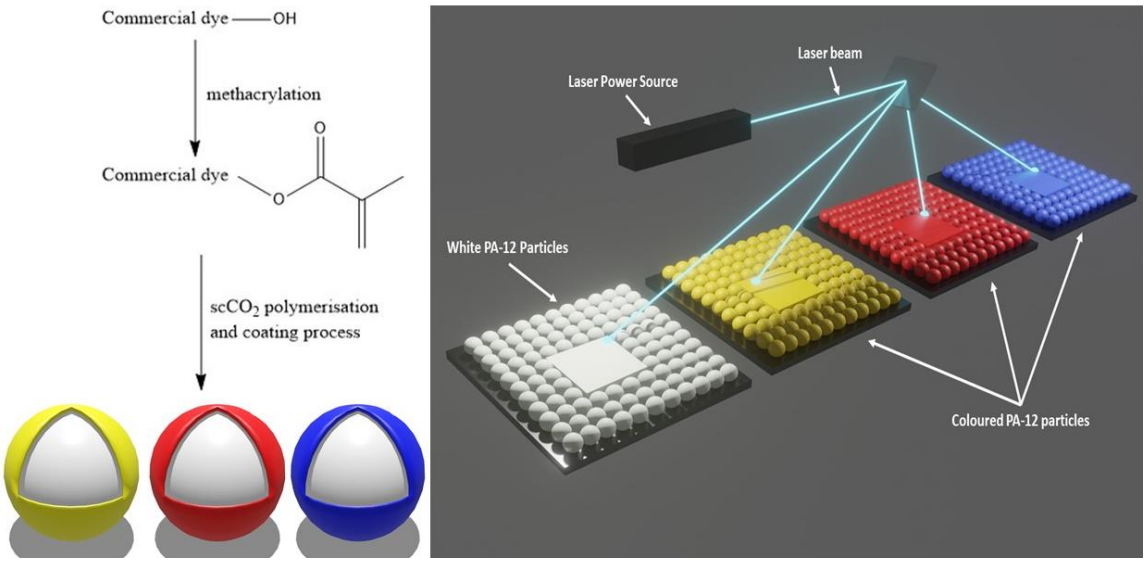


Figure 2 – Schematic diagram for colour addition onto polymers, and subsequent coloured SLS.

Dye screening:

The process of the synthesis of red, blue, and yellow monomers started with the screening of commercial dyes. The dyes were evaluated through six criteria:

1.) The molecule needs to have an alcohol group preferably a primary alcohol.

2.) The dye cannot be very expensive.

3.) The dye molecule cannot be too large.

4.) Preferably the dye should not have other reactive functional groups.

5.) The dye must have the correct colour.

6.) The dyes should not contain halogens.

The dye molecule needs to have an alcohol group for a variety of reasons. The main reason is that in many of the possible synthesis routes an alcohol group is used to react with a chloride/ester/acid group to attach the methacrylate onto the molecule.[5,27,28] A primary alcohol is preferable to a secondary or tertiary alcohol, as it offers less steric hindrance in the reaction.[28] The enzymes used in the methacrylation reactions are selective towards primary alcohols, so having other alcohols (secondary/tertiary) would automatically rule out potential synthetic routes to the target molecules.[28]

The dye cannot be overly expensive, largely because, if these dye monomers are to be used for SLS; large scales of coloured polymers will be used. Therefore, even if the dye monomer colour is very intense, a relatively large amount will still be used to create 1 Kg batches, ruling out any dyes that are sold in milligram quantities and/or cost hundreds of GBP per gram. The other factor is that the aim of the project is to create a commercially viable product. In order to create a product that consumers would purchase, the price needs to be in line with current products while also taking into account the added value of the product in question. The most widely used polymeric particle material used in the industry is PA-12 and its price is ~70-80 GBP per Kg depending on the supplier. To obtain coloured materials, the user often needs to send the part to a specialized company for dyeing/painting of SLS parts. This leads to added cost and time, and sometimes loss in part efficiency, as the painting process can alter the dimensions of the part. The pricing can greatly vary depending on part size, colour, and quality of finish required. Larger entities have purchased and installed dyeing equipment in house however the cost of this is ~75,000£ per machine excluding

working and training time needed to operate them and return on invest is only seen for parts that have a high volume and the dyes are an added cost. The target product of this project would remove the need to send parts to companies for dyeing or purchasing expensive equipment, as the starting material would be coloured. This would benefit the user as the dimensions of the part would not be affected by the painting process; and the cost and time needed to get coloured parts would be eliminated. Therefore, the dyes should be selected in an effort to make a coloured polymeric particle material whose cost is similar or lesser to PA-12 and the final painting process.

The third requirement is that the dye should not have a molecular structure that is very large. This is a vague, but important consideration as some dyes have structures with hundreds of atoms. These large structures lessen the likelihood that the dye monomer would become part of the polymer chain even if it has a methacrylate functionality. This is because the pendant group could sterically hinder the addition of further monomer units onto the chain, leading to inefficient reactions as only a very small amount of dye monomer units would be added onto the polymer chain. Effectively a smaller pendant group would aid in the polymerisation of the dye monomer.

The fourth is that the dyes should preferably not have reactive functional groups, with the exception of a single primary alcohol. This is because the synthesis route could yield various by products as the chlorides/esters/acids used in possible reactions can react with a wide range of functional groups, yielding products without methacrylate groups, or methacrylate groups in an undesirable place, or multiple methacrylate groups on the same molecule. Polymerisations with such products could lead to no

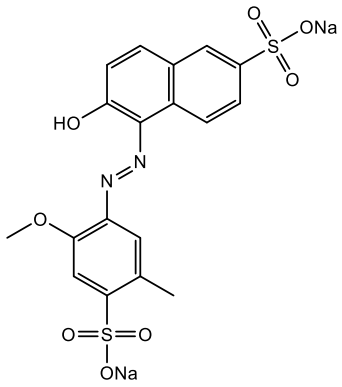
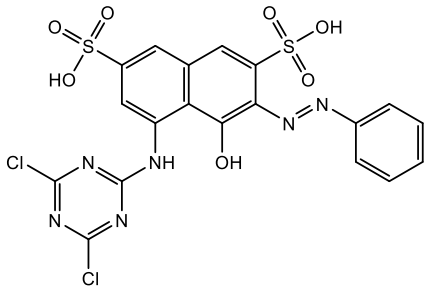
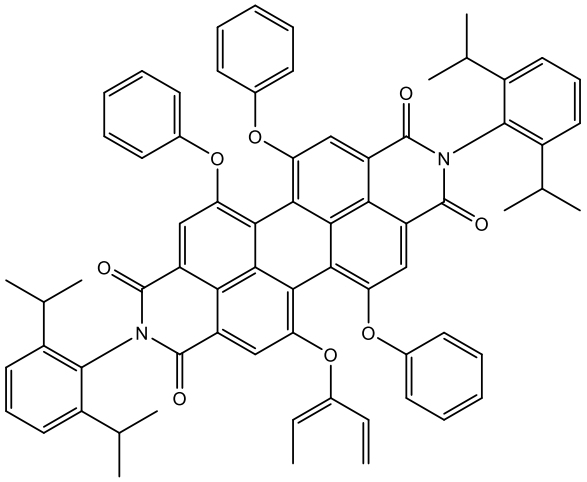
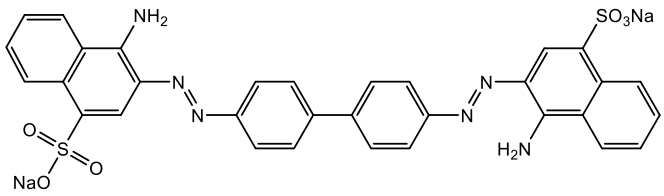
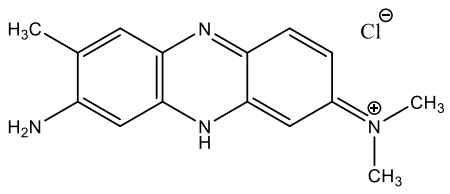
conversion of monomer, hyperbranched, or crosslinked polymers. Therefore, to limit this uncertainty it is preferable to limit the amount of competitively reactive functional groups on the dye molecule as much as possible.

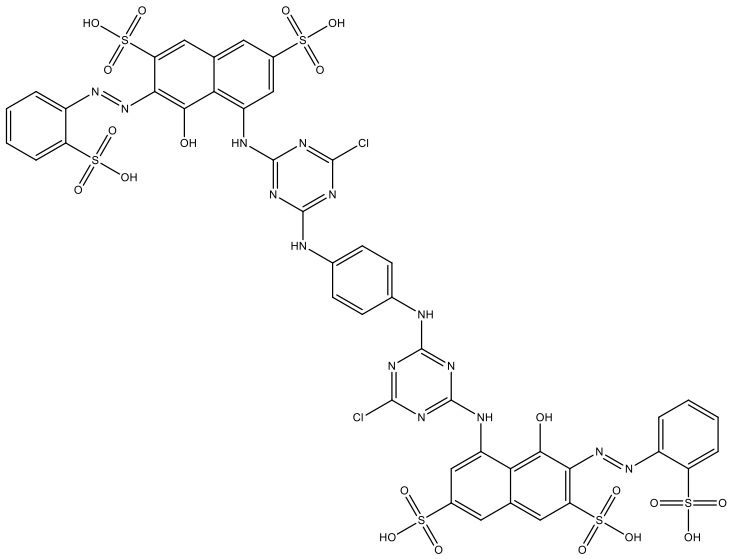
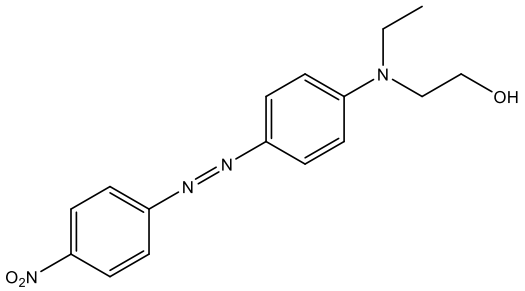
The fifth requirement is that the dyes must have the correct colour. To establish a CMYK colour mixing system three dye monomers needed to be synthesized, red (magenta), blue (cyan), and yellow.

The sixth and final requirement for the dyes is that they cannot have any halogens. This is an important safety concern, as the polymerisation reactions will be performed in $scCO_2$. To work with $scCO_2$ an autoclave is needed, because of the high pressures involved. The autoclaves are made of 316L stainless steel, which when exposed to halogens can corrode leading to pickering.[29–32] This can result in spontaneous leaks or explosions, so for this reason the dye cannot have halogens in its structure.

The first colour dye that was searched for was red. There are a multitude of red dyes available all with different structures, applications, and prices. Seven different commercial red dyes were found (table 1).

Table 1 – Structures of seven Red dye molecules with their IUPAC and commercial names

Structure of Red Dye molecules	Names
	disodium;6-hydroxy-5-[(2-methoxy-5-methyl-4-sulfonatophenyl)diazenyl]naphthalene-2-sulfonate (Allura Red AC)
	disodium;5-[(4,6-dichloro-1,3,5-triazin-2-yl)amino]-4-hydroxy-3-phenyldiazenylnaphthalene-2,7-disulfonate (C.I. reactive red 2)
	7,18-bis[2,6-di(propan-2-yl)phenyl]-11,14,22,26-tetraphenoxy-7,18-diazaheptacyclo[14.6.2.2^{2,5}.0^{3,12}.0^{4,9}.0^{13,23}.0^{20,24}]hexacosa-1(22),2(26),3,5(25),9,11,13,15,20,23-decaene-6,8,17,19-tetrone (Perylene Red)
	disodium;4-amino-3-[[4-[4-[(1-amino-4-sulfonatonaphthalen-2-yl)diazenyl]phenyl]phenyl]diazenyl]naphthalene-1-sulfonate (Congo Red)
	8-*N*,8-*N*,3-trimethylphenazine-2,8-diamine;hydrochloride (Neutral Red)

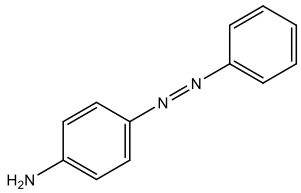
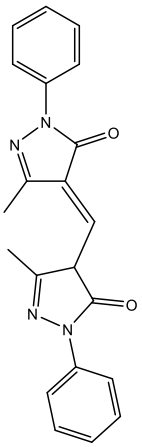
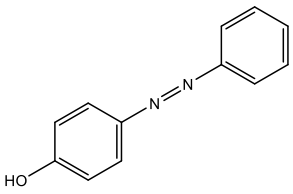
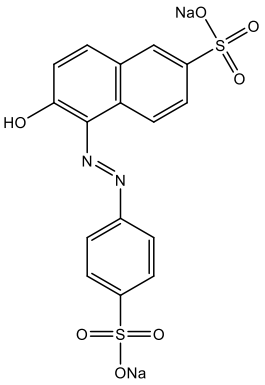
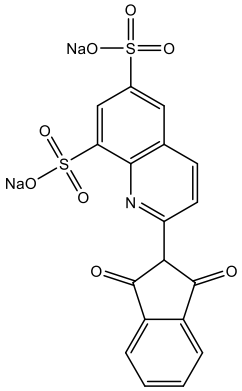
Structure of Red Dye molecules	Names
	5-[[4-chloro-6-[4-[[4-chloro-6-[[8-hydroxy-3,6-disulfo-7-[(2-sulfophenyl)diazenyl]naphthalen-1-yl]amino]-1,3,5-triazin-2-yl]amino]anilino]-1,3,5-triazin-2-yl]amino]-4-hydroxy-3-[(2-sulfophenyl)diazenyl]naphthalene-2,7-disulfonic acid (Reactive Red 120)
	2-[*N* -ethyl-4-[(4-nitrophenyl)diazenyl]anilino]ethanol (Disperse Red 1)

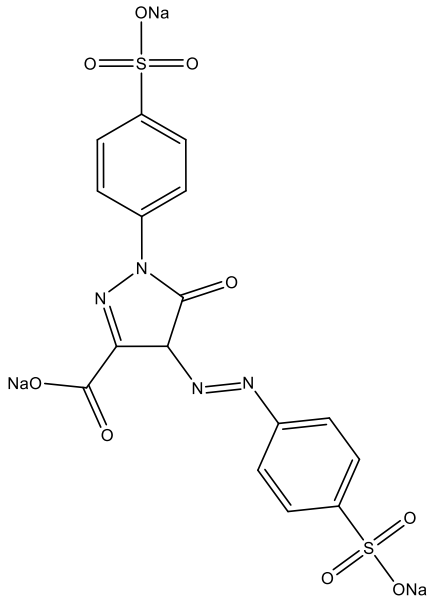
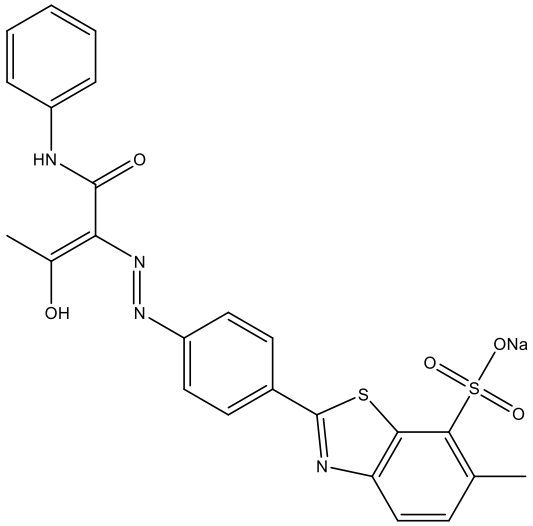
From these structures it can be seen that a large quantity of dyes can be immediately ruled out, because they of are too large. The fact that they are too large is a limiting factor as they can cause steric hindrance during the polymerisation, and as a fact of this the conversion of the dye monomer could be lower than desired. Others were eliminated as they do not possess a primary alcohol, or they have competitive functional groups or halogens. Lastly the cost of the dyes was examined. After taking all the requirements into consideration, disperse red 1 was chosen as the ideal candidate for methacrylation, as it is relatively small, has a primary alcohol, and is reasonably priced (5 g for 70.30£).

The next coloured dye to be identified was yellow. Much like red dyes, there are a large variety of yellow dyes with different structures, properties, and prices (table 2).

From the commercially available yellow dyes, 4-phenyldiazenylphenol/solvent yellow 7/ Yellow 1 was chosen. A large quantity of the dyes were ruled out because they were too large, had too many functional groups, did not have a primary alcohol, or were considered too expensive. 4-phenyldiazenylphenol/solvent yellow 7/ Yellow 1 was chosen as it contains a single alcohol group, no other reactive functional groups, is quite small, does not contain halogens, and is inexpensive (25 g for 80.00 £).

Table 2 – Structures of seven Yellow dye molecules with their IUPAC and commercial names.

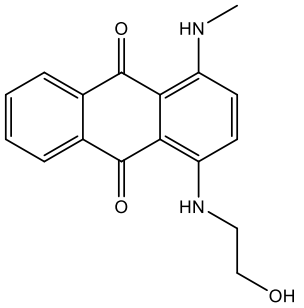
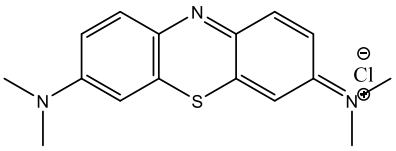
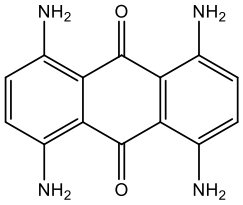
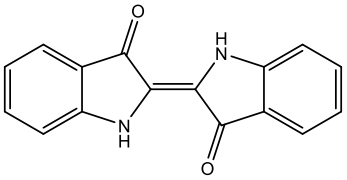
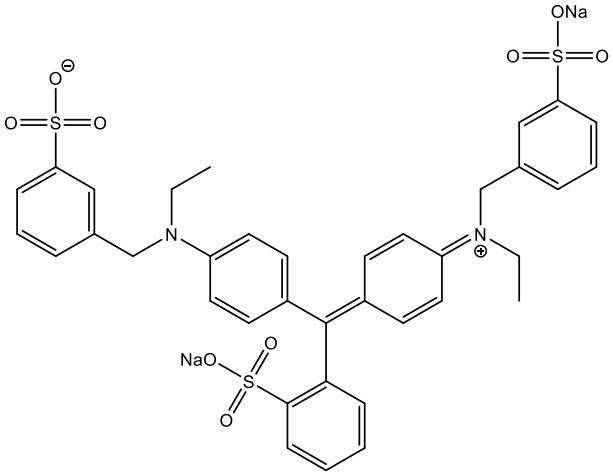
Structures of Yellow Dye molecules	Names
	4-phenyldiazenylaniline (Aniline yellow)
	(4*E*)-5-methyl-4-[(5-methyl-3-oxo-2-phenyl-1*H*-pyrazol-4-yl)methylidene]-2-phenylpyrazol-3-one
	4-phenyldiazenylphenol (Solvent yellow 7/ Yellow 1)
	disodium;6-hydroxy-5-[(4-sulfonatophenyl)diazenyl]naphthalene-2-sulfonate (Sunsent Yellow FCF)
	2-(1,3-dioxoinden-2-yl)quinoline-6,8-disulfonic acid (C.I. Acid Yellow 3)

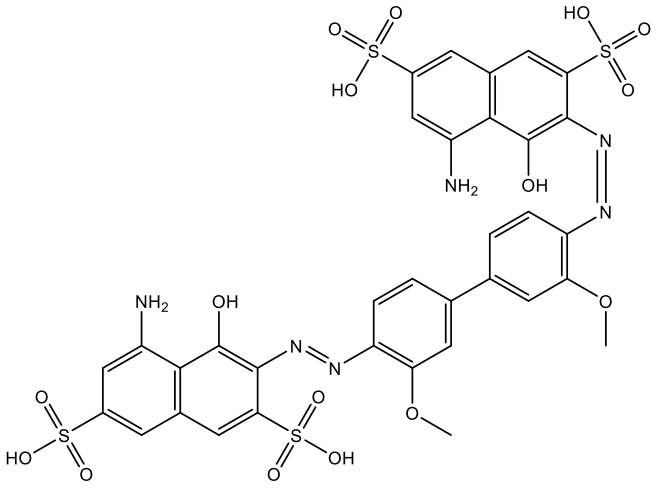
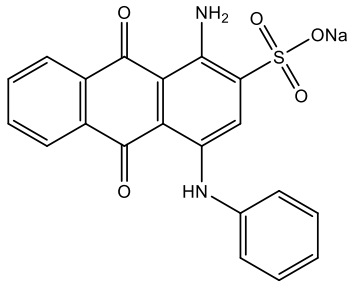
Structures of Yellow Dye molecules	Names
	trisodium;5-oxo-1-(4-sulfonatophenyl)-4-[(4-sulfonatophenyl)diazenyl]-4*H*-pyrazole-3-carboxylate (Tartrazine)
	sodium;2-[4-[[(*Z*)-1-anilino-3-hydroxy-1-oxobut-2-en-2-yl]diazenyl]phenyl]-6-methyl-1,3-benzothiazole-7-sulfonate (Direct Pure Yellow)

The selection of a blue dye for methacrylation posed more issues than the red and yellow dyes. The majority of blue dyes are larger and have more functional groups than the aforementioned yellow and red dyes (table 3). The dyes with the required structural features were very expensive, so compromises had to be made when selecting a blue dye for methacrylation. The compromises were in between choosing a dye molecule which only had an alcohol group vs. choosing one that was reasonably priced. The outcome was choosing a molecule that had more functional groups, but

could in theory be selectively methacrylated at the alcohol moiety, whilst still being at an industrially viable price point.

Table 3 – Structures of seven Blue dye molecules with their IUPAC and commercial names

Structure of Blue Dye molecules	Names
	1-(2-hydroxyethylamino)-4-(methylamino)anthracene-9,10-dione (Disperse Blue 3)
	[7-(dimethylamino)phenothiazin-3-ylidene]-dimethylazanium;chloride (Methylene Blue)
	1,4,5,8-tetraaminoanthracene-9,10-dione (Disperse Blue 1)
	(E)-1H,1'H,3H,3'H-[2,2'-biindolylidene]-3,3'-dione (Indigo)
	disodium;2-[[4-[ethyl-[(3-sulfonatophenyl)methyl]amino]phenyl]-[4-[ethyl-[(3-sulfonatophenyl)methyl]azaniumylidene]cyclohexa-2,5-dien-1-ylidene]methyl]benzenesulfonate (Brilliant Blue FCF)

Structure of Blue Dye molecules	Names
	tetrasodium;5-amino-3-[[4-[4-[(8-amino-1-hydroxy-3,6-disulfonatonaphthalen-2-yl)diazenyl]-3-methoxyphenyl]-2-methoxyphenyl]diazenyl]-4-hydroxynaphthalene-2,7-disulfonate (Direct Blue 15)
	sodium 1-amino-9,10-dioxo-4-(phenylamino)-9,10-dihydroanthracene-2-sulfonate (Acid Blue 25)

The process for producing the dye monomers starts with the selection of appropriate dyes onto which the methacrylate functionality is added. The dyes can change colour due to the addition of the methacrylate moiety.[33,34] The shift could be either bathochromic or hypsochromic. A bathochromic shift is a shift to a longer wavelength, a hypsochromic shift is a shift to a shorter wavelength. These shifts can occur for a variety of reasons including a change in π-conjugation, a change in functional groups, or a variation in chemical environment (figure 3).[33,34]

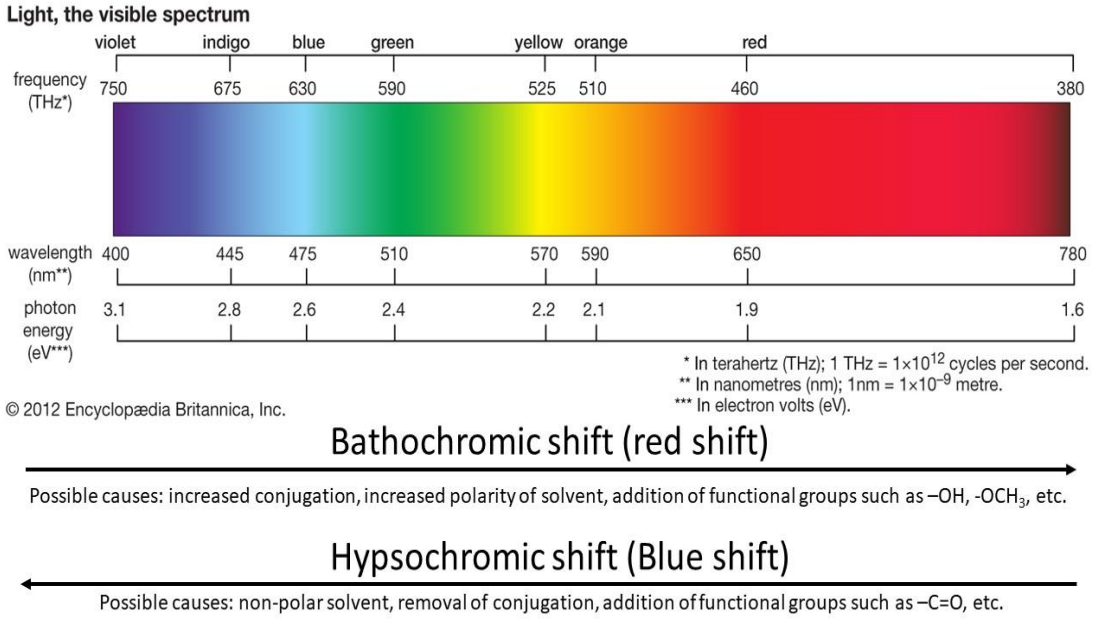


Figure 3 – Batho and hypso-chromic shifts. Bathochromic shifts can occur due to increased conjugation, increased polarity of solvent, addition of functional groups such as -OH, -OCH_3, etc. Hypsochromic shifts can occur due to non-polar solvents, removal of conjugation, addition of functional groups like -C=O, etc.

This change can be predicted computationally. A multitude of studies have been done on the prediction of colour for different classes of dyes.[35–40] Several approaches for this type of problem have been taken in the past starting with large-scale highly correlated ab initio approaches, such as CAS-PT2 and MR-CI.[37] These calculate the λ_{max} of dyes using post-Hartree-Fock methods, which are based on the Hartree-Fock method, which approximates the wavefunction and the energy at a quantum many-body system in a stationary state. However, instead of averaging repulsion between electrons the post Hartree-Fock method adds electron correlation, which is more accurate. These methods are accurate but time consuming and can encounter problems with increasing molecular size. The second type of computational calculation that has been done is a semiempirical method such as CNDO/S and

INDO/S. However, these are not as accurate. Recently, time-dependent density functional theory (TD-DFT) calculations have oft been used as they strike a good balance between accuracy and computational time.[35,37,40] DFT calculations have the downside of being expensive, but this is typically only for large scale systems and not individual molecules. Quantitative structure-property-relationship (QSPR) approaches have been experimented with, leading to faster process times, but slightly diminished accuracy.[38]

The TD-DFT methodology seems to give the best results coupled with reasonable computational cost, but the possible DFT functionals, solvation methods, and basis sets are large.[35] Mahmood et. al. tested the accuracy of different functionals such as Becke three-parameter Lee-Yang-Parr correlation functional (B3LYP), Coulomb attenuated B3LYP functional (CAM-B3LYP), Long range corrected BLYP (LC-BYLP), Becke-half-and-half-LYP (BHandHLYP), and Perder-Burke-Ernzerhof exchange-correlation functional (PBE0).[35] These findings showed that all the functionals gave results with margins smaller than 15 nm, with the best accuracy going from PBE0 > BHandHLYP > LCBLYP > CAM-B3LYP.[35] Different basis tests were also tested with the best being the 6-311++G basis set. All four of the tested solvation methods polarizable continuum model (PCM), implicit PCM (I-PCM), self-consistent isodensity PCM (SCI-PCM), and integral equation formalism PCM (IEF-PCM)) showed similar results. The studies showed that the λ_{max} of the dye molecules can be predicted to a 15 nm or better accuracy with a reasonable computational scope.[35] Through the proper selection of commercial dyes, computational methods, and reaction routes, the synthesis of red, yellow, and blue dye monomers can be achieved.

Methacrylation methods:

In the literature there are several methods for the addition of a methacrylate onto a molecule. Acik et. al. used an alternative method when synthesizing sugar-based methacrylates (figure 4).[41] The reaction was two-step, which inevitably leads to lower total yield and adds to total synthesis time and cost. The reaction begins with epichlorohydrin reacting with an alcohol to attach an epoxide to the molecule, the epoxide then reacts with methacrylic acid in the presence of triethylamine (TEA) to give the corresponding methacrylate monomer.[41]

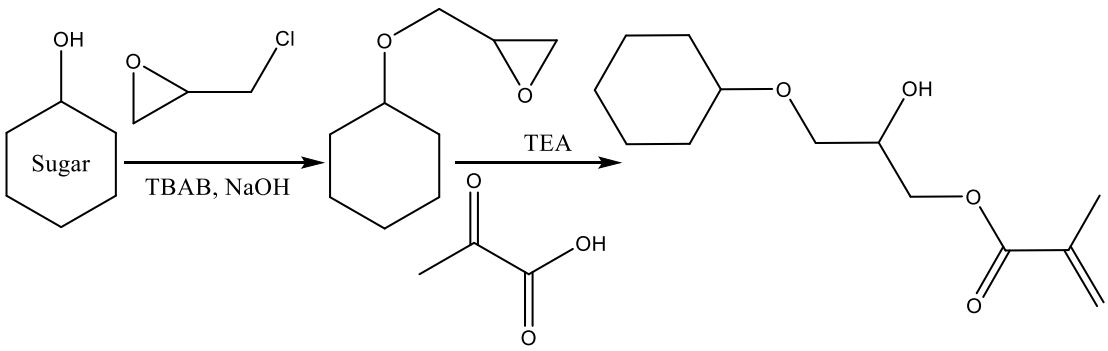


Figure 4 – Synthesis of sugar-based methacrylates by Acik et. al.[41] Abbreviations TBAB and TEA mean tetrabutylammonium bromide and triethylamine respectively.

This reaction is attractive because it gives a method for the synthesis of 'greener' monomers. However, there are several downsides such as the use of epichlorohydrin and dimethylformamide which are toxic, corrosive, etc. Also, the reaction is multistep and has low yields (~ 70%).[41] The reaction adds a larger functional group than a methacrylate, which could induce a greater colour change in the dye monomer.[33,34,41]

Microwave reactions have been used in the synthesis of methacrylate-based monomers by Dundas et. al.[42] This system utilizes microwaves to heat a solventless

reaction (figure 5). This transesterification uses microwells at 160° C with a titanium butoxide catalyst to synthesize novel monomers.[42] This system has many positives, as it is solventless, has been shown to work for a variety of alcohols, and it can react alcohols that are hard to methacrylate with conventional methods due to the heating system.[42] Also, the conversions are relatively high (~80 %). The drawbacks are that the reactor system is highly specialized and although it is theoretically scalable, at present the largest scale is 15 mL.[42]

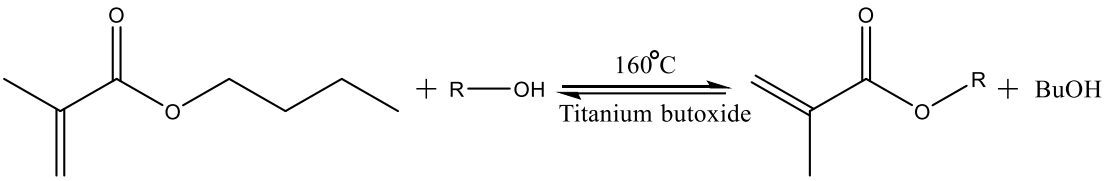


Figure 5 – Methacrylation via microwell (microwave) reactor system.[42]

Gunes et. al. showed that methacrylate-based monomers can be synthesized via boron ester acidolysis (figure 6).[43] This reaction uses boric acid to produce boric esters, which are reacted with methacrylic acid yielding methacrylate monomers.[43] This reaction was shown to be robust and applicable for a wide variety of alcohols.[43] However, this synthesis route necessitates multiple steps, and the reaction is heated at 160° C for extended periods of time (≥ 24 hrs). Lastly the yield of this reaction is low (between 41 – 71%).[43]

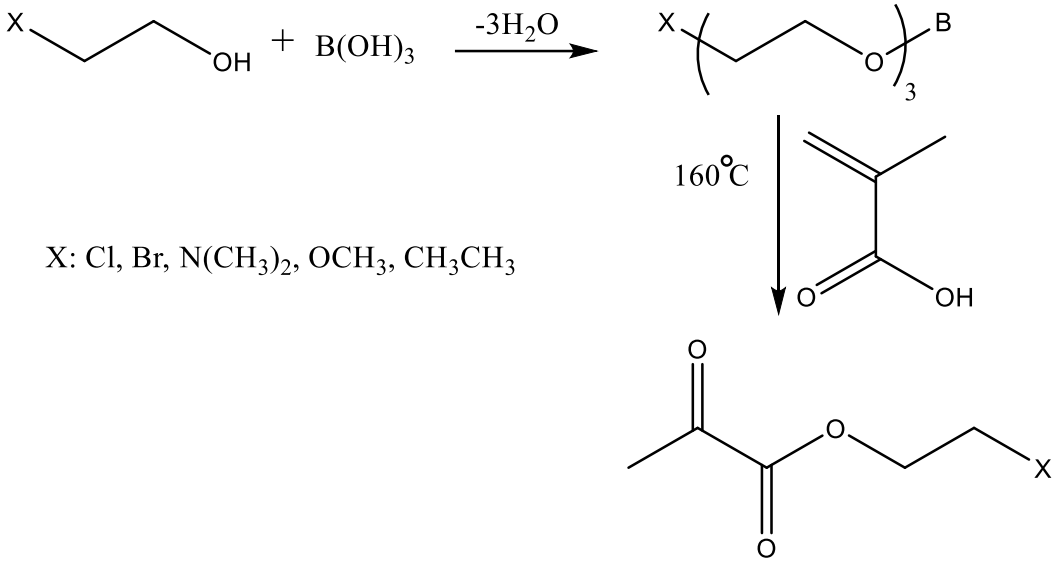


Figure 6 – Synthesis of methacrylate based functional monomers via boron ester acidolysis.[43]

In 2019, Soykan et. al. showed that methacrylates can be made via a myriad of reaction routes.[44] The first of which, was the synthesis of methacrylates from arylacetylhalide compounds (figure 7).[44] This two-step reaction, starts with the reaction of an aryl-alcohol with chloroacetyl chloride in the presence of potassium carbonate yielding an alpha-chloroarylacetamide.[44] This product is subsequently reacted with sodium methacrylate, yielding the methacrylate-based monomer.[44]

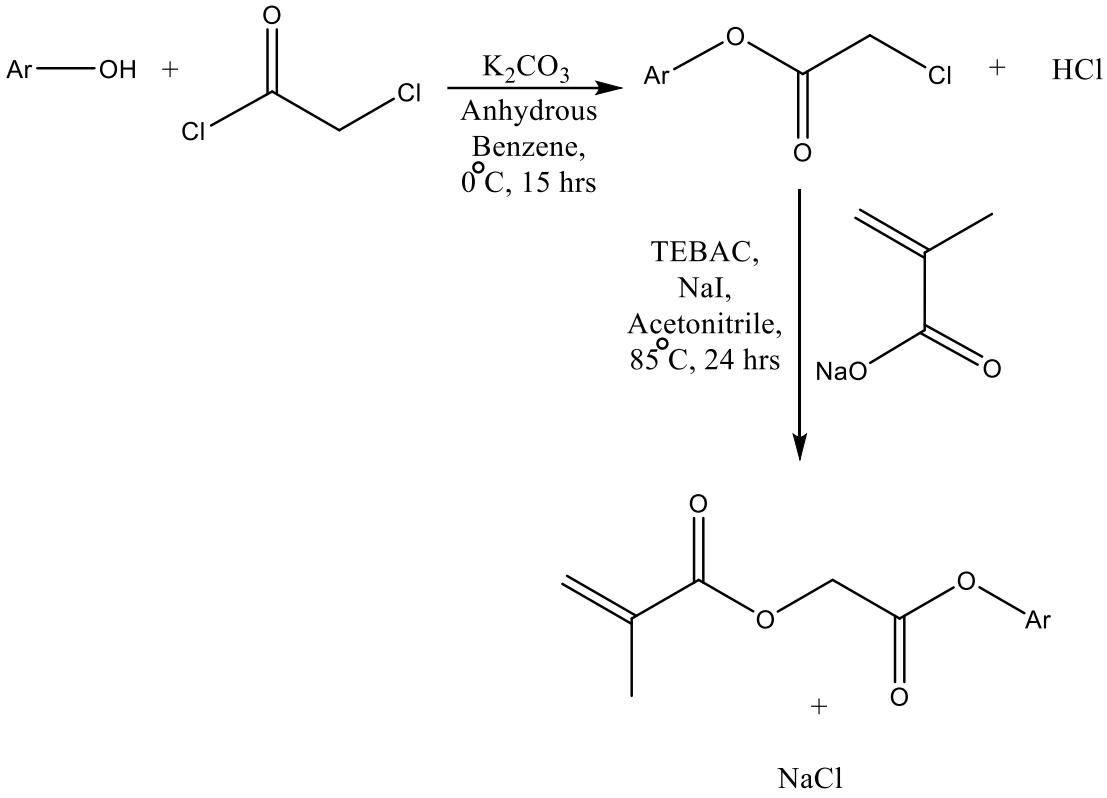


Figure 7 – Synthesis of methacrylate monomers from arylacetylhalide compounds[44]

The main benefit of this reaction is that it gives high yields (~85%).[44] However, it uses chloroacetylchloride, has several synthesis steps, and multiple purification steps.[44] Also, the final group that is added is larger than just the methacrylate, which could result in a larger than expected colour change to the dye.[44]

Methacrylate monomers were also synthesized from aryl-1,3-dioxolane compounds (figure 8).[44] This two-step reaction shows that different classes of molecules can be utilized to make methacrylate monomers.

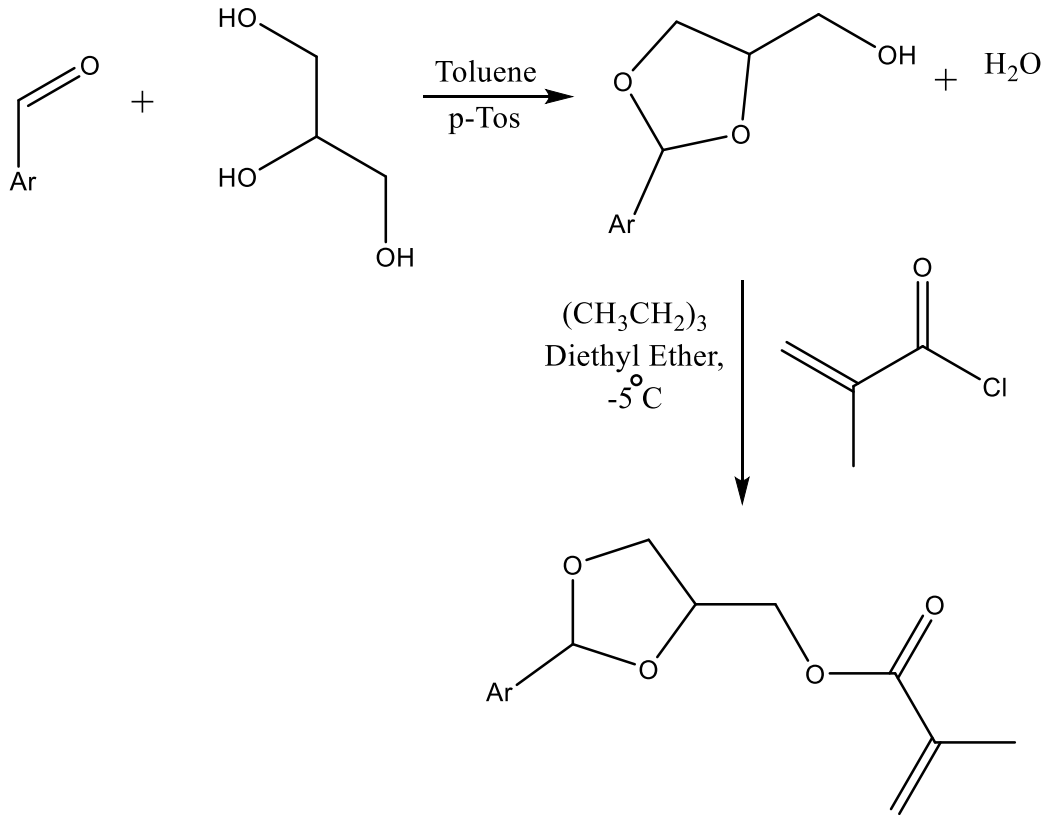


Figure 8 – Methacrylation of aryl-1,3-dioxolane compounds via cyclic acetal formation and subsequent reaction with methacryloyl chloride, with p-Tos abbreviation meaning p-toluene sulfonic acid [44]

Besides the fact that this shows the methacrylation of a different class of molecule there are not many positives. The authors do not mention a final yield, the reaction has two steps, with multiple purification steps and the reactions are ~24 hrs long.[44] The reaction, also uses methacryloyl chloride which is highly toxic, corrosive, carcinogenic, etc.

Through another synthesis route, acetyl benzofuryl methacrylate was synthesized (figure 9).[44] This was a three-step synthesis, so although all the steps have high yields (80-85 %) the total yield is low (~60 %).[44] The reaction uses bromine and has a long

reaction time with multiple purification steps, which make it ill-suited for the production of industrial quantities of monomer.[44]

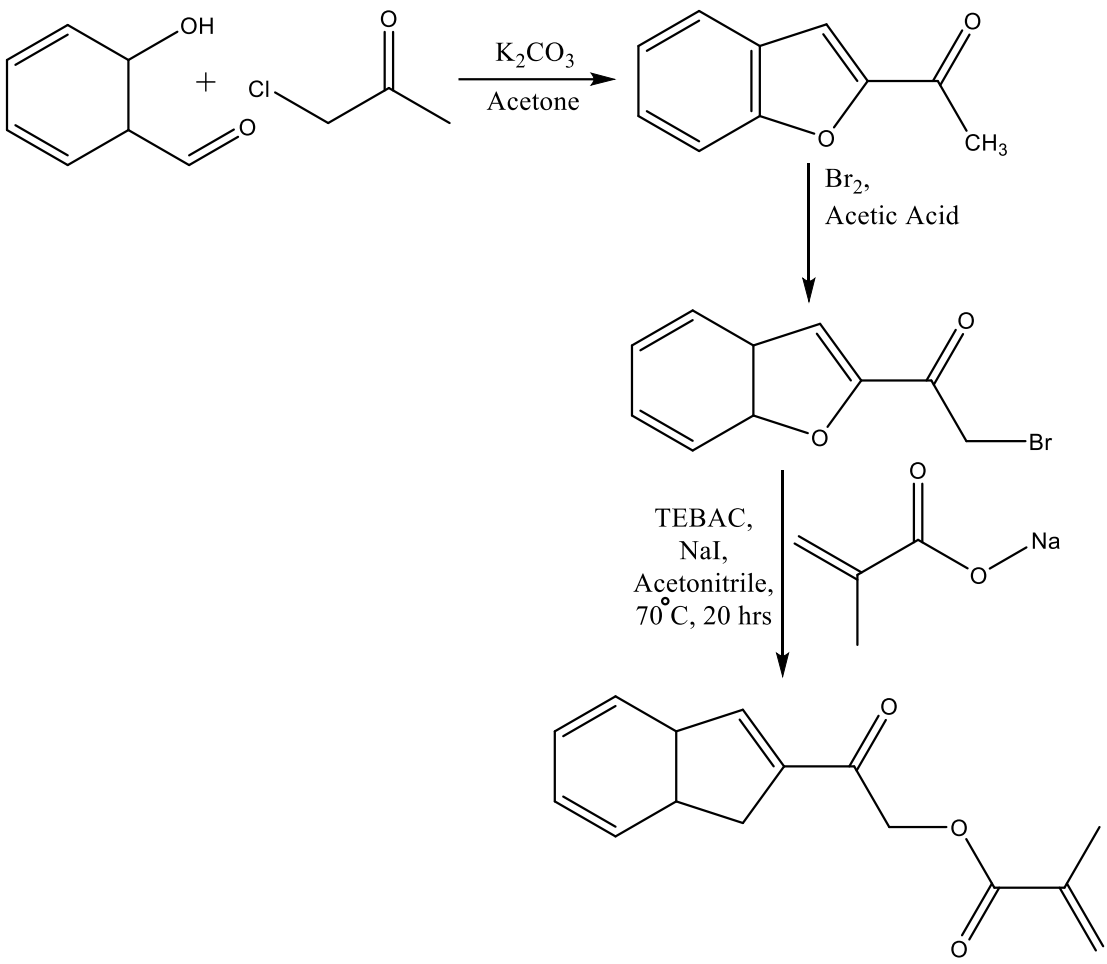


Figure 9 – Synthesis of acetyl benzofuryl methyl methacrylate, through a three step mechanism[44]

Another route is the synthesis of methacryloxyphenyl-methoxystyrylketone (figure 10).[44] This reaction uses a two-step route with methacryloyl chloride to achieve high total yields of 85 %.[44] However, the reaction is long (≥ 36 hrs), uses methacryloyl chloride, and has multiple purification steps.[44] This reaction also adds large functional groups onto the alcohol, which could greatly change the colour of the dye.[33,34,44]

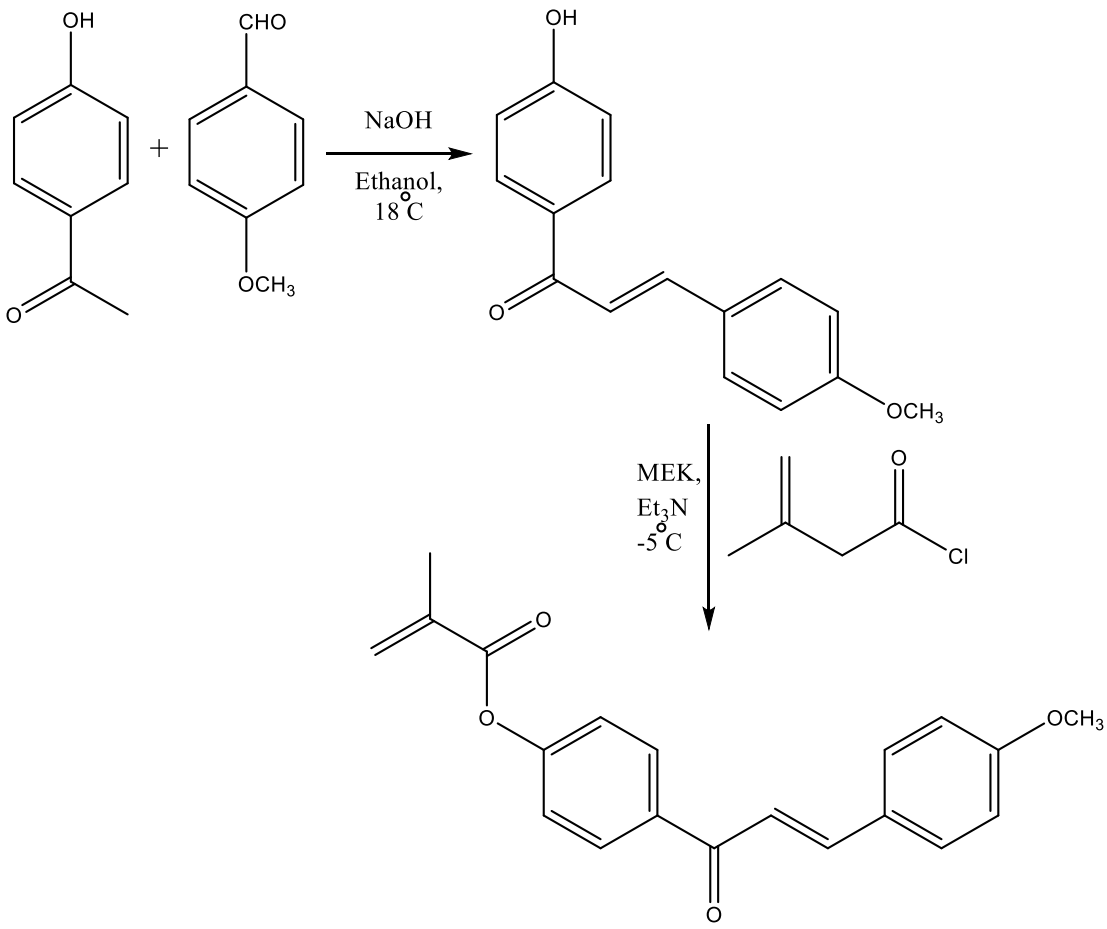


Figure 10 – Synthesis of methacryloxyphenyl-methoxystyrylketone, with MEK abbreviation meaning methyl ether ketone.[44]

One reaction route that is frequently used is a nucleophilic substitution in which methacryloyl chloride reacts with the alcohol on the target molecule (figure 11).[5,27,28] This reaction has several benefits, one of which is a fast reaction time (2-4 hrs).[5,27,28] This reaction is one step and has simple purification steps. Literature has shown the potential for high yields (≥ 90%) and the reaction has been shown to be scalable.[5,27,28]

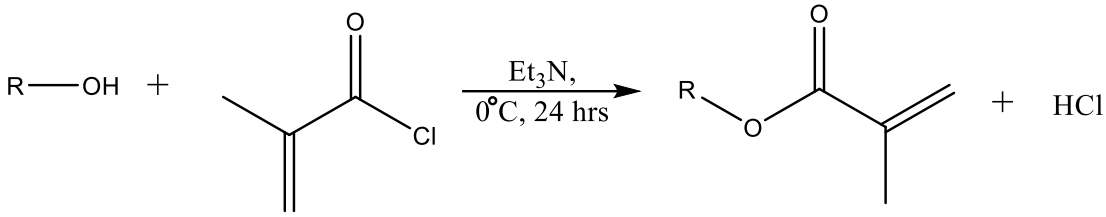


Figure 11 – Addition of a methacrylate functionality through nucleophilic substitution with methacryloyl chloride.[28]

However, it has significant drawbacks as methacryloyl chloride is toxic, flammable, carcinogenic, corrosive, a lachrymator, and the solvent used is dichloromethane (DCM). This reaction is very efficient, fast, and scalable but does not follow several of the principles of green chemistry.

Another method for the methacrylation of a molecule is the enzymatic transesterification using Novozym 435 and methyl methacrylate (MMA) or methacrylic acid (MA), which is a greener reaction than the aforementioned reactions.[45–48] Tetrahydrofuran (THF) is used as the solvent, which is less toxic than DCM, and instead of methacryloyl chloride; MMA or MA are used. MMA and MA are less harmful than methacryloyl chloride, and do not produce hydrochloric acid (HCl) as a by-product. It has been shown that MMA and MA can be produced from renewable sources such as acetone, isobutanol, ethanol, lactic, itaconic, and citric acids.[49] Another benefit is that this reaction is very selective as the enzyme primarily reacts with primary alcohols, and it is one step.[45–48] The drawbacks for this reaction are that the reaction is relatively long (~24 hrs), and the reagents are expensive, specifically Novozyme 435, but it can potentially be reused.

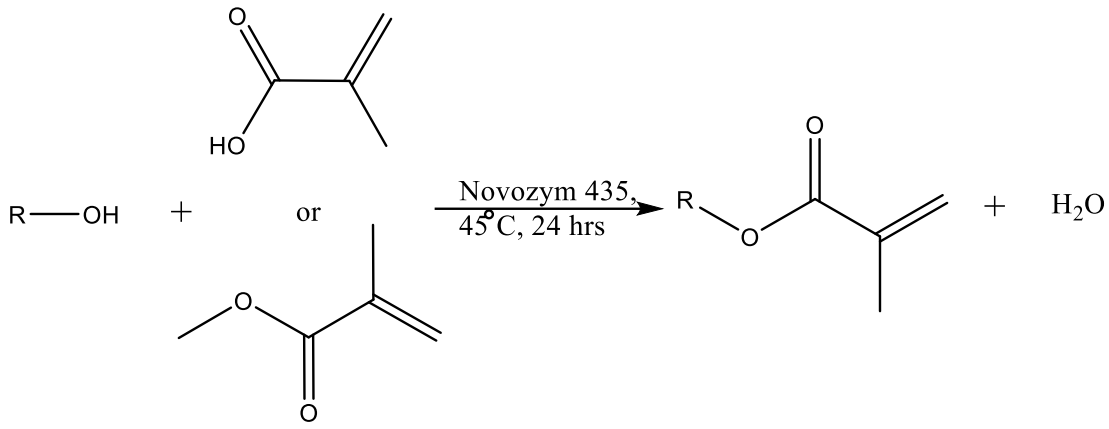


Figure 12 – Methacrylation via enzymatic transesterification[47]

From this set of reactions, it can be seen that the reactions with a nucleophilic substitution with methacryloyl chloride and the enzymatic transesterification (figures 11 and 12 respectively) are the most suitable reaction schemes. As the reaction with methacryloyl chloride has very high yields, is one step, is fast (2-4 hrs), scalable, and only adds the methacrylate group without additional carbon bonds, which could further change the colour of the dye in question. The enzymatic route is one-step and is a 'green' route as it uses less toxic reagents and is catalysed by an enzyme, but is more expensive. It was decided that both of these reactions should be trialled as they are one-step, have high yields, are theoretically scalable, and should hopefully minimize the effect of methacrylation on the colour of the dye.

Results and Discussion:

Computational modelling of colour

The purpose of the computational model was to check if the addition of the methacrylate functionality would cause the chosen dyes to undergo significant hypso or bathochromic shifts (blue or red shift). This would help the project, because large amounts of time could be lost (among other resources) in the synthesis of dye monomers, if the addition of a methacrylate causes a significant colour change, leading to undesirable colours. This model ensures that the correct dyes are chosen.

Various computational methods have been used in the past to predict the λ_{max} of dye molecules. The modelling technique that was chosen was TDDFT, as it is known to yield accurate results with a reasonable computational cost.[35,37] Within TDDFT there are differing approaches that can be taken, as the user can choose different functionals, basis sets, and solvation methods.[35] The basis set that was chosen was B3LYP as it is known to give accurate λ_{max} values for azobenzene dyes.[35] The basis set 6-311+g was chosen, because it has previously been used in literature for similar applications.[35] However, it has been shown that 6-311++g basis sets give slightly better results,[35] 6-311+g was chosen as the computational costs are lower, and the improvement in accuracy of 6-311++g over 6-311+g is minimal for this application.[35] The solvation method chosen was a C-PCM gas-phase model, as it is a basic model that should mimic the conditions of the dye in the solid state. However other solvation models might work better, as the UV spectrum of the dye is not measured in a gas-phase, but rather when it is dissolved in a solvent. This is an important factor as the dye molecule can interact with the solvent in such a way that the λ_{max} of the dye is

slightly altered. The chosen TDDFT method is a B3LYP/6-311+g (d,p) calculation with a PCM gas-phase solvation model. The geometries are optimized to a B3LYP/6-311+g (d,p) level of theory. The first dye tested was 4-phenyl azophenol, results showed that the transition responsible for the colour is the π to π* transition.

In the gas phase, the λ_{max} of Y1 (Solvent Yellow 7 or 4-phenyl azophenol) was predicted to be 308.6 nm, and the actual λ_{max} is 344 nm, so the calculation was off by 35.4 nm. In the gas-phase the λ_{max} of Y1MA was predicted to be 305.6 nm, hence a slight red-shift is predicted by TDDFT calculations. The experimental result showed a λ_{max} of 324 nm. The B3LYP/6-311+G (d,p) calculations in the gas phase predicted the correct type of shift but the value was out by 20-35 nm. The calculations were then performed with an implicit solvent model (I-PCM) of DCM, which gave more accurate results. The prediction for Y1 was 321.5 nm, so the result was 4% closer to the experimental result. For Y1MA (Yellow 1 methacrylate), the result with a DCM solvent model was 313.8 nm, which was 2.5% more accurate than the gas phase. This seemingly minimal change in accuracy is quite important as small changes in λ_{max} can have a visible impact in colour. TDDFT calculations done with DCM instead of in the gas phase gave a predicted λ_{max} with a 10-20 nm accuracy. From this it can be said that the model is accurate enough to aid in the selection of dyes used for the synthesis of dye monomers.

Disperse blue 3 was the blue dye that was selected for methacrylation. It has a vastly different structure than Y1 or DR1 (both azobenzene based), as its molecular structure is based on anthraquinone. The anthraquinone group and the additional functional groups (eg. secondary amines) in DB3 might be the reason why a loss of accuracy is observed for DB3 and DB3MA, another possible reason is that the conformer seen

experimentally is different from the one that the computation was done on. This inevitably leads to complications when the same modelling technique is applied to DB3 as was to Y1 and DR1. These complications can result in skewed theoretical values for the λ_{max} of DB3 and DB3MA. However, the impact of the methacrylate group on the λ_{max} should be measurable, and the model should predict if the shift will be hypso or bathochromic. The C-PCM DCM model was used, as it was shown to be more accurate than the gas-phase model. The λ_{max} of DB3 and DB3MA were predicted through the same TDDFT methods and the geometries optimized to the B3LYP/6-311+g level.

The predicted λ_{max} of DB3 was 479 nm, which is quite far from the experimental value of 595 nm. The predicted λ_{max} of DB3MA was 477 nm (experimental 593 nm), this means that the addition of a methacrylate group caused a red shift of 2 nm in both the predicted and measured values. The accuracy of the model in relation to the experimental values is low (~ 80%), but the predicted change between DB3 and DB3MA was accurate. The results also showed that the excitation state responsible for the colour is the π to π^* transition. Considering the results, it is suggested that DB3MA could be a suitable blue monomer.

The dyes showed that the addition of a methacrylate functionality did not drastically change their λ_{max}, hence it was decided to take these commercial dyes onto the synthesis stage and produce three methacrylate-based dye monomers.

Dye monomer synthesis:

Disperse red 1 is well suited for methacrylation as it has a primary alcohol, is red, does not have halogens, and is of a reasonable cost. The reaction route chosen for the synthesis of DR1MA was a nucleophilic substitution with methacryloyl chloride. This reaction produced high yields of product (70-88%) (figure 13).

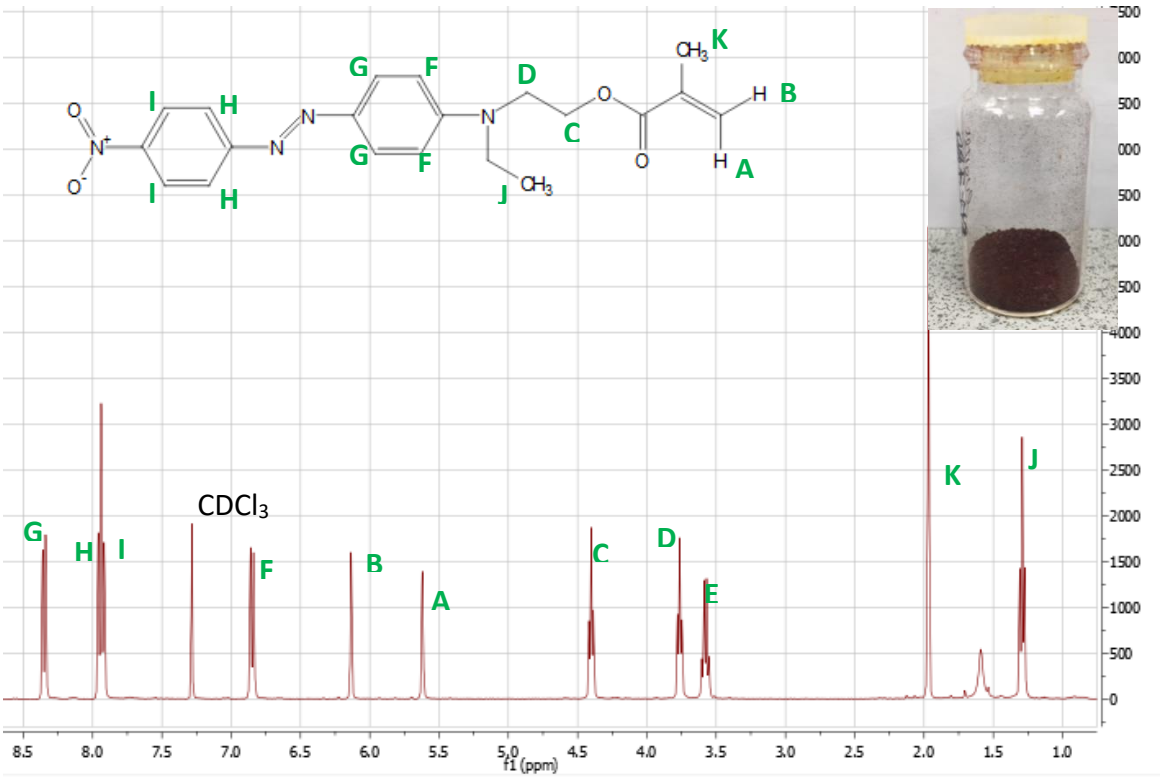


Figure 13 – ^{1}H NMR of Disperse Red 1 methacrylate in $CDCl_3$

The ^{1}H NMR shows the alcohol peak has disappeared and the characteristic methacrylate peaks in the 5.5-6.5 region have appeared. The colour of the dye monomer confirms that DR1MA can be used as red/magenta dye monomer. This reaction was done in multiple scales from 0.5 g to 15 g, showing the scalability of the reaction. The reaction has many positives, however efforts should be made to make

it more environmentally friendly as methacryloyl chloride and DCM were used. The intensity of the colour should allow for the formation of coloured co-polymers with minimal amounts (~2.5 wt%) of dye monomer in comparison to the other methacrylate monomer.

The yellow commercial dye that was chosen for methacrylation was 4-phenyldiazenylphenol (an azobenzene based dye). The first reaction route used to synthesize Y1MA was a nucleophilic substitution with methacryloyl chloride (analogous reaction to the synthesis of DR1MA). The conversion and structure of Y1MA was determined through ^{1}H NMR analysis (figure 14). Analysis revealed that after purification there was a notable side product, however the overall yield was high (≥90%).

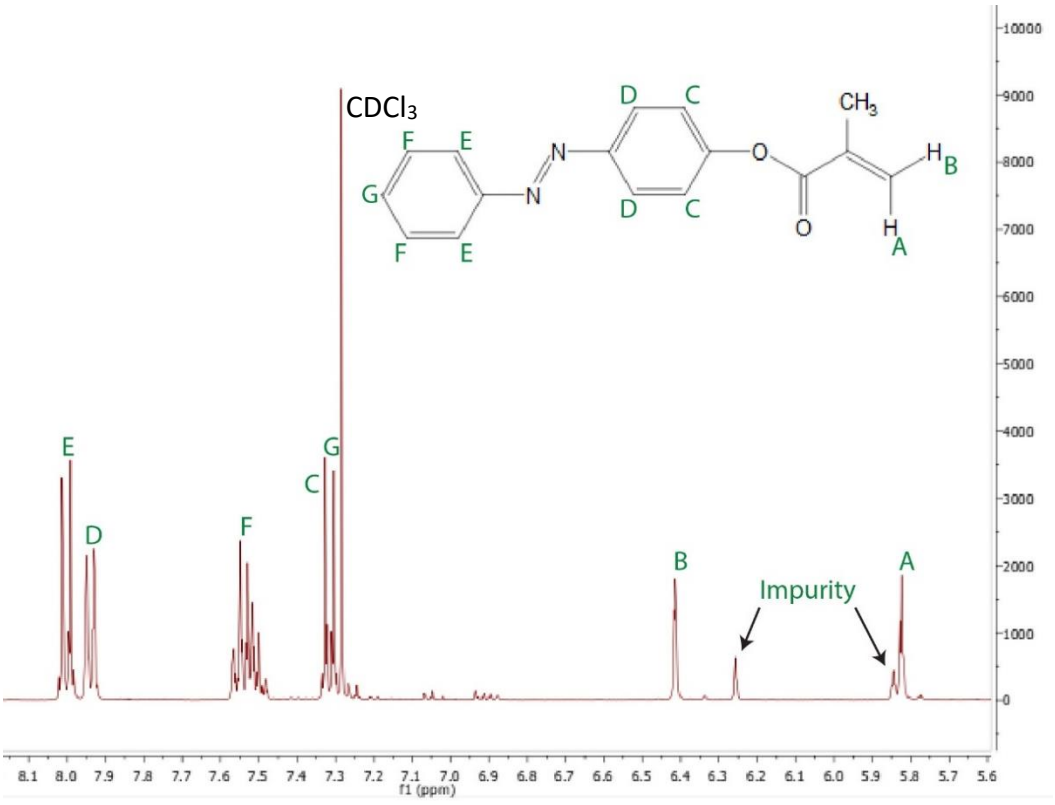


Figure 14 – ^{1}H NMR of Yellow 1 methacrylate

The impurity was found to be methacrylic anhydride via NMR and IR analysis, which usually is an undesirable side-product in monomer synthesis as it can act as a crosslinker, leading to crosslinked or hyperbranched polymers.[50] This is impractical as crosslinked polymers can have different physical, rheological, and mechanical properties than their non-crosslinked counterparts. As predicted from TDDFT calculations, Y1MA showed a hypsochromic shift of ~20 nm (from 344 nm to 324 nm). The effect is likely due to the change in electron conjugation along the aromatic structure and change in the chromophore species. This was a good result as even though 4-phenyldiazenylphenol is yellow it can be perceived by some to have a greener aspect in its solid form. The addition of the methacrylate has a positive effect as Y1MA has a bright yellow colour when solid (figure 15). The colour Y1MA is more suitable for 3D printing applications as it is notably yellow in its solid form unlike 4-phenylazophenol.

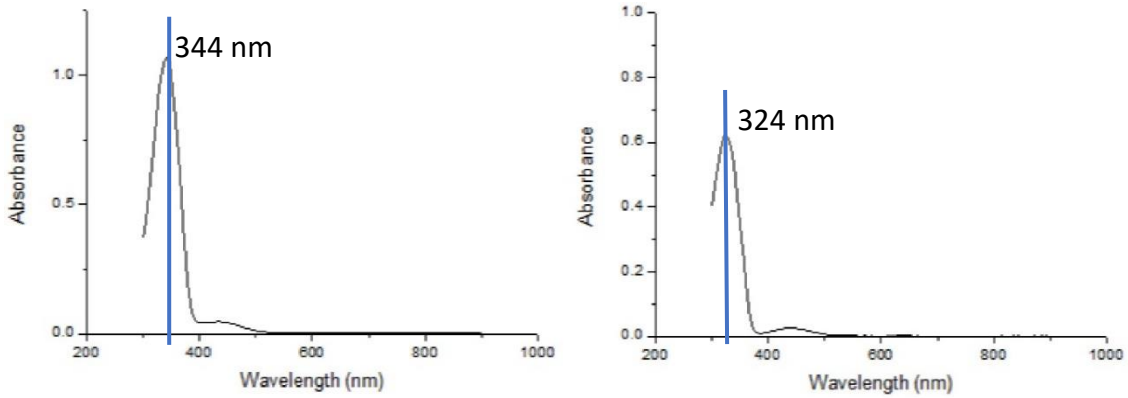


Figure 15 – UV/Vis spectra of 4-phenylazophenol (left) and Yellow 1 methacrylate (right), showing a shift after the methacrylation as 4-phenylazophenol has a λ_{max} of 344 nm and Yellow 1 methacrylate of 324 nm.

Because of the potential issues due to the impurity, further purification techniques were used. The impurity was removed by passing Y1MA through a basic alumina flash column, as methacrylic anhydride was bound to the basic alumina. Y1MA along with the eluent pass through the column, once the eluent is evaporated, pure Y1MA was obtained (figure 16). ^{1}H NMR analysis shows the purification of Y1MA, as the methacrylic anhydride peaks have disappeared leaving only the methacrylate peaks. This purified bright yellow monomer can be used for the synthesis of yellow polymers without unwanted side-effects.

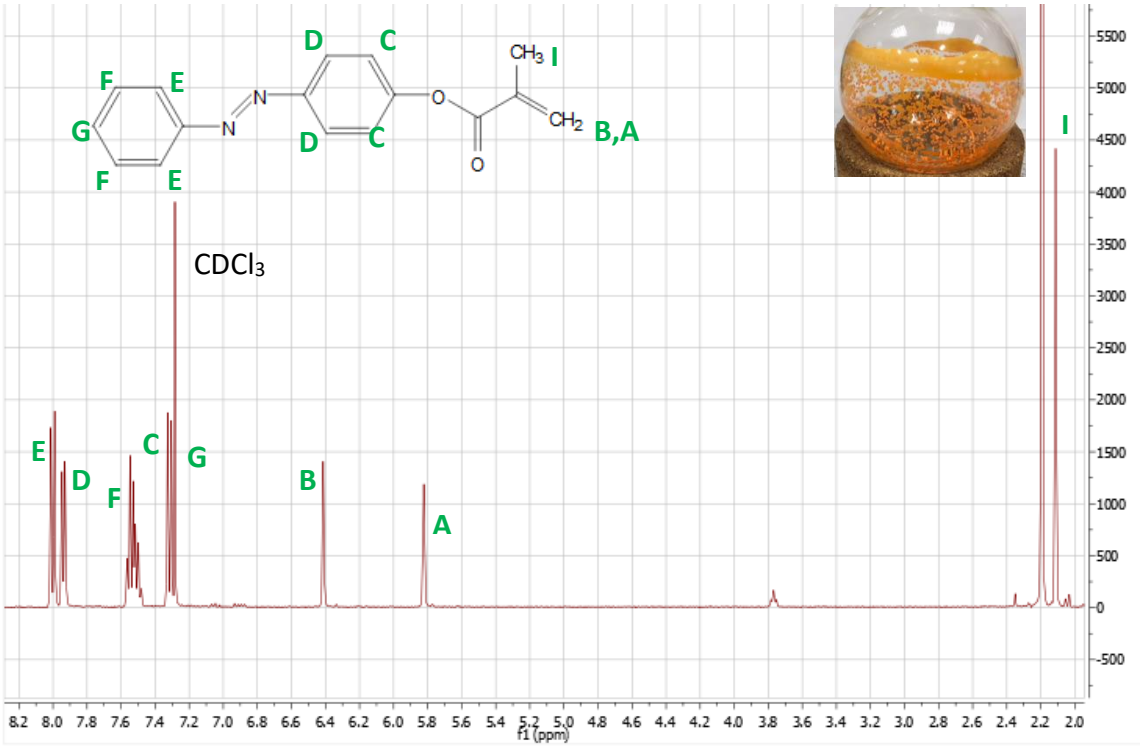


Figure 16 - ^{1}H NMR of purified Yellow 1 methacrylate in $CDCl_3$

The selection of the blue dye for further methacrylation was more complicated than the others as previously stated. The chosen dye was disperse blue 3 (DB3), with the resulting monomer being disperse blue 3 methacrylate (DB3MA). The first synthetic route that was attempted was the nucleophilic substitution with methacryloyl chloride, which was shown to work for Y1MA and DR1MA. The synthesis did not yield the wanted monomer as the ^{1}H NMR showed no methacrylate peaks (figure 27). The hypothesis is that methacryloyl chloride reacted with another group from DB3 such as the secondary amines that are present in the molecule, changing the methacrylate.

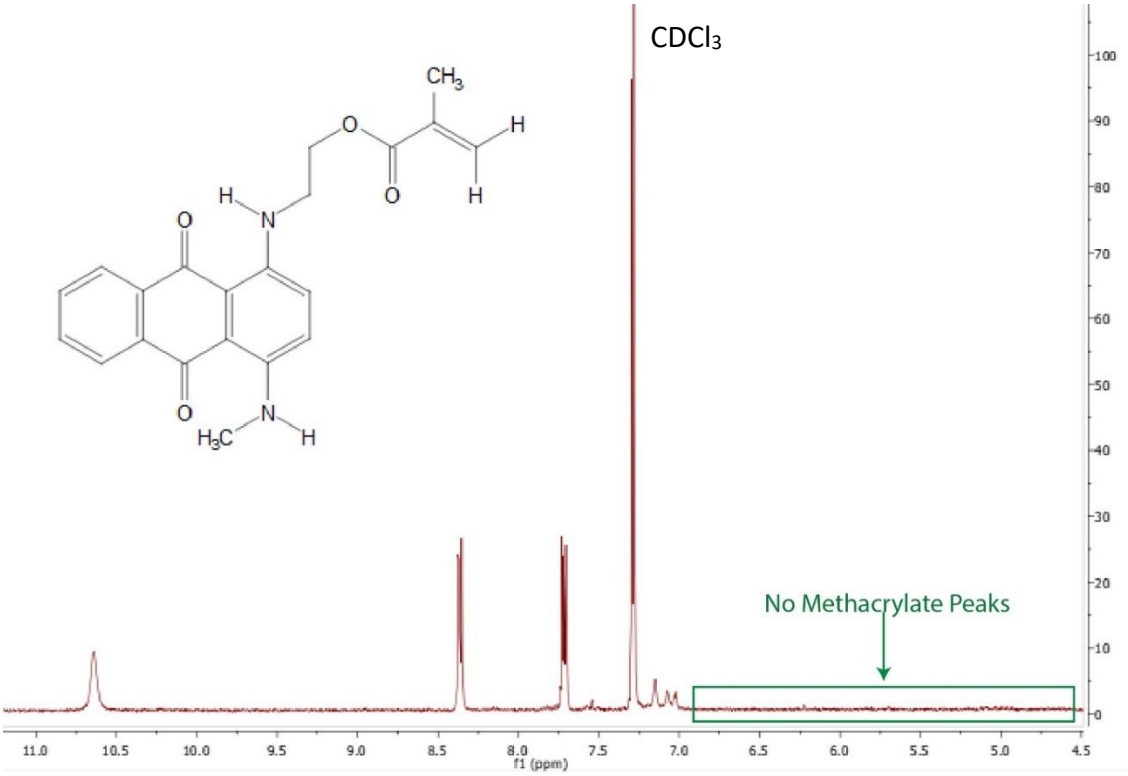


Figure 17 - ^{1}H NMR of purified Disperse Blue 3 methacrylate via nucleophilic substitution with methacryloyl chloride in $CDCl_3$.

The reaction needed greater selectivity as DB3 has multiple functional groups (eg. secondary amine groups), which can react with methacryloyl chloride. To combat this a transesterification using Novozym 435 was performed, in an effort to target a reaction between methacrylic acid and the alcohol on DB3. Methacrylic acid was used instead of MMA, in an effort to make the reaction more environmentally friendly. However this yielded a similar result, as the product had no methacrylate peaks. Novozym 435 has been known to react with acids before, but it is more efficient and more commonly used for reactions between esters and alcohols. Methyl methacrylate (MMA) was then used instead of MA, as it is an ester. This reaction proved fruitful, as the product had methacrylate peaks (figure 18).

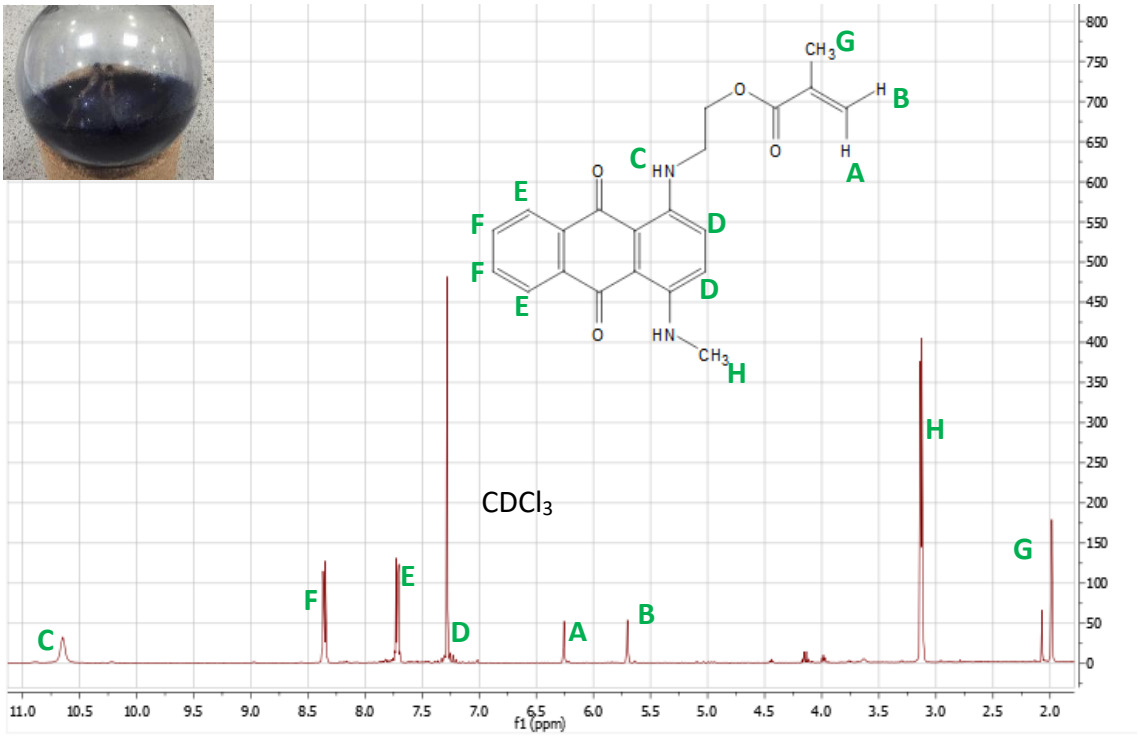


Figure 18 - ^{1}H NMR of purified Disperse Blue 3 methacrylate via enzymatic Transesterification in $CDCl_3$

The peaks are unique to DB3MA, because they are in a different place than the peaks of MMA, and the alcohol peak is also not visible. The product was subsequently further purified resulting in a blue monomer. This monomer could be used to synthesize blue/cyan polymers. The resulting monomer did not change colour as was theoretically calculated, because even though the computational model was incorrect in the λ_{max} of the dye and dye monomer, it was correct in that the hypso or bathochromic shift between the dye and the dye monomer would be minimal (2 nm). DB3MA has a quinone moiety, which can be detrimental to free radical based polymerisations.[51,52] This is because quinones are very good radical scavengers, and could stop the radical initiators or monomers from reacting with the methacrylate

group on DB3MA.[51,52] This effect is enhanced in the presence of H_2O/O_2, so the polymerisation of DB3MA or any quinone is very hard to perform with conventional solvents/techniques.[51,52] However, chapters two and appendix 1 show a work around via a $scCO_2$ based polymerisation method to polymerise DB3MA.

Conclusion:

In this project, three novel dye monomers have been synthesized. To start a screening of the available commercial dyes was undertaken, and by applying certain criteria three candidates were chosen (one for each colour). TD-DFT calculations were executed, in an effort to predict the colour change brought on by the methacrylation of the commercial dyes, showing minimal shift, so the dye monomers were subsequently synthesized. Both Y1MA and DR1MA were produced via a nucleophilic substitution with methacryloyl chloride, and DB3MA was synthesized through an enzymatic transesterifcation. The reactions had high yields (77 - 95%), were scaled up from the 0.5g to the 15g scale and had relatively fast reaction times. A drawback of the reactions using methacryloyl chloride, is that the reactions are not environmentally friendly. The enzymatic transesterification requires more expensive reagents such as Novozym 435. In short, the reactions gave products in good yields, but they could be improved. The reusability of the enzyme in the enzymatic transesterification should be investigated. Greener alternatives to the methacryloyl chloride reaction route should also be investigated further. These brightly coloured dye monomers, with methacrylate functionalities should allow for the creation of coloured polymers and polymeric particles for use in PBF (SLS) systems (figure 19).

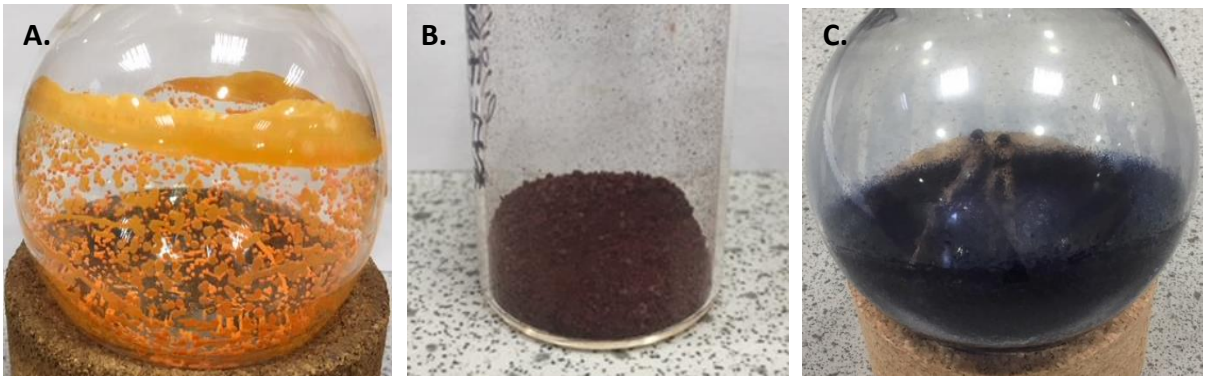


Figure 19 – Images of the brightly coloured dye monomers. A.) Yellow one methacrylate. B.) Disperse red one methacrylate. C.) Disperse blue three methacrylate.

Materials and Methods:

Materials:

Methyl methacrylate (MMA) (99 %) was obtained from Kaneka Belgium N.V. Isobornyl methacrylate (IBMA) (> 80 %) (CPDT) (97 %) was purchased from Sigma Aldrich. 2,2'-Azobis(2-methylpropionnitrile) (AIBN) was purchased from Fluorochem. CO_2 was purchased from Air Products. Disperse Red 1 methacrylate, Yellow 1 methacrylate, Disperse Blue 3 methacrylate were used as synthesised. Triethylamine, petroleum ether, acetone, chloroform, hexane, and toluene were purchased from Fischersci. Dichloromethane (DCM), ethyl acetate, 4-phenylazophenol, (E)-2-(ethyl(4-((4-nitrophenyl)diazenyl)phenyl)amino)ethan-1-ol, and 1-(dimethylamino)-4-((2-hydroxyethyl) (methyl)amino)anthracene-9,10-dione, were purchased from Sigma Aldrich. Methacryloyl chloride was purchased from Acros Organics and Novozyme 435 was purchased from Novozymes.

Methods:

Synthesis of Disperse Red 1 Methacrylate (DR1MA)

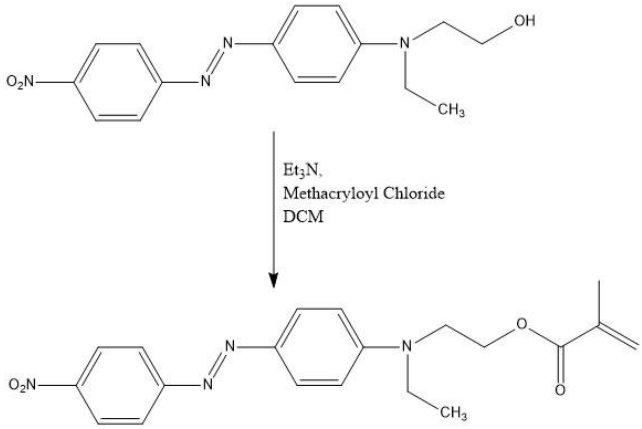


Figure 20 **–** Reaction scheme for the synthesis of Disperse Red 1 Methacrylate

To a cold solution (0^oC) of (E)-2-(ethyl(4-((4-nitrophenyl)diazenyl)phenyl)amino)ethan-1-ol (3.35g, 0.0107 mol) in dichloromethane (83.75 mL) triethylamine (2.43g, 0.024 mol) was added. To the resulting solution, Methacryloyl chloride (1.569g, 0.159 mol) was added dropwise, and left stirring at 500 rpm for 2 hours. The reaction vessel was connected to a sodium hydroxide bubbler and sealed. The final mixture was quenched with saturated sodium carbonate solution (33 mL). The aqueous layers were extracted with dichloromethane, and the combined organic layers were washed with brine, finally the organic solvent was evaporated under reduced pressure. The resulting red powder was dissolved in petroleum ether/ethyl acetate (40%/60%) and purified through a silica gel column adopting the same eluent mixture to yield a red powder (after solvent evaporation) of disperse red 1 methacrylate.

Synthesis of Yellow 1 Methacrylate (Y1MA)

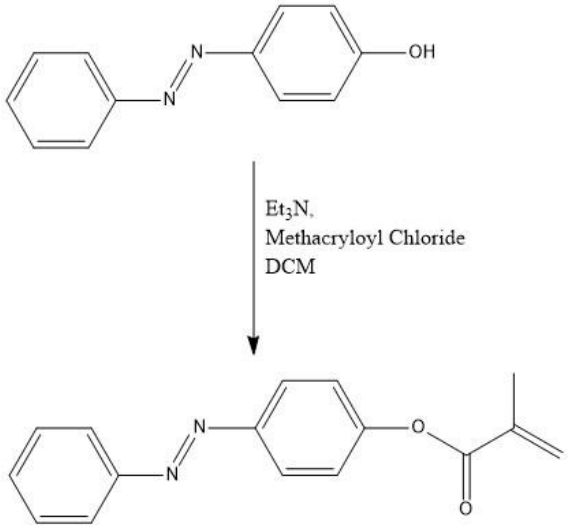


Figure 21 - Reaction scheme for the synthesis of Yellow 1 Methacrylate

To a cold solution (0°C) of (E)-4-phenyl azophenol (5g, 0.025 mol) in dichloromethane (200 mL) triethylamine (5.78g, 0.057 mol) was added. The reaction vessel was connected to a sodium hydroxide bubbler and sealed. To the solution, methacryloyl chloride (3.711g, 0.355 mol) was added dropwise, and left stirring at 500 rpm for 4 hours. The solution was quenched with saturated sodium carbonate solution (79 mL). The aqueous layers were extracted with dichloromethane, and the combined organic layers were washed with brine, and the solvent was evaporated. The resulting yellow-brown powder was dissolved in petroleum ether. The solution was purified through a silica gel column with petroleum ether as eluent, and the solvent was then evaporated. The product was then columned through basic alumina with petroleum ether, to yield a yellow powder of yellow 1 methacrylate.

Synthesis of disperse blue 3 methacrylate (DB3MA) 1

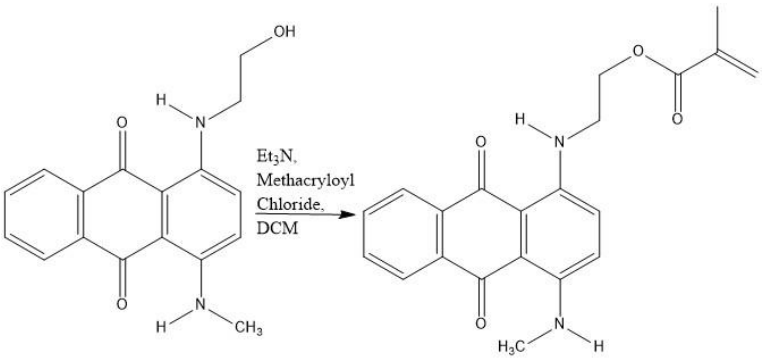


Figure 22 - Reaction scheme for the synthesis of Disperse Blue 3 Methacrylate 1

To a cold solution ($0^{o}C$) of 1-(dimethylamino)-4-((2-hydroxyethyl) (methyl)amino)anthracene-9,10-dione (0.5g, 0.0017 mol) in dichloromethane (14.1 mL) triethylamine (0.4g, 0.0039 mol) was added. The reaction vessel was connected to a sodium hydroxide bubbler and sealed. To the solution, Methacryloyl chloride (0.25g, 0.0024 mol) was added dropwise, and left stirring at 500 rpm for 24 hours. The reaction was quenched with saturated sodium carbonate solution (5.53 mL). The aqueous layers were extracted with dichloromethane, and the combined organic layers were washed with brine, and the solvent was evaporated. The resulting purple powder was dissolved in petroleum ether/ethyl acetate (90%/10%). The solution was purified through a silica gel column with petroleum ether/ethyl acetate (90%/10%) to yield a purple powder.

Synthesis of disperse blue 3 methacrylate (DB3MA) 2

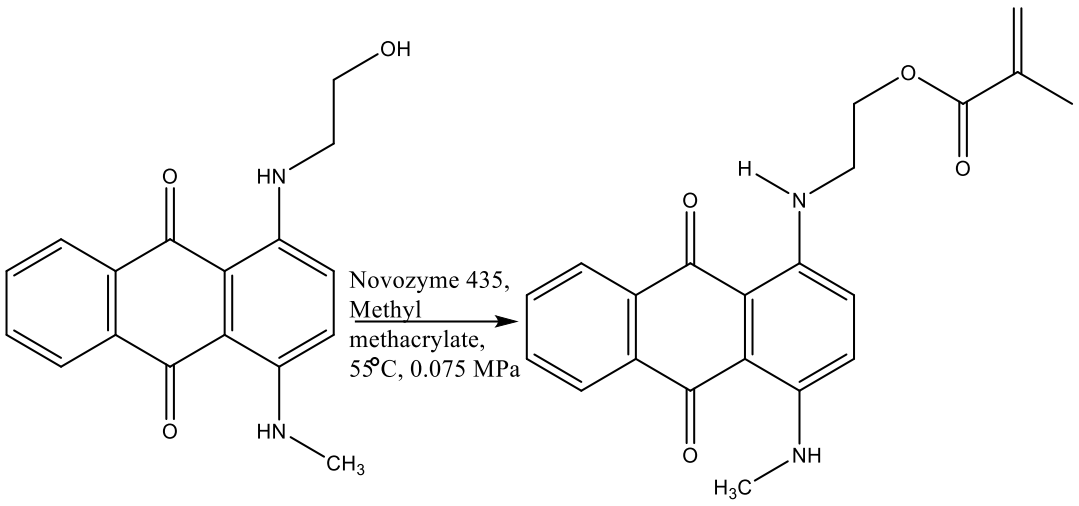


Figure 23 - Reaction scheme for the synthesis of Disperse Blue 3 Methacrylate 3

1-(dimethylamino)-4-((2-hydroxyethyl) (methyl)amino)anthracene-9,10-dione (0.25g, 0.0008 mol) was dissolved in toluene (5 mL); Novozyme 435 (0.5g) and methyl methacrylate (1.02g, 0.0119 mol) were added to the solution. The solution was raised to 55°C and put under a vacuum of 0.075 MPa, and was left for 24 hours. The solution was filtered, and washed with dichloromethane, the solvent was then evaporated. The resulting blue powder was purified through a silica gel column with an ethyl acetate eluent, yielding a blue powder of disperse blue 3 methacrylate.

Analysis:

Nuclear Magnetic Resonance (NMR):

The samples were analysed by ^{1}H NMR, using a Bruker 400 Ultrashield (400 MHz NMR), and all the samples were dissolved in deuterated chloroform. The ^{1}H NMR spectra were used to identify the polymers formation and to calculate the monomers conversion. The conversions were obtained with equation 1.

$$Conversion = \frac{AUCP}{AUCP + 1}$$

Equation 1

In this equation AUCP is the area under the curve of the polymer peak when compared to the area under the curve of the monomer peak.

Chapter 2: In-situ Polymerisation/Coating and Scale-Up:

Introduction:

To address some of the problems of the PBF (SLS) technique, novel polymers had to be designed and synthesized. The properties of polymers can be greatly modified by changing a variety of factors. Their properties can be modified by altering the structure of the monomers. This affects both homopolymers and copolymers. The properties of copolymers are highly dependent on the architecture of the polymer chain and the relative size of each block and/or constituent. Through the advancement of polymer science, a range of polymer architectures are available such as: diblock, triblock, brush, star, comb, ring, etc. (figure 1).

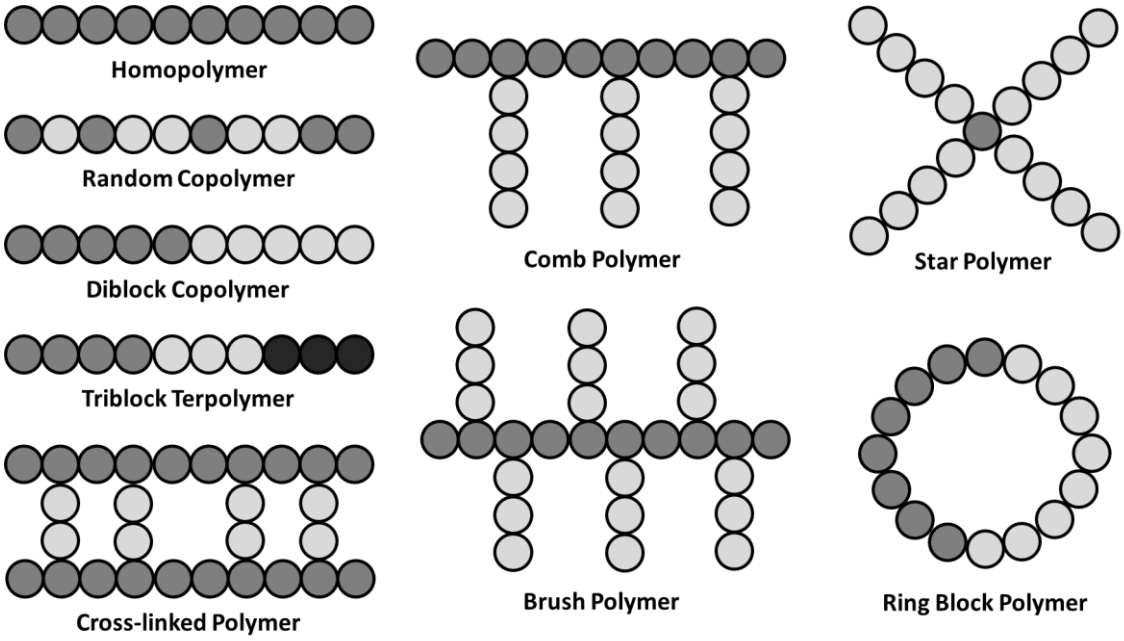


Figure 1 – Basic copolymer architectures

Polymers can be synthesized from several methods, all within two main mechanistic classes: chain growth (e.g. free radical polymerisation (FRP)) and step growth (e.g.

polycondensation)). This project utilized different types of radical polymerisation. Free radical polymerisation is a method of polymerisation, which forms a polymer through the successive addition of free-radical building blocks (monomers).[53–55] The reaction starts by the activation of an initiator, during which it decomposes into free radical containing molecules once an external stimulus is applied. The external force can be light, heat, and many others. One of the most widely used initiators is azobisisobutyronitrile (AIBN), a thermally-activated initiator.[56–58] Once the initiator is homolytically decomposed into two free radicals, these react with a monomer, converting the monomer into a radical species. The radical monomer reacts with other monomers, thereby starting the propagation of the polymer chain. The reaction continues until termination and/or until all the monomer is consumed (figure 2).

$I_2 \rightarrow 2I^{\bullet}$	*(Initiator Decomposition)*
$I^{\bullet} + M \rightarrow IM^{\bullet}$	*(Initiation)*
$IM^{\bullet} + nM \rightarrow P_{n+1}^{\bullet}$	*(Propagation)*
$P_n^{\bullet} + P_m^{\bullet} \rightarrow P_{n+m}$	*(Combination)*
$P_n^{\bullet} + P_m^{\bullet} \rightarrow P_n + P_m$	*(Disproportionation)*

Figure 2 – Free Radical polymerisation reaction mechanism, in which "I" stands for the initiator, M for monomer, and P for polymer chain.

FRP is possibly the most common polymerisation strategy with ~50 % of industrially manufactured polymers being produced via FRP.[59] Thanks to the high tolerance towards chemical functionality of this technique, it is well suited to a wide variety of monomers and solvents.[60] This robustness gives FRP an advantage over other more

sensitive polymerisation techniques such as ionic methods and step growths, as it is less sensitive to chemical impurities.[60]

At the moment, the vast majority (~90 %) of material used for SLS is based on Nylon 12 (Polyamide 12 or PA-12).[61] PA-12 is predominately made via polycondensation or ring opening polymerisation (ROP), with ROP being the preferred route for industry.[61] To synthesize PA-12 industrially; laurolactam undergoes ROP at 260 – 300 ^{o}C, with either cationic or anionic initiators.[61] After polymerisation PA-12 goes through a series of post-processing steps (extrusion, milling, drying, etc.) in order to produce PA-12 particles suitable for SLS.[61] The polymeric particles must have the prerequisite intrinsic and extrinsic properties needed for SLS:[14,61,62]

Intrinsic:

- Can absorb radiation at the wavelength of the laser
- Have thermal properties that result in a ≥ 10°C sintering window

Extrinsic:

- The particles need to be spherical or potato-shaped
- The particles must be of the desired size (normally 50-80 µm)
- The particles must flow adequately

The strategy employed to introduce colours into polymers and make coloured polymer particles relies on the synthesis (chapter 1), and subsequent polymerisation of dye monomers (figure 3). The methacrylate containing dye monomers, can undergo copolymerisation with other methacrylates to yield coloured polymers.[63]

Use of copolymers is advantageous compared to the homopolymers of the dye monomers for two main reasons. Firstly, co-polymerisation allows the for thermal and mechanical properties to be tuned to facilitate SLS. Secondly, use of inexpensive commercial methacrylate comonomers decreases the overall cost, as a smaller fraction of costly dye monomer is required to obtain the target effect. Copolymerisations such as these are possible in traditional solventsT.[64,65] In order to produce well-defined spherical uniform coloured polymeric particles for PBF (SLS), free radical dispersion polymerisation (FRDP) in $scCO_2$ can be used (Appendix 1).[22,66–71] FRP in $scCO_2$ is highly flexible and can be used in conjunction with a variety of monomers (figure 3). The FRP coating technique allows the user to synthesise an extensive variety of polymeric outer shells on polymeric particles such as PA-12 particles.

Polymerisation and coating of polymeric particles in $scCO_2$:

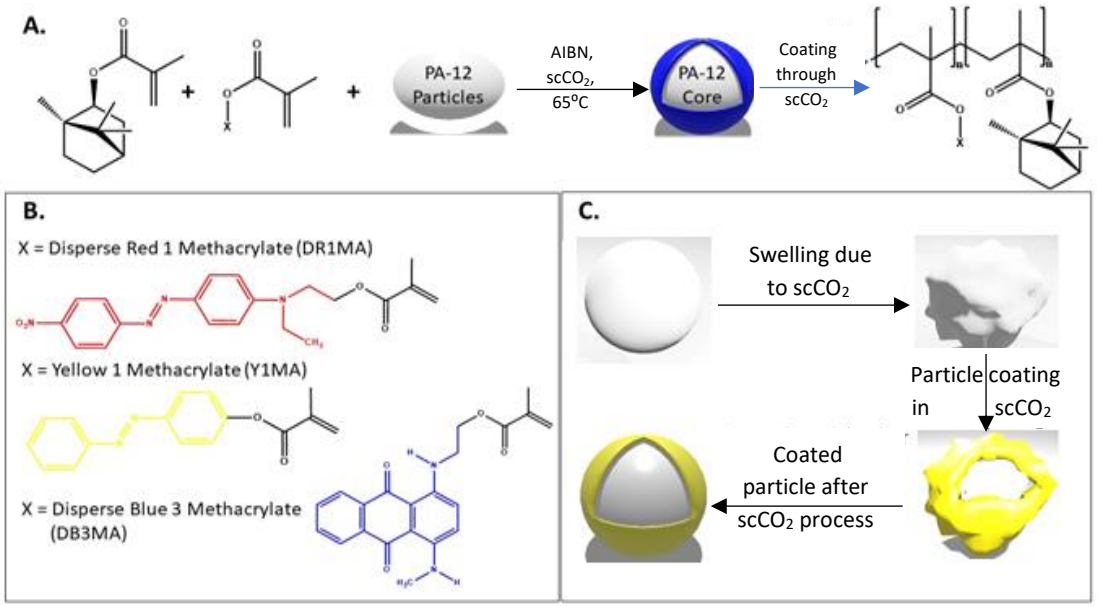


Figure 3 – Strategy used for the production of well-defined spherical coloured particles. A.) Reaction route for the coating of PA-12 with a copolymeric outer shell

consisting of P(Isobornyl methacrylate-dye monomer methacrylate). B.) Structure of dye monomers. C. Schematic of coating procedure in $scCO_2$, in which the $scCO_2$ swells the amorphous regions of the polymeric particle (PA-12 particle) thereby enabling the outer shell to penetrate the surface of the particle.

$ScCO_2$ has been used previously to create polymeric particles through FRDP in $scCO_2$, but it is also possible to coat already existing particles in $scCO_2$, with an outer shell (figure 4). In the past polymeric particles and polymers of different shapes have been coated and impregnated with a range of substances using $scCO_2$. Polymers that are amorphous or semicrystalline can be efficiently coated via $scCO_2$ as the amorphous regions in the polymer particles swell/deform allowing for partial impregnation of the coating species into the core polymeric particle. Literature has shown that polyethylene, polytetrafluoroethylene, polyvinyl acetate, poly methyl methacrylate, etc. can be swollen with $scCO_2$ at varying conditions.[72–75] More specifically and pertaining to this work $scCO_2$ has been shown to swell polyamide materials.[76–79] This process has been used to dope a variety of polymers.[80–86] Polyamide materials have been impregnated with substances such as dyes and pharmaceutical agents.[76–79] This property allows for the physical formation of shells on particles, enabling the synthesis of core shelled particles without the need for covalent bonding.

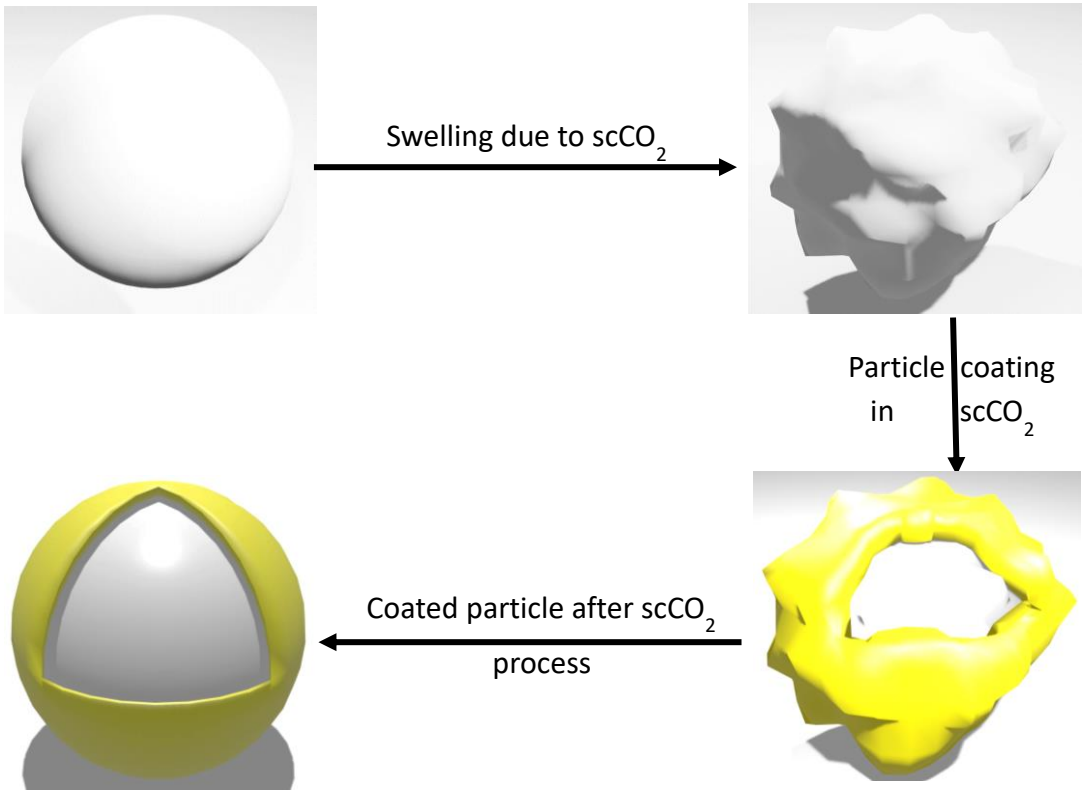


Figure 4 – Schematic of polymeric particle coating through free radical polymerisation in $scCO_2$. In $scCO_2$ a polymeric particle (e.g. PA-12 particles) will have its amorphous regions swollen, by introducing a dopant or a polymer the surface of the polymeric particle can be coated and slightly impregnated (Supporting information figure 13 and table 3). Upon depressurisation, the particles should return to their previous shape albeit with increased size due to the outer shell.

The formation of the polymeric outer shells on top of PA-12 particles should work, as the PA-12 particles act as the reaction locus for the polymerisation. PA-12 particles act as the locus for polymerisation encouraging shell formation. Initially the monomer and initiator are soluble in $scCO_2$, and initiation and initial propagation stages of the polymerisation occur in the $scCO_2$ phase. At this point the polymer chains can go into the swollen parts of the polymeric core (e.g. PA-12), then when a certain chain length

of polymer is reached the polymer chains are no longer soluble in $scCO_2$ and the reaction finishes on the outer shell of each particle. This is analogous to FRP dispersion polymerisations in $scCO_2$ in which the polymerisation finishes in the formed particles as the rest of the monomer is consumed. Then once the pressure is lowered by venting the $scCO_2$ out of the reactor the particles revert to their natural shape, along with their new coating (figure 4). With this method the user is able to coat PA-12 particles adequately and reliably with a variety of polymeric outer shells, given that the monomer is initially soluble in $scCO_2$. One of the main benefits of $scCO_2$ for this application is that the CO_2 is removed in a facile process by reverting to ambient pressure, yielding dry and pure coated polymeric particles. This is important for PBF (SLS) as the particulate powder needs to be very dry. When $scCO_2$ is used the benefits can be significant in both monetary and environmental costs as $scCO_2$ is cheap, can be recycled, and is a green solvent as it is non-toxic, non-flammable, and avoids energy intensive drying and purification steps.[22,68–71,87] The main advantages of this type of polymerisation and coating process are:

1. it is a green polymerisation process as it is performed in $scCO_2$.

2. $scCO_2$ swells the PA-12 so that all the particles can be wholly and uniformly coated

3. This process is versatile as long as the monomers are soluble in $scCO_2$, which allows for new materials to be produced for SLS printing.

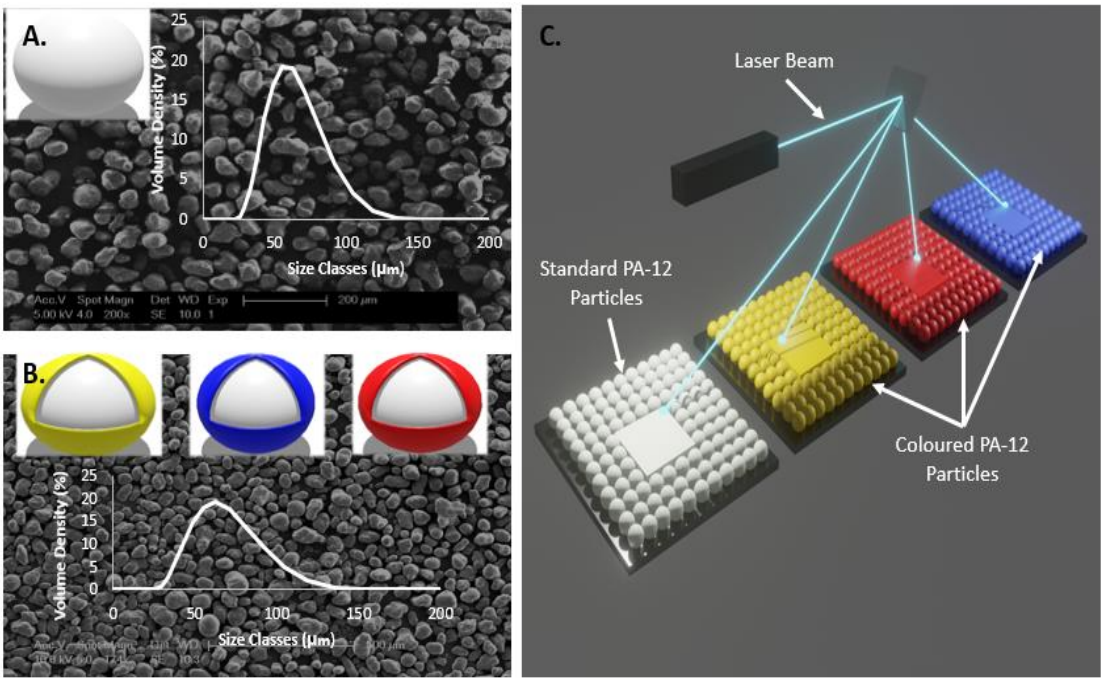


Figure 5 – Desired polymeric particles for coloured SLS. A.) SEM image and LDS spectrum of PA-12 P2200 particles. B.) SEM image and LDS spectrum of PA-12 particles coated with P(IBMA-Dye monomer). C.) Schematic of SLS printing in colour.

The aim for this work was to synthesize a variety of coloured polymeric particles and other polymer particles suitable for SLS (figure 5). The primary goal was to coat commercial PA-12 particles with random-copolymers of P(Isobornyl methacrylate-dye monomer) to synthesize coloured core-shelled particles. IBMA was chosen as it has similar thermal properties to that of PA-12, so the resulting particles should have similar properties to the industry gold standard that is PA-12.[61] PA-12 was chosen to be the core, because it is the industry standard for SLS.

Results and Discussion:

Commercial PA-12 particles were coated with three different copolymers to yield coloured PA-12 based particles suitable for SLS. The polymerisation and coating

process was conducted in $scCO_2$ via FRP. The coatings consist of a major monomer of IBMA as it possesses similar thermal properties to PA-12, and the minor monomers are the respective dye monomers (Chapter 1). This allows for the production of SLS printable uniformly coated coloured PA-12 particles via a simultaneous polymerisation and coating FRP process in $scCO_2$.

Synthesis of PA-12 particles coated with Poly (Isobornyl methacrylate-Yellow 1 methacrylate)

The coating of PA-12 particles with IBMA and Y1MA was the first set of polymerisations attempted. IBMA was chosen, because it has a T_g of ~180^oC, which is close to the T_m of PA-12 (178-180^oC).[12,61] This is important, because IBMA comprises the majority of the outer shell. The similarity between the T_g of IBMA and the T_m of PA-12 allows for even sintering of the particles during SLS printing. The first three reactions used Y1MA before the removal of a methacrylic anhydride impurity (chapter 1). This resulted in polymers with high dispersities (table 1), shown by GPC and ^1H NMR analysis conducted on the copolymeric outer shell. The outer shell was extracted by dissolving the shell in DCM, which is suitable as the coating is soluble, whereas the core is not. The shell was extracted in order to ascertain it's composition by and conversion quantitatively. The DCM layer was subsequently filtered to remove the remaining PA-12 particles and evaporated leaving a film composed of the copolymeric outershell, which could be analysed by ^1H NMR and GPC analysis ($CDCl_3$ and THF respectively).

Table 1 – Results for synthesis of PA-12 coated with P(IBMA-Y1MA)

Polymer	Conversion of IBMA (%)[a]	Appearance	M_n (KDa)[b]	M_w (KDa)[b]	Dispersity (Đ)	T_c (^oC)[c]	T_m(^oC)[c]
P1 Yellow	54.0	Yellow Powder	18	162	8.7	147.2	175.4
P2 Yellow	85.1	Yellow Powder	20	148	7.4	146.5	175.2
P3 Yellow	70.0	Yellow Powder	19	117	6.1	146.1	175.7

[a] Calculated from ^1H NMR spectra of the reaction mix. [b] Measured from GPC in THF using a pMMA triple detection. [c] Calculated from the second heating cycle of DSC.

From the results in Table 1, it is evident that the Đ values were very high for all three polymers (>6) compared to the expected Đ for a FRP polymerisation in $scCO_2$ (between 1.5 and 3). The observed Đ values could result from branched polymers, caused by the presence of methacrylic anhydride.[50] The high Đ of these samples, suggest that there is a lot of variation in the polymer in terms of molecular weight and heterogeneity. This indicates that these samples might not be suitable for SLS printing, as it has been shown that there is a correlation between the T_g of a polymer and its M_n (the higher M_n, the higher T_g).[88] One positive aspect of the GPC data is that

the UV signal matches the DRI signal and LS signal, indicating that the dye monomer has been integrated into the polymer chain (Figure 6). The UV signal measures the UV response of the polymer in question, if the polymer is not compatible with the wavelength (e.g. white or colorless) a signal does not appear, and if it is then a signal will show the molecular weight of the polymer, via a signal at that timepoint. The dRI measures the molecular weight of a polymer as a change in refractive index compared to the eluent used. If the time points for the dRI and UV signals are the same, this proves that the molecular weight of the polymer is the same, hence the colour monomer is integrated into the polymeric chain.

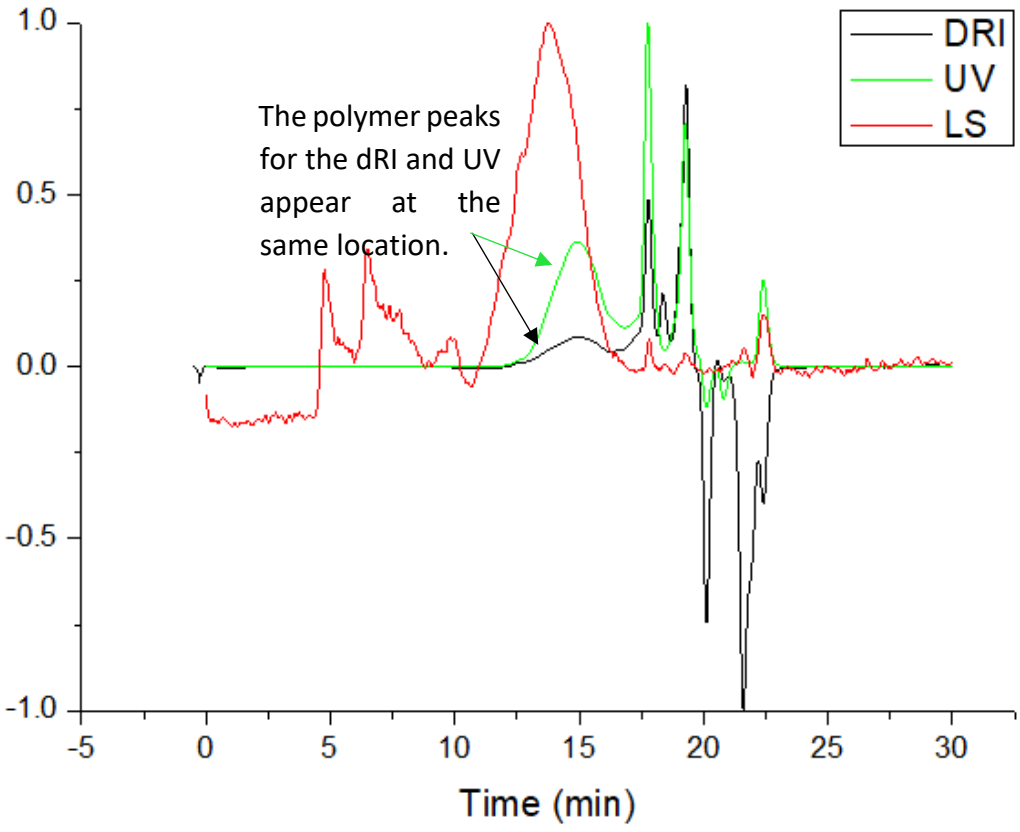


Figure 6 – GPC Chromatogram of P(IBMA-Y1MA). In the GPC chromatogram it can be seen that the UV and dRI signals appear at the same timepoint, hence the dye monomer has integrated into the polymer. The UV signal measures the ultraviolet-visible response of the polymer in question, if the polymer is not compatible with the wavelength (e.g. white or colorless) a signal does not appear, and if it is then a signal will show the molecular weight of the polymer. The dRI measures the molecular weight of a polymer as a change in refractive index compared to the eluent used. If the time points for the dRI and UV signals are the same, this proves that the molecular weight of the polymer is the same, hence the colour monomer is integrated into the polymeric chain. Light scattering (LS) in GPC is performed by irradiating the material with a laser beam and measuring the intensity of the scattered light, hence when the polymer is present the scattered light will be different from that of the eluent (Dawn 8+ Wyatt technology). DRI measures the refractive index difference between the polymer sample and the eluent (1260 RID Agilent Technologies). UV measures the UV-vis response from the eluting sample, exhibiting the differences between the polymeric sample and the eluent (1260 Infinity Variable Wavelength detector Agilent Technologies). The results are compiled and represented as difference of detector voltage (V) (Y-axis).

The conversion of IBMA to P(IBMA) was calculated from the relevant peaks (peaks A and B) of the ^{1}H NMR of the polymers (figure 7).

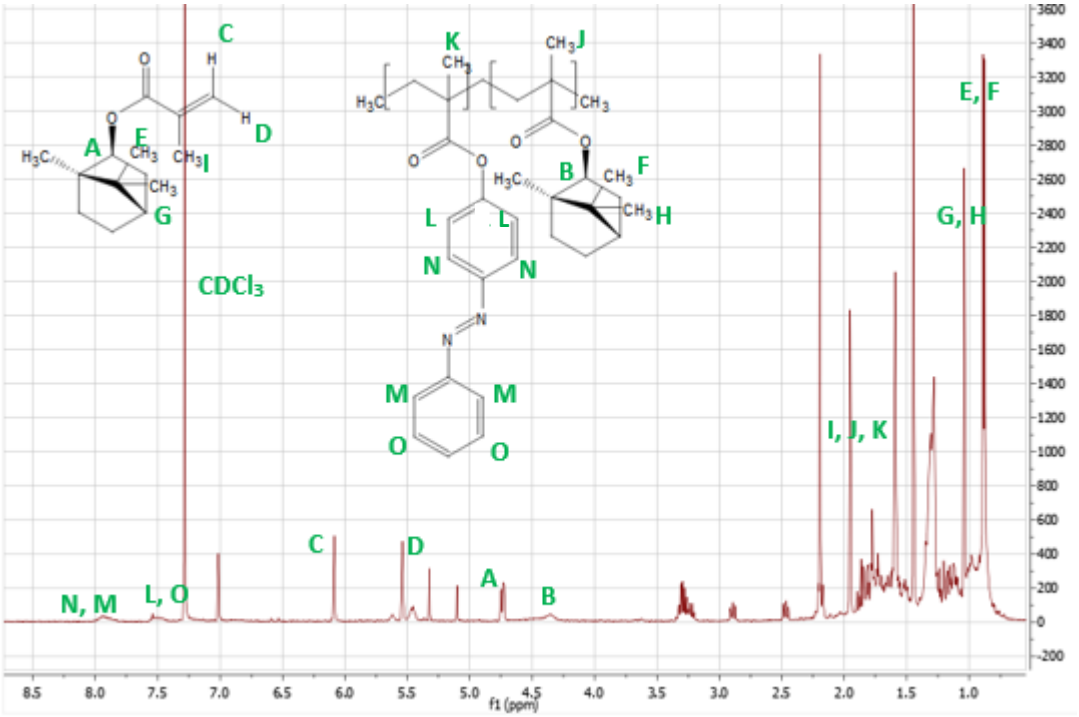


Figure 7 – ^{1}H NMR of P(IBMA-Y1MA), showing residues of IBMA and the corresponding polymer peaks for P(IBMA-Y1MA).

The conversion of Y1MA to PY1MA was not calculated, because the peaks of PY1MA and the monomer tended to overlap in the ^{1}H NMR spectra leading to unreliable results, however the observed broadening of the 1H-NMR signals is characteristic of polymer formation it is evident that the polymer has formed since the peaks have become broader as is characteristic for polymers.

The T_c and T_m (with the T_g matching the T_m as predicted) are far apart (>20°C) for all three polymers, showing that samples P1-P3 Yellow have a good sintering window (table 1). However due to the large polydispersity a differential in melting point onset could be observed because of the large differences in molecular weight (table 1). The samples have a variety of C-H bonds so they can absorb radiation at the wavelength of a CO_2 laser.[17,18] The introduction of the dye monomer allows the polymer to absorb

radiation at a wavelength suitable for UV lasers so, in theory these polymers could possibly be printed via an HRSLS printer (Appendix 1). All three samples were yellow powders (figure 8).

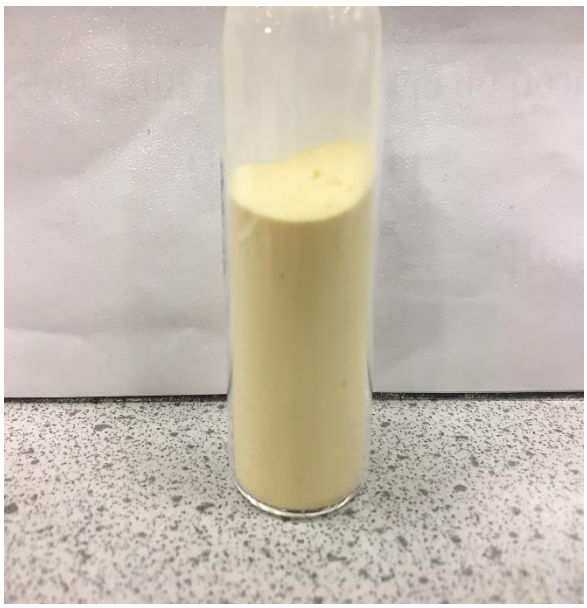


Figure 8 – Picture of PA-12 coated with P(IBMA-Y1MA), showing that it is a yellow powder.

SEM analysis was conducted, and the images showed that the polymer powder was composed of discrete particles with an average size of 62.5 µm. The particles pack into monolayers and do not aggregate, which is ideal for SLS printing (figure 9). The polymeric powders flow and pack well, which allows for uniform deposition by the recoater arm to yield uniformly packed layers. As a result of uniformly packed layers, the parts will be defect free and avoid the presence of stress points or other negative features.

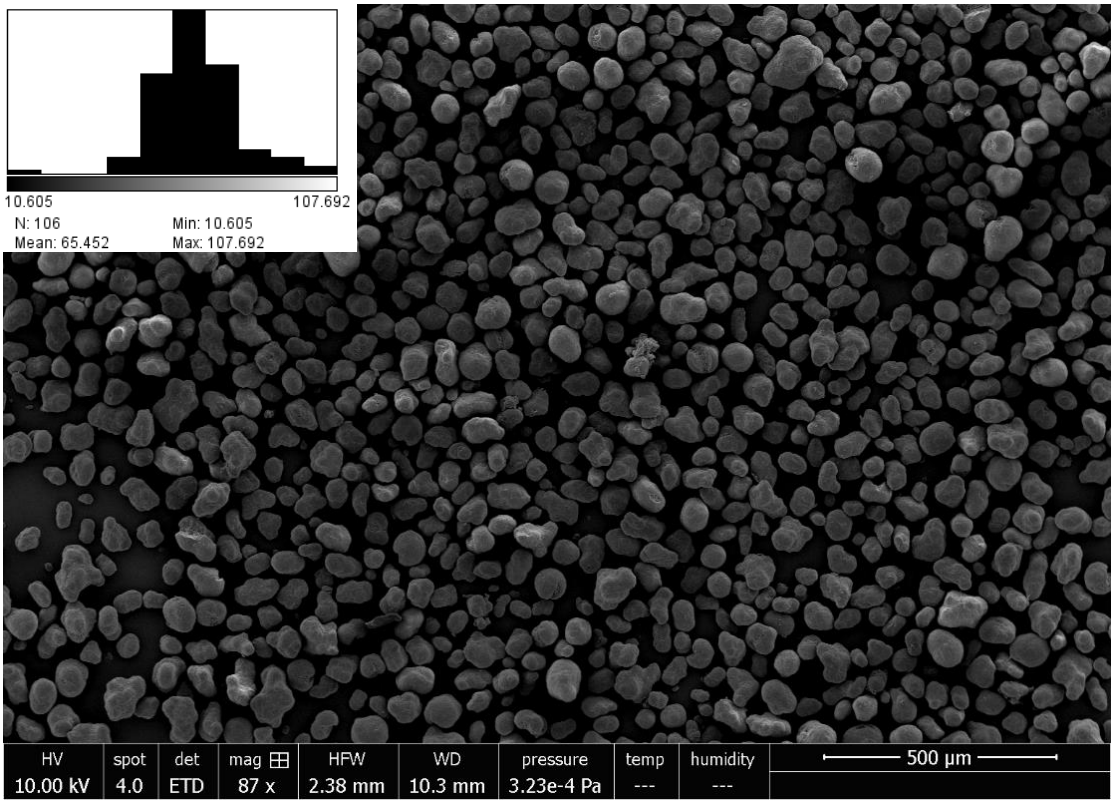


Figure 9 – SEM image of PA-12 coated with P(IBMA-Y1MA) particles, showing that they are potato shaped and of a size ~60 µm, with the uncoated PA-12 particles having a size of 58 µm (± 0.63%).

Further particle size analysis was conducted with laser diffraction particle size analysis (LDS), to analyse a larger portion of the samples than by SEM. LDS showed that the average particle size was 61.5 µm (± 0.82%), corroborating the results from SEM (figure 10). LDS was conducted as it is a particle sizing technique performed on the dry powder, as an alternative to DLS which requires the particles to be suspended in solution. Performing particle sizing in solution could give misleading results as being in a suspension could separate particles which tend to aggregate in the solid and dry state. This is significant as the application (PBF (SLS) printing) is conducted on dry polymeric powders, so the particle size must be known in this state. The size of 61.5 µm (± 0.82%) shows that these particles have increased in size from the commercial

PA-12 ones (58 µm) (± 0.63%), demonstrating that the coating is present. The SEM and LDS data show that after the coating of P(IBMA-Y1MA) is formed these particles increase in size, but retain their potato shape, hence they keep the extrinsic properties of PA-12 and flow and pack well.

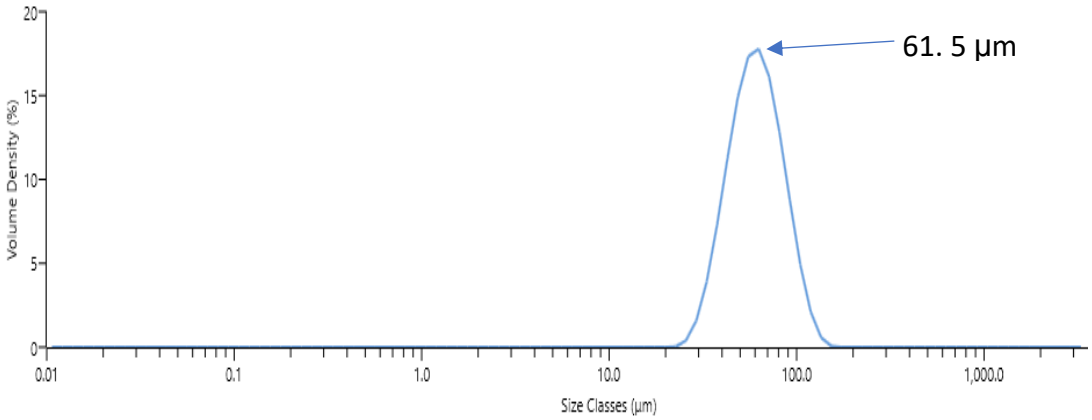


Figure 10 – Particle size distribution of PA-12 coated with P(IBMA-Y1MA) particles. The peak indicates that the majority of the particles are of the size of 61.5 µm (± 0.82%), and the uncoated PA-12 particles have an average size of 58 µm (± 0.63%).

These samples had several positive results, the first of which is that the resulting polymers were yellow powders. The polymers were composed of discrete particles which packed into monolayers and had wide sintering windows. However, the coatings on the samples had very high Đs, which could alter the properties of the particles such as their thermal properties. The large polydispersity doesn't not appear to influence the overall T_g of the polymer (table 1), however if one of the particles has a higher or lower T_g due to significant differences in molecular weight, this could lead to improper sintering and introduce stress points. To create PA-12 particles coated with P(IBMA-Y1MA) suitable for SLS, the Đ of the polymeric coatings needed to be lowered. To narrow the Đ three reactions were performed with Y1MA purified via a

basic alumina column removing methacrylic anhydride impurities. These reactions followed the same procedure used to make polymers P1-P3 but they showed lower Đs than the aforementioned polymers (table 2).

Table 2 – Results for synthesis of PA-12 coated with P(IBMA-Y1MA) (after purification of Y1MA monomer)

Polymer	Conversion of IBMA (%)[a]	Appearance	M_n (KDa)[b]	M_w (KDa)[b]	Polydispersity (Đ)	T_c (°C)[c]	T_m(°C)[c]
P4 Yellow	61.0	Yellow Powder	120	224	1.8	148.5	175.2
P5 Yellow	56.0	Yellow Powder	40	57	1.5	147.6	175.2
P6 Yellow	57.0	Yellow Powder	9	23	2.5	146.2	174.4

[a] Calculated from ^{1}H NMR spectra of the reaction mix. [b] Measured from GPC in THF using a PMMA triple detection. [c] Calculated from the second run of DSC (Supporting Information Figures 1-3).

From table 2, it can be seen that the properties of P4-P6 Yellow are more consistent with the expected Đ values than the ones related to P1-P3 Yellow. The conversion of IBMA for P4-6 Yellow ranges from 56% to 61% and was calculated using the same method used for P1-P3 Yellow.

The GPC results show that the Đ of the samples is narrower than before, as the lowest Đ for P4-P6 Yellow is 1.5 and the highest is 2.5, which is nearly 3 times lower than the Đs observed for P1-P3 Yellow. However, the M_n and M_w vary by a wide margin as P4 Yellow had a M_n and M_w of 120 KDa and 224 KDa respectively, while P6 Yellow had a M_n and M_w of 9 KDa and 23 KDa respectively. The GPC data showed that the UV signal matched the DRI signal, signifying that Y1MA is in the polymer chain. Although this is a marked difference in molecular weight the T_c, T_m, and T_g are consistent and have a large sintering window. Also, like P1-P3 Yellow, samples P4-P6 Yellow can absorb radiation of both the wavelength for CO_2 and UV laser. All 3 samples were composed of yellow powders. From this data, it is seen that P4-P6 Yellow have the appropriate intrinsic properties for use in SLS printing. Samples P4-P6 Yellow were analysed via SEM, to gain an understanding of size, shape, and packing of the polymer particles. The shape of the particles was the typical (for PA12) potato-like-shape, they pack into monolayers, and there is no evident agglomeration (figure 11). The average particle size of PA-12 particles coated with P(IBMA-Y1MA) (purified) was found to be 60.5 µm from SEM.

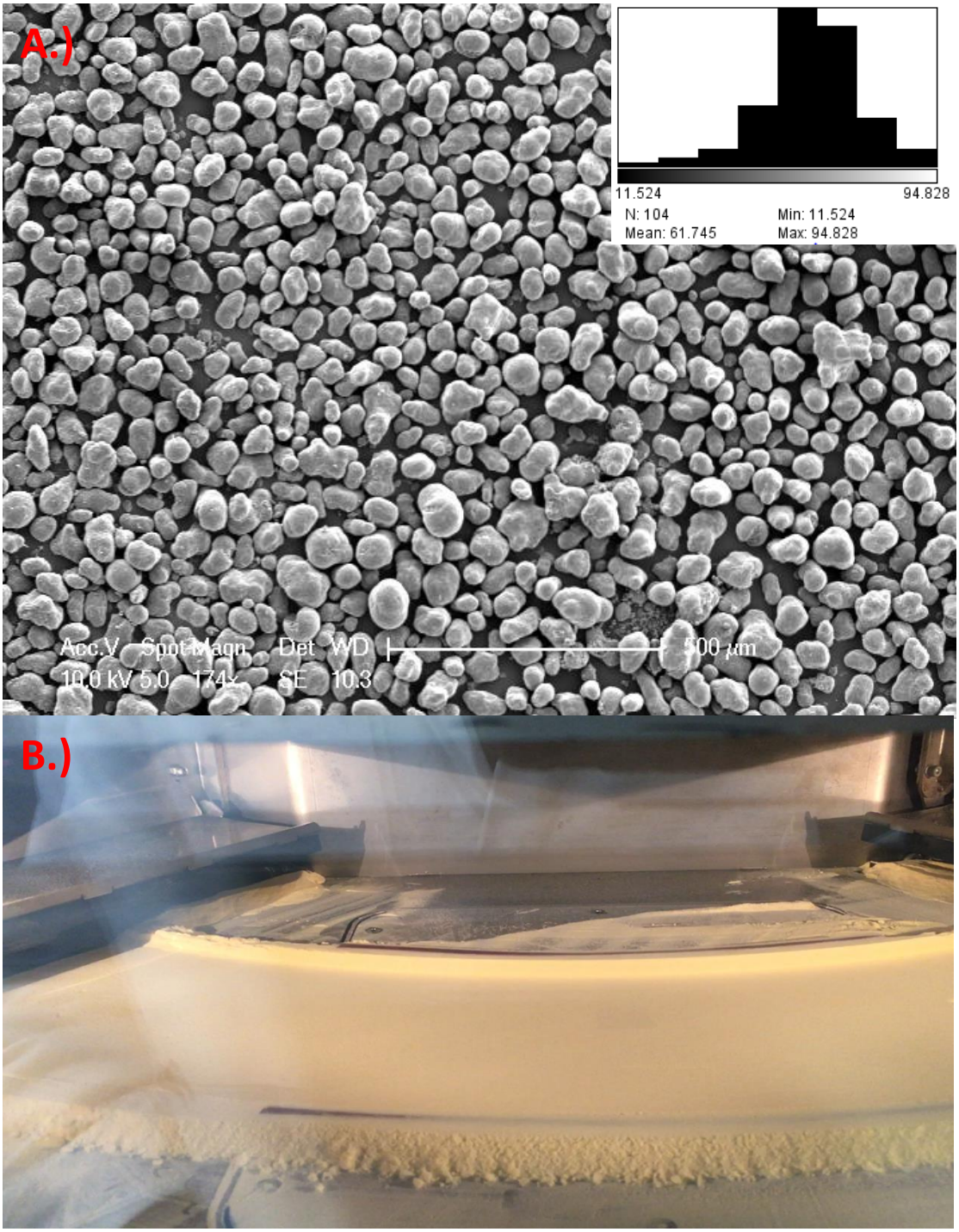


Figure 11 – Shape and flow images of coated PA-12 particles. A. SEM image of PA-12 particles coated with P(IBMA-Y1MA) (purified), showing that the particles are potato shaped and of a size ~60 µm. B.) Image showing good layer formation of PA-12 particles coated with P(IBMA-Y1MA) via SLS powder deposition method.

LDS analysis was used to confirm the average size of the particles. The average particle size obtained from LDS was 62.0 µm (± 0.74%), which is similar to the particle size calculated from SEM analysis, and to polymers P1-P3 (figure 12). As before, SEM images confirmed the particles were potato shaped, and the LDS that the particle size of the coated particles when dry was 62.0 µm, showing that they have increased slightly in size but are not agglomerating.

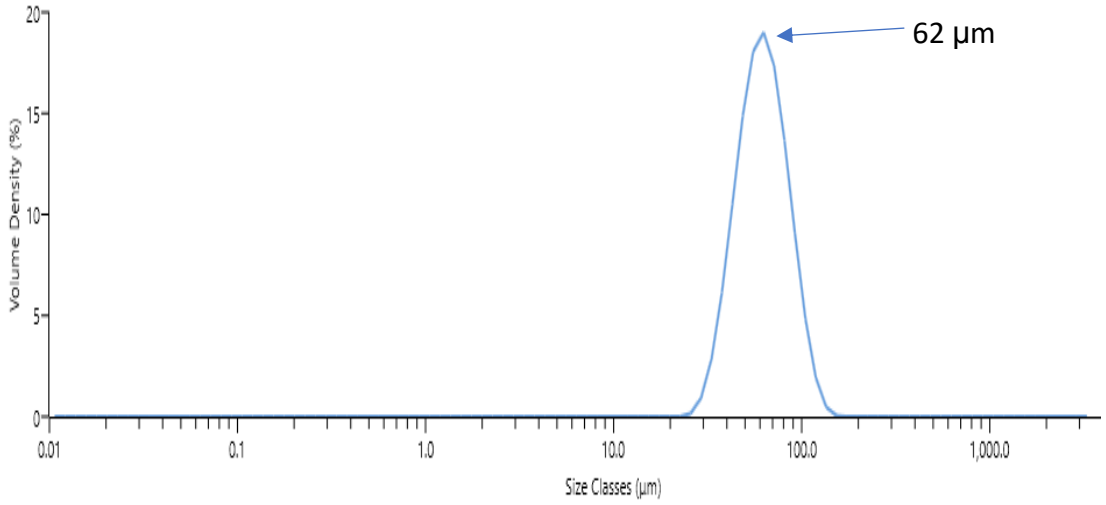


Figure 12 – Particle size distribution of PA-12 particles coated with P(IBMA-Y1MA)(purified) particles. The peak indicates that the majority of the particles are of the size of 62.0 µm (± 0.74%), with the average size of uncoated PA-12 particles being ~58 µm (± 0.63%).

These samples can be said to be ideal for SLS printing, as they possess the appropriate extrinsic and intrinsic properties. Namely, a wide sintering window, a narrow dispersity, and absorb radiation at the wavelength of the laser. The particles are discrete and pack into monolayers. Following the successful synthesis of yellow PA 12 particles suitable for SLS printing, the next step was to produce magenta (red) PA-12 particles.

Synthesis of PA-12 particles coated with Poly (Isobornyl methacrylate-Disperse Red 1 methacrylate)

To produce red PA-12 particles for SLS, an analogous strategy to the one used for the production of yellow PA-12 particles was used. The major monomer of the outer shell was IBMA as the thermal properties are similar to those of PA-12, and the minor monomer (dye monomer) used to impart the red colour was DR1MA. Several polymerisations were attempted to produce red PA-12 particles for SLS printing. These particles were made by coating PA-12 particles with IBMA and DR1MA via FRP in $scCO_2$. It was desired to see if the reactions for these coatings could be controlled or tailored through varying the concentration of initiator used, in an effort to achieve control over the molecular weight of P(IBMA-DR1MA)(Table 3).[89]

Table 3 – Results for synthesis of PA-12 particles coated with P(IBMA-DR1MA)

Polymer	Amount of AIBN (wt%)	Conversion of IBMA (%)[a]	Appearance	M_n (KDa)[b]	M_w (KDa)[b]	Đ	T_c (^oC)[c]	T_m(^oC)[c]
P7 Red	5.0	73.0	Red Powder	85	265	3.1	149.5	177.4
P8 Red	7.5	70.0	Red Powder	65	290	4.4	148.8	177.2
P9 Red	10.0	75.0	Red Powder	58	133	2.3	146.2	175.4

P10 Red	12.5	74.0	Red Powder	25	40	1.7	146.4	175.2

[a] Calculated from ^{1}H NMR spectra of the reaction mix. [b] Measured from GPC in THF using a pMMA triple detection. [c] Calculated from the second run of DSC (Supporting Information Figures 1-3).

The GPC data show that the M_n of the polymer can be controlled by changing the amount of AIBN. The trend is that there is a decrease in M_n with increasing quantities of AIBN, as would be expected, as fewer polymer chains are formed, so each polymer chain will contain more monomer units, and vice versa. These results could be extrapolated to give a wider range of molecular weights, which could then be used for printing, and subsequently tested to see if the mechanical properties of the parts could be altered by having outer shells of different molecular weights. The Đ for these samples ranges from 1.7 to 4.4 for P7-P10, which aligns with values for FRP. Much like the yellow PA-12 particles, samples P7-10 Red have matching UV and DRI signals in their GPC chromatograms (figure 13). This shows that the dye monomer has been successfully integrated into the polymer chain as the UV signal coming from the dye monomer/polymer is at the same location as the dRI signal coming from the polymer chains.

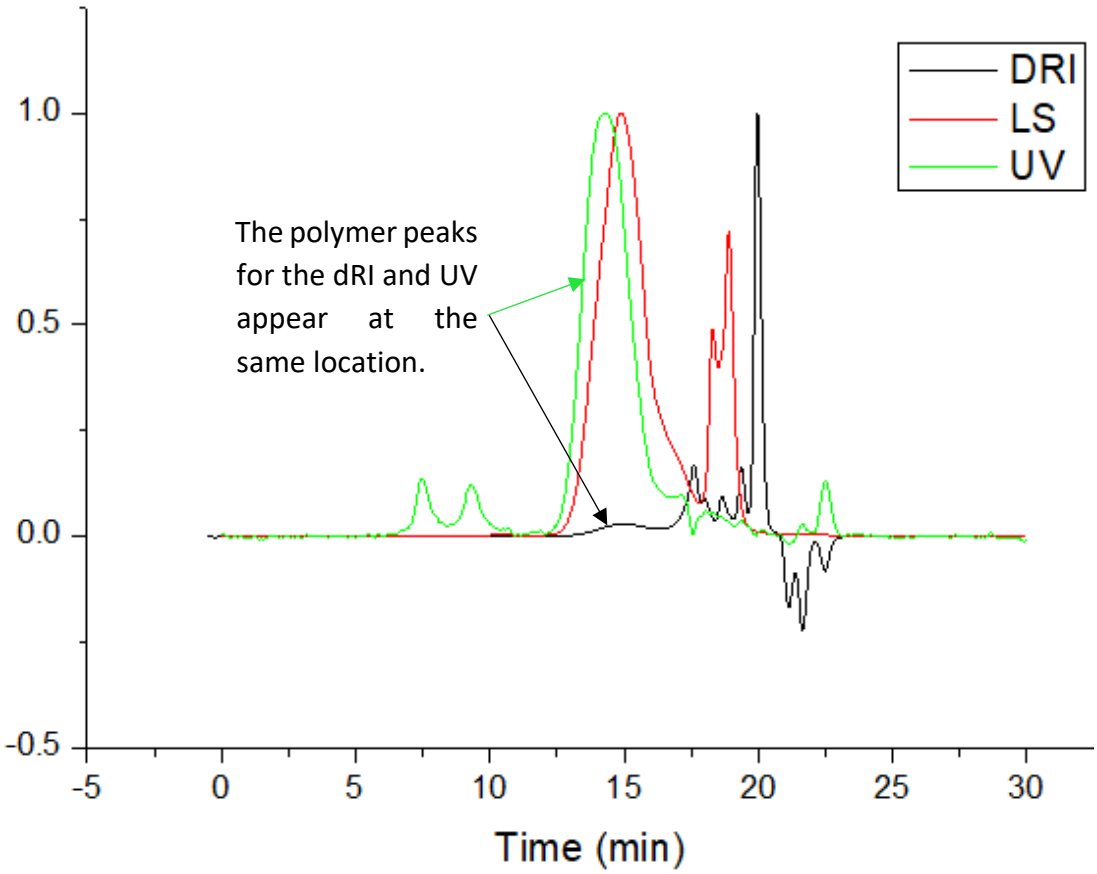


Figure 13 - GPC Chromatogram of P(IBMA-DR1MA). Showing that UV and dRI peaks correspond to the same species, demonstrating successful co-polymerisation.

The conversion of IBMA was calculated from the ^{1}H NMR spectrum (Figure 14) from the relevant peaks for IBMA. The conversion of DR1MA was not calculated as the polymeric DR1MA peaks overlap with the monomer peaks. The observed peak broadening does suggest that DR1MA has undergone polymerisation.

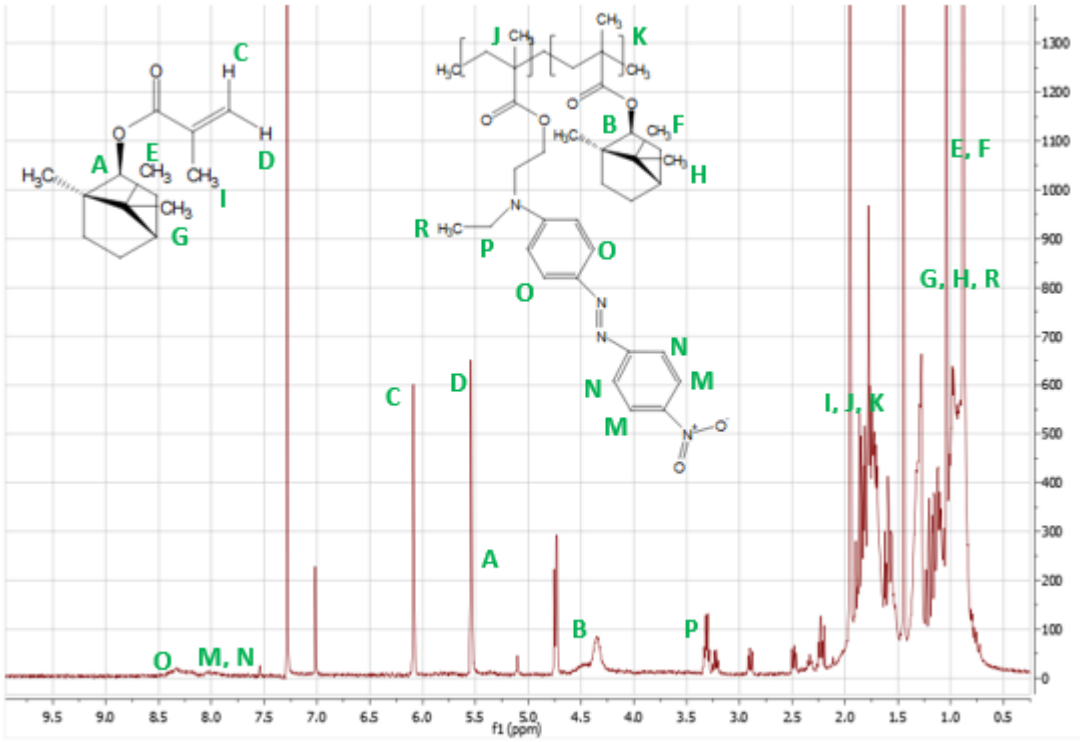


Figure 14 – ^{1}H NMR of P(IBMA-DR1MA) in $CDCl_3$ showing residues of IBMA.

The conversions of IBMA are consistent (70%-75%) for all the samples, and the polymers are composed of red free-flowing powders (Figure 15). The T_c and T_m of the samples were quite similar across the different samples, with average gap between them of about 20°C, indicating that the polymers P7-10 Red have a wide sintering window (>10°C), suggesting that the samples P7-P10 Red have the appropriate intrinsic properties for SLS.



Figure 15 – PA-12 particles coated with P(IBMA-DR1MA), showing that they are red powders.

These samples, like samples P1-P6 Yellow, showed promising properties when analysed via SEM, as they were discrete monodisperse particles that formed monolayers (figure 16). The average particle size obtained from the SEM images was ~60 µm. SEM analysis showed that the particles retained their potato shape after the coating process (figure 16).

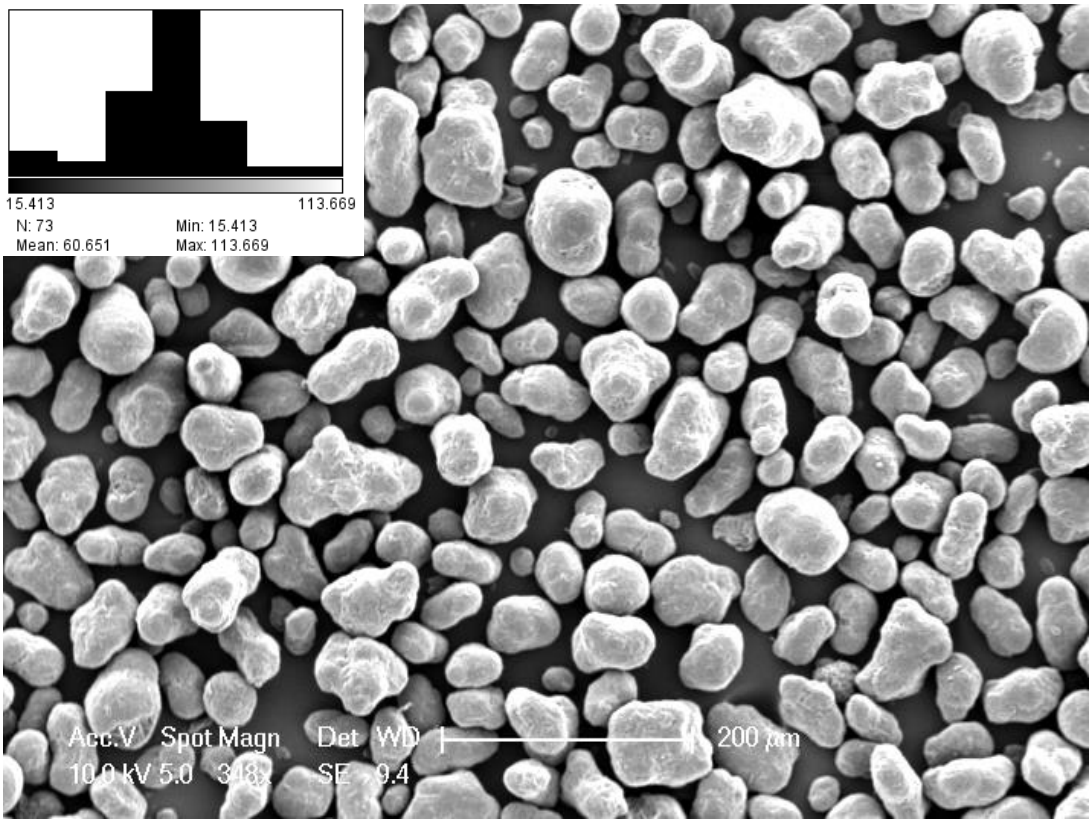


Figure 16 - SEM image of PA-12 particles coated with P(IBMA-DR1MA), showing that the particles are potato shaped and of a size ~60 µm.

In order to confirm the particle size of the samples, LDS was used, revealing an average particle size of 63.2 µm (± 1.63%) (figure 17). From the LDS and SEM analysis one can conclude that the extrinsic properties of this coated PA-12 based material are appropriate for SLS, as the particles retain their potato shape, and increase slightly in size.

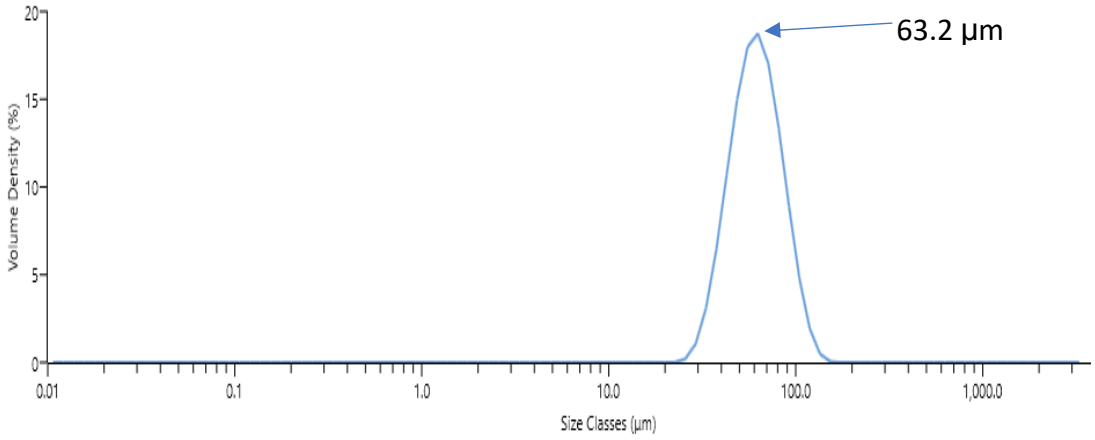


Figure 17 – Particle size distribution of PA-12 particles coated with P(IBMA-DR1MA). The peak indicates that most of the particles are of the size of 63.2 µm (± 1.63%), with the average size of uncoated PA-12 being ~58 µm (± 0.63%).

Polymers P7-P10 Red like samples P4-P6 Yellow are suitable for SLS printing, as they possess the correct intrinsic and extrinsic properties. This is because the copolymeric coating has similar thermal properties to that of PA-12 hence the sintering of the core and shell should occur at the same time. Also, the copolymeric coating can absorb the radiation of a CO_2 laser, enabling sintering, and the size and shape of the particle imply that the red PA-12 particles should have similar flow and packing to the uncoated commercial PA-12.

The colour was manipulated by varying the amount of DR1MA used in the coating of PA-12 particles with P(IBMA-DR1MA). A range of weight percentages (2.5 – 12.5 wt.%) of DR1MA to IBMA were tested. The colour of the resulting polymers was studied with a NIX colour sensor. This sensor allows the user to get the colour values for any material. These colour values directly relate to the colour that is perceived by humans. This study showed that as more DR1MA is added, the redder the final material (table 4).

Table 4 – Colour of PA-12 coated with P(IBMA-DR1MA) depending on weight percentage of IBMA and DR1MA. Colour was determined through NIX colour analysis.

Sample	Amount of IBMA (wt%)	Amount of DR1MA (wt%)	Colour (appearance)	Cyan (CMYK values)	Magenta (CMYK values)	Yellow (CMYK values)	Black (CMYK values)
Red PA-12 (1)	15	2.5	Orange	7	96	100	1
Red PA-12 (2)	15	5	Orange	7	96	100	1
Red PA-12 (3)	15	10	Red	9	100	100	6
Red PA-12 (4)	15	12.5	Red	13	100	100	7

It was observed that when a low weight percentage (2.5 – 5 wt.%) of DR1MA is used the colour of the powder is orange (table 4). Upon increasing dye monomer loading to 10 and 12.5 wt.% the colour of the powder produced was red. To produce magenta/red polymeric particles, a minimum of 10 wt.% of DR1MA is needed on the outershell. This shows that different colours can be obtained by simply changing the weight percentage of the dye monomer in the polymeric outershell.

Synthesis of PA-12 particles coated with Poly (Isobornyl methacrylate-Disperse Blue 3 methacrylate)

DB3MA was the chosen blue dye monomer, for the reasons previously mentioned (Chapter 1). However, DB3MA contains a quinone group, which are known for being prolific radical scavengers. Especially in the presence of O_2/H_2O the quinone group can affect many free radical species (figure 18).[90–92] Solution polymerisations were performed to confirm the radical scavenging capability of DB3MA.

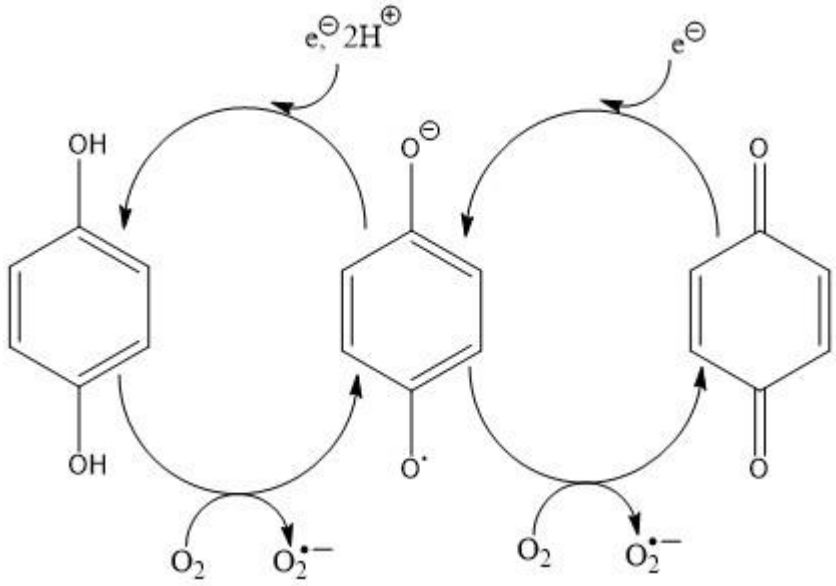


Figure 18 – Radical scavenging mechanism of quinones, showing that the radical scavenging cycle is dependent on the presence of O_2/H_2O.

The attempted synthesis of P(MMA-DB3MA) was conducted in toluene using AIBN as an initiator. The conditions employed are known to work for a variety of methacrylate-based monomers.[93] However, it can be seen that DB3MA did not polymerise, and only MMA polymerised. Consequently, the DB3MA remained in solution upon precipitation of the polymeric species (figure 19). This showed that

conventional solvents and methods are unsuitable for the polymerisation of DB3MA, and alternative methodology would have to be utilised.

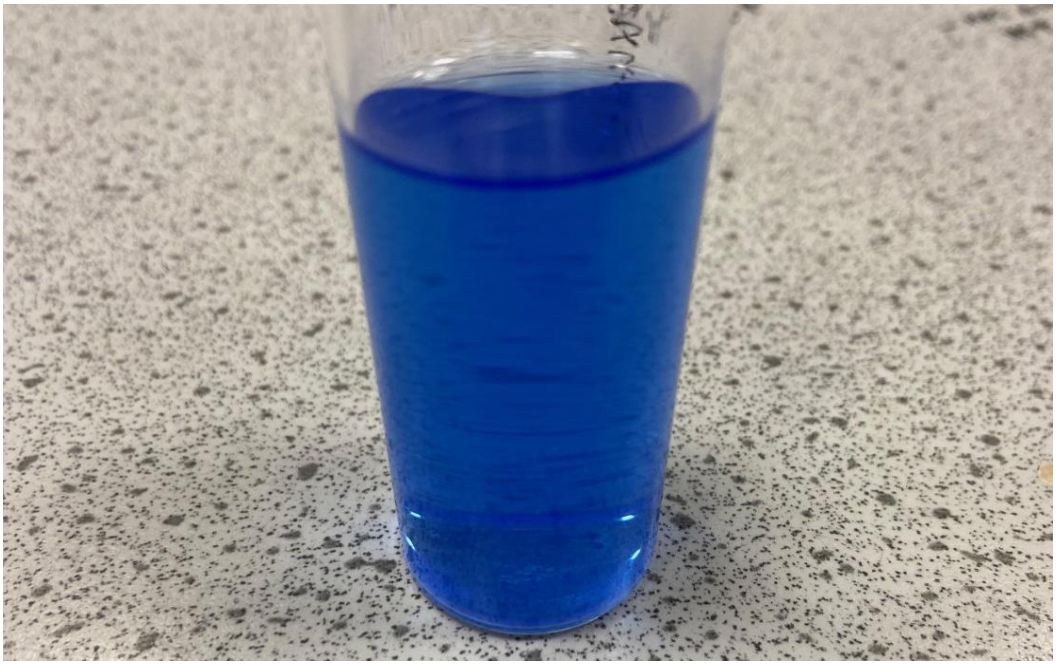
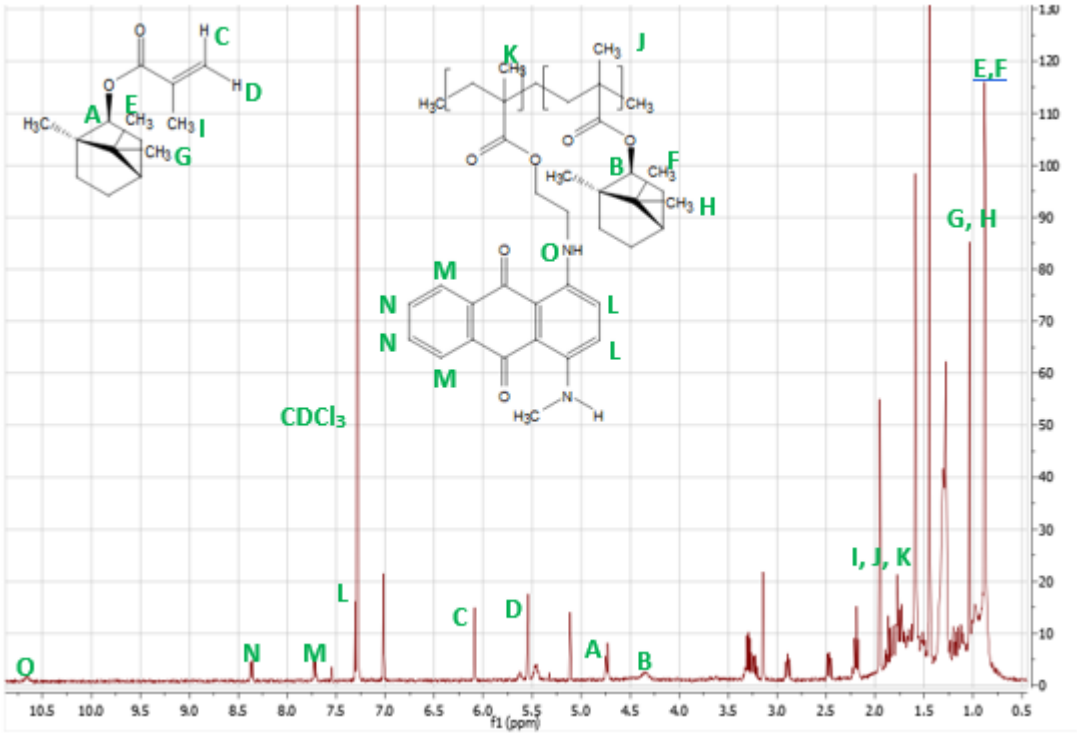


Figure 19 – Image of filtrant used for polymer precipitation. The bright blue colour indicates that DB3MA has not reacted and stayed in the solvent medium instead of polymerising with MMA to yield a P(MMA-DB3MA) monomer.

It was the decided to try free radical dispersion polymerisation (FRDP) in $scCO_2$ with MMA and DB3MA in an attempt to synthesize P(MMA-DB3MA) particles, to see if it was possible to produce a polymer with DB3MA in $scCO_2$ (Appendix 1). MMA was chosen as the first copolymer to test, as MMA polymerisations via FRDP in $scCO_2$ have been studied extensively. This was done as $scCO_2$ has very little if any O_2/H_2O (≤0.00009 %), hence the quinone scavenger cannot cycle back after it has reacted with one free radical, so the free radical scavenging property of DB3MA should be greatly impeded through the use of $scCO_2$ P(MMA-DB3MA) polymeric particles were produced (Appendix 1), the particles had sizes ranging from 0.5 µm to 5 µm. Particles

composed of P(MMA-DB3MA) were used to perform high resolution SLS, the results of this synthesis are explained and expanded upon in Appendix 1. It was seen that DB3MA was part of the polymer chain, as there was a UV peak that matched directly with the DRI and LS peaks in the GPC chromatograms (Appendix 1).

After this success it was decided to synthesize P(IBMA-DB3MA) and coat PA-12 particles with said polymer. The polymerisation was repeated in triplicate at the 60 mL scale. The results were analogous to that of the P(IBMA-Y1MA) and P(IBMA-DR1MA) with conversions of IBMA ranging from 69-72% (figure 20) (table 6). GPC and ^{1}H NMR analysis were performed on the outer shell. GPC analysis showed that DB3MA had incorporated into the polymer chain as the LS, DRI, and UV signals had a polymer peak at the same region (figure 20) (table 5). The overlap of UV and dRI signals demonstrates that the polymer is UV active, implying that the dye has successfully been copolymerised.



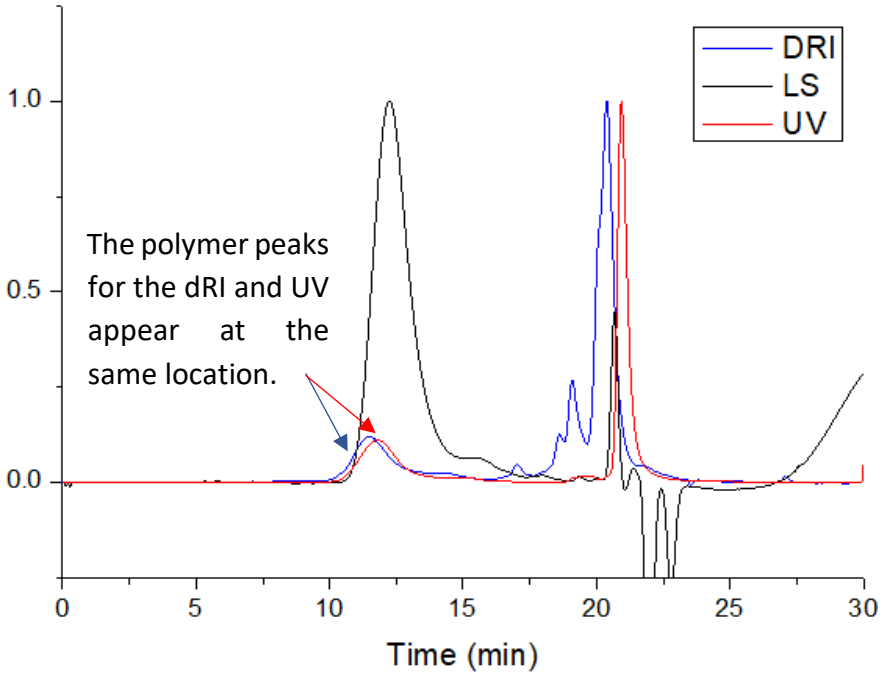


Figure 20 – Results of synthesis of PA-12 particles coated with P(IBMA-DB3MA) via FRP in $scCO_2$. A.) ^1H NMR spectrum in $CDCl_3$ showing the formation of P(IBMA-DB3MA) and residues of IBMA B.) GPC chromatogram of P(IBMA-DB3MA). Showing that UV and dRI peaks correspond to the same species, demonstrating successful co-polymerisation.

Table 5 – Results of synthesis of PA-12 particles coated with P(IBMA-DB3MA) via FRP in $scCO_2$.

Sample	Conversion (%)[a]	M_w (Da)[b]	M_n (Da)[b]	$Đ$	T_g (°C)[d]	T_m (°C)[d]	T_c (°C)[d]
Blue PA-12 (1)	72	82	48	1.7	166.3	175.8	147.6
Blue PA-12 (2)	70	94	55	1.7	167.4	175.4	146.4
Blue PA-12 (3)	69	83	50	1.7	166.9	175.5	146.7

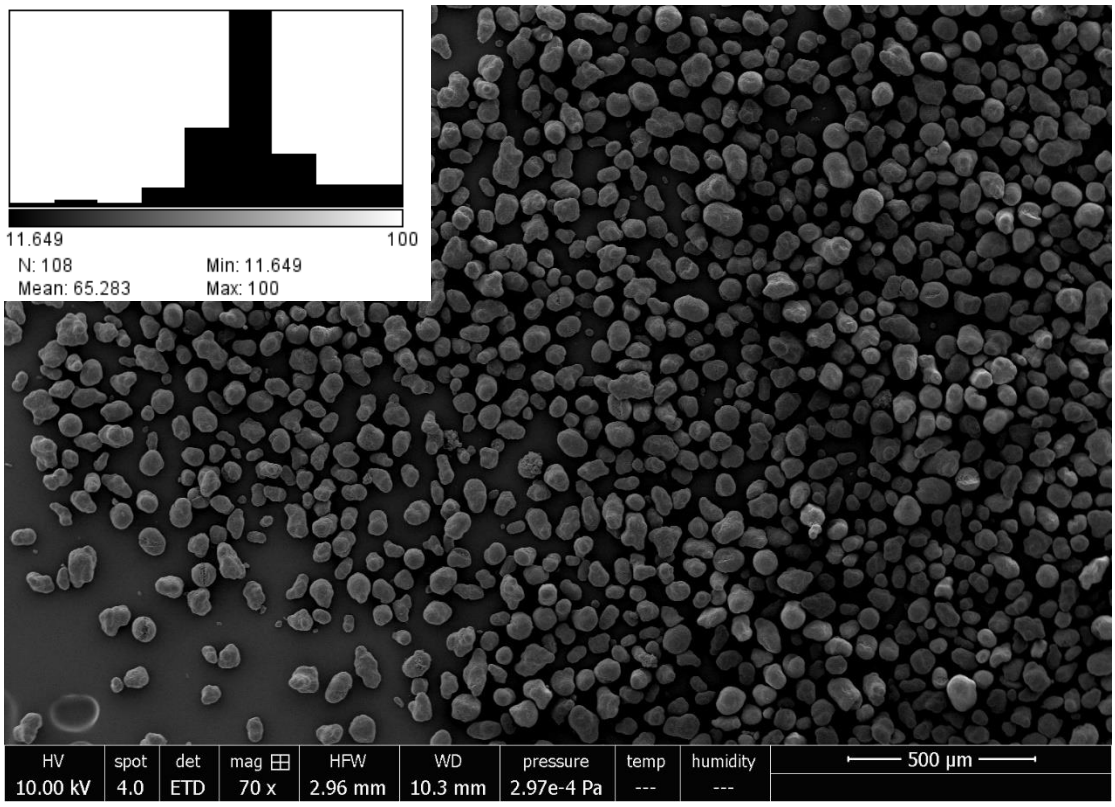
[a] Calculated from ^1H NMR spectra of the reaction mix. [b] Calculated from GPC in THF using a pMMA triple detection. [c] Calculated from the second run of DSC.

The polymers showed promising thermal properties with a T_g similar to the T_m of PA-12, ensuring a wide sintering window (≥10°C) (DSC spectra: Supporting Information Figures 1-3). The polymers had an intense bright blue colour (figure 21).



Figure 21 – Picture of PA-12 coated with P(IBMA-DB3MA)

The size and shape of the particles were analysed via SEM and LDS revealing that the particles were potato shaped and had a particle size of 60.1 µm (± 1.45%)(figure 22). Therefore, these particles should have the appropriate extrinsic and intrinsic properties needed for SLS.



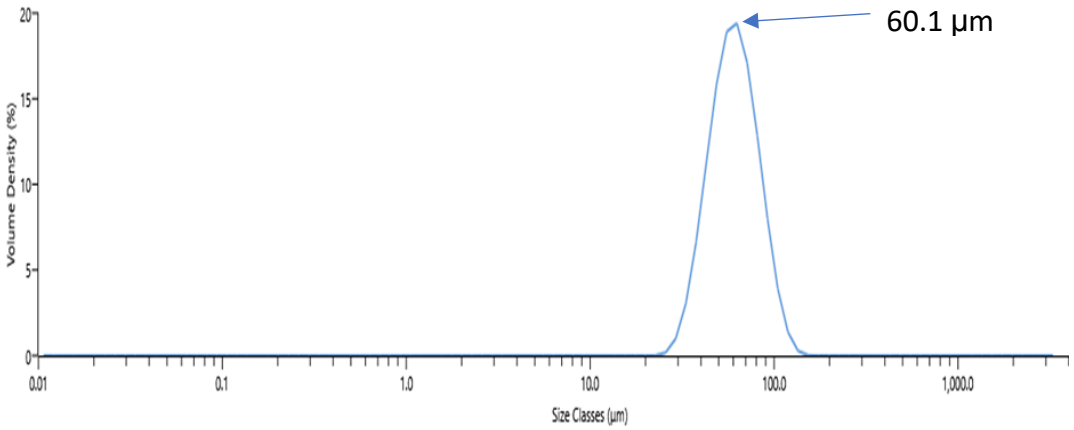


Figure 22 – Particle size and shape analysis of PA-12 particles coated with p(IBMA-DB3MA) A.) SEM image of PA-12 particles coated with P(IBMA-DB3MA) showing their

potato shape B.) LDS analysis of PA-12 particles coated with P(IBMA-DB3MA) revealed an average particle size of 60.1 μm (± 1.45%), with the uncoated PA-12 particles having an average size of ~58 μm (± 0.63%).

These results are very similar to that of the other coloured PA-12 particles that were synthesized. The analysis shows that these particles have the necessary intrinsic and extrinsic properties needed for SLS. The intrinsic properties are suitable as the thermal properties of the outer and core shells are similar ensuring adequate sintering. The copolymeric outer shell can absorb the radiation of a CO_2 laser, hence sintering should be possible. The extrinsic properties should be as desired as the particles retained their potato shape, although increased in size, hence they should flow and pack similarly to commercial PA-12. These factors indicate that the blue PA-12 material should be printable via SLS.

Scale up (1L) of coloured PA-12 particle synthesis:

At this point all the coloured core-shelled particles had been produced (blue, yellow, and red PA-12 based particles) using a 60 mL autoclave. The polymers all showed the appropriate extrinsic and intrinsic properties needed for SLS. Most of the commercial SLS printers need one to three kg of material per print run, using a 60 mL autoclave for such amounts would be impractical (~10g of product per reaction). For this reason, the polymerisations were scaled up to the 1L scale using a 1L autoclave (~150g of product per reaction) (figure 23), with no change to reaction conditions.

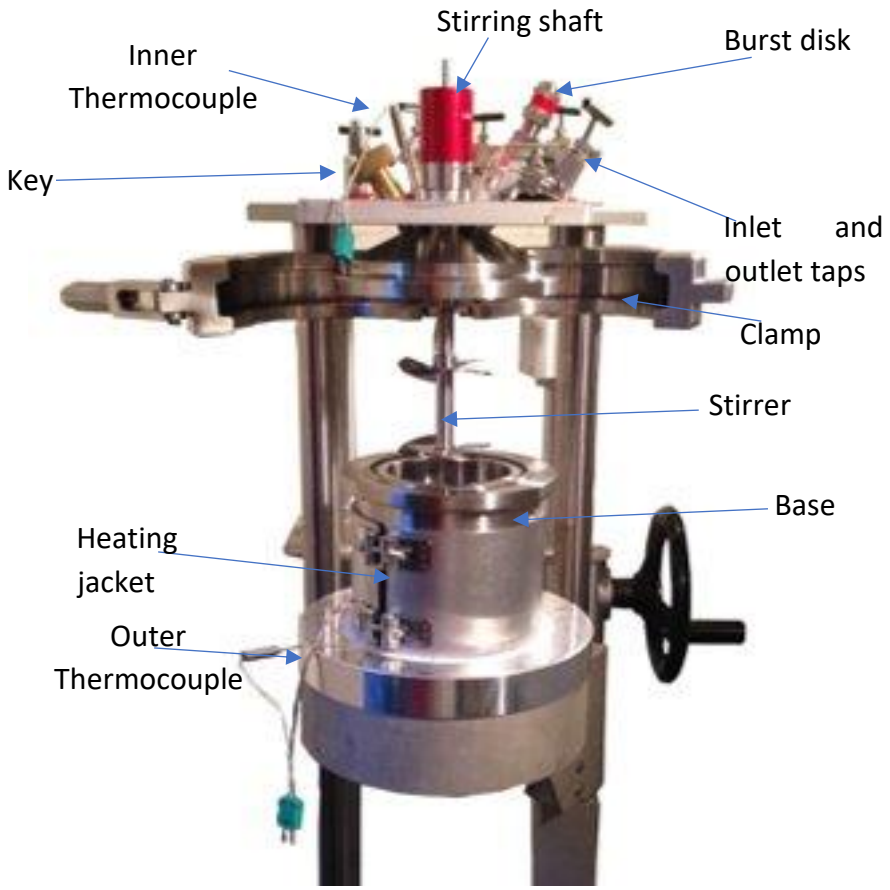


Figure 23 – Image of 1L autoclave, showcasing the integral elements of the setup.

The first reactions that were performed at the 1L scale were the coatings of PA-12 with P(IBMA-Y1MA). Identical stoichiometry was used on scale up. The reactions yielded free-flowing yellow powders comprised of PA-12 based particles coated with P(IBMA-Y1MA) (figure 24).

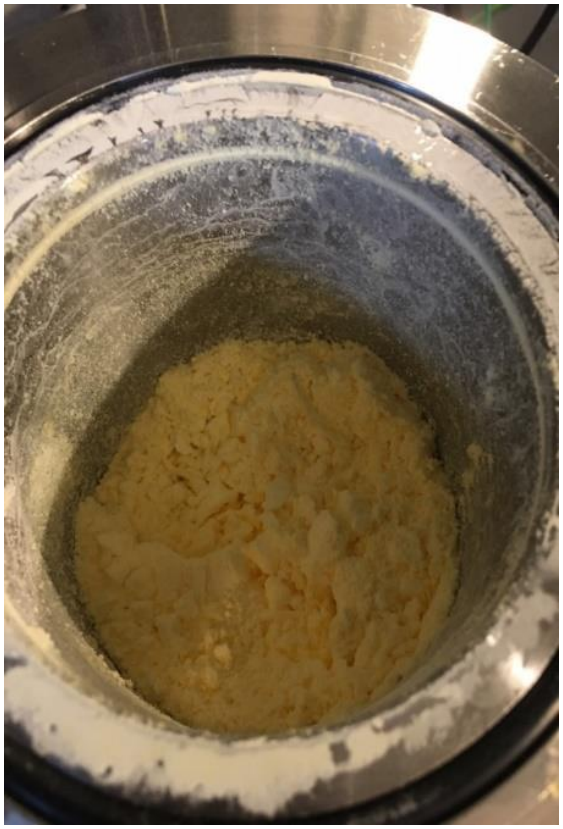


Figure 24 – Image of PA-12 coated with P(IBMA-Y1MA) at the 1L scale.

The conversion of IBMA was measured by ^{1}H NMR spectroscopy and was found to be similar to that of the 60 mL reactions, as were the molecular weights, dispersities, and thermal properties (Supporting Information figures 4-12). The conversion of IBMA was ~60% and the GPC chromatograms showed that the dye monomer had incorporated into the polymer chain as in the 60 mL autoclave, as the UV and dRI signals had peaks at the same time points (Supporting Information figures 4-12). The other extrinsic and intrinsic properties matched the results from the 60 mL autoclave, so the scale up was considered a success. As well as coating virgin PA-12, recycled PA-12 (unsintered PA-12 from SLS printing) was utilized for the polymerisation and coating reactions in the 1L scale, showing little to no difference between recycled and virgin materials. It is important to test with coated recycled PA-12 and coated virgin

PA-12 in order to know that the coating and polymerisation process is versatile and robust. It is also important from an environmental perspective as successful coating and subsequent printing of recycled PA-12 adds further uses to recycled polymeric materials for SLS and shows the extensive recyclability of the unsintered powder. The same was done for the reactions which coated PA-12 particles with either P(IBMA-DR1MA) or P(IBMA-DB3MA) yielding blue and red PA-12 particles at the 1L scale, and the results matched the ones observed at the 60 mL scale (Supporting Information figures 4-12).

The experiments performed at the 1L scale were crucial, as they showed that greater quantities of coloured PA-12 particles can be produced utilizing the same reaction conditions and stoichiometry as before. This scale enables us to produce enough coloured polymeric particles to test on commercial SLS printers. The facile scale-up process is indicative of a robust methodology suitable for potential further scale up to industrial quantities. The next step was to produce a sufficient quantity of material so that printing on an EOS Formiga P100 printer could be performed. In addition, other polymeric particles were created to expand the library of materials available for SLS and their potential applications (Chapter 6 and Appendix 1).

Conclusion:

Utilizing a novel coating process and innovative dye monomers, coloured core-shelled particles were synthesized. These red, blue, and yellow particles have the prerequisite extrinsic and intrinsic properties needed for SLS. The process was scaled up from the 60 mL to the 1L scale, showing the scalability of the process. It was shown

that the colour of the materials can be easily varied through altering the amount of dye monomer present during polymerisation. The resulting particles were used to print coloured polymers via SLS for the first time and develop the first colour mixing system for SLS (Chapters 4 and 5). The synthesis process of these particles is relatively cheap (Supporting information tables 1 and 2), which allows these materials to be industrially viable as the added cost is not much more than the cost of standard PA-12. This will address key issues facing the SLS technique, as currently the post sintering dyeing process is expensive, time consuming, can lessen the quality and performance of the part, and is environmentally consequential. It should be noted that through the use of FRP in $scCO_2$ a copolymer was successfully synthesized, in which one of the monomers has a quinone moiety. This is noteworthy, because with traditional methods and solvents this is hard to accomplish as the free radical scavenging properties of the quinone group impede the reaction.

Future Work:

In the future a wide variety of novel polymeric materials with active and functional surfaces could be produced utilizing the same process. This could be polymers with enhanced mechanical properties, anti-microbial properties, elevated thermal properties, different physical properties such as elasticity, etc. This would greatly expand the scope of SLS technology. Lastly the process of the polymer synthesis could be improved by implementing a flow $scCO_2$ system instead of a one-pot batch process, however this would require the design and manufacture of a new $scCO_2$ rig. The maximum loadings of the autoclave should also be investigated, this would make

the process more efficient as more coloured polymeric particles could be made with every reaction.

Materials and Methods:

Materials:

Methyl methacrylate (MMA) (99 %) was obtained from Kaneka Belgium N.V. Isobornyl methacrylate (IBMA) (> 80 %), 2,2'-Azobis(2-methylpropionnitrile) (AIBN) and PDMS-MA (10 kDa) were purchased from Fluorochem. CO_2 was purchased from Air Products. Disperse Red 1 methacrylate, Yellow 1 methacrylate, Disperse Blue 3 methacrylate were used as synthesised. PA-12 was purchased from EOS.

Methods:

Synthesis of PA-12 coated with P(IBMA-dye monomer) (60 mL autoclave):

PA-12 (10 g), IBMA (0.5 g, 0.0022 mol), Dye monomer (0.05 g), and AIBN (0.025 g, 0.1522 mmol) were degassed in the autoclave for 15 min, by flushing it with CO_2 at a constant pressure between 0.27 – 0.41 MPa. The key was then shut rapidly, and the pressure was slowly increased to 5.51 MPa, subsequently the temperature was increased to 50°C, and after stabilising the autoclave was pressurized to 13.79 MPa, with subsequent heating to 65°C. Once stable at 65°C the reaction is pressurized to 20.7 MPa and left stirring at 450 rpm for 24 hours. The autoclave is allowed to cool <30°C and the CO_2 is vented slowly, and the autoclave is opened to reveal the product. A variety of reaction conditions were used for these reactions.

Synthesis of PA-12 coated with P(IBMA-dye monomer) (1L autoclave):

PA-12 (120 g), IBMA (19.5 g, 0.0022 mol), Dye monomer (0.5 g), and AIBN (0.2 g, 0.00122 mol) were degassed in the autoclave for 15 min, by flushing it with N_2 at a constant pressure between 0.27 – 0.41 MPa. The key was then shut rapidly, and the pressure was slowly increased to 5.51 MPa, subsequently the temperature was increased to 50°C, and after stabilising the autoclave was pressurized to 13.79 MPa, with subsequent heating to 65°C. Once stable at 65°C the reaction is pressurized to 20.7 MPa and left stirring at 450 rpm for 24 hours. The autoclave is allowed to cool <30°C and the CO_2 is vented slowly, and the autoclave is opened to reveal the product. A variety of reaction conditions were used for these reactions.

Synthesis of P(MMA-DB3MA) in solution:
MMA (5 g, 0.05 mol), DB3MA (0.25 g), and AIBN (0.315 g, 0.194 mol) were dissolved in 10 mL of THF. The mixture was degassed with argon for 15 min, and subsequently heated to 65 ^{o}C and stirred at 450 rpm for 24 hrs. The mixture was then cooled and precipitated into ice cold methanol, and vacuum filtered. The product was subsequently dried and collected.

Synthesis of P(MMA-DB3MA) in scCO_2:

MMA (10 g, 0.1 mol), IBMA (0.5 g, 0.0022 mol), DB3MA (0.05 g), AIBN (0.025 g, 0.1522 mmol), and PDMS-MA (10 kDa) (1.05 g) were degassed in the autoclave for 15 min, by flushing it with CO_2 at a constant pressure between 0.27 – 0.41 MPa. The key was then shut rapidly, and the pressure was slowly increased to 5.51 MPa, subsequently the temperature was increased to 50°C, and after stabilising the autoclave was

pressurized to 13.79 MPa, with subsequent heating to 65°C. Once stable at 65°C the reaction is pressurized to 20.7 MPa and left stirring at 450 rpm for 24 hours. The autoclave is allowed to cool <30°C and the CO_2 is vented slowly, and the autoclave is opened to reveal the product. A variety of reaction conditions were used for these reactions.

Analysis:

^{1}H NMR analysis (NMR):

The samples were analysed by ^{1}H NMR spectroscopy, using a Bruker 400 Ultrashield (400 MHz NMR), and all the samples were dissolved in deuterated chloroform. The ^{1}H NMR spectra were used to identify the polymers formation and to calculate the monomers conversion. The conversions were obtained with equation 1.

$$Conversion = \frac{AUCP}{AUCP + 1}$$

Equation 1

In this equation AUCP is the area under the curve of the polymer peak when compared to the area under the curve of the monomer peak.

Gel Permeation Chromatography (GPC):

GPC was performed in order to obtain the M_n, M_w, and dispersity (Đ) values for all the synthesised polymers. These values were produced using pMMA standards. All the measurements were performed on an Agilent 1260 Infinity HPLC using HPLC grade

THF as eluent at 40°C with 2 x Agilent PL-gel mixed-D column at 1 mL min^{-1} flow rate, connected to a differential refractive index (dRI) detector and MALLS detector.

Scanning Electron Microscopy (SEM) and particle size analysis:

SEM was used to see if the polymer materials were composed of discrete monodisperse particles, and it was performed using a Philips XL30 electron microscope. The samples were prepared by putting the polymer powder on a carbon tab mounted onto an SEM stub, which were then coated with Platinum for 180 seconds at 12 mA and 2.2 kV using an Emitech SC7640 sputter coater. The average size of the polymer particles was calculated by taking the area of 100 particles from a SEM image and then taking the average area of the particles exploiting ImageJ software.

Laser Diffraction Spectrometry (LDS):

LDS was used to analyse the particle size of a large segment of the samples. This was done by using a Malvern Mastersizer 3000. Initially, the samples (1 g) were loaded onto a dispenser. Dispenser vibration moved the polymeric powder evenly into an air jet, which inserted the sample into the detector. Mastersizer 3000 software was then used to obtain the average particle size.

Differential Scanning Calorimetry (DSC):

DSC was used to detect polymers thermal transitions such glass temperature transition (Tg), temperature of crystallisation (Tc), and temperature of melting (Tm). The samples were prepared by weighing out circa 5 mg of sample into a DSC pan,

which was then closed with a lid and tested from 0°C to 250°C. The Tc was determined by finding the maximum point of the curve if any was present, the Tm by finding the minimum point if any was present, and the Tg by finding a change in the slope of the line if any was present.

Chapter 3: Coloured PBF Printing

Introduction:

One of the largest issues with SLS printing, until this moment, is that the technique does not allow for printing in colour.[61] The parts built via SLS are mostly white as that is the colour of PA-12 and other SLS materials.[61] It is possible to print in grey to black, through the addition of carbon black to the PA-12 particulate powder.[8,9] Currently as has been mentioned previously, colour is added post-printing to parts via a series of dyeing steps.[10,94–96] These include the application of several coats of paint and drying steps to achieve the wanted colours.[10,94–96] These colouring processes are detrimental to the printing process for a variety of reasons:

1.) It adds cost

2.) Addition of time to the overall manufacturing process.

3.) The paint can affect the dimensions of the part.

4.) The paint can be scratched off the part.

5.) The painting process has negative environmental consequences.[10,94–96]

The process adds cost to the overall build as in most cases the part needs to be sent to a company, which does the painting, so that the part has the desired aesthetic appeal.[10,95,96] The cost of the process depends on the level of the finish, the type of paint, and the size of the part. Otherwise larger entities such as EOS and Stratasys have partnered with dyeing companies such as Dye Mansion, to purchase machines

so that dyeing can be performed in house. This adds a large initial cost (75,000 £) and necessitates dedicated professionals to tend to the dyeing process. This adds significant equipment and personnel costs on top of the cost of the dyes used. Our strategy provides already coloured materials which would allow users to reduce costs, as it is estimated that our coloured materials will cost ~125£ per Kg (taking into account economies of scale) compared to the 70-80£ per Kg of commercial PA-12 along with the high added costs of dyeing services.

The dyeing process add significant post-processing time (days) defeating one of the key benefits of SLS, which is rapid prototyping, as the process could take several days if not more. This is because if you have the facilities to accommodate in house dyeing the dyeing process takes at least 2 hrs on top of which there is a 24 hr drying period. When parts are sent to be dyed by specialist companies the shipping time must also be taken into account, which will at least be 2 days as the part needs to be sent there and back. Either of the current solutions adds a large period of time to the production process, and our method can eliminate the need for such post-processing steps.

The dimensions of the part are affected by the process as the layers of paint can make the part marginally thicker.[10,94–96] For most applications this will not matter, but if the dimensions of the part need to be very precise, the paint could worsen the performance of said part. This can be accounted for in the design of the part if the manufacturer knows the exact thickness of the painted coating. The paint can be scratched off the part, revealing the white PA-12 underneath the surface. The maximum depth that the paint can get to in a part is about 4 mm.[10,94–96] For parts dyed with such intensity it would be difficult to get to the white interior. However,

most paint finishes are not that deep and a slight scratch could remove the outer covering. The last disadvantage of the dyeing process is that it has negative environmental consequences. The process involves soaking the parts at elevated temperatures (≥ 80 ^{o}C) in a vat of paint for hours and/or spray painting the parts.[10,94–96] After each coat the part is left to dry in an oven and the process is repeated several times.[10,94–96] This is a very energy intensive process, and the shipping of the part also imparts significant environmental costs. The answer to solve all of these problems is to print already coloured polymeric particles via SLS, hence there would be no need for the aforementioned painting process.

In the previous chapter, the synthesis of coloured coated PA-12 particles was explained. It was shown that one could synthesize red, yellow, and blue PA-12 based particles by coating PA-12 particles with P(IBMA-Disperse Red 1 Methacrylate), P(IBMA-Yellow 1 Methacrylate), and P(IBMA-Disperse Blue 3 Methacrylate) respectively. These three materials were shown to have the necessary extrinsic and intrinsic properties needed for SLS. The extrinsic properties are appropriate, as the powder flows and packs well due to the size and shape of the particles (~60 μm and potato shaped).[14,61,97–99] The intrinsic properties are suitable as the polymeric coating can absorb the radiation of a CO_2 laser, ensuring that sintering is possible.[17,18] The thermal properties are suitable as the T_g of the coating is similar to the T_m of PA-12, so the materials still have a large sintering window.[12,14,16,61,62,97,99] This should allow the coloured materials to be printed with the same conditions as PA-12, which are: powder bed temperature of 172 ^{o}C, a chamber temperature of 150 ^{o}C, a hatching laser power of 21 W, a contour laser power of 16 W, and a hatching speed of 2500

mm/s. These conditions have been used to print PA-12 parts for a variety of application in varying fields.

The three colours (red, yellow, blue) were chosen because of their potential to be used in a CMYK colour mixing system. CMYK colour mixing uses Cyan, Magenta, Yellow, and Black to produce any other colour when the 4 'inks' are mixed in the correct ratios.[23,25,100–102] This is the main colour mixing system used in modern paper inkjet printers.[103] Most paper printers use a black ink, but the black colour can be made by mixing the other three colours together. For this reason, it was decided that it was appropriate to use red, blue, and yellow PA-12 based powders, as red can be viewed to be magenta, and cyan is a type of blue.[26] To begin the three powders must be printed separately to show that printing in colour with these powders is in fact possible (figure 1).

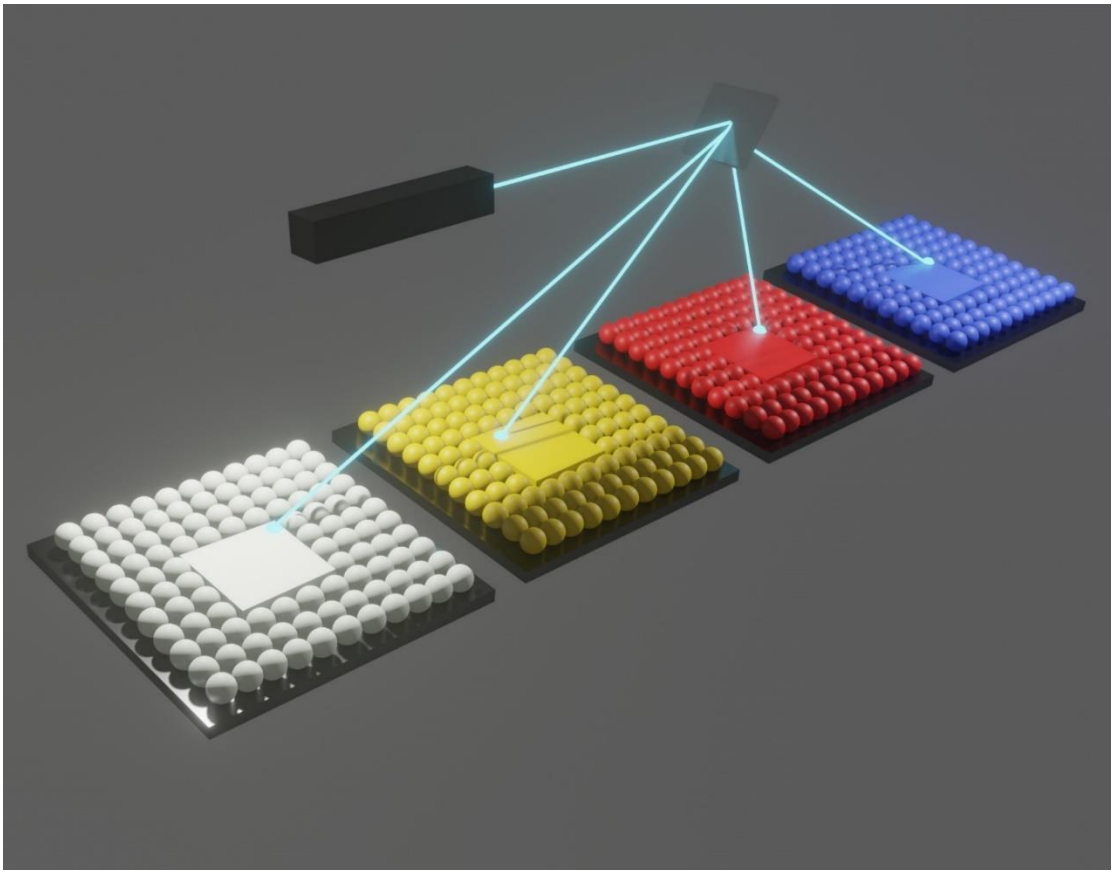


Figure 1 – SLS printing in colour

This would be the first time that coloured polymeric particles are used to print wholly coloured parts via SLS. Once it is shown that these three colours can be printed, these 'inks' could be used to create the first colour mixing system for SLS. This would be simple as one could physically premix the 'inks' before printing to achieve the desired colour, and then print with the mixed powder.

Results and Discussion:

Printing with virgin PA-12:

The first material that was printed was pure virgin PA-12. This material was chosen, as it is the most frequently used material and the gold standard for SLS

printing.[14,16,61,97,99] The parts made from this material have desirable properties, such as relatively good thermal and chemical resistance and good mechanical properties.[104,105] The conditions used to print PA-12 have been optimized in previous research, and have been found to be a: powder bed temperature of 172 ^{o}C, a chamber temperature of 150 ^{o}C, a hatching laser power of 21 W, a contour laser power of 16 W, and a hatching speed of 2500 mm/s. These conditions have been used to print PA-12 parts for a variety of application in varying fields.[106–108] These conditions were used to print a 5x20x20 mm square out of virgin PA-12, and several dog bones. The square was built in order to compare to the squares built out of the other coloured polymeric materials, and a square is an excellent shape to test the curling properties of the material, as the edges tend to curl easily, thereby allowing for printing optimisation. Dog bones were built in order to test the mechanical strength and compare to the novel synthesized materials (figure 2).

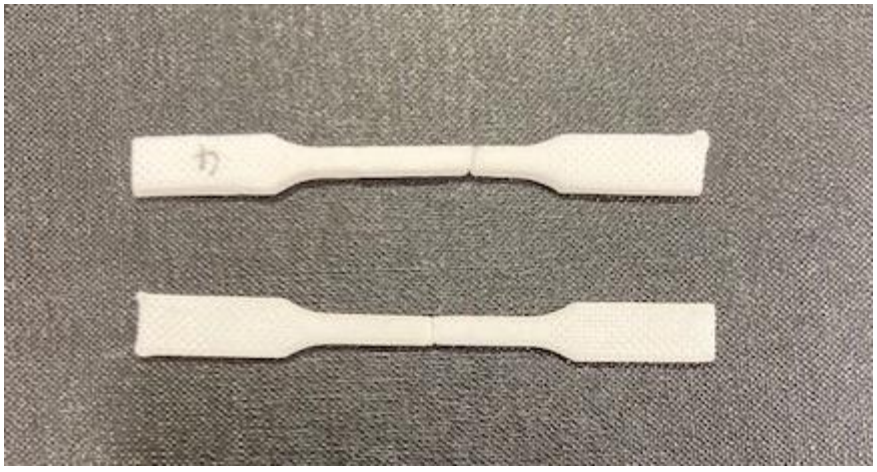


Figure 2 – Images of SLS printed parts composed of virgin PA-12: Dog bones

From the images it can be seen that there is a minimal warp factor in the built parts as the square is 5x20x20 mm or exactly the desired dimensions. The dog bones exhibit

slightly more warpage but it is minimal, hence the parts have desirable dimensions. The parts have a noticeable white colour which is characteristic of virgin PA-12 parts (figure 3).

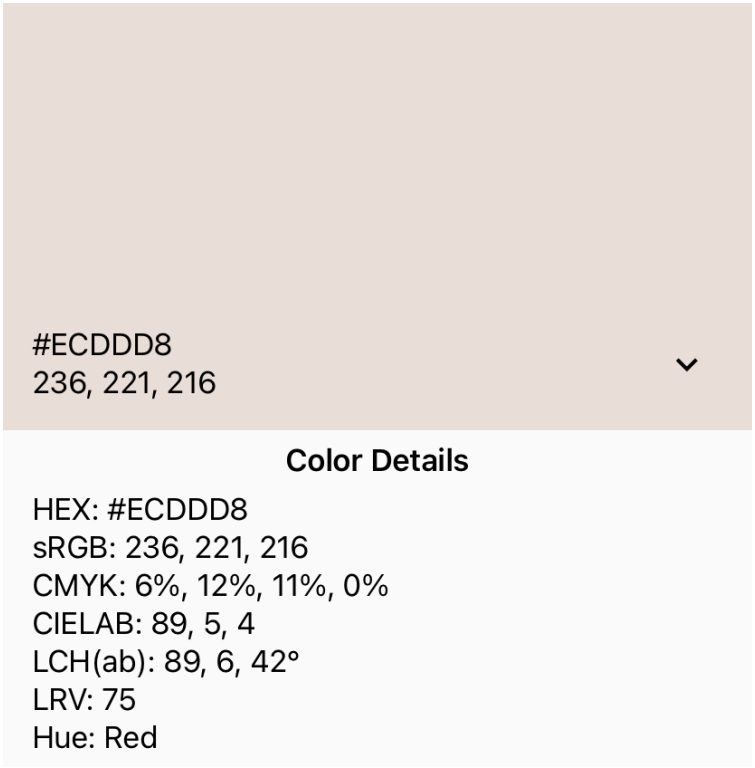


Figure 3 – NIX colour analysis of SLS printed parts composed of virgin PA-12. On the top of the figure there is square which is a photo representation of the colour of the part that was analysed via NIX colour analysis. On the bottom of the figure there is a variety of values which are numerical representations of the colour of the part. HEX, sRGB, CMYK, CIELAB, LCH (ab), and LRV are different units used for the valuation of colours with CMYK and CIELAB being key values for the targeted colour mixing and colour valuation. At the bottom the Hue of the part is stated. HEX is a six-digit order of numbers and letters used to define colour in values of red, green, and blue. sRGB refers to the colour coordinates defined by standard red, green, and blue space, with each value representing red, green, or blue. It is commonly used for additive colour

mixing and colours in visual displays such as computer monitors. LCH refers to lightness, chroma, and hue using cylindrical colour models which are designed to represent human perception. LRV is the light reflectance value of a colour. It refers to the amount of visible and usable light reflecting from a painted surface. CMYK refers to the colour coordinates defined by a colour space of cyan, magenta, yellow, and black. Each value represents on of these four colours, and it is commonly used for subtractive colour mixing, such as in colour mixing in paper printers. CIELAB refers to a colour expressed as L, A, B values if a colour space defined by the International Commission on Illumination (CIE), therefore CIELAB. L represents perpetual lightness, whilst A and B represent red, green, yellow, and blue which are deemed to be the four unique colours of human vision. It is frequently used in industry for identifying minute differences in colour.

The colour analysis shows that the resulting parts are white, however slightly off-white, with a tinge of red. This is simply because it is rare for an object to be perfectly white, and while appears white to the human eye, it can have slight tinges of different colours.[109] These imperfections could be the result of impurities in the powder mix such as dust or other contaminants.

SEM analysis was undertaken to show proper sintering of PA-12. The particles are sintered so that the surface is a homogenous layer with no particles left, this ensures that there has been good fusion across the part and prevents the formation of weak spots across the part (figure 4).

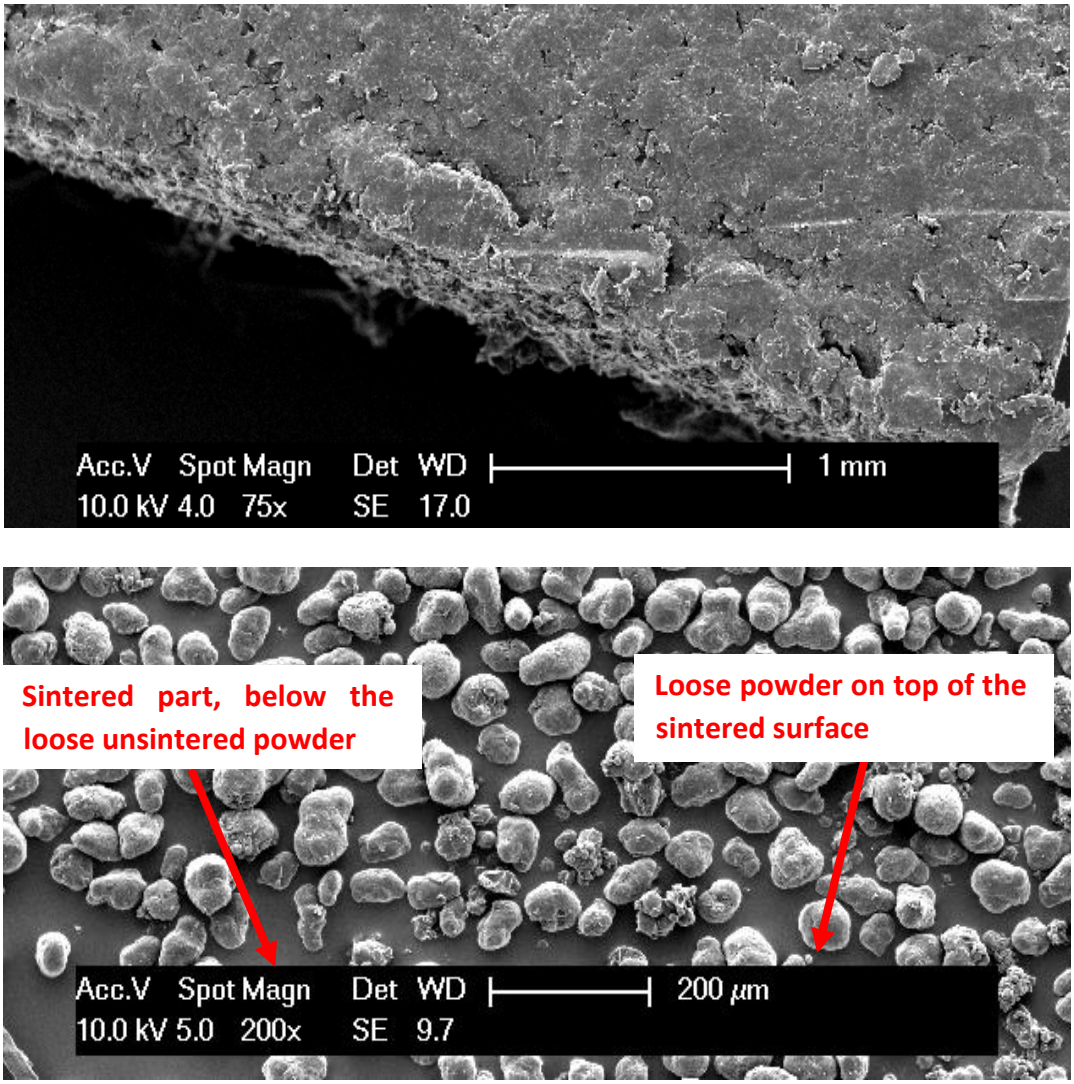


Figure 4 – SEM image of part (pure virgin PA-12) printed via SLS A.) SEM image at a magnification of 75x of a part printed via SLS composed of pure virgin PA-12, showing sintering of the particles to form a structure. B.) SEM image at magnification of 200x of a part printed via SLS composed of pure virgin PA-12, showing the loose powder (polymeric particles) remaining on top of the sintered surface after SLS.

The coloured PA-12 materials were printed and compared to the aforementioned PA-12 parts. The aim is that we should be able to print parts out of the coloured materials that have similar properties to those built from virgin PA-12.

Printing with Yellow PA-12 (PA-12 coated with P(IBMA-Y1MA):

The first coloured polymeric particles that were printed via SLS, were PA-12 coated with P(IBMA-Y1MA) or yellow PA-12 for short. The first variety that was tested was recycled PA-12 coated in the yellow random co-polymer. It is important to test printing and coating of recycled and virgin PA-12 for various reasons including: proving recyclability of unsintered material and testing the synthetic process and printing for versatility and robustness. From the DSC it was seen that the recycled PA-12 has slightly different thermal properties as the T_m has an initial large dip at around 162-166 ^oC. This means that the powder bed temperature (PBT) must be lower than for virgin PA-12, as a PBT of 172 ^oC would partially melt a significant percentage of the polymer (~ 20 %).

To begin the first conditions that were used to test the printability of yellow PA-12 were a PBT of 158 ^oC, a chamber temperature (CT) of 150 ^oC, a hatching laser power (HLP) of 21 W, a contour laser power (CLP of 16 W), and a hatching speed (HS) of 2500 mm/s. These conditions were chosen because only the PBT has been changed (lowered) from the conditions used for PA-12. However, the use of these conditions caused the part to sinter well, but the part curled massively. This likely occurred, because the yellow coating can absorb the radiation from the CO_2 laser more effectively than the virgin PA-12, causing more energy to be absorbed into the part thereby causing curling or possibly due to the core-shelled particles having altered crystallisation kinetics compared to PA-12.[97,110] An alternative or synergistic reason could be that the recycled PA-12 has different thermal properties to the virgin PA-12 causing it to curl at different conditions.[111–113] The different thermal process could be

due to the heating and cooling cycles that the recycled PA-12 has been exposed to. Another reason for curling is that the heat caused due to the laser contact and the PBT is very different, which caused the hotter sintered surface to contract when exposed to the colder PBT.[114] They could all be acting synergistically to cause the observed lack of control during sintering, so the conditions were changed accordingly (table 1).

Structure	Powder Bed Temperature (°C)	Chamber Temperature (°C)	Laser Power (W)	Hatching speed (mm/s)	Hatching Distance (mm)	Energy density (ψ) (W/mm^3s^1)	Scan Type
Square	158	150	21.5	2500	0.25	0.344	Single
Square	160	150	21	2500	0.25	0.336	Single
Square	158	150	19	2500	0.25	0.304	Single
Square	158	150	17.5	2500	0.25	0.280	Single
Square	158	150	16.5	2500	0.25	0.264	Single
Square	158	150	15.5	2500	0.25	0.248	Single
Square	158	150	14.5	2500	0.25	0.232	Single
Square	158	150	13.5	2500	0.25	0.216	Single
Square	158	150	12.5	2500	0.25	0.200	Single

Table 1 – Printing conditions for recycled PA-12 coated with P(IBMA-Y1MA). Energy density (ψ) obtained from equation 1 : $\psi = \frac{P}{V \times H \times D}$, where P is laser power, V is hatching speed, H is hatching distance, and D is depth of powder layer (100 μm).

To begin the PBT was raised by 2 °C to 160 °C, to see if the curling was due to the temperature difference between the sintered powder and the chamber. This did not alleviate any of the curling so more conditions were tested. The PBT was lowered to 158 °C and the HLP to 19 W (from 21 W), but curling was still significant. Hence the HLP was lowered to 17.5 W, whilst the other conditions were kept the same. This lowered the amount of curling in the part. From this it was seen that the decrease in laser power, helps lower the curling seen in the part. The laser power was lowered by 1 W with each test, until satisfactory part building was observed. With each watt that was lowered the amount of warping decreased until a laser power of 14.5 W was

used. This gave no curling and allowed for a 50 layered square (5x20x20 mm) to be built (figure 5).

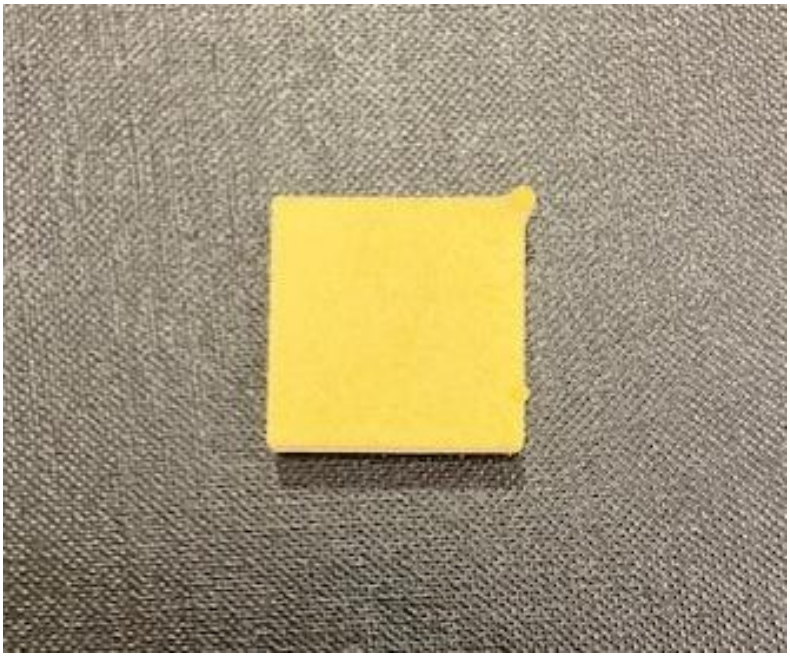


Figure 5 – Image of square (5x20x20 mm) composed of recycled PA-12 coated with P(IBMA-Y1MA).

The successful building of a part composed of Yellow PA-12, was the first step in optimizing the printing of yellow PA-12. The recycled PA-12 coated in yellow PA-12 was not compared with the virgin PA-12, as it was seen that the thermal properties of recycled PA-12 were different from virgin PA-12, hence so should the mechanical properties. Because of this virgin PA-12 was coated with P(IBMA-Y1MA), so that the yellow PA-12 could be compared to the virgin PA-12 material (Appendix 2). The printing of this material was optimised through the testing of many sets of conditions (table 2). Many tests were conducted in an effort to find printing conditions which lead to the least amount of warpage with the best mechanical properties. The issue is it often in order to increase the mechanical properties of a part the part needs to

be exposed to higher laser powers or more energy, however, this can lead to warping.[115,116]

Structure	Powder bed temperature (°C)	Chamber temperature (°C)	Laser Power (W)	Hatching speed (mm/s)	Hatching distance (mm)	Energy density (ψ) (W/mm^3s^1)	Scan type
dog bone	159	164	14.5	2500	0.25	0.232	single
dog bone	164.5	145	21	2500	0.25	0.336	single
dog bone	164.5	145	21	2500	0.25	0.336	double
square box	167	150	21	2500	0.25	0.336	single
square box	170	150	21	2500	0.25	0.336	single
square box	172	150	21	2500	0.25	0.336	single
square box	173	150	21	2500	0.25	0.336	single
square box	172.5	150	21	2500	0.25	0.336	double
square box	173	150	20	1500	0.25	0.533	double
square box	173	150	20	2000	0.25	0.400	double
square box	173	150	20	2250	0.2	0.444	double
square box	173	150	20	2250	0.22	0.404	double
square box	174	150	20	2250	0.22	0.404	double
square box	174	150	19	2250	0.22	0.384	double
square box	174.5	150	19	2250	0.22	0.384	double
square box	175	150	19	2250	0.22	0.384	double
square box	175	150	18	2250	0.22	0.364	double
square box	175	150	18	2250	0.25	0.320	double
square box	175	150	18	2500	0.22	0.327	double
square box	175	150	18	2500	0.25	0.288	double
square box	175.5	150	18	2500	0.22	0.327	double
square box	176	150	18	2500	0.22	0.327	double
square box	176	150	18	2250	0.25	0.320	double
square box	176	150	20	2500	0.25	0.320	double
square box	176.5	150	20	2500	0.25	0.320	double
square box	177	150	20	2500	0.25	0.320	double
square box	177	150	20	2500	0.25	0.320	double

Table 2 – Printing conditions used to print a 5x20x20 mm square composed of virgin PA-12 coated in P(IBMA-Y1MA). Energy density (ψ) obtained from equation 1 : $\psi = \frac{P}{V \times H \times D}$, where P is laser power, V is hatching speed, H is hatching distance, and D is depth of powder layer (100 μm).

The first printing conditions used were the optimal conditions used for the recycled PA-12 coated in yellow copolymer. This attempt did not curl, but it was remarkably weak, in fact it turned to dust when it was handled. This is most likely due to the difference in thermal properties between recycled and virgin PA-12. The virgin PA-12 has a higher T_m with a much sharper onset, so at the current conditions the sintering of the PA-12 core would be minimal causing the observed weakness. Because of this

the PBT and the laser power were increased. The PBT was raised to 167 ^{o}C and the laser power to 21 W, this resulted in a part that could be retrieved, but was still very weak. From this it was seen that increased PBT and LP bettered the mechanical properties of the part, so the PBT was increased to 173 ^{o}C, which resulted in slightly improved part strength. Another way of increasing sintering in a part is to scan each layer twice instead of once. This increases the total time that each layer is exposed to the laser, so sintering should be improved, and so should the mechanical properties. This resulted in a part that was stronger, but still weaker than the one printed with recycled yellow PA-12. The next condition utilized a PBT of 173 ^{o}C, a LP of 20 W, a HS of 1500 mm/s, and a double scan, resulting in significant curling. This would normally be a negative, but it showed us the upper boundary for the conditions used for this material.

The curling most likely occurred due to the large decrease in HS from 2500 mm/s to 1500 mm/s, this greatly increased laser exposure time. When the HS was raised to 2000 mm/s the part curled less, so it was decided that the effect of hatching distance (HD) should also be tested. The HD was decreased from 0.25 mm to 0.2 mm and the HS raised to 2250 mm/s, which cause significant curling. The decrease in HD led to curling as there are more hatching lines as the gap between each hatching line in the grid is smaller, thereby leading to greater laser exposure. The HD was increased to 0.22 mm, which led to less curling as 20 layers were printed before the part curled and was taken by the recoater arm. The PBT was increased to 174 ^{o}C, with the same result. Then the laser power was lowered to 19 W and the build finished, however even though it was mechanically stronger than the previous attempts, it was

noticeably weaker than the parts built from the other two materials (Appendix 2). The PBT was increased gradually until 175 ^{o}C, which led to warping, but subsequent lowering of the laser power to 18 W allowed for the build to be finished. When the HD was raised to 0.25 mm the strength of the part decreased, indicating that a smaller HD is crucial to improving the mechanical properties of the part. The HD was lowered again to 0.22mm and the PBT raised to 176 ^{o}C and the HS raised to 2500 mm/s, which resulted in a slightly stronger part, then lowering the HS to 2250 mm/s and raising the HD to 0.25 mm led to warping after 18 layers. The laser power was then raised to 20 W with the HS and HD at 2500 mm/s and 0.25 mm respectively, which led to a stronger part. After subsequent testing the optimum conditions to build a 5x20x20 mm square with pure virgin PA-12 coated in P(IBMA-Y1MA) were found to be 177 ^{o}C PBT, a CT of 150 ^{o}C, a LP of 20 W, HS of 2500 mm/s, and a HD of 0.25 mm, with a double scan. Afterward dog bones were built with these materials. The dog bones were built with a variety of conditions based on the optimum conditions found for the building of the aforementioned squares.

The dog bones were built with the intention of testing them through mechanical testing to reveal their tensile strength, and other mechanical properties, however due to COVID-19 restrictions these could not be tested. The conditions used to build these dog bones are seen in table 3.

Structure	Powder bed temperature (°C)	Lower chamber temperature (°C)	Laser Power (W)	Hatching speed (mm/s)	Hatching distance (mm)	Energy density (ψ) (W/mm^{3}s^1)	Scan type
dog bone	177	150	18	2500	0.25	0.288	double
dog bone	177	150	19	2500	0.25	0.304	double
dog bone	177	150	20	2500	0.25	0.320	double
dog bone	177	150	21	2500	0.25	0.336	double
dog bone	177	150	21.5	2500	0.25	0.344	double
dog bone	177	150	22	2500	0.25	0.352	double
dog bone	177	150	22.5	2500	0.25	0.360	double
dog bone	177	150	23	2500	0.25	0.368	double
dog bone	177	150	22	2500	0.23	0.383	double
dog bone	177	150	22.5	2500	0.23	0.391	double
dog bone	177	150	22	2300	0.23	0.416	double
dog bone 4x	177	150	22	2300	0.23	0.416	double
dog bone	177	150	22	2400	0.23	0.399	double
dog bone	177	150	22	2500	0.23	0.383	double
dog bone 4x	177	150	22	2500	0.23	0.383	double

Table 3 – Printing conditions used to print dog bones composed of pure virgin PA-12 coated with P(IBMA-Y1MA) Energy density (ψ) obtained from equation 1: $\psi = \frac{P}{V \times H \times D}$, where P is laser power, V is hatching speed, H is hatching distance, and D is depth of powder layer (100 µm).

As can be seen in table 3 different PBTs, HSs, HDs, and LSs were used. From touch the strength of the dog bones varied with differing conditions, but they were all weak, with the seemingly strongest resulting from the following conditions: PBT of 177 °C, CT of 150 °C, LP of 22 W, HS of 2300 mm/s, and a HD of 0.23 mm. These conditions did not cause the dog bone to warp and led to stronger parts. These were supposed to be tested but due to Covid-19 related issues sample delivery resulted in loss of said samples before testing was possible. SEM images show that the surfaces of the printed parts are sintered (figure 6). The particles are successfully fused together, showing that the part was built well through SLS, and that the mechanical issues are caused by coating the materials, and not by faulty printing.

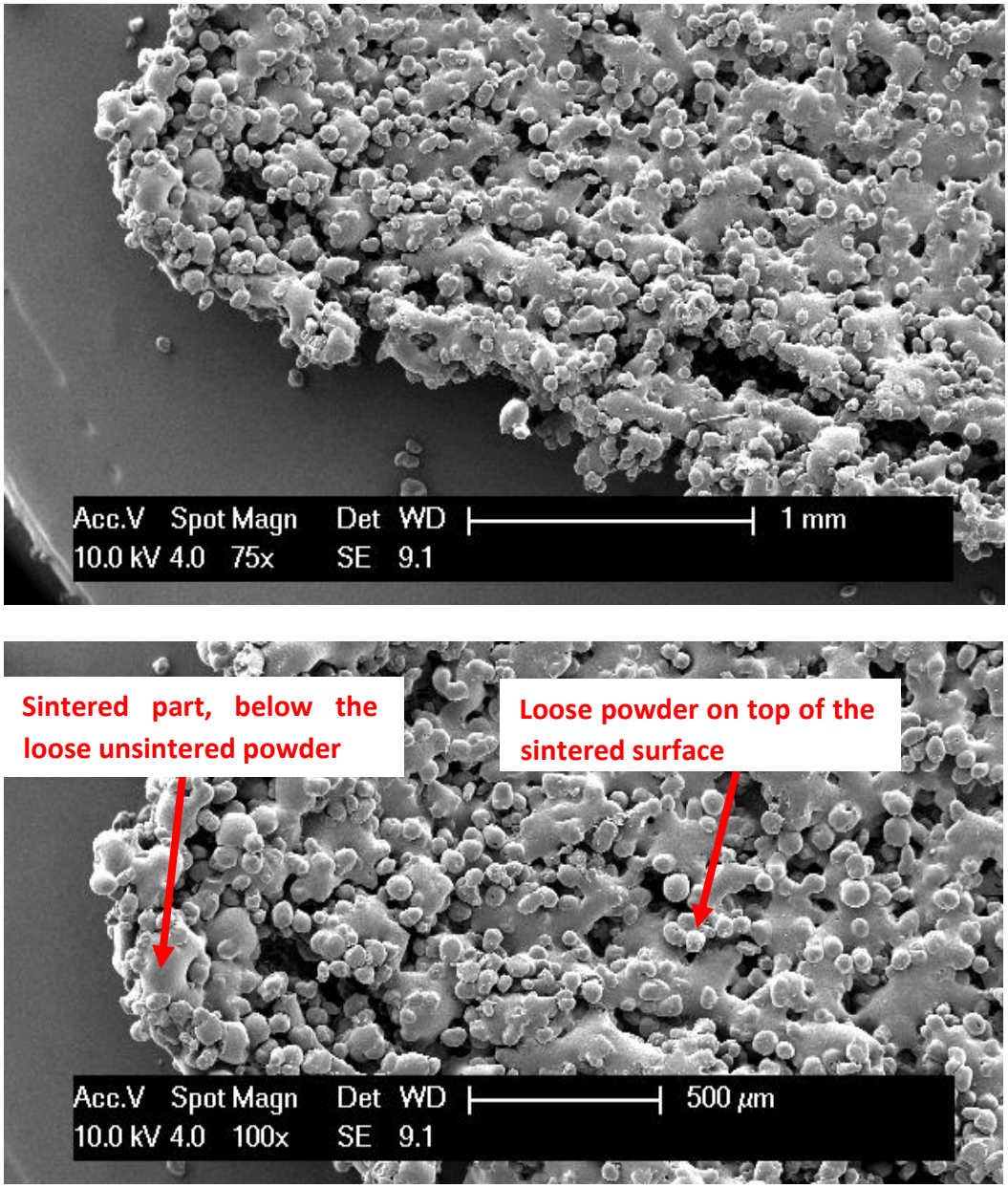


Figure 6 – SEM images of parts built via SLS, which are composed of virgin PA-12 coated in P(IBMA-Y1MA).

The parts were also analysed via NIX colour sensor analysis, confirming that the parts built with this material are yellow (figure 7). The powders were mixed in different ratios of commercial PA-12 to yellow PA-12 to test if the yellow colour could be maintained, this resulted in coloured parts which have similar mechanical properties as commercial PA-12 (Appendix 2).

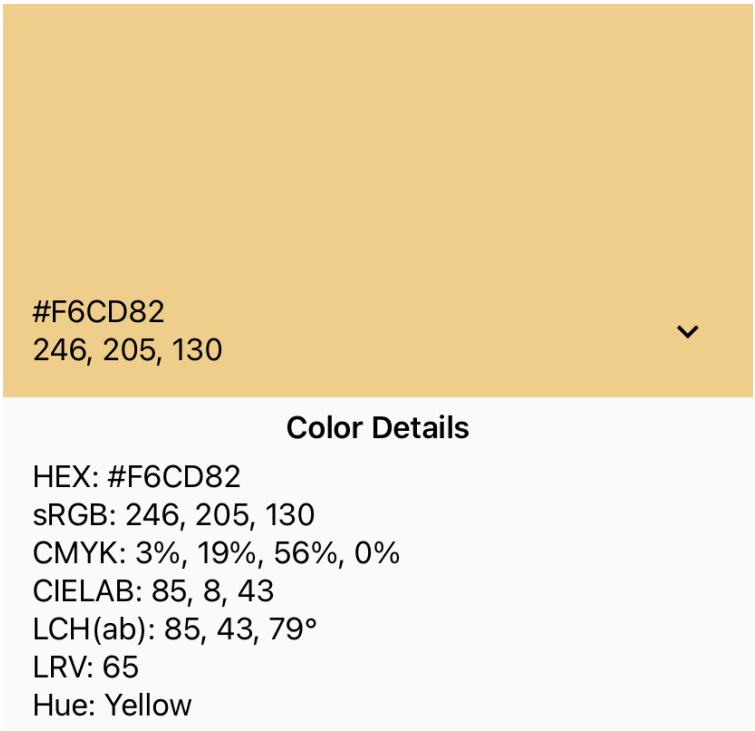


Figure 7 – NIX colour sensor analysis of SLS built parts composed of virgin PA-12 coated in P(IBMA-Y1MA). On the top of the figure there is square which is a photo representation of the colour of the part that was analysed via NIX colour analysis. On the bottom of the figure there is a variety of values which are numerical representations of the colour of the part. HEX, sRGB, CMYK, CIELAB, LCH (ab), and LRV are different units used for the valuation of colours, and at the bottom the Hue of the part is stated.

Synthetic strategies were taken in an effort to further increase the mechanical properties of the synthesized novel materials. These methods are explained in chapter 5 of the thesis. Once the yellow PA-12 had been printed via SLS and optimized, the other coloured PA-12 powders had to be printed.

Printing with red PA-12 (PA-12 coated with P(IBMA-DR1MA):

The second material that was printed was recycled PA-12 coated with P(IBMA-DR1MA). The random copolymeric coating of Isobornyl methacrylate and disperse red 1 methacrylate gave the PA-12 based particles their red appearance. The printing conditions used for this material were based on the printing conditions used for the printing of recycled PA-12 coated with P(IBMA-Y1MA). This is because it is the most analogous material that had been printed via SLS, as it has very similar thermal properties.

The first print was executed with the following conditions: PBT of 158 ^{o}C, HLP of 14.5 W, CLP of 14.5 W, CT of 150 ^{o}C, HS of 2500 mm/s, and an HD of 0.25 mm. This yielded a build that curled after 6 layers, so the conditions needed to be modified (table 4).

Structure	Powder Bed Temperature (^{o}C)	Chamber Temperature (^{o}C)	Laser Power (W)	Hatching speed (mm/s)	Hatching distance (mm)	Energy density (ψ) (W/mm^{3}s^{1})	Scan Type
Square	158	150	14.5	2500	0.25	0.232	Single
Square	159	150	14.5	2500	0.25	0.232	Single
Square	158.5	150	14.5	2500	0.25	0.232	Single
Square	158	150	14	2500	0.25	0.224	Single
Square	159	150	14	2500	0.25	0.224	Single
Square	159.5	150	14	2500	0.25	0.224	Single
Square	159.5	150	14	2500	0.25	0.224	Single

Table 4 – Printing conditions used to print a 5x20x20 mm square composed of recycled PA-12 coated in P(IBMA-DR1MA). Energy density (ψ) obtained from equation 1: $\psi = \frac{P}{V \times H \times D}$, where P is laser power, V is hatching speed, H is hatching distance, and D is depth of powder layer (100 μm).

The laser power was decreased to 14 W and the PBT was gradually raised to 159.5 ^{o}C, until satisfactory conditions were found for the printing of 'red PA-12'. This allowed for the building of squares with the dimensions of 5x20x20 mm (figure 8).

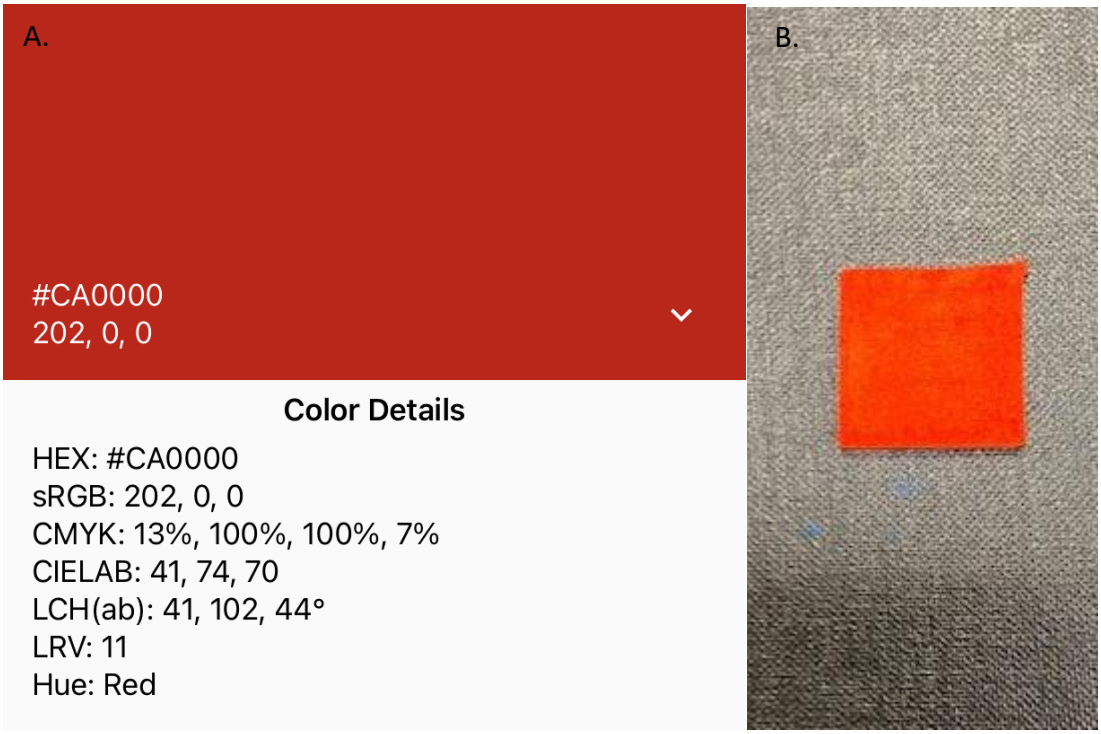


Figure 8 – Images and colour analysis of 5x20x20 mm squares printed via SLS composed of recycled PA-12 coated with P(IBMA-DR1MA). A.) NIX colour sensor analysis of printed part B.) Image of 5x20x20 mm square. On the top of the part A. there is square which is a photo representation of the colour of the part that was analysed via NIX colour analysis. On the bottom of part A there is a variety of values which are numerical representations of the colour of the part. HEX, sRGB, CMYK, CIELAB, LCH (ab), and LRV are different units used for the valuation of colours, and at the bottom the Hue of the part is stated.

This print yielded bright red squares, which are evidently red via sight, and the colour is confirmed through NIX colour analysis (figure 8). SEM analysis was done to show that the material had sintered well (figure 9).

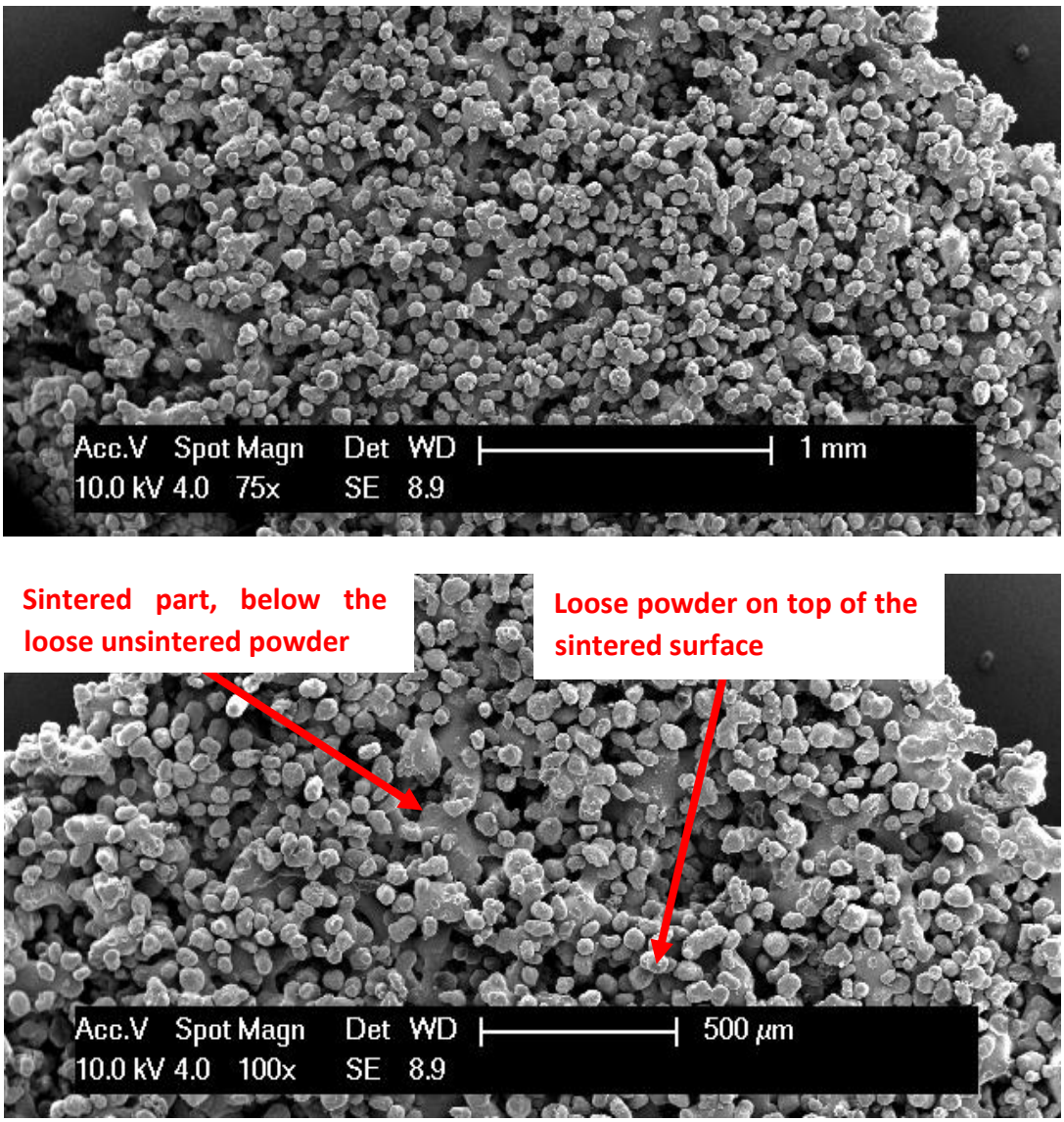


Figure 9 – SEM images of part printed via SLS composed of recycled PA-12 coated in P(IBMA-DR1MA).

The particles have been successfully printed showing that the sintering process has been adequate (figure 9). The mechanical properties of this material should be

analogous to those observed for the yellow PA-12 material. With the red and yellow PA-12 particulate powders having been printed successfully, the 'Blue PA-12' needed to be printed.

Printing with Blue PA-12 (PA-12 coated with P(IBMA-DB3MA):

The final-coloured material that was printed was virgin PA-12 coated with P(IBMA-DB3MA). The random copolymeric outer shell composed of Isobornyl methacrylate and Disperse Blue 3 Methacrylate gives the particles their blue visage. The particles used for these experiments were virgin PA-12 particles, so the most analogous material is the virgin PA-12 coated with P(IBMA-Y1MA), hence the printing conditions of the later should be used as a starting point for the optimization of the printing of blue PA-12. However, at the point of printing the blue PA-12 the printing of the yellow virgin PA-12 had not been conducted, so the recycled yellow PA-12 was used as a baseline. The first conditions that were used were a PBT of 159 ^{o}C, a CT of 150 ^{o}C, a laser power (LP) of 14.5 W a HS of 2500 mm/s, and a HD of 0.25 mm. This print yielded a part that disintegrated when part retrieval was attempted, which matches up with that was seen for the yellow virgin PA-12 material. Several different conditions were used until a satisfactory part was built (table 5).

Structure	Powder Bed Temperature (^{o}C)	Chamber Temperature (^{o}C)	Laser Power (W)	Hatching speed (mm/s)	Hatching distance (mm)	Energy density (ψ) (W/mm^{3}s^{1})	Scan Type
Square	159	150	14.5	2500	0.25	0.232	Single
Square	159	150	17.5	2500	0.25	0.280	Single
Square	159	150	19	2500	0.25	0.304	Single
Square	159	150	21	2500	0.25	0.336	Single
Square	159	150	21	2000	0.25	0.420	Single
Square	159	150	21	2000	0.2	0.525	Single
Square	159	150	21	2000	0.23	0.457	Single
Square	159	150	21	2200	0.23	0.415	Single

Table 5 – Printing conditions used to print a 3x20x20 square composed of virgin PA-

12 coated with P(IBMA-DB3MA). Energy density (ψ) obtained from equation 1: $\psi = \frac{P}{V \times H \times D}$, where P is laser power, V is hatching speed, H is hatching distance, and D is depth of powder layer (100 µm).

The laser power was gradually increased to 21 W, and with each increase of laser power the parts became stronger, however they were still quite weak. The next step taken was to decrease the HS to 2000 mm/s, this strengthen the part, but it was still weaker than the parts made with coloured recycled PA-12 materials. The optimal conditions were found to be a PBT of 159 ^{o}C, a CT of 150 ^{o}C, LP of 21 W, HS of 2200 mm/s, and a HD of 0.23 mm. This was the optimum condition as it was the highest amount of laser exposure the part could receive before smoking or curling, giving maximum part density. The parts built with this material were blue (figure 10).

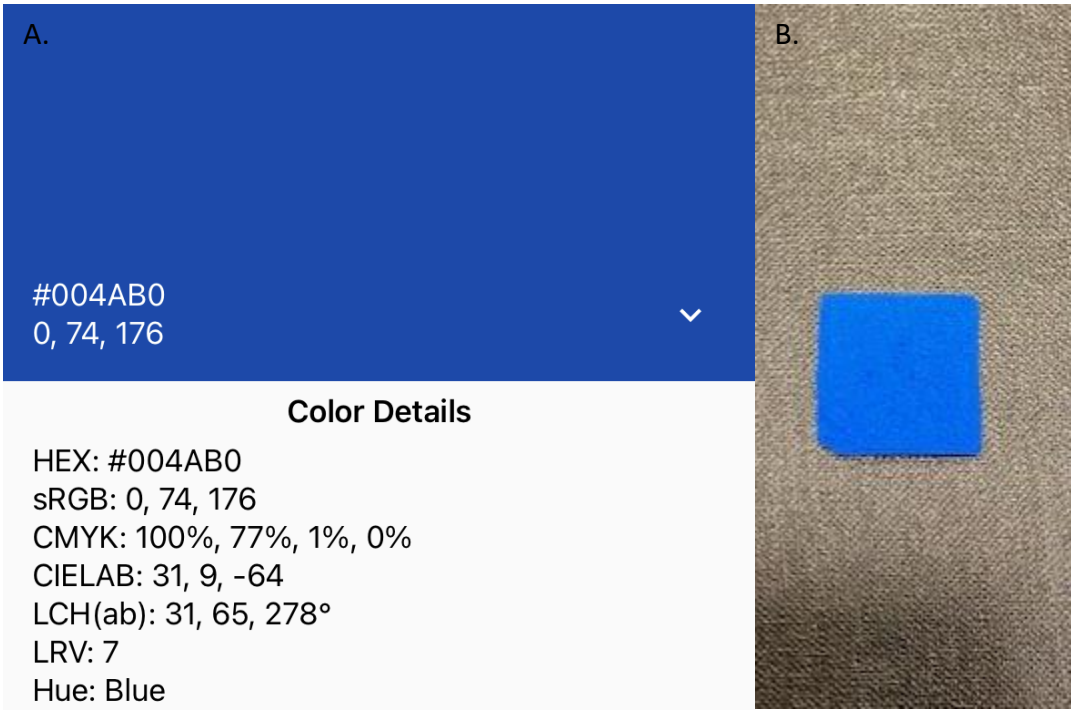
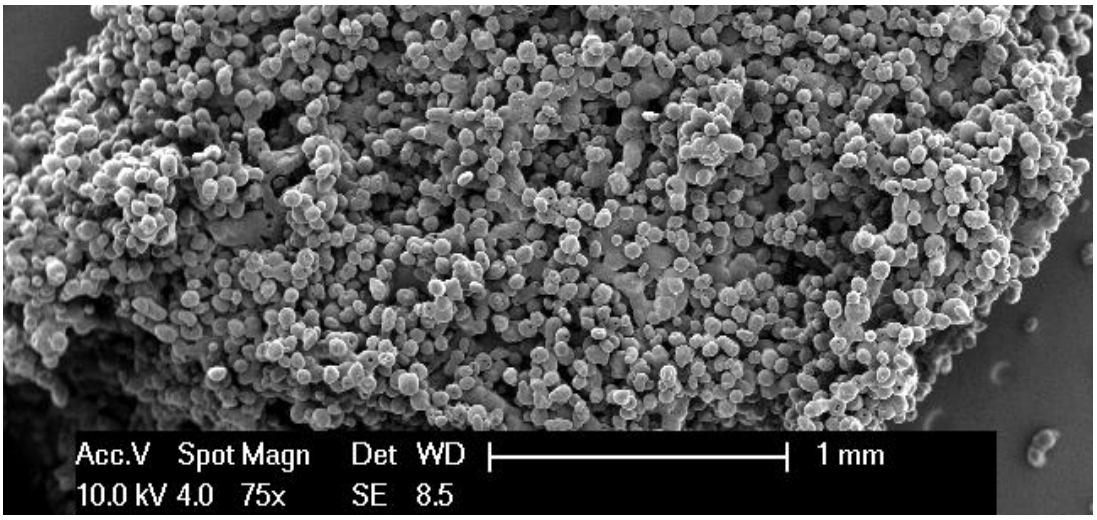


Figure 10 - Images and colour analysis of 3x20x20 mm squares printed via SLS composed of recycled PA-12 coated with P(IBMA-DB3MA). A.) NIX colour sensor

analysis of printed part B.) Image of 5x20x20 mm square. On the top of the part A. there is square which is a photo representation of the colour of the part that was analysed via NIX colour analysis. On the bottom of part A there is a variety of values which are numerical representations of the colour of the part. HEX, sRGB, CMYK, CIELAB, LCH (ab), and LRV are different units used for the valuation of colours, and at the bottom the Hue of the part is stated.

The printed parts are blue, as was confirmed by the NIX colour analysis (figure 10). SEM analysis was performed to see if adequate sintering had taken place (figure 11).



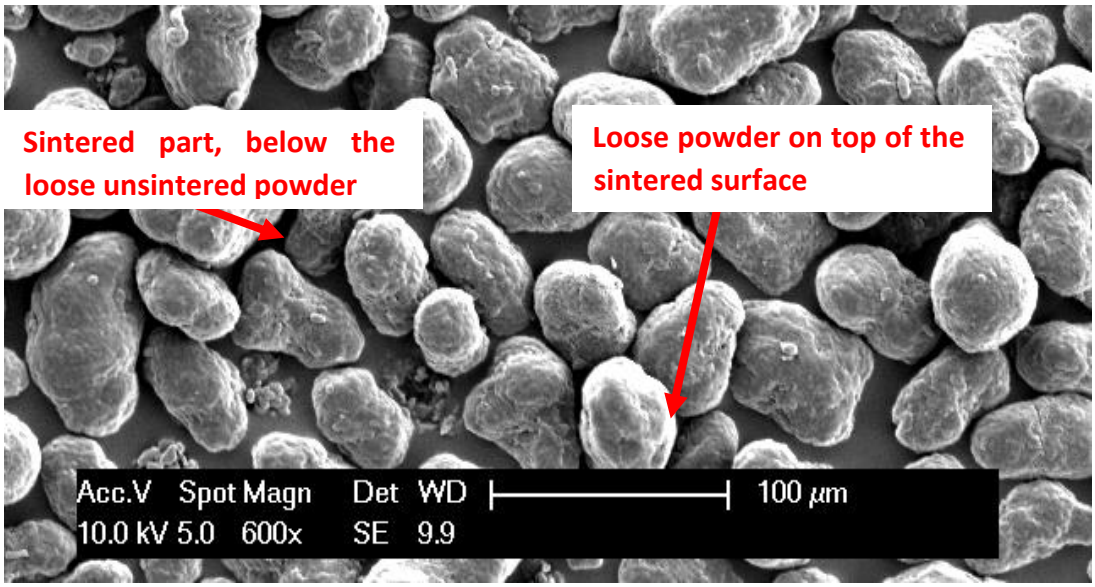


Figure 11 – SEM images of part printed via SLS composed of recycled PA-12 coated in P(IBMA-DB3MA).

From the SEM it can be seen that the particles are fused together, showing that proper sintering had taken place. Mechanical analysis was not performed on parts built from this material, but it can be assumed that they would be similar to those exhibited by the yellow virgin PA-12 material (Appendix 2). This is because both materials have similar thermal behaviour and show the same printing trends, when optimized for both. The successful printing of this material proved that we could successfully print blue, red, and yellow polymeric materials through SLS. This process would address many of the issues that are intrinsic to the SLS process currently used to obtain coloured parts. These materials could also be used to create a CMYK colour mixing system for SLS.

Initial colour mixing in SLS:

Initial testing was performed on the topic of the development of a CMYK colour mixing system for SLS. To begin the blue and yellow PA-12 powders were physically mixed in different ratios (both using the virgin PA-12 as the core shell). The mixing of these powders yielded green powders. These green powders are composed of a mixture of yellow and blue particles. During printing the particles will sinter together and when well mixed the yellow and blue particles will melt together to form a green surface. This type of colour mixing is called subtractive colour mixing, it is used extensively in the mixing of inks and it is the basis of coloured paper printing. If mixing is not satisfactory this can lead to agglomerations of a certain colour, resulting in

zones in which one colour is dominant. These powders were then printed at the conditions used to print the yellow PA-12 composed of virgin PA-12 coated with P(IBMA-Y1MA). Three ratios were used: 90 wt% yellow Pa-12 and 10 wt% blue PA-12, 87.5 wt% yellow Pa-12 and 12.5 wt% blue PA-12, 85 wt% yellow Pa-12 and 15 wt% blue PA-12. The majority of the composition is yellow PA-12 as the blue PA-12 is more intense, thereby the blue PA-12 can dominate the colour of the mix. These three powder mixes were printed and analysed via NIX colour analysis revealing that each part had a unique colour (different shades of green) (figure 12).

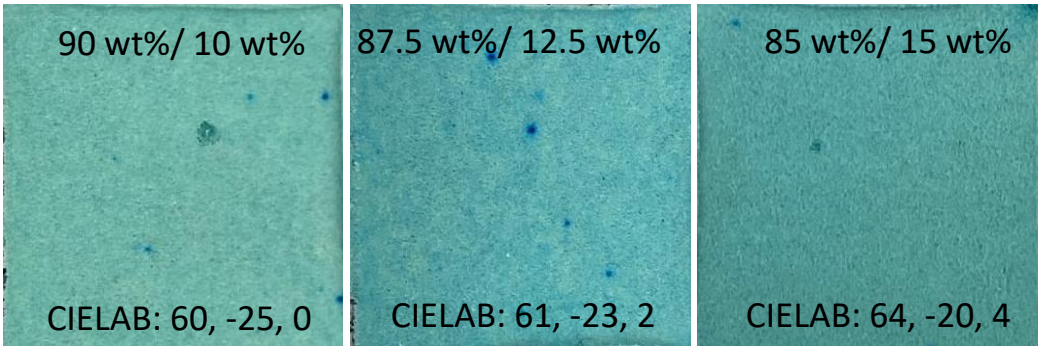


Figure 12 – Initial results of colour mixing for SLS, images of parts printed from the yellow and blue PA-12 mixes.

Further colour mixing was attempted during the initial development of the CMYK colour mixing system for SLS. To test if this process worked for other colour mixtures, the red and yellow PA-12 powders were mixed in a ratio of 75 wt% PA-12 coated with P(IBMA-Y1MA) and 25 wt% PA-12 coated with P(IBMA-DR1MA), and subsequently printed with the conditions used for the yellow PA-12 material. This yielded a 5x20x20 mm orange block (figure 13).



Figure 13 – Initial results of colour mixing A.) NIX colour analysis of orange part B.) Orange part printed which is composed of 75 wt% PA-12 coated with P(IBMA-Y1MA) and 25 wt% PA-12 coated with P(IBMA-DR1MA). On the top of the part A. there is square which is a photo representation of the colour of the part that was analysed via NIX colour analysis. On the bottom of part A there is a variety of values which are numerical representations of the colour of the part. HEX, sRGB, CMYK, CIELAB, LCH (ab), and LRV are different units used for the valuation of colours, and at the bottom the Hue of the part is stated.

The colour analysis indicates that through simple physical mixing of the coloured PA-12 particles it is possible to print parts in unique colours. Through this novel synthesis and printing process, the first colour mixing system for SLS has been developed.

Tof-Sims analysis of parts:

The printed parts were analysed via Time-of-flight Secondary ion mass spectroscopy (Tof-Sims) in order to prove the presence of the copolymeric coatings on the surface of the printed parts. ToF-SIMS is a surface analytical tool, which utilizes a pulsed ion beam (e.g. Gallium) to remove molecules from the sample surface. These molecules are accelerated into a mass spectrometer, in which their mass is measured. At first this analysis was performed on parts composed of pure PA-12 and parts composed of PA-12 particles coated with PIBMA. The analysis revealed that ions characteristic of IBMA are present on the surface of the parts composed of PA-12 coated with PIBMA whilst only a small amount of ions corresponding to PA-12 are present, thereby proving that the intended coating is on the surface (figure 14). The part composed of PA-12 shows no signal corresponding to the IBMA ion and a large signal for the PA-12 ion, proving that the PA-12 part has no PIBMA on its surface.

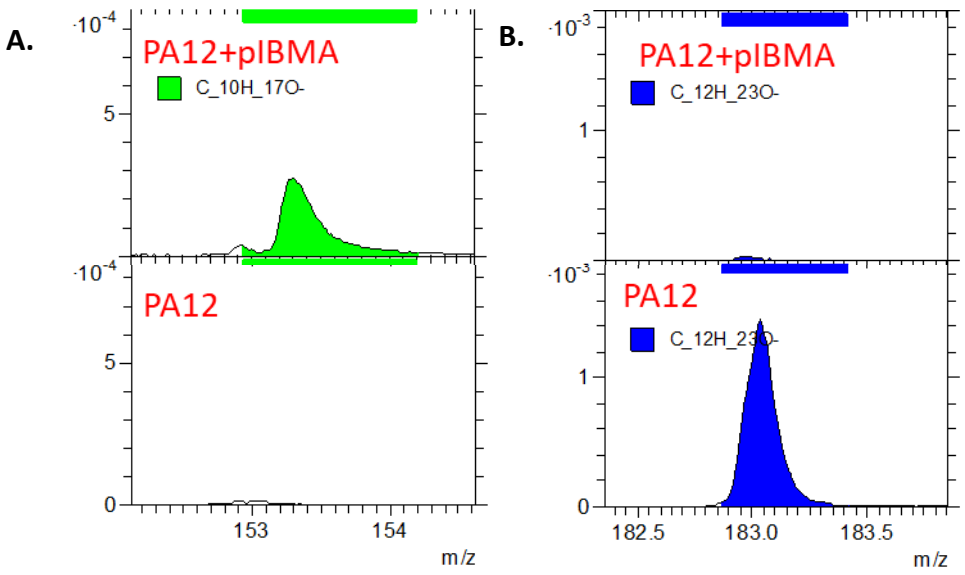


Figure 14 – Tof-Sims results of PBF printed parts. A.) PBF printed part composed of PA-12 particles coated with PIBMA, showing the presence of a PIBMA peak and the

lack of PA-12 peaks. B.) PBF printed part composed of PA-12 particles, showing the lack of PIBMA peaks and the presence of PA-12 peaks.

Similar analysis was undertaken to map a region of the printed parts composed of PA-12 coated with PIBMA and parts composed purely of PA-12. This analysis allowed for the mapping data corresponding to the IBMA ions signals and the PA-12 ion signals to be overlayed, giving a holistic view of the surface of each part. The part composed of PA-12 coated with PIBMA was mapped showing that the majority of the surface is composed of PIBMA, with small areas of PA-12, which can be clearly seen in figure 15 part C, in which the IBMA ions are illustrated by the red regions and the PA-12 ions by the green regions. The opposite can be seen for the part composed purely of PA-12 as the part is mostly covered by the green showing that the part is composed of PA-12 (Figure 15C).

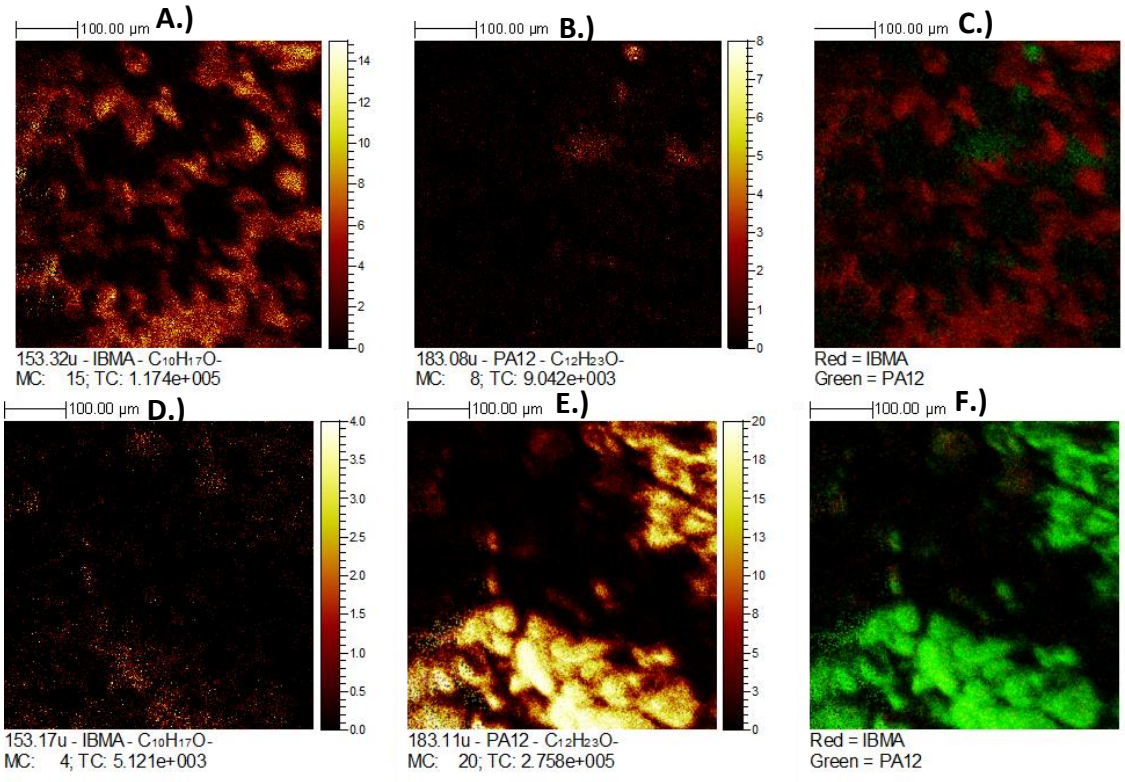


Figure 15 – Tof-Sims results displayed in image form. A.) The areas belonging to the characteristic PIBMA peak, showing the presence of PIBMA on the surface of the part composed of PA-12 particles coated with PIBMA, B.) The areas belonging to the characteristic PA-12 peak, showing the lack of PA-12 on the surface of the part composed of PA-12 coated with PIBMA. C.) An overlayed image of the characteristic PIBMA (red) and PA-12 (green) peaks on the part composed of PA-12 coated with PIBMA, showing that the majority of the surface is PIBMA, with a small percentage of PA-12. D.) The areas belonging to the characteristic PIBMA peak, showing the lack of PIBMA on the part composed of PA-12. E.) The areas belonging to the characteristic PA-12 peak, showing the presence of PA-12 on the surface of the part composed of PA-12. F.) An overlayed image of the characteristic PIBMA (red) and PA-12 (green) peaks showing that the part composed of PA-12, show no red signifying that there is no PIBMA and the green shows that there is PA-12 on the surface.

Tof-Sims was performed on parts composed of PA-12 coated with P(IBMA-Y1MA), in an effort to see if PY1MA was evenly spread out through the part. The characteristic ion for Y1MA was found on the region of the part that was analysed, showing that there is PY1MA on the surface of the part, and from the mapping image corresponding to the Y1MA ion it can be said that it is spread out evenly throughout the part (figure 16A). The part was analysed for the PA-12 ion and from both the data and the mapping image it could be seen (figure 16B). However, both ions for PA-12 and for Y1MA have roughly the same molecular weight, hence the peaks appear in the same location, from the data it can be seen that the Y1MA ion peak is of greater intensity and a different shape to that of the PA-12 ion, which suggests the presence

of P(IBMA-Y1MA) on the surface of the part (figure 16). This evidence revealed that the intended copolymer was probably on the surface, but the peak placement does not allow for it to be conclusive, so a part composed of PA-12 coated with P(IBMA-DR1MA) was analysed, as it has characteristic peaks that are not in the region of the peaks belonging to PA-12 or IBMA.

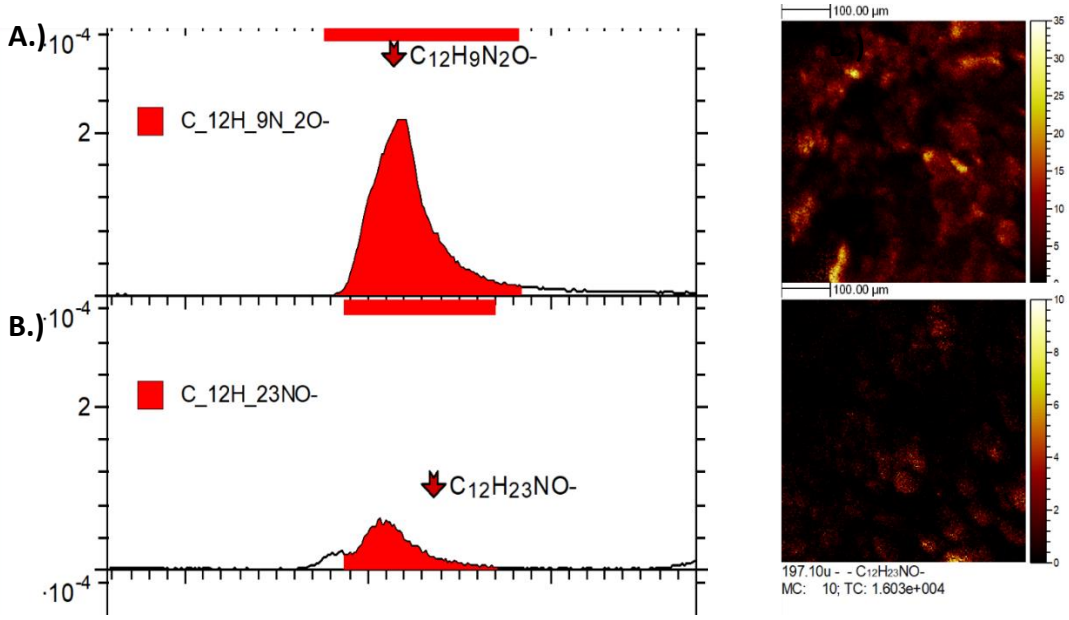


Figure 16 – Tof-Sims results of PBF printed parts composed of PA-12 coated with P(IBMA-Y1MA). A.) Characteristic peak of the Y1MA segment in P(IBMA-Y1MA) showing that Y1MA is on the surface of the printed part composed of PA-12 coated with P(IBMA-Y1MA). This is seen as the peak is of a greater intensity and different shape than the PA-12 peak. B.) Characteristic peak of PA-12 in a part composed PA-12 coated with P(IBMA-Y1MA), showing the presence of PA-12 on the surface.

The next sample that was analysed and mapped via Tof-Sims was a part composed of PA-12 particles coated with P(IBMA-DR1MA). This sample was chosen as DR1MA has a NO_2^- ion present that does not appear for any of the other components in the

system, therefore if the ion is present, it proves that DR1MA is a component of the part. Tof-Sims showed that there was a clear NO_2^- ion peak in the sample with DR1MA, and no peaks (small peaks can be impurities) in the other samples (Figure 17).

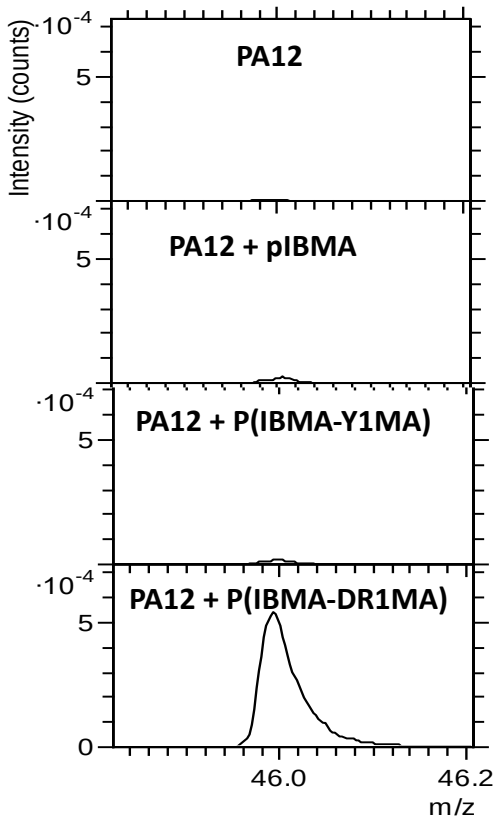


Figure 17 – Tof - Sims results for the NO_2^-, which is belonging to the DR1MA segment of the PA-12 particles coated in P(IBMA-DR1MA). Tof-Sims indicate that there are no NO_2^- ions present in the part composed of PA-12 as there is no peak present. For the part composed of PA-12 coated with PIBMA there is a slight peak, which could be due to impurities, as is the case for the part composed of PA-12 coated with P(IBMA-Y1MA). The presence of a large peak at 47 m/z for the sample composed of PA-12 coated with P(IBMA-DR1MA) proves that there are NO_2^- ions present on the surface

of the material, indicating that DR1MA is part of the polymeric coating that has been sintered.

The part composed of PA-12 particles with P(IBMA-DR1MA) was mapped for the presence of three ions (PA-12 ion, IBMA ion, DR1MA ion). One of these ions corresponds to DR1MA and the mapping proves that DR1MA is spread out evenly across the part (figure 18A). The second ion that was analysed was the IBMA ion, which is also shown to be spread out evenly across the mapped region (figure 18B). When the mapped regions for the DR1MA and IBMA ions are compared, it can be seen that the highlighted regions are in very similar positions, this is conclusive proof that the P(IBMA-DR1MA) copolymer is spread out evenly across the part (figure 18A and B). The ion corresponding to PA-12 was analysed, showing that a very small percentage of the surface is composed of PA-12 and not P(IBMA-DR1MA) (figure 18C and D).

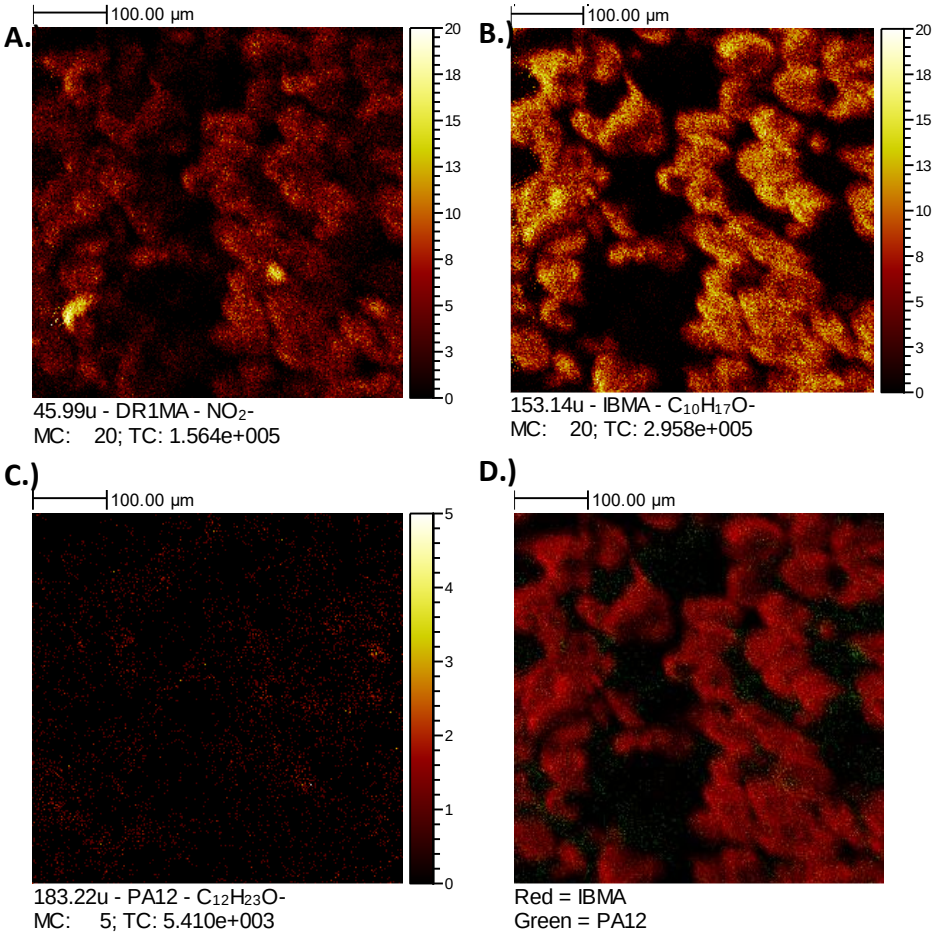


Figure 18 – Tof-Sims results displayed in image form. A.) Tof-sims results for the presence of NO_2^- ions on the surface of a part composed of PA-12 coated with P(IBMA-DR1MA). The NO_2^- is characteristic of the DR1MA, hence it should confirm the presence of the red coating on the part. The mapping image indicates that DR1MA is spread across the entire surface of the part. B.) Tof-sims results for the presence of $C_{10}H_{17}O^-$ ions on the surface of a part composed of PA-12 coated with P(IBMA-DR1MA). The $C_{10}H_{17}O^-$ ion is characteristic of IBMA, hence its presence would confirm the presence of the red coating (P(IBMA-DR1MA). The mapping image shows that the IBMA ions are present on the surface of the part indicating that PIBMA is present. The mapping images of the IBMA and DR1MA ions are similar and appear in the same

regions of mapped space, indicating that P(IBMA-DR1MA) is coating the surface. C.) Tof-sims results for the presence of $C_{12}H_{23}O^-$ ions (characteristic of PA-12) on the surface of a part composed of PA-12 coated with P(IBMA-DR1MA). The mapping image shows that there is small quantity of the characteristic PA-12 ions present on the surface, indicating that even though the surface is mostly covered with P(IBMA-DR1MA) there is a small amount of PA-12 on the surface of the part. D.) Overlayed image of the mapping corresponding to the IBMA ion (red) and the PA-12 ion (green) showing that the majority of the surface is covered in IBMA, and a small percentage by PA-12.

The evidence gathered from Tof-Sims analysis conclusively illustrates that the intended coloured coatings are on the surface of the printed parts, thereby showing that the particles were coated and sintered successfully, in order to produce wholly and evenly coloured parts.

Conclusions:

In this chapter, it was shown that it is possible to print in colour via SLS, through the use of coloured polymeric particles. Red, Blue, and Yellow PA-12 based particles with coloured random copolymeric coatings P(IBMA-r-Dye monomer) were printed and the printing was subsequently optimized. 5x20x20 mm squares were made using each coloured material. This showed that it was possible to print multi-layered structures, and that there was minimal curling and warpage once the appropriate printing conditions were found.

The mechanical properties of the coloured materials could be improved through blending them with virgin PA-12, this is because preliminary testing showed that virgin PA-12 had greater mechanical properties. This can be a positive as the colour of the material does not change greatly due to physical mixing with virgin PA-12, this could result in coloured powders for SLS that are very close in price to commercial PA-12. This was the first time that the printing of coloured polymeric particles has been performed in SLS. This is important as this process can address many of the shortcomings of the colouring process currently used for SLS parts. The problems that are addressed could help potential users of this technology to save cost and time. The dimensions of the parts could also be considered to be more accurate than that of the parts that are painted, thereby assuring effectiveness of the parts. Tof-Sims analysis showed that the printed parts were composed of the desired components as the coloured copolymeric coatings were spread out evenly across the surface of the parts. The process produces wholly coloured parts, which means that unlike the dyed parts the colour cannot be scratched off, and lastly the use of these materials would mitigate many of the environmental consequences of the painting process as shipping, dyeing, and drying steps would be eliminated from the production of the parts. Through the use of these materials the yellow and blue PA-12 powders were physically mixed in varying ratios and printed. This yielded three different hues of green, indicating that these materials can be used to the develop the first colour mixing system for SLS.

Future Work:

In the future several experiments should be undertaken in an effort to gain a better understanding of the printing system. In this chapter it can be seen that there was a clear difference between the virgin and the recycled PA-12. The effect of the thermal process should be further studied, and their properties as single and core-shelled materials investigated. As well further optimization and mechanical testing should be performed for the red and blue PA-12 powders and parts.

Materials and Methods:

Materials:

PA-12 (P2200) was purchased from EOS GmbH. PA-12 coated with P(IBMA-DB3MA) (Blue PA-12 ink), PA-12 coated with P(IBMA-DR1MA) (Red PA-12 ink), and PA-12 coated with P(IBMA-Y1MA) (Yellow PA-12 ink) were produced in house.

Printing and Fabrication of Primary coloured parts:

Squares and dog bones were designed (Magics). The powder of PA-12 coated with P(IBMA-Dye monomer) was sieved through a 200 μm mesh and dried for 1 hr at 100 ^{o}C. The powders were sintered on an EOS Formiga P100, with varying conditions. The parts were left overnight and collected. The parts were cleaned and the powder was collected so it could be reused.

Physical mixing of powders:

The calculated amounts of red and/or blue and/or yellow and/or white PA-12 based powders were added to a glass vial. The vial was physically mixed via a vortex mixed

for 10 min, and subsequently left on a roller overnight, to ensure appropriate physical mixing.

Printing of colour-mixed structures:

The coloured powder mixtures were deposited onto the build platform of an EOS Formiga P100 SLS printer. A powder bed temperature of 172° C, a chamber temperature of 150° C, a hatching laser power of 20 W, a contour laser power of 20 W, a hatching speed of 2500 mm/s, a hatching distance of 0.25 mm, and a double scan were used for the printing of the coloured structures. Once cooled the structures were removed for visual inspection and colour analysis.

Analysis:

Colour of printed parts:

The coloured parts were removed from the printer and placed onto a white sheet of paper. An image of the surface of the square is taken with a NIX© colour sensor, and the data is compiled. The NIX© colour sensor is one of the available tools used for colour analysis.[117–119] This sensor can be linked to a smartphone and provide readings through an app almost instantaneously.[117–119] The read out includes a picture of the colour and the colour's values in a variety of units. This allows the user to thoroughly analyse the perceived colour of an object, paint, etc.

Scanning Electron Microscopy (SEM):

SEM was used to determine the size and shape of the discrete monodisperse particles, a Phillips XL30 electron microscope was used. The samples were prepared

by adding powder to a carbon tab mounted onto a SEM stub, which were then coated with Platinum for 180 seconds at 12 mA and 2.2 kV using an Emitech SC7640 Sputter coater. An average particle size was calculated by taking the area of 100 particles from a SEM image and finding the average, performed using ImageJ. The thickness of the polymeric particle layer was measured by removing a segment of the layer revealing the surface of the stub, the height difference between the stub and the particle tops equals the thickness of the particle layer.

Time-of-flight Secondary Ion Mass Spectrometry (Tof-Sims): ToF-SIMS data were acquired using a ToF-SIMS IV instrument (ION-TOF GmbH., Münster, Germany).Primary ion beam was a bismuth liquid metal ion gun (Bi3+) run at 25 kV (pulsed target current of ~1 pA).For each sample, data were acquired over 3 regions of 500 µm x 500 µm at 256 x 256 pixels resolution for 20 scans. Data acquisition and analysis was performed using SurfaceLab 7 software (IONTOF GmbH). Selected spectra (area 1 of each sample) were normalised for comparison and identical Y scales were used.

Chapter 4: Developing a Colour Mixing System for SLS

Acknowledgements:

I would like to acknowledge Prof. Fabricio Machado, for his help in the creation of a predictive system used for the formulation of polymeric powder mixes to yield specific colours for SLS printed parts. His help and expertise were invaluable in the development of this predictive algorithm.

Introduction:

The aim of the work in this chapter was to develop a colour mixing system for SLS. Colour mixing is a desirable tool, as it allows the user to obtain any colour from a set of three or four primary colours.[120–122] The field of colour science has intrigued scientists, artists, philosophers, etc. for many years. In fact, one of the earliest recorded theories of colour mixing and general colour theory can be seen in Aristotle's Metereologica.[123–125] The basis of his findings laid the ground for the future of the field, as he postulated that there are primary colours which can be mixed together to create all other colours.[123–125] However, he said white, yellow, red, purple, green, blue, and black were the primary colours.[123–125] This was later found to not be the case, as the primary colours are yellow, cyan (blue), and magenta (red).[25,100,120–122]

Colour Mixing:

There are two main types of colour mixing: additive and subtractive mixing. Additive colour mixing is a colour model that is used to mix and predict the appearance of colours made by coincident component light i.e., the perceived colour can be predicted by summing the numeric representation of the component colours (figure 1).[126–128] Additive colour mixing is mainly used in electronic displays and sometimes when mixing differently coloured solid objects such as powders.[103] Subtractive colour mixing predicts the resultant spectral power distribution of light filtered through overlaid partially absorbing materials on a reflecting or transparent surface.[23,25,100,101] Each layer partially absorbs some wavelengths of light from the illumination spectrum, whilst letting others pass through, thus giving a coloured appearance.[23,25,100,101] The resultant spectral power distribution is predicted by sequentially taking the product of the spectral power distributions of the incoming light and transmissivity at each filter (figure 1).[23,25,100,101] Subtractive colour mixing is used in dye, paint, and ink mixing for coloured printing and photography.[103]

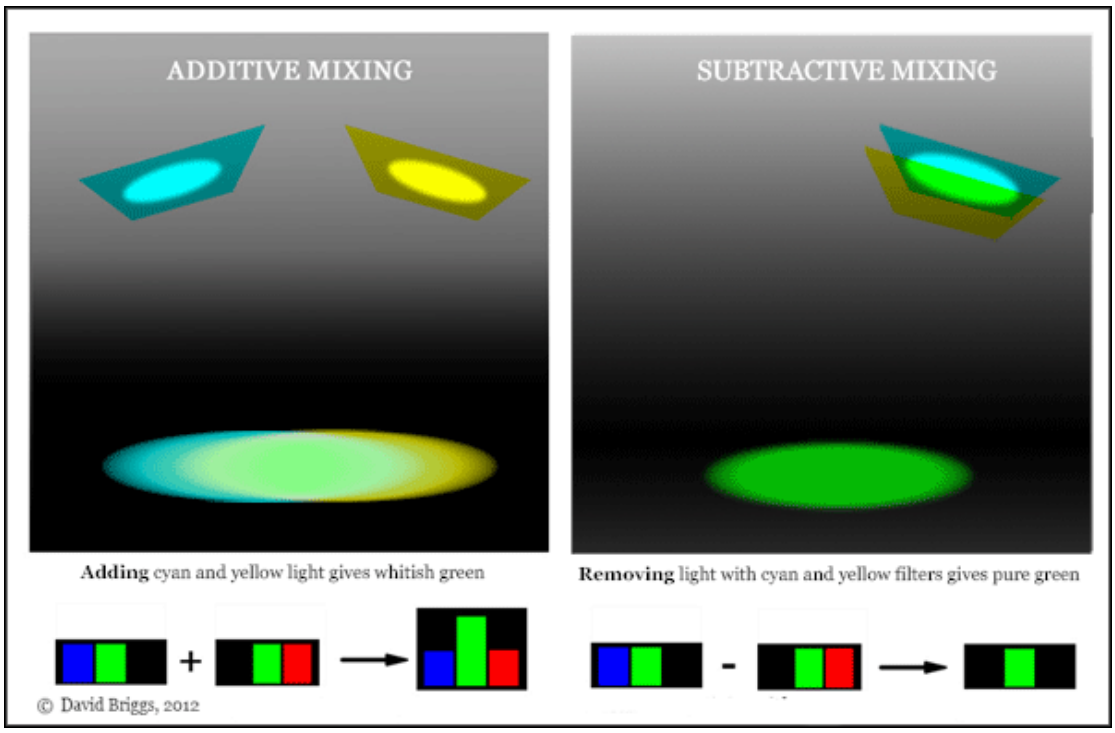


Figure 1 – Schematic of additive and subtractive colour mixing.[129]

In theory, these colour mixing techniques should be simple and when tracked on digital displays, trackable mixing patterns can be found with relative ease.[129,130] However, it becomes increasingly difficult in real world applications, largely because most paints, dyes, etc. are not perfectly formed of a simple colour.[129] They possess impurities of different colours, which affects colour mixing, as they can cause the addition or subtraction to be different than if the colours were 'perfect'.[129] Also, the effects of different types of light can dramatically affect the colour (figure 2).[130] The perceived colour of an object can change greatly due to light, as the illuminated side of the sphere has a light green colour and the non-illuminated side has a dark green colour, although both parts of the sphere are identical.

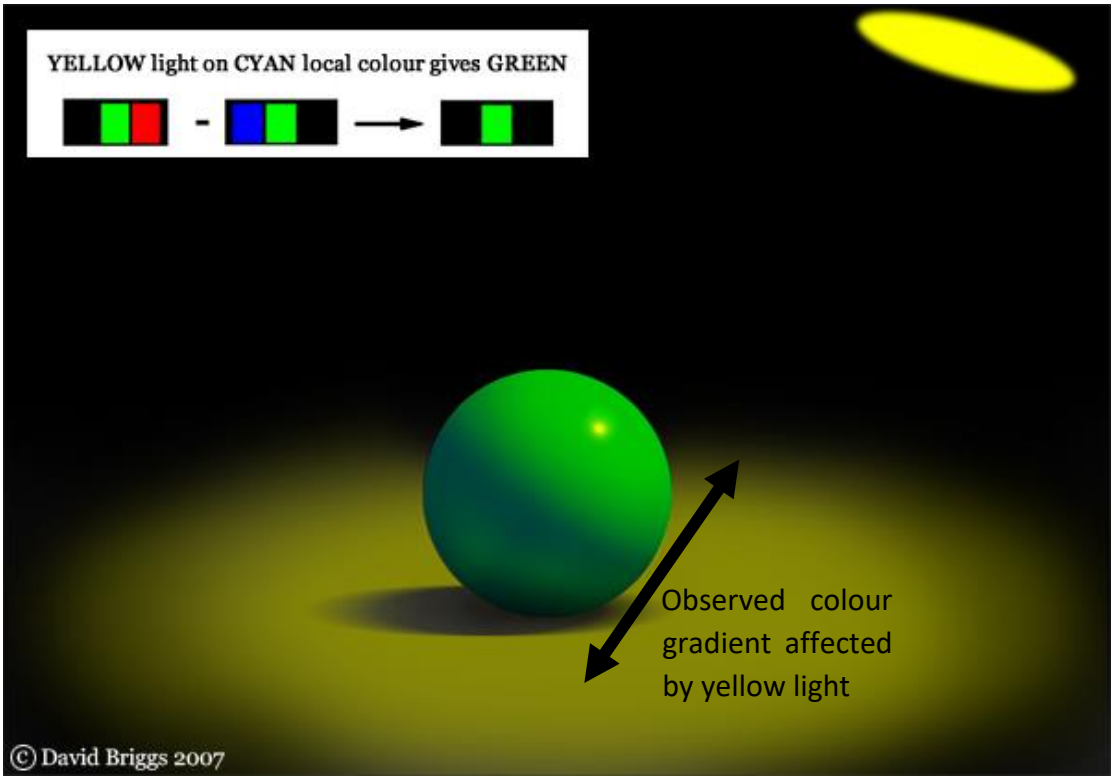


Figure 2 – Influences of light on colour mixing, showing that where the light is hitting the ball appears to have a light green colour, and the area of ball which has less contact with the light appears to have a dark green colour.[130]

In order to decide on the colour mixing process for this project, many factors had to be considered. The different coloured powders are mixed together, which would normally use additive colour mixing. This should also be applicable for the colour of the powder mixes. However, the colour mixing of the sintered part is desirable as the colour of the printed part is the objective and not the colour of the mixed powder. There can be differences in these as when sintered the colour could change due to changes in density of material. The colour mixing of the sintered part would be determined through subtractive colour mixing, because when the laser sinters the desired area, the particles will melt, and the liquid will mix together forming one solid

colour. Hence, during SLS printing the coloured polymeric particles act like inks when they mix together in the melt phase.

Measurement of Colour:

Colour mixing and colour can also be complicated by the actual wavelength (UV-vis absorption curves) and the perceived colour.[131] When colour mixing is used, the resulting mixture will have individual UV-vis absorption maxima for each colour, instead of the colour for the mixture, hence it is not feasible to study the perceived colour via UV-vis absorption. For example, if you mix blue and yellow inks, the resulting UV-vis absorption curve will have two peaks one representing blue and another yellow, but the sample in question will look green to the viewer. This poses the following question, what is more relevant, the UV-vis data or the perceived colour? The decision was taken that perceived colour was more relevant for the end applications (which are consumer based). This decision allowed us to focus on the actual perceived colours that can be produced and the methods for obtaining target colours. Another benefit of using this technique in comparison to solid state UV-vis measurements is that the measurement is quick, accurate, and does not require a large amount of sample.

There have been significant problems in analysing the perceived colour of materials and paints in the past, arising from a lack of standardization of colour units (HEX, LCH, CIELAB, etc.), and because it was challenging to accurately calculate the colour of objects without computational aid.[132] Until quite recently, the way to compare and match colours was to use a colour palette.[133,134] Paint manufactures have databases,

which include millions of variations based on hues, brightness, intensity, texture, etc. and people would go through these databases to compare and match to the colour required (figure 3).[135,136] Recently, sensors for colour analysis have been produced, which allow for rapid and on-site colour analysis.

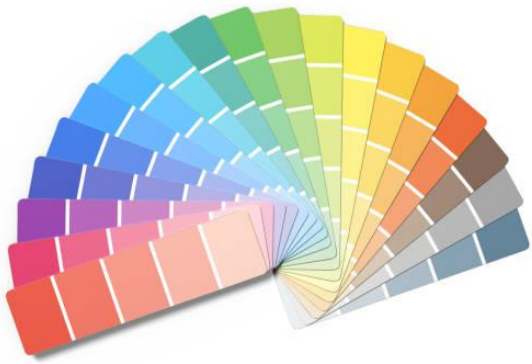


Figure 3 – Colour analysis via colour palettes and swatches.

The NIX© colour sensor is one of the available tools used for colour analysis.[117–119] This sensor can be linked to a smartphone and provide readings through an app almost instantaneously.[117–119] The read out includes a picture of the colour and the colour's values in a variety of units. This allows the user to thoroughly analyse the perceived colour of an object, paint, etc. (figure 4).

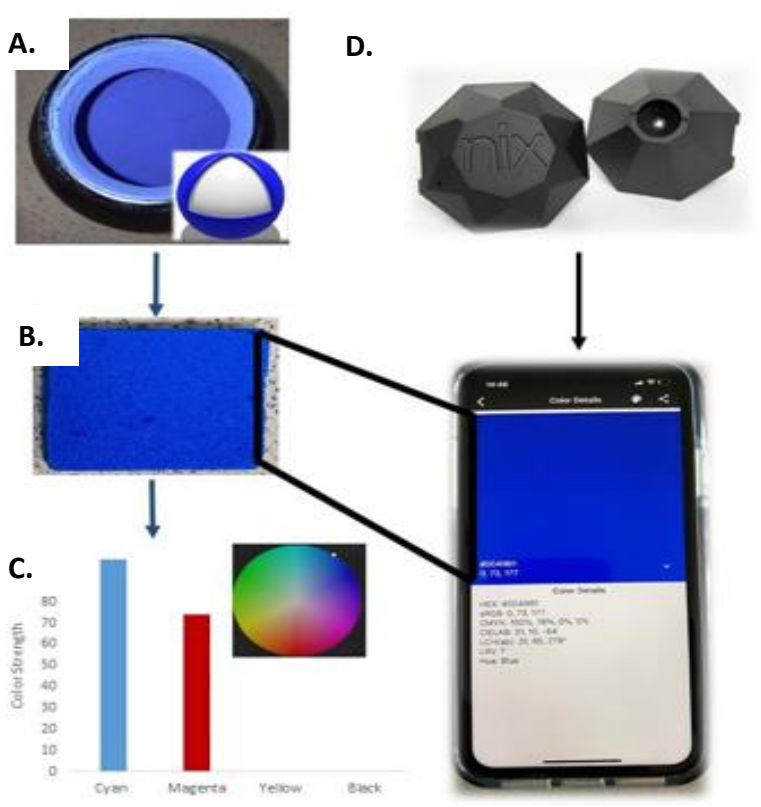


Figure 4 – Colour analysis via NIX colour sensor. A.) Blue powder composed of PA-12 particles coated with P(IBMA-DB3MA). B.) SLS printed part composed of PA-12 particles coated with P(IBMA-DB3MA). C.) CMYK values of the blue part obtained via NIX colour analysis. D.) NIX colour analyser and in app results readout.

Cyan, Magenta, Yellow, and Black (CMYK) colour mixing:

The colour mixing system that we wanted to emulate was the CMYK mixing used by paper inkjet printers.[103] This is a tried and tested system used throughout the world. CMYK stands for Cyan, Magenta, Yellow, and Black.[101,102] This is suitable for this project as we have synthesized red, blue, and yellow polymers that can be printed via SLS.[26,101,102] Red is suitable as magenta can be defined as a range of colours from red to mauve to purple, and Cyan is a shade of blue.[26,101,102] Also, black ink is often used,

but is not integral to the system as the other three inks can be mixed to make black.[101,102] This colour mixing system works by mixing two or more of the inks to get the target colour.[101,102] For example, if the user wanted to print in green, the blue and yellow inks would be used in unison.

Paper inkjet printers that use CMYK colour mixing use liquid inks that are mixed when liquid and dried on the paper to give the wanted colour.[103] The 'inks' that are in our system are solid polymeric particulate-based powders, but the process can be emulated. The powders can be physically mixed pre-printing, so that the colour will be uniform throughout the part. At this point at a microscopic level the colour difference can be seen, but from a distance it looks like it is all one solid colour. As it sinters, the particles should melt and the colours should mix in the melt phase. The resulting part should thereby be composed of one solid colour (figure 5).

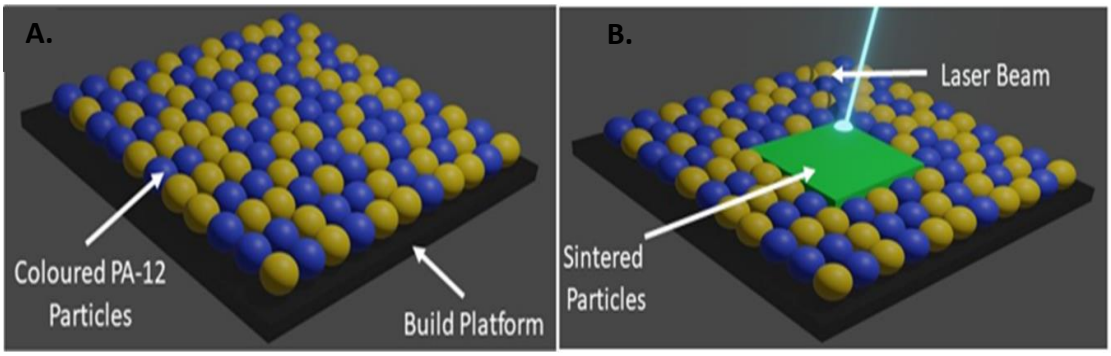


Figure 5 – Schematic of CMYK colour mixing in SLS. A.) Green powder mix on build platform before printing showing that the green powder mix is composed of individual yellow and blue particles. B.) SLS printing of green powder mix showing that when in the melt pool the two colours (yellow and blue) mix to form one new colour green, whilst the unsintered powder remains unchanged.

Once the colour mixing system was proven in concept, it had to be optimised. The broadness of colour definitions throughout colour theory and the many variables affecting the true colour and perceived colour of objects, makes it difficult to optimise such a system. In industry, paint manufacturers compile millions of data points in order to produce models to accurately predict the formulations needed for a target colour. The need for optimization arises from the fact that trying to obtain a target colour through trial and error can waste kilos of material, because it is difficult to extrapolate the formulations needed for new colours. However, in the research lab we do not have hundreds of SLS printers and/or enough time to gather the necessary data points needed to fill the colour sphere via trial and error (figure 6). For example, to run one test on an SLS printer such as an EOS Formiga P100, at least 600 grams of material is needed, and if that polymeric-powder mix is not of the desired colour then that powder is wasted.

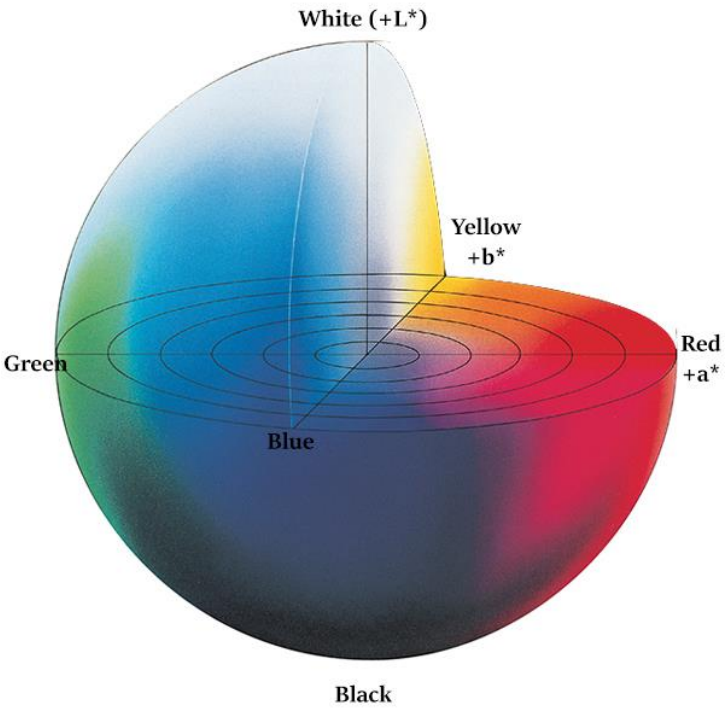


Figure 6 – Schematic of colour space, representing colour space as a sphere with the variables L, A, and B. The top and bottom of the sphere represent white and black respectively, showing that the top and bottom of the sphere dictate the brightness of the colour. Whilst the colours are on the A and B axis, Green, Blue, Red and Yellow are evenly spread out at 90-degree intervals on the horizontal plane.

Instead, a predictive model can be produced to aid in the creation of formulations for different colours. In previous research, such models have been made for the mixing of paints, with accuracy of colour prediction of a formulation ranging between 70-80% and the highest accuracies being reported as 90-92.5%.[137–140] This would aid in the development of new colour mixes as the precise formulation could be predicted, or at least the possible formulation could be narrowed down. However, the sintering process imparts increased complexity to the problem. This is because the colour can become darker and/or more intense after printing, as was seen in the previous

chapter, and not all colours change equally during the sintering process. For example, the blue PA-12 ink darkens more than the yellow PA-12 ink. This means that the premixed powder could have a vastly different colour than the printed part. The predictive algorithms that are used, should be able to find trends in the data to accurately predict the formulations needed for target colours of the printed parts.

Predictive models used for colour prediction:

Different types of computational methods have been used in attempts to predict the results of colour mixing. In a recent paper, genetic algorithms were used to predict colour mixing.[140]This paper attempted to simulate and predict colour mixing on cotton, however the general approach could be used for other types of colour mixing.[140] It claimed to have achieved a 92.5% level of accuracy, which in the field of colour mixing is high.[140] A genetic algorithm was used to achieve this, and it is a method for solving both constrained and unconstrained optimization problems, based on a natural selection process that mimics biological evolution (figure 7).[141–144] The method relies on biologically inspired operators such as mutation, crossover, and selection, and belongs to the larger class of evolutionary algorithms.[141–144]

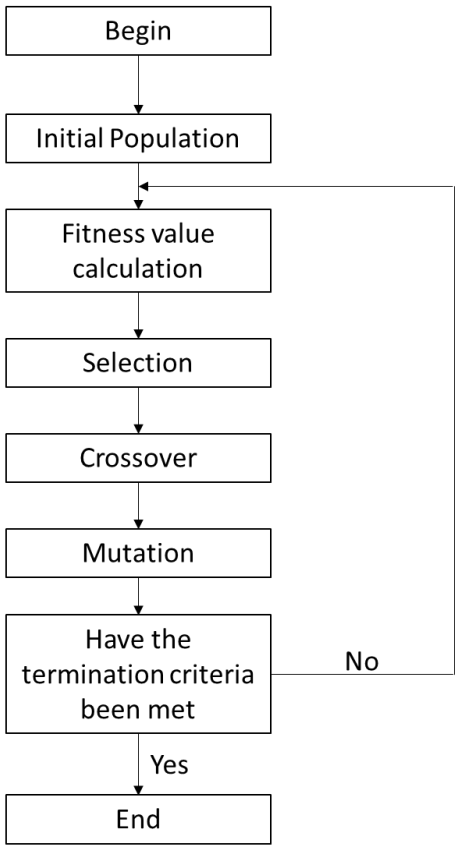


Figure 7 – Schematic of a genetic algorithm. A genetic algorithm commences with the development of an initial population of values that could be possible solutions to the problem at hand. The fitness scores of each of the population values are calculated and then the best are selected. The values of the population are then interchanged to give new possible solutions (a second population), and some of the values of the second population are mutated to be further altered. If the termination criteria are met then the process ends, but if it does not this process continues until a set number of iterations have been completed or the termination criteria are met.

There are other optimization techniques that could be used to predict colour mixing for SLS. One is particle swarm optimization (PSO), which is a method that optimizes a problem by iteratively trying to improve a candidate solution with regard to a given measure of quality.[145,146] It solves a problem by having a population of candidate

solutions, dubbed particles, and moving these particles around in search space according to mathematical formulae describing the particle's position and velocity.[145,146] Each particle's movement is influenced by its local best-known position and is also guided by the best-known positions in the search space, which are updated as better positions are found by other particles.[145,146] This moves the particle swarm towards the best solutions (figure 8).

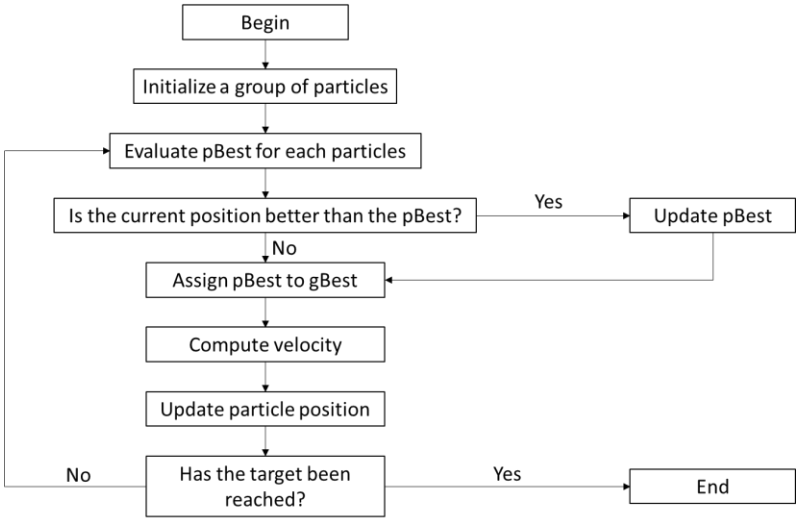


Figure 8 – Schematic of a particle swarm optimization (PSO). A PSO beings with a group of particles representing possible solutions being generated. Then the position of the particles are analysed to see which particles are closest to a desired solution. The particles then explore space and gradually move towards the solution based on the previous best results. The process of particle position evaluation and movement continues until a target result is reached or a set number of iterations are completed.

The other approach that could be used is a multivariable analysis and simplex lattice design to predict and follow the results of colour mixing. Simplex lattices can be used

to treat a wide variety of mixture problems.[147] For example, in the most general mixture problems in which the component proportions must satisfy the constraints:

$$x_i \geq 0, x_i + x_2 + \cdots x_q = 1.0$$

Each component proportion x_i can take values from zero to unity, and all blends among the ingredients are possible.[147] The fitting of mathematical equations to model the response surfaces over the entire simplex space can be done, so that empirical prediction of the response to any mixture over the entire simplex space is possible.[147] Modelling in this case means postulating an equation which represents the response surface.[147] A design is chosen in which it is possible to collect data at different points and the equation is fitted to these points.[147] Then the equation (model) is tested, until the fitted equation is decided to be a satisfactory prediction tool. Modelling using a simplex lattice method was first developed and used in the late 1950s and early 60s.[147] It is often used today, however more complex polynomials can utilize the same general methods.[147] All three of these techniques have merits and could be useful in the development of a prediction tool for CMYK colour mixing in SLS. All three will be tested and the results compared, in order make a satisfactory prediction tool.

Results and Discussion:

Colour prediction via Modified Genetic algorithm:

The first prediction modelling tool that was used was a modified genetic algorithm approach. The term modified is used because in this case the fitness score for evaluation of a possible result will still be used as will most of the other factors,

however a mutation step will be avoided. This was done to increase processing speed, and instead a large number (2000-5000) randomly generated number combinations were tested in each run and their fitness score retrieved and analysed. The system is based on finding the closest colour values to the target colour and basing the fitness score on the calculated difference between the randomly generated colours and the target colour. From equation 1-16 the derivation of the fitness score can be seen.

Equation 1	$if\ 164\ \leq H1\ \leq 345\ T_{func} = \big(0.56 + abs(0.2\cos(H1 + 168))\big)$ $else: T_{func} = \big(0.36 + abs(0.4\cos(H1 + 35))\big)$	Equation for T_func
Equation 2	$if\ H \geq 0\ H1_{func} = H$ $else: H1_{func} = (H + 360)$	Equation for H1_func
Equation 3	$if\ L1 < 16\ SL_{func} = 0.511$ $else: SL_{func} = \frac{0.040975L1}{0.01765L1}$	Equation for SL_func
Equation 4	$c1 = \sqrt{a1^2 + b1^2}$	Equation for C1
Equation 5	$c2 = \sqrt{a2^2 + b2^2}$	Equation for C2
Equation 6	$Delta_C = c1 - c2$	Equation for Delta_C

Equation 7	$Delta_L = L1 - L2$	Equation for Delta_L
Equation 8	$Delta_a = a1 - a2$	Equation for Delta_a
Equation 9	$Delta_b = b1 - b2$	Equation for Delta_b
Equation 10	$Delta_H = \sqrt{Delta\_a^2 + Delta\_b^2 - Delta\_C^2}$	Equation for Delta_H
Equation 11	$S_C = \frac{0.0638c1}{1 + \frac{0.0131}{c1}} + 0.638$	Equation for S_C
Equation 12	$F = \sqrt{\frac{c1^4}{c1^4 + 1900}}$	Equation for F
Equation 13	$H = arctan\left(\frac{b1}{a1}\right)$	Equation for H
Equation 14	$SH = S\_C\left((FT\_func(H1)) + 1 - F\right)$	Equation for SH
Equation 15	$Delta_E = \sqrt{\frac{Delta\_L}{2SL_{func}(L1)}^2 + \frac{Delta\_C^2}{2.6453} + \frac{Delta\_H^2}{SH}}$	Equation for Delta_E
Equation 16	$Fitness_{Function} = \frac{1}{Delta_E + 10^{-6}}$	Equation for fitness_score

Table 1 – Equations for derivation of Fitness Score. There are several key parameters in the derivation of this equation L, A, B, C, C1, C2, and H. L is a representation of the perpetual lightness of a colour and ΔL is the difference in lightness between two colours. A represents the value of a colour on a scale between red and green, hence ΔA is the difference in redness or greenness between two colours. B represents the value of a colour on a scale between blue and yellow, hence ΔB is the difference in blueness or yellowness between two colours. C represents chroma (saturation of the colour, with C1 and C2 being the chroma of colour 1 and 2 respectively. H is the hue which is represented as the angle of the colour in 360° colour space.

The next step for this modified genetic algorithm was to correlate the results that yielded good fitness scores to actual formulations of white, red, yellow, and blue PA-12 powders. For this to work, equations had to be made to find the relationships between the amount of colour used and the colour values (L, A, B, C, and H(Standard colour values)). The influence of each colour on every colour value was modelled giving equations that represent Red vs. L, Red vs. A, Red vs. B, Red vs. C, and Red vs. H and the same for the other two colours (blue and yellow) (equations 16-39).

Equation 17	$y_1 = (-0.4218L2) + 35.52$	Red vs. L
Equation 18	$y_2 = (0.4978a2) + 10.969$	Red vs A
Equation 19	$y_3 = (0.3955b2) + 16.429$	Red vs B
Equation 20	$y_4 = (0.3665c2) + 5.5016$	Red vs C

Equation 21	$y_5 = (-0.1004H2) + 10.969$	Red vs H
Equation 22	$Red_{Amount} = \frac{(y_1 + y_2 + y_3 + y_4 + y_5)}{5}$	Amount of Red PA-12 powder needed for a formulation
Equation 23	$y_6 = 0.00002L2^4 - 0.004L2^3 + 0.2778L2^2 - 5.4945L2 + 36.843$	Blue vs. L
Equation 24	$y_7 = (-0.6195a2) + 42.968$	Blue vs A
Equation 25	$y_8 = (-0.6593b2) + 37.775$	Blue vs B
Equation 26	$y_9 = (-0.3855c2) + 46.94$	Blue vs C
Equation 27	$y_{10} = -0.000000009H2^4 - 0.00008H2^3 + 0.0228H2^2 - 1.8083H2 + 42.327$	Blue vs H
Equation 28	$Blue_{Amount} = \frac{(y_6 + y_7 + y_8 + y_9 + y_{10})}{5}$	Amount of Blue PA-12 powder needed for a formulation

Equation 29	$y_{11} = (1.0495L2) + 16.344$	Yellow vs. L
Equation 30	$y_{12} = (-.2656a2) - 26.539$	Yellow vs A
Equation 31	$y_{13} = (0.4447b2) + 17.351$	Yellow vs B
Equation 32	$y_{14} = (0.049c2) + 19.641$	Yellow vs C
Equation 33	$y_{15} = (-0.077H2) + 34.579$	Yellow vs H
Equation 34	$Yellow_{Amount} = \frac{(y_{11} + y_{12} + y_{13} + y_{14} + y_{15})}{5}$	Amount of Yellow PA-12 powder needed for a formulation
Equation 35	$y_{16} = 0.00005L2^4 + 0.0091L2^3 - 0.5553L2^2 + 10.257L2 + 27.216$	White vs. L
Equation 36	$y_{17} = (0.3884a2) - 19.43$	White vs A
Equation 37	$y_{18} = (-0.1802b2) + 28.368$	White vs B
Equation 38	$y_{19} = (-0.027c2) + 27.726$	White vs C
Equation 39	$y_{20} = (0.1591H2) - 0.154$	White vs H

Equation 40	$White_{Amount} = \frac{(y_{16} + y_{17} + y_{18} + y_{19} + y_{20})}{5}$	Amount of White PA-12 powder needed for a formulation

Table 2 – Influence of each colour on each colour value

From equations 17 – 40, it can be seen that the equations do not follow linear relationships and the r^2 values (average 0.254) of these equations show that the equations do not fit well with the experimental data well (Supporting Information figures 13-32 and tables 4-5). This is largely because there are not many data points. This makes it challenging to find a pattern among the data. The amount of each colour to be used is then found by using these equations and inserting a target colour value then the amounts calculated for each value are summed and averaged to give an approximate value to be used for each colour.

It is evident that there are faults in the model as the model yields suboptimal fitness scores (table 3). In a genetic algorithm, a fitness equation is used to show how good a solution is (an appropriate fitness value is 1). In our genetic algorithm the fitness equation is equation 16, which is composed of several values (eq. 1-16).

This model works by generating thousands of colours with L, A, B, C, H values, and predicting formulations for them, and producing fitness scores showing how well they match up to a target colour. From table 3 it can be seen that the fitness scores for the predicted target colours and their respective predicted formulations are not optimal. The fitness scores for the predicted formulations are not optimal as the best 5 of the

2000 different variations (possible solutions) have an average fitness score of 0.62 (table 3).

Formulation	L1	L2	A1	A2	B1	B2	C1	C2	H1	H2	Fitness score
1686	19	19	51	49	-16	-15	53	49	343	49	1.162686
1881	19	17	51	50	-16	-15	53	80	343	193	0.549501
1537	19	19	51	46	-16	-16	53	93	343	42	0.497342
513	19	18	51	46	-16	-16	53	10	343	347	0.457467
248	19	19	51	51	-16	-12	53	14	343	95	0.441429
…											
211	19	10	51	1	-16	59	53	65	343	199	0.019006
64	19	14	51	1	-16	60	53	4	343	114	0.018982
1853	19	2	51	7	-16	60	53	48	343	320	0.018966
111	19	0	51	0	-16	55	53	36	343	209	0.018836
1775	19	4	51	3	-16	60	53	100	343	337	0.018709

Table 3 – Results of fitness score calculations for the prediction of formulations for target colours.

From the examples in table 4, it can be seen that the model can at times predict a formulation for the target colour which gives a logical amount of each colour with the sum of all four colours (red, yellow, blue, and white) being 100. However, the model can fail significantly, this is seen as the model can give values for the amount of the inks used that do not sum to 100, and in fact are quite a bit over 100, with some being at ≥120 (table 1). This shows that this model is not finding the relationship between the colours in a reliable and/or accurate way.

Target colour					Predicted Formulation				
L	**A**	**B**	**C**	**H**	**Red**	**Blue**	**Yellow**	**White**	**Total**
19	51	-16	53	343	20.31	19.76	17.48	42.36	99.91
29	61	-6	63	353	21.78	21.89	6.01	43.03	92.71
39	71	4	73	360	23.32	26.28	20.09	43.28	112.97
49	81	14	83	360	25	30.22	22.3	42.49	120.01
59	91	24	93	360	26.67	32.77	26.16	34.54	120.14
69	101	34	103	360	28.35	32.78	9.39	40.93	111.44
79	111	44	113	360	30.02	30.64	29.47	40.1	130.23
-1	31	-36	33	323	17.362	32.59	11.5	39.56	101.01
-21	11	-56	13	303	14.41	38.24	15.57	40.3	108.52
-41	-9	-76	-7	283	11.46	49.98	3.18	26.68	91.3
-61	-29	-96	-27	263	8.517	65.49	7.47	39.14	120.62
50	19	80	-20	333	17.01	34.22	21.76	32.94	105.93

Table 4 – Results for predicted formulations of target colours.

In short, the literature posed a genetic algorithm as a possible method to predict the formulations needed to obtain target colours. However, the correlation between predicted and experimental data, expressed as a correlation coefficient (r^2) values obtained when the behaviour of the colours was modelled was not ideal as the average r^2 value was 0.254, which is a very small correlation (ideally the r^2 value is ≥0.90). Stemming from this, some of the predicted data gave amounts that summed to more than unity, which is not possible in practice. This could be addressed by increasing the amount of experimental data used to make the model. As the amount of data points increase, the easier it should be to find equations which fit the data

better. The other negative of this model is that the fitness scores were suboptimal. This can be addressed by using mutation and crossover modifiers, so that an infinite number of values can be produced until values with high fitness scores are found. However, these changes might not overcome the limitations of the GA method. For this reason, an alternative technique was used, which utilized particle swarm optimization and simplex-lattice/centroid designs to predict the formulations for target colours.

Colour prediction via mixture design approaches:

The second method utilized particle swarm optimization and simplex-lattice/centroid designs. A {q,m} simplex lattice design for q components consists of points defined by specific coordinate settings in which each component takes the m+1 equally spaced values from 0 to 1, and all possible combinations (mixtures) of the proportions from this equation are used (eq. 41) [147]

$$x_1 = 0, \frac{1}{m}, \frac{2}{m}, \dots 1 \; for \; i = 1, 2, \dots, q$$

Equation 41 – Equation used for values of simplex lattice design[147]

It should be noted that in the standard Simplex lattice design, all the design points are on the boundaries of the simplex.[147] The standard simplex lattice for a three-component system uses the mixture design seen in figure 9.

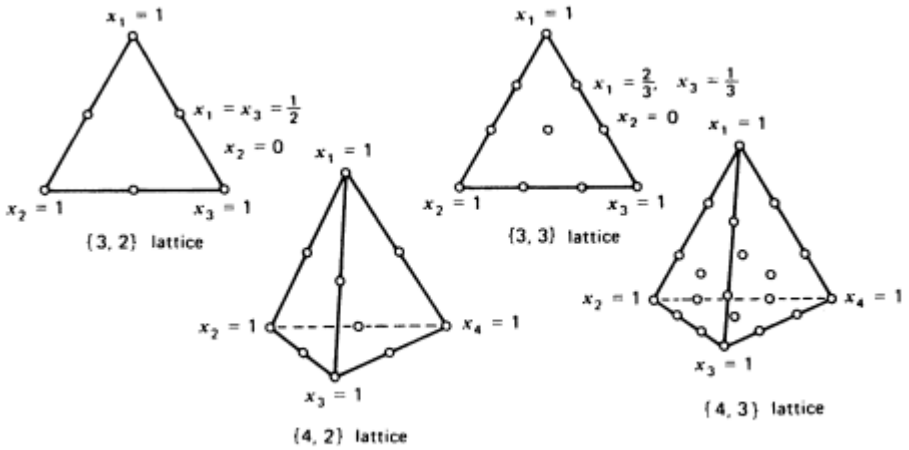


Figure 2.1 Some $\{3, m\}$ and $\{4, m\}$ simplex-lattice arrangements, $m = 2$ and $m = 3$.

Figure 9 – Configuration of design runs for a {3,m} and {4,m} with m = 2 and m = 3 simplex lattice design[147]

The standard simplex lattice design gave better results than the GA method. The r^2 value was 0.9896, which is very good and none of the points were outliers (figure 10). The standard effect of all the constituents were estimated (figure 10). The effect of the components matched the experimental observations as the blue and red coated PA-12 'inks' had a greater effect on the colour of the powder mixture than the yellow or white PA-12 particles.

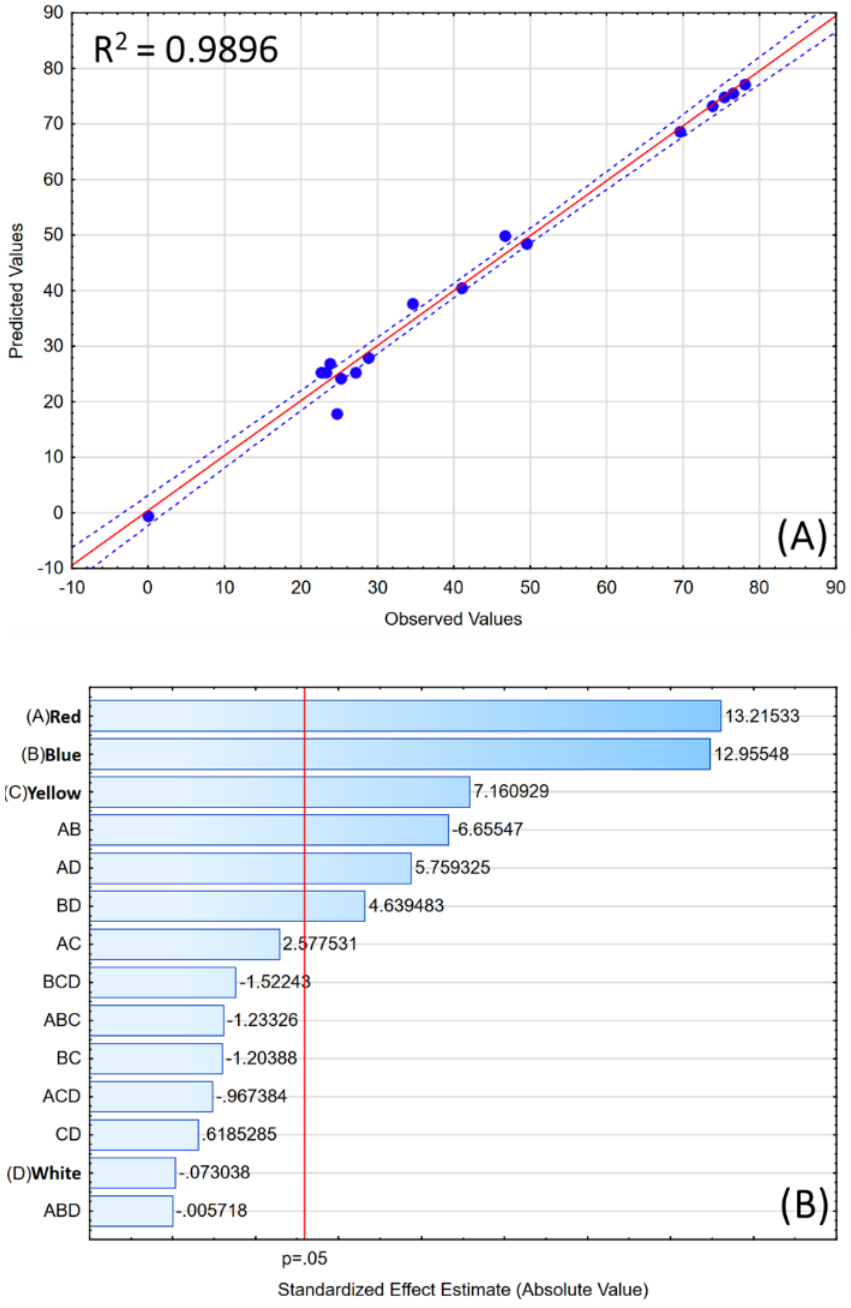


Figure 10 – Simplex lattice cubic model prediction. A.) Estimated vs predicted results B.) Pareto chart for standardized effects with respect to the model variables

This was a positive result as the model was following the general trends seen experimentally. The simplex space was mapped for the different colours against each other, and plots were produced (figure 11). From these plots, it can be seen that the

simplex lattice method yields values that are between 0 and 100, meaning that the Δ E values fall between 0 and 100.

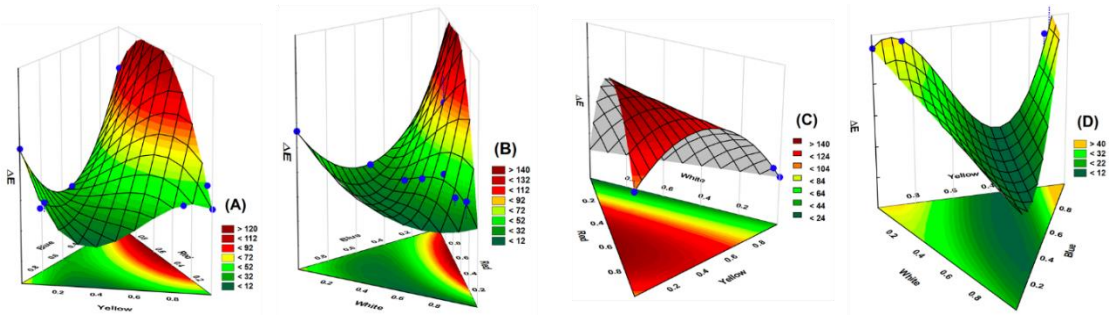


Figure 11 – Standard simplex lattice fitted surface for the different colours. A.) Red: Blue: Yellow B.) Red: Blue: White C.) Blue: Yellow: White D.) Red: Yellow: White

This model was starting to yield positive results, however an attempt to better the model was made, by adding eight more data points. These eight data points were based on formulations that were obtained from the model, and subsequently printed and analysed and then the results reinserted into the model. Therefore, more data points were added in order to see if the model would work for the entire colour space. The same simplex-lattice method was used with eight added points. The r^2 value was high (0.9863) and effect estimates of the differing coloured PA-12 particles matched up with the previous simplex-lattice model and the experimental method (figure 12).

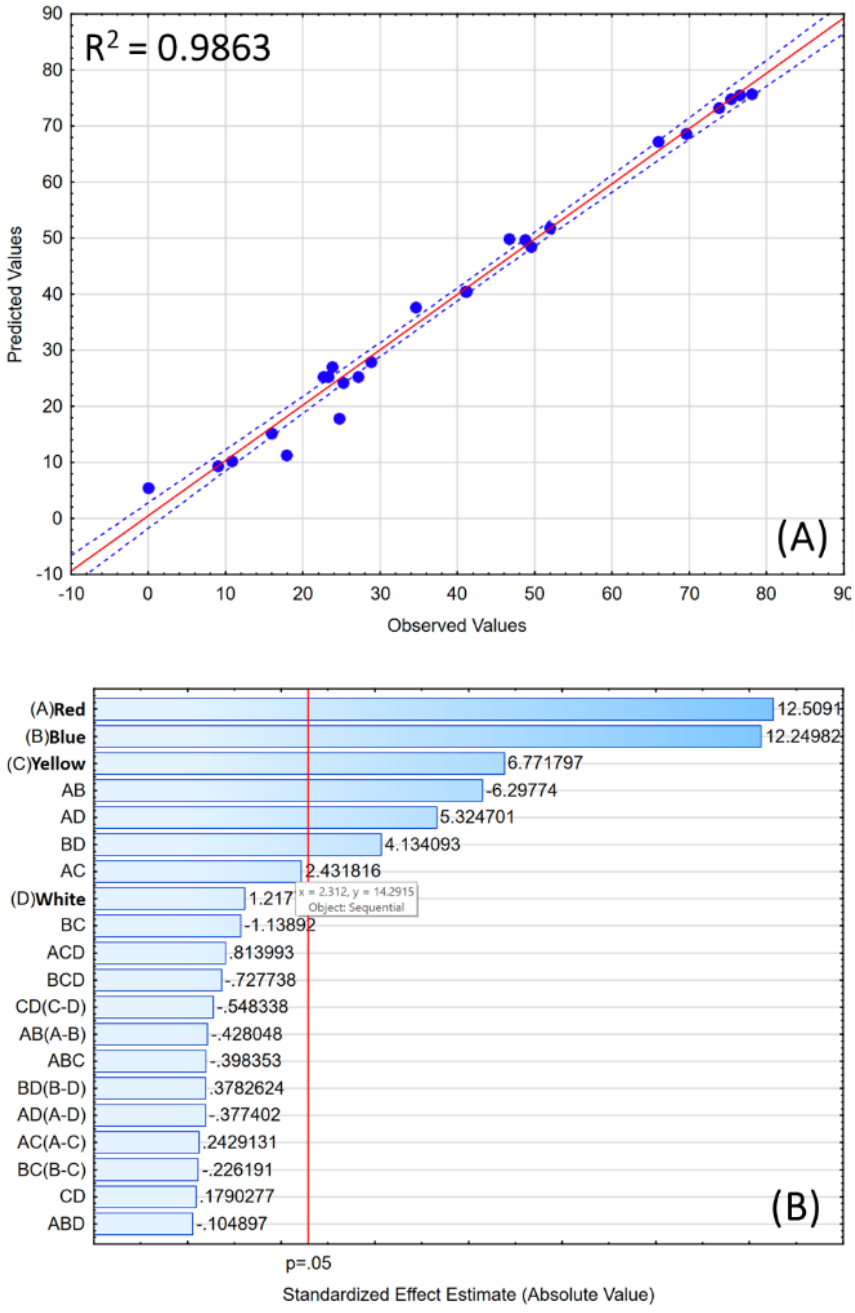


Figure 12 – Simplex-lattice plus eight points cubic model prediction. A.) Estimated vs. predicted results B.) Pareto chart for standardized effects with respect to model variables

However, the simplex lattice model does fail when more points are added as is evident from figure 13. It can be seen that the values relating to the amount of each

colour are not reliable as there are several values above 100, signifying that the model cannot adequately predict the formulations needed to achieve a target colour.

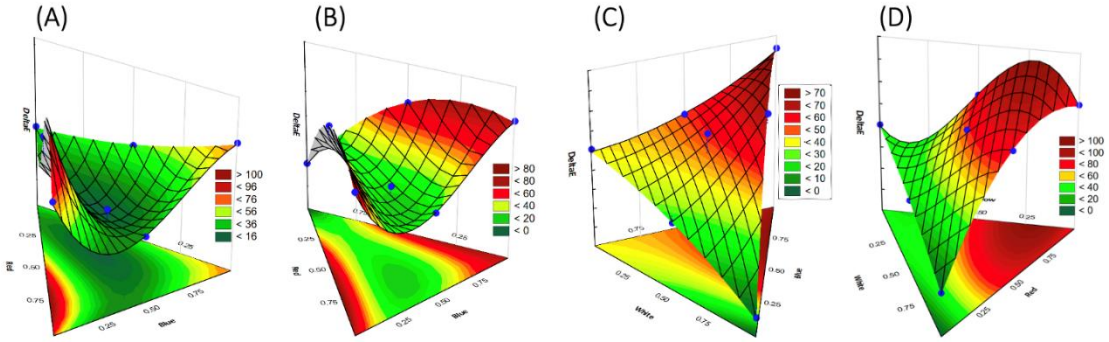


Figure 13 – Simplex lattice plus eight points fitted surface for the different colours. A.) Red: Blue: Yellow B.) Red: Blue: White C.) Blue: Yellow: White D.) Red: Yellow: White

To combat the issues with the simplex lattice design, a simplex centroid approach was tested. Simplex centroid design differs from simplex lattice in several ways. In the q-component in simplex centroid design, the number of distinct points is 2q – 1. The points correspond to different possible mixtures of the components. For a three-component system they would be the single component blends (1, 0, 0), the doublet mixtures (0.5, 0.05, 0) or all binary mixtures (1/3, 1/3, 1/3), and this can continue for all the components such that (1/q, 1/q, 1/q, …) the overall centroid point is reached.[147] For a three-component system, the simplex centroid method uses a special cubic instead of a standard cubic like in the simplex lattice (eq. 42).[147]

$$E(Y) = \sum_{i=1}^{q} B_i X_i + \sum_{i=1}^{q} \sum_{i>j}^{q} B_{ij} X_i X_j + \sum_{K=1}^{q} \sum_{j<K}^{q} \sum_{i<j}^{q} B_{ij} K X_i X_j X_K$$

Equation 42 – Special cubic model used in simplex centroid design[147]

The basic simplex centroid experimental points were used, and the model was made. The r^2 was quite high (0.9550), but lower than seen for the simplex lattice, and the estimated effects of the three main components were the same as aforementioned, as red and blue were of equal importance to the overall colour of the mixture, whilst the yellow was less influential (figure 14).

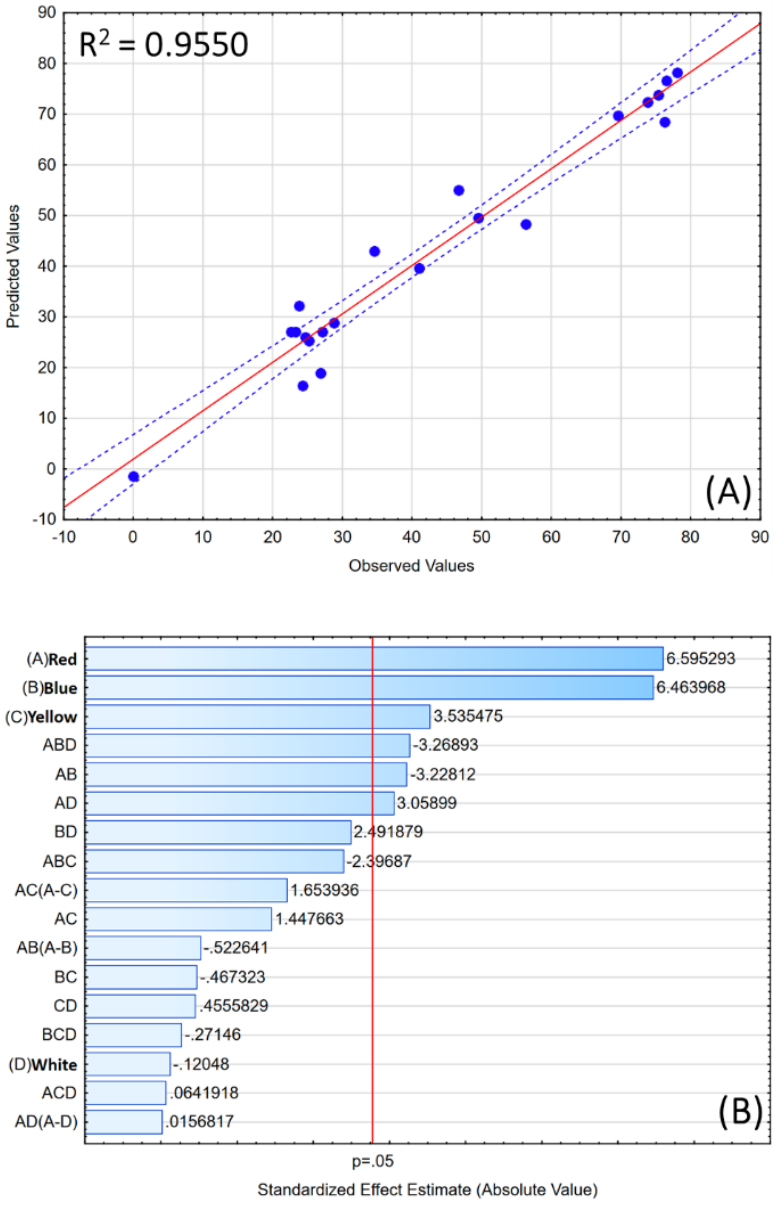


Figure 14 – Simplex centroid special cubic model prediction A.) Estimated vs. predicted results B.) Pareto chart for standardized effects with respect to the model variables

The relationship between the differing main components was further examined through contour mapping of simplex space. The results were positive as all the values relating to the amount of the colours were between 0 and 100, making this model sound (figure 15).

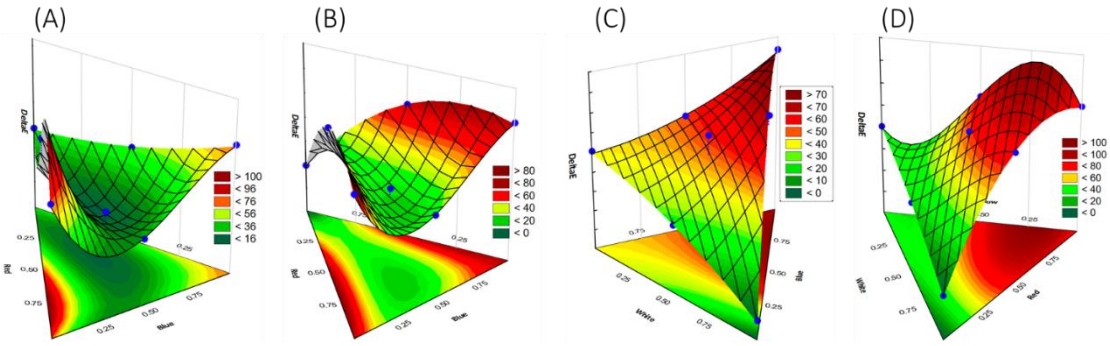


Figure 15 – Simplex centroid fitted surface for differing colours A.) Red: Blue: Yellow B.) Red: Blue: White C.) Blue: Yellow: White D.) Red: Yellow: White

The next step was to see if the addition of further data points would damage the model and cause it to fail. The r^2 value for the simplex centroid plus eight was 0.9521, which is satisfactory, and the estimated effect of the main components was the same as seen previously (figure 16). The eight points that were added were obtained from model predicted formulations which were subsequently printed and analysed and reinserted into the model.

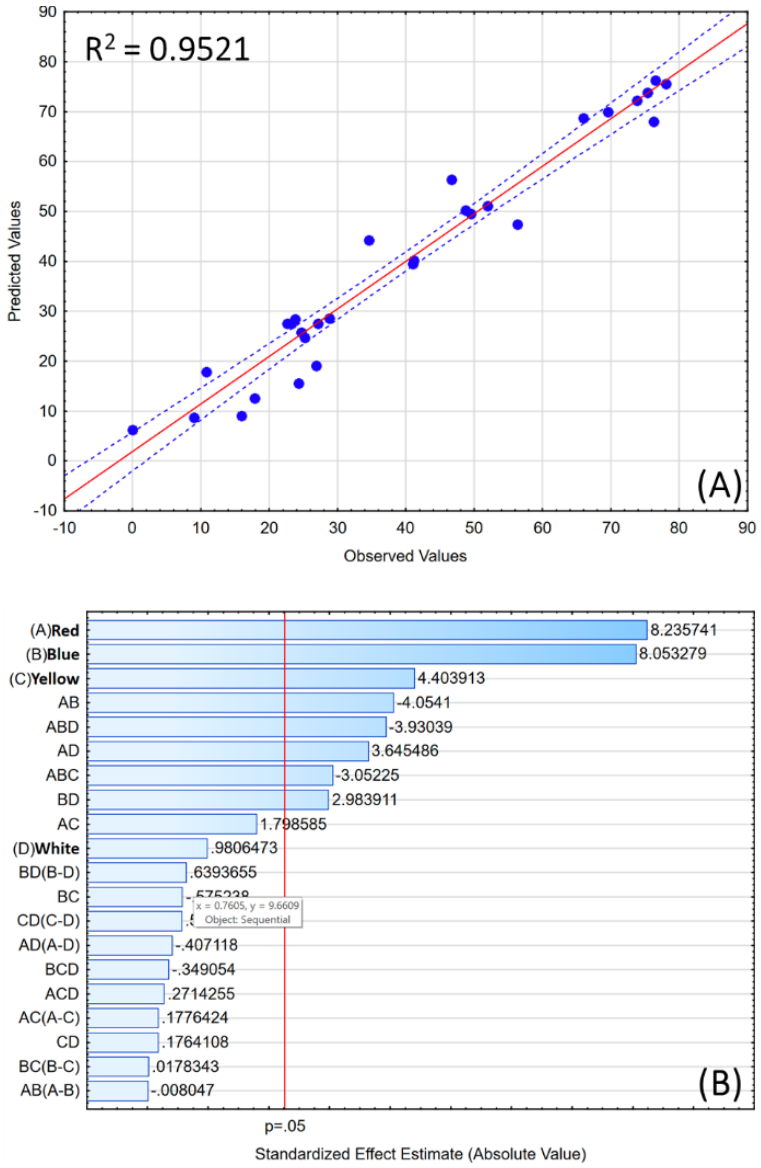


Figure 16 – Simplex centroid plus eight points special cubic model prediction. A.) Estimated vs. predicted values B.) Pareto chart for standardized effects with respect to the model variables

However, the simplex lattice plus eight points was also satisfactory up to this point of analysis, and its failures were only seen once the contour maps were analysed. This was a more positive result as all of the values were between 0 and 100, showing the increased reliability and accuracy of this model (figure 17).

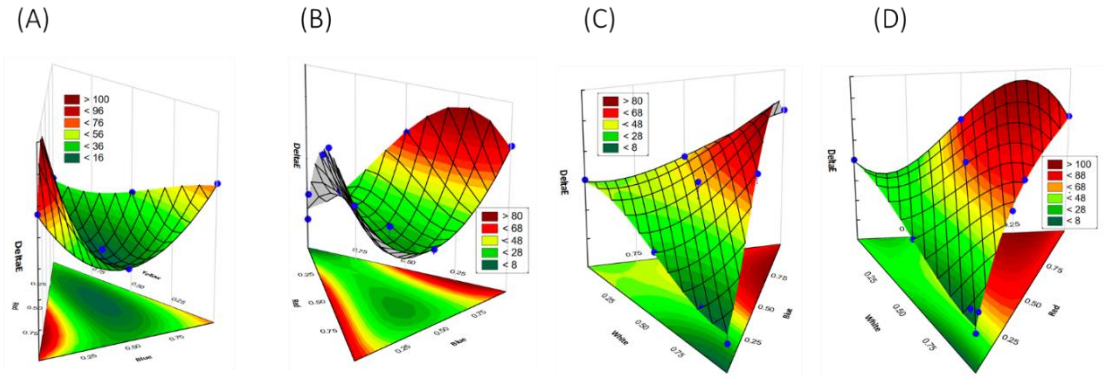


Figure 17 – Simplex centroid plus eight points fitted surface for different colours. A.) Red: Blue: Yellow B.) Red: Blue: White C.) Blue: Yellow: White D.) Red: Yellow: White

This was a positive result, which meant that the model could be used to predict the formulations for target colours for SLS printed parts. However, before printing more colour formulations, a model based on all the data points compiled up until that point was created. This model was made to see if the relationship between the colours maintained accuracy, even when more data was added. In total, 67 mixtures were used. The r^2 value was 0.9229, which is lower but still deemed acceptable, and the estimated effects of the main colours matched up with what had been seen experimentally. In previous models the red and blue PA-12 inks were the most influential, whilst the yellow powder was about 50 % as influential (figure 18).

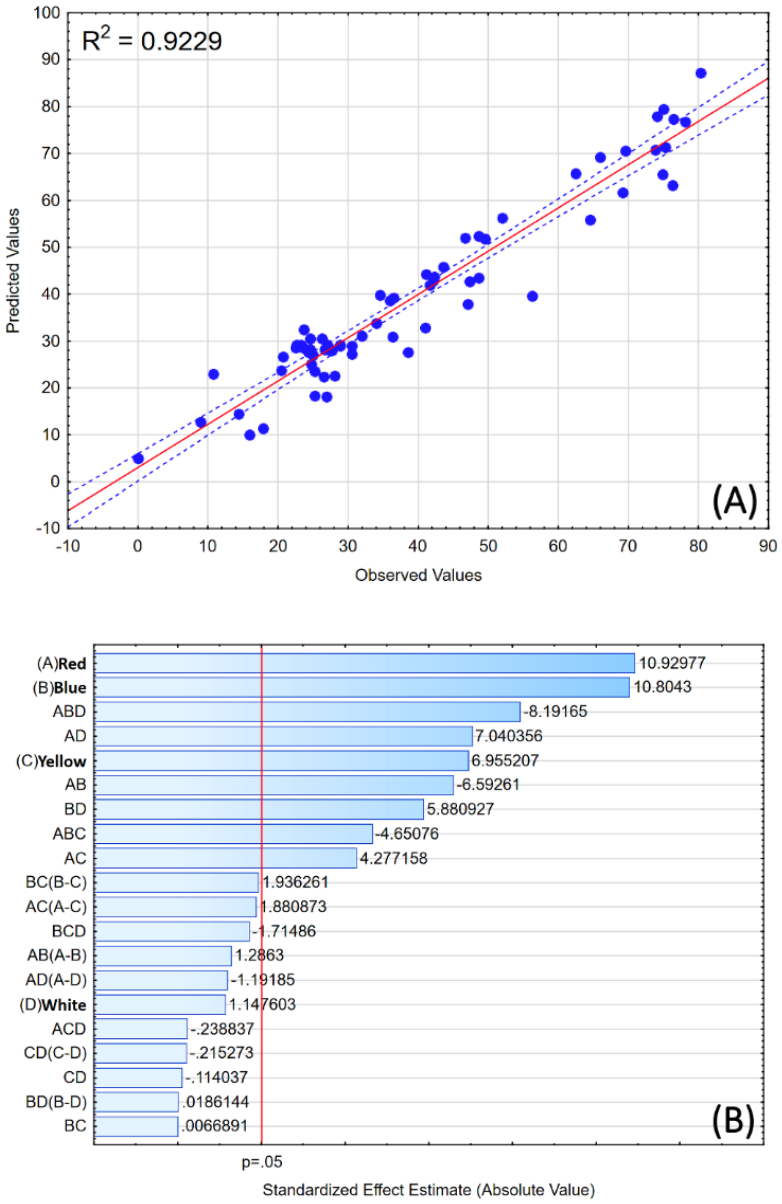


Figure 18 – Mixture design (67 points) cubic model prediction. A.) Estimated vs. predicted values B.) Pareto chart for standardized effects with respect to the model variables

The contour maps show that this type of model could adequately be used to predict the formulation of target colours as the values on the fitted curves were between 0 and 100 (figure 19).

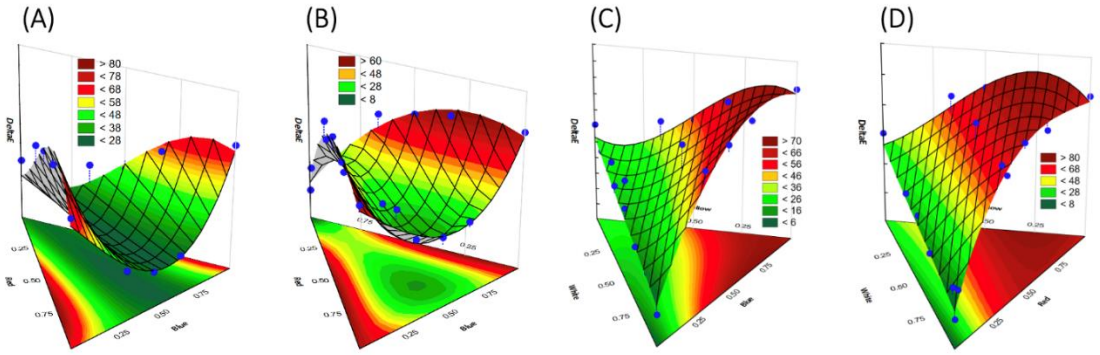


Figure 19 – Mixture design (67 points) fitted surface for the different colours. A.) Red: Blue: Yellow B.) Red: Blue: White C.) Blue: Yellow: White D.) Red: Yellow: White

From these preliminary results, it was decided that the simplex centroid special cubic model would be tested via predicting the formulation of several target colours and observing if the resulting printed parts had the desired target colours. From this point, the data gathered from this model was fed into a particle swarm optimizer to yield predicted formulations with the four component 'inks' (red, blue, yellow, and white). The combination of these two techniques would rapidly produce estimated formulations for target colours. The formulations for nine target colours were predicted with the simplex centroid special cubic model plus particle swarm optimizer. In these nine colours, three of them were green, two were blue, two were red, and two were brown (table 5).

Colour Target	Colour fraction (wt)				Results			
	Blue	Red	Yellow	White	L	A	B	Colour
Green	0.0626	0.0000	0.6418	0.2956	62	-13	5	green
Green	0.0987	0.0653	0.6055	0.2306	45	6	16	brown
Green	0.0877	0.0133	0.6255	0.2735	57	-6	6	green
Blue	0.7033	0.2333	0.0604	0.0030	19	5	-12	violet
Blue	0.6609	0.1550	0.1587	0.0255	22	-3	-13	Blue
Red	0.0574	0.8409	0.0714	0.3030	32	61	50	red
Red	0.0553	0.8006	0.0848	0.0594	30	50	48	red
Brown	0.2786	0.2917	0.0000	0.4297	27	10	15	brown
Brown	0.1428	0.5783	0.1070	0.1719	24	31	31	orange

Table 5 – Results from predicted formulations for the target colour of SLS printed parts.

From the table, it can be seen that several of the formulations were predicted correctly as two out of the three green targets were green. The blue and brown targets both correctly predicted one out of two of the targets. The red target also yielded positive results and both of the predicted formulations produced red parts. The results can be viewed in a positive light as the formulations that missed, resulted in colours close to the targets. This is evident as the formulation that failed to make blue yielded a violet part, and the brown formulation gave an orange part; these misses are quite close in colour space to the desired target. The model could be improved through a simple method. Boundary conditions could be introduced into the particle swarm optimization method, which automatically removes certain predicted formulations. An example would be that for a target red, there should always be a minimum amount of red, so that the mixture does not yield a part in another colour such as brown. Another example is that when targeting a green colour, only yellow PA-12 should encompass the majority of the mixture as both red and blue are more dominant. Also, there should be a very small percentage or no red at all. Boundary conditions such as these could greatly aid in making the model more

accurate. The modelling process with the combined simplex centroid plus particle swarm optimization yielded other notable observations.

From the formulations predicted by the model, it was seen that a variety of different formulations could potentially be used to produce the same target colour. This could have a beneficial impact on the commercial appeal of the project, as this could serve as a cost minimization tool. As is widely known, different paints cost varying amounts, as the ingredients to produce them can vary. The same applies in this project as each of the coloured PA-12 'inks' are more expensive than standard PA-12, as there is cost from the dye monomers and IBMA, and each of the dye monomers differ in value as well. This makes the use of the white component (standard PA-12) in formulations appealing as it can lower the cost whilst giving the same colour. By using this method, several formulations could be tested in ordered to determine the best compromise between results and cost. This could also be improved by adding the boundary conditions.

Conclusions:

In conclusion, via simple physical mixing of the coloured PA-12 coated particles with P(IBMA – Dye monomer), it was possible to create different colours, and subsequently print with them to establish the first colour mixing system for SLS. In total, 81 uniquely coloured parts were made through this method, and in this chapter, it was shown that it is also possible to predict the formulations needed to build parts with target colours (figure 20).

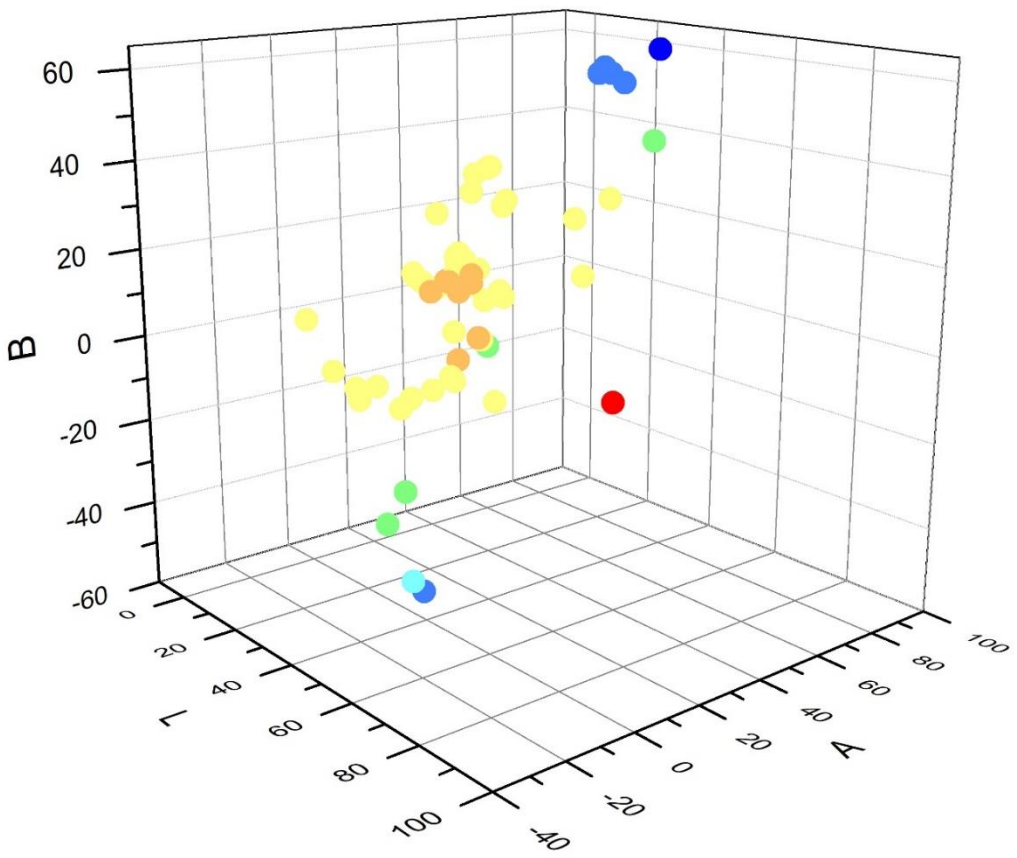


Figure 20 – Colours of printed parts in LAB colour space.

Figure 20 shows that through the CMYK colour mixing system that has been developed, it is possible to target a wide array of colours throughout colour space. However, when trying to target specific colours experimentally, there was a large amount of spent time and materials as the relationships between the 'inks' and the final printed colour were not clear. For this reason, two methods were tested in an attempt to model this colour mixing system. Simplex centroid design plus particle swarm optimizer was chosen as the best model to predict the formulations needed to target certain colours.

This model had satisfactory r^2 values and experimentally sound pareto charts and contour maps. When the model was used for formulation prediction the results were positive, but more work needs to be done to improve the accuracy of the model. It was also shown that the model has the potential to be used as a cost optimisation tool. In this segment of the project, a novel CMYK colour mixing system for SLS was optimized, and a modelling tool for formulation prediction and cost optimisation was developed.

Future Work:

In the future, a wider array of colours should be printed, and an updated library of available colours should be constructed. This would resemble the colour palette libraries of paint manufacturers, thereby making the process more user friendly. The colour model should also be further improved with more boundary conditions so that the accuracy of the model will improve. This will enable a potential user to predict the formulation of a desired product, produce a powder mixture, and subsequently print a structure with the target colour.

Materials and Methods:

Materials:

PA-12 (P2200) was purchased from EOS GmbH. PA-12 coated with P(IBMA-DB3MA) (Blue PA-12 ink), PA-12 coated with P(IBMA-DR1MA) (Red PA-12 ink), and PA-12 coated with P(IBMA-Y1MA) (Yellow PA-12 ink) were produced in house.

Methods:

Physical mixing of powders:

The calculated amounts of red and/or blue and/or yellow and/or white PA-12 based powders were added to a glass vial. The vial was physically mixed via a vortex mixer for 10 min, and subsequently left on a roller overnight, to ensure appropriate physical mixing.

Printing of coloured structures:

The coloured powder mixtures were deposited onto the build platform of an EOS Formiga P100 SLS printer. A powder bed temperature of 172° C, a chamber temperature of 150° C, a hatching laser power of 21 W, a contour laser power of 16 W, a hatching speed of 2500 mm/s, and a hatching distance of 0.25 mm were used for the printing of the coloured structures. Once cooled the structures were removed for visual inspection and colour analysis.

Analysis:

Colour of printed parts:

The coloured parts were removed from the printer and placed onto a white sheet of paper. An image of the surface of the square is taken with a NIX colour sensor, and the data are compiled.

Modelling and Optimisation of Colour Mixture

Colour Difference Method – Δ E CMC:

Basically, the colour difference method allows for the evaluation of the colour difference (ΔE) between two samples, based on the general model (Equation 1).

$$\Delta E = \sqrt{\left(\frac{\Delta L}{l \cdot S_L}\right)^2 + \left(\frac{\Delta C}{c \cdot S_C}\right)^2 + \left(\frac{\Delta H}{S_H}\right)^2} \quad (1)$$

ΔE is a pre-defined two-parameter model (*l* and *c*) widely used to evaluate the colour difference between the reference colour and the desired colour formulated by using a predicted recipe. Equation 1 is typically associated to the Colour Measurement Committee (CMC), typically expressed as CMC(*l*:*c*). When using a lightness weight (*l*) of 2.0 and a chroma weight I of 1.0, Equation 1 is intended for use with acceptability data (CMC(2:1)) whereas for perceptibility, CMC(1:1), l and c are assumed to be 1 and 1, respectively.

According to Equation 1 CMC colour tolerance is based on CIELAB, accounting for lightness (*L*), chroma I and hue (*H*), expressed as differences between sample colour possessing the L_2, a_2, and b_2 values and a reference colour L_1, a_1 and b_1 values, as follows:

$$\Delta L = L_1 - L_2 \quad (2)$$

$$\Delta C = C_1 - C_2 \quad (3)$$

$$\Delta H = \left(\Delta a^2 + \Delta b^2 - \Delta c^2\right)^{\frac{1}{2}} \quad (4)$$

with

$$C_1 = \left(a_1^2 + b_1^2\right)^{\frac{1}{2}} \tag{5}$$

$$C_2 = \left(a_2^2 + b_2^2\right)^{\frac{1}{2}} \tag{6}$$

$$\Delta a = a_1 - a_2 \tag{7}$$

$$\Delta b = b_1 - b_2 \tag{8}$$

The S_L, S_C, and S_H, corresponding to the weighting functions for the lightness, chroma, and hue components, respectively, are strongly dependent on the positions of the sample pair in the CIELAB colour space (Equations 9 to 11).[148]

$$S_L = \begin{cases} 0.511, & \text{if } L_1 < 16 \\ \dfrac{0.0409 \cdot L_1}{1 + 0.01765 \cdot L_1}, & \text{if } L_1 \geq 16 \end{cases} \tag{9}$$

$$S_C = \frac{0.0638 \cdot C_1}{1 + 0.0131 \cdot C_1} + 0.638 \tag{10}$$

$$S_H = S_C\left(F \cdot T + 1 - F\right) \tag{11}$$

where

$$F = \sqrt{\frac{C_1^4}{C_1^4 + 1900}} \tag{12}$$

$$T = \begin{cases} 0.56 + \left|0.2\cos\left(H_1 + 168°\right)\right|, & \text{if } 164° \leq H_1 \leq 345° \\ 0.36 + \left|0.4\cos\left(H_1 + 35°\right)\right|, & \text{otherwise} \end{cases} \tag{13}$$

$$H_1 = \begin{cases} H, & if\ H \geq 0° \\ H + 360°, & \text{otherwise} \end{cases} \quad (14)$$

with

$$H = \arctan\left(\frac{b_1}{a_1}\right) \quad (15)$$

Regression Model:

A multiple linear regression model, expressed as a third-degree polynomial (Equation 16), can be a useful tool to predict the composition of components in a colour formulation.

$$\Delta E_k^{\mathrm{RM}} = \sum_{i=1}^{m} \beta_i z_i + \sum_{i=1}^{m}\sum_{\substack{j=1 \\ i<j, i\neq j}}^{m} \beta_{ij} z_i z_j + \sum_{i=1}^{m}\sum_{j=1}^{m}\sum_{\substack{k=1 \\ i<j<k, i\neq j\neq k}}^{m} \beta_{ijk} z_i z_j z_k + \sum_{i=1}^{m}\sum_{\substack{j=1 \\ i<j, i\neq j}}^{m} \alpha_{ij} z_i z_j \left(z_i - z_j\right) + \varepsilon_k \quad (16)$$

where ΔE_k^{RM} represents the dependent variable (response) in the experimental condition *k*, β_i, β_{ij} and α_{ij} (*I* = 1, ..., *m* and *j* = 1, ..., *m,* where *m* stands for the number of components in the colour mixture) are the linear regression coefficients, z_i are the independent variables (colour *m*) and ε_k is the error associated with each experimental condition *k*.

In Equation (15), the model response (ΔE_k^{RM}) corresponds to the difference between the predict (desired) colour and reference colour (white). In order to estimate the regression coefficients β_i, β_{ij} and α_{ij}, the least square method was employed, and the function to be minimized is expressed as follows:

$$\Im = \sum_{k=1}^{n} \varepsilon_k^2 = \sum_{k=1}^{n} \left(\Delta E_k^{EXP} - \Delta E_k^{RM} \right)^2 \quad (17)$$

where ΔE_k^{EXP} is the experimental data in the condition *k*, computed in relation to the reference colour based on Equation 1. It is worth mentioning that the white colour is strategically assumed to be the reference colour (L_1 = 89, a_1 = 5 and b_1 = 4) in order to enhance the regression model ability to predict the true effect of the other colours in the mixture, for instance red, blue and yellow.

Optimisation Techniques:

The main challenge in colour formulation is to define the correct amount of each colour in order to achieve the desired colour target. In this work, two strategies have been adopted based on Genetic Algorithm (GA) and Particle Swarm Optimisation (PSO).

Genetic Algorithm

The modified genetic algorithm was employed to find formulations for target colours. The process relied on calculating a fitness score (eq. 16) based on the value of Δ E (eq. 15) for each of the randomly generated colour values. The highest scores were then analysed via equations 17-40, to yield formulations for the target colours.

Particle Swarm Optimisation

The optimisation procedure based on the swarm optimization (PSO) has been employed to determine the optimum mixture formulation.[146,149]

The numerical tasks basically consisted of the parameter estimation (colour composition z_i – Equation 16), in such way that the optimization problem can be defined as (Equation 18):

$$\min_{\underline{z}} \ \Im = \left(\Delta E^{\mathrm{RM}} - \Delta E^{\mathrm{Target}}\right)^2$$

(18)

subject to:

$$\sum_{i=1}^{m} z_i = 1$$

(19)

where $\Delta E^{\mathrm{Target}}$ is the desired value of the colour difference computed based on Equation 1, ΔE^{RM} corresponds to cubic regression model (Equation 16) used to evaluate the optimal estimated composition values (z_i), and *m* is the number of components (colours).

The sequential optimization procedure employed for determination of colour composition based on PSO technique try find the best candidates for the cubic regression model (Equation 16) by minimization of Equation 18. Basically, PSO considers that *n* particles (candidates) moving along a multidimensional search space exchange information with other particles iteratively to find the minimum of the objective function (Equation 18). Equations 20 to 22 are used to compute the velocity (*v*) and position (*x*) of the particles in the swarm, which are stochastically updated at each iteration as follows:

$$v_k^{(i+1)} = w^{(i)} v_k^{(i)} + c_1 \lambda \left(x_k^{best} - x_k^{(i)}\right) + c_2 \mu \left(x_{global} - x_k^{(i)}\right)$$

(20)

$$x_k^{(i+1)} = x_k^{(i)} + v_k^{(i+1)}$$

(21)

$$w^{(i)} = w_{max} - \frac{\left(w_{max} - w_{min}\right)}{1 + e^{\left[-\xi_1 (i - \xi_2)\right]}} \quad (22)$$

where c_1 and c_2 are particle acceleration constants, λ e μ random numbers with uniform distribution in the interval [0, 1], x_k^{best} is the best position of particle *k* in the swarm, x_{global} corresponds to the best position found considering all particles in the swarm, *k* denotes the particle and *i* is related to the iteration number. $v_k^{(i+1)}$ correspond to the velocity and $x_k^{(i+1)}$ is the position of each particle *k* in the swarm. $W^{(i)}$ is the inertia weight represented as a nonlinear decreasing sigmoidal function. w_{max} and w_{min} are the maximum and minimum values of the inertia weight $W^{(i)}$ in the interaction *i*, respectively, i_{max} is the maximum number of iterations (starting from iteration 1), ξ_1 and ξ_2 are related to i_{max} in the follow way $\xi_1 = 10/i_{max}$ and $\xi_2 = i_{max}/2$.

Chapter 5: Further Developments for SLS

In the previous chapters, several developments and improvements to the SLS technique have been made. We have shown that it is possible to print in colour and to print in higher resolutions. These are significant improvements to the SLS technique, but there are still major issues that plague this technique, thereby hampering it from its potential universal use. In this chapter, the aim is to start to address a few of the other problems areas of SLS. There are three deficiencies that were investigated:

1.) The prevention of biofouling on SLS printed parts.

2.) Printing with more than one material in a single build (multimaterial printing).

3.) Increasing or improving the mechanical properties of materials for SLS.

By addressing these three issues the areas of potential use for SLS produced parts could expand exponentially.

Materials which prevent the formation of biofilm for SLS

Introduction:

Anti-attachment materials are vital for the expansion of SLS, as PA-12 is prone to microbial attachment and biofouling.[150] In fact, PA-12 is used in a variety of applications, in which it is damaged by a range of biological organisms.[150–152] PA-12 is frequently used to produce water filters, due to its optimal filtering performance, but

it is rapidly fouled by waterborne organisms such as *Pseudomonas aeruginosa*, cutting the lifetime of PA-12 filters drastically.[150,153] PA-12 parts are often used for prototypes instead of consumer ready parts for a variety of reasons; one of them being that PA-12 fouls more rapidly than other polymeric materials. If a material was synthesized that was PA-12 based but coated with a polymer that prevents the growth of fouling organisms, the use of SLS made parts could be expanded and used in consumer products. The attachment mechanism of biological organisms can vary and is dependent on the organism, but they all follow a general mechanism, followed by biofilm formation (Figure 1). In order for a material to be made that prevents microbial attachment, it must be tested against a variety of organisms with different attachment mechanisms, rather than model organisms such as *E. coli*, better reflecting the natural environment.

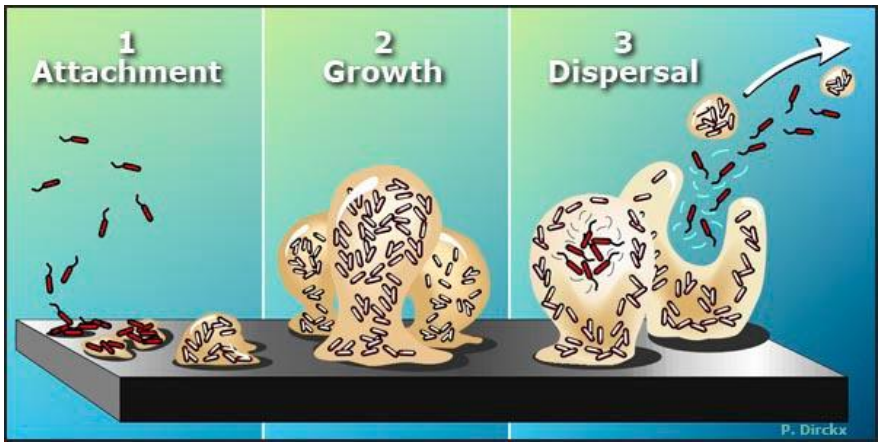


Figure 1 – General mechanism for the growth of biofilm. Step 1 is the attachment of the biological organism onto the substrate. Step 2 is the growth or proliferation of the organism of the substrate including the production of extracellular products, forming an immature biofilm. Step 3 is the formation of a mature biofilm on the surface of the substrate, which allows for dispersal of the microbes into the environment.[154]

One type of microorganism that can attach to PA-12 based parts and form biofilms is bacteria such as *P. aeruginosa*,[150,155] a human pathogen that is frequently found in a range of environments, including in water-based environments where PA-12 filters are used.[150,155,156] The attachment of bacteria generally causes a two-pronged detriment to the part. Firstly, the bacteria can spread diseases to people, this is often seen in biomedical devices such as catheters, resulting in a shorter shelf-life of the part.[155,157] Secondly the creation of the biofilm can affect the dimensions (through growth or degradation) of a part such as a water filter, thereby decreasing its efficiency.[158]

There are two generally accepted theories as to how bacteria attach onto abiotic surfaces. One is a where the initial attachment is localised, quite weak, and mainly due to Van der Waals, electrostatic, and hydrophobic forces, although specific protein-surface interactions can occur.[159] During this early phase of attachment, the bacteria can be removed relatively easily.[159] After the initial attachment, the bacteria excrete an extracellular matrix, commonly consisting of exopolysaccharides and eDNA. This attachment can be seen as irreversible, and to remove the resulting biofilm the surface must be scraped and chemically treated.[159]

The second theory is a three-step process, which is the same as above, with an additional interaction step prior to attachment. Bacteria first interact with the solid substrate through Lifshitz-Van der Waals forces at around 100 nm distance.[159] Then at a distance of ~20 nm electrostatic interactions start to occur, strengthening the adhesion, and finally at 5 nm the process of irreversible adhesion takes place.[159] It has

been reported that the speed of transition from reversible to irreversible attachment can be quite fast (1-5 min).[159]

Another type of microorganism that can attach to PA-12 is yeast, a morphological type of fungi. Two examples of this are *Candida albicans* and *Candida glabrata*. There are several differences between yeast and bacteria; yeasts are eukaryotes, have a different cell wall composition, slower growth, and have vastly different metabolisms.[160] Both species can form biofilms on abiotic surfaces, frequently this occurs on biomedical devices such as catheters and implants.[161–165] It has been shown that there is a pattern of increased biofilm with human diseases, as it is estimated that 65% of all human infections are of biofilm aetiology.[162] The formation of biofilm based on these yeast organisms is normally a 3-step process:

1. Early Stage – Adhesion of the yeast cells on the surface
2. Intermediate stage – Differentiation of yeast cells to hyphal cells (for *C. albicans*)
3. Maturation stage – An increase in the cell matrix

The adhesion stage occurs when the Candida cells are nearby the abiotic surface, and the adhesion is typically due to a series of proteins called adhesins; in *C. glabrata* these are the EPA proteins.[161–163,165] These three stages are seen often in biomedical devices as they are generally in favourable growth media, so adequate nutrition is provided for the growth of the yeast cells. Therefore, by making materials that discourage the growth and/or attachment of such organisms, biomedical devices could be printed via SLS.

Fungi such as *Chaetomium globosum* and *Colletotrichum gloeosporioides* are filamentous fungi, and such fungi can attach to PA-12.[151,166,167] Both fungi form spores, which allows the proliferation of the fungi to new environments. *C. gloeosporioides* is known as a food spoilage organism, causing the spoilage of citrus fruits such as oranges and lemons, as well as avocados, reducing crop yields and contributing to food waste.[168–171] *C. globosum* is an indoor contaminant that can be found on many surfaces, and it contributes to indoor air pollution via release of volatile organic compounds (VOCs).[166,172–174] The release of VOCs occurs in both household and industrial settings, which can have health implications and causes indoor air pollution. [166,172–174] Both species can attach on wide array of abiotic surfaces such as food packing, kitchen surfaces, bathrooms tiles, etc. Additionally, the attachment of these organisms, and subsequent growth, causes material damage on the surface that it is attached on, leading to repairs or replacements needing to be carried out. Therefore, preventing the spore attachment of these organisms in these different environments can both improve material function, as well as reducing food spoilage and indoor air pollution.

There are many other types of biological organisms that readily attach to PA-12, but the ones mentioned above serve as an example. By limiting the growth of these species on PA-12 parts, SLS parts could start to be used for more end consumer parts as the risk of biofilm growth would no longer be as high. In the past there have been a multitude of approaches used to combat biofilm growth and subsequent biofouling.

The treatments against biofilm formation can be classed into two groups the toxic (fatal) and non-toxic treatments. The fatal methods are most commonly used and can

be utilized after the biofilm has formed or can be inserted into the material itself. These treatments generally operate by exposing the biofilm to chemicals which are toxic to said species, thereby killing the organism. This can also be done through the incorporation of drugs and or metal nanoparticles (e.g. silver nanoparticles) into the material (e.g. plastics) so that the microorganisms are killed immediately.[175,176] However, there are problems with this method as the rate of release of the toxic element can occur rapidly, this can result in materials that are also toxic to humans.[177,178] Another important issue is that the constant exposure of these organisms to drugs can cause the organisms to become resistant to the drugs, thereby making these treatments less effective in the future and leading to fewer treatments available.[177–179] Other 'fatal' methods can be used as well to kill biofilms or to sterilise materials include ultrasonication and UV irradiation.[180,181] The non-fatal, or passive, methods can be described generally as coatings or materials, which can prevent the attachment of the biological organisms.[175,182] The properties by which materials can be anti-attachment can be attributed to several reasons: hydrophobicity, surface charge, topology, etc., as all of these could stop the initial interaction between the organism and the abiotic substrate.[183,184] An example of such a material is a paint used on the hulls of ships which limits the Van der Waals forces thereby stopping the attachment of marine organisms.[185] The non-toxic approach is advantageous as it allows the materials to be used for consumer applications that involve contact with humans, reduces the active antimicrobials in use and so damages the environment less, as well as reducing the likelihood of antimicrobial resistance to occur. Also, as these materials prevent attachment in a passive manner, there is no selection

pressure exerted on the microorganisms, reducing the likelihood of bacteria or fungi that can evolve to attach to these surfaces.

A frequent method to assessing whether a material is anti-attachment or fatal is by conducting a series of bioassays against biological organisms to determine if the growth of the species is inhibited. With this method one can determine if the inhibition of growth is because the samples kill the organism or because it stops its attachment to the substrate, because if it is killing the species then it is toxic.

The aim of this part of the project is to create materials which prevent the formation of biofilm for SLS. To do this a similar strategy to the one used to produce coloured PA-12 particles (chapter 2) can be used. It was shown that this strategy produced coated PA-12 particles that could be printed via SLS (chapter 3). The process is a simultaneous polymerisation and coating reaction which takes place in a $scCO_2$ reaction medium. This process is ideal as it produces uniform polymeric coatings on each PA-12 particle, and after the reaction the CO_2 is vented, leaving dry product that can be printed via SLS.(Chapters 2 and 3)[22,69,71] Also, $scCO_2$ is a green solvent as it is renewable, recyclable, non-toxic, and non-flammable.[22,69,186–188] However, instead of coating with P(IBMA-dye monomer) a coating of P(IBMA-biologically active monomer) would be used. Having IBMA as the main component would ensure that the resulting particles can be printed (chapter 3). The biologically active monomer in the coating would give the material the anti-attachment properties that are desired. There are several requirements that the biologically active monomer should have:

1. Does not contain halogens
2. Is an acrylate or methacrylate
3. Is known to have biological activity
4. Is soluble in $scCO_2$

The minor component should not contain halogens, as halogens can damage the steel autoclave that is used as the reaction vessel, and they are frequently not environmentally friendly.[30–32] The monomers should be acrylates or methacrylates, so that they can readily copolymerise with IBMA to form a coating on the PA-12 particles. There must be evidence that the minor monomer is biologically active, because if it is not then the resulting copolymeric coating will not have the desired anti-attachment property. Lastly, the monomers must be soluble in $scCO_2$ at the same reaction conditions used to coat PA-12 particles with IBMA (chapter 2), to ensure that the minor monomer is integrated into the polymer chain, and that the synthesized copolymer forms a coating on the PA-12 particles.[12]

Six monomers were chosen as potential biofilm preventing monomers. Four of which belong to a class of molecules known as terpenes. Terpenes have been shown to be biologically active and anti-attachment in some cases, and they can be easily acrylated or methacrylated.[5,6,189–192] The two other monomers are modified acid acrylates, which have been shown to have biological activity in past research conducted in the research group. All these monomers are $scCO_2$ soluble, and do not contain halogens. Another positive is that they can all be sourced from renewable sources and or waste streams.[193] Via the $scCO_2$ polymerisation and coating process PA-12 can be coated with P(IBMA-terpene methacrylate) or P(IBMA-modified acid

acrylate) to possibly yield biofilm preventing materials for SLS (figure 2). Once copolymerised with PIBMA, these biologically active monomers should be thermally stable as the polymer as a whole; will have the thermal properties necessary for SLS, therefore the biologically activity should remain after SLS, imparting anti-fouling/attachment properties to the printed part.

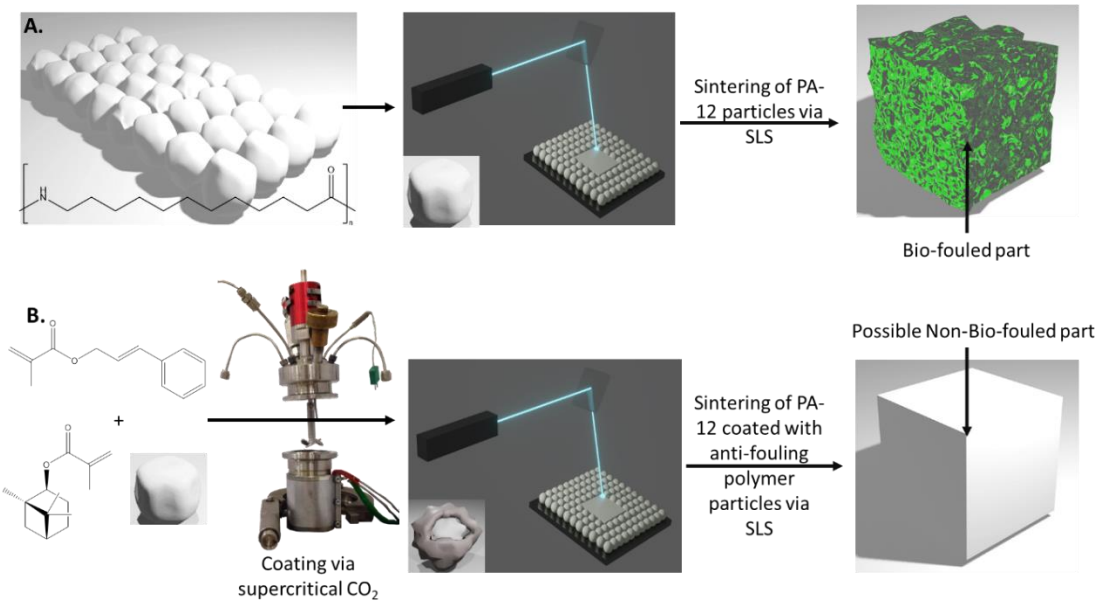


Figure 2 – Schematic for production of biofilm preventing materials for SLS. A.) Printing of standard PA-12 particles leading to a part that can be fouled. B.) Coating of PA-12 and subsequent printing of PA-12 particles coated with P(IBMA-biologically active monomer) to yield a part that does not suffer from biofilm formation or biofouling.

Results and Discussion:

To produce PA-12 particles coated with polymers with biofilm preventing properties, a small library of materials was created via the aforementioned $scCO_2$ process. A total of six different coatings were produced, four of which have the principal formula

P(IBMA-terpene monomer) and two P(IBMA-modified acid acrylate) (figure 3). IBMA was chosen as the major component of the coating as it has similar thermal properties to PA-12 ensuring that both the core and outer shell of the particles sinter at the same time.[12] The six minor monomers were selected as they can polymerise in $scCO_2$ and they have shown biological activity.

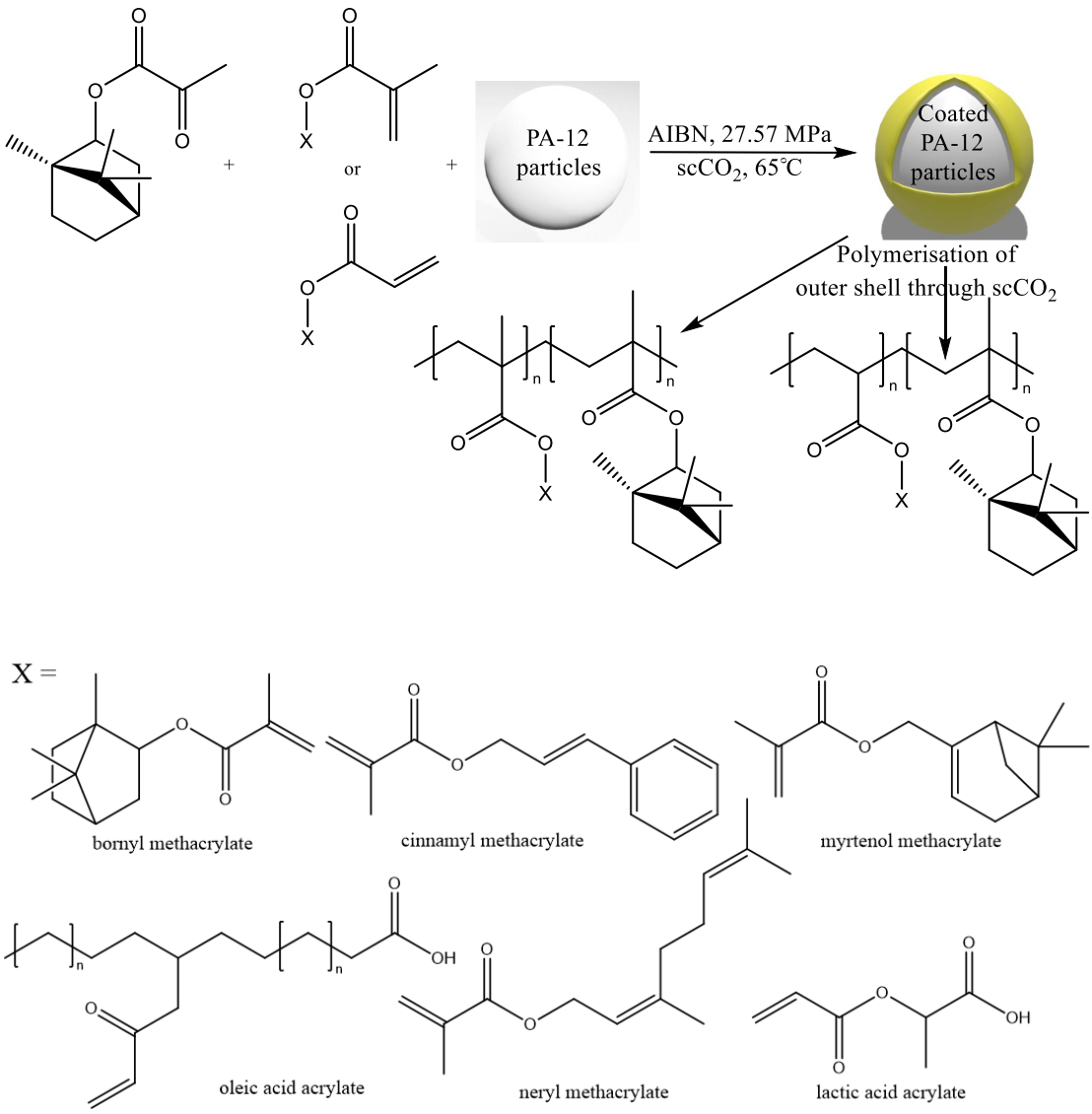


Figure 3 – Schematic for the synthesis of anti-attachment materials for SLS. A.) Reaction process for the coating of PA-12 particles with P(IBMA-biologically active

(meth)acrylate) via a $scCO_2$ process. B.) The structure of the six chosen biologically active monomers for the production of anti-attachment materials for SLS.

The coatings were made with three different concentrations (10, 20, 30 wt% of the minor component to amount of IBMA) for each of the biologically active monomers. This was done to see if the polymerisation and coating was successful at different concentrations of the minor monomer. The first copolymeric coating made was of P(IBMA-bornyl methacrylate). From the ^{1}H NMR it can be seen that the polymer peaks for each respective polymer have formed, albeit the conversion cannot be assessed (Supporting Information Figure 35). The conversion cannot be assessed as the monomer and polymer peaks overlap with each other; therefore, the amount of monomer and polymer present cannot be quantified via ^{1}H NMR. The polymers had reasonably consistent M_n, M_w, the Đ ranged from 2.40-5.88. These values are in line with what is frequently seen for FRP. ^{1}H NMR and GPC analysis had added preparation steps as the outer shell was extracted from the particle. This was done by dissolving the outer shell in dichloromethane (DCM), the coatings are soluble in DCM and the PA-12 core is not. The liquid was extracted and filtered, thereby separating the dissolved coating from the PA-12 cores. The DCM was then evaporated leaving a film of the coating, which can then be dissolved in the appropriate solvents ($CDCl_3$ and THF) for ^{1}H NMR and GPC analysis (figure 4). ^{1}H NMR and GPC were performed to ascertain the composition, conversion, and molecular weight, and dispersity of the coating in order to sure the coating was of sound quality for SLS.

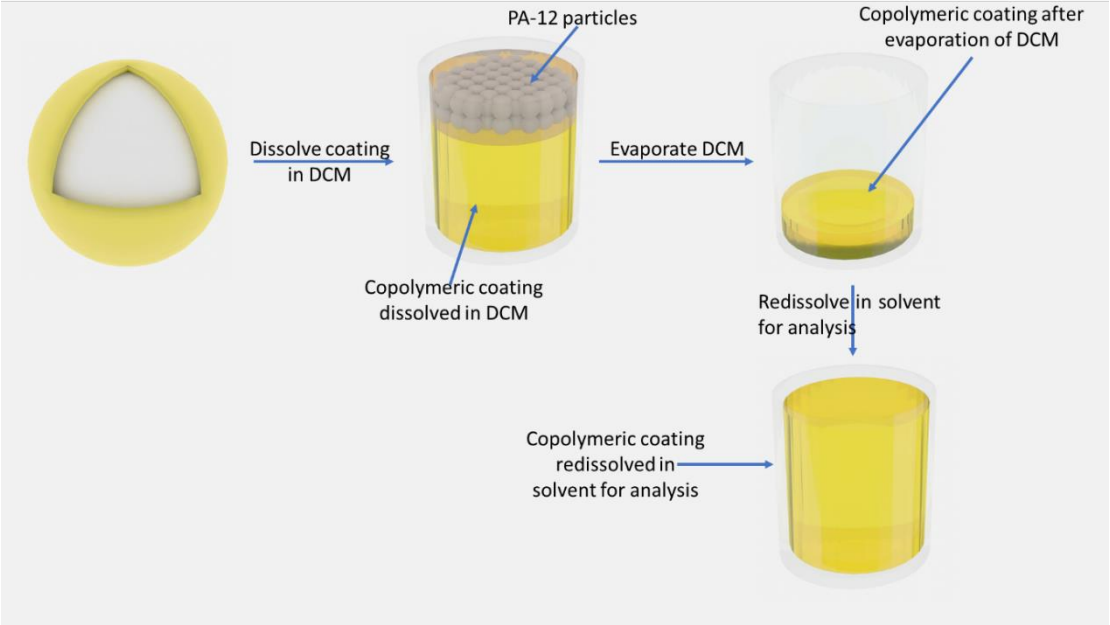


Figure 4 – Process of extraction of copolymeric outer shell from the PA-12 particles for further analysis.

DSC analysis indicated that the polymers were suitable for printing, as the T_g of the copolymeric coating was similar to the T_m of PA-12, this was previously explained in detail (chapters 2-3). This analysis was done for all the coatings and showed that each of the 10, 20, and 30 wt% coatings had the desired results. The ^1H NMR and GPC analysis showed that the copolymers had formed with M_n, M_w, the Đ typical of FRP, and the DSC analysis revealed that all have similar thermal properties (SI), as they all have the same major component (IBMA). All three wt% classes showed similar results, so the 30 wt% samples were chosen for analysis, as the polymerisation and coating was successful, and they have the largest amount of biologically active monomer, hence there is a greater chance that they will have activity towards biological organisms (table 1).

Sample	**co-polymer formation[a]**	**M_n (KDa)[b]**	**M_w (Kda)[b]**	**Đ[b]**	**T_g (^oC)[c]**	**T_m (^oC)[c]**	**T_c (^oC)[c]**
PA-12 coated with P(IBMA-bornyl methacrylate) 30wt%	Yes	25	56	2.2	139.2	172.7	140.3
PA-12 coated with P(IBMA-cinnamyl methacrylate) 30wt%	Yes	8	44	5.6	142.0	175.6	144.2
PA-12 coated with P(IBMA-neryl methacrylate) 30wt%	Yes	19	47	2.5	147.2	175.3	147.6
PA-12 coated with P(IBMA-myrtenol methacrylate) 30wt%	Yes	21	112	5.3	142.9	171.9	143.2
PA-12 coated with P(IBMA-modified oleic acid acrylate) 30wt%	Yes	29	149	5.1	147.9	176.1	149.4
PA-12 coated with P(IBMA-modified lactic acid acrylate) 30wt%	Yes	18	69	3.9	151.2	176.4	151.7

Table 1 – Results from coating PA-12 with P(IBMA-biologically active monomer) with 30wt% of biologically active monomer to IBMA. [a] Copolymer formation was

investigated via ^{1}H NMR. [b] M_n, M_w, Đ were measured via GPC analysis. [c] T_g, T_m, T_c were investigated via DSC analysis.

Once their composition and thermal properties were analysed confirming their suitability for SLS; their biofilm preventing properties were investigated. To test the biofilm preventing properties, these materials were printed via melt pressing instead of SLS printing. In melt pressing the user inserts a sample into a mould with the desired shape, and then this mould is pressed between two plates, which are heated slightly above the T_g and T_m of the polymer (Figure 5).[194] Melt pressing was chosen as the printing technique, because it is analogous to SLS as it takes the polymer through a similar thermal process, but instead of using a laser it uses heated plates.[194] The only difference is that there is a sharp temperature peak when the laser sinters the material, whilst melt pressing holds the material for a longer period of time at a temperature slightly lower than the peak temperature used in SLS. This means that the materials would be exposed to similar thermal treatment, hence the potential changes to the copolymeric coating due to heating would be the same, so if a part is made via melt pressing and shows anti-attachment properties it should do the same when printed via SLS. The major benefit of melt pressing is that small amounts of material (≤ 1 g) are needed to make multiple parts depending on the size (≥ 10 parts sized below 1 cm^3), so it was ideal for anti-attachment screening, because if SLS were to be used all the coatings would need to be scaled up, and at least 600 g of each sample produced, so to avoid waste and long optimisation steps, melt pressing was chosen as the production method. The parts printed via melt pressing were discs with a thickness of 1.5 mm and a diameter if 5 mm. These dimensions were chosen as they

allow for the discs to be placed into 96 well plates, in which bioassays are frequently performed.

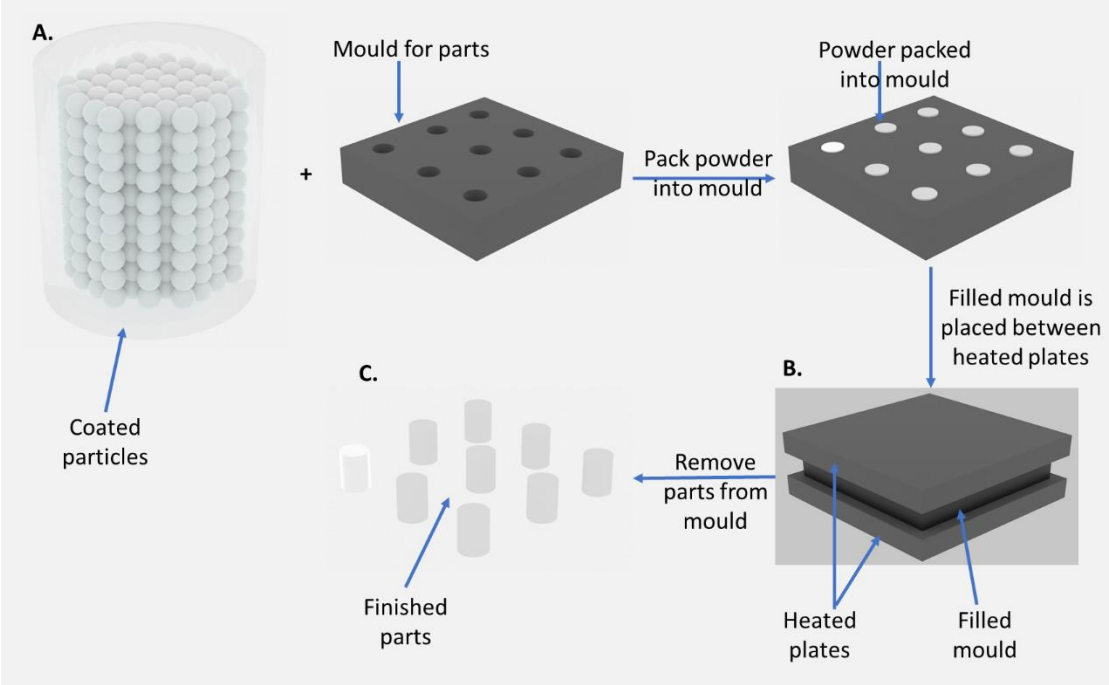


Figure 5 – Method of production of melt pressed parts for bioassays. A.) Step one is packing the coated PA-12 particles into the mould. B.) Step two is placing the mould between the two heated plates and applying pressure to the mould by closing the gap between the heated top and bottom plates. C.) Step 3 after the appropriate amount of time the sample is cooled and then removed from the mould, these can then be inserted into the 96 well plates.

The first assay conducted; tested the activity of the samples against the growth of *P. aeruginosa*. This bacterium was chosen as it is a common human pathogen seen on a multitude of devices such as catheters and water filters, but especially because it is known to attach to PA-12. Often PA-12 water filters can become fouled due to the attachment of *P. aeruginosa*. This assay was conducted in triplicate in a 96 well plate

with the 30 wt% minor monomer disc samples produced via melt pressing. The results show that these copolymeric coatings can limit the growth of *P. aeruginosa* (Figure 6).

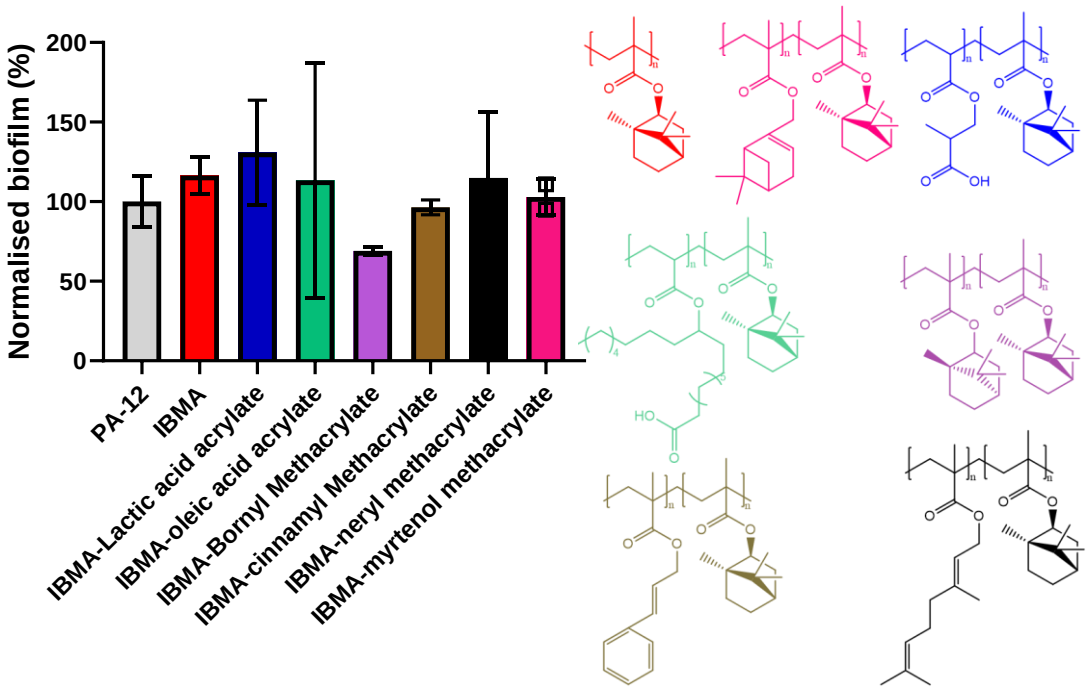


Figure 6 – Bioassay of printed parts (discs 1.5 mm in thickness and 5 mm in diameter) testing their activity against the attachment of *P. aeruginosa*. The control used was a disc made of 100% PA-12, the attachment of the bacteria to the coated samples was compared to the attachment of *P. aeruginosa* on the PA-12 control, so the PA-12 control has a value of 100% attachment. Assays were performed in triplicate.

In this test the control used was PA-12 and the attachment of the bacteria on the samples was compared to the attachment of *P. aeruginosa* on the PA-12 control, so the PA-12 control is known as 100% growth. A coating of just PIBMA was tested to check if it was the minor (biologically active) component imparting the effect or also the major component PIBMA. Large error bars are seen for the some of the samples (eg. P(IBMA-modified oleic acid acrylate)), because of a variety of possible reasons

(Figure 6). One is biological variation between replicas, as some might attach better than others, also this could be caused by experimental errors as for example a small difference in the size of the sample, or the fragility of the sample, could lead to variation.[195,196] It is evident that the discs made of PA-12 coated with P(IBMA-bornyl methacrylate) showed a reduced attachment of *P. aeruginosa,* by ~40% relative to PA-12 alone (Figure 6). The sample coated with just PIBMA showed no decrease in attachment of *P. aeruginosa*, confirming that the effect seen is due to the presence of bornyl methacrylate in the copolymeric outer shell. The reduction in attachment of this sample is significant as it could for example be used to extend the lifetime of PA-12 based water filters.

The next assay conducted was on *C. glabrata*, it was chosen as *C. albicans* does not attach to PA-12, but *C. glabrata* does. Although the exact mechanism of attachment is unknown, *C. glabrata* is likely to attach to the abiotic surface through a different mechanism by that of *P. aeruginosa* and bacteria. The fact that it has a different attachment mechanism is important, as the desired anti-attachment material should have inhibitory effects against organisms with a multitude of attachment mechanisms, as depending on the application the printed part could be exposed to different organisms. This assay was also conducted in triplicate as is standard for these assays. The results indicate that several of the samples can significantly reduce the attachment of *C. glabrata* compared to the PA-12 (control) (Figure 7).

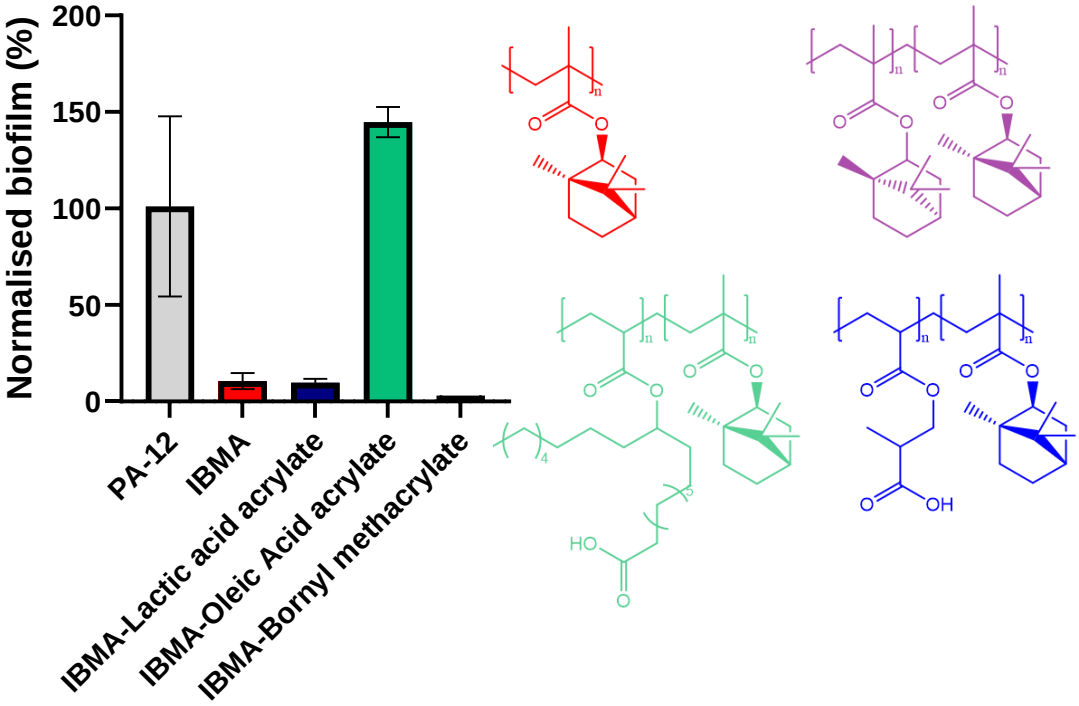


Figure 7 – Bioassay of printed parts (discs 1.5 mm in thickness and 5 mm in diameter) testing their activity against the attachment of *C. glabrata*. The control used was a disc made of 100% PA-12, the attachment of the bacteria to the coated samples was compared to the attachment of *C. glabrata* on the PA-12 control, so the PA-12 control has a value of 100% attachment. Assays were performed in triplicate.

Surprisingly one of the samples (P(IBMA-modified oleic acid acrylate)) showed an increase in the growth of *C. glabrata* as it had 150% attachment compared to the control which was PA-12 (Figure 7). This result could be due to the aforementioned variability of the assay due to biological variance and/or experimental error.[195,196] However, more likely it is because the polymer acts as a stimulus and/or food source for *C. glabrata* , as the error bars are small. This is speculation and further research into the mechanism of attachment must be done to ascertain the reason for this result. The other three samples showed a significant decrease in the attachment of

the yeast compared to PA-12. The sample composed of PA-12 coated in PIBMA and the sample coated in P(IBMA-modified lactic acid acrylate) had the same effect (~90% decrease in attachment), so it could be said that just the PIBMA has a very strong inhibitory effect towards the attachment *C. glabrata* (figure 7). The sample containing P(IBMA-bornyl methacrylate) showed almost complete inhibition of attachment of *C. glabrata* relative to *PA-12* , so the bornyl methacrylate segment of the copolymeric coating decreases the attachment of *C. glabrata* more so than PIBMA alone (Figure 7). This is similar to the result seen in the *P. aeruginosa* assay, showing that the samples with bornyl methacrylate have inhibitory properties towards the attachment of *C. glabrata*.

The activity of the samples towards the attachment of *C. gloesporioides* was performed as this organism is a fungus which forms spores; hence it has a different attachment mechanism to *P. aeruginosa* and *C. glabrata*. *C. gloesporioides* is known as a food spoilant, especially of citrus fruits, so if a printable material was made that decreased the attachment of this fungus, then printing food packaging via SLS could be advantageous. This assay was conducted in triplicate with PA-12 as the control. The assay showed that the samples decreased the attachment of the fungus by varying amounts (Figure 8).

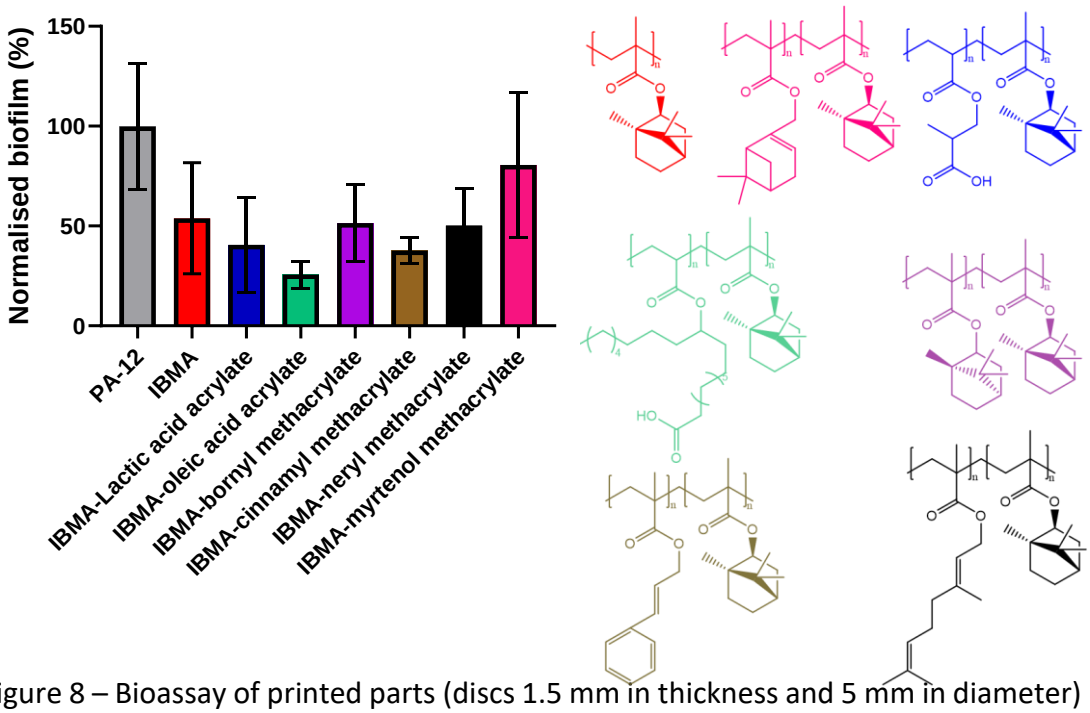


Figure 8 – Bioassay of printed parts (discs 1.5 mm in thickness and 5 mm in diameter) testing their activity against the growth of *C. gloesporioides*. The control used was a disc made of 100% PA-12, the attachment of the bacteria to the coated samples was compared to the attachment of *C. gloesporioides* on the PA-12 control, so the PA-12 control has a value of 100% attachment. Assays were performed in triplicate.

The sample coated with PIBMA showed a ~50% decrease in the attachment of *C. gloesporioides* relative to PA-12, which is significant (Figure 8). Other samples P(IBMA-neryl methacrylate) and P(IBMA-bornyl methacrylate) showed a ~50% decrease as well, which could mean that the main inhibitory effect in these samples stems from the IBMA and not the neryl methacrylate or bornyl methacrylate (Figure 8). Interestingly, the sample containing P(IBMA-myrtenol methacrylate) saw a decrease of activity of 25% which is less than the PIBMA sample, so myrtenol methacrylate could be acting as a stimulant and/or food source for the fungus (Figure 8). Three samples (P(IBMA-cinnamyl methacrylate), P(IBMA-modified oleic acid acrylate), and P(IBMA-modified lactic acid acrylate) showed a greater decrease in

attachment (~60%-80% decrease), hence they have a stronger inhibitory effect than the PIBMA samples, indicating that cinnamyl methacrylate, modified oleic acid acrylate, and modified lactic acid acrylate have a strong inhibitory effect towards the attachment of *C. gloesporioides* (Figure 8).

The last assay was conducted on *C. globosum* (another spore-based fungus), as it is known to attach to PA-12, and unlike *C. gloesporioides*, this fungus is an indoor contaminant and contributes to air pollution. The air contamination is a result of the fungal spores releasing volatile organic chemicals (VOCs), and much like the other three organisms its attachment can lead to the formation of biofilm and subsequent biofouling. This fungus can not only grow on household surfaces such as bathroom and kitchen surfaces, but also in industrial settings. This fungus can spread quickly as the wind can carry the spores onto a new surface and if the surface encourages the growth of the fungus, then a new colony can grow. A material that inhibits the growth of such a fungus could be used to make household products such as kitchen storage units, bathroom features, etc. This assay used PA-12 as the control and was run in triplicate. The assay showed that all the samples had an inhibitory effect towards the attachment of *C. globosum* to varying degrees (Figure 9). However, since a large error bar is seen for the myrtenol methacrylate containing sample, that result could be inaccurate possibly due to biological variance and/or experimental error (Figure 9).

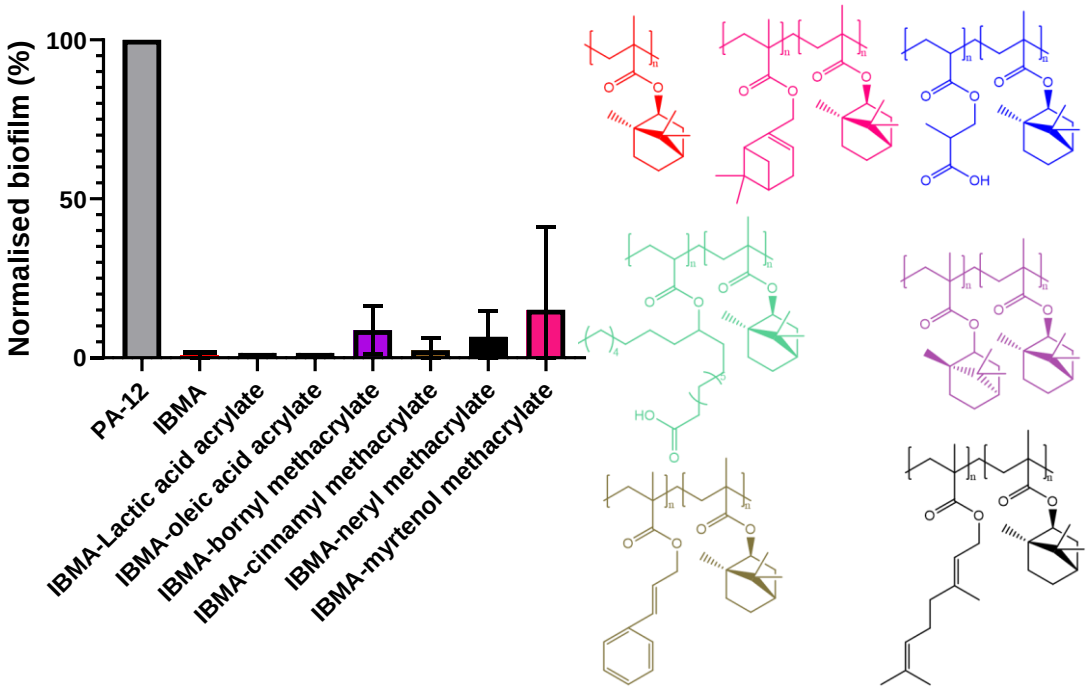


Figure 9 – Bioassay of printed parts (discs 1.5 mm in thickness and 5 mm in diameter) testing their activity against the growth of *C. globosum*. The control used was a disc made of 100% PA-12, the attachment of the bacteria to the coated samples was compared to the attachment of *C. globosum* on the PA-12 control, so the PA-12 control has a value of 100% attachment. Assays were performed in triplicate.

The sample containing just PIBMA as the coating had a very strong inhibitory effect (decreased attachment by ~99% relative to PA-12) (Figure 9). There are three samples that had a lesser effect on the attachment of *C. globosum* as they lowered the attachment of the fungus to ~5-15%, which is a strong effect, but since PIBMA alone provides a stronger effect than the minor components of the outer shell of these samples could be stimulating the fungus or counteracting the effect of the PIBMA (Figure 9). The sample with P(IBMA-cinnamyl methacrylate had a very similar effect to that of PIBMA (Figure 9). The acid acrylate containing samples showed almost complete inhibition of the attachment of *C. globosum*, hence the acid acrylate

segments could be providing a greater inhibitory effect, but the result is similar to that of PIBMA (Figure 9).

These four assays show that the printed samples had a significant effect on all of the tested organisms. This shows that the samples can be used to combat the attachment of a variety of organisms which have vastly different attachment mechanisms, as one is a bacterium, one if a type of yeast, and the last two are spore-based fungi. Several samples showed very strong inhibitory effects against particular organisms, such as the acid acrylate containing samples on *C. globosum*. The sample containing P(IBMA-bornyl methacrylate) showed inhibitory effects against all four organisms, showing great potential, but some of the other samples showed better results against particular organisms. This suggests that an optimal material could be made via mixing these materials pre-printing, as synergistic effects could be present. However, the goal of this segment of the project was to synthesize anti-attachment materials for SLS, and at this point the inhibitory effects of these novel materials had been proven, but it was not known if they were in fact anti-attachment or were toxic towards the tested organisms.

To ascertain if the samples were toxic or anti-attachment/biofilm preventing toxicity studies were performed on each of the previously assayed biological organisms. If the samples show toxicity towards these organisms, then their mechanism of action is killing the organism, hence they would not be anti-attachment or biofilm preventing. If the samples show no toxicity towards the organisms, then they are anti-attachment as they are just stopping the attachment of the organisms to the abiotic surface instead of killing the organisms.

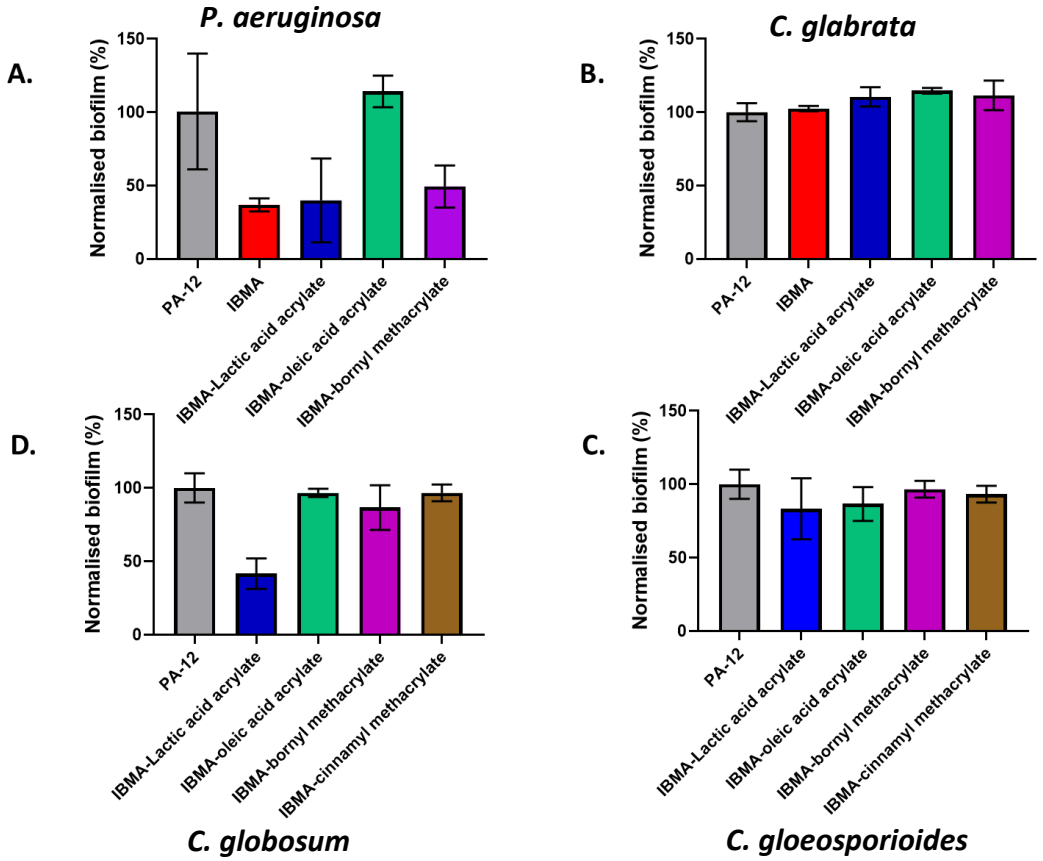


Figure 10 – Toxicity tests of the printed discs (1.5 mm in height and 5 mm in diameter) A.) Toxicity test of samples against *P. aeruginosa*. B.) Toxicity test of samples against *C. glabrata*. C.) Toxicity test of samples against *C. gloeosporioides*. D.) Toxicity test of samples against *C. globosum*. Assays were performed in triplicate.

There is a slight reduction (~60%) of Pseudomonas aeruginosa when in the presence of the samples containing PIBMA, P(IBMA-modified lactic acid acrylate), and P(IBMA-bornyl methacrylate). However, this is not necessarily a negative as only samples which reduce growth by more than 75% are considered toxic in this assay, so their samples could be said to just reduce the growth of *P. aeruginosa*, but they are not inhibitory or toxic to *P. aeruginosa* (Figure 10A). The samples are not toxic to *C. glabrata*, as none of them have values below 100%, in fact they are marginally higher (Figure 10B). The fact that the values are over 100% be due to biological variance

and/or experimental error. There is no decrease in the growth of *C. glabrata*, which proves that they are non-toxic and acts as an anti-attachment material towards *C. glabrata*. The samples were non-toxic towards *C. gloeosporioides* as all the samples had growth of about ~100%, the same as the PA-12 control (Figure 10C). Lastly, the samples were largely non-toxic against *C. globosum* as they exhibited about 100% growth (equal to PA-12 control), with the exception of the modified lactic acid acrylate containing sample, which reduced the growth of the fungus slightly (Figure 10D). From this toxicity screening it can be concluded that these materials and samples are non-toxic towards the tested organisms, hence they act through anti-attachment mechanisms rather than toxic/fatal mechanisms. This shows that the monomers and the polymers have different toxicities as the monomers are known to be toxic. Through the use of these anti-attachment materials, parts could be printed via SLS that can be used for household, biomedical, food packaging, etc. products. The mechanisms of biofilm prevention are not known for these materials and could differ for each active monomer, for example the bornyl methacrylate and modified oleic acid acrylate could have different mechanisms of anti-attachment. It is hypothesized that the reason for this property could be due to a change in hydrophobicity, surface charge, topology, etc., the nature of the mechanism requires further research.

Conclusions:

Through a novel $scCO_2$ polymerisation and coating process; PA-12 particles were coated with six different copolymeric outer shells consisting of P(IBMA-terpene methacrylate) or P(IBMA-modified acid acrylate). It was shown that these coatings

could be made reliably and with different concentrations of the biologically active monomers. These samples were subsequently printed into discs via melt pressing (analogous thermal process to SLS), the discs were then used to conduct bioassays in 96-well plates. The bioassays revealed that the discs had an inhibitory effect towards the growth of a diverse group of biological organisms. Depending on the tested organism, different materials had varying inhibitory effects, an example of this is the material containing modified oleic acid acrylate, because it encouraged the growth of *C. glabrata* and completely inhibited the growth of *C. globosum*. The sample containing bornyl methacrylate had an inhibitory effect against all four tested organisms. Toxicity tests revealed that the novel materials were not toxic towards the biological organisms used for the bioassays, hence the materials are anti-attachment. The use of such materials could lead to PA-12 based parts printed via SLS, which can be used as end consumer products for a variety of industries such as the biomedical industry (eg. Catheters, stents, implants, etc.).

Future Work:

There are several key experiments that must be performed to finalize this project. The reactions of the six different active monomers should be scaled up to the 1L scale, as was done with the coatings of P(IBMA-dye monomer)(Chapter 2). This will allow for the SLS printing of these anti-attachment materials. SLS printing of these materials must be optimized and their mechanical properties tested, as was done with the coloured PA-12 particles (Chapter 3). Prototypes of possible products should be constructed, such as an anti-attachment implant or food storage part. The diversity of the biological organisms tested against should be widened even further, to include

species such as marine organisms. The differently coated materials should be physically mixed, and their anti-attachment activity tested, in order to see if there are any synergistic effects. These materials should be mixed with the coloured PA-12 particles (Chapters 2-3), and the resulting parts tested, to see if coloured anti-attachment materials could be printed via SLS. Through these experiments this project would come closer to producing materials ready for consumer use.

Materials for improved mechanical properties

Introduction:

One of the current problems with PA-12 based parts built via SLS is that they do not possess excellent mechanical properties when compared to materials used for high performance parts. When compared to other polymers such as polystyrene or PMMA, PA-12 parts do have favourable mechanical properties. However, they are significantly weaker than materials such as carbon fibre and steel.[197–201] Therefore PA-12 is not used to build parts for 'high-performance' applications such as crucial aeronautics parts, engine parts for automobiles, and construction materials. There are currently several approaches towards the improvement of the mechanical properties of PA-12 based parts for SLS.

Generally, this has been done by coating or impregnating PA-12 particles with a variety of dopants. Such dopants could be glass (silica) particles, metal fillers, carbon nanotubes, ceramics, etc. (Figure 1) One of the methods used for improving the mechanical properties of PA-12 for Additive Manufacturing has been to add glass beads to the powder mix. The addition of the glass beads increased the tensile and flexural modulus by 85% and 36% respectively. But lowered the tensile and flexural

strength by 39% and 15% respectively.[202] Other properties such as decomposition temperature were changed, as the glass bead/PA-12 mix had a decomposition temperature of 390 ^{o}C, which is higher than that of PA-12.[203] The results were quite similar when hybrid ceramics were blended with PA-12 as the tensile strength of hybrid filled PA-12 are slightly lower than that of unfilled PA-12, but the tensile modulus and impact strength were increased compared to unfilled PA-12.[204] Depending on the blend of PA-12/carbon nanotubes the tensile strength, impact strength and flexural strength were changed by different amounts (-5%-50%, -40%-125%, 41%-151% respectively).[205] In the past composite particles composed of nickel/PA-12 have been developed in an attempt to improve the mechanical properties of PA-12 materials for additive manufacturing. When printed under the same conditions, a PA-12 part had a tensile strength, bending strength, and elongation at break of 42 MPa, 44 MPa, and 20% respectively whilst a nickel/PA-12 composite had 50 MPa, 60 MPa, and 10% respectively.[206] These are significant improvements to PA-12 used for SLS and other forms of AM, but the improvements have not been large enough to compete with materials such as steel and carbon fibre as they possess tensile strengths of 450-2350 MPa and 3500-5500 MPa respectively.[197–201] It is evident that this doping strategy does improve PA-12 based materials, but other routes must be taken in order to increase properties such as tensile strength more significantly.

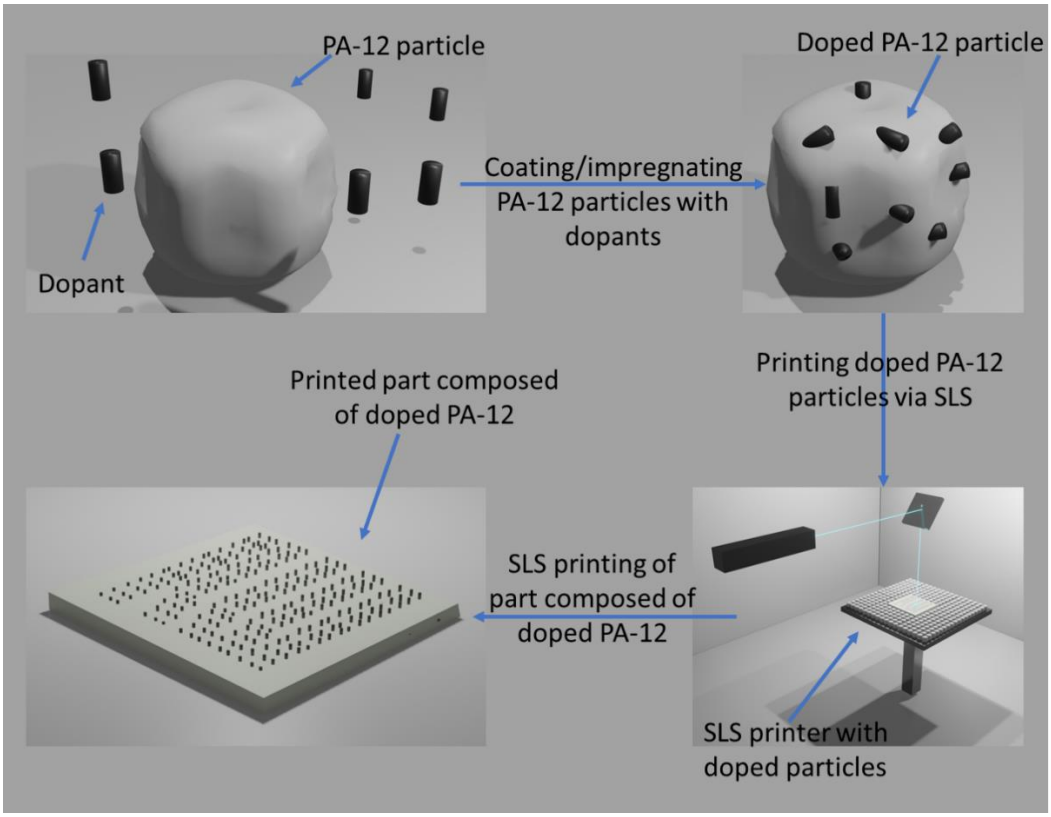


Figure 1 – Schematic of current strategies used for improving the mechanical properties of PA-12 for SLS and other Additive manufacturing techniques. PA-12 particles are coated through a variety of methods, depending on the dopant (glass beads, ceramic particles, metal particles, carbon nanotubes, etc.). These non-uniformly coated particles are then printed via SLS, yielding parts with the dopant unevenly spread throughout the part.

The strategy that we propose is to form a copolymeric outer shell on the PA-12 particles that can crosslink in situ during SLS printing (Figure 2). During sintering most of the coated particles will melt and a crosslinked polymer network can form in the melt pool, which should be evenly spread throughout the part. This is advantageous as the previous strategies can leave gaps in which no dopant is present, which can lead to stress points in which the part has a lower tensile strength than the rest of the

part. Crosslinking is known to increase the mechanical strength of polymers as it forms a network of bonded polymer chains that is more rigid than its non-crosslinked alternative.[207–212] Not only does it increase mechanical strength, but it changes other properties such as solubility, as the crosslinked polymer should no longer be soluble.[213] Therefore, in theory printing a part composed of a crosslinked network, should enable PA-12 based parts to have improved mechanical and physical properties, such as increased tensile strength.

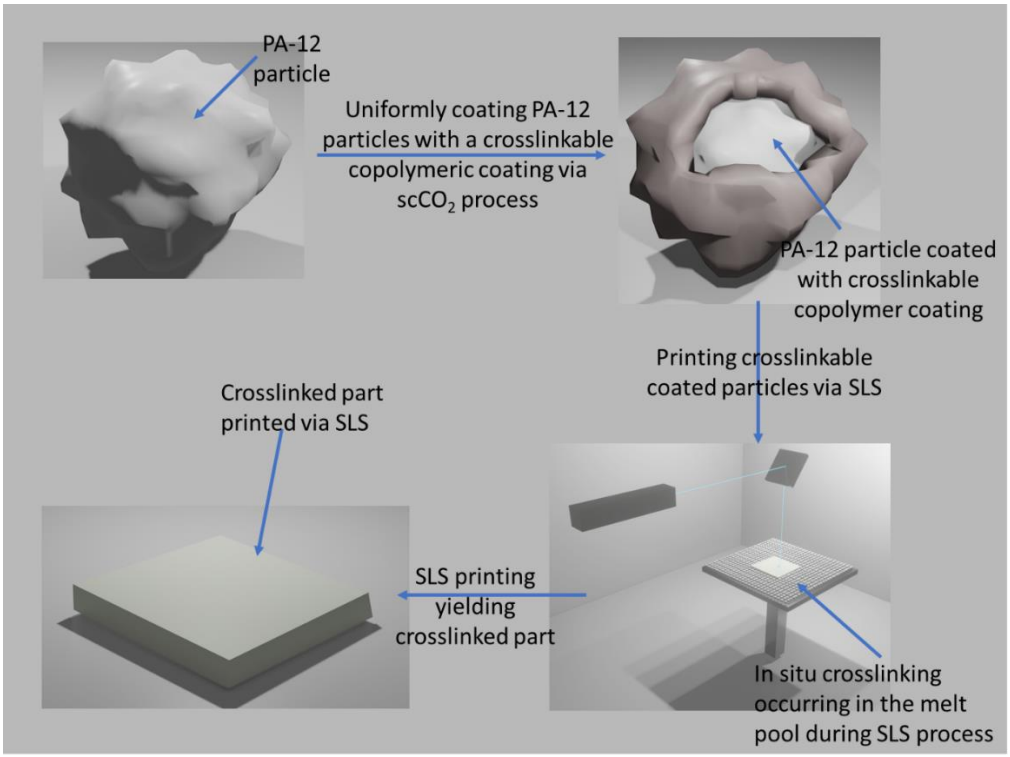


Figure 2 – Schematic for improving mechanical properties of parts via a copolymeric outershell which allows for in situ crosslinking to occur during printing. The copolymeric coating of the PA-12 particles can be added through the $scCO_2$ process used to create the coloured and anti-attachment particles for SLS (Chapter 4 and 6). These particles have active functional groups on the outer shell, enabling them to react and crosslink during SLS printing, to yield crosslinked parts with improved

mechanical properties. Crosslinking occurs through a variety of methods, three examples are:

1.) double bonds (eg. Vinyl groups) are present in the pendant groups of a polymer chain

2.) Hydrogen backbiting

3.) Epoxide – alcohol reactions [214–219]

The double bonds (eg. Pendant vinyl groups) can react with each other, or possibly other groups in a polymer chain to link two chains, and this process continues so that a network of bonded polymer chains forms.[216,217] Crosslinking can also form through different reactions such as hydrogen 'backbiting', this is when a mid-chain radical from an active polymer chain nucleophilicly attacks another polymer chain thereby linking the two polymer chains together.[214,215] The reaction between an epoxide and alcohol moieties can lead to crosslinking. This occurs when one segment of the polymer has an epoxide which is opened by an alcohol group. This reaction can create a bond between two polymer chains, which can lead to a crosslinked network.[218,219]

The correct type of crosslinking reaction must be chosen as frequently crosslinking can occur during the synthesis of a polymer or copolymer, and also at room temperature during the storage of said polymer. This is because the functional groups on these monomers and polymers are active, so they can react to branch and inevitably crosslink the polymer. It is desired for crosslinking to occur during the sintering process and not before. This is because if crosslinking occurs before then each individual particle will be coated with a crosslinked shell, so the strength that

comes from having a crosslinked network through the part would not exist as each individual particle would have its own network, hence the mechanical properties of the part would not be improved (Figure 3). What is needed is that the functional groups responsible for the crosslinking are stable enough that they do not react during the reaction or at slightly elevated temperatures. The functional groups must be able to be initiated by heat, so that when the laser sintering process occurs then the crosslinking process will happen in the melt pool, resulting in a part composed of a crosslinked network (Figure 3).

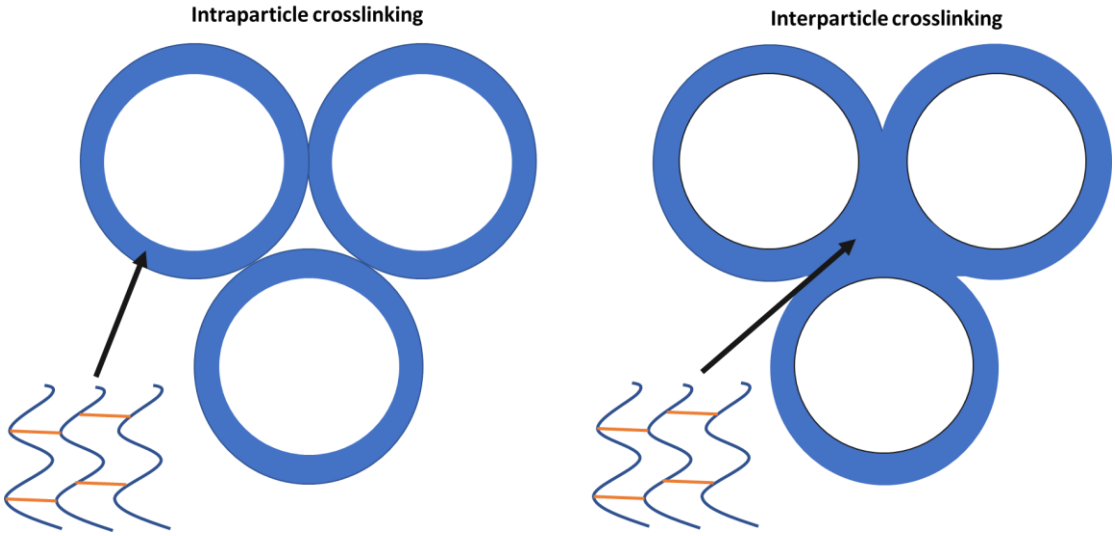


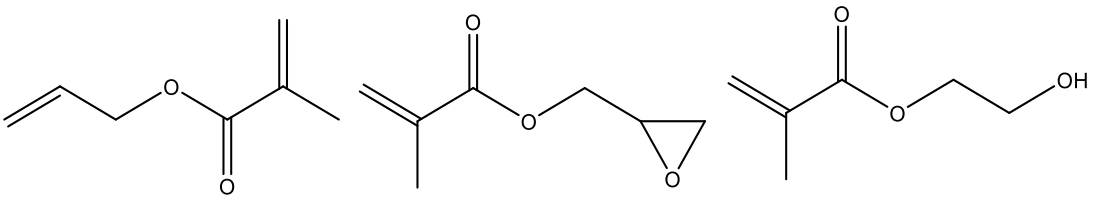
Figure 3 – Difference between intra and inter particle crosslinking. Particles whose outershell is crosslinked pre-sintering, will not result in a crosslinked network, what will occur is a part composed of individually crosslinked particles. Particles which can crosslink in-situ during sintering will result in parts with interparticle crosslinking, thereby having a crosslinked network throughout the part, resulting in improved mechanical properties.

To coat PA-12 particles with the aforementioned polymers a $scCO_2$ based polymerisation and coating process was used (Chapter 3). This system was also used to coat PA-12 particles in a variety of copolymeric coatings for the synthesis of anti-attachment materials for SLS. The system coats each PA-12 particle evenly with a coating composed of a copolymer with a major monomer and an active minor monomer. As was the case for the coloured and anti-attachment PA-12 particles, IBMA was used as the major component of the coating. This was because PIBMA has very similar thermal properties to PA-12, hence the sintering of the core and outer shell should occur at the same time.[12] $ScCO_2$ as the reaction medium is advantageous as when the reaction is completed the CO_2 is vented leaving a product that is dry and ready for use.[68–70] The minor (active) monomers were selected according to several aforementioned criteria. The active monomer must possess functional groups such as an active double bond on the pendant group or alcohol or epoxide groups, so that the resulting copolymeric outer shells can crosslink during sintering. The active monomer should contain an acrylate or methacrylate group, so that they can readily form a random copolymer with IBMA. The monomers must be soluble in $scCO_2$, so that the polymerisation and coating process can occur, as the monomer has to first be soluble in $scCO_2$ to form the copolymeric coating, and once a certain chain length is reached the copolymer will no longer be soluble in $scCO_2$. Two different routes towards the synthesis of crosslinked PA-12 based parts were taken:

- Route 1.) The use of allyl methacrylate (AMA) as the minor copolymer in the copolymeric outer shell (Figure 4). AMA has a pendant double bond, which is known to react and cause crosslinked polymers.

- Route 2.) Coating PA-12 particles with an outer shell which contains a minor monomer that contains an alcohol group (eg. 2-hydroxy ethyl methacrylate (HEMA)) and others an epoxide group (eg. Glycidyl methacrylate (GMA)) (Figure 4).

Allyl methacrylate was chosen as it does not contain any halogens and it possesses a pendant double bond which is known to cause crosslinking in polymers. It is also a methacrylate, so it should readily copolymerize with PIBMA, and it is soluble in $scCO_2$. HEMA was chosen as one of the components of route two, as it does not contain halogens, and it has an alcohol moiety which can be used to cause crosslinking when reacted with an epoxide. HEMA has a methacrylate and is soluble in $scCO_2$, hence it should readily copolymerise with IBMA and form an outer shell on the PA-12 particles.[67] GMA was chosen as the second component of route two, as it does not contain halogens, has an epoxide moiety, which should cause crosslinking when exposed to the alcohol moiety from HEMA (when exposed to heat ~200°C).[66,220] It has a methacrylate and is soluble allowing for the P(IBMA-GMA) copolymeric outer shell to form on PA-12 particles.



Allyl methacrylate Glycidyl methacrylate 2-hydroxy ethyl methacrylate

Figure 4 – Structures of monomers to be used as active monomers for the synthesis of coated PA-12 particles which can be crosslinked in-situ during sintering.

Route one towards crosslinkable PA-12 based particles depends on the synthesis of PA-12 particles coated in P(IBMA-AMA) (Figure 5). This polymer could be formed through FRP in $scCO_2$, but this reaction procedure could have an unwanted product as AMA can crosslink during FRP when performed in traditional organic solvents. However, $scCO_2$ is known to change the reaction kinetics of polymerisations which are normally conducted in traditional organic solvents, and the amount of active monomer used is small (≤5wt% compared to IBMA), so this copolymeric coating could be synthesized through FRP in $scCO_2$ without experiencing crosslinking.

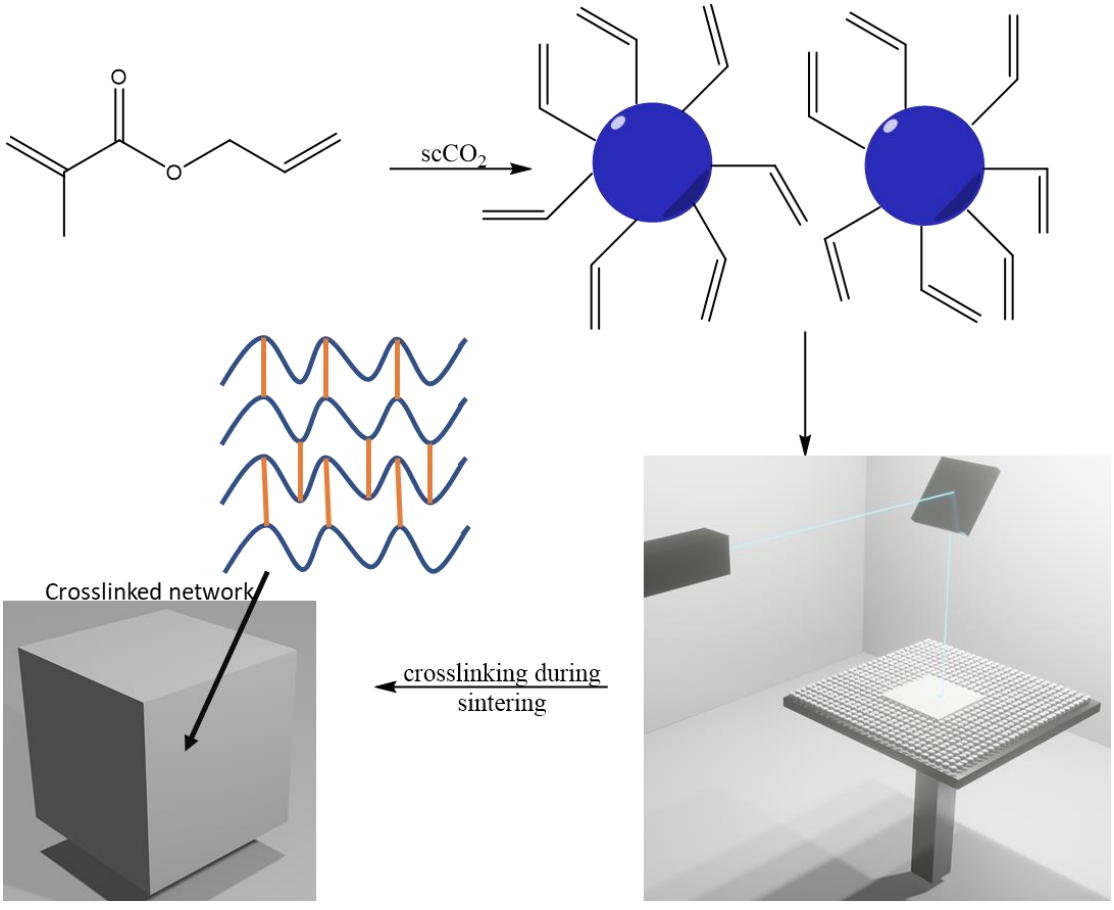


Figure 5 – Schematic of route one towards crosslinkable PA-12 based particles. Allyl methacrylate can be copolymerized with IBMA in $scCO_2$, in order to coat PA-12 particles, which have pendant vinyl groups on the outer shell of the particle. These

particles can then be printed via SLS, during which the pendant vinyl groups can react forming a crosslinked interparticle network, yielding a crosslinked part.

If crosslinking is seen during the synthesis of the coated PA-12 particles, different types of polymerisation techniques can be used to retard the reaction and thereby stop the crosslinking from occurring. Reversible addition fragmentation chain transfer (RAFT) is a polymerisation technique that could be used to address the possible crosslinking of AMA.[221] RAFT is a type of living polymerisation which utilizes a RAFT agent, which acts as a mediator for the reaction (Figure 6).

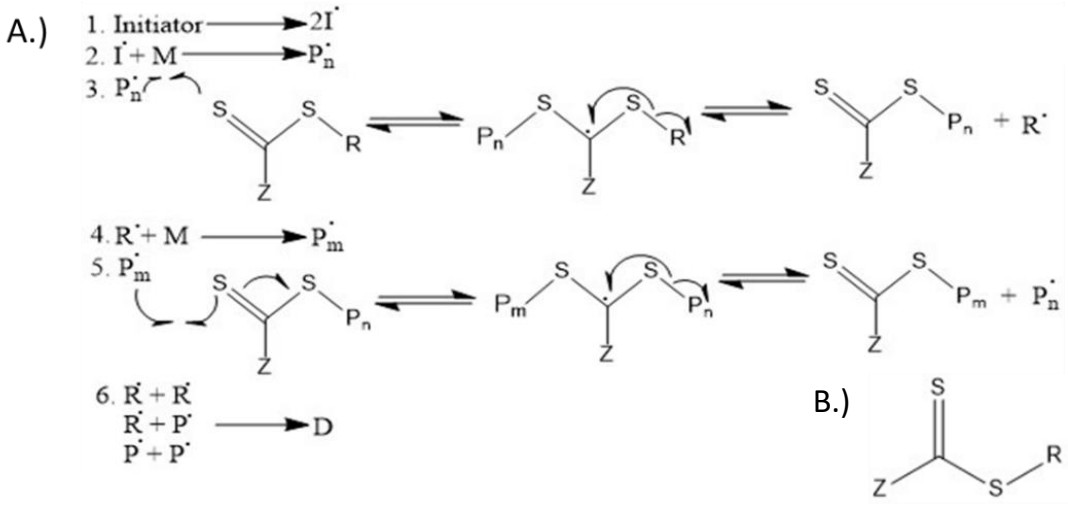


Figure 6 – Reaction mechanism for RAFT polymerisation. A.) Mechanism of RAFT polymerisation. The first step is the decomposition of the initiator into two radicals. In the second step a radical reacts with a monomer, which can start propagation of the polymer chain. The growing polymer chain with a radical then reacts with the RAFT agent, in a process where the R group on the RAFT agent is substituted with the polymer chain. The R group can then react with a monomer, starting another polymer chain, and the new polymer chain (Pm) can substitute the previous polymer chain

(Pn). This process continues until the reaction terminates. B.) General structure of RAFT agents, in which the Z and R groups can be tailored to suit particular monomers.

RAFT has been utilized in $scCO_2$ to synthesize block co-polymers with targeted molecular weights and low dispersities, but in this case would be simply used to stop the crosslinking from happening, via the retardation of the polymerisation.[87,221–224] The key element for RAFT to occur in $scCO_2$ is that the RAFT agent must be soluble in $scCO_2$, and the RAFT agent must be suitable for the chosen monomers.[87] Pacheco *et. al.* showed that RAFT agents such as CPDT can be used in $scCO_2$ to control the polymerisation of methacrylate monomers.[87]

Route two towards coated PA-12 which can crosslink during SLS hinges on the synthesis of two different coated PA-12 particles (Figure 7). One of which is coated with P(IBMA-HEMA) and the other with P(IBMA-GMA). These copolymeric coatings can be produced via FRP in $scCO_2$. However, to prevent crosslinking due to the reaction between HEMA and GMA, the synthesis of these coatings is performed in two separate autoclaves. Because even though it is known that the crosslinking reaction between these functional groups occurs at elevated temperatures, $scCO_2$ can sometimes lower the temperatures needed for reaction to occur reactions, which could mean that the crosslinking reaction could occur at a lower temperature in $scCO_2$ than in traditional solvents.[225,226] Also, it is practical to keep these products separate, to ensure that the coatings of each particle are uniform and that an even amount of each active monomer is present.

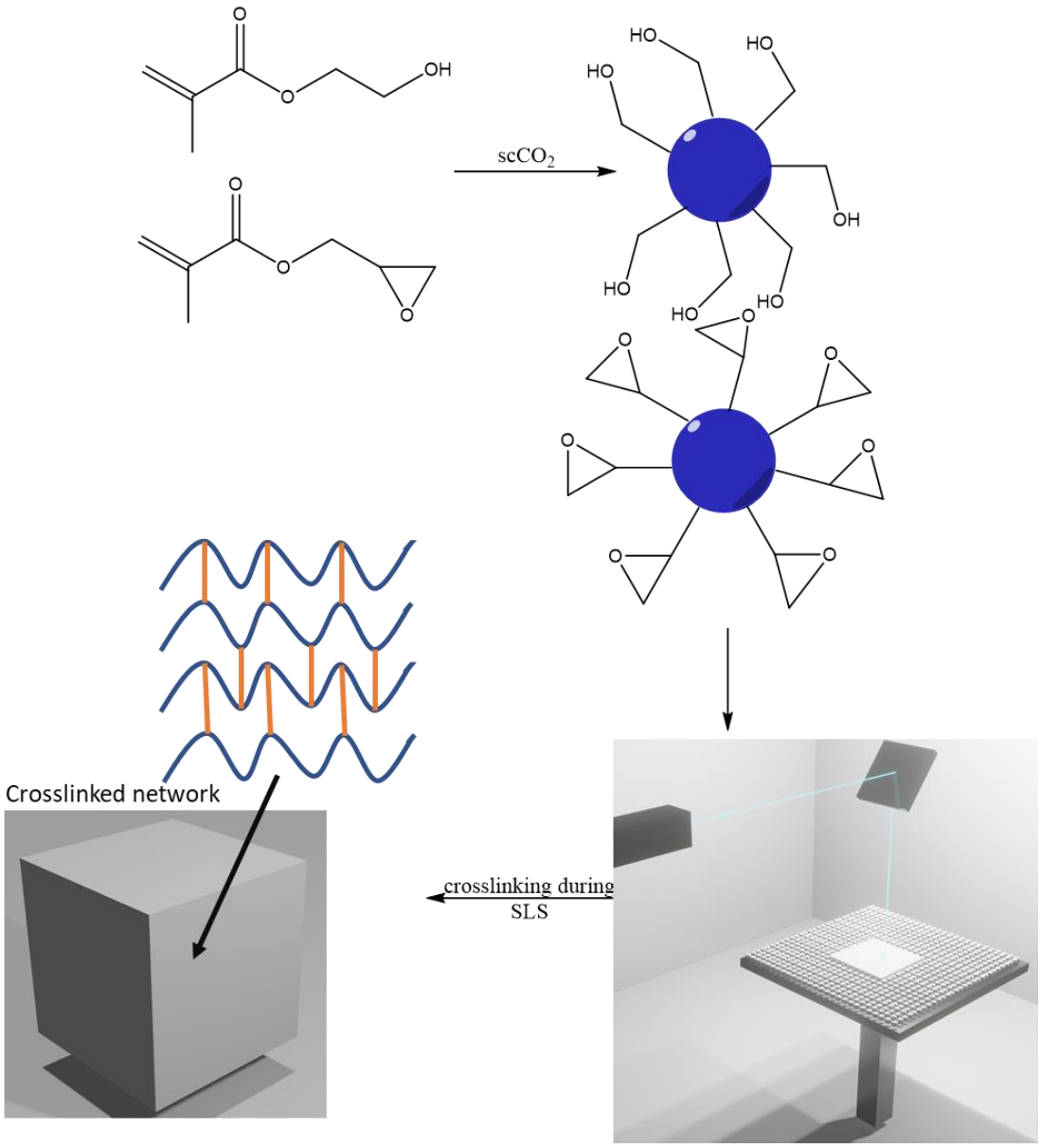


Figure 7 – Schematic of route two towards coated PA-12 particles which can crosslink during SLS. PA-12 particles can be coated with copolymers of P(IBMA-GMA) and P(IBMA-HEMA) via the use of $scCO_2$ as a reaction medium. These coated particles can then be physically mixed and then printed via SLS. During the printing the energy given by the laser can cause the alcohol and epoxide groups to react, yielding a crosslinked network and part. This process should ensure interparticle crosslinking instead of the intraparticle alternative.

The aim with this route is that after the coated polymers are produced, they can be physically mixed as was done with the coloured PA-12 particles to create different colours (Chapters 4-5), this blend of PA-12 particles coated in P(IBMA-GMA) and P(IBMA-HEMA) can then be printed via SLS. In theory once the laser hits the energy barrier for this reaction to occur should be passed and crosslinking should occur in the melt pool, resulting in a crosslinked part.

Results and Discussion:

Route one towards PA-12 based particles which can crosslink in situ during SLS – Coating PA-12 in P(IBMA-AMA):

The first route taken towards the synthesis of PA-12 particles that can be crosslinked in situ during SLS was the synthesis of PA-12 particles coated with P(IBMA-AMA). AMA was chosen as it has a methacrylate group, and a double bond on the pendant group. Having this co-polymer would leave multiple double bonds on the pendant groups of the polymer chain, thereby allowing for simple post-synthesis heat-based crosslinking. The double bond on the surface of these particles could in theory also be used for other purposes such as post-synthesis functionalization, as the double bond opens a host of possible chemical reactions.

At first the synthesis of the AMA containing outer shell was attempted through FRP in $scCO_2$. This reaction was performed in triplicate with a 5:95 wt% loading of AMA compared to IBMA, and all three reactions yielded crosslinked polymeric particles. The crosslinking was determined via submerging the reaction product (particulate powder) in DCM in an attempt to extract the coating (as is done for ^{1}H NMR and GPC

sample preparation), if there was no product extracted into the DCM, then it was determined that the outer shell was crosslinked. This is because the non-crosslinked P(IBMA-AMA) is soluble in DCM but the crosslinked is not. The fact that all the FRP reactions yielded crosslinked polymers is not promising, as the aim is not to make particles coated in crosslinked polymers, but to make coatings which can crosslink during SLS. To produce a non-crosslinked outer shell of P(IBMA-AMA) on PA-12, the reaction was attempted via RAFT. RAFT was used to try to minimize the crosslinking during the reaction, so that crosslinking does not occur during synthesis. The RAFT agent used was 2-cyano-2-propyl dodecyl trithiocarbonate (CPDT) as it has been shown to work adequately for the synthesis of methacrylate-based polymers in $scCO_2$. Three different reactions were performed via RAFT in $scCO_2$, the difference between the three was the theoretical degree of polymerisation (DP) (120 units, 60 units, and 30 units). Theoretical DP is a value for how many monomer units should be in each polymer chain and is determined by the amount of RAFT agent (the smaller the DP, the greater amount of RAFT agent needed). The reaction which had a theoretical DP of 120 still experienced crosslinking. This could be because there was not enough RAFT agent to retard the reaction, meaning that the pendant double bonds still reacted to form a crosslinked network inside the outer shell on the PA-12 particles. The theoretical DP was then halved, in an effort to produce a non-crosslinked copolymeric outer shell. This worked as the outer shell was dissolved in DCM, which allowed for GPC analysis, from which one can see that the M_n does not match the theoretical DP and the Đ (2.55) was significantly higher than what is typical of successful RAFT polymerisation (1.0 – 1.30). This is not of much importance to the product as the use of RAFT in this case is not to make a polymer with a narrow Đ, but

to retard the reaction enough, so that crosslinking is minimized, and in this the reaction scheme was successful. However, the reaction vented spontaneously, which is not desired, as a spontaneous vent is not controlled by the user and brings with it safety and reliability issues. The sudden vent of the reaction is not safe, as the pressurized contents are released from the reaction quickly and without the user's knowledge. The reliability of this reaction is also brought into question as the time of the vent is not known, so the reaction length is also not known, which can cause issues with conversion. The sudden vent of this reaction occurred from the O-ring which seals the autoclave system, this could be due to the AMA/RAFT agent mixture degrading the O-ring (Figure 8). One last set of reaction conditions were attempted for the RAFT mediated synthesis of the coated PA-12 particles. This reaction had a theoretical DP of 30, this was chosen as it could decrease the Đ of the copolymer to be more in line with what is expected of RAFT. Also, the addition of excess RAFT agent can be used to test if the AMA/RAFT agent mixture does in fact degrade the O-ring in the autoclave leading to a spontaneous vent. The positive result from this reaction is that the copolymeric coating of P(IBMA-AMA) did not crosslink, but negatively it did vent spontaneously. GPC analysis was not performed for this sample, as it had vented during the reaction, hence this reaction was not successful.

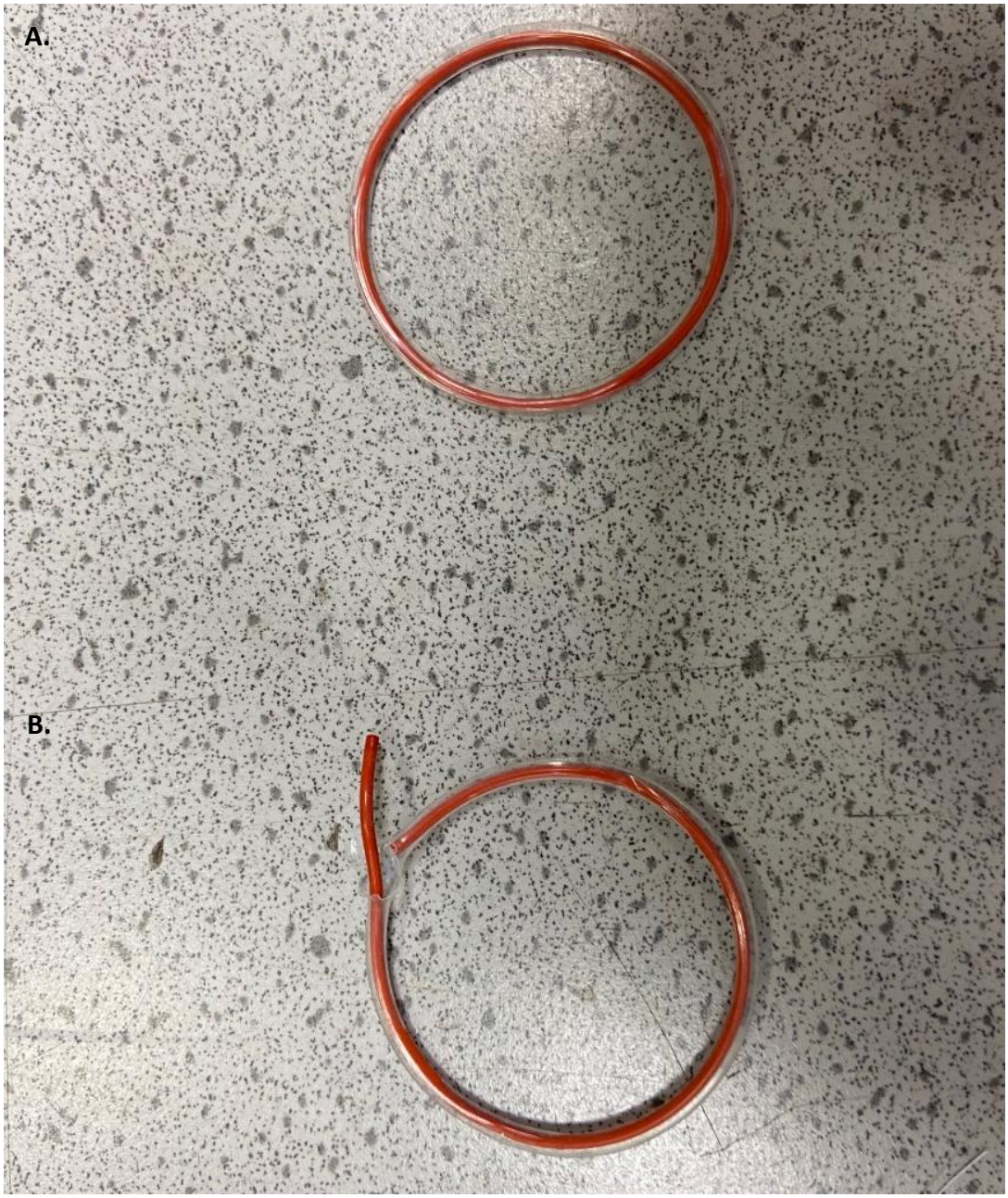


Figure 8 – Degradation of O-rings during RAFT synthesis of P(IBMA-AMA) coating on PA-12 A.) Image of normal O-ring after a reaction. B.) Image of O-ring after RAFT synthesis of P(IBMA-AMA) coating on PA-12. Example of reaction performed in triplicate.

From the results it can be concluded that both the FRP and RAFT attempts at the synthesis of a P(IBMA-AMA) coating on PA-12 were not successful. This is because the

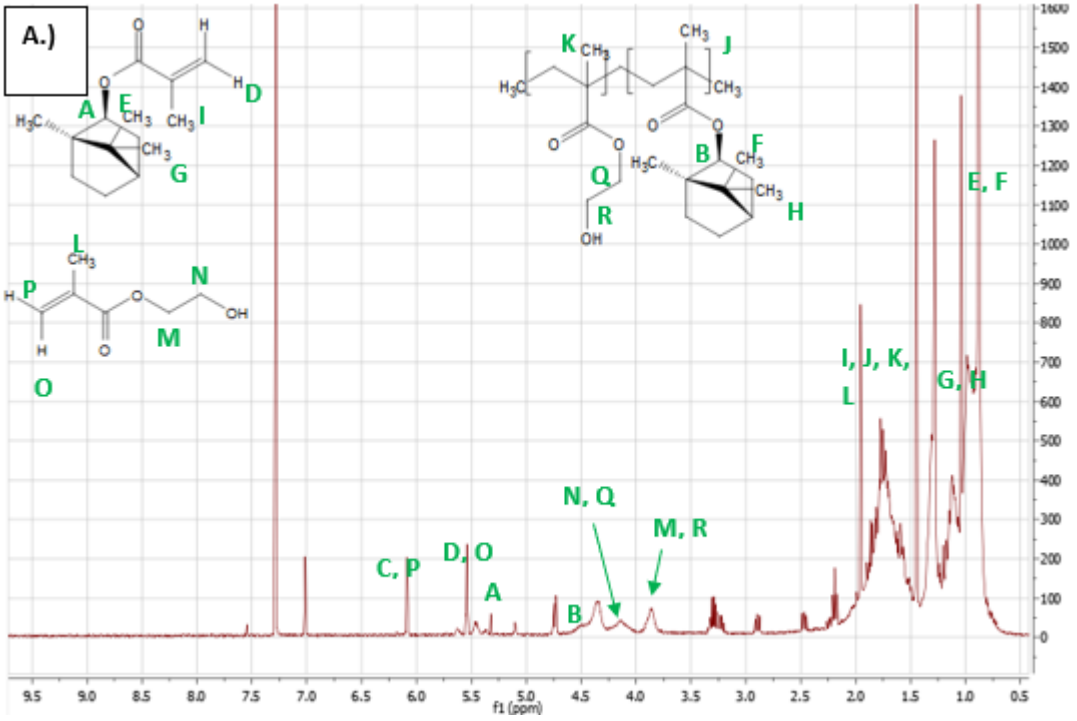
FRP reactions consistently yielded polymers that were crosslinked. RAFT polymerisation was able to minimize the reaction enough to yield coated polymeric particles that were not crosslinked. However, the reactions spontaneously vented during the polymerisation process, which is both unsafe and causes these reactions to be unreliable. For this reason, another synthetic strategy towards crosslinkable PA-12 particles was taken.

Route two towards PA-12 based particles which can crosslink in situ during SLS – Coating PA-12 in P(IBMA-GMA) and P(IBMA-HEMA):

The second strategy used to synthesize PA-12 based particles which can crosslink in situ during SLS, is based on coating PA-12 particles with P(IBMA-GMA) and P(IBMA-HEMA).

HEMA was chosen as one of the active monomers as it has an alcohol group, is soluble in $scCO_2$, does not contain halogens, and has a methacrylate. GMA was chosen for the same reasons as HEMA, but instead of an alcohol group it has an epoxide group. This strategy utilizes the reaction between the alcohol group on HEMA and the epoxide group on GMA to crosslink the polymer during printing to build a crosslinked part. The two coatings were synthesized separately to avoid crosslinking during the reaction. These coatings were made via the FRP $scCO_2$ process used to produce coloured and anti-attachment PA-12 based materials for SLS (Chapters 3 and 6(Synthesis of anti-attachment materials for SLS)) (Table 1). The synthesis of these products was reliable, as the resulting copolymeric coatings were not crosslinked and successfully made copolymers of P(IBMA-HEMA) and P(IBMA-GMA) (Figures 9A/B

and 10A/B respectively) (Table 1). Importantly in stark contrast to the polymers made via route one, these reactions did not vent. These copolymers were analysed via ^{1}H NMR and GPC revealing the composition of said co-polymers (Figures 9A/B and 10A/B respectively) (Table 1). The copolymeric coatings were analysed via ^{1}H NMR and GPC after the coatings were extracted with DCM, and subsequently filtered, dried, and redissolved in the appropriate solvent for analysis (Chapter 3 and 6(Synthesis of anti-attachment materials for SLS)).



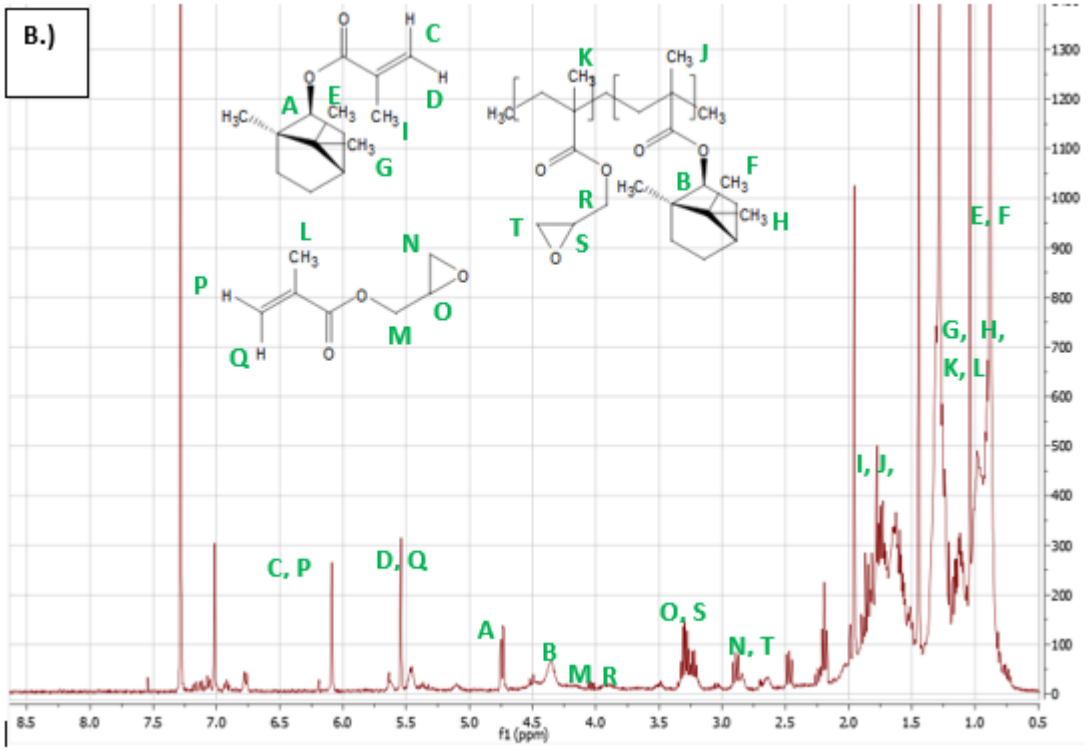
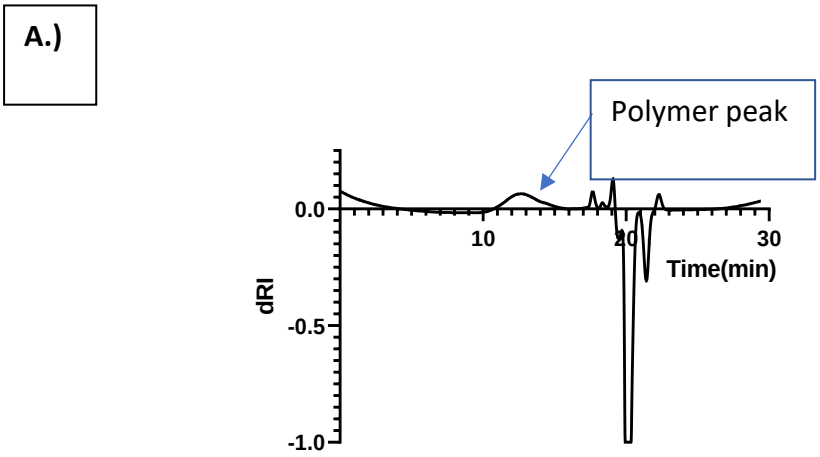


Figure 9 – ^{1}H NMR spectra of PA-12 coatings for second crosslinking strategy A.) P(IBMA-HEMA) B.) P(IBMA-GMA)



B.)

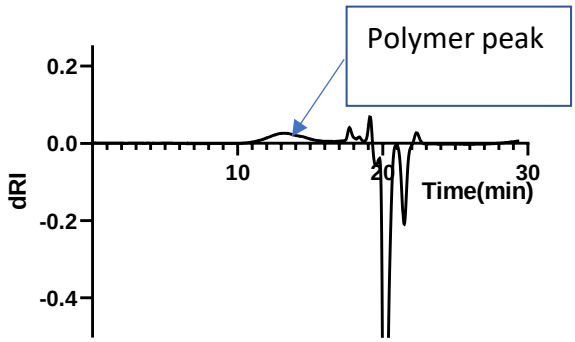


Figure 10 – GPC chromatograms showing the dRI signals of the PA-12 coatings for route two A.) Extracted P(IBMA-HEMA) coating from coated PA-12 particles B.) Extracted P(IBMA-GMA) coating from coated PA-12 particles

Sample	**Conversion of IBMA (%)[a]**	**Conversion of minor monomer (%)[b]**	**Mn (KDa)[b]**	**Mw (KDa)[b]**	**Đ[b]**
PA-12 coated with P(IBMA-HEMA) 1	84.4	50.9	40	83	2.1
PA-12 coated with P(IBMA-GMA) 1	74.3	71.9	27	42	1.5
PA-12 coated with P(IBMA-HEMA) 2	81.4	45.6	41	9	2.2
PA-12 coated with P(IBMA-GMA) 2	78.5	59.5	26	63	2.4

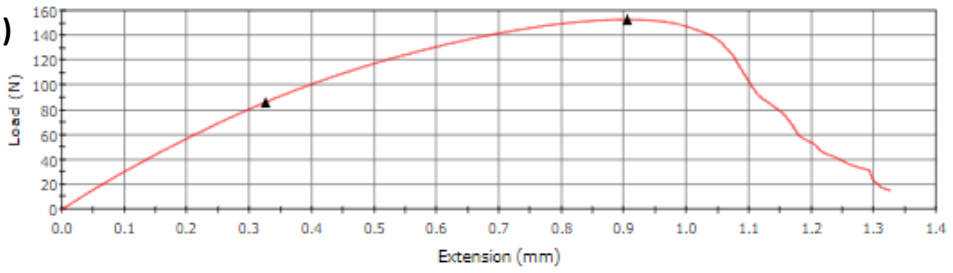
Table 1 – Results of the synthesis of PA-12 coated with P(IBMA-HEMA) and P(IBMA-GMA). A.) [a] Conversion of IBMA and minor monomer were determined via ^{1}H NMR B.) [b] M_n, M_w, Đ were determined via GPC analysis.

The results show that the synthesis of the P(IBMA-HEMA) and P(IBMA-GMA) coatings were successful, as none of the samples were crosslinked and all contained the desired alcohol and epoxide functionalities (Table 1). This strategy has a more reliable, safer, and cheaper synthetic procedure than the AMA route. It is more reliable and safer as it does not vent spontaneously, and it is cheaper as it does not use the expensive RAFT agents needed to stop the P(IBMA-AMA) coating from crosslinking. These particles show the same thermal properties as the other materials made through this novel coating process (eg. Coloured materials) (Supporting information Figures 52 and 53), for this reason their printing was assumed to be viable, and due to COVID-19 printing time was short, so another method of examining their mechanical properties had to be found. The most analogous method to analyse the effect of this coating on the mechanical strength of PA-12 was found to be the production of tensile bars via melt pressing and their subsequent analysis.[194] Melt pressing was chosen as the production method for the tensile bars as it is a temperature-based process much like SLS, but instead of a laser to sinter particles together, it uses heat plates to melt the particles which are placed in a mould which has the shape of the desired part. This method is used because it raises the material above the T_g and T_m of the core and outer shells, much like what occurs when the laser hits the material during SLS, so if crosslinking does occur in the melt pool during melt pressing it should also occur during SLS.[194] Using the melt press to produce

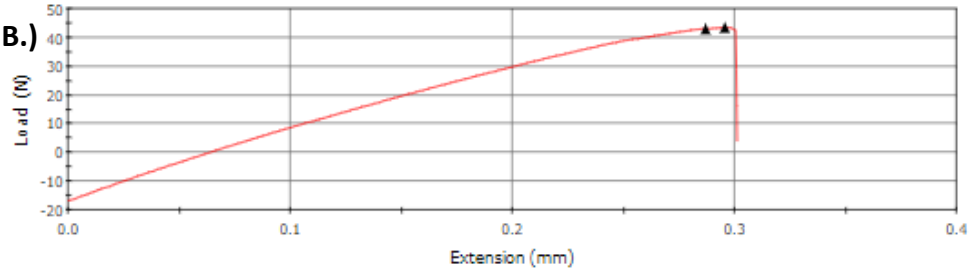
tensile does not only save time (which was limited due to Covid-19), but it also allows for these materials to be tested before they are scaled up to the 1L scale, because 0.35 g of material can be used to produce one tensile bar instead of the 600 g needed to print via SLS.

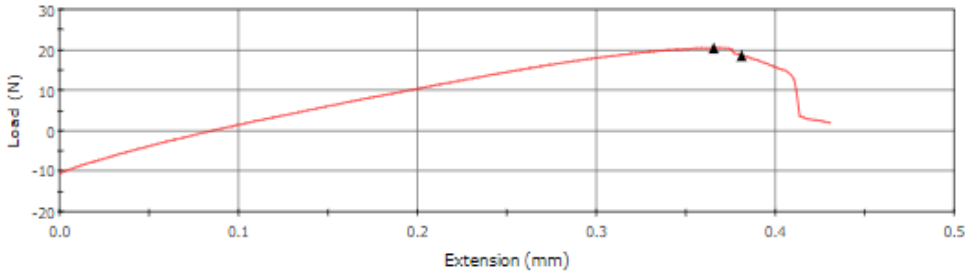
Three different types of tensile bars were produced, one utilized 100% PA-12, another 100% PA-12 coated with PIBMA, and the third was a mixture composed of 50 wt% PA-12 coated with P(IBMA-HEMA) and 50 wt% PA-12 coated with P(IBMA-GMA). The sample of 100% PA-12 was used as a control, and the PA-12 coated with PIBMA was made in order to see if the crosslinking strategy would harden it. If that is the case GMA and HEMA could be integrated into the coloured coatings (produced in Chapter 3 and printed in Chapter 4), as a way to increase their mechanical strength chemically rather than by blending with commercial PA-12. The mechanical tests show that the second crosslinking strategy did not increase the mechanical strength of PA-12, but it did increase the mechanical strength of the samples composed of virgin PA-12 coated with PIBMA (figure 11) (table 2). The results of the route two samples were quite different, and this could be the result of varying amounts of interparticle crosslinking occurring between samples (Table 2). This should be investigated in the future.

A.)

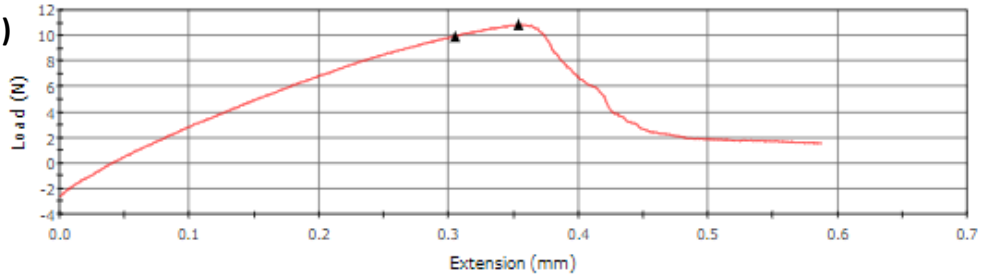

Load (N)
160
140
120
100
80
60
40
20
0
0.0
0.1
0.2
0.3
0.4
0.5
0.6
0.7
0.8
0.9
1.0
1.1
1.2
1.3
1.4
Extension (mm)

B.)


Load (N)
50
40
30
20
10
0
-10
-20
0.0
0.1
0.2
0.3
0.4
Extension (mm)


Load (N)
30
20
10
0
-10
-20
0.0
0.1
0.2
0.3
0.4
0.5
Extension (mm)

C.)


Load (N)
12
10
8
6
4
2
0
-2
-4
0.0
0.1
0.2
0.3
0.4
0.5
0.6
0.7
Extension (mm)

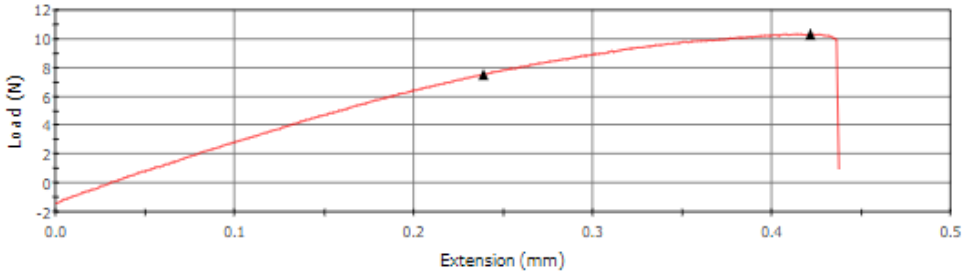

Load (N)
12
10
8
6
4
2
0
-2
0.0
0.1
0.2
0.3
0.4
0.5
Extension (mm)

Figure 11 – Results of tensile strength testing for second crosslinking strategy. A.) 100% PA-12. B.) mixture composed of 50 wt% PA-12 coated with P(IBMA-HEMA) and 50 wt% PA-12 coated with P(IBMA-GMA 100%. C.) PA-12 coated with PIBMA.

Sample	**Maximum Load (N)[a]**	**Modulus (MPa)[a]**	**Elongation at break (%)[a]**
PA-12 tensile bar melt press	152.6	1086.3	3.0
PA-12 coated with P(IBMA-HEMA) and P(IBMA-GMA) (50/50 wt%) tensile bar melt press (1)	43.4	1526.0	0.9
PA-12 coated with P(IBMA-HEMA) and P(IBMA-GMA) (50/50 wt%) tensile bar melt press (2)	20.5	389.1	1.2
PA-12 coated with PIBMA tensile bar melt press (1)	10.8	182.3	1.2
PA-12 coated with PIBMA tensile bar melt press (2)	10.3	149.3	1.4

Table 2 – Results of tensile strength testing for second crosslinking strategy. A.) [a] Tensile bars were tested via ASTM standard methods.

The results although not as positive as hoped showed promise, because even though these materials did not increase the mechanical strength of PA-12, it does allow for greater freedom in the pursuit of the development and optimisation of a colour mixing system for SLS. This is because the addition of chemical crosslinking into the coloured particles would allow for the production of coloured parts with relatively high tensile strength without the need for the addition of virgin PA-12, this could lead to parts with brighter colours.

Conclusions:

Two different routes were used to try to make materials that could crosslink in situ during SLS, which could lead to parts with improved mechanical properties. The first route taken aimed at utilizing the available pendant double bonds on a P(IBMA-AMA) outer shell to cause the polymer to crosslink as it sinters during the SLS process. However, the synthesis of this outer shell did not work. First the synthesis was attempted via FRP in $scCO_2$, but the reaction yielded copolymeric coatings which were already crosslinked. RAFT polymerisation in $scCO_2$ was used to try to slow the reaction, in an attempt to stop the shell from crosslinking during the reaction. The crosslinking was stopped during this reaction, but an unintended consequence was that the O-rings which seal the reactions degraded during the reaction causing spontaneous leaks. The second route taken involved coating PA-12 particles in P(IBMA-HEMA) and P(IBMA-GMA) separately via the same $scCO_2$ process. These reactions yielded the desired products which were then physically blended before printing via melt pressing. The results showed that the parts composed of a blend of PA-12 coated with P(IBMA-HEMA) and P(IBMA-GMA) had higher tensile strengths than parts composed of PA-12 coated with PIBMA but were weaker than part composed of standard PA-12. Therefore, this strategy did not yield PA-12 based materials that were stronger than PA-12, but through the addition of HEMA and GMA the PIBMA coated parts can be improved. This gives another route for the strengthening of coloured parts (Chapter 4). With this route more brightly coloured parts could be made, as the parts would not need to be blended with standard PA-12 in order to have desirable physical properties.

Future Work:

There are several studies to be done if materials with improved mechanical properties are to be made for SLS. To see if the addition of HEMA and GEMA could improve the mechanical properties of the coloured PA-12 parts, PA-12 should be coated with P(IBMA-HEMA-Dye monomer) and P(IBMA-GMA-Dye monomer). These materials should then be mixed and used to build tensile bars via melt pressing, which can then be tested to get their mechanical properties such as tensile strength. If these materials allow for the building of parts which have higher tensile strength than the coloured PA-12 ones, then these reactions should be scaled up (1L) and then printed via SLS. A potential material could be made which is coloured, anti-attachment, and has improved mechanical properties by coating PA-12 with P(IBMA-HEMA-Bornyl methacrylate-Dye monomer) and P(IBMA-GMA-Bornyl methacrylate-Dye monomer). In order to produce polymeric particles for SLS that have better mechanical properties than PA-12 a different approach might need to be taken. Using cores composed of different polymers (that can crosslink in situ during SLS) should be researched, as having a completely crosslinked part could lead to parts with improved mechanical properties.

Multimaterial PBF printing

Introduction:

In order to accomplish multimaterial printing in SLS, the solution was not chemical but a mechanical one. To be able to print with more than one material the powder delivery mechanism needs to be changed. Current SLS printers spread powder out of

two wells onto the build platform, and then the recoater arm returns to its initial position and repeats the process.[7,98,227] This makes multimaterial printing with sharp interfaces impossible as the different materials would mix with every layer, and the powder in the well would also be mixed as a part of the unused powder get taken back to the powder well with every layer (figure 1). What is needed is a method to deliver a specific material during a set of layers, without it mixing with the materials used in the previous layers. This would enable the user to build a part out of different materials with sharp interfaces.

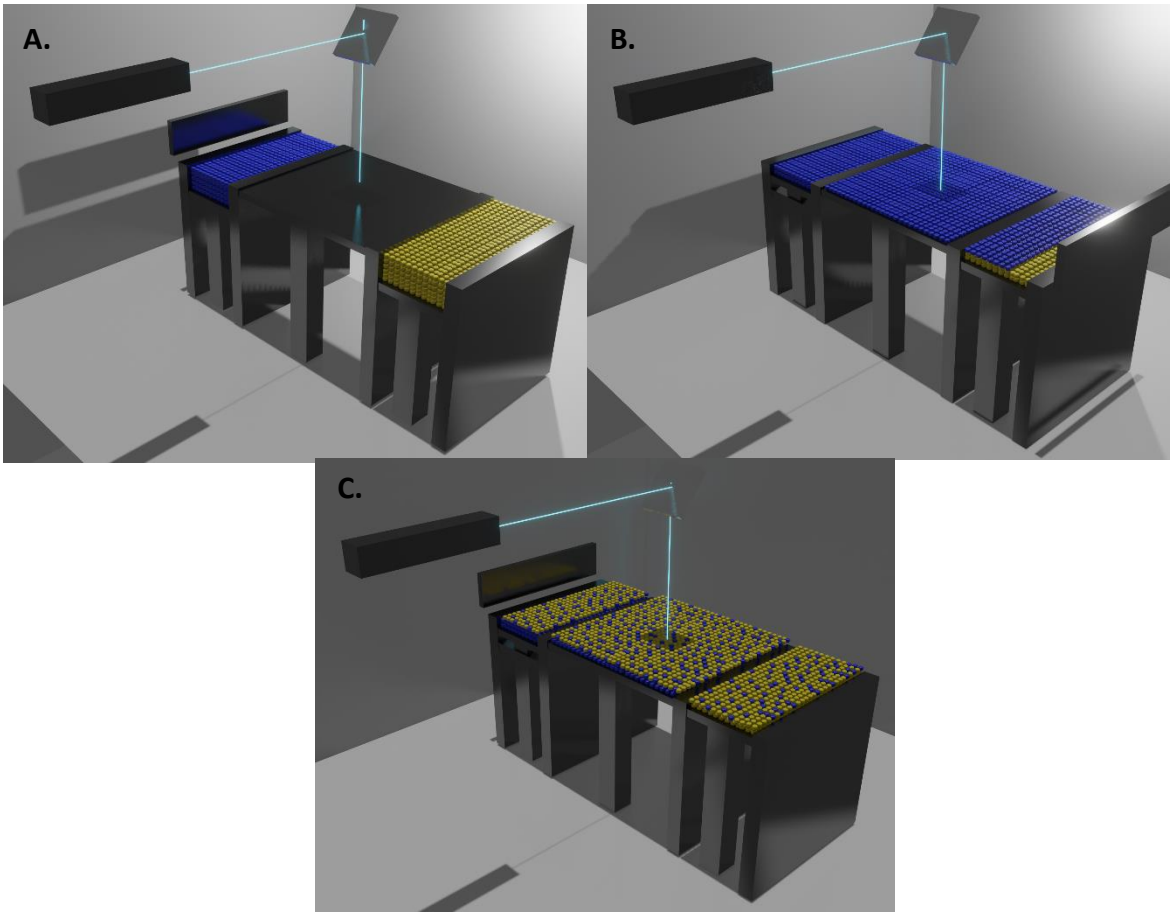


Figure 1 – Schematic of powder delivery system in standard SLS printers. A.) The materials are added to the powder reservoirs, in this diagram one side is filled with blue powder and the other with yellow powder. B.) The first layer is deposited by the recoater arm as it spreads a layer of the blue powder from the powder reservoir

across the build platform and into the other powder reservoir. C.) The second layer is spread by the recoated arm starting from the reservoir containing the yellow power. However, powder from the other reservoir has contaminated the second reservoir as the recoater arm spread blue powder across the machine. The result is a 2nd layer that is a slight mix of yellow and blue powder. This effect continues over time until of powder reservoirs are mixed and contain both powders.

There were two methods that were explored for the construction of multimaterial parts. One was using a mask system; the mask would shield a part of the building object from the spreading powder allowing for an exact number of layers to be built. The unused powder could then be collected, and the new material added, thereby ensuring a good interface between the segments of the part. However, the use of such a mask would mean that the powder must be collected as the build is in progress which is impractical. Another method that could be used is to create a multi-hopper system that dispenses a select powder on demand. This would stop the need for powder collection, that would be needed in the mask method, and should still have a good interface which should only be mixed for the first few layers as a print job. However, this route relies on the design of a new hopper and powder deposition system, which is a more significant change to the SLS technique than the mask strategy. This is because the previous powder is on the build platform, but as the layers progress the materials should switch over. Both methods have positives and negatives.

Results and Discussion:

Multimaterial printing via SLS is currently not viable, for one reason, and that is the powder reservoirs and spreading system.[7,98,228] Most printers work with a system using one or two powder reservoirs and a recoater arm which takes the powder from these reservoirs and delivers it to the build platform allowing for the SLS process. However, this means that the introduction of any new powder will cause a blend of materials, as the excess material is brought back to the powder wells. The first method that was used to print multimaterial objects via SLS was using a mask system. This involved placing a mask around the object being built, so that no unsintered powder was beside it. This was done so that powders would not mix on the build platform and ensuring that the part being built is always in the correct place, whilst sintering. This is an important factor, as the part could shift during the collection of the unsintered powder, which must be done before the insertion of the second material. The first masks and multimaterial objects printed via this method (figure 2).

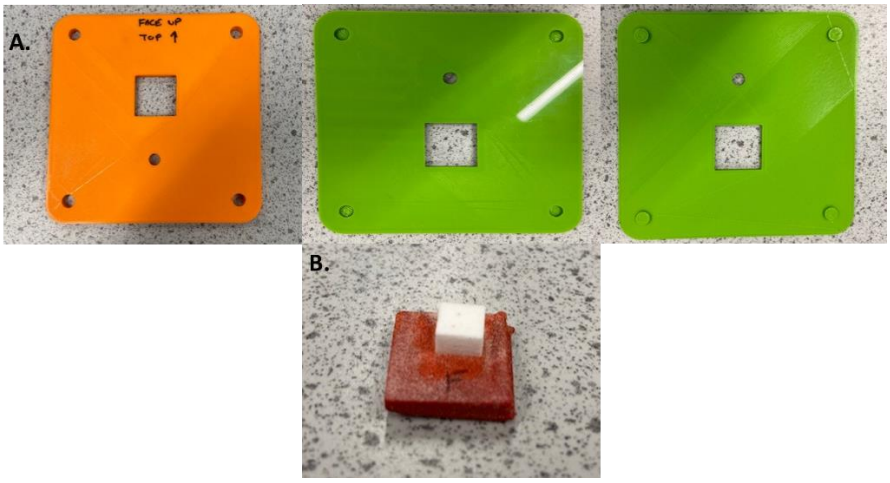


Figure 2 – Multimaterial SLS printing via mask method A.) The structure of the masks that hold the part in place during printing B.) Image of the first multimaterial object

that was built via the mask method. The bottom layer is a red square, on which a white cube was built via the addition of a secondary material and the use of the mask system.

It can be seen that a smaller white cube was built on a red platform in a single build (Figure 2). The bottom red layer was composed of PA-12 coated with P(IBMA-DR1MA) and the white layer is PA-12. This proved the concept that multimaterial printing is possible in SLS as long as the materials used have similar thermal properties and the correct precautions are taken for powder delivery. This was expanded upon and a tri-layer structure was built with a red-white-red structure (Figure 3).

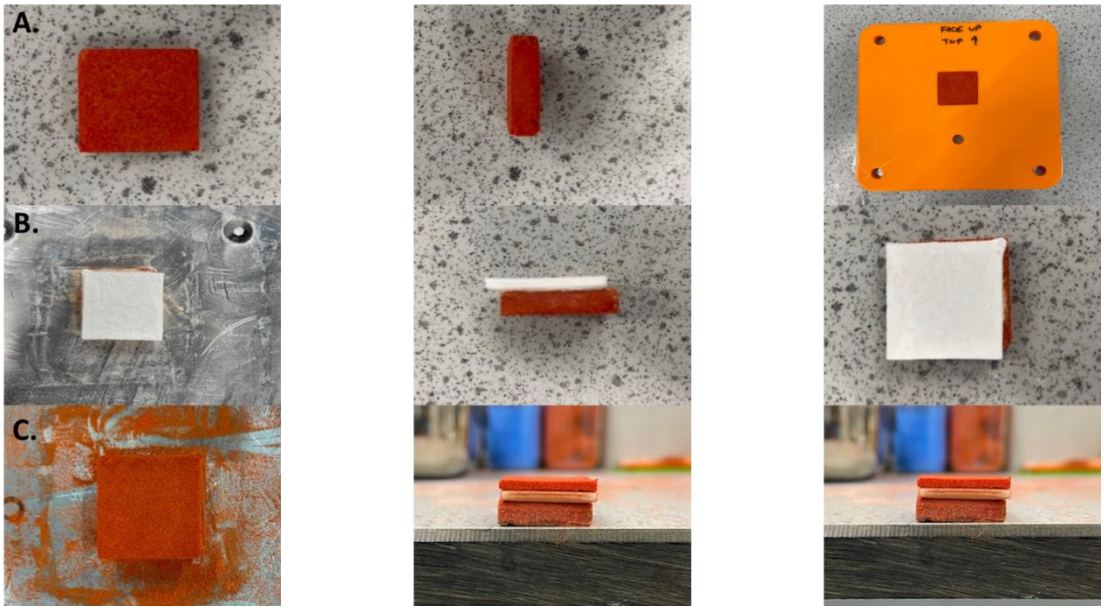


Figure 3 – Building of a tri-layered multimaterial structure composed of a bottom and top layer of PA-12 coated with P(IBMA-DR1MA) and a middle layer of PA-12. A.) Construction and images of first layer B.) Construction and images of second layer C.) Construction and images of third layer

This was a promising result, but it was wanted to be seen if more complex parts could be built with the same process. The design chosen for this was similar to the famous Star Wars character Grogu (“Baby Yoda”). This design was chosen as it is familiar to people, it has complex shapes, and overhanging angles, so it would be a good proof of concept for the technique. A similar protocol was followed, but the materials used were PA-12 and PA-12 coated with carbon black (dark black appearance). This yielded a part with a white bottom half and a black top half (figure 4).



Figure 4 – Multimaterial part (Grogu) built via SLS composed of PA-12 (bottom half) and PA-12 coated with carbon black (top half)

The series of prints shows that it is possible to print with more than one material in a single build via SLS. The problem facing the aforementioned process is that the used powder (first material) needs to be collected and the second material added during

the build. This results in a time loss and a temperature gradient, as the second material is not at the same temperature as the first material when it is added. For this reason, the powder delivery system was redesigned. A double hopper system was added to the top of the recoater arm (figure 5). The hoppers were placed on either side of the arm, and both have spreaders (blades) attached, which then spread the powder evenly. At the bottom of each of the hoppers there is a latch that can be flipped open, opening a gap at the bottom of the hopper to let the powder out. The printing process would involve having one hopper open at the start. Then once that select segment of the part is sintered, the latch is closed, and the other hopper is opened. For the first series of layers (3-5 layers) the powder is mixed, but after that the powder on the top layer is evidently composed majorly of the second material.

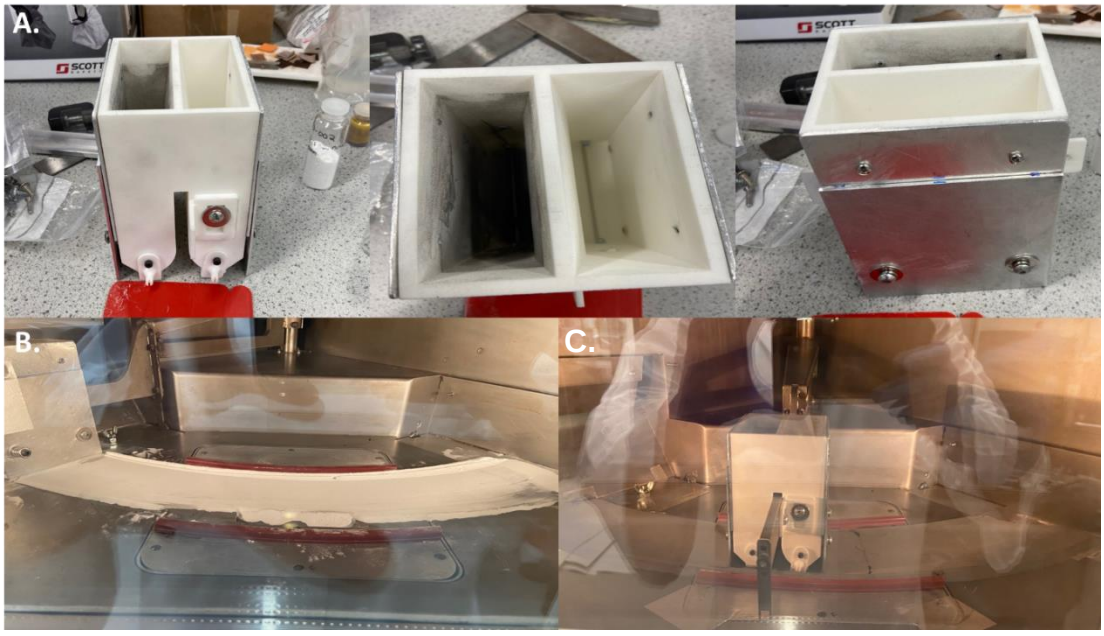


Figure 5 – Dual-hopper system for multimaterial SLS A.) Hopper design B.) Deposition and spreading of first material C.) Deposition and spreading of second material

This system worked well at room temperature, but once the machine was taken to printing conditions (172 ^{o}C), the hoppers no longer deposited powder. Powder bridging was occurring at the bottom of the hopper near the exit gap, thereby blocking the rest of the powder from exiting. This could be caused by a variety of reasons: the angle of the hopper not being steep enough, greater attraction to the PA-12 interior causing bridging, elevated temperature morphing the part leading to a smaller exit gap during printing.[229,230] These issues could be alleviated by constructing a dual hopper system made entirely of stainless steel with a sharper angle at the exit gap to encourage powder exit and deposition, lessen powder attraction to the interior walls, and lessen the impact of temperature on the hoppers.[229,230] These initial trials have proven that multimaterial printing can be done with SLS as long as the materials and powder deposition systems are appropriate. This could lead to parts with a multitude of interesting applications, as different segments of the part could have different chemical, physical, mechanical, etc. properties.

Conclusion:

Two different methods were used to try to print multimaterial structures with sharp interfaces via SLS. These methods both dealt with modifying the powder deposition system used in SLS printers. This is because it is not possible to build multimaterial parts with sharp interfaces via the current deposition method, as the different materials mix in the powder reservoirs during the recoating process. The first strategy used was to build a mask, for the part that is being printed. The mask serves to keep the part in place during printing, and the mask height is determined by the wanted thickness of the segment of the part. This allows for the user to simply add the

subsequent mask for the next step of printing. This strategy yielded parts that were multimaterial with sharp interfaces, but the technique had a few disadvantages one of which was, that the primary powder must be collected before the addition of the secondary material. This causes significant problems:

1. Added time to the build process as the primary powder must be collected, and the second deposited.
2. The machine undergoes rapid cooling as the door must be opened to collect the primary powder.

These two issues result in increased build time and a large temperature change being experienced by the part, which could cause the part to warp. The second strategy used attempted to address the issues with the mask technique, by using a dual hopper which could be opened and closed selectively and was attached to the recoater arm. This allowed for powder to be spread out of one hopper, that hopper could be closed and the second one opened, allowing for the release of a second material. This system worked well at room temperature but at printing conditions the hoppers warped, and the powder bridged preventing the powder from exiting the hopper. These strategies showed that it is possible to build multimaterial parts via SLS with sharp interfaces, however the dual hopper system attached to the recoater arm needs to be optimised. Multimaterial parts built via SLS could be used for a variety of applications ranging from household goods such as kitchen utensils to implants to sensors.

Future Work:

The first task that must be undertaken is the improvement of the dual hopper system. To improve it a new design has been created, but it has not been made or tested. The design has a screw pump at the bottom of each hopper, which is turned by the wheels which are on the outside of the hoppers (figure 6). The screw pump should keep the powder from bridging as it will move the powder which is at the bottom of the hopper. Along the inside of the hoppers there are several pegs, these pegs will allow the powder to move in the hopper, as well as lessening the weight on the powder, which is at the bottom of the hopper, thereby helping to stop bridging. The angle of the hoppers at the exit point have been steepened, which should encourage powder flow. The final improvement of this new design is that it should be made of steel. Steel will interact less with the polymeric particles than the PA-12 hopper and have a smoother finish, which should encourage powder flow. The steel hopper should also not warp under heat as readily as the PA-12 hopper. These improvements should allow for accurate and reliable multimaterial printing via SLS.

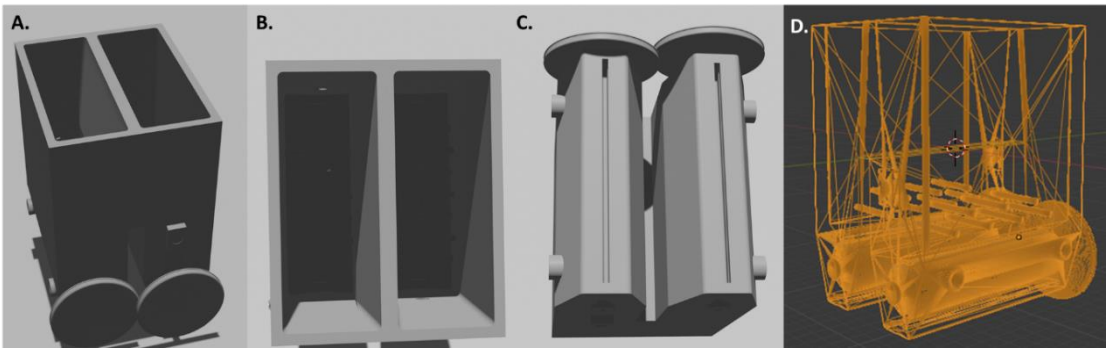


Figure 6 – Design of new dual hopper system for improved thermal stability and powder flow. A.) Side on view of the model for the dual hopper system, showing the wheels at the bottom of the hoppers. B.) Topside view of the model for the dual

hopper system, displaying the inside of the hoppers. C.) Bottom side view of the model for the dual hopper system, showing the exit gaps. D.) Wireframe design of the model for the dual hopper system, showing the pegs and screw pump on the inside.

Materials and Methods:

Materials:

Allyl methacrylate (AMA) (99 %), 2-hydroxy ethyl methacrylate (HEMA) (99%), glycidyl methacrylate (GMA) (99%), and 2-Cyano-2-propyl dodecyl trithiocarbonate (CPDT) (97 %) were obtained from Sigma Aldrich. Isobornyl methacrylate (IBMA) (> 80 %) and 2,2'-Azobis(2-methylpropionnitrile) (AIBN) were purchased from Fluorochem. CO_2 was purchased from Air Products. Terpene acrylate/methacrylate and modified acid acrylate were used as synthesised. PA-12 was purchased from EOS.

Methods:

Synthesis of PA-12 coated with p(IBMA-x monomer):

PA-12 (7.5 g), IBMA (1.1255 g, 0.005 mol), x monomer (10, 20 , or 30 wt% compared to IBMA), and AIBN (0.0124 g, 0.0755 mmol or 0.0135 g, 0.0822 mmol or 0.0145 g, 0.0883 mmol) were degassed in the autoclave for 15 min, by flushing it with CO_2 at a constant pressure between 0.27 – 0.41 MPa. The key was then shut rapidly, and the pressure was slowly increased to 5.51 MPa, subsequently the temperature was increased to 50°C, and after stabilising the autoclave was pressurized to 13.79 MPa, with subsequent heating to 65°C. Once stable at 65°C the reaction is pressurized to 20.7 MPa and left stirring at 450 rpm for 24 hours. The autoclave is allowed to cool

<30°C and the CO_2 is vented slowly, and the autoclave is opened to reveal the product.

Multimaterial printing with mask strategy:

A mask of the object being printed is made and inserted into the powder, so that it can not move. The first powder is added to the printer, and the design is printed at the optimum conditions for the material. The first material is rapidly removed leaving the mask and the printed part in place, and the second material is added. The machine is warmed up to temperature, and the printing is continued. Once printing is completed the printer is left to cool and the part and mask are removed.

Multimaterial printing with dual hopper:

The dual hopper is attached to the recoater arm and levelled, to make sure the blades on either side are level. The respective powders (50 g) are added to their designated hopper. The hopper containing the first material to be used is opened and the machine is warmed up to optimum conditions and subsequently printing is commenced. Once the area designated for the first material has finished building, the print is paused, and the first hopper is closed and the second is opened and the print is restarted. Once the print is finished the machine is left to cool and the part is collected.

Powder mixing:

The calculated amounts of PA-12 and coated PA-12-based powders were added to a glass vial. The vial was physically mixed via a vortex mixer for 10 min, and subsequently left on a roller overnight, to ensure appropriate physical mixing.

Tensile bar production:

PA-12 or coated PA-12 particles (0.35 g) were added and packed into a mould. The mould was pre-sprayed with Teflon grease, once packed the mould with the powder was placed on a heat melt press (180 ^{o}C) and tightened and left for 30 min. The melt press was left to cool, and the tensile bars collected.

Analysis:

^{1}H NMR analysis (NMR):

The samples were analysed by ^{1}H NMR, using a Bruker 400 Ultrashield (400 MHz NMR), and all the samples were dissolved in deuterated chloroform. The ^{1}H NMR spectra were used to identify the polymers formation and to calculate the monomers conversion. The conversions were obtained with equation 1.

$$Conversion = \frac{AUCP}{AUCP + 1}$$

Equation 1

In this equation AUCP is the area under the curve of the polymer peak when compared to the area under the curve of the monomer peak.

Gel Permeation Chromatography (GPC):

GPC was performed in order to obtain the M_n, M_w, and dispersity (Đ) values for all the synthesised polymers. These values were produced using calibration standards of PMMA. All the measurements were performed on an Agilent 1260 Infinity HPLC using HPLC grade THF as eluent at 40°C with 2 x Agilent PL-gel mixed-C column at 1 mL min^{-1} flow rate, connected to a differential refractive index (dRI) detector and MALLS detector.

Scanning Electron Microscopy (SEM):

SEM was used to see if the polymer materials were composed of discrete monodisperse particles, and it was performed using a Philips XL30 electron microscope. The samples were prepared by putting the polymer powder on a carbon tab mounted onto an SEM stub, which were then coated with Platinum for 180 seconds at 12 mA and 2.2 kV using an Emitech SC7640 sputter coater.

Average Particle Area calculations:

The average size of the polymer particles was calculated by taking the area of 100 particles from a SEM image and then taking the average area of the particles exploiting ImageJ software.

Laser Diffraction Spectrometry (LDS):

LDS was used to analyse the particle size of a large segment of the samples. This was done by using a Malvern Mastersizer 3000. Initially, the samples (1 g) were loaded onto a dispenser. Dispenser vibration moved the polymeric powder evenly into an air

jet, which inserted the sample into the detector. Mastersizer 3000 software was then used to obtain the average particle size.

Dynamic Scanning Calorimetry (DSC):

DSC was used to detect polymers thermal transitions such glass temperature transition (Tg), temperature of crystallisation (Tc), and temperature of melting (Tm). The samples were prepared by weighing out circa 5 mg of sample into a DSC pan, which was then closed with a lid and tested from 0°C to 250°C. The Tc was determined by finding the maximum point of the curve if any was present, the Tm by finding the minimum point if any was present, and the Tg by finding a change in the slope of the line if any was present.

Biological assays:

Biofilm metabolic activity was measured by the XTT (Sigma-Aldrich) reduction assay. For *C. glabrata* and *P. aeruginosa* (for *P. aeruginosa*, single colonies were used to inoculate TSB broth cultures incubated overnight), single colonies were used to inoculate YPD broth cultures in Erlenmeyer flasks and incubated overnight at 37°C with orbital shaking at 150 revolutions min^{-1}. Cultures were washed twice in RPMI 1640 and diluted to 125,000 cells ml^{-1}. Aliquots (100 μl) of the cell suspension were transferred to 96-well microtiter plates (Greiner Bio-One, Stonehouse, UK), either coated with the polymers of interest or containing coupons 3D-printed with polymer as described above and then incubated statically for 2 hours. Similarly, 100 μl of fungal spores (2.5×106 spores $ml{-}1$ in PDB) from 7-day-old PDA plates were transferred to coated 96-well plates for 6 hours at room temperature. In all cases,

coupons were subsequently transferred to fresh 96-well plates. Nonadherent cells or spores were removed by three gentle washes with PBS; then, 100 μl of fresh medium was added to each well, and plates were incubated at 37°C up to 24 hours after inoculation. Coupons were again transferred to fresh plates. The wells were washed three times with PBS, and the XTT reaction was initiated by adding XTT and menadione to RPMI (for *C. glabrata* and *P. aeruginosa*) to final concentrations of 210 μg ml−1 and 4.0 μM, respectively, or to PBS (for *C. globosum* and *C. gloeosporioides*) to final concentrations of 400 μg ml−1 and 25 μM (final volume per well, 200 μl; PBS was used instead of PDB, as the XTT reaction does not work in PDB medium). After 2 and 6 hours, respectively, 100 μl of the reaction solutions was transferred to fresh 96-well plates, and the absorbance at 490 nm was measured using a BioTek EL800 microplate spectrophotometer. To assess the impact of the polymers on fungal growth, washing steps were omitted as presented in Fig. 3. Contrary to RPMI and as mentioned above, the XTT reaction cannot be performed in PDB medium, and fungi are not able to grow in PBS. Therefore, *C. globosum* and *C. gloeosporioides* was cultivated for 15 days on the polymers in the presence of PDB, and growth effects were assessed visually.

Mechanical Testing:

A 5kN load cell on a benchtop instron universal testing machine (Instron 5969) was used with bluehill 2 testing software. The grips were pneumatic rated to 2kN, the sample was placed in the top grip and then the top and bottom grips were closed. Then the sample was tested until a breakpoint and it was removed from the grips.

Conclusions

Throughout this project the goal has been to improve multiple facets of selective laser sintering (SLS) otherwise known as Powder bed fusion (PBF). SLS is a widely used technique and it has many advantages associated with its use. These advantages include:

1.) the ability to print objects without support structures

2.) the possibility of recycling the unused material

3.) rapid prototyping

4.) the potential to use a wide range of materials

5.) the ability to build parts with relatively good mechanical properties (used for prototypes)

These advantages have led to SLS being used in many fields for rapid prototyping and some end-user parts as well. SLS has also been used in the fashion, automotive, and aerospace industries, but its shortcomings prevent its use from becoming widespread. Several limitations of SLS have been addressed in this work:

1.) Parts can only be printed in black and white.

2.) Maximum feature resolution for a part is only ~100µm.

3.) PA-12 based parts bio-foul readily

4.) The tensile strength of PA-12 is too low for high-performance parts

5.) SLS can only print with one material at a time.

The first drawback of SLS that was addressed was the fact that parts can only be printed in black and white. As previously mentioned, this is because PA-12 is white and carbon black can be added to the PA-12 powder in order to impart a grey/black visage. To overcome this limitation, the strategy taken to impart colour was to create dye monomers which could be co-polymerised with IBMA to make a SLS compatible outer shell on PA-12 particles (Chapters 1 and 2). Three dye monomers were synthesized: yellow one methacrylate, disperse red 1 methacrylate, and disperse blue 3 methacrylate (Chapter 1). These dyes were chosen as these three colours can be used to create a CMYK colour mixing system. Once monomer synthesis was optimized, the monomers were copolymerised with IBMA using a novel $scCO_2$ based FRP process, which simultaneously polymerises the monomers and uniformly coats the PA-12 particles (Chapter 2). The polymer synthesis and coating process was scaled up from the 60 mL scale to the 1 L scale (Chapter 2). The coloured polymeric particulate powders were ready for use after venting of the CO_2, as it dries the product. The printing conditions for each of the blue, red, and yellow PA-12 based particles were optimized and cubes of each material printed, and the mechanical properties analysed (Chapter 3 and Appendix 2). This allowed for the creation of coloured polymeric parts via SLS for the first time (figure 1). These coloured polymeric particles were then used to create the first colour mixing system for SLS (Chapters 3 and 4).

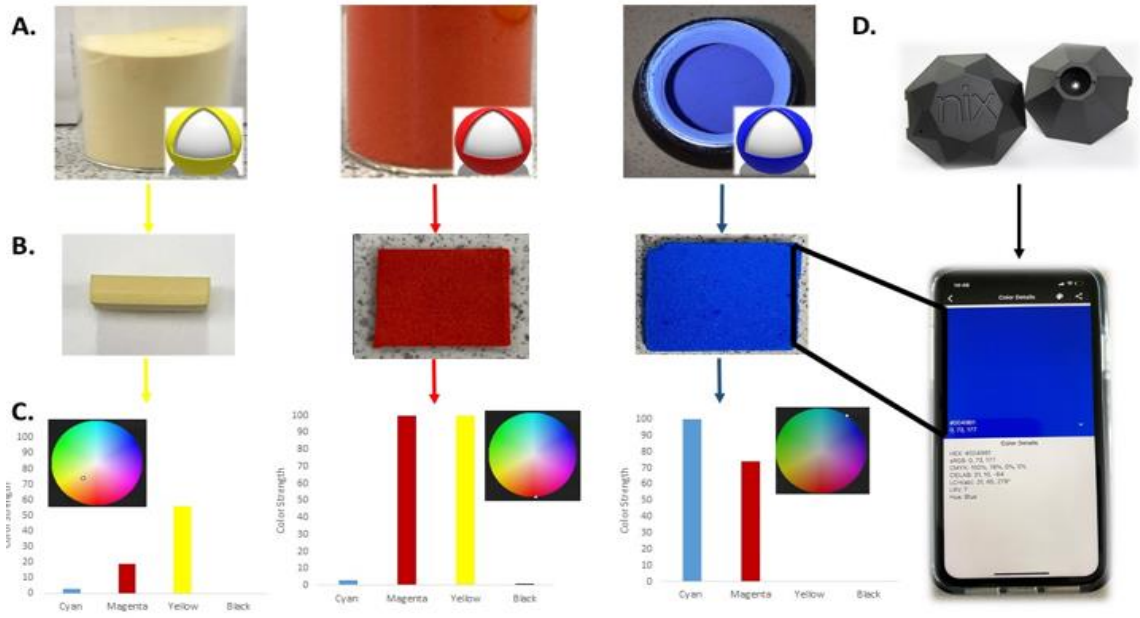


Figure 1 – Coloured parts printed via SLS A.) Red PA-12 based part. B.) Yellow PA-12 based part C.) Blue PA-12 based part. D.) NIX colour analysis

A CMYK colour mixing system was designed and created for SLS by utilizing the aforementioned colour coated PA-12 particles (Chapters 3 and 4). The system was used to make a variety of colours throughout colour space (figure 2)(Chapter 4). To optimize the acquisition of target colours, a programme was created which suggests possible formulations for a target colour. This programme is based on multivariable analysis and particle swarm optimization (Chapter 4). The accuracy of this programme is not fool proof, but it can adequately predict colours on different ends of the colour sphere such as green or red (Chapter 4). The accuracy of this system could be increased by adding additional data points and boundary conditions. This programme can also be used as a cost optimization tool, as it provides many possible formulations for the target colour, then the formulation that is the least expensive based on powder ratios could be used instead of the more costly alternatives.

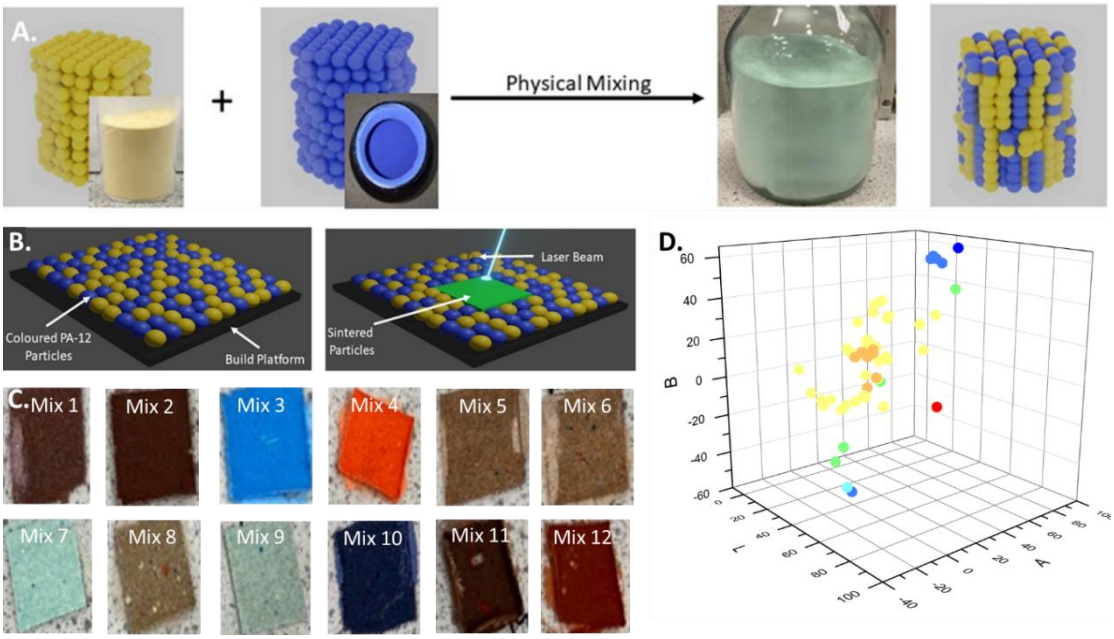


Figure 2 – CMYK colour mixing in SLS. A.) Example of physical mixing of coloured powders leading to a different colour. B.) Schematic of colour mixing when not melted vs when melted. C.) Selection of colours that have been made D.) Graph showing the range of colour space covered by computational modelling.

In addition to colour mixing and computational modelling, the resolution of the SLS process has been improved through a two-pronged approach (Appendix 1). A series of novel micron sized polymeric particles were produced in an effort to create printed parts with a resolution of ~10 µm. The particles were synthesized through FRDP in $scCO_2$. The particles that were found to be suitable were composed of a random copolymer of P(MMA-DB3MA) (Appendix 2). Particles composed of this copolymer formed flat layers with a depth of about ~10µm. Utilizing an in-house built printer, which uses a UV (405 nm) laser the particle layers were sintered in a track pattern (Appendix 2). After optimization, one layered tracks with a resolution of 10-15µm were printed (figure 3) (Appendix 2). Although this is a vast improvement over the

previous maximum resolutions for SLS, only one layer was printed at that resolution. Subsequent layer deposition was not successful as the part underneath moved during powder deposition and spreading. Several steps must be taken in order to achieve multi-layered printing at this higher resolution. Firstly, the printer must be modified with a vacuum chuck, similar to that used by Roy *et al.* the purpose of this is to keep the bottom layers from moving during the deposition of subsequent layers. The reason for the monolayer formation with particles composed from P(MMA-DB3MA) should also be studied using macro (analysis of packing density of the deposited layers) and micro (colloidal probe technique AFM) methods.

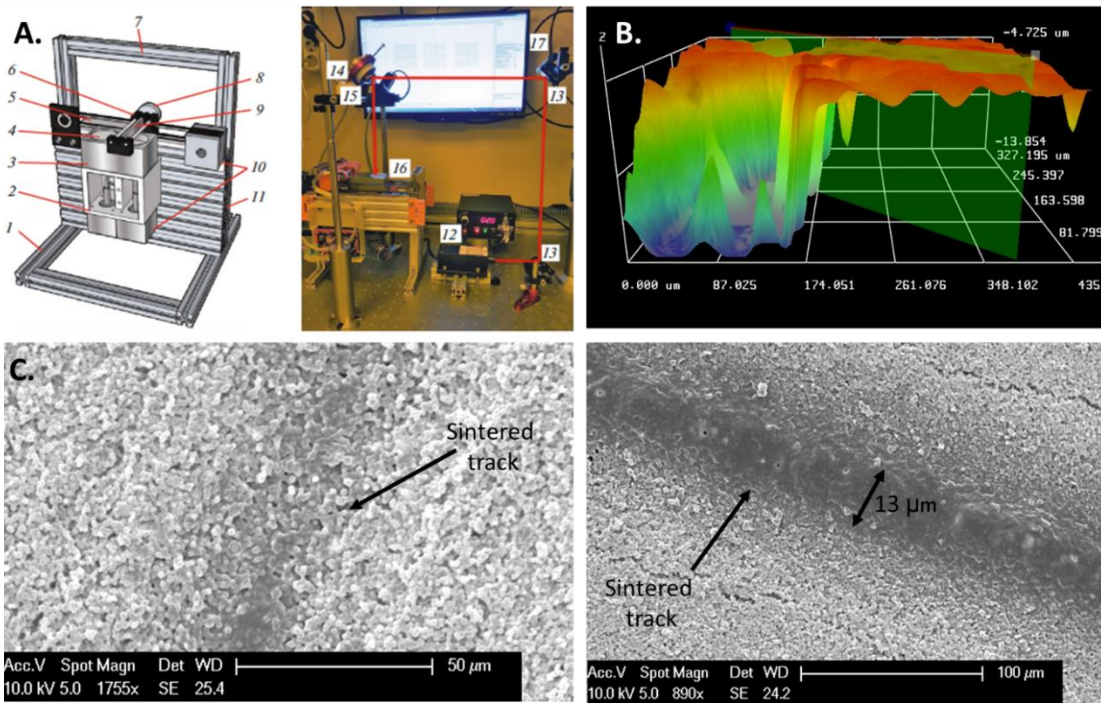


Figure 3 – High resolution SLS. A.) Schematic and image of novel SLS printer B.) Depth mapping of layer formed with P(MMA-DB3MA) particulate C.) SEM images of printed tracks (lower laser power (left)(higher laser powder (right))

The third problem with SLS that was investigated is the propensity of PA-12 based parts to undergo biofilm formation and bio-foul. Not only can biofilm formation decrease the lifespan and efficiency of printed parts, but it can also result in disease spread in parts used for biological applications. In order to overcome these limitations, a strategy was developed to coat PA-12 particles in copolymers that are known to exhibit anti-attachment properties (Chapter 5). The achieve this, a process similar to that used in the colour coating of PA-12 particles was utilised (Chapter 5). The anti-attachment coating allows for the printing of objects which are inherently anti-attachment thereby preventing biofilm formation. A library of random copolymer coated PA-12 particles was made with the major component of the polymer being IBMA and the minor 'active' part was either a terpene (meth)acrylate or a modified acid acrylate (Chapter 5). These monomers were chosen as they have previously been shown to exhibit antimicrobial/bacterial/fungal properties. Additionally, they can be derived from sustainable sources and, in some parts, can be obtained from waste streams.

Six different copolymeric coatings were made with terpene (meth)acrylate or a modified acid acrylate as minor components. These coatings were printed via melt pressing (analogous to SLS) to make discs that could be used for bioassays conducted in 96-well plates (Chapter 5). The discs were tested against four different microorganisms which have varied attachment and growth mechanisms. The assays showed that several of these samples had reduced attachment of the microorganisms compared to PA-12, as was seen in the test conducted with *C. gloesporioides*, in which several of the samples had reduced attachment of the fungus (figure 4) (Chapter 5).

The toxicity of these samples towards the assayed microorganisms was tested, revealing that these materials are non-toxic towards the microorganisms, hence these materials are anti-attachment (Chapter 5). Potentially such materials could be used to produce household products especially in kitchen and bathroom settings, food packaging, water filters, etc.

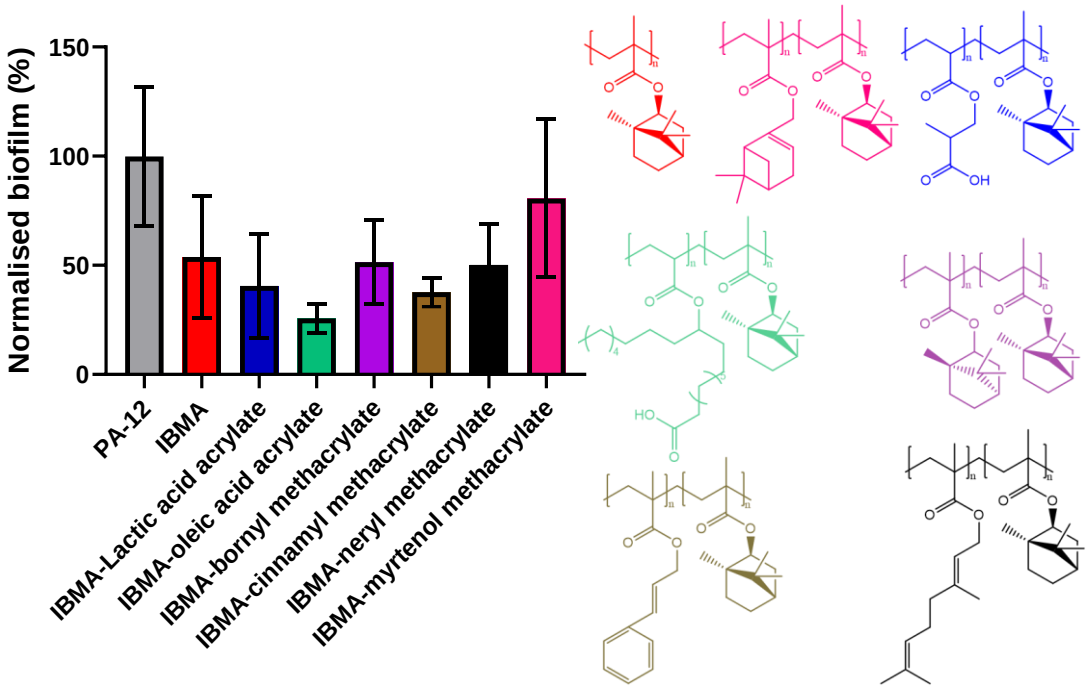


Figure 4 – Bioassay of printed parts (discs 1.5 mm in thickness and 5 mm in diameter) testing their activity against the growth of *C. gloesporioides*. The control used was a disc made of 100% PA-12, the attachment of the bacteria to the coated samples was compared to the attachment of *C. gloesporioides* on the PA-12 control, so the PA-12 control has a value of 100% attachment.

In an effort to broaden the possible applications of SLS to include the manufacture of high-performance parts, the mechanical properties of PA-12 were attempted to be improved in this work. The strategy taken to increase the tensile strength of PA-12

based parts was to coat PA-12 particles with a polymer capable of crosslinking during the printing process (Chapter 5). Two methods were used to attempt in-situ SLS crosslinking (Chapter 5). The first relied on the unreacted double bond pendant groups on the allyl methacrylate segment of the polymer to react and crosslink. However, the synthesis had a variety of issues, which resulted in this method being ruled as unreliable (Chapter 5). The second method relied on the reaction between the alcohol and epoxide groups on HEMA and GMA to crosslink during SLS. PA-12 was coated with P(IBMA-HEMA) and P(IBMA-GMA), the powders were physically mixed before the production of the parts (Chapter 5). The parts composed of this material were not stronger than the parts composed of PA-12 but were stronger than the parts composed of PA-12 particles coated with PIBMA (Chapter 5). This was not the expected result, but it can be viewed in a positive light, as it allows for the strengthening of the coloured materials without the need of physical blending with PA-12. This affords the user greater freedom in the pursuit of target colours with improved mechanical properties. In the future, different strategies could be used to enhance the mechanical strength off PA-12, such as altering the core of the particle, so that it can be crosslinked in situ during printing as well, in an attempt to make parts that are wholly crosslinked instead of just the outer shell.

The last facet of SLS that was improved during this work was the powder delivery system. The powder delivery was changed in two ways in an attempt to print parts composed of more than one material with sharp interfaces (Chapter 5). One method used involved making a mask for the part in question and splitting it into different heights (Chapter 5). Thereby allowing for the powders to be replaced mid print

without affecting the part being built. Using this method, squares containing two different segments composed of different materials were printed (figure 5) (Chapter 5). This method was also utilized to print multimaterial figures with sharp interfaces (figure 5) (Chapter 5).

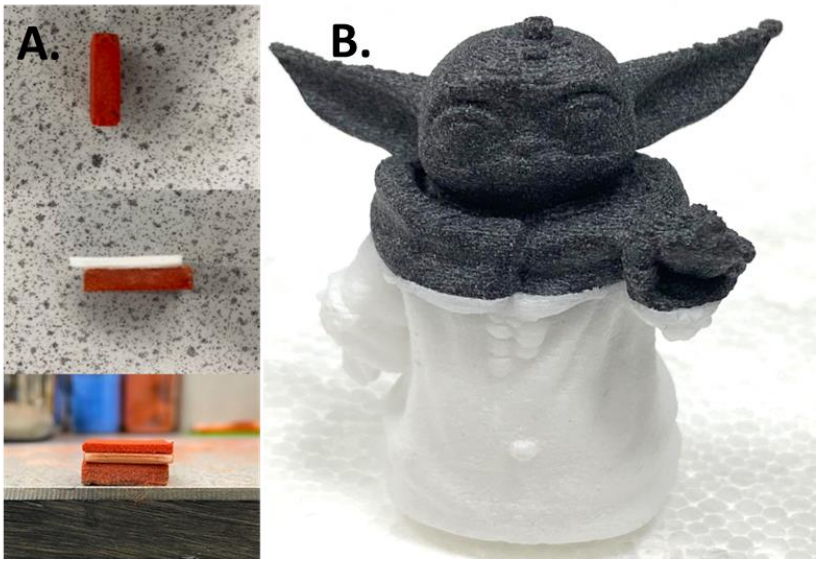


Figure 5- Multimaterial SLS printing via mask method A.) Segmented square composed of red-white-red PA-12 respectively for the layers B.) Baby Yoda composed of a white bottom and a black top.

The parts built via this method demonstrated the desired properties: sharp interfaces and multi-material (Chapter 5). However, the method required the collection of unprinted material and subsequent deposition of the next material. This was not efficient as the printer temperature would drop while this process was executed, lengthening the print time. Temperature variations are also not ideal whilst parts are being built as they increase the risk of curling and warping. The second strategy sought to fix this by attaching two hoppers to the recoater arm. This worked at room temperature, but at printing conditions the hoppers composed of PA-12 warped

minimally causing powder to bridge, hence the exit gaps of the hoppers were blocked (Chapter 5). This could be fixed through a variety of methods such as constructing the hoppers out of steel and steepening the inner angles of the hopper. With minor fixes, multimaterial parts with sharp interfaces could readily be built via SLS. This is not only for aesthetic purposes, but one could build parts in which varying segments of the part have different properties, such as hydro-phobic or philic, super or antireflective, magnetic, varying chemical sensitivities, etc.

In short, many facets of SLS have been advanced through this project in an effort to improve the technique and the products created by it. Through this project it was shown that coloured printing, higher resolutions, anti-attachment parts, and multimaterial printing are possible in SLS. To achieve these advancements, both engineering and chemical challenges were confronted, as novel monomers, polymers and polymerization processes were designed that were both sustainable and imparted new functionality. Novel modifications to SLS printers were made as seen by the high resolution SLS printer and the dual hopper system. The advancements made should enable a wide variety of new and exciting parts to be made through SLS.

Appendix 1: Development of a novel High Resolution SLS process

Acknowledgements:

In order to take steps towards high resolution SLS (HRSLS) work was carried out with Professor Vladimir Popov and Mariya Syachina, who were indispensable for this project as they designed and constructed the printer used for HRSLS testing and conducted many of the printing tests.

Introduction:

The aim of this part of the project is to better the resolution of selective laser sintering printers. Currently the highest resolution that can be reached in commercial SLS printers is about ~100 µm.[231] This resolution limit is caused by both the polymeric material used for printing and the actual printers.[231] The vast majority (~95%) of the printing material used is composed of Nylon-12.[14,15] The PA-12 particles used for SLS have a size ranging from ~50 – 80 µm.[14,15,30] This limits the max resolution to the size of the particles (~50 – 80 µm). There are two main factors of the printer design that restrict the resolution from betterment. The first is the laser spot size, which depending on the printer can range from 50 – 200 µm and is often a CO_2 laser.[232] The resolution can only be as small as the spot size, because the spot size will dictate the smallest space that can be sintered.[232] The second technological area that affects resolution is the movement of the build platform. As has been previously mentioned, after every sintered layer the build platform moves down by a set distance and allows the recoated arm to spread a new layer of powder on top of the sintered layer. Hence, the resolution in the z-direction of the part built via SLS is heavily influenced by the

build platform, as it can only be as small as the smallest controlled movement that the build platform can make in the z-direction.[231] Our aim is to print via SLS with a resolution of ~10 – 20 μm, thereby improving the resolution tenfold. In order to do this; novel materials were synthesized, which were suitable for SLS and had a much smaller particle size (500 nm – 2 μm). A new SLS printer was produced which had a smaller laser spot size (~ 10 μm), and better control over the build platform in the z-direction (~ 5 μm). These improvements to the SLS process could allow the user to print tracks at a resolution of ~ 15 μm, which would be significantly improved from the previous max resolution for SLS.

Modern selective laser sintering systems with high productivity and fairly good (approximately 100 μm) spatial resolution allow for the production of 3D objects of varying architectures according to their designed computer models.[231] At the same time, the potential abilities of this technology to use polymeric materials are far from being fully achieved. One of the main reasons for this is the limited choice of polymers suitable for SLS. The vast majority of the SLS industry utilizes PA-12 particles and a small range of other polymers such as other polyamides and their composites.[61] These polymer particles are imperfect spheres ('potato' shaped) and they usually have sizes ranging from 50 – 80 μm.[61] The resulting polymer-based powders have large size distributions and varying optical and rheological properties.[61] In selective laser sintering it has not been possible to print at resolutions higher than 60 – 100 μm. The resolution limit of the SLS process is imposed by a variety of factors:

1.) Size of polymeric particles

2.) Size of laser spot size

3.) Control of the build platform in the z-direction (figure 1).

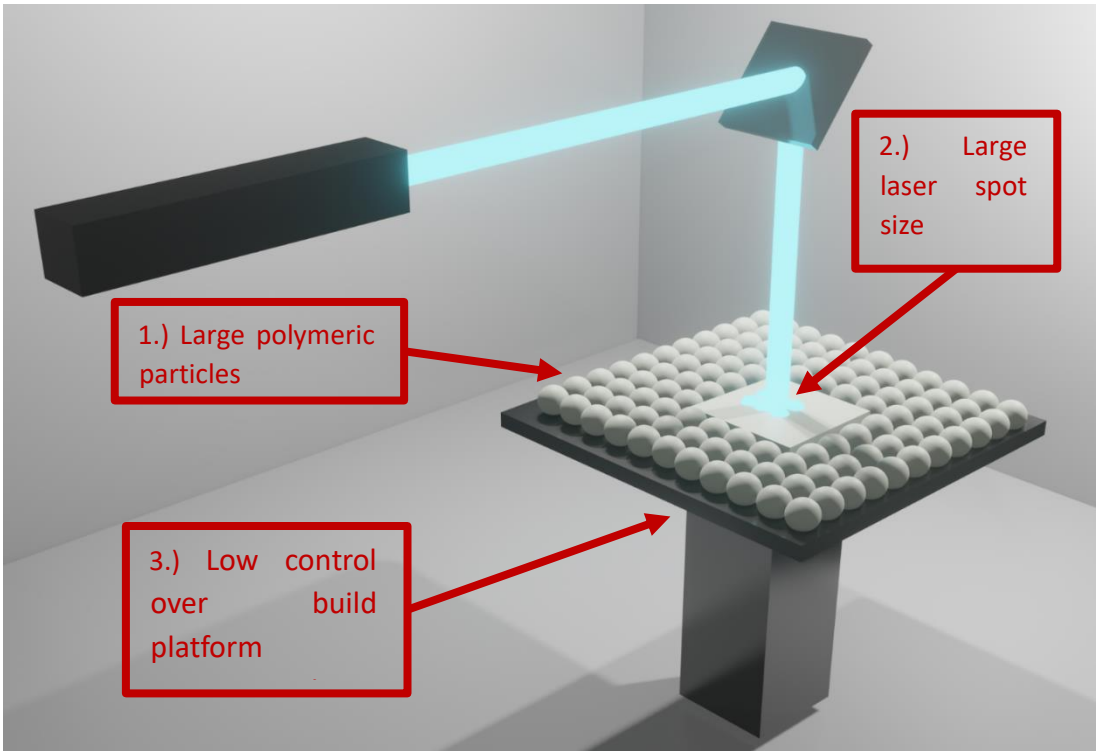


Figure 1 – Areas of the SLS process limiting the resolution of SLS printing. 1.) The size of the polymeric particles (normally ~60-80 µm) limits the resolution. 2.) The laser spot size limits resolution as CO_2 lasers are used (wavelength is 10.6 µm, spot size is usually ~100-200 µm). 3.) The control over the build platform in the z-direction will dictate how thick each layer is thereby limiting resolution.

The most common polymeric particles used are composed of Poly amide-12 (PA-12) and these particles have an average size of 50 - 80 µm.[61] Other polymers have been used such as: polyether ether ketone (PEEK), polyether ketone ketone (PEKK), PA-11, etc. but these all have similar particle sizes.[14,15,233] Thereby, limiting the resolution to

the particle size. This is because the entire outside of the particle will melt, so the minimum feature resolution is the size of the particle. SLS requires particle size to be well-defined in both size and shape. The majority of the PA-12 particles made for SLS have the aforementioned size and are potato shaped. The two main methods for producing these particles are by precipitation or mechanical grinding, although there are more methods available (figure 2).[61] Many processes also add fillers/additives to PA-12 particles such as carbon black. The most common way to produce PA-12 particles of this size is to conduct the anionic ring opening polymerisation of lauryl lactam in organic solvents at 300° C (figure 2-3).[234–239] The process can also be done hydrolytically, in which water or a metal-organic compound catalyses the ring-opening polymerisation (figure 2).[234–236,240] The particles are then made via precipitation in methanol. Another route taken by Arkema is the anionic ring-opening precipitation polymerisation of lauryl lactam in the presence of 0.1 wt% silica nucleating agent.[241] Lim et. Al. showed that PA-12 particles could be produced via conducting the polymerisation of lauryl lactam in a mixture of water and ethanol at elevated temperatures and pressures.[242] Lim et. Al. showed that the particle size could be controlled through the temperature and pressure.[242] Cryogenic milling of PA-12 has also been used to produce said particles.[243] However, the structure of such particles is more jagged than the particles made from precipitation (figure 3).[61] Emulsion polymerisation of insoluble monomers has been used to create particles for SLS, however this yields slightly smaller particles ~50 µm, which are spherical (figure 2-3).[241] Other polymers such as PA-11 can be processed in similar ways; as other polyamide powders can be prepared via precipitation from polymer solutions such as AB and A/AB type amide copolymers with a chain length of 6 - 13 carbon atoms,

polyamide homopolymers with 7 – 10 carbon atoms, and coprecipitated polyamide powders AB and AABB type such as PA-12 and PA-10/13.[244] However, it should be noted that powders produced through this method are not available commercially.[61] Spray drying is used to synthesize particles for SLS in the case of PA-6 with layered silicates (figure 2).[245] By utilizing smaller polymeric particles we can attain a better resolution because the minimum feature resolution will theoretically be the size of the particles used.

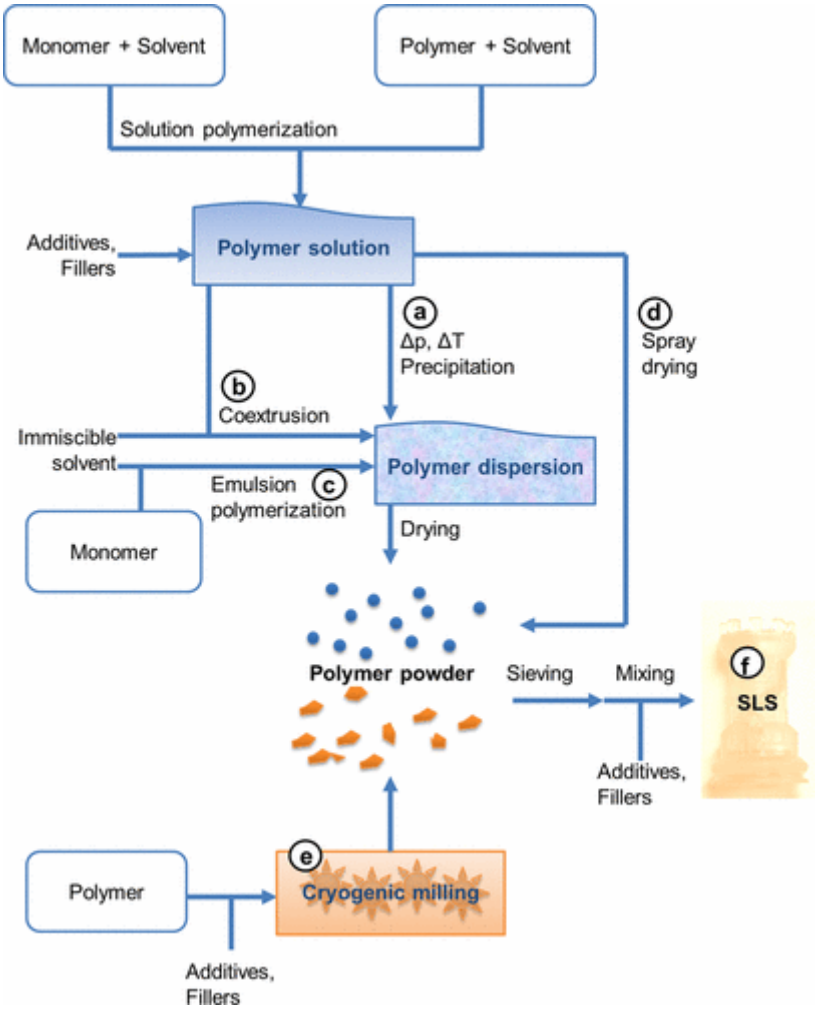


Figure 2 – Methods for the fabrication of SLS powders A.) precipitation of polymer B.) coextrusion of polymer solution with immiscible solvent C.) emulsion polymerisation

of water insoluble monomers D.) Spray drying of polymer solution E.) Cryogenic milling of polymer powders F.) SLS processing of powders. [61]

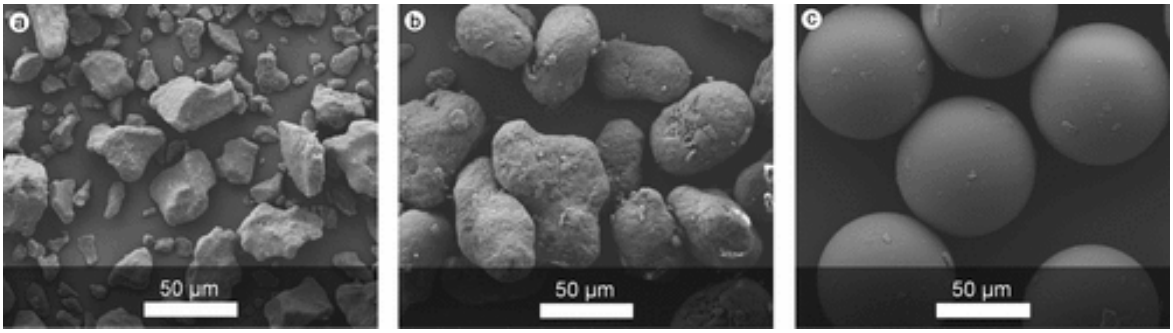


Figure 3 – Morphology of commercial powders for polymer-based SLS A.) cryogenically ground, jagged particles (PA-11 powder, PA1101 from EOS GmBH) B.) Potato shaped particles precipitated from ethanol solution (PA-12 powder, PA2200 from EOS GmBH) C.) Spherical particles produced via emulsion polymerisation (PS powder Primecast 101 from EOS GmBH)[61]

The spot size of the laser in an SLS system can dictate the resolution of the built part in the x and y directions.[232] The laser will scan over the polymer particles sintering them in a pattern specified by a computer model, and the width of this scan is the spot size of the laser. Therefore, if you use particles that are 1 µm in size, using a laser with a spot size of 200 µm, would lead to a resolution of ~200 µm, as every particle that comes into contact with the laser is sintered, so by utilizing a laser with a smaller spot size the user can reach a higher resolution (figure 4).

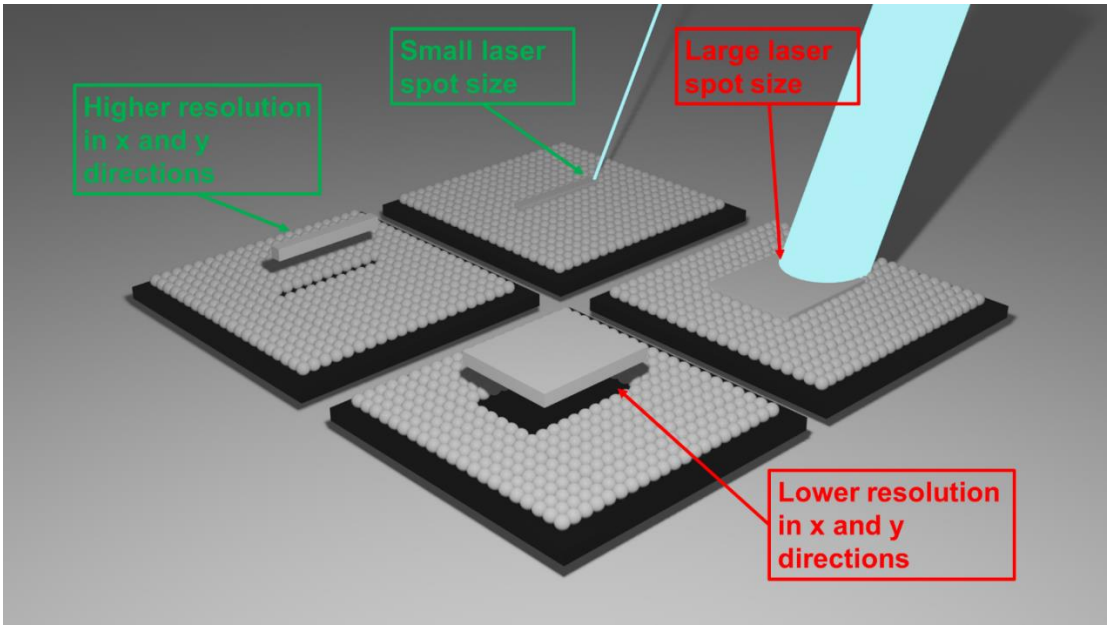


Figure 4 – Effect of laser spot size on resolution of part built via SLS. A laser with a small spot size will sinter a smaller segment of the particles thereby allowing for a higher resolution. A large laser spot size will sinter a larger segment of the particles, even if the particles are smaller, as everything the laser touches will sinter, thereby resulting in a lower resolution.

The smallest spot size that may be in theory achieved with conventional SLS printers is around 10.6 µm. This is because CO_2 lasers are used in SLS systems and they have a wavelength of 10.6 µm.[232] These lasers often have a spot size of 200 µm because the spot size is also dependent on different parts of the laser array, and the spot size can be found using equation 1.

$$Wf = \frac{\lambda f}{\pi Wo}$$

Equation 1 – Determining focal point spot size of a laser. Wf is the focal point spot size. Wo is the diameter of the beam before focusing. F is the distance of the focal point. λ is the wavelength of the laser.

As is seen from eq. 1 the wavelength of the laser is proportional to the spot size, as the smaller the wavelength the smaller the possible wavelength. The wavelength of a CO_2 laser is 10.6 µm that is why ~10.6 µm is the theoretical limit for the spot size of a CO_2 laser. By using a laser with a smaller wavelength, it should be possible to reach a smaller spot size, for example a UV laser with a wavelength of 405 nm can theoretically reach a ~ 405 nm spot size. However, it is very difficult to reach this theoretical limit, as when using the SLS the laser passes through a series of mirrors and travels a considerable distance through the machine, thereby increasing the laser spot size.[246]

The control over the build platform will dictate the resolution in the z-axis of the built part. This is, because the control over the z-axis controls the thickness of each layer (composed of particles). Hence even if the particle size and laser spot size give you the desired resolution in the x and y axis; bad control over the build platform would result in an undesirable resolution in the z axis, thereby limiting the total feature resolution of the part (figure 5).

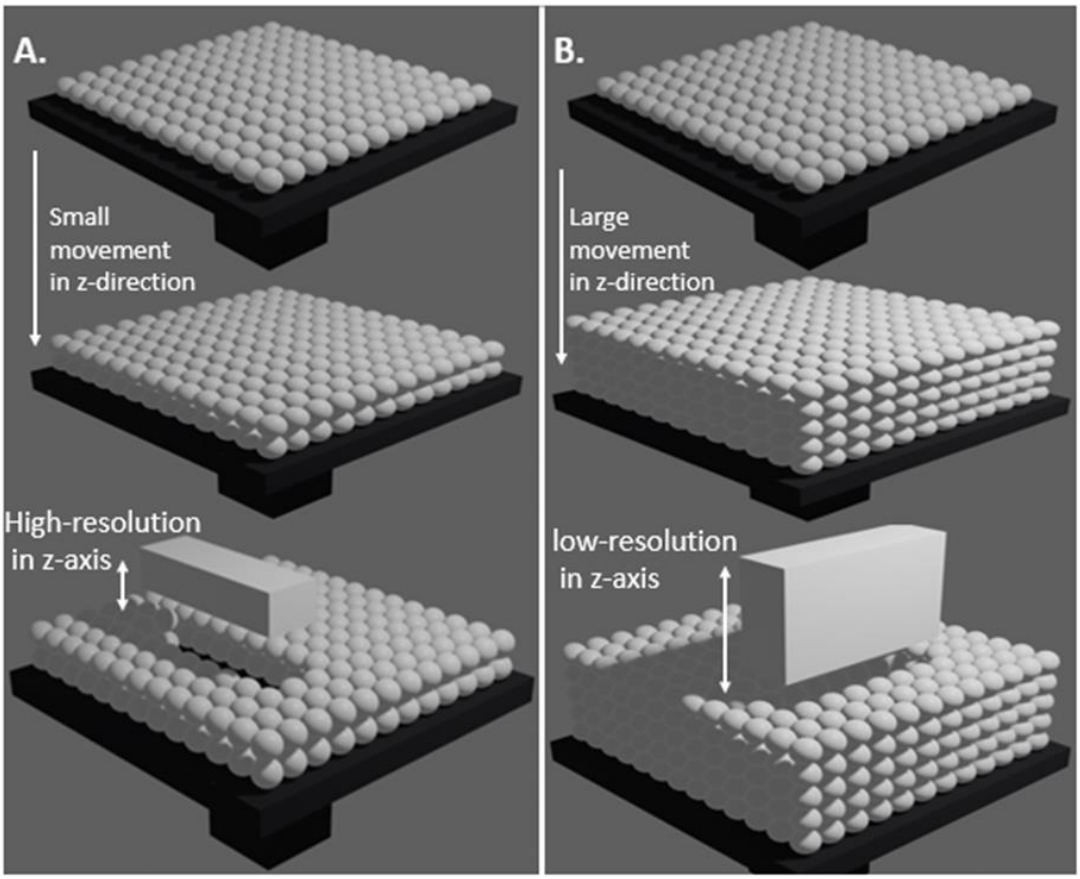


Figure 5 - The effect of the build platform on the resolution of a part. A.) Schematic of higher controller over movement of the build platform in the z-direction leading to higher-resolution. B.) Schematic of lower controller over movement of the build platform in the z-direction leading to lower-resolution.

The control over the build platform in the z-direction varies from machine to machine; high-end printers can reach movement control between 50 – 200 µm.[231] By using a build platform that can move with a precision of ≤ 10 µm, a printer should be able to form layers that are ~10 µm thick if particles of the appropriate size are used. For the aforementioned reasons commercial printers can only reach max resolutions of ~100 µm.

There have been attempts to improve the resolution of SLS printers. The most successful has been a SLS printer built by Roy et. al. and others such as H. Ko *et. al*. have also managed to print in high resolutions.[247,248] The printer built by Roy *et. al.* had several notable alterations, which increased its maximum resolution to 10 µm.[247] The high resolution was achieved by using a particulate slurry composed of sub-micron metal particles and a surfactant to deposit a metallic particle layer.[247] The system included a vacuum built into the build platform, which was used to drain the liquid used to create the slurry and ensure that the particles stay in their position during the deposition of subsequent layers.[247] The laser would then sinter the layer once the liquid was drained and the process repeats for each layer until the part is finished.[247] This rig also used a micromirror array on the laser to reach a laser spot size of ~10 µm, and a laser with a wavelength of 532 nm.[247] However, this process and the one developed by H. Ko *et. al.* deviated significantly from conventional SLS printing and used metallic particles instead of polymer-based particles.[247,248] Not only was it needed to produce a printer suited towards higher resolution, but also small polymeric particles (0.5 – 10 µm), which can be produced through free radical dispersion polymerisation in $scCO_2$.

Free Radical Dispersion Polymerisation in $scCO_2$

Dispersion polymerisation in $scCO_2$ was used to produce several of the target polymers, when the target particle size was between 0.5 µm to 10 µm. Dispersion polymerisation is a type of heterogenous polymerisation in which the polymer precipitates out of the solvent ($scCO_2$).[249] This polymerisation requires a solvent and

a stabilizer, and the monomer must be soluble in the solvent but the polymer cannot be.[249]

To start the reaction an initiator (eg. AIBN) is needed. The initiator decomposes into free radicals, which subsequently react with the monomer, to produce monomer radical species (step 1, figure 6). At this stage the monomer starts to propagate, and until the polymer chains reach a critical molecular weight they remain in the solution (step 2, figure 6). After the threshold of the critical point is crossed, the polymer chains precipitate out (step 3, figure 6) and coagulate until stabilized particles are formed (step 4, figure 6). Stabilisation happens, because the stabilizer (PDMS-MA) is covalently bonded to the polymer particle. The growth of the polymer continues as the monomers add onto stabilized particles. Then the polymerisation ends as the monomer has been depleted.

The stabilizer is essential to the reaction as one end has an affinity toward the solvent and the other to the polymer, hence the stabilizer keeps the polymer particles in the solvent, so that monomer addition can continue.[249] The stabilizer also forms a layer around the particles that prevents particle coagulation.[250,251] This reaction has been utilized in the past to produce particles of PMMA of varying sizes.[250,251] Many other polymeric particles such as polystyrene have been made through dispersion polymerisation in $scCO_2$.[66–70]

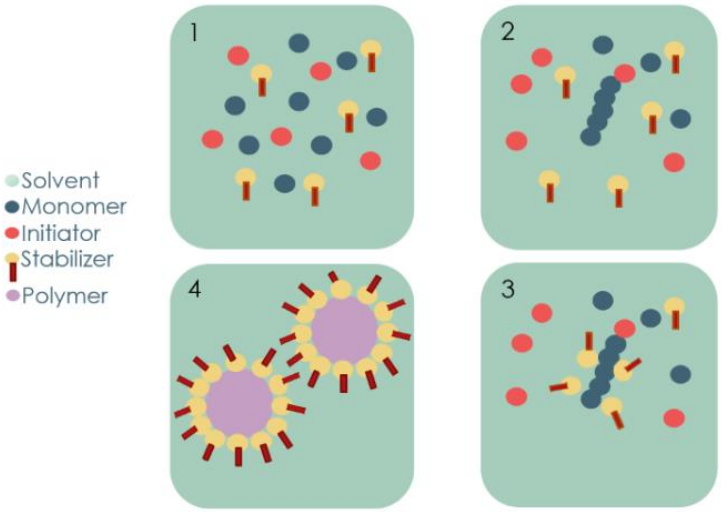


Figure 6 – Reaction scheme of dispersion polymerisation. In step one the reagents are dissolved in the reaction. In step two the initiators have decomposed into free radical species and have reacted with the monomers, starting the propagation stage of polymerisation. In the third step the polymer chain has reached a critical mass, at which it interacts with the stabilizer and starts to form particles. In step 4 the particles have formed and the reaction finishes inside said particles as the remaining monomer is consumed.

The stabilizer used for this project is PDMS-MA, however there are different types of stabilizer available. The two main types of stabilizers are: graft type stabilizers and stabilizers which interact to the polymer through Van der Waals forces.[250,251] The graft-type stabilizers covalently bond to the polymer particles as a graft co-polymer, so the interaction is very strong.[250,251] In stark contrast, the other type of stabilizers bind through much weaker forces.[250,251] Each of these stabilizers have benefits, because the graft-type stabilizers bind strongly they can assure good dispersion of the polymer particle in the reaction medium, however it is hard to remove form the finished product. The Van der Waals type stabilizer binds weakly, therefore the bond

between the stabilizer and the polymer can break causing the polymer to crash out of the reaction medium, which can occur due to excessive stirring. The main benefit of dispersion polymerisation in $scCO_2$ is that the reaction yields polymer particles that are discrete and monodisperse.

Through FRDP polymerisation in $scCO_2$, particles with sizes ranging from 0.2 µm to 7 µm can be synthesized, it is possible to coat larger particles as well, and a wide variety of polymer and particle architectures can be obtained.[68–70] This can be done in other reaction media, however CO_2 has several key benefits that make it the preferred reaction media. The main advantages of this type of polymerisation are:

1. It is a green polymerisation process as it is performed in $scCO_2$.

2. The dispersion aspect of the reaction allows the polymer to be composed of discrete monodisperse particles.

3. By using the aforementioned types of polymerisations several new polymers can be made, which could be suitable for SLS printing.

Our aim is to create a polymer SLS system that can print with a maximum resolution of ~10 µm. This would be a big advancement for SLS and 3D printing technology as parts with high resolution could be printed quickly with a large variety of complex geometries. In order to achieve this a new SLS rig needed to be built and custom polymer particles were synthesized. The SLS printer needs to have a laser spot size of ≤ 10 µm and excellent control over the movement of the build platform in the z-axis (≤ 10 µm). Small spherical polymeric particles (1 – 5 µm) were synthesized, which have the necessary extrinsic and intrinsic properties needed for SLS printing.

Results and Discussion:

Initial small polymeric particle synthesis:

The problem area that was addressed first, in regard to high-resolution SLS, was the synthesis of small polymeric particles suitable for SLS. Several possible methods were considered such as emulsion polymerisation in organic solvents and dispersion polymerisations in $scCO_2$. Dispersion Polymerisations can be conducted in $scCO_2$ if the monomer is soluble, and the polymer is insoluble.[22,69,186] The technique necessitates a surfactant and an initiator, which should be soluble in $scCO_2$.[22,68,69,186] During the free-radical dispersion polymerisations the initiator breaks down into radicals, which subsequently react with the monomer and start the propagation step. Once a certain chain length is reached the polymer chains that interact with the surfactant start to become particles, and the reaction terminates in these particles. $ScCO_2$ allows the user to employ a multitude of polymerisation techniques, for these particles free radical dispersion polymerisation (FRDP) was used.[22,68,69,186] This allows for the synthesis of polymer particles of sizes ranging from 0.5 – 5 µm.[68,69] The size of the particles can be controlled via the amount of stabilizer used during the polymerisation , with PDMS-MA the weight of percentage (wt%) can be increased up to 20 wt% decreasing the particle size as the wt% of PDMS-MA is increased.[68,69] Along with particle size Molecular weight (M_n) can be controlled, however through varying the amount of initiator used, as a lower amount of initiator will lead to longer polymer chains hence higher M_n. $ScCO_2$ offers other benefits, one of which is extremely beneficial for SLS purposes, as once the polymerisation has finished the CO_2 can be

vented yielding a dry and pure product that can be immediately used in an SLS printer.[188,252,253]

The first particles that were produced for high-resolution SLS were Poly methyl methacrylate (PMMA) particles were synthesized via FRDP in $scCO_2$. The aim was to make particles that had a size ranging between 0.5 – 5 µm. PMMA was chosen as the monomer, as it has been shown to polymerize and form particles well in $scCO_2$. PMMA also has the intrinsic properties needed for SLS, as it can absorb the radiation of the lasers normally used for SLS, has a Tg of about 100 – 120° C, and can flow adequately.[68,69] The conversion of the polymers was calculated from the ^{1}H NMR (figure 7) of the polymers using equation 2.

$$conversion = \frac{AUCP}{1 + AUCP}$$

Equation 2 – Determining the conversion of the polymers. AUCP is the area under the curve of the polymer peak when compared to the area under the curve of the monomer peak. Hence by dividing AUCP by the peak plus one, one obtains the conversion of the monomer, if species in questions has the same number of hydrogens as a polymer and monomer.

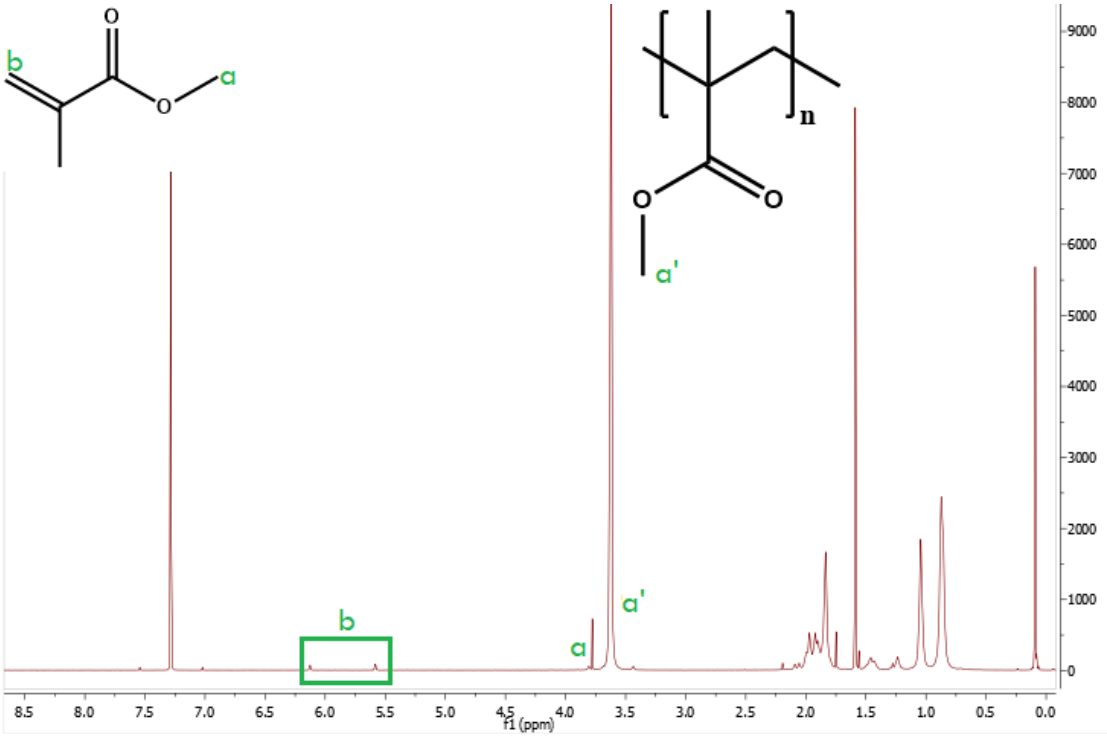


Figure 7 – ^{1}H NMR spectrum of PMMA and MMA residues. a' peak is belonging to PMMA whilst a belongs to MMA. Peaks related to b are of MMA, as they are the vinyl bond which reacts to form the PMMA polymer.

The conversion of PMMA is greater than 95%, and the dispersity ranges from 1.4 - 2.0 (measured via GPC). Glass transition temperature (T_g) was measured via DSC and was found to be between 114 – 119 ^{o}C (table 1).

Table 1 – Synthesis of pMMA particle.

Sample	Conversion (%)[a]	M_w (KDa)[b]	M_n (KDa)[b]	$Đ$[b]	T_g (^oC)[c]	Effective Particle size (µm)[d]
PMMA 1	96	327	194	1.7	114.3	23.7
PMMA 2	99	125	88	1.4	118.7	22.9
PMMA 3	99	152	109	1.4	116.4	22.2
PMMA 4	99	310	155	2.0	115.3	22.8

a. Conversion measured from ^1H NMR spectrum. b. M_w, M_n, $Đ$ obtained from GPC chromatograms. c. T_g, T_m, T_c values obtained from DSC analysis. d. Effective Particle size (Size of agglomerates formed when in the solid state) obtained from LDS analysis and further corroborated with SEM which was utilized for particle size and shape analysis.

Particles sizes were obtained from both SEM and LDS techniques (figure 8). SEM analysis was used to detect the size of individual particles while LDS measured the size of the agglomerates formed because of Van der Waals forces imposed on the PMMA particles. LDS was used instead of DLS as LDS measures the particle size when the powder is dry instead of suspended in a solution. Hence, LDS gives a more representative measurement of the size of the particles whilst printing via SLS. The particle size of the PMMA particles obtained from SEM analysis ranges from 1 – 5 µm (figure 8). LDS analysis showed that PMMA particles agglomerate into larger clusters with sizes ranging between 22.2 µm – 23.7 µm.

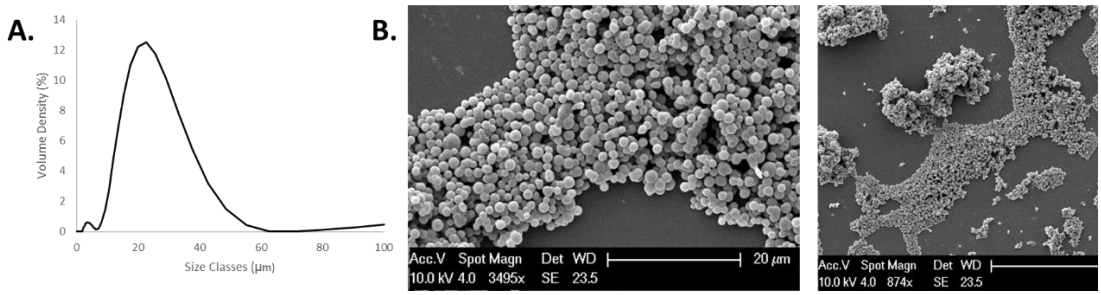


Figure 8 – Particle size analysis of PMMA particles. A.) LDS spectra of PMMA particles, showing that the formed agglomerates (secondary structures) are between 22.2 µm – 23.7 µm, whilst the primary particles are between 1-2 µm. B.) SEM image of PMMA particles this image shows that the particles are agglomerating into larger clusters instead of forming monolayers

Even though the particle clusters had a larger size than desired, they were later used to print a grid with the in-house built SLS rig. The particles consistently agglomerate into clusters (secondary structures), because the attractive Van der Waals forces between the individual particles are stronger than the gravitational force imposed on them, once the clusters reach a size of 20 µm the gravitational forces start the be favoured instead of the Van der Waal's forces (figure 9).[254,255] This behaviour has been observed for many types of sub 20 µm particles (metal, glass, and polymer).[254,255]

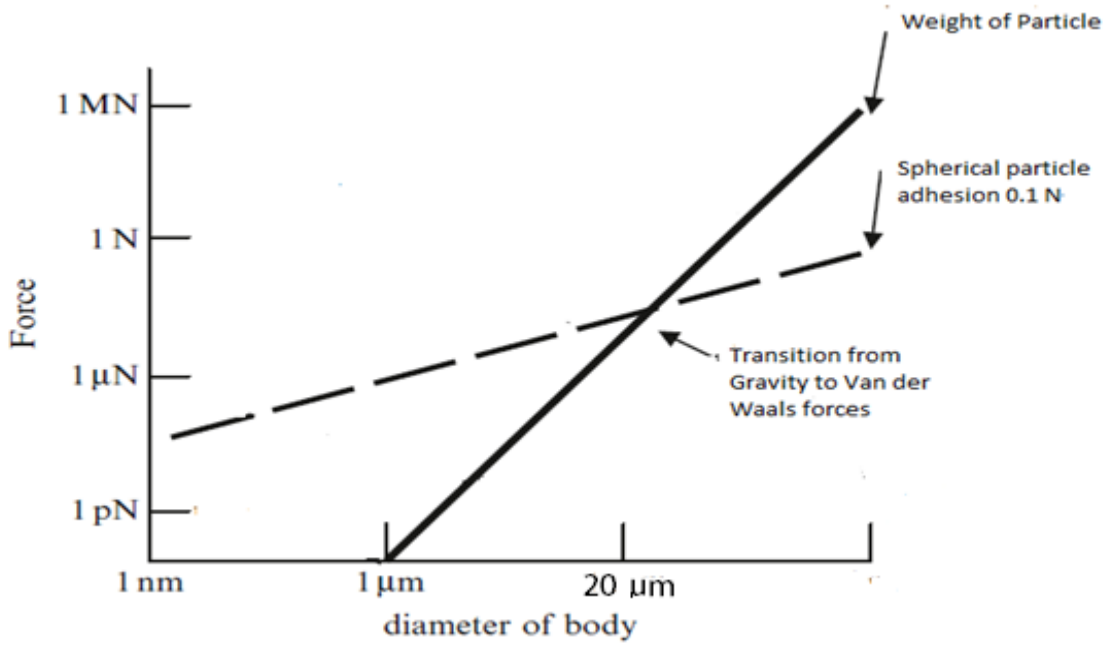


Figure 9 – Strength of gravitational and Van der Waal's forces imposed on spherical particles depending on size. Showing that there is a crossover point at ~20 µm, where the dominant force stops being gravity and starts being Van der Waals forces.

Production and testing of novel SLS rig for high-resolution printing:

A novel SLS printer was developed, manufactured, and debugged. This new system allows us to study the processes of selective laser sintering of various new polymeric materials of micron and sub-micron particles.[256] The operating principle of the apparatus is based on the formation of a 3D object by layer-by-layer laser induced fusion of finely dispersed (0.3 µm – 5 µm) polymer particles. A thin layer of the initial powder (the thickness is adjustable in the range of 5 µm – 100 µm) is transferred from the loading surface to the working surface using a specialized device (figure 10, part a). In the powder layer, local fusion of particles, by a focused laser beam is carried out along a part corresponding to a specific section of a digital model (figure 10, part b). After finishing printing one layer, the next layer is applied; the cycle is repeated as

long as necessary. This approach allows one to obtain three-dimensional structures of almost any geometry.[256] Hence with this novel design, we can utilize the same SLS process, but aim at printing with resolutions improved by as much as ten-fold.

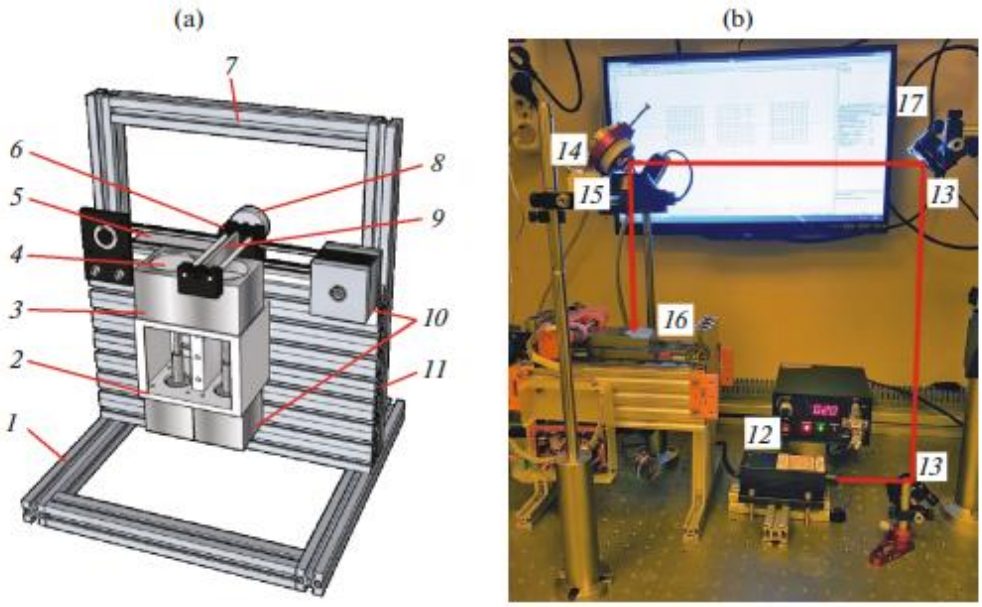


Figure 10 – A.) The scheme of the module for the formation of layers of fine powders in an apparatus for SLS. B.) Image of the laser scanning module. 1.) Frame 2.) Piston drive house 3.) Block of working chambers 4.) pistons 5.) unit power supply 6.) levelling device housing 7.) fastening of the laser scanning module (galvanic scanner) 8.) mechanical or piezoelectric levelling device actuator 9.) The working element of the levelling device 10.) step drives 11.) microcontroller 12.) laser 13.) mirrors 14.) galvanoscanner 15.) lens 16.) the working layer of powder 17.) control computer.[256]

The module for the deposition of polymeric particle layers has two essential parts, a roller to spread the powder onto the build stage and the pistons which move both the build stage and the powder reservoir in the z-direction (figure 10a).[256] Its basis is a block (3) made of corrosion-resistant steel containing two cylindrical chambers with

pistons (4). Each piston has a diameter of 36 mm and is equipped with an individual step drive (10) that provides a maximum movement along the vertical axis (Z-axis) of 30 mm and a minimum step of 5 μm. The contacting surfaces of the working chambers and pistons have a surface finish of grade 10 and are ground with a gap not exceeding 5 μm. This ensures movement of micron sized polymer particles without loss. One of the chambers acts as a reservoir and dosing device, while the piston of the second chamber is the working surface for the SLS process, whose movement determines the required thickness of the powder layer. Powder transfer and the formation of a homogeneous and dense layer on the working surface are carried out by a specialized device that consists of an electronically insulated housing (6) on which a mechanical or piezoelectric activator is fixed. The device has a working element, polished shaft (9), which is 8 mm in diameter, made of 08KKh18N10 stainless steel, which rotates at the required speed around the axis. To suppress surface electrostatic effects (leading to agglomeration and sticking of polymer particles to the surfaces of the levelling device), components of the levelling device (6,8,9) and the blocks with pistons (3,4,6) are electronically isolated from the housing of the rest of the apparatus and grounded. Potential can also be applied to them, varying within +- 36 V. The electromechanical drives of the apparatus are controlled by an Atmol ATmega 2560 micro controlled with an electronic strapping similar to that described previously in that it provides the operation of four unipolar stopper motors with rated operating currents of up to 1.8 A.[256]

The printer and laser scanning module were built in such a way that the UV laser can be focused through a mirror array, so that the laser spot is small (~10 μm) when it

hits the build platform (figure 10b). For sintering, continuous radiation from a DP55 laser MDL-III-405 was used (12) at a wavelength of 405 nm. This laser was used as the wavelength is considerably lower, and previous work has shown that it is possible to print via SLS with UV lasers. Laser radiation was focused on the working surface of the sintered powder layer using mirrors (13) and on LScan xy single mirror galvanic scanning system (14) with a TSL-405-29-55Q F-theta lens (15). The optical system allows one to collect laser radiation with a power of up to 100 mW into a spot with a diameter of 10 μm, as well as to move it along the necessary path along the surface of the formed layer (16) at a speed of 0.1 to 100 mm/s.[256] The spot size is considerably smaller than what is achieved with a CO_2 laser, as the CO_2 laser will pass through a series of mirror array enlarging the spot size frequently to about 200 μm. The spot size is this large, because the laser passes through the mirror array and a considerable distance before reaching the powder that is sintered.

Automatic control of the laser part of the system is provided by a computer (17) with preinstalled LDesigner SLS software; control of its mechanical part occurs using the original software of our own development. This software allows the preparation of a control program with which the apparatus preforms the process for the required object according to the computer 3D model (STL file).[256]

A microcamera equipped with a telescopic lens can also be placed in the optical path for the operator's convenience and control of the behaviour of polymer microparticles during the formation of new powder layers. With its use, it is possible to carry out visual control at the sintering event of polymer particles in the laser

exposure zone and study its dependence on sintering parameters (laser reduction power, scanning speed, etc.). [256]

The aforementioned small PMMA particles with an individual particle size of 0.5 – 5 µm, and agglomerates of ~20 µm, were used to test the printer. This resulted in grids with resolutions between 80 – 100 µm (figure 11), which was larger than the expected resolution of ~20 µm (given by the effective particle size ~20 µm and the use of a 405 nm laser for printing) .[257] It is thought that the lack of resolution is caused by the size of the secondary structures, and not the printer, since the laser worked consistently and the control over the build platform was as desired. The lack of resolution most likely occurred because the large clusters can diminish the flow and packing quality of the products.

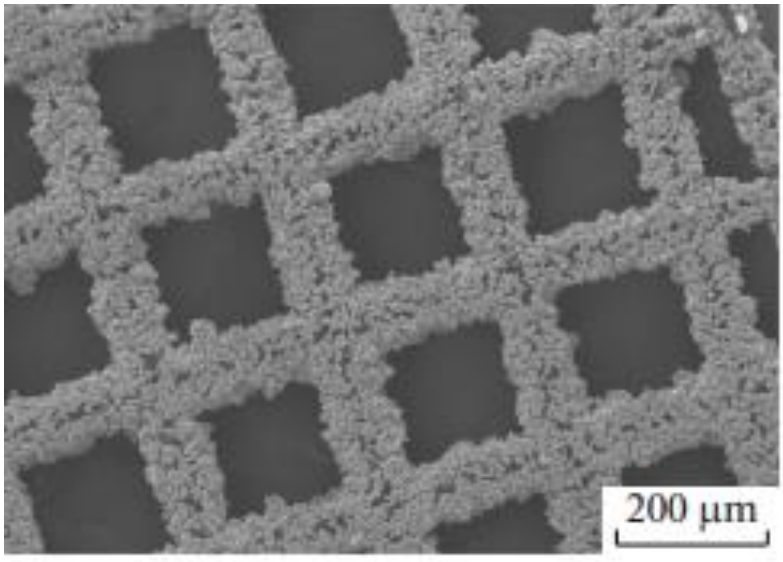


Figure 11 – Results from SLS printing of PMMA particles. The pattern printed is of a grid and the resolution of the produced grid is between 80 – 100 µm.

The packing and flow properties of the PMMA clusters is not satisfactory because the shape of the clusters is very irregular and sometimes very far from spherical. The

combination of different shapes found in the particulate powder prevent the powders from rolling easily thereby producing polymeric particle layers that have a low Z-resolution and frequently small gaps caused by the uneven rolling.

Production of micron-sized particles for SLS via milling:

Studies have shown that roughening of the spherical particles can reduce the impact of the Van der Waal's forces on the particles.[258] Because of this PMMA particles were ball milled to see if the agglomerates could be broken, and the particles roughened enough to weaken the Van der Waals forces, thereby allowing for the formation of smaller and stable agglomerates (figure 12).

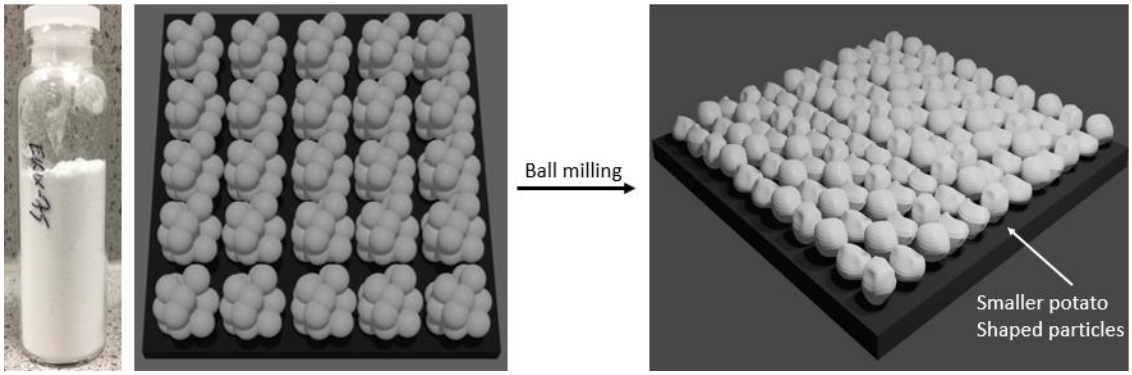


Figure 12 – Theoretical result of ball milled PMMA particles. Through ball milling the particulate clusters should be crushed into smaller potato shaped particles, which should have the desired size and flow properties.

PMMA particles were ball milled for three different periods of time (1 min, 5 min, and 10 min). The particles that were ball milled, showed a decrease in size in both SEM and LDS analysis, with LDS analysis showing that the particles decreased to 14.7 µm (figure 13) after 1 min of ball milling. SEM showed that there was a minimal change

to the shape of the particles (figure 13). The resulting particles were statically charged, which made collection and testing impractical.

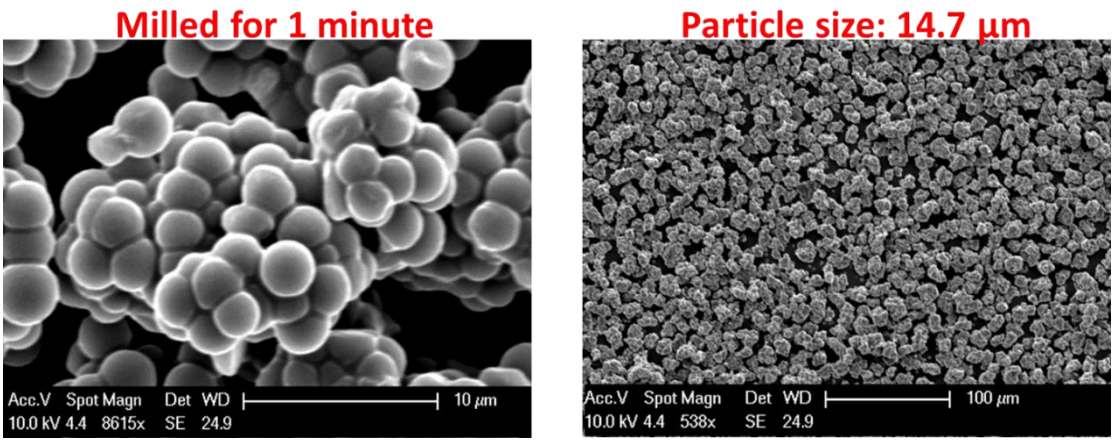


Figure 13– Results of ball milling PMMA particles for 1 min. SEM images of the ball milled (1 min) PMMA particles. The SEMs show that the individual particles have largely kept their shape, whilst the particulate clusters have decreased in size to 14.7 µm (obtained from LDS analysis).

The particles showed greater shape change (albeit still minimal) after 5 min of ball milling (figure 14). This was a promising result as the particles were rougher and had a size of 14.7 µm (figure 14). However, the particles were statically charged and still did not have the desired size of ~ 10 µm.

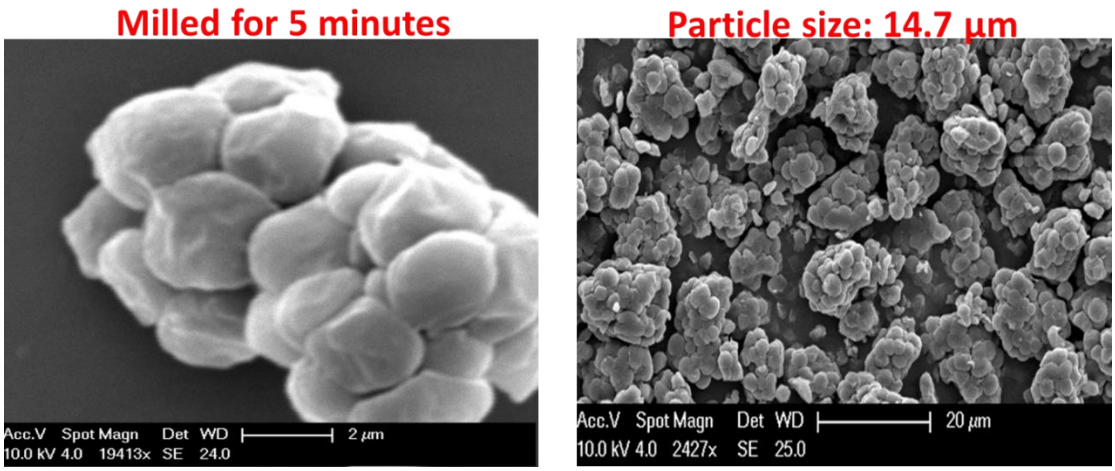


Figure 14 - Results of ball milling PMMA particles for 5 min. SEM images of the ball milled (5 min) PMMA particles. SEM images show that the particles are starting to lose their shape, and the decrease in size (to 14.7 µm) was the same as the sample that was ball milled for 1 min (obtained from LDS analysis).

Finally, PMMA particles were ball milled for 10 min, yielding small particles with greater change in shape. The particles aggregates showed an average particle size of 11.7 µm (figure 15). The shape of the particles was greatly changed as some particles agglomerated and some separated entirely, while others showed slight loss of the morphology. The inconsistent shapes made the packing less efficient, and the particles were also statically charged, further investigations into powder density could grant more information about the nature of the statics. Hence the resulting particles were unsuitable for use as SLS polymer.

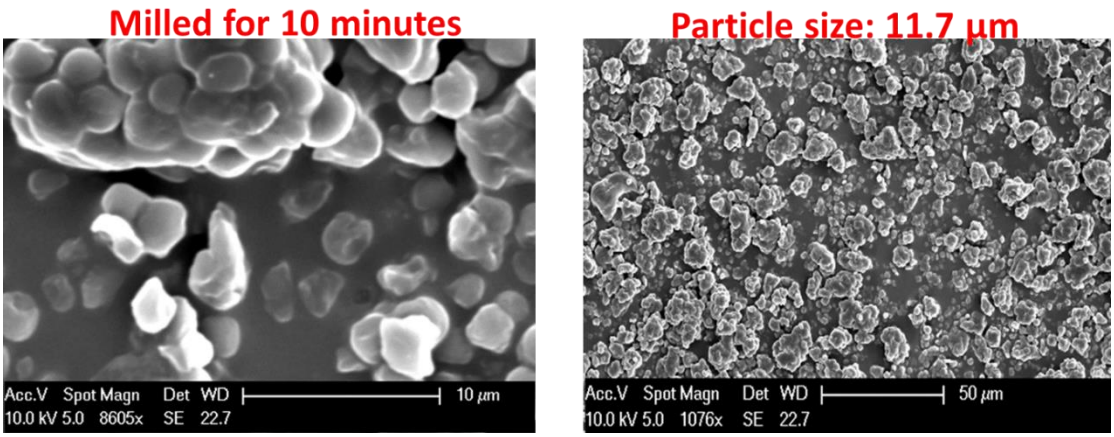


Figure 15 - Results of ball milling pMMA particles for 10 min. SEM images of the ball milled (10 min) PMMA particles. After ten minutes of ball milling the particles have almost completely lost their shape and the size of the particulate clusters has decreased to 11.7 µm (obtained from LDS analysis).

The expectation was to see smaller particles as milling time increased, which was shown by the LDS data. However, the downside to increased milling time was that the particles got hotter as a high number of collisions occurred for an extended period of time. This led to complete loss of the spherical shape of the particles instead of just roughening the particles to yield 'potato' shaped particles (figure 16).

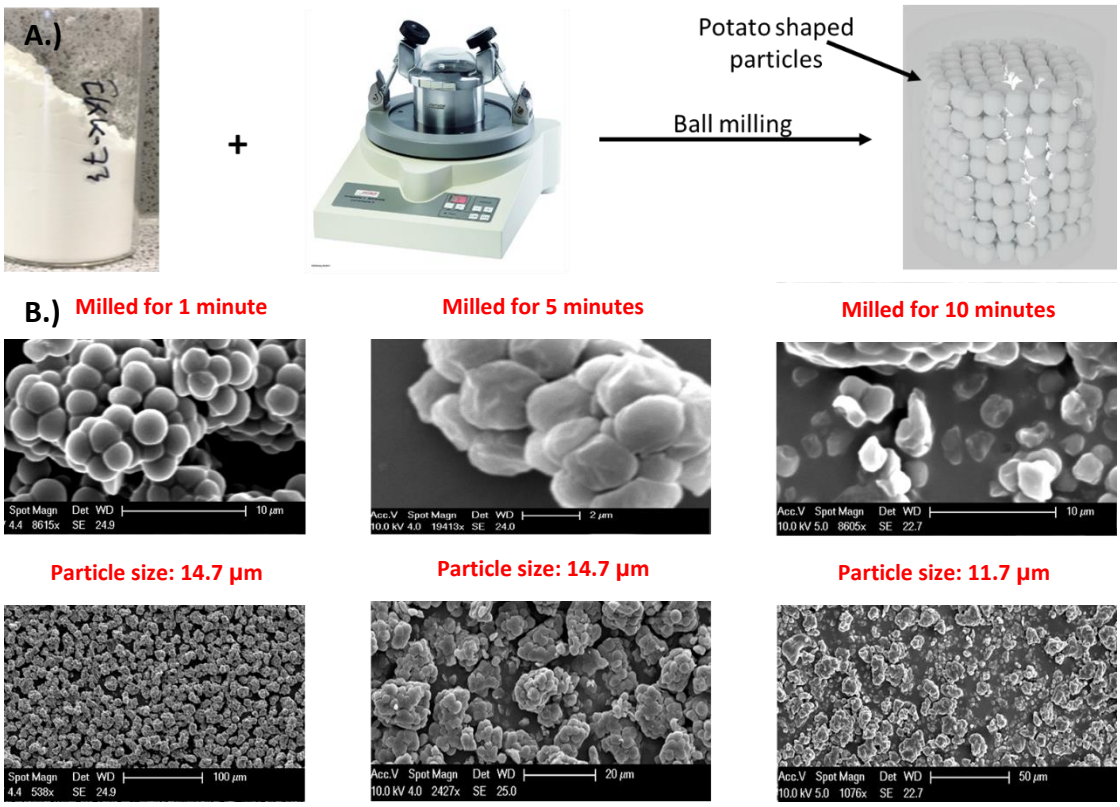


Figure 16 – Results of Ball milling PMMA particles for 1, 5, and 10 minutes. A.) Schematic for production of smaller potato shaped particles via ball milling. B.) SEM images of PMMA particles ball milled for 1, 5, and 10 minutes.

Ball milling succeeded in decreasing the size of the particles, however the particle shape was altered greatly, and they melted together (figure 16). Production of printable layers was attempted by manual and mechanical procedures, as was done with the standard PMMA particles. All the ball milled samples from 1 min to 10 min had several factors which prevented adequate layer formation. The main factor being that the particles had a static charge, which complicated their handling. Also, the flow properties was worsened, as the particles had completely lost their shape after 10 min, which also affected the packing structure. This was seen qualitatively as there

were large gaps in the sintered layers, and the particles flew when layer spreading was attempted.

In order to address these issues, the particles were cryogenically milled (cryo-milled). This strategy should keep the temperature low enough to prevent the particles from melting.[259] Cryogenic milling decreased the size of the clusters to 3.6 µm (measured via DLS) and SEM analysis showed that the change in shape resulted in particles that were 'potato' shaped (figure 17). However, cryogenic milling failed in improving the other SLS pertaining properties of the PMMA particles, as the particles still had a static charge and bad flow, this effect could be further studied through powder density measurements. Because of this, a different route, based on a chemical alteration rather than a physical manipulation was taken in order to produce a printable layer with higher resolutions.

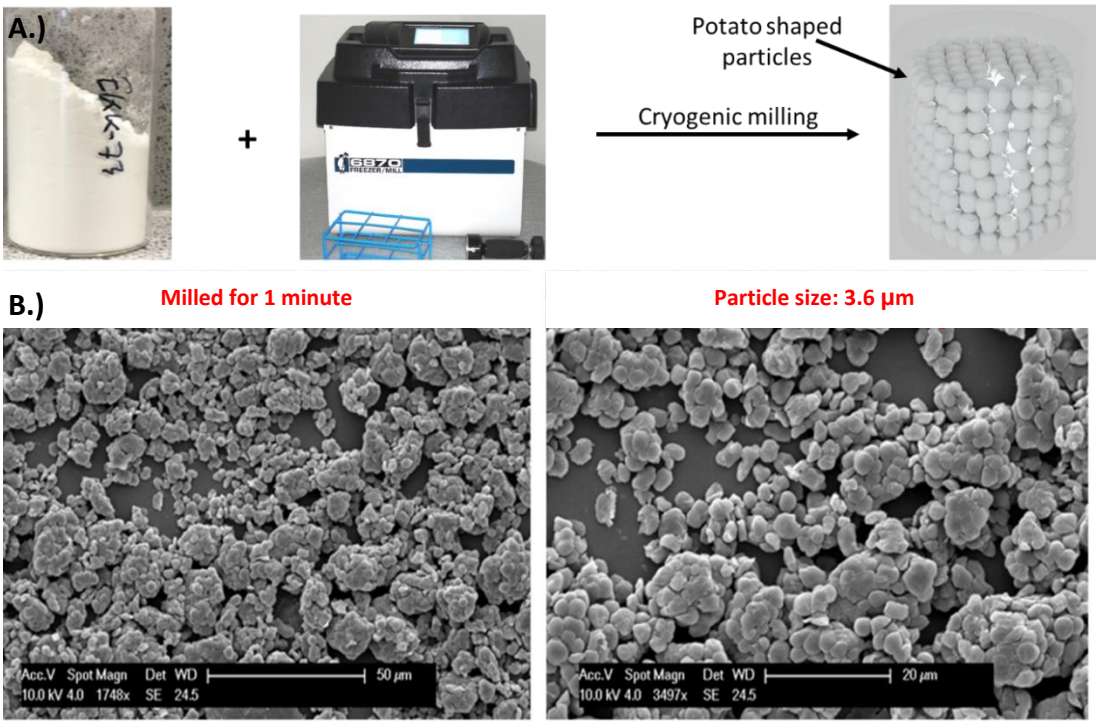


Figure 17 – Results of cryogenic milling PMMA particles. A.) Schematic of production of smaller potato shaped PMMA particles through cryo-milling B.) SEM images of cryogenically milled PMMA particles (1 min). The SEM images show that the particles have changed shape and a large decrease in particulate cluster size was seen (to 3.6 µm).

Even though the ball milling and cryo-milling strategies succeeded in decreasing the size of the PMMA clusters, the ball-milling strategy changed the shape of the polymeric particles too much, and the cryo-milling strategy produced particles of the wanted shape and size but the particles were too statically charged for practical SLS powder deposition. For this reason an alternate route to producing small polymeric particles for SLS needed to be taken.

Production of micron-sized particles for SLS via chemical means:

To be able to consistently produce monolayers of small polymeric particles an alternative synthesis route had to be taken. It was decided that to reduce the agglomeration of the particles and fix the flow issues a co-polymeric particle would be synthesized consisting of P(MMA-X). The non-MMA polymer would have to impart the necessary functionality, which in this case is to reduce the Van der Waals forces between the particles, so that they prefer to form a monolayer instead of agglomerating into clusters. At the same time P(MMA-DB3MA) particles were being synthesized for an alternative purpose, and it was observed that this polymeric powder flowed well and made consistent layers when spread, so this material was investigated further. A variety of co-polymeric particles were produced with differing amounts of DB3MA. Between 0 – 2.5 wt% of DB3MA was used in the synthesis of the polymers. The polymers with varying amounts of the compound were compared via flow tests, which were conducted by eye. As the presence of DB3MA was shown to influence the flow behaviour of the polymers.

Particles composed of a P(MMA-disperse blue 3 methacrylate (DB3MA)) random co-polymer were synthesized via FRDP in $scCO_2$. These particles showed a conversion of ≥95% for PMMA (table 2). In ^1H NMR the monomer peaks of DB3MA coincide with the polymer peaks of pDB3MA hence the conversion cannot be measured (figure 18).

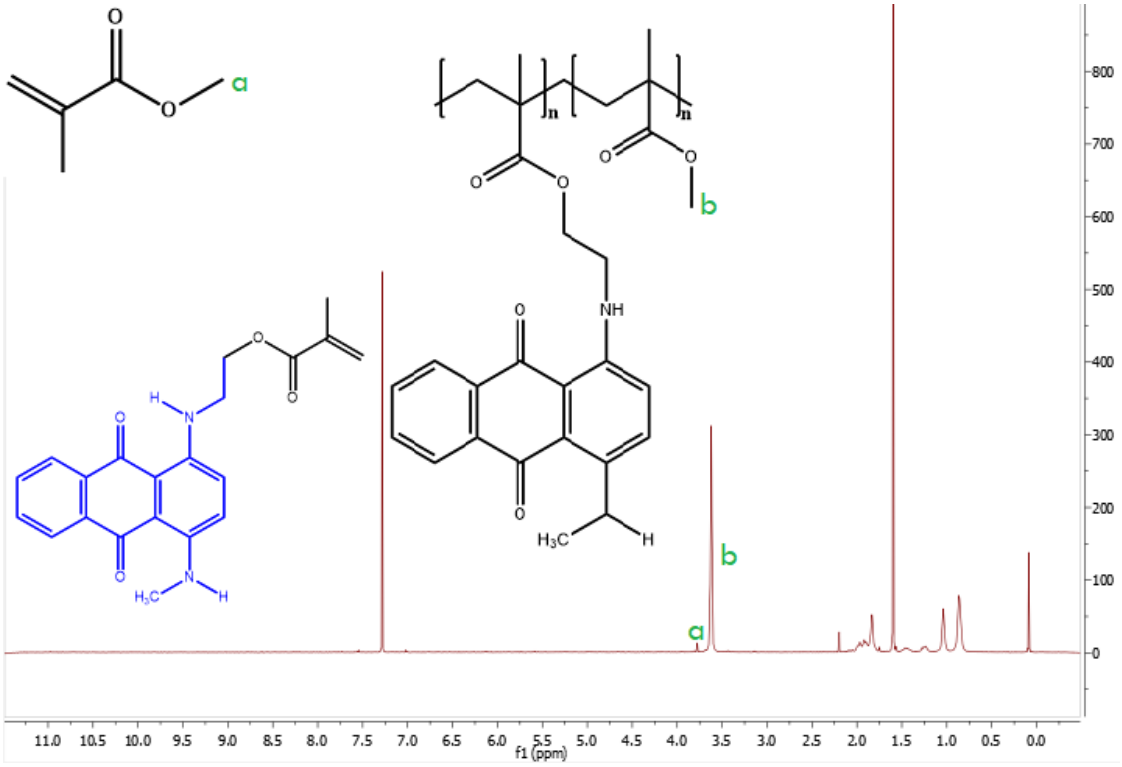


Figure 18 – ^{1}H NMR spectra of P(MMA-DB3MA) showing residues of MMA.

GPC analysis proved that DB3MA was part of the polymer chain as the UV trace of the polymer matched with the dRI and LS trace (figure 19).

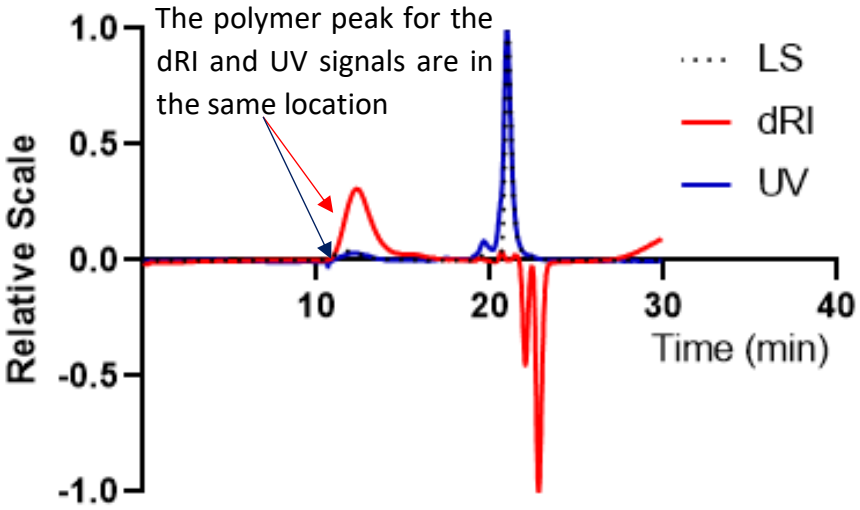


Figure 19 – GPC chromatogram of P(MMA-DB3MA). In the GPC chromatogram it can be seen that the UV and dRI signals appear at the same timepoint, hence the dye monomer has integrated into the polymer. The UV signal measures the ultraviolet-visible response of the polymer in question, if the polymer is not compatible with the wavelength (e.g. white or colorless) a signal does not appear, and if it is then a signal will show the molecular weight of the polymer. The dRI measures the molecular weight of a polymer as a change in refractive index compared to the eluent used. If the time points for the dRI and UV signals are the same, this proves that the molecular weight of the polymer is the same, hence the colour monomer is integrated into the polymeric chain.

The molecular weights of the polymers were consistently high M_w ≥200 kDa and the dispersities ranged from 1.2 – 1.9. The high molecular weight guarantees consistent thermal properties as after 40 kDa the T_g stops increasing. This can be seen from the DSC analysis as the T_g ranges from 108.6 – 111.3^oC (Table 2).

Table 2 – Synthesis of P(MMA-DB3MA) particles.

Sample	Amount of DB3MA (wt%)	Conversion (%)[a]	M_w (kDa)[b]	M_n (KDa)[b]	*Đ*[b]	T_g (^oC)[c]	Effective Particle size (μm)[d]
P(MMA-DB3MA) 1	1	98	232	136	1.7	111.3	25.8
P(MMA-DB3MA) 2	1.5	99	357	211	1.6	108.6	25.5
P(MMA-DB3MA) 3	0.5	99	340	175	1.9	109.4	26.1
P(MMA-DB3MA) 4	0.5	99	199	161	1.2	NA	NA
P(MMA-DB3MA) 5	0.5	99	284	213	1.3	NA	NA
P(MMA-DB3MA) 6	0.75	99	207	130	1.6	NA	NA

a. Conversion measured from ^{1}H NMR spectrum. b. M_w, M_n, *Đ* obtained from GPC chromatograms. c. T_g, T_m, T_c values obtained from DSC analysis. d. Particle size obtained from SEM and LDS analysis. n/a for thermal and particle size analysis for polymers P(MMA-DB3MA) 4-6 as the initial triplicate had proved repeatability and the remaining samples were sent to collaborators for high resolution SLS testing.

SEM and LDS analysis showed that the P(MMA-DB3MA) particles behaved in a similar way to the PMMA particles, the samples had the same spherical shape (analysed via SEM), and agglomerated into clusters of the same size (table 2) (figure 20).

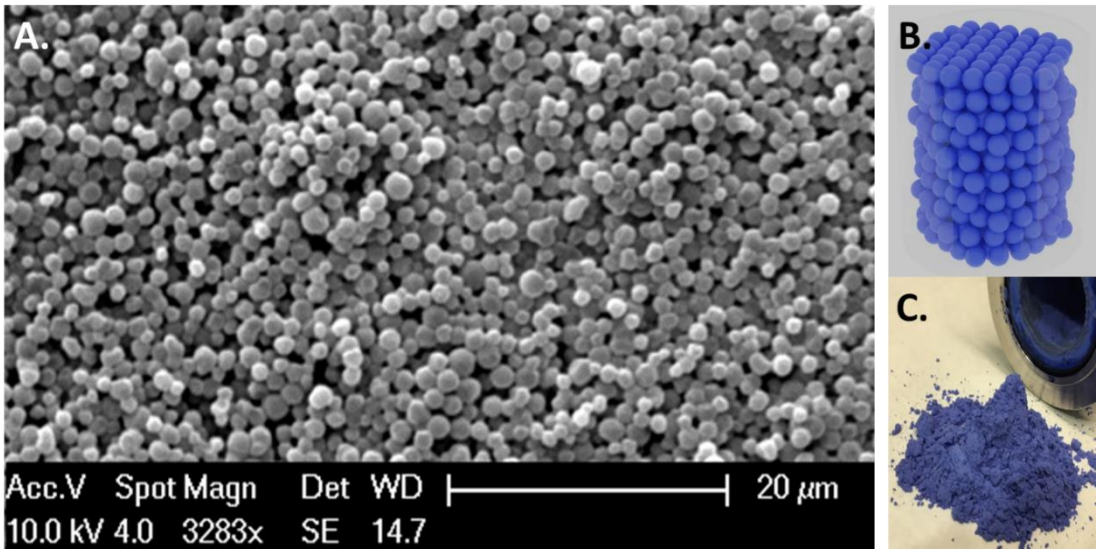


Figure 20 – Images of P(MMA-DB3MA) particles. A.) SEM image of P(MMA-DB3MA) particles, showing that the particles of P(MMA-DB3MA) pack in a form more similar to a monolayer than the PMMA particles, and that no secondary structures (agglomeration of particles in the solid state) are formed, with primary particle size of ~ 1 µm. B.) Schematic of P(MMA-DB3MA) particles C.) Image of P(MMA-DB3MA) powder straight after the CO_2 is vented after the synthesis was conducted.

However, the particles showed improved flow properties, and the material could be made into printable layers both manually and mechanically. The thickness of the layers was found to be ~ 10 µm (figure 21). This was promising as a layer with the wanted thickness and packing structure was formed.

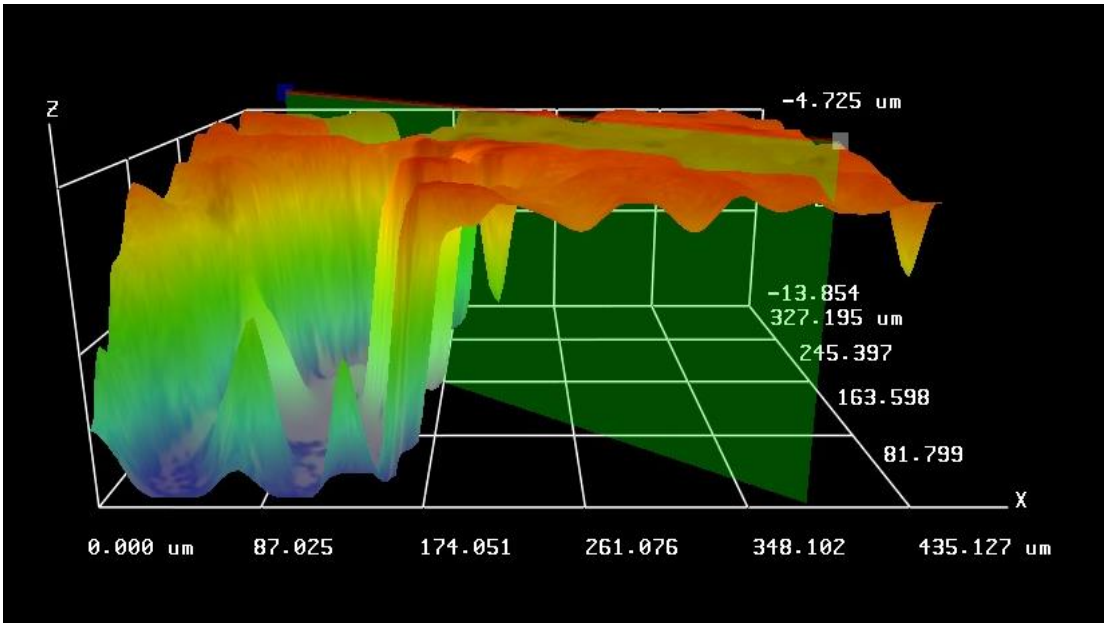


Figure 21 – SEM thickness mapping of a layer of P(MMA-DB3MA) particles spread on the build platform of the novel SLS rig, showing that the layer of powder spread is ~10 µm, the blue is the surface of the build platform and the red is the top of the P(MMA-DB3MA), hence their difference in height is the thickness of the layer that is deposited on the build platform.

It is hypothesized that the improved flow behaviour and packing structure, is due to the molecular structure of the disperse blue 3 methacrylate segment of the polymer. There are a variety of structural factors that might aid the flow behaviour: 1.) The π-π stacking of the anthracene moieties on the particle surfaces could be creating a repulsive force between the particles.[260] This could cause the Van der Waals forces between the particles to be lower than the ones for the PMMA particles. 2.) The charge provided by the molecule could offset the static charge of the PMMA.[261] There is no conclusive proof that these reasons are responsible for the improved flow and packing behaviour of P(MMA-DB3MA) particles, hence this should be researched further.

The correct ratio of DB3MA in the copolymer was found to be 1.5 wt% DB3MA, different ratios were attempted, but this consistently gave the polymer powder layers with no gaps and the best thickness (~10 µm). Sintering was done at varying laser powers (10 mW – 80 mW), in order to produce sintered tracks, that were wholly melted, high laser powers needed to be utilized. This caused the polymer in the proximity of the track to partially melt as well. The resulting tracks had a resolution of 30 – 50 µm. This was not the desired resolution. The reasons for this failure were investigated, and it was found that the polymer powder was not absorbing the laser radiation well at 405 nm, so an excess of laser power was needed. Using more laser power can cause the spot size of the laser to increase, leading to lower-than-expected resolutions.

To see in which wavelength region the P(MMA-DB3MA) particles were absorbing radiation, solid state UV was performed on several samples with varying loadings of DB3MA in the polymer chain (0 – 2.5 wt%). Solid state UV confirmed that these polymeric particles were not absorbing at 405 nm (laser radiation). The analysis showed that the absorbance at 405 nm was minimal compared to its absorption at other wavelengths in the UV-vis region. The lambda max (λmax) of P(MMA-DB3MA) particles ranged from 570 – 580 nm (figure 22). This showed that the polymeric powder needed to be modified in order to better absorb the laser's radiation (405 nm). At this point a method of introducing a substance that absorbs radiation at 405 nm to the P(MMA-DB3MA) powder was needed.

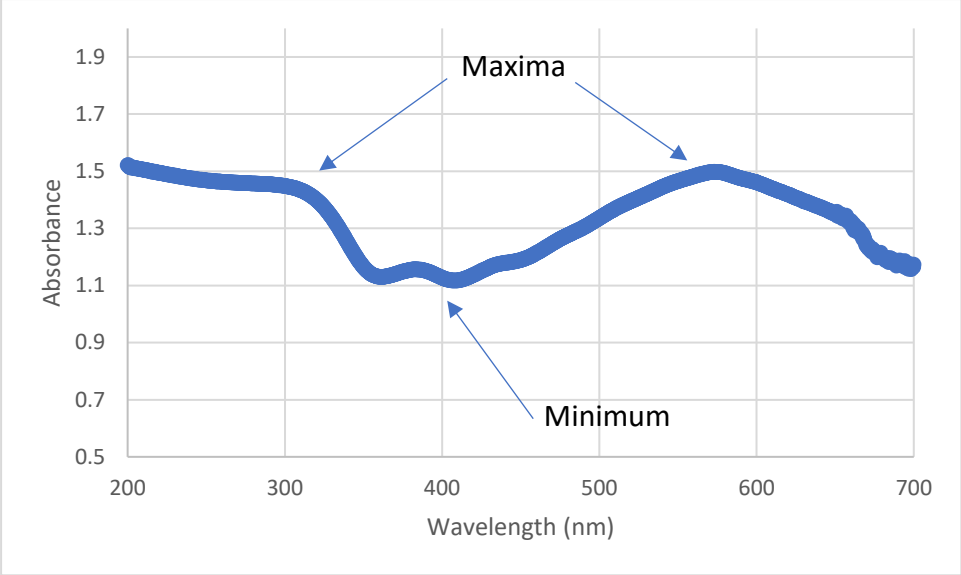


Figure 22 – Solid State UV spectrum of P(MMA-DB3MA) particles shows that there is a decrease of absorbance in the 405 nm region, which implies that the P(MMA-DB3MA) particles do not absorb the radiation of a 405 nm laser well.

The first approach that was investigated was the possibility to replace the DB3MA monomer, with another dye monomer that has a λ_{max} at 405 nm. This route was not taken considering some crucial reasons. First of which, is that since we do not fully understand why P(MMA-DB3MA) particles have better flow and packing properties than PMMA, changing DB3MA for another dye monomer might hinder the flow and packing of the resulting powder. The second is that once a methacrylate group is added to a potential dye, the dye monomer can suffer from a hypso or bathochromic shift.[34] The third reason is that there are only a few dyes that have a λ_{max} of 405 nm and have a primary alcohol (these dyes are very expensive). The cost of the dyes makes it not industrially viable to use them as a dye monomer, because the cost of the resulting particles would be too high for SLS purposes. For these reasons another approach was utilized.

Previous studies have shown that carbon black can be introduced into polymeric particles systems, in order to increase the absorbance of the particulate powder.[262–264] Carbon black has been shown to absorb radiation at 405 nm well, thereby allowing for the particles in the powder to sinter better at a lower laser power.[262–264] The carbon black particles are very small (≤ 1 μm), so they are suitable for the target resolution of ~10 μm. Carbon black has good flow properties and does not affect the flow or packing of polymer particles detrimentally. This was tested on PA-12 particles, which are much larger (50 – 80 μm), so its effect on small particles (1 – 10 μm) is unknown. For this reason, amounts varying from 0.25 - 2.5 wt% of carbon black were added to the P(MMA-DB3MA) powder, through dry mixing.

The most successful being at 0.5 wt% carbon black, after mixing the powder changed colour to a slightly greyer blue. The powder mix made layers of the wanted thickness, so their printability was tested. The samples were printed with varying laser powers (0.01 – 0.08 W). At the lower end of the laser power range the sintering in between particles was not complete, and there were gaps in between the sintered tracks (figure 23). This resulted in very brittle weak parts that fell apart when touched, however they had exceptional resolution for SLS 7 – 10 μm. Higher laser powers were used to make solid tracks that could be moved without falling apart. The laser power used was 0.08 W resulting in more thorough sintering and particle fusion. The tracks had a resolution of ~10 – 15 μm as the thickness was 10 μm and the width was 10 – 15 μm depending on the region of the track (figure 23).

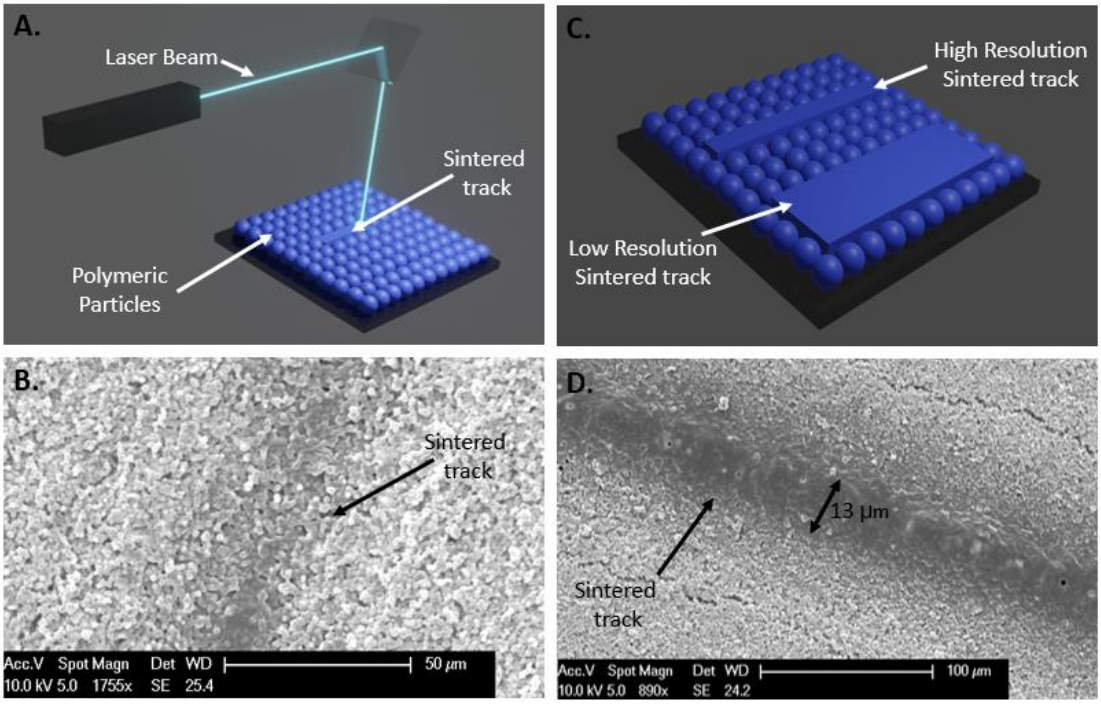


Figure 23 – High resolution SLS printing on one layer of polymeric particles. A.) Scheme of SLS printing. B.) Image of high-resolution (7-10 µm) track produced with a low laser power, however this track was very brittle C.) Scheme comparing a low-resolution track versus a high-resolution track, showing how laser spot size can influence the resolution of a part even if the build platform and material used are the same D.) SEM image of high-resolution produced tract with a high laser power, which has a resolution of ~13 µm, but was not as brittle as the 7-10 µm track.

This shows that SLS printers can reach a resolution of ~10 µm if the correct materials and rig are used. However, when the deposition of a second layer was attempted, the results were inconsistent. This is because the position of the track in the bottom layer would be change due to the deposition of the second layer. A possible cause is the pressure inflicted by the cylinder roller, therefore the pressure with which the cylinder rolls the 2nd layer was varied, but the results were not as desired. At times,

the powder would become static and fly, or have large gaps, or move the track or pattern below. The highest resolution reached for a two layer track was 80 – 100 µm. The reason for this low resolution is due to the method of layer deposition, as very weak forces can distort the very thin layer below. In the future this could be addressed by utilizing similar features as the aforementioned high resolution metal SLS printer.

Conclusions:

This project yielded several promising results. The first is that a SLS printer was built which has a step size of 5 µm and a laser spot size of ≤ 10 µm, thereby overcoming the resolution limitations imposed by conventional SLS systems. Spherical PMMA particles (1 – 5 µm) were synthesized via $scCO_2$, with the necessary extrinsic and intrinsic properties needed for conventional SLS. However, these particles were unsuitable for high resolution SLS as the particles tended to form aggregates of sizes ranging from 20 to 30 µm. The particles were then modified post synthesis via ball and cryogenic milling. Both milling techniques resulted in smaller particles; ball milling caused the particles to lose their shape because of the heat generated during the milling process. Cryogenic milling resulted in particles of adequate size and shape, but the particles were statically charged which led to problems during product collection and subsequent layer formation. When a chemical alteration route was taken the results were more positive. When P(MMA-DB3MA) particles with 0.5 wt% carbon black were used our SLS rig printed solid tracks with a resolution of ~10µm. This proved that by utilizing smaller spherical polymeric particles and a SLS rig with a small laser spot size and good build platform control better resolutions can be

reached for SLS. This is a step forward for selective laser sintering, but the deposition and subsequent printing of a second layer was not successful. Future work should be undertaken so that subsequent layers can be printed with a resolution of ~ 10 µm. Different approaches could be taken, such as adding a flow agent, so that the second layer will not cause as much friction with the first layer, thereby allowing the first layer to stay intact. The printer can be modified, in an effort to mimic the powder deposition method used by the printer made by Roy *et. al.* The reasons why the placement of DB3MA in the polymer chain helped the flow and packing properties of the powder should be investigated.

Parts produced with a resolution of 10 µm with SLS, would have a variety of potential applications. This technology could potentially be used in the biomedical field, possibly resulting in detailed and customized scaffolds and implants. This would also suit the purpose of any electrical or mechanical part that necessitates a high-resolution, as this method would yield accurate parts in a short period of time.

Future Work:

There are several studies to be done in order to fully finish developing a high-resolution SLS process. One of the studies needed is the investigation of spreading of the second and subsequent layers onto the build platform. The printer created by Roy *et. al.* used a vacuum built into the build platform to make sure that the layer stayed intact during layer deposition.[247] This printer worked by depositing a slurry of particles in solution on the build platform.[247] Then using a vacuum to get rid of the solvent, and then the vacuum could ensure the integrity of the layer (figure 24).[247]

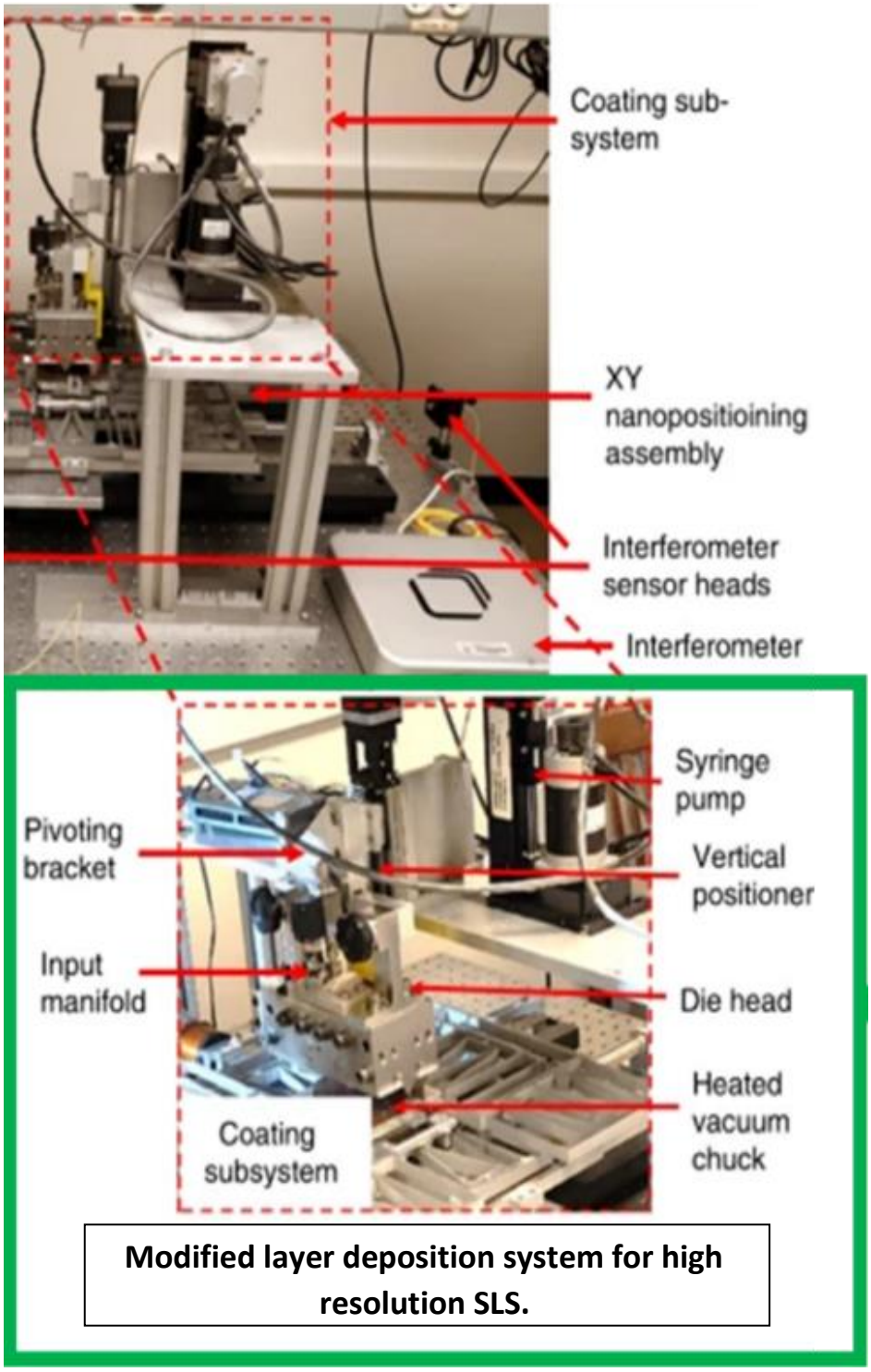


Figure 24 – Microscale SLS printer (Roy *et. al.*) with highlighted layer formation mechanism. The addition of the heated vacuum pump and syringe pump could solve the movement of the first layer during deposition of the second layer.[247]

The vacuum could also work on solid particulate system, such as ours, however this could have issues with agglomeration. The vacuum would ensure the position of the first layer, this would stop the track from moving, thereby aiding in the formation of a second and subsequent layers. If this does not work, creating a slurry of the P(MMA-DB3MA) particles with carbon black and then depositing the slurry to make a layer should be attempted, this method is less likely to form agglomerates. Although it is unusual to form a slurry of polymer particles for SLS, slurries of polymers are used in other forms of 3D printing yielding successful results.[265,266] The slurry formulation would have to be optimised for both solvent and polymer concentration, so that the slurry is compatible with the printer and the particles could be dispersed well at a concentration which yields a monolayer. This would mimic the layer deposition system that was shown to work for small metal-based particles. The effects of DB3MA on the flow behaviour of the polymeric particles must be investigated.

In order to investigate the relationship between the dye monomer (DB3MA) and the improved flow behaviour of the P(MMA-DB3MA) based particulate powder the macro and micro flow behaviour of the polymer must be studied. To assess the macro flow behaviour of the blue powder vs other PMMA powders, a technology developed by Van den Eyde *et. al*. should be used (figure 25).[267] This analysis technique is based on analysing the packing density of each layer.[267] The technique mimics SLS powder spreading, and it weighs the solid build platform after every layer, in order to find the packing density and to see how reliable layer formation is.[267] Ideally one would have high and consistent packing density throughout the layers.

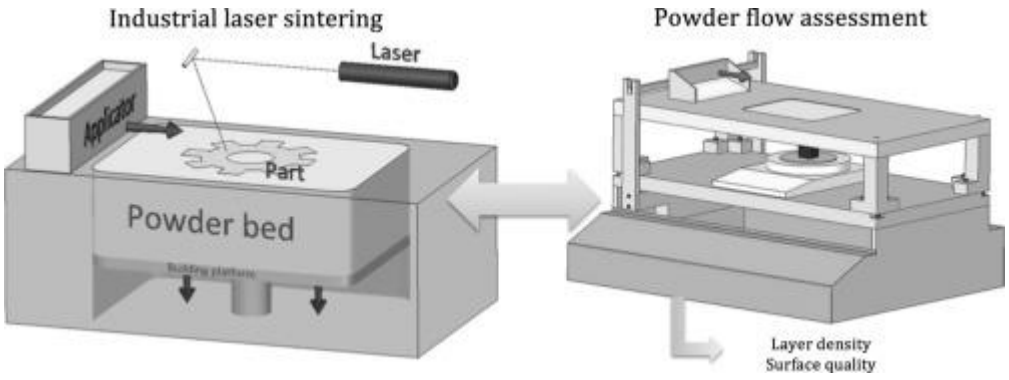


Figure 25 – Schematic illustration of powder density and flow analyser.[267] On the left a schematic of standard SLS printer is shown, and on the right the powder density and flow analyser can be seen. This analyser replicates the method of layer formation and polymer particle deposition, to give an accurate measurement of the consistency and density of each of the deposited layers.

To study the effect of DB3MA on the particle-particle interactions a variation of AFM can be used. Ducker *et. al.* showed that through the use of colloidal probe technique AFM, the Van der Waals forces between particles could be identified and quantified (figure 26).[268]

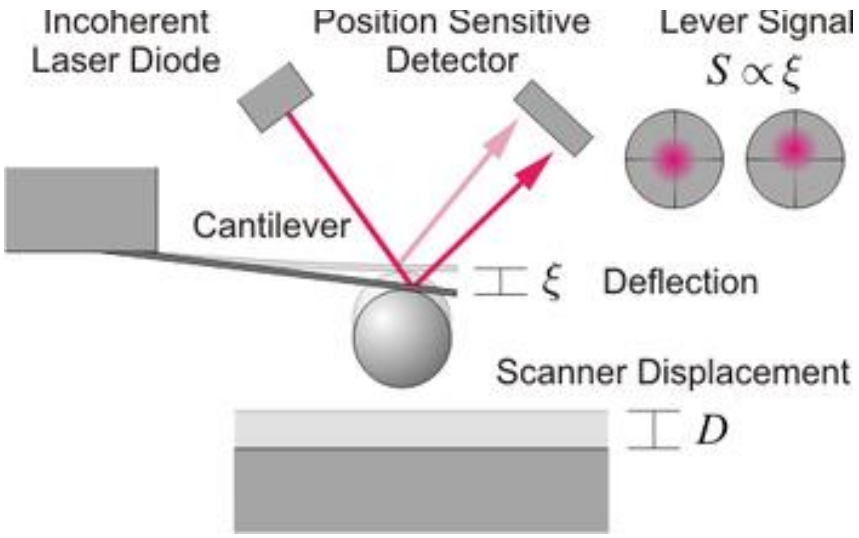


Figure 26 – Schematic illustration of colloidal probe technique AFM.[268]

This technique has been used for a variety of materials ranging from silica, paper, polymer, *etc.* particles.[268] The quantification of the Van der Waals forces exhibited by the different polymer particles could elucidate why the blue monomer is affecting flow. If the Van der Waals forces for the blue powder are lower than for the other PMMA powders it means that gravity is having a stronger effect beforehand compared to the interparticle interactions, therefore leading to less agglomeration and more consistent monolayer formation. The use of these two techniques would help obtain information regarding the reasons behind the differing flow behaviours of the polymers. The enhanced understanding of flow behaviours and the development of an advanced powder delivery system such as that built by Roy *et. al.* would enable the development of an SLS process that would consistently allow the user to print multi-layered structures at high resolutions (~ 10 μm).

Materials and Methods:

Materials:

Methyl methacrylate (MMA) (99 %) was obtained from Kaneka Belgium N.V. 2,2'-Azobis(2-methylpropionnitrile) (AIBN) and poly(dimethylsiloxane)-methacrylate 10000Da were purchased from Fluorochem. CO_2 and Argon were purchased from Air Products. Disperse Blue 3 methacrylate was used as synthesised.

Methods:

Synthesis of PMMA particles:

MMA (10 g, 0.998 mol), AIBN (0.01 g, 0.6089 mmol), and PDMS-MA (10 kDa) (0.5 g, 0.05 mmol) were degassed in a vial for 30 min with Argon, and the autoclave for 30 min, by flushing it with CO2 at a constant pressure between 0.27 – 0.41 MPa. The reaction mixture was injected through the key, and the key was then shut rapidly, and the pressure was slowly increased to 5.51 MPa, subsequently the temperature was increased to 50°C, and after stabilising the autoclave was pressurized to 13.79 MPa, with subsequent heating to 65°C. Once stable at 65°C the reaction is pressurized to 20.7 MPa and left stirring at 300 rpm for 6 hours. The autoclave is allowed to cool <30°C and the CO_2 is vented slowly, and the autoclave is opened to reveal the product. ^{1}H NMR (400 MHz, $CHCl_3$-d_3, δ): 3.50-3.75 (mp, 3H, CH_3)

Synthesis of P(MMA-DB3MA) particles:

MMA (10 g, 0.998 mol), DB3MA (0.25 g, 0.9385 mmol) , AIBN (0.01 g, 0.6089 mmol), and PDMS-MA (10 kDa) (0.5 g, 0.05 mmol) were degassed in a vial for 30 min with Argon, and the autoclave for 30 min, by flushing it with CO_2 at a constant pressure between 0.27 – 0.41 MPa. The reaction mixture was injected through the key, and the key was then shut rapidly, and the pressure was slowly increased to 5.51 MPa, subsequently the temperature was increased to 50°C, and after stabilising the autoclave was pressurized to 13.79 MPa, with subsequent heating to 65°C. Once stable at 65°C the reaction is pressurized to 20.7 MPa and left stirring at 300 rpm for 6 hours. The autoclave is allowed to cool <30°C and the CO2 is vented slowly, and the

autoclave is opened to reveal the product. ^{1}H NMR (400 MHz, $CHCl_3$-d_3, δ): 3.50-3.75 (mp, 3H, CH_3), 7.28 (D, 2H, ArH), 7.73-7.75 (mp, 2H, ArH), 8.34-8.38 (mp, 2H, ArH), 10.65 (S, NH)

Ball Milling of PMMA particles:

PMMA particles (1g) and steel balls are inserted into the milling chamber, which is then closed. The timer is set to a particular duration. After milling the chamber is opened and the product is collected, and the chamber is cleaned with water. Performed in a Retsch MM301 mixer mill.

Cryogenic Milling of PMMA particles:

PMMA particles (2.5 g) and steel tube are inserted into the milling chamber, which is then closed. The mill is filled with liquid nitrogen and cooled for 10 min, thereby starting the milling period. Once finished, the mill is opened and allowed to heat to room temperature. After which the milling chamber is removed and the product is collected. The milling chamber is cleaned with water. Performed in a Spex Sampleprep 6870 Freezer/Mill.

Analysis:

^{1}H NMR:

The structure of the dye monomers and polymers was analysed via ^{1}H NMR (Bruker 400 Ultrashield (400 MHz NMR)), all samples were dissolved in deuterated chloroform. The ^{1}H NMR spectra were used to identify the polymer formation, and to calculate the monomers conversion using equation 2.

$$Conversion = \frac{AUCP}{AUCP + 1}$$

Equation 2

In this equation AUCP is the area under the curve of the polymer peak when compared to the area under the curve of the monomer peak.

Gel Permeation Chromatography (GPC):

M_n, M_w, and Đ values were obtained for all synthesized polymers via GPC. The values were calculated using standards of PMMA. All measurements were performed on an Agilent 1260 Infinity HPLC using HPLC grade THF as eluent at 40°C with 2 x Agilent PL-gel mixed-c column at 1 mL/min flow rate, connected to a differential refractive index (dRI) and MALLS detector.

Laser Diffraction Spectrometry (LDS):

Laser Diffraction Particle Sizing (LDS) was used to analyse the particle size, performed on a Malvern Mastersizer 3000.

Scanning Electron Microscopy (SEM):

SEM was used to determine the size and shape of the discrete monodisperse particles, a Phillips XL30 electron microscope was used. The samples were prepared by adding powder to a carbon tab mounted onto a SEM stub, which were then coated with platinum for 180 seconds at 12 mA and 2.2 kV using an Emitech SC7640 Sputter coater. An average particle size was calculate by taking the area of 100 particles from a SEM image and finding the average, performed using ImageJ.[269] The thickness of

the polymeric particle layer was measured by removing a segment of the layer revealing the surface of the stub, the height difference between the stub and the particle tops equals the thickness of the particle layer.

Appendix 2: Mechanical properties of coloured PA-12 parts:

Mechanical analysis of commercial PA-12 based SLS printed parts was conducted in order to be able to compare it to parts composed of the novel coloured materials. PA-12 based dog bones were printed and tested in duplicate to find and confirm their mechanical properties (Table 1).

Sample	Maximum Load (N)	Modulus (MPa)	Elongation at break (%)
100 % PA-12 (1)	259.96	1251.38	11.3
100 % PA-12 (2)	260.52	1204.58	12

Table 1 – Mechanical data of SLS printed parts composed of virgin PA-12

The maximum load of the two pure virgin PA-12 dog bones were 259.96 N and 260.52 N, which are very similar showing the reliability of the materials and the printing technique. The modulus was shown to be 1251.38 MPa and 1204.58 MPa for both parts. These results show that pure virgin PA-12 produces parts with excellent mechanical properties. The parts have about a 11.3 – 12% elongation at break as the parts are 30 mm long and they elongated by 3.4 and 3.6 mm respectively (figure 1). The consistency of the mechanical properties show that the results can be reproduced from build to build.

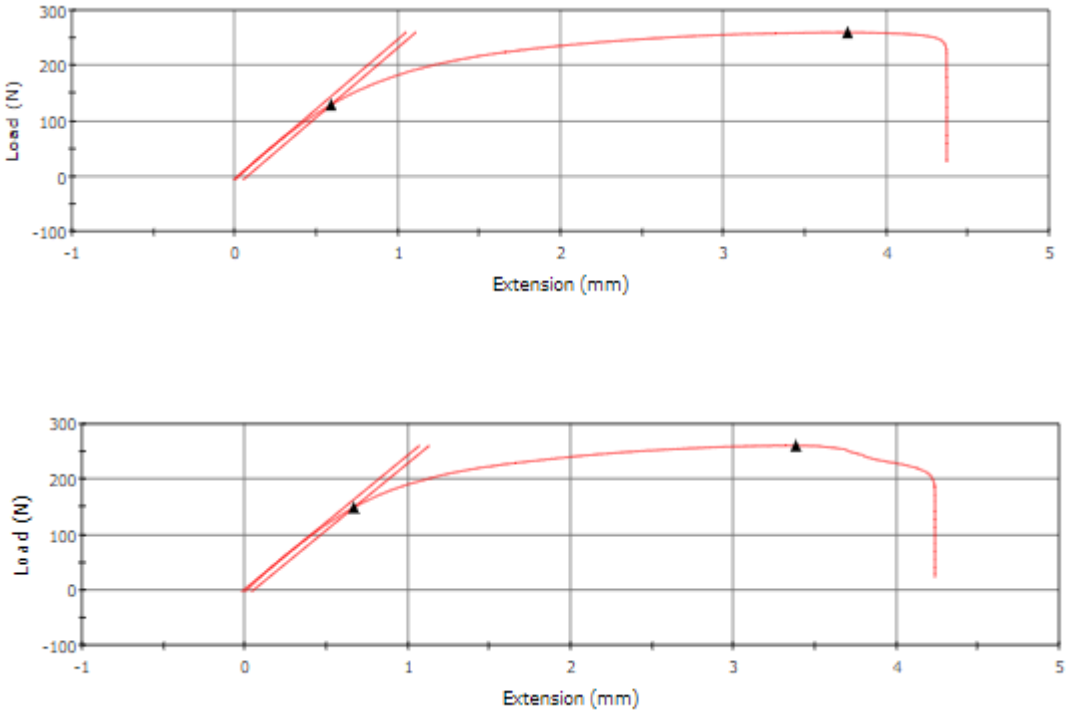


Figure 1 – Tensile strength (N) vs extension (mm) till break A.) Dog bone 1 B.) Dog bone 2.

The physical properties of 100% yellow PA-12 parts printed via SLS was found to be weak, and could be broken by hand, in order to improve this yellow PA-12 was blended with commercial PA-12 in an effort to create a coloured PA-12 based mixed powder which had good mechanical properties.

Improving the mechanical properties of yellow PA-12 parts via physical blending:

The mechanical properties of the yellow PA-12 based parts were improved by physically mixing virgin PA-12 with the virgin PA-12 particles coated in P(IBMA-Y1MA) in varying ratios.

Sample	Maximum Load (N)	Modulus (MPa)	Elongation at break (%)
100 % PA-12 (1)	259.96	1251.38	11.3
100 % PA-12 (2)	260.52	1204.58	12
75 % PA-12 / 25 % Yellow PA-12 (1)	126.02	1078.9	5.7
75 % PA-12 / 25 % Yellow PA-12 (2)	115.92	1082.37	4.1
50 % PA-12 / 50 % Yellow PA-12 (1)	30.35	148.45	7.9
50 % PA-12 / 50 % Yellow PA-12 (2)	31.59	131.09	6.1
25 % PA-12 / 75 % Yellow PA-12 (1)	3.75	130.62	2.5

Table 2 – Physical mixing of virgin PA-12 and virgin PA-12 coated with P(IBMA-Y1MA) used for SLS printing and mechanical testing results. Two repeats were done per sample, this limitation was imposed due to Covid-19 regulations.

These mixes were chosen, so that the best mix in terms of both colour and mechanical properties could be found. The mixes were made by physically mixing for several hours. As a large percentage of the mixes was composed of pure virgin PA-12, the conditions chosen for the parts to be built with were a PBT of 172 ^{o}C, a CT of 150 ^{o}C, HLP of 21 W, CLP of 16 W, HS of 2500 mm/s, and a HD of 0.25 mm (these are the optimal conditions for printing PA-12).

The first mix that was printed was the sample composed of 50 wt% virgin PA-12 coated with P(IBMA-Y1MA) and 50 wt% virgin PA-12. The dog bones built from this mix are yellow as can be seen by eye and NIX colour analysis (figure 2)



Figure 2 – Image and colour analysis of SLS built part composed of 50 wt% virgin PA-12 coated with P(IBMA-Y1MA) and 50 wt% virgin PA-12. A.) NIX colour analysis of the dog bones B.) Image of the dog bone. On the top of the part A. there is square which is a photo representation of the colour of the part that was analysed via NIX colour analysis. On the bottom of part A there is a variety of values which are numerical representations of the colour of the part. HEX, sRGB, CMYK, CIELAB, LCH (ab), and LRV are different units used for the valuation of colours, and at the bottom the Hue of the part is stated.

The dog bones were shown to have a maximum load of 30.35 N and 31.59 N a modulus of 148.45 and 131.09 MPa, and an extension of 2.38 mm (7.9 %) and 2.01 mm (6.07%) (figure 3).

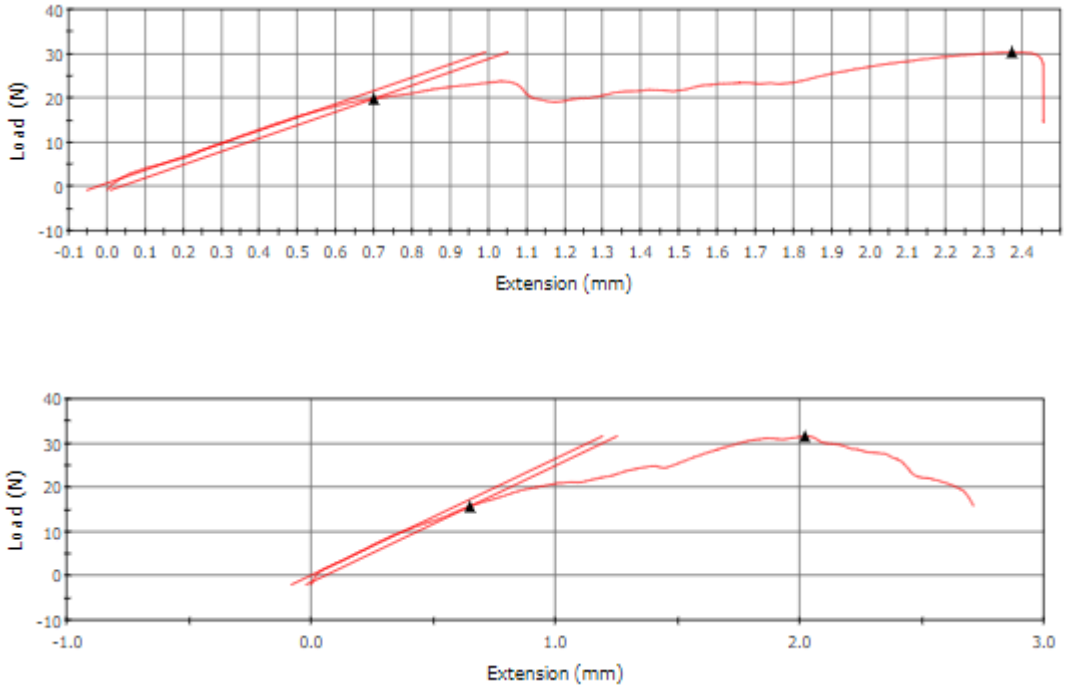


Figure 3 – Tensile strength (N) vs. Extension (mm) till break. A.) Dog Bone 1 of 50 wt% virgin PA-12 coated with P(IBMA-Y1MA) and 50 wt% virgin PA-12. B.) Dog Bone 2 of 50 wt% virgin PA-12 coated with P(IBMA-Y1MA) and 50 wt% virgin PA-12.

These are relatively good mechanical properties, but noticeably weaker than parts built out of 100 % virgin PA-12. As the maximum load is on average only 11.9% of that of pure virgin PA-12, the modulus is 11.4%, and the extension is half of that of the parts built with pure virgin PA-12. Also, as can be seen from the broken dog bones the inside of the part is wholly coloured, which proves that this method produces completely coloured parts (figure 4). In order to further improve the mechanical properties more virgin PA-12 was needed to be used in the powder mix.

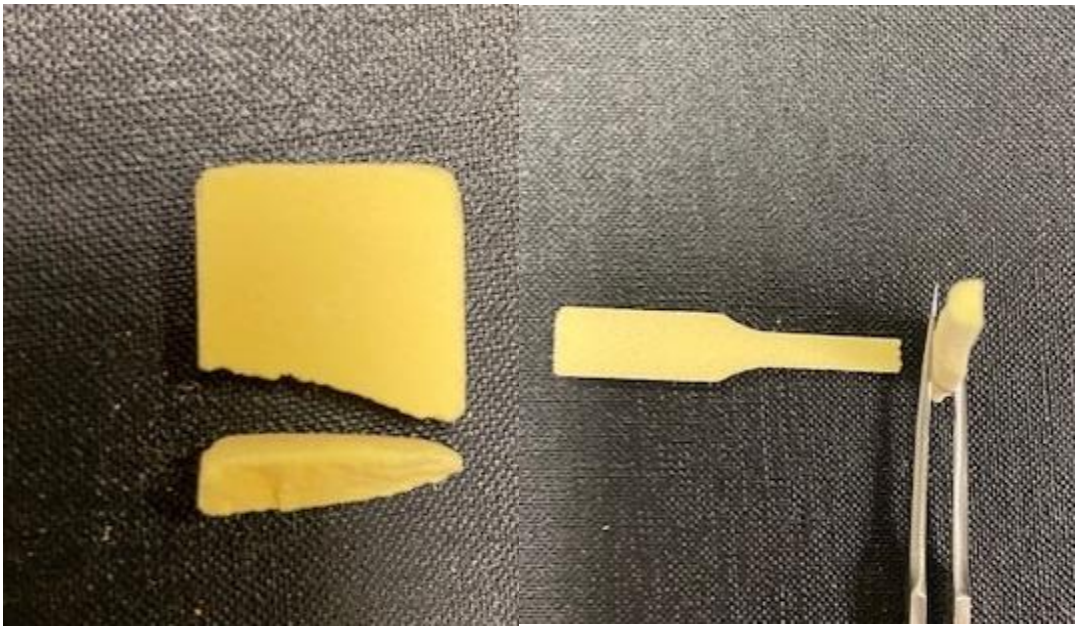


Figure 4 – Image of the break points of yellow PA-12 based materials. A.) Dog bone composed of 50 wt% virgin PA-12 coated with P(IBMA-Y1MA) and 50 wt% virgin PA-12. B.) Square composed of 100 % PA-12 coated with P(IBMA-Y1MA)

The next mix that was printed was a 25 wt% virgin PA-12 coated with P(IBMA-Y1MA) and 75 wt% virgin PA-12. The dog bones composed of this material were printed with the same conditions used for standard virgin PA-12. The resulting dog bones were yellow to the naked eye and the NIX sensor (figure 5).



Figure 5 - Image and colour analysis of SLS built part composed of 25 wt% virgin PA-12 coated with P(IBMA-Y1MA) and 75 wt% virgin PA-12. A.) NIX colour analysis of the dog bones B.) Image of the dog bones. On the top of the part A. there is square which is a photo representation of the colour of the part that was analysed via NIX colour analysis. On the bottom of part A there is a variety of values which are numerical representations of the colour of the part. HEX, sRGB, CMYK, CIELAB, LCH (ab), and LRV are different units used for the valuation of colours, and at the bottom the Hue of the part is stated.

Mechanical testing was conducted, which revealed that the properties of this mix were very close to the properties of pure virgin PA-12. The maximum load of the tested dog bones were 126.02 N and 115.92 N respectively, which is 46.5 % that of the value of pure virgin PA-12. The moduli for each dog bone was 1078.90 and 1082.37 MPa, so the moduli for the parts composed of 25 wt% virgin PA-12 coated

with P(IBMA-Y1MA) and 75 wt% virgin PA-12 is 88% of the value for pure virgin PA-12, and the elongation at break was 1.48 mm on average, which is about one third the elongation of the PA-12 parts (figure 6).

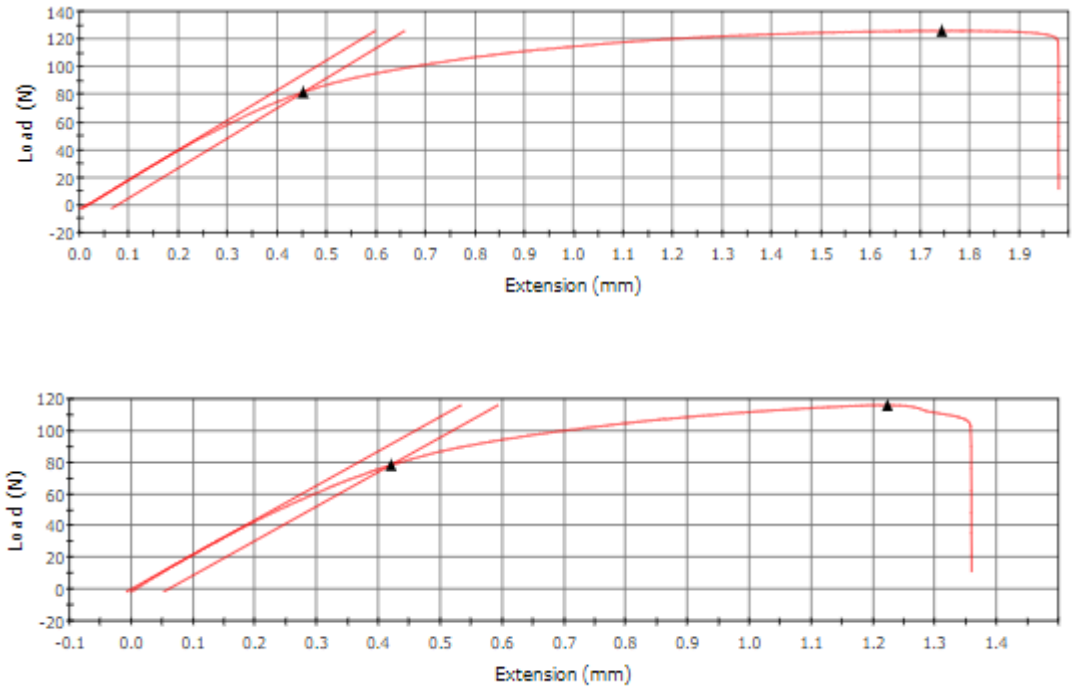


Figure 6 - Tensile strength (N) vs. Extension (mm) till break. A.) Dog Bone 1 of 25 wt% virgin PA-12 coated with P(IBMA-Y1MA) and 75 wt% virgin PA-12. B.) Dog Bone 2 of 25 wt% virgin PA-12 coated with P(IBMA-Y1MA) and 75 wt% virgin PA-12.

These values are vastly improved from the 50/50 mix, and they are quite close to the values seen from pure PA-12 whilst maintaining the desired yellow colour. This can be seen as an advantage, as this allows the user to produce coloured parts, whilst using less coloured PA-12, which is more expensive than standard PA-12. This reduces the cost of this novel colouring process making it potentially appealing to industry.

The last mix that was printed was a composition of 75 wt% virgin PA-12 coated with P(IBMA-Y1MA) and 25 wt% virgin PA-12. This mix was printed with the same

conditions as the previous two mixes. This produced clearly yellow dog bones (figure 7).

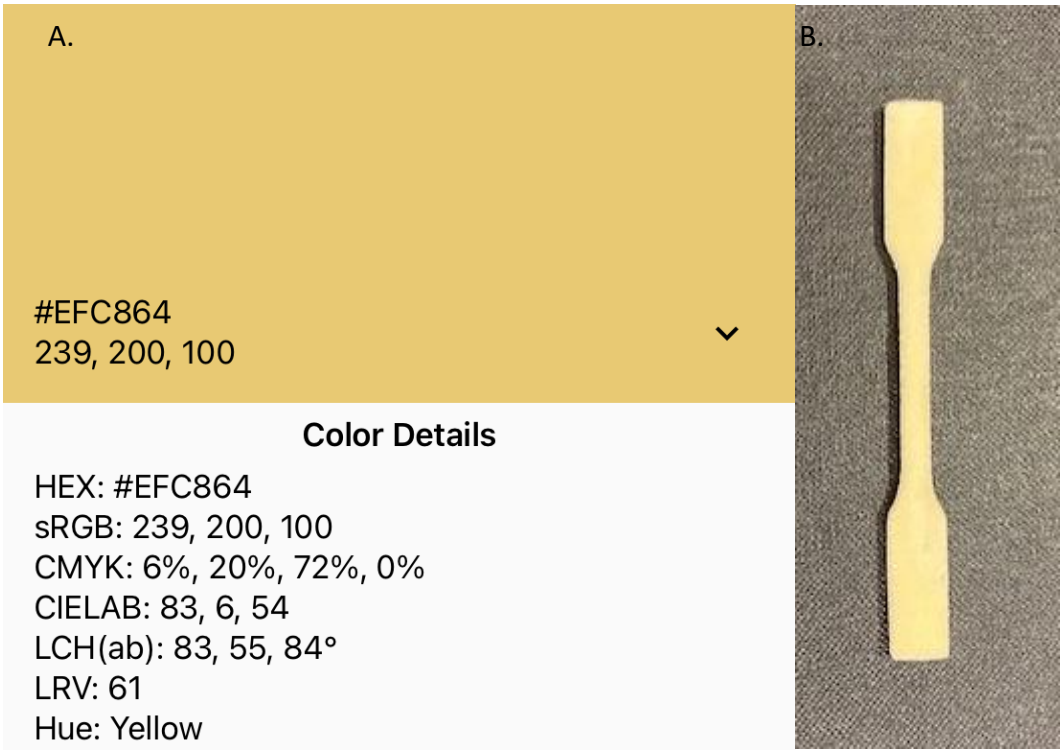


Figure 7 - Image and colour analysis of SLS built part composed of 75 wt% virgin PA-12 coated with P(IBMA-Y1MA) and 25 wt% virgin PA-12. A.) NIX colour analysis of the dog bones. B.) Image of the dog bones. On the top of the part A. there is square which is a photo representation of the colour of the part that was analysed via NIX colour analysis. On the bottom of part A there is a variety of values which are numerical representations of the colour of the part. HEX, sRGB, CMYK, CIELAB, LCH (ab), and LRV are different units used for the valuation of colours, and at the bottom the Hue of the part is stated.

The mechanical testing revealed that the dog bones made using this mix were considerably weaker than the other two variants. The first one snapped while it was

being loaded and the second one had a maximum load of 3.75 N, a modulus of 130.62 MPa and an elongation of break of less than 1 mm (figure 8).

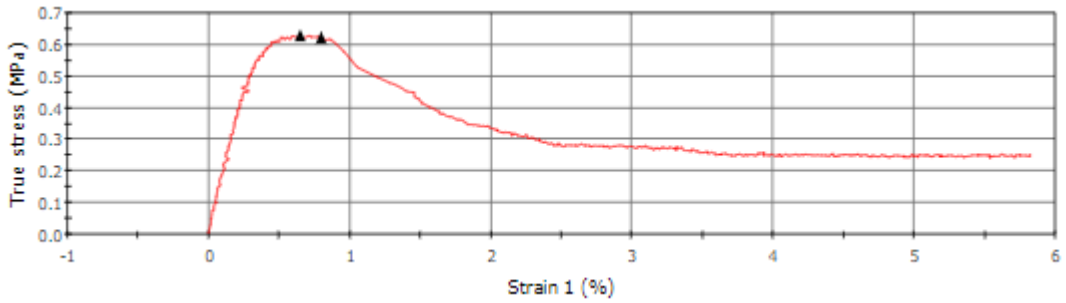


Figure 8 - Tensile strength (N) vs. Extension (mm) till break. A.) Dog Bone 1 of 75 wt% virgin PA-12 coated with P(IBMA-Y1MA) and 25 wt% virgin PA-12.

These are worse than the other two, so it is clear that there is a trend of improvement as more virgin PA-12 is added. With the mix of 25 wt% virgin PA-12 coated with P(IBMA-Y1MA) and 75 wt% virgin PA-12 parts can be produced which are both yellow and have desirable mechanical properties.

Materials and Methods:

Mechanical Testing:

A 5kN load cell on a benchtop instron universal testing machine (Instron 5969) was used with bluehill 2 testing software. The grips were pneumatic rated to 2kN, the sample was placed in the top grip and then the top and bottom grips were closed. Then the sample was tested until a breakpoint and it was removed from the grips.

References:

1. Solmaz, A., Ilter, Z. & Kaya, I. Synthesis, Characterization, Thermal Behavior, and Dielectric Properties of Methacrylate Polymers Containing Imine Bonding. *J. Electron. Mater.* **50**, 5348–5358 (2021).

2. Persico, P. *et al.* Synthesis and nonlinear optical properties of methacrylate polymers based on 2-[4-(N-methyl,N-hydroxyethylamino)phenylazo]-phenyl-6-nitrobenzoxazole chromophore. *J. Polym. Sci. A. Polym. Chem.* **41**, 1841–1847 (2003).

3. Worzakowska, M. High chemical and solvent resistant, branched terpene methacrylate polymers—Preparation, thermal properties, and decomposition mechanism. *Polym. Adv. Technol.* **29**, 1414–1425 (2018).

4. Sahagún Aguilar, L. O., Ceja Andrade, I., Alvarado Mendoza, A. G., Puig Arevalo, J. E. & Rabelero Velasco, M. Tunable mechanical properties of core-shell polymers of poly(hexyl methacrylate) and poly(methyl methacrylate) by semicontinuous heterophase polymerization. *Polym. Eng. Sci.* **59**, 365–371 (2019).

5. Sainz, M. F. *et al.* A facile and green route to terpene derived acrylate and methacrylate monomers and simple free radical polymerisation to yield new renewable polymers and coatings. *Polym. Chem.* **7**, 2882–2887 (2016).

6. Atkinson, R. Terpene-derived, hard-soft block copolymers as sustainable thermoplastic elastomers. (2021).

7. Ligon, S. C., Liska, R., Stampfl, J., Gurr, M. & Mülhaupt, R. Polymers for 3D Printing and Customized Additive Manufacturing. *Chem. Rev.* **117**, 10212–10290 (2017).

8. Espera Jr., A. H. *et al.* 3D Printing of a Robust Polyamide-12-Carbon Black Composite via Selective Laser Sintering: Thermal and Electrical Conductivity. *Macromol. Mater. Eng.* **304**, 1800718 (2019).

9. Hong, R., Zhao, Z., Leng, J., Wu, J. & Zhang, J. Two-step approach based on selective laser sintering for high performance carbon black/ polyamide 12 composite with 3D segregated conductive network. *Compos. Part B Eng.* **176**, 107214 (2019).

10. Redwood, B. Post processing for SLS printed parts. *3D Hubs* (2020).

11. Powell, A. W., Stavrinadis, A., de Miguel, I., Konstantatos, G. & Quidant, R. White and Brightly Colored 3D Printing Based on Resonant Photothermal Sensitizers. *Nano Lett.* **18**, 6660–6664 (2018).

12. Fu, X. *et al.* Use of short isobornyl methacrylate building blocks to improve the heat and oil resistance of thermoplastic elastomers via RAFT emulsion polymerization. *J. Appl. Polym. Sci.* **134**, 45379 (2017).

13. Stanley R. Sandler, Wolf Karo, M. P. S. *Polymer Synthesis: Volume 1*. (Gulf Professional Publishing, 1992).

14. Schmid, M., Amado, A. & Wegener, K. Polymer powders for selective laser sintering (SLS). *AIP Conf. Proc.* **1664**, 160009 (2015).

15. Schmid, M. & Wegener, K. Thermal and molecular properties of polymer powders for Selective Laser Sintering (SLS). *AIP Conf. Proc.* **1779**, 100003 (2016).

16. Schmid, M., Kleijnen, R., Vetterli, M. & Wegener, K. Influence of the Origin of Polyamide 12 Powder on the Laser Sintering Process and Laser Sintered Parts. *Appl. Sci.* **7**, 462 (2017).

17. Canestri, F. Optical absorption coefficient, time of thermal relaxation, time of surface threshold, and time of heat incubation for PMMA samples at the CO2 laser-beam wavelength of 10.6 microm. *Photomed. Laser Surg.* **24**, 655–659 (2006).

18. Bonardi, A.-H., Dumur, F., Gigmes, D., Xu, Y.-Y. & Lalevée, J. Light-Induced Thermal Decomposition of Alkoxyamines upon Infrared CO2 Laser: Toward Spatially Controlled Polymerization of Methacrylates in Laser Write Experiments. *ACS Omega* **5**, 3043–3046 (2020).

19. McAllister, T. D., Farrand, L. D. & Howdle, S. M. Improved Particle Size Control for the Dispersion Polymerization of Methyl methacrylate in Supercritical Carbon Dioxide. *Macromol. Chem. Phys.* **217**, 2294–2301 (2016).

20. Zong, M., Thurecht, K. J. & Howdle, S. M. Dispersion polymerisation in supercritical CO2 using macro-RAFT agents. *Chem. Commun.* 5942–5944 (2008). doi:10.1039/b812827h

21. Huo, Z. Y. *et al.* In situ synthesis of fluorinated diblock copolymer nanoparticles

via {RAFT} dispersion polymerization in supercritical carbon dioxide. *{IOP} Conf. Ser. Mater. Sci. Eng.* **479**, 12107 (2019).

22. Woods, H. M., Nouvel, C., Licence, P., Irvine, D. J. & Howdle, S. M. Dispersion polymerization of methyl methacrylate in supercritical carbon dioxide: An investigation into stabilizer anchor group. *Macromolecules* **38**, 3271–3282 (2005).

23. Pepper, J. Ready set print. *Presentations* **14**, 79 (2000).

24. Hodges, E. S. *The Guild Handbook of Scientific Illustration*. (John Wiley & Sons, 2003).

25. Jay A. Siegel. *Forensic Chemistry: Fundamentals and Applications*. (John Wiley & Sons, 2015).

26. Rosi, T., Malgieri, M., Onorato, P. & Oss, S. What are we looking at when we say magenta? Quantitative measurements of RGB and CMYK colours with a homemade spectrophotometer. *Eur. J. Phys.* **37**, 65301 (2016).

27. Kalirajan, C., Dukle, A., Nathanael, A. J., Oh, T.-H. & Manivasagam, G. A Critical Review on Polymeric Biomaterials for Biomedical Applications. *Polymers (Basel).* **13**, 3015 (2021).

28. Kohsaka, Y. Conjugate substitution reaction of α-(substituted methyl)acrylates in polymer chemistry. *Polym. J.* **52**, 1175–1183 (2020).

29. Zhang, W. *et al.* Halogen-Substituted Acridines as Highly Effective Corrosion

Inhibitors for Mild Steel in Acid Medium. *J. Phys. Chem. C* **122**, 25349–25364 (2018).

30. Holthoff, J. M., Engelage, E., Kowsari, A. B., Huber, S. M. & Weiss, R. Noble Metal Corrosion: Halogen Bonded Iodocarbenium Iodides Dissolve Elemental Gold—Direct Access to Gold–Carbene Complexes. *Chem. – A Eur. J.* **25**, 7480–7484 (2019).

31. Whorlow, K; Hutto, F [1]; Woolridge, E. [2]. Effect of halogens and inhibitors on the external stress corrosion cracking of Type 304 austenitic stainless steel. *U.S. Dep. Energy Off. Sci. Tech. Inf.* (1997).

32. Kappes, M. A. Localized corrosion and stress corrosion cracking of stainless steels in halides other than chlorides solutions: a review. *Corros. Rev.* **38**, 1–24 (2020).

33. Nassau, Kurt, A. A. *et al.* Physical and chemical causes of colour. *britannica.com* (2021).

34. Sklar, A. L. Theory of Color of Organic Compounds. *J. Chem. Phys.* **5**, 669–681 (1937).

35. Mahmood, A., Khan, S. U.-D. & ur Rehman, F. Assessing the quantum mechanical level of theory for prediction of UV/Visible absorption spectra of some aminoazobenzene dyes. *J. Saudi Chem. Soc.* **19**, 436–441 (2015).

36. Haghdani, S., Davari, N., Sandnes, R. & Åstrand, P.-O. Complex frequency-dependent polarizability through the $\pi \rightarrow \pi^*$ excitation energy of azobenzene

molecules by a combined charge-transfer and point-dipole interaction model. *J. Phys. Chem. A* **118**, 11282–11292 (2014).

37. Jacquemin, D. *et al.* Absorption spectra of azobenzenes simulated with time-dependent density functional theory. *Int. J. Quantum Chem.* **111**, 4224–4240 (2011).

38. Xu, X., Luan, F., Liu, H., Cheng, J. & Zhang, X. Prediction of the maximum absorption wavelength of azobenzene dyes by QSPR tools. *Spectrochim. Acta Part A Mol. Biomol. Spectrosc.* **83**, 353–361 (2011).

39. Ali, M. *et al.* DFT Study for the Spectroscopic and Structural Analysis of p-Dimethylaminoazobenzene. *J. Spectrosc.* **2018**, 9365153 (2018).

40. Chen, P. C., Chieh, Y. C. & Wu, J. C. Theoretical study of the electronic spectra of azobenzene dyes. *J. Mol. Struct.* **715**, 183–189 (2005).

41. Acik, G. Synthesis and Characterization of Sugar-based Methacrylates and Their Random Copolymers by ATRP. *eXPRESS Polym. Lett.* **11**, (2017).

42. Dundas, A. A. *et al.* Methodology for the synthesis of methacrylate monomers using designed single mode microwave applicators. *React. Chem. Eng.* **4**, 1472–1476 (2019).

43. Gunes, D., Karagoz, B. & Bicak, N. Synthesis of Methacrylate-Based Functional Monomers via Boron Ester Acidolysis and Their Polymerization. *Des. Monomers Polym.* **12**, 445–454 (2009).

44. Soykan, C. New Methods in the Synthesis of (Meth)AcrylatesNo Title. *IntechOpen B. Ser.* (2020). doi:10.5772/intechopen.89767

45. Sayed, M., Gaber, Y., Bornadel, A. & Pyo, S.-H. Multi-steps green process for synthesis of six-membered functional cyclic carbonate from trimethylolpropane by lipase catalyzed methacrylation and carbonation, and thermal cyclization. *Biotechnol. Prog.* **32**, 83–88 (2016).

46. Park, D.-W. *et al.* Enzymatic esterification of beta-methylglucoside with acrylic/methacrylic acid in organic solvents. *J. Biotechnol.* **107**, 151–160 (2004).

47. Ortiz, C. *et al.* Novozym 435: the “perfect” lipase immobilized biocatalyst? *Catal. Sci. Technol.* **9**, 2380–2420 (2019).

48. Chowdhury, A. & Mitra, D. A kinetic study on the Novozyme 435-catalyzed esterification of free fatty acids with octanol to produce octyl esters. *Biotechnol. Prog.* **31**, 1494–1499 (2015).

49. Darabi Mahboub, M. J., Dubois, J.-L., Cavani, F., Rostamizadeh, M. & Patience, G. S. Catalysis for the synthesis of methacrylic acid and methyl methacrylate. *Chem. Soc. Rev.* **47**, 7703–7738 (2018).

50. Barnes, C. E. Resin of interpolymerized substances comprising acrylic or methacrylic anhydride. (1939).

51. de la Vega-Hernández, K., Antuch, M., Cuesta-Rubio, O., Núñez-Figueredo, Y. & Pardo-Andreu, G. L. Discerning the antioxidant mechanism of rapanone: A

naturally occurring benzoquinone with iron complexing and radical scavenging activities. *J. Inorg. Biochem.* **170**, 134–147 (2017).

52. Norma Francenia Santos-Sánchez, Raúl Salas-Coronado, C. V.-C. and B. H.-C. Antioxidant Compounds and Their Antioxidant Mechanism. *IntechOpen B. Ser.* (2019). doi:10.5772/intechopen.85270

53. Lamaoui, A., García-Guzmán, J. J., Amine, A., Palacios-Santander, J. M. & Cubillana-Aguilera, L. Chapter 4 - Synthesis techniques of molecularly imprinted polymer composites. in *Molecularly Imprinted Polymer Composites* (eds. Sooraj, M. P., Nair, A. S., Mathew, B. & Thomas, S.) 49–91 (Woodhead Publishing, 2021). doi:https://doi.org/10.1016/B978-0-12-819952-7.00002-0

54. Barner-Kowollik, C., Vana, P. & Davis, T. P. The Kinetics of Free-Radical Polymerization. in *Handbook of Radical Polymerization* 187–261 (John Wiley & Sons, Ltd, 2002). doi:https://doi.org/10.1002/0471220450.ch4

55. Moad, G. & Solomon, D. H. 2 - Radical Reactions. in *The Chemistry of Radical Polymerization (Second Edition)* (eds. Moad, G. & Solomon, D. H.) 11–48 (Elsevier Science Ltd, 2005). doi:https://doi.org/10.1016/B978-008044288-4/50021-2

56. Sanchez, J. & Myers, T. N. Initiators (Free-Radical). in *Van Nostrand's Encyclopedia of Chemistry* (John Wiley & Sons, Ltd, 2005). doi:https://doi.org/10.1002/0471740039.vec1367

57. Kita, Y. & Matsugi, M. Radical Initiators. in *Radicals in Organic Synthesis* 1–10

(John Wiley & Sons, Ltd, 2001). doi:https://doi.org/10.1002/9783527618293.ch1

58. Mechanisms of Decomposition of Initiators. in *Handbook of Free Radical Initiators* 1–15 (John Wiley & Sons, Ltd, 2003). doi:https://doi.org/10.1002/0471721476.ch1

59. Hakkarainen, M. *Update on Polylactide Based Materials*. (Smithers Information Limited, 2011).

60. COOTE, M. L. & DAVIS, T. P. 12.2 - SOLVENT EFFECTS ON FREE RADICAL POLYMERIZATION. in *Handbook of Solvents (Second Edition)* (ed. Wypych, G.) 811–833 (ChemTec Publishing, 2014). doi:https://doi.org/10.1016/B978-1-895198-64-5.50021-0

61. Ligon, S., Liska, R., Stampfl, J., Gurr, M. & Mülhaupt, R. Polymers for 3D Printing and Customized Additive Manufacturing. *Chem. Rev.* **117**, (2017).

62. Schmid, M. & Wegener, K. Thermal and molecular properties of polymer powders for Selective Laser Sintering (SLS). *AIP Conf. Proc.* **1779**, (2016).

63. Zaremba, D. *et al.* Methacrylate-Based Copolymers for Polymer Optical Fibers. *Polymers (Basel).* **9**, (2017).

64. Jiang, S., Deng, J. & Yang, W. Block Copolymers Prepared by Free Radical Polymerization Using α-Methylstyrene-containing Precopolymer as Macroinitiator. *Polym. J.* **40**, 543–548 (2008).

65. Elarbe, B., Elganidi, I., Abdullah, N., Yusoh, K. & Ridzuan, N. Optimization and modeling of reactive conditions for free radical solution polymerization of SA-co-BA copolymer based on the yield using response surface methodology. *Malaysian J. Fundam. Appl. Sci.* **17**, 50–55 (2021).

66. Shiho, H. Dispersion Polymerization of Acrylonitrile in Supercritical Carbon Dioxide. *Macromolecules* **33**, (2000).

67. Shiho, H. & DeSimone, J. M. Dispersion polymerization of 2-hydroxyethyl methacrylate in supercritical carbon dioxide. *J. Polym. Sci. Part A Polym. Chem.* **38**, 3783–3790 (2000).

68. Kortsen, K., Pacheco, A. A. C., Lentz, J. C., Taresco, V. & Howdle, S. M. On-line polymerisation monitoring in scCO2: a reliable and inexpensive sampling method in high pressure applications. *J. Supercrit. Fluids* **167**, 105047 (2021).

69. McAllister, T. D., Farrand, L. D. & Howdle, S. M. Improved Particle Size Control for the Dispersion Polymerization of Methyl methacrylate in Supercritical Carbon Dioxide. *Macromol. Chem. Phys.* **217**, 2294–2301 (2016).

70. Mcallister, T. Expanding the scope of free-radical dispersion polymerisations in supercritical CO2. (The University of Nottingham, 2017).

71. Christian, P. *et al.* Free Radical Polymerization of Methyl Methacrylate in Supercritical Carbon Dioxide Using a Pseudo-Graft Stabilizer: Effect of Monomer, Initiator, and Stabilizer Concentrations. *Macromolecules* **33**, (2000).

72. Zhu, R. *et al.* Surface properties and depth analysis of

polyethylene/polydimethylsiloxane composite prepared by using supercritical carbon dioxide. *Polym. J.* **42**, 562–566 (2010).

73. Houben, M., van Geijn, R., van Essen, M., Borneman, Z. & Nijmeijer, K. Supercritical CO2 permeation in glassy polyimide membranes. *J. Memb. Sci.* **620**, 118922 (2021).

74. Nalawade, S. P., Picchioni, F. & Janssen, L. P. B. M. Supercritical carbon dioxide as a green solvent for processing polymer melts: Processing aspects and applications. *Prog. Polym. Sci.* **31**, 19–43 (2006).

75. Bonavoglia, B., Storti, G., Morbidelli, M., Rajendran, A. & Mazzotti, M. Sorption and swelling of semicrystalline polymers in supercritical CO2. *J. Polym. Sci. Part B Polym. Phys.* **44**, 1531–1546 (2006).

76. Nowak, M., Misic, D., Trusek, A. & Zizovic, I. Polymeric Microfiltration Membranes Modification by Supercritical Solvent Impregnation—Potential Application in Open Surgical Wound Ventilation. *Molecules* **26**, (2021).

77. Zizovic, I., Trusek, A., Tyrka, M., Moric, I. & Senerovic, L. Functionalization of Polyamide Microfiltration Membranes by Supercritical Solvent Impregnation. *J. Supercrit. Fluids* **174**, 105250 (2021).

78. Elmaaty, T. A., El-Aziz, E. A., Ma, J., El-Taweel, F. & Okubayashi, S. Eco-Friendly Disperse Dyeing and Functional Finishing of Nylon 6 Using Supercritical Carbon Dioxide. *Fibers* **3**, 309–322 (2015).

79. Chang, Y. *et al.* Supercritical CO2 assisted processing of polystyrene/nylon 1212

blends and CO2-induced epitaxy on nylon 1212. *J. Appl. Polym. Sci.* **92**, 2023–2029 (2004).

80. Milovanovic, S., Stamenic, M., Marković, D., Jasna, I. & Zizovic, I. Supercritical impregnation of cellulose acetate with thymol. *J. Supercrit. Fluids* **97**, 107–115 (2015).

81. Thomas Gamse, Rolf Marr , Christian Wolf, K. L. Supercritical CO2 Impregnation of Polyethylene Components for Medical Purposes. *Hem. Ind. = Chem. Ind.* **61**, 229–232 (2007).

82. Champeau, M., Thomassin, J.-M., Tassaing, T. & Jérôme, C. Drug loading of polymer implants by supercritical CO2 assisted impregnation: A review. *J. Control. Release* **209**, 248–259 (2015).

83. Rojas, A., Torres, A., José Galotto, M., Guarda, A. & Julio, R. Supercritical impregnation for food applications: a review of the effect of the operational variables on the active compound loading. *Crit. Rev. Food Sci. Nutr.* **60**, 1290–1301 (2020).

84. Zizovic, I. *et al.* Functional Modification of Cellulose Acetate Microfiltration Membranes by Supercritical Solvent Impregnation. *Molecules* **26**, (2021).

85. Li, D. & Han, B. Impregnation of Polyethylene (PE) with Styrene Using Supercritical CO2 as the Swelling Agent and Preparation of PE/Polystyrene Composites. *Ind. Eng. Chem. Res.* **39**, 4506–4509 (2000).

86. Üzer, S., Akman, U. & Hortaçsu, Ö. Polymer swelling and impregnation using

supercritical CO2: A model-component study towards producing controlled-release drugs. *J. Supercrit. Fluids* **38**, 119–128 (2006).

87. Pacheco, A. A. C. *et al.* Influence of structure and solubility of chain transfer agents on the RAFT control of dispersion polymerisation in scCO2. *Chem. Sci.* **12**, 1016–1030 (2021).

88. Brady, J., Dürig, T., Lee, P. I. & Li, J.-X. Chapter 7 - Polymer Properties and Characterization. in *Developing Solid Oral Dosage Forms (Second Edition)* (eds. Qiu, Y., Chen, Y., Zhang, G. G. Z., Yu, L. & Mantri, R. V) 181–223 (Academic Press, 2017). doi:https://doi.org/10.1016/B978-0-12-802447-8.00007-8

89. Wei-Fang Shu. Radical Chain Polymerization. in *Principles of Polymer Design and Synthesis* 137–183 (Springer, Berlin, Heidelberg, 2013). doi:https://doi.org/10.1007/978-3-642-38730-2_7

90. Bagh, M. B. *et al.* Quinone and oxyradical scavenging properties of N-acetylcysteine prevent dopamine mediated inhibition of Na+, K+-ATPase and mitochondrial electron transport chain activity in rat brain: implications in the neuroprotective therapy of Parkinson's disease. *Free Radic. Res.* **42**, 574–581 (2008).

91. Mukai, K., Morimoto, H., Kikuchi, S. & Nagaoka, S. Kinetic study of free-radical-scavenging action of biological hydroquinones (reduced forms of ubiquinone, vitamin K and tocopherol quinone) in solution. *Biochim. Biophys. Acta - Gen. Subj.* **1157**, 313–317 (1993).

92. Polonik, N. S., Sabutskii, Y. E. & Polonik, S. G. Free Radical Scavenging Activity of Synthetic and Naturally Occurring Polyhydroxy-, Aminohydroxynaphthazarins and Related Compounds. *Nat. Prod. Commun.* **13**, 1934578X1801301021 (2018).

93. Hook, J. P. Van & Tobolsky, A. V. The Solution Polymerization of Styrene and Methyl Methacrylate. *J. Phys. Chem.* **62**, 257–260 (1958).

94. Dizon, J. R. C., Gache, C. C. L., Cascolan, H. M. S., Cancino, L. T. & Advincula, R. C. Post-Processing of 3D-Printed Polymers. *Technologies* **9**, (2021).

95. David Cameron, A. B. Dyeing SLS Parts. *Interact. Res. Stud.* 1–64 (2014).

96. Achieving vivid colours for your SLS prints. *Autonomous Manufacturing* (2017). Available at: https://amfg.ai/2017/05/19/colours-sls/. (Accessed: 22nd December 2021)

97. Hui, D., Goodridge, R. D., Scotchford, C. A. & Grant, D. M. Laser sintering of nano-hydroxyapatite coated polyamide 12 powders. *Addit. Manuf.* **22**, 560–570 (2018).

98. Beitz, S. *et al.* Influence of Powder Deposition on Powder Bed and Specimen Properties. *Mater. (Basel, Switzerland)* **12**, (2019).

99. Brandt, M. *Laser Additive Manufacturing: Materials, Design, Technologies, and Applications*. (Elsevier Science, 2016).

100. Elaine R. S. Hodges. *The Guild Handbook of Scientific Illustration*. (John Wiley &

Sons, 2003).

101. Gilbert, P. U. P. . Chapter 8 - Subtractive color mixing. in (ed. Gilbert, P. U. P. . B. T.-P. in the A. (Third E.) 147–168 (Academic Press, 2022). doi:https://doi.org/10.1016/B978-0-12-824347-3.00008-X

102. Celko, J. Chapter 15 - Colors. in (ed. Celko Measurements and Standards in SQL, J. B. T.-J. C. D.) 145–146 (Morgan Kaufmann, 2010). doi:https://doi.org/10.1016/B978-0-12-374722-8.00015-3

103. Kang, H. R. *Color Technology for Electronic Imaging Devices*. (SPIE Optical Engineering Press, 1997).

104. EOS. Polyamide 12 for 3D Printing. *EOS* (2021). Available at: https://www.eos.info/en/additive-manufacturing/3d-printing-plastic/sls-polymer-materials/polyamide-pa-12-alumide. (Accessed: 10th December 2021)

105. 14 - Nylon 12 (PA 12). in *Plastics Design Library* (eds. Woishnis, W. A. & Ebnesajjad, S. B. T.-C. R. of T.) 1813–1874 (William Andrew Publishing, 2012). doi:https://doi.org/10.1016/B978-1-4557-7896-6.00014-5

106. Almansoori, A., Abrams, K. J., Ghali Al-Rubaye, A. D., Majewski, C. & Rodenburg, C. Novel plasma treatment for preparation of laser sintered nanocomposite parts. *Addit. Manuf.* **25**, 297–306 (2019).

107. Nar, K., Majewski, C. & Lewis, R. A comprehensive characterisation of Laser Sintered Polyamide-12 surfaces. *Polym. Test.* **106**, 107450 (2022).

108. Pilipović, A., Rujnić-Sokele, M. & Šercer, M. Impact of ageing, different share of recycled material and orientation on SLS polyamide product hardness. *AIP Conf. Proc.* **1779**, 100001 (2016).

109. Department, U. S. W. *War Department Technical Manual*. (U.S. Government Printing Office, 1940).

110. Wiria, F. E., Leong, K. F., Chua, C. K. & Liu, Y. Poly-epsilon-caprolactone/hydroxyapatite for tissue engineering scaffold fabrication via selective laser sintering. *Acta Biomater.* **3**, 1–12 (2007).

111. Simha Martynková, G. *et al.* Polyamide 12 Materials Study of Morpho-Structural Changes during Laser Sintering of 3D Printing. *Polymers (Basel).* **13**, 810 (2021).

112. Dadbakhsh, S. *et al.* Effect of PA12 powder reuse on coalescence behaviour and microstructure of SLS parts. *Eur. Polym. J.* **92**, (2017).

113. Weinmann, S. & Bonten, C. Recycling of PA12 powder for selective laser sintering. *AIP Conf. Proc.* **2289**, 20056 (2020).

114. Sivadas, B. O., Ashcroft, I., Khlobystov, A. N. & Goodridge, R. D. Laser sintering of polymer nanocomposites. *Adv. Ind. Eng. Polym. Res.* **4**, 277–300 (2021).

115. Craft, G., Nussbaum, J., Crane, N. & Harmon, J. P. Impact of extended sintering times on mechanical properties in PA-12 parts produced by powderbed fusion processes. *Addit. Manuf.* **22**, 800–806 (2018).

116. Czelusniak, T. & Amorim, F. L. Influence of energy density on polyamide 12 processed by SLS: from physical and mechanical properties to microstructural and crystallization evolution. *Rapid Prototyp. J.* **27**, 1189–1205 (2021).

117. NIX. NIX-mini. *NIX* (2021). Available at: https://www.nixsensor.com/nix-mini/. (Accessed: 20th November 2021)

118. NIX. Nix Pro. *NIX* (2021). Available at: https://www.nixsensor.com/nix-pro/. (Accessed: 20th November 2021)

119. NIX Color Sensor. *NIX* (2021). Available at: https://www.nixsensor.com/. (Accessed: 16th December 2021)

120. Wyszecki, G. & Stiles, W. Color Science: Concepts and Methods, Quantitative Data and Formulae, 2nd Edition. *Color Sci. Concepts Methods, Quant. Data Formulae, 2nd Ed. by Gunther Wyszecki, W. S. Stiles, pp. 968. ISBN 0-471-39918-3. Wiley-VCH , July 2000.* (2000).

121. Tsuboi, A., Nakamura, K. & Kobayashi, N. Multicolor Electrochromism Showing Three Primary Color States (Cyan–Magenta–Yellow) Based on Size- and Shape-Controlled Silver Nanoparticles. *Chem. Mater.* **26**, 6477–6485 (2014).

122. Yang, G. *et al.* Three primary color (cyan/magenta/yellow) switchable electrochromic devices based on PEDOT:PSS and 'electrobase/electroacid' theory. *New J. Chem.* **43**, 8410–8413 (2019).

123. Sayili, A. M. The Aristotelian Explanation of the Rainbow. *Isis* **30**, 65–83 (1939).

124. Ierodiakonou, K. Aristotle and Alexander of Aphrodisias on Colour BT - The Parva naturalia in Greek, Arabic and Latin Aristotelianism: Supplementing the Science of the Soul. in (eds. Bydén, B. & Radovic, F.) 77–90 (Springer International Publishing, 2018). doi:10.1007/978-3-319-26904-7_4

125. Sorabji, R. Aristotle, Mathematics, and Colour. *Class. Q.* **22**, 293–308 (1972).

126. Choudhury, A. K. R. 4 - Principles of colour perception. in (ed. Choudhury, A. K. R. B. T.-P. of C. and A. M.) 144–184 (Woodhead Publishing, 2014). doi:https://doi.org/10.1533/9780857099242.144

127. Mumby, R. 19 - Printing for packaging. in (eds. Emblem, A. & Emblem, H. B. T.-P. T.) 441–489 (Woodhead Publishing, 2012). doi:https://doi.org/10.1533/9780857095701.3.441

128. Parraman, C. 18 - Colour printing techniques. in *Woodhead Publishing Series in Textiles* (ed. Best, J. B. T.-C. D.) 497–531 (Woodhead Publishing, 2012). doi:https://doi.org/10.1533/9780857095534.3.497

129. Briggs, D. 5.2 Ideal Subtractive Primaries. *The Dimensions of Colour* (2012). Available at: http://www.huevaluechroma.com/052.php. (Accessed: 16th December 2021)

130. Briggs, D. 5.1 SUBTRACTIVE MIXING PROCESSES. *The Dimensions of Colour* (2012). Available at: http://www.huevaluechroma.com/051.php. (Accessed: 16th December 2021)

131. Gigahertz-Optik. II.9. The perception of color. *Measurement of Light* •

Measurement with Light (2021). Available at: https://light-measurement.com/perception-of-color/. (Accessed: 10th December 2021)

132. Minolta, K. *Precise Color Communication*. (2007).

133. Tigwell, G. W., Flatla, D. R. & Archibald, N. D. ACE: A Colour Palette Design Tool for Balancing Aesthetics and Accessibility. *ACM Trans. Access. Comput.* **9**, (2017).

134. Lai, P. & Westland, S. Machine learning for colour Palette extraction from fashion runway images. *Int. J. Fash. Des. Technol. Educ.* **13**, 334–340 (2020).

135. Williams, S. Colours. *Sherwin Williams* (2021). Available at: https://www.sherwin-williams.com/homeowners/color. (Accessed: 15th December 2021)

136. PPG. Color. *PPGPaints* (2021). Available at: https://www.ppgpaints.com/color. (Accessed: 15th December 2021)

137. Furferi, R. & Carfagni, M. Colour Mixing Modelling and Simulation: Optimization of Colour Recipe for Carded Fibres. *Model. Simul. Eng.* **2010**, 487678 (2010).

138. Yang, Y.-P. & Tian, X. Combining Users' Cognition Noise with Interactive Genetic Algorithms and Trapezoidal Fuzzy Numbers for Product Color Design. *Comput. Intell. Neurosci.* **2019**, 1019749 (2019).

139. Wu, M., Guan, X., Li, W. & Huang, Q. Color spectra algorithm of hyperspectral

wood dyeing using particle swarm optimization. *Wood Sci. Technol.* **55**, 49–66 (2021).

140. Chaouch, S., Moussa, A., Ben Marzoug, I. & Ladhari, N. Application of genetic algorithm to color recipe formulation using reactive and direct dyestuffs mixtures. *Color Res. Appl.* **45**, 896–910 (2020).

141. Yang, X.-S. Chapter 6 - Genetic Algorithms. in (ed. Yang, X.-S. B. T.-N.-I. O. A. (Second E.) 91–100 (Academic Press, 2021). doi:https://doi.org/10.1016/B978-0-12-821986-7.00013-5

142. Chau, T., Burovskiy, P., Flynn, M. & Luk, W. Chapter Two - Advances in Dataflow Systems. in (eds. Hurson, A. R. & Milutinović, V. B. T.-A. in C.) **106**, 21–62 (Elsevier, 2017).

143. Roetzel, W., Luo, X. & Chen, D. Chapter 6 - Optimal design of heat exchanger networks. in (eds. Roetzel, W., Luo, X. & Chen, D. B. T.-D. and O. of H. E. and their N.) 231–317 (Academic Press, 2020). doi:https://doi.org/10.1016/B978-0-12-817894-2.00006-6

144. Saeed, G. 16 - Structural Optimization for Frequency Constraints. in (eds. Gandomi, A. H., Yang, X.-S., Talatahari, S. & Alavi, A. H. B. T.-M. A. in S. and I.) 389–417 (Elsevier, 2013). doi:https://doi.org/10.1016/B978-0-12-398364-0.00016-4

145. Sahab, M. G., Toropov, V. V & Gandomi, A. H. 2 - A Review on Traditional and Modern Structural Optimization: Problems and Techniques. in (eds. Gandomi,

A. H., Yang, X.-S., Talatahari, S. & Alavi, A. H. B. T.-M. A. in S. and I.) 25–47 (Elsevier, 2013). doi:https://doi.org/10.1016/B978-0-12-398364-0.00002-4

146. Kennedy, J. & Eberhart, R. Particle swarm optimization. in *Proceedings of ICNN'95 - International Conference on Neural Networks* **4**, 1942–1948 vol.4 (1995).

147. Cornell, J. *A Primer on Experiments with Mixtures*. (2011). doi:10.1002/9780470907443

148. Luo, M. R., Cui, G. & Rigg, B. The development of the CIE 2000 colour-difference formula: CIEDE2000. *Color Res. Appl.* **26**, 340–350 (2001).

149. Shi, Y. & Eberhart, R. A modified particle swarm optimizer. in *1998 IEEE International Conference on Evolutionary Computation Proceedings. IEEE World Congress on Computational Intelligence (Cat. No.98TH8360)* 69–73 (1998). doi:10.1109/ICEC.1998.699146

150. Kucera, J. Biofouling of Polyamide Membranes: Fouling Mechanisms, Current Mitigation and Cleaning Strategies, and Future Prospects. *Membranes (Basel).* **9**, 111 (2019).

151. Deguchi, T., Kitaoka, Y., Kakezawa, M. & Nishida, T. Purification and characterization of a nylon-degrading enzyme. *Appl. Environ. Microbiol.* **64**, 1366–1371 (1998).

152. Rogalsky, S., Bardeau, J.-F., Tarasyuk, O. & Fatyeyeva, K. Fabrication of new antifungal polyamide-12 material. *Polym. Int.* **61**, (2012).

153. L., W. T. *et al.* Living biofouling-resistant membranes as a model for the beneficial use of engineered biofilms. *Proc. Natl. Acad. Sci.* **113**, E2802–E2811 (2016).

154. Biofilm basics: Section 1. *Montana State University* Available at: https://biofilm.montana.edu/biofilm-basics/what_are_biofilms.html.

155. Palmer, J., Flint, S. & Brooks, J. Bacterial cell attachment, the beginning of a biofilm. *J. Ind. Microbiol. Biotechnol.* **34**, 577–588 (2007).

156. Diggle, S. P. & Whiteley, M. Microbe Profile: Pseudomonas aeruginosa: opportunistic pathogen and lab rat. *Microbiology* **166**, 30–33 (2020).

157. J., C. S. *et al.* Catheter-Associated Urinary Tract Infection by Pseudomonas aeruginosa Is Mediated by Exopolysaccharide-Independent Biofilms. *Infect. Immun.* **82**, 2048–2058 (2014).

158. Cabrera, J. N., Rojas, G., D'Accorso, N. B., Lizarraga, L. & Negri, R. M. Membranes based on polyacrylamide coatings on metallic meshes prepared by a two-steps redox polymerization. Performance for oil-water separation and biofouling effects. *Sep. Purif. Technol.* **247**, 116966 (2020).

159. Kreve, S. & Reis, A. C. Dos. Bacterial adhesion to biomaterials: What regulates this attachment? A review. *Jpn. Dent. Sci. Rev.* **57**, 85–96 (2021).

160. Monroy Salazar, H. *et al.* YEAST: DESCRIPTION AND STRUCTURE. in 4–13 (2016).

161. Cavalheiro, M. *et al.* From the first touch to biofilm establishment by the

human pathogen Candida glabrata: a genome-wide to nanoscale view. *Commun. Biol.* **4**, 886 (2021).

162. Atriwal, T. *et al.* Mechanistic Understanding of Candida albicans Biofilm Formation and Approaches for Its Inhibition. *Front. Microbiol.* **12**, (2021).

163. Alim, D., Sircaik, S. & Panwar, S. L. The Significance of Lipids to Biofilm Formation in Candida albicans: An Emerging Perspective. *Journal of Fungi* **4**, (2018).

164. Valotteau, C., Prystopiuk, V., Cormack, B. P. & Dufrêne, Y. F. Atomic Force Microscopy Demonstrates that Candida glabrata Uses Three Epa Proteins To Mediate Adhesion to Abiotic Surfaces. *mSphere* **4**, e00277-19 (2019).

165. Hassan, Y., Chew, S. Y. & Than, L. T. L. Candida glabrata: Pathogenicity and Resistance Mechanisms for Adaptation and Survival. *J. fungi (Basel, Switzerland)* **7**, 667 (2021).

166. Fogle, M. R., Douglas, D. R., Jumper, C. A. & Straus, D. C. Growth and mycotoxin production by Chaetomium globosum. *Mycopathologia* **164**, 49–56 (2007).

167. Kamle, M. *et al.* Identification and phylogenetic correlation among Colletotrichum gloeosporioides pathogen of anthracnose for mango. *Biocatal. Agric. Biotechnol.* **2**, 285–287 (2013).

168. Weir, B. S., Johnston, P. R. & Damm, U. The Colletotrichum gloeosporioides species complex. *Stud. Mycol.* **73**, 115–180 (2012).

169. Tang, L. *et al.* Antifungal effects of dimethyl trisulfide against Colletotrichum gloeosporioides infection on mango. *J. Phytopathol.* **167**, 445–450 (2019).

170. Iñiguez-Moreno, M., Ragazzo-Sánchez, J. A., Barros-Castillo, J. C., Sandoval-Contreras, T. & Calderón-Santoyo, M. Sodium alginate coatings added with Meyerozyma caribbica: Postharvest biocontrol of Colletotrichum gloeosporioides in avocado (Persea americana Mill. cv. Hass). *Postharvest Biol. Technol.* **163**, 111123 (2020).

171. De la Rosa-García, S. C. *et al.* Antifungal Activity of ZnO and MgO Nanomaterials and Their Mixtures against *Colletotrichum gloeosporioides* Strains from Tropical Fruit. *J. Nanomater.* **2018**, 3498527 (2018).

172. C., F. M. *et al.* Threats Posed by the Fungal Kingdom to Humans, Wildlife, and Agriculture. *MBio* **11**, e00449-20 (2022).

173. Haleem Khan, A. A. & Mohan Karuppayil, S. Fungal pollution of indoor environments and its management. *Saudi J. Biol. Sci.* **19**, 405–426 (2012).

174. Green, B. J. *et al.* Production of a Chaetomium globosum enolase monoclonal antibody. *Monoclon. Antib. Immunodiagn. Immunother.* **33**, 428–437 (2014).

175. Nurioglu, A. G., Esteves, A. C. C. & de With, G. Non-toxic{,} non-biocide-release antifouling coatings based on molecular structure design for marine applications. *J. Mater. Chem. B* **3**, 6547–6570 (2015).

176. Brzezinska, M. S. *et al.* Antifungal Activity of Polyhexamethyleneguanidine Derivatives Introduced into Biodegradable Polymers. *J. Polym. Environ.* **27**,

1760–1769 (2019).

177. Hook, A. L. *et al.* Discovery of Novel Materials with Broad Resistance to Bacterial Attachment Using Combinatorial Polymer Microarrays. *Adv. Mater.* **25**, 2542–2547 (2013).

178. Hook, A. L. *et al.* Combinatorial discovery of polymers resistant to bacterial attachment. *Nat. Biotechnol.* **30**, 868–875 (2012).

179. Singh, N. *et al.* Dual bioresponsive antibiotic and quorum sensing inhibitor combination nanoparticles for treatment of Pseudomonas aeruginosa biofilms in vitro and ex vivo. *Biomater. Sci.* **7**, 4099–4111 (2019).

180. Song, M., Im, S. J., Jeong, D. & Jang, A. Reduction of biofouling potential in cartridge filter by using chlorine dioxide for enhancing anti-biofouling of seawater reverse osmosis membrane. *Environ. Res.* **180**, 108866 (2020).

181. Pasmore, M. *et al.* Effects of ultrafiltration membrane surface properties on Pseudomonas aeruginosa biofilm initiation for the purpose of reducing biofouling. *J. Memb. Sci.* **194**, 15–32 (2001).

182. Magin, C. M., Cooper, S. P. & Brennan, A. B. Non-toxic antifouling strategies. *Mater. Today* **13**, 36–44 (2010).

183. Palmer, J. S., Flint, S. H., Schmid, J. & Brooks, J. D. The role of surface charge and hydrophobicity in the attachment of Anoxybacillus flavithermus isolated from milk powder. *J. Ind. Microbiol. Biotechnol.* **37**, 1111–1119 (2010).

184. Mohamad, A. johari, Zhu, X., Liu, X., Pfleging, W. & Torge, M. *Effect of surface topography on hydrophobicity and bacterial adhesion of polystyrene*. (2013). doi:10.1109/3M-NANO.2013.6737421

185. Dafforn, K. A., Lewis, J. A. & Johnston, E. L. Antifouling strategies: History and regulation, ecological impacts and mitigation. *Mar. Pollut. Bull.* **62**, 453–465 (2011).

186. Giles, M. R., Hay, J. N., Howdle, S. M. & Winder, R. J. Macromonomer surfactants for the polymerisation of methyl methacrylate in supercritical CO2. *Polymer (Guildf).* **41**, 6715–6721 (2000).

187. Gong, S., Chen, H., Zhou, X. & Gunasekaran, S. Synthesis and applications of MANs/poly(MMA-co-BA) nanocomposite latex by miniemulsion polymerization. *R. Soc. Open Sci.* **4**, (2017).

188. Nurlybayeva, A., Sakhy, M., Negim, E. S., Rustem, E. & Shinibekova, A. Synthesis and research of copolymers on the basis of methyl methacrylate and their application in paint and varnish coverings. *Int. J. Chem. Sci.* **13**, 922–934 (2015).

189. O'Brien, D. M. *et al.* Epoxy–amine oligomers from terpenes with applications in synergistic antifungal treatments. *J. Mater. Chem. B* **7**, 5222–5229 (2019).

190. Rao, A., Zhang, Y., Muend, S. & Rao, R. Mechanism of antifungal activity of terpenoid phenols resembles calcium stress and inhibition of the TOR pathway. *Antimicrob. Agents Chemother.* **54**, 5062–5069 (2010).

191. Mahizan, N. A. *et al.* Terpene Derivatives as a Potential Agent against

Antimicrobial Resistance (AMR) Pathogens. *Molecules* **24**, 2631 (2019).

192. Guimarães, A. C. *et al.* Antibacterial Activity of Terpenes and Terpenoids Present in Essential Oils. *Molecules* **24**, 2471 (2019).

193. Wilbon, P. A., Chu, F. & Tang, C. Progress in Renewable Polymers from Natural Terpenes, Terpenoids, and Rosin. *Macromol. Rapid Commun.* **34**, 8–37 (2013).

194. Ammann, K. R., Li, M., Hossainy, S. & Slepian, M. J. The Influence of Polymer Processing Methods on Polymer Film Physical Properties and Vascular Cell Responsiveness. *ACS Appl. bio Mater.* **2**, 3234–3244 (2019).

195. Ren, S. & Frymier, P. D. Reducing bioassay variability by identifying sources of variation and controlling key parameters in assay protocol. *Chemosphere* **57**, 81–90 (2004).

196. Stauber, J. L. & Davies, C. M. Use and limitations of microbial bioassays for assessing copper bioavailability in the aquatic environment. *Environ. Rev.* **8**, 255–301 (2000).

197. 15 - Fibre–polymer composites for aerospace structures and engines. in (ed. Mouritz, A. P. B. T.-I. to A. M.) 338–393 (Woodhead Publishing, 2012). doi:https://doi.org/10.1533/9780857095152.338

198. Feih, S. & Mouritz, A. P. Tensile properties of carbon fibres and carbon fibre–polymer composites in fire. *Compos. Part A Appl. Sci. Manuf.* **43**, 765–772 (2012).

199. Bhatt, Pooja; Goe, A. Carbon Fibres: Production, Properties and Potential Use. *Mater. Sci. Res. India* (2017). doi:http://dx.doi.org/10.13005/msri/140109

200. Calaf Chica, J., Bravo Díez, P. M. & Preciado Calzada, M. A New Prediction Method for the Ultimate Tensile Strength of Steel Alloys with Small Punch Test. *Mater. (Basel, Switzerland)* **11**, 1491 (2018).

201. Pavlina, E. J. & Van Tyne, C. J. Correlation of Yield Strength and Tensile Strength with Hardness for Steels. *J. Mater. Eng. Perform.* **17**, 888–893 (2008).

202. O' Connor, H. J. & Dowling, D. P. Comparison between the properties of polyamide 12 and glass bead filled polyamide 12 using the multi jet fusion printing process. *Addit. Manuf.* **31**, 100961 (2020).

203. Guo, B., Xu, Z., Luo, X. & Bai, J. A detailed evaluation of surface, thermal, and flammable properties of polyamide 12/glass beads composites fabricated by multi jet fusion. *Virtual Phys. Prototyp.* **16**, S39–S52 (2021).

204. Abdullah, A. M. *et al.* Mechanical and cytotoxicity properties of hybrid ceramics filled polyamide 12 filament feedstock for craniofacial bone reconstruction via fused deposition modelling. *Dent. Mater.* **34**, e309–e316 (2018).

205. Qi, S. *et al.* Effect of carbon nanotubes on mechanical properties of polyamide 12 parts by fused filament fabrication. *Polymer (Guildf).* **247**, 124784 (2022).

206. Gui, C., Chen, Z., Yao, C. & Yang, G. Preparation of nickel/PA12 composite particles by defect-induced electroless plating for use in SLS processing. *Sci. Rep.* **8**, 13407 (2018).

207. Sun, J.-Y. *et al.* Highly stretchable and tough hydrogels. *Nature* **489**, 133–136 (2012).

208. Xie, B., Liu, Y., Ding, Y., Zheng, Q. & Xu, Z. Mechanics of carbon nanotube networks: microstructural evolution and optimal design. *Soft Matter* **7**, 10039–10047 (2011).

209. Thompson, J. I. & Czernuszka, J. T. The effect of two types of cross-linking on some mechanical properties of collagen. *Biomed. Mater. Eng.* **5**, 37–48 (1995).

210. Patermann, S. & Altstädt, V. Influence of different crosslinking systems on the mechanical and morphological properties of thermoplastic vulcanizates. *AIP Conf. Proc.* **1664**, 120002 (2015).

211. Costa, L. & Bracco, P. Chapter 21 - Mechanisms of Crosslinking, Oxidative Degradation and Stabilization of UHMWPE. in (ed. Kurtz, S. M. B. T.-U. B. H. (Second E.) 309–323 (Academic Press, 2009). doi:https://doi.org/10.1016/B978-0-12-374721-1.00021-3

212. EVERAERTS, A. I. & CLEMENS, L. M. Chapter 11 - Pressure sensitive adhesives. in (eds. Dillard, D. A., Pocius, A. V & Chaudhury, M. B. T.-A. S. and E.) 465–534 (Elsevier Science B.V., 2002). doi:https://doi.org/10.1016/B978-044451140-9/50011-1

213. Arima, T., Hamada, T. & McCabe, J. F. The effects of cross-linking agents on some properties of HEMA-based resins. *J. Dent. Res.* **74**, 1597–1601 (1995).

214. Schier, J. E. S., Cohen-Sacal, D., Larsen, O. R. & Hutchinson, R. A. The Effect of

Hydrogen Bonding on Radical Semi-Batch Copolymerization of Butyl Acrylate and 2-Hydroxyethyl Acrylate. *Polymers* **9**, (2017).

215. Welsch, N. & Lyon, L. A. Oligo(ethylene glycol)-sidechain microgels prepared in absence of cross-linking agent: Polymerization, characterization and variation of particle deformability. *PLoS One* **12**, e0181369–e0181369 (2017).

216. Satav, S. S., Karmalkar, R. N., Kulkarni, M. G., Mulpuri, N. & Sastry, G. N. Formation of linear polymers with pendant vinyl groups via inclusion complex mediated polymerization of divinyl monomers. *J. Am. Chem. Soc.* **128**, 7752–7753 (2006).

217. Zhou, C., Yan, J. & Cao, Z. Postcrosslinking of macroporous styrene–divinylbenzene copolymers via pendant vinyl groups: Effect of the starting copolymers on the pore structure of the postcrosslinked products. *J. Appl. Polym. Sci.* **83**, 1668–1677 (2002).

218. Lovett, J. R. *et al.* A Robust Cross-Linking Strategy for Block Copolymer Worms Prepared via Polymerization-Induced Self-Assembly. *Macromolecules* **49**, 2928–2941 (2016).

219. Shen, H., Chen, J. & Taha, M. Cross-linking and damping properties of poly(caprolactone-co-glycidyl methacrylate). *Polym. J.* **46**, 598–608 (2014).

220. Brunner, G. H. *Supercritical Fluids as Solvents and Reaction Media*. (Elsevier Science, 2004).

221. Tan, J., Rao, X., Yang, J. & Zeng, Z. Monodisperse highly cross-linked “living”

microspheres prepared via photoinitiated RAFT dispersion polymerization. *RSC Adv.* **5**, 18922–18931 (2015).

222. Hawkins, G., Zetterlund, P. B. & Aldabbagh, F. RAFT polymerization in supercritical carbon dioxide based on an induced precipitation approach: Synthesis of 2-ethoxyethyl methacrylate/acrylamide block copolymers. *J. Polym. Sci. Part A Polym. Chem.* **53**, 2351–2356 (2015).

223. Jennings, J. *et al.* Advantages of Block Copolymer Synthesis by RAFT-Controlled Dispersion Polymerization in Supercritical Carbon Dioxide. *Macromolecules* **46**, 6843–6851 (2013).

224. Gregory, A. M., Thurecht, K. J. & Howdle, S. M. Controlled Dispersion Polymerization of Methyl Methacrylate in Supercritical Carbon Dioxide via RAFT. *Macromolecules* **41**, 1215–1222 (2008).

225. Zhao, F., Ikushima, Y., Chatterjee, M., Sato, O. & Arai, M. Hydrogenation of an α,β-unsaturated aldehyde catalyzed with ruthenium complexes with different fluorinated phosphine compounds in supercritical carbon dioxide and conventional organic solvents. *J. Supercrit. Fluids* **27**, 65–72 (2003).

226. Chouchi, D., Gourgouillon, D., Courel, M., Vital, J. & Nunes da Ponte, M. The Influence of Phase Behavior on Reactions at Supercritical Conditions: The Hydrogenation of α-Pinene. *Ind. Eng. Chem. Res.* **40**, 2551–2554 (2001).

227. Gan, X. *et al.* Powder quality and electrical conductivity of selective laser sintered polymer composite components. in *Woodhead Publishing Series in*

Composites Science and Engineering (eds. Friedrich, K., Walter, R., Soutis, C., Advani, S. G. & Fiedler, I. H. B. B. T.-S. and P. of A. M. P. C.) 149–185 (Woodhead Publishing, 2020). doi:https://doi.org/10.1016/B978-0-12-819535-2.00006-5

228. Deshmukh, K. *et al.* Chapter 17 - Fundamentals and applications of 3D and 4D printing of polymers: Challenges in polymer processing and prospects of future research. in (eds. Sadasivuni, K. K., Deshmukh, K. & Almaadeed, M. A. B. T.-3D and 4D P. of P. N. M.) 527–560 (Elsevier, 2020). doi:https://doi.org/10.1016/B978-0-12-816805-9.00017-X

229. Greg Mehos, Dave Morgan, J. & J. Hopper Design Principles. *Chem. Eng. essentials CPI Prof.* (2016).

230. Schulze, D., Schwedes, J. & Carson, J. W. Powders and bulk solids: Behavior, characterization, storage and flow. *Powders Bulk Solids Behav. Charact. Storage Flow* 1–511 (2008). doi:10.1007/978-3-540-73768-1

231. Koslow, T. SLS 3D Printer Buyer's Guide. *All3DP.pro* (2019).

232. Walker, J. L. & Santoro, M. 9 - Processing and production of bioresorbable polymer scaffolds for tissue engineering. in *Bioresorbable Polymers for Biomedical Applications* (eds. Perale, G. & Hilborn, J.) 181–203 (Woodhead Publishing, 2017). doi:https://doi.org/10.1016/B978-0-08-100262-9.00009-4

233. Lexow, M. M. & Drummer, D. New Materials for SLS: The Use of Antistatic and Flow Agents. *J. Powder Technol.* **2016**, 1–9 (2016).

234. Griehl, W. & Ruestem, D. Nylon-12-Preparation, Properties, and Applications.

Ind. Eng. Chem. **62**, 16–22 (1970).

235. Udipi, K., Davé, R. S., Kruse, R. L. & Stebbins, L. R. Polyamides from lactams via anionic ring-opening polymerization: 1. Chemistry and some recent findings. *Polymer (Guildf).* **38**, 927–938 (1997).

236. Klaus-Rudolf Dipl-Ing Dr MeyerKarl-Heinz Dr HornungRainer Dr FeldmannHans-Juergen Dipl-In Smigerski. Verfahren zur Herstellung von pulverfoermigen Beschichtungsmitteln auf der Basis von Polyamiden mit mindestens 10 aliphatisch gebundenen Kohlenstoffatomen pro Carbonamidgruppe. (1979).

237. Sylvia Monsheimer, Franz-Erich Baumann, Maik Grebe, J. L. Polymerpulver mit polyamid, verwendung in einem formgebenden verfahren und formkörper, hergestellt aus diesem polymerpulver. (2004).

238. Sylvia Monsheimer, Franz-Erich Baumann, Maik Grebe, J. L. Polymer powder comprising polyamide use thereof in a moulding method and moulded body made from said polymer powder. (2004).

239. Franz-Erich Baumann, Wolfgang Diekmann, Beatrice Küting, Heike Stemmer, Maik Grebe, Kristiane Warnke, Sylvia Monsheimer, H. H. Polymerpulver auf der basis von polyamiden, verwendung in einem formgebenden verfahren und formkörper, hergestellt aus diesem polymerpulver. (2010).

240. Heinz Dr. Scholten, W. C. Use of a polyamide 12 for selective laser sintering. (1997).

241. Karine Loyen, Holger Senff, F.-X. P. Process for the manufacture of polyamide-

12 powder with a high melting point. (2005).

242. Lim, B.-S., Kim, H.-I., Bang, Y.-K. & Kim, D.-S. Manufacture of polymer powders for the industrial SFF system by using SLS process. in *2007 International Conference on Control, Automation and Systems* 2573–2577 (2007). doi:10.1109/ICCAS.2007.4406800

243. Schultz, J. P., Martin, J. P., Kander, R. G. & Suchicital, C. T. A. Selective Laser Sintering of Nylon 12-PEEK Blends Formed by Cryogenic Mechanical Alloying. in *2000 International Solid Freeform Fabrication Symposium* (2000).

244. Sylvia Monsheimer, Maik Grebe, Stefan Altkemper, Sigrid Hessel-Geldmann, Franz-Erich Baumann, Kristiane Warnke, Heike Stemmer, Joachim Mügge, Michael Türke, U. S. Copolyamide powder and its production, its use in a moulding method and object made of this copolyamide powder. (2008).

245. Wahab, M. S., Dalgarno, K., Cochrane, R. & S, H. Development of Polymer Nanocomposites for Rapid Prototyping Process. *Lect. Notes Eng. Comput. Sci.* **2177**, (2009).

246. Forbes, M. D. E., Jarocha, L. E., Sim, S. & Tarasov, V. F. Chapter One - Time-Resolved Electron Paramagnetic Resonance Spectroscopy: History, Technique, and Application to Supramolecular and Macromolecular Chemistry. in (eds. Williams, I. H. & Williams, N. H.) **47**, 1–83 (Academic Press, 2013).

247. Roy, N. K., Behera, D., Dibua, O. G., Foong, C. S. & Cullinan, M. A. A novel microscale selective laser sintering (μ-SLS) process for the fabrication of

microelectronic parts. *Microsystems Nanoeng.* **5**, 64 (2019).

248. Ko, S. H. *et al.* Air stable high resolution organic transistors by selective laser sintering of ink-jet printed metal nanoparticles. *Appl. Phys. Lett.* **90**, 141103 (2007).

249. Seigou Kawaguchi, K. I. Dispersion polymerization. in *Polymer particles* (ed. Okubo, M.) 299–328 (Springer, Berlin, Heidelberg, 2005). doi:https://doi.org/10.1007/b100118

250. Zong, M., Thurecht, K. J. & Howdle, S. M. Dispersion polymerisation in supercritical CO2 using macro-RAFT agents. *Chem. Commun.* 5942–5944 (2008). doi:10.1039/B812827H

251. O'Neill, M. L., Yates, M. Z., Johnston, K. P., Smith, C. D. & Wilkinson, S. P. Dispersion Polymerization in Supercritical CO 2 with Siloxane-Based Macromonomer. 2. The Particle Formation Regime . *Macromolecules* **31**, 2848–2856 (2002).

252. He, G. *et al.* A facile route to bespoke macro- and mesoporous block copolymer microparticles. *Polym. Chem.* **9**, 3808–3819 (2018).

253. Park, S. Il, Lee, S. I., Hong, S.-J. & Cho, K. Y. Suspension polymerization and characterization of transparent poly(methyl methacrylate-co-isobornyl methacrylate). *Macromol. Res.* **15**, 418–423 (2007).

254. Hartley, P. A., Parfitt, G. D. & Pollack, L. B. The role of the van der Waals force in the agglomeration of powders containing submicron particles. *Powder*

Technol. **42**, 35–46 (1985).

255. Sasai, K. Direct Measurement of Agglomeration Force Exerted between Alumina Particles in Molten Steel. *ISIJ Int.* **54**, 2780–2789 (2014).

256. Minaev, N. V *et al.* An Apparatus for Research on Processes of Selective Laser Sintering of Powder Materials with High Spatial Resolution. *Instruments Exp. Tech.* **63**, 288–290 (2020).

257. Syachina, M., Minaeva, S., Krumins, E., Howdle, S. & Popov, V. Novel materials for high-resolution three-dimensional printing using surface-selective laser sintering. *{IOP} Conf. Ser. Mater. Sci. Eng.* **848**, 12086 (2020).

258. Mishra, D. P. & Azam, S. Experimental investigation on effects of particle size, dust concentration and dust-dispersion-air pressure on minimum ignition temperature and combustion process of coal dust clouds in a G-G furnace. *Fuel* **227**, 424–433 (2018).

259. Loh, Z. H., Samanta, A. K. & Sia Heng, P. W. Overview of milling techniques for improving the solubility of poorly water-soluble drugs. *Asian J. Pharm. Sci.* **10**, 255–274 (2015).

260. Zhao, R. & Zhang, R. A new insight into π-π stacking involving remarkable orbital interactions. *Phys. Chem. Chem. Phys.* **18**, 25452–25457 (2016).

261. Müller, K. H. *et al.* The effect of particle agglomeration on the formation of a surface-connected compartment induced by hydroxyapatite nanoparticles in human monocyte-derived macrophages. *Biomaterials* **35**, 1074–1088

(2014).

262. Liu, F. *et al.* Review of recent literature on the light absorption properties of black carbon: Refractive index, mass absorption cross section, and absorption function. *Aerosol Sci. Technol.* **54**, 33–51 (2020).

263. Shamjad, P. M., Tripathi, S. N., Thamban, N. M. & Vreeland, H. Refractive Index and Absorption Attribution of Highly Absorbing Brown Carbon Aerosols from an Urban Indian City-Kanpur. *Sci. Rep.* **6**, 37735 (2016).

264. Miqdad, H. Effect of Carbon Black Nanoparticles on the Optical Properties of poly (ethylene oxide) Films. **13**, 4333–4341 (2018).

265. Mühler, T. *et al.* Slurry-Based Powder Beds for the Selective Laser Sintering of Silicate Ceramics. *J. Ceram. Sci. Technol.* **6**, 113–117 (2015).

266. Chen, Z. *et al.* 3D printing of ceramics: A review. *J. Eur. Ceram. Soc.* **39**, 661–687 (2019).

267. Van den Eynde, M., Verbelen, L. & Van Puyvelde, P. Assessing polymer powder flow for the application of laser sintering. *Powder Technol.* **286**, 151–155 (2015).

268. Ducker, W. A., Senden, T. J. & Pashley, R. M. Direct measurement of colloidal forces using an atomic force microscope. *Nature* **353**, 239–241 (1991).

269. Mazzoli, A. & Favoni, O. Particle size, size distribution and morphological evaluation of airborne dust particles of diverse woods by Scanning Electron

Microscopy and image processing program. *Powder Technol.* **225**, 65–71 (2012).

Supporting Information:

This project had several goals throughout its duration:

1. Synthesize coloured PA-12 based materials for SLS
2. Develop a colour mixing system for SLS
3. Synthesize anti-attachment PA-12 based materials for SLS
4. Synthesize materials with improved tensile strength for SLS
5. Develop a method for multimaterial printing via SLS

In order to accomplish (or attempt to meet) these aims, the materials synthesized were characterised mostly through ^{1}H NMR, GPC, and DSC, SEM, and LDS. The spectra and chromatograms not present (referred to SI) in the thesis chapter (Chapter 2) can be seen in the sections:

- Supporting information for Polymer Synthesis and Scale up
- Supporting information for Further Developments to SLS

The basis and data used to make the modified genetic algorithm (Chapter 4) is in the section:

- Supporting information for Developing a Colour Mixing System for SLS

Supporting information for Polymer Synthesis and Scale up:

To produce coloured materials PA-12 based materials for SLS, PA-12 particles were coated with P(IBMA-dye monomer) through a novel and versatile $scCO_2$ based polymerisation and coating system. At first these reactions were tested and optimized in autoclaves which had a reactor volume of 60 ml. Model DSC chromatograms can be seen for PA-12 coated in P(IBMA-DR1MA), P(IBMA-Y1MA), and P(IBMA-DB3MA) (figures 1-3).

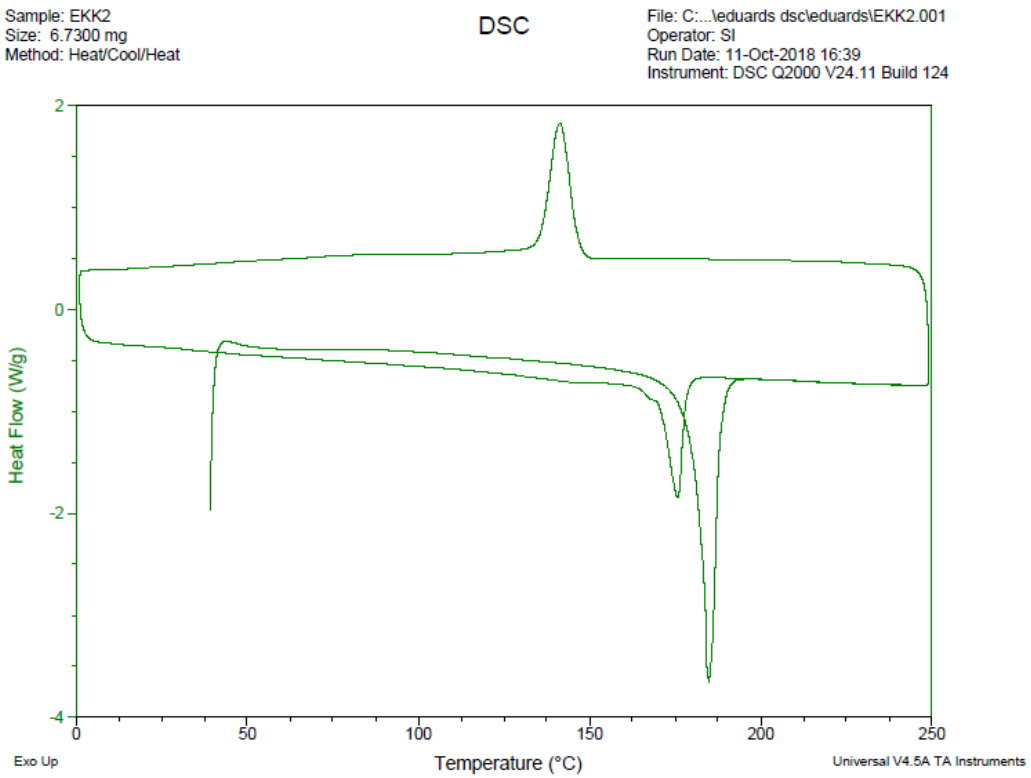


Figure 1 - DSC chromatogram of PA-12 coated with P(IBMA-DR1MA) synthesized in a 60 ml autoclave

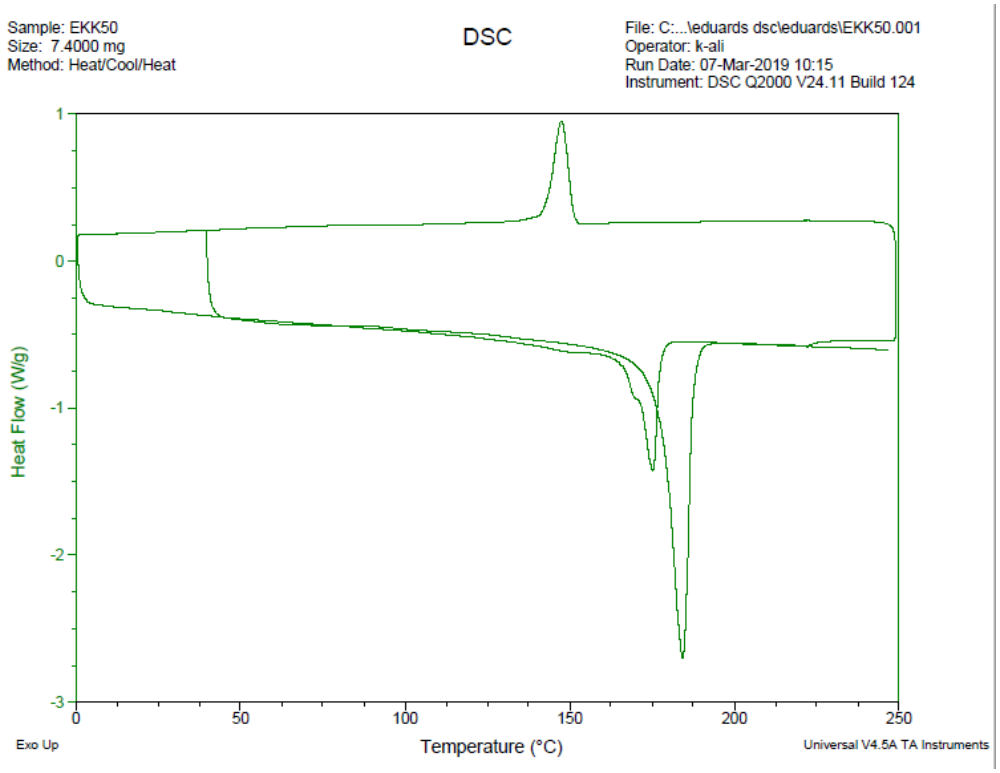


Figure 2 - DSC chromatogram of PA-12 coated with P(IBMA-Y1MA) synthesized in a 60 ml autoclave

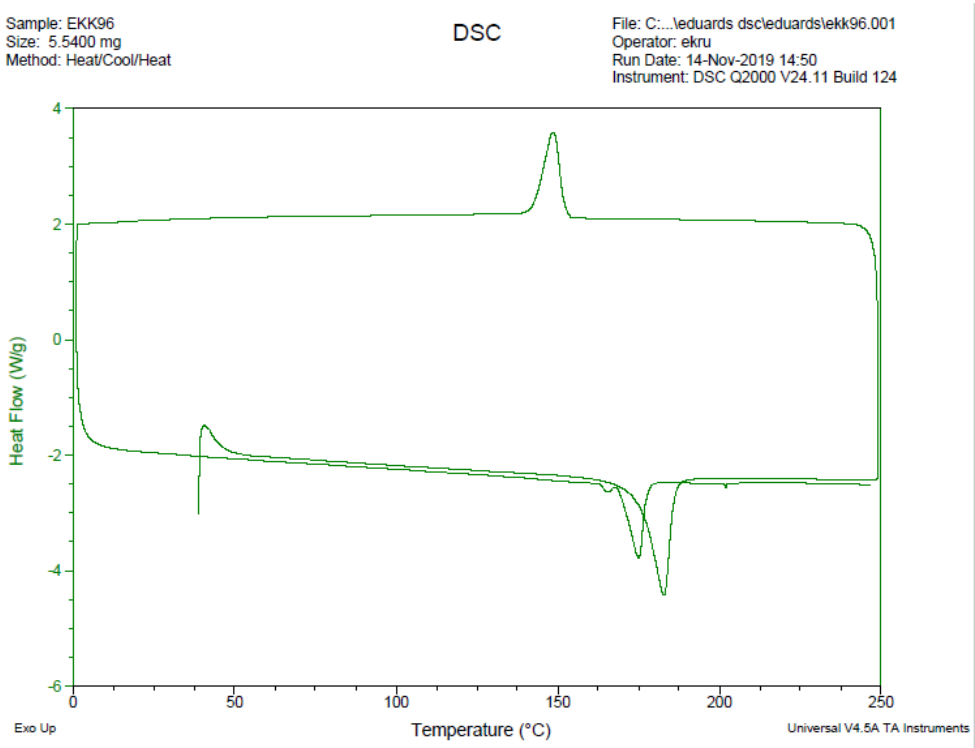


Figure 3 - DSC chromatogram of PA-12 coated with P(IBMA-DB3MA) synthesized in a 60 ml autoclave

In order to print via SLS with a commercial printer (eg. Formiga P100) at least 600 grams of material are needed to operate the printer. Therefore it was impractical to produce such amounts with a 60 mL autoclave, so the synthesis of PA-12 coated with P(IBMA-dye monomer) was scaled up using a 1 L autoclave. The results were analogous to that seen in the 60 ml reactions and this was shown through GPC, DSC, and ^{1}H NMR (figures 4-12).

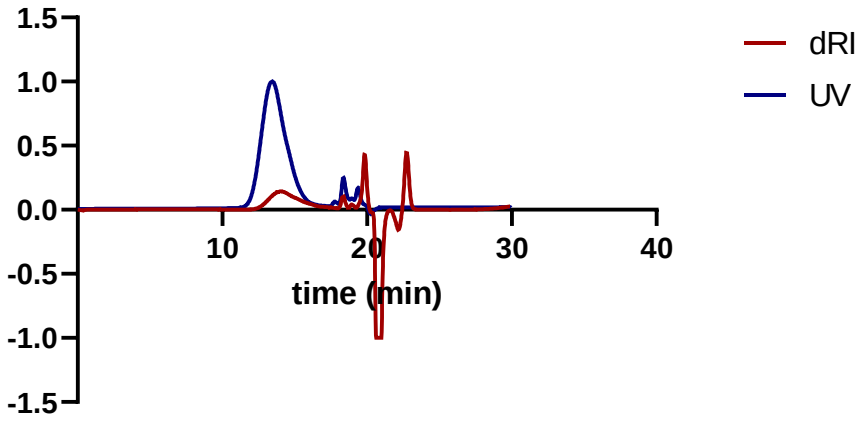


Figure 4 - GPC chromatogram of P(IBMA-DR1MA) outer coating extracted from PA-12 particles coated with P(IBMA-DR1MA) synthesized in a 1 L autoclave.

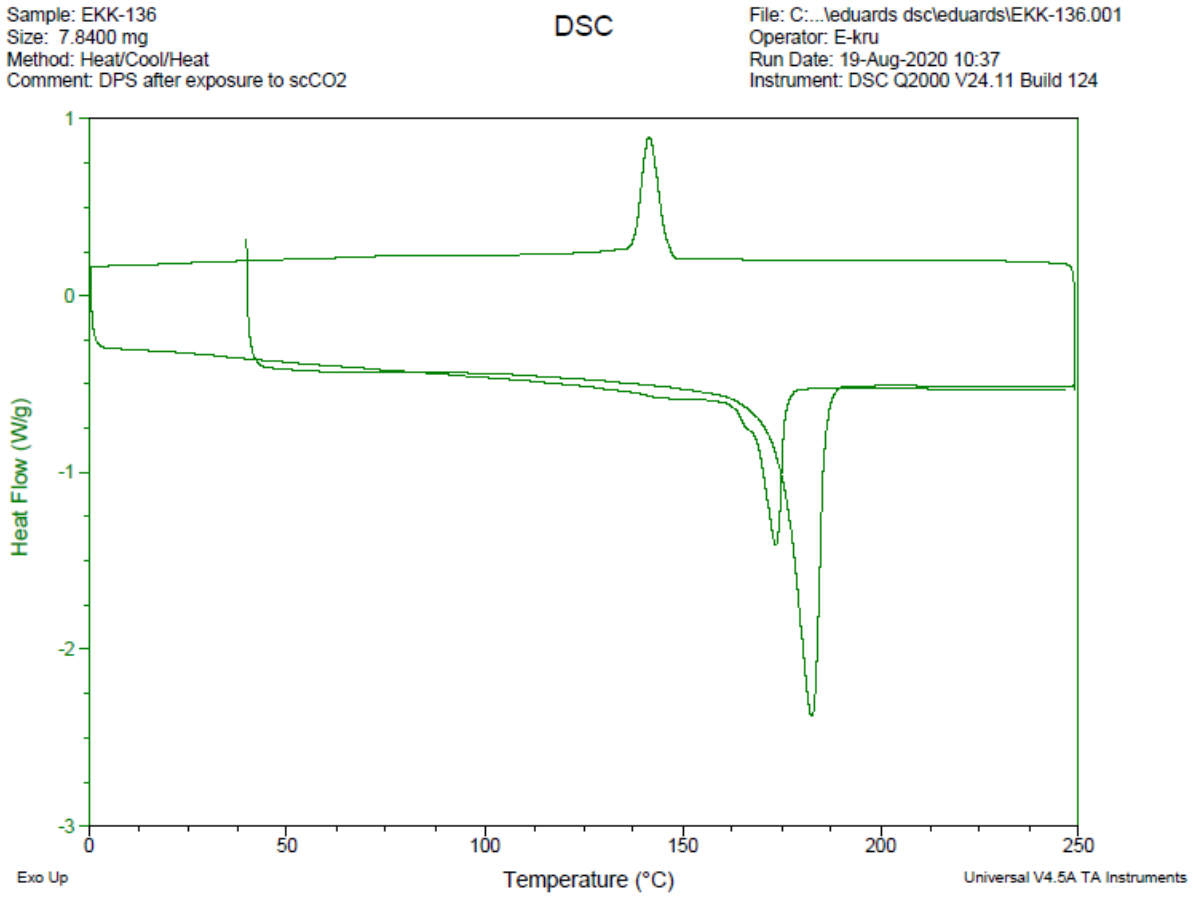


Figure 5 - DSC chromatogram of PA-12 coated with P(IBMA-DR1MA) synthesized in a 1 L autoclave

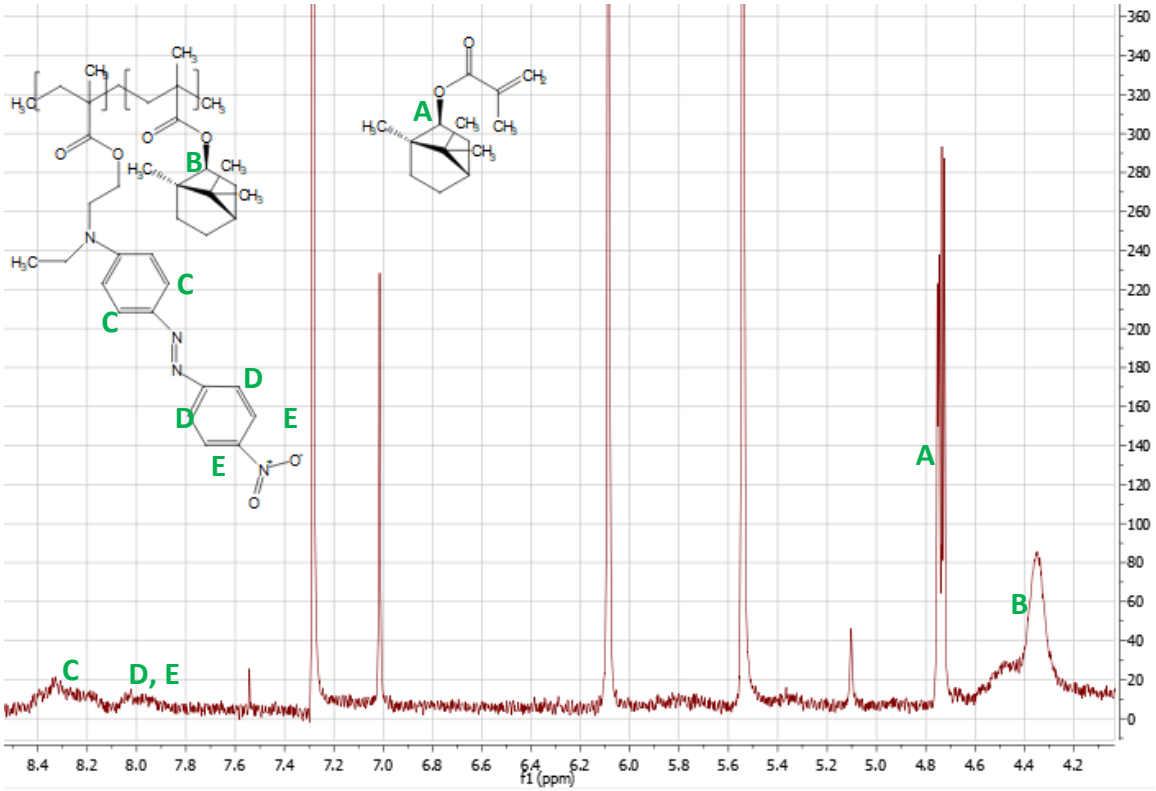


Figure 6 - ^{1}H NMR of P(IBMA-DR1MA) outer shell synthesized in 1L autoclave. ^{1}H NMR (400 MHz, $CHCl_3$-d_3, δ): 4.30-4.60 (mp, 1H, CH), 7.90-8.10 (mp, 2H, ArH)(mp, 2H, ArH), 8.10-8.40 (mp, 2H, ArH)

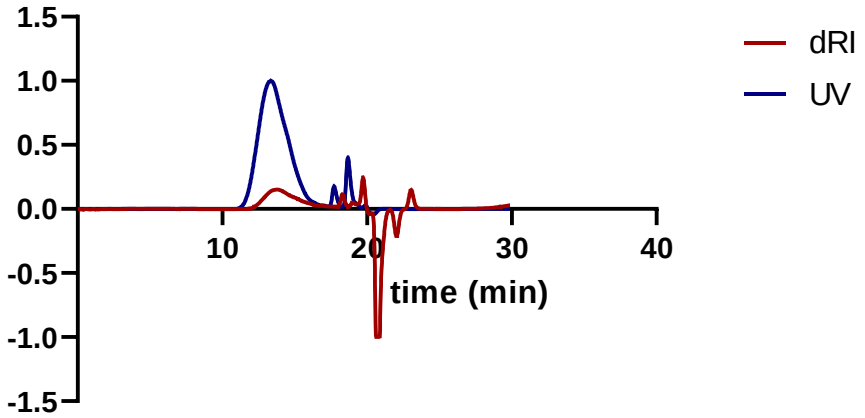


Figure 7 - GPC chromatogram of P(IBMA-Y1MA) outer coating extracted from PA-12 particles coated with P(IBMA-Y1MA) synthesized in a 1 L autoclave.

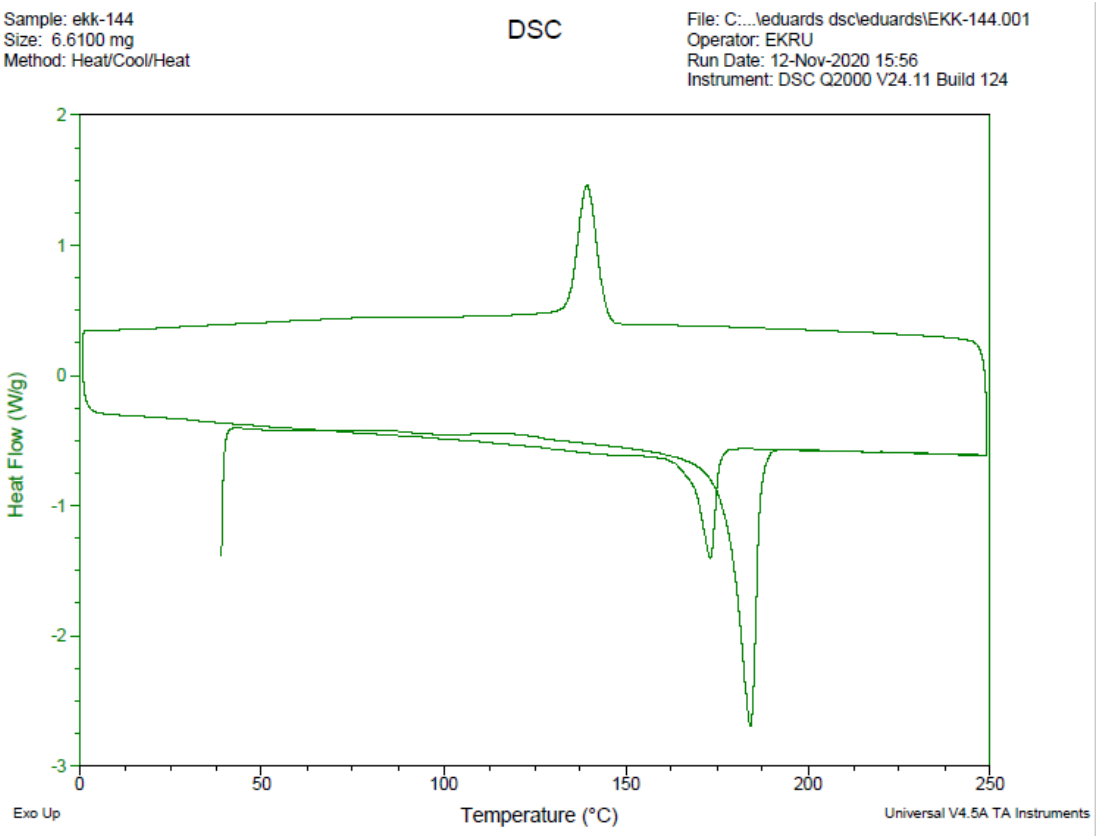


Figure 8 - DSC chromatogram of PA-12 coated with P(IBMA-Y1MA) synthesized in a 1 L autoclave

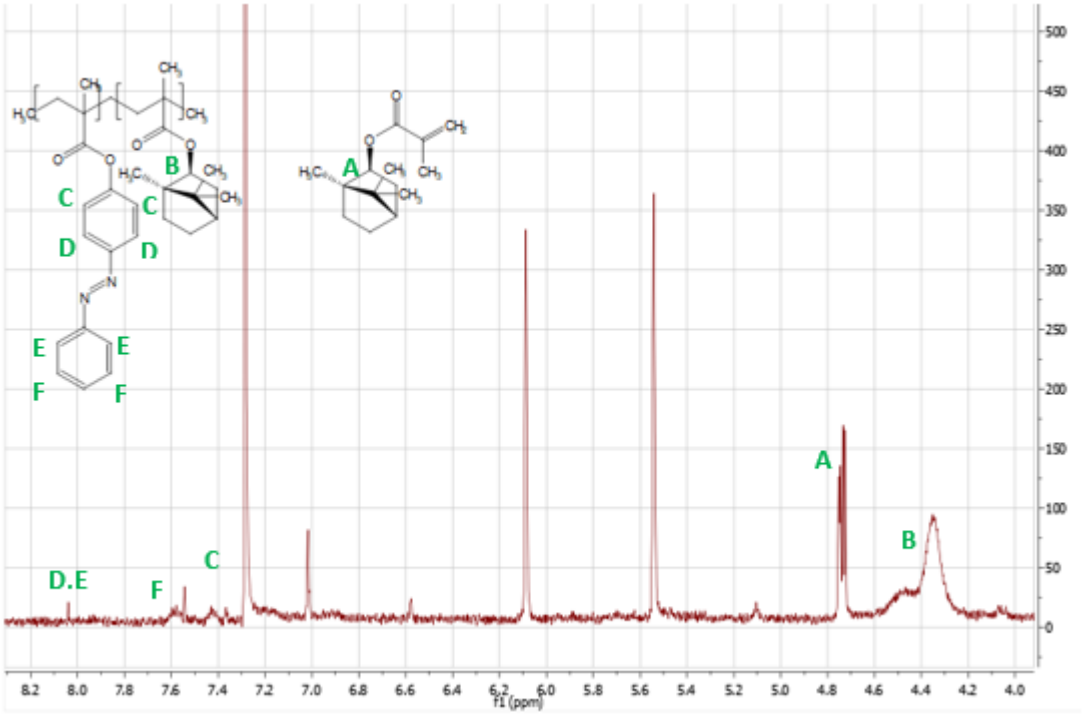


Figure 9 - ^{1}H NMR of P(IBMA-Y1MA) outer shell synthesized in 1L autoclave. ^{1}H NMR (400 MHz, $CHCl_3$-d_3, δ): 4.30-4.60 (mp, 1H, CH), 7.39-7.47 (mp, 2H, ArH), 7.48-7.63 (mp, 2H, ArH), 7.80-8.00 (mp, 2H, ArH)(mp, 2H, ArH)(Need to zoom in on Mestrenova)

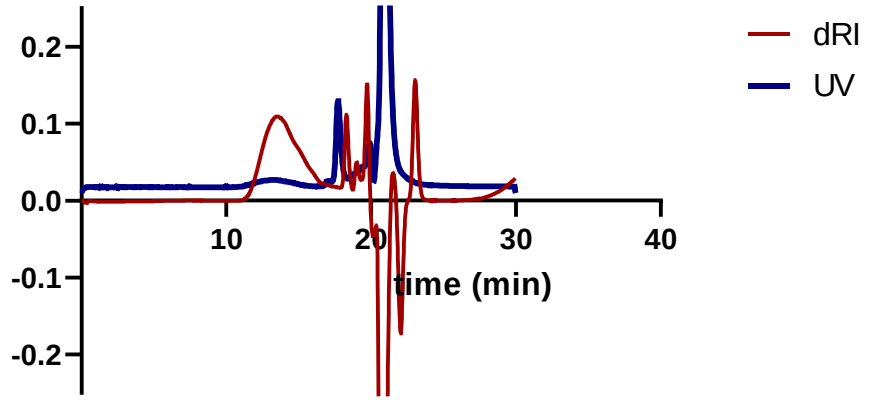


Figure 10 - GPC chromatogram of P(IBMA-DB3MA) outer coating extracted from PA-12 particles coated with P(IBMA-DB3MA) synthesized in a 1 L autoclave.

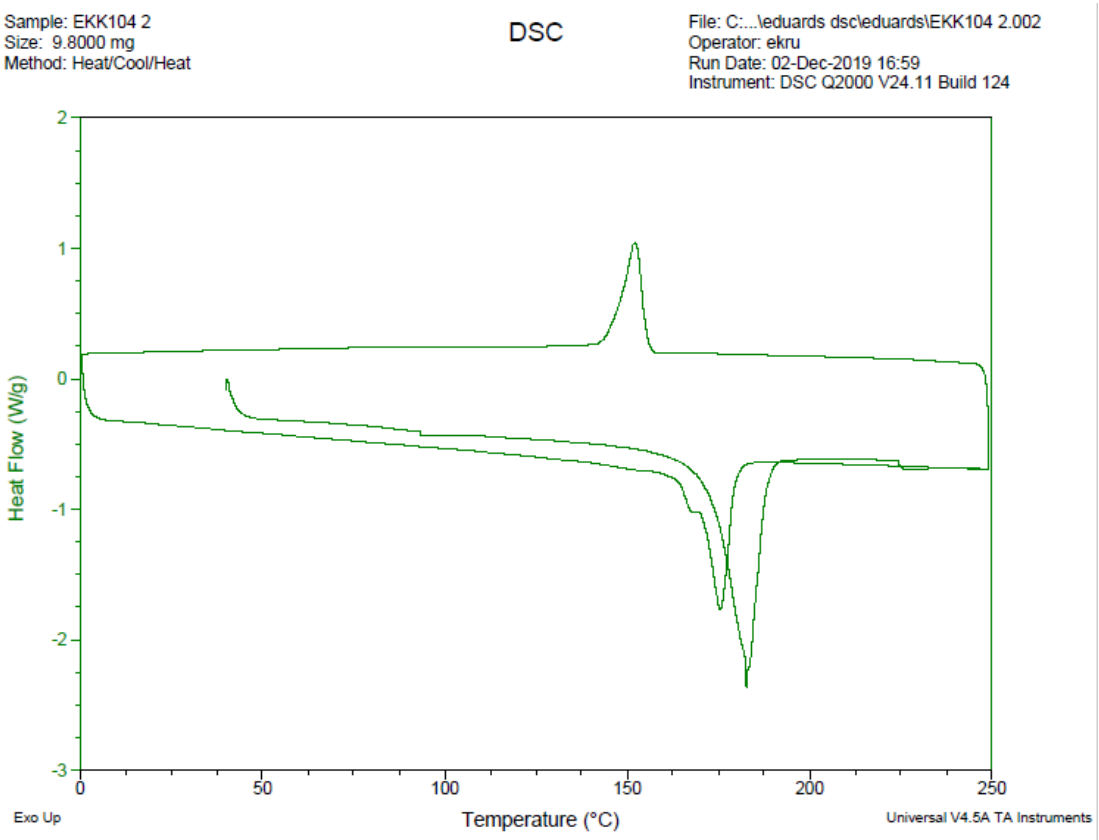


Figure 11 - DSC chromatogram of PA-12 coated with P(IBMA-DB3MA) synthesized in a 1 L autoclave

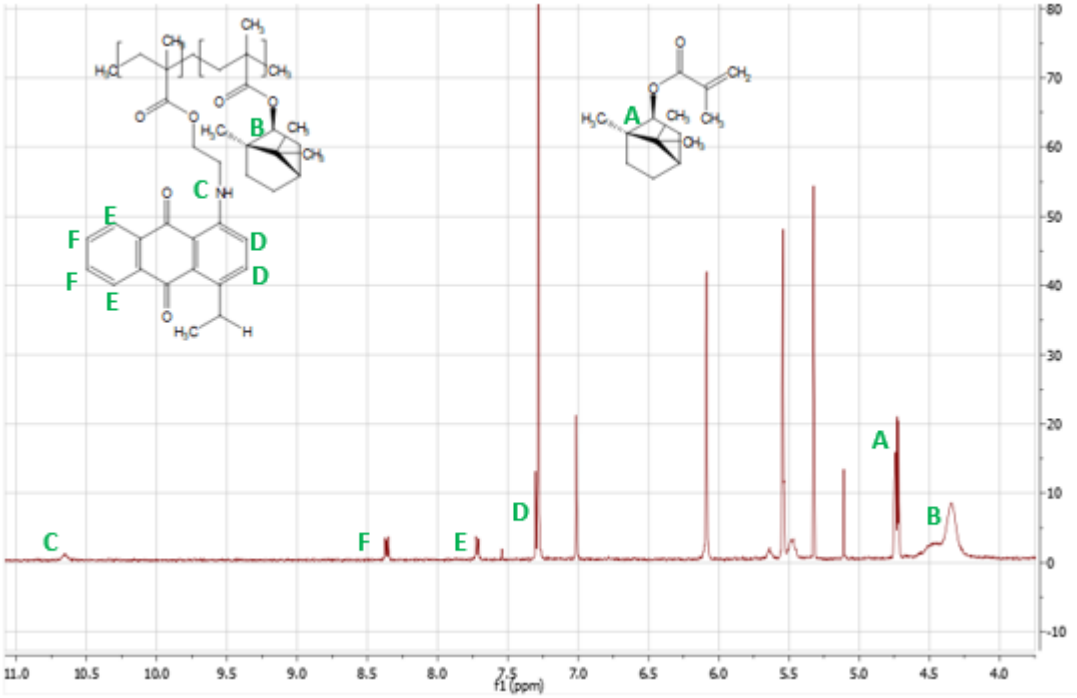


Figure 12 - ^{1}H NMR of P(IBMA-DB3MA) outer shell synthesized in 1L autoclave. ^{1}H NMR (400 MHz, $CHCl_3$-d_3, δ): 4.30-4.60 (mp, 1H, CH), 7.28 (D, 2H, ArH), 7.73-7.75 (mp, 2H, ArH), 8.34-8.38 (mp, 2H, ArH), 10.65 (S, NH)

When conducting the dye screening, one of the criteria that was used to decide a potential dye was cost. This was because, it was desired that the coloured materials for SLS would potentially be commercially viable, so the added cost of the coloured shell could not be significant. The cost of the outer shell needed to be low, so that the cost would be similar to standard PA-12 and lower than what is paid for the current dyeing process. A preliminary cost analysis was done to compare the cost of the novel coloured PA-12 materials and standard PA-12 (tables 1 and 2).

Cost of DB3MA Synthesis			**Cost of DR1MA Synthesis**			**Cost of Y1MA Synthesis**		
Reagents	Amount used (g)	Price (£)	Reagents	Amount used (g)	Price (£)	Reagents	Amount used (g)	Price (£)
Disperse Blue 3	4	5.76	Disperse Red 1	3.35	22.38	Yellow 1	5	10.8
Methyl Methacrylate	16	1.06	Methacryloyl Chloride	1.57	1.76	Methacryloyl Chloride	3.71	0.97
Novozyme 435	0.2	19.02	Triethyl amine	2.43	24.52	Triethyl amine	5.78	15.92
Price per gram = 5.17 £			Price Per gram = 4.90 £			Price per gram = 2.12 £		

Table 1 – Cost analysis for the synthesis of dye monomers.

Added cost for Blue PA-12		Added cost for Red PA-12		Added cost for Yellow PA-12	
Reagents	Price for producing 150 g (£)	Reagents	Price for producing 150 g (£)	Reagents	Price for producing 150 g (£)
PA-12	NA	PA-12	NA	PA-12	NA
Isobornyl Methacrylate	5.25	Isobornyl Methacrylate	5.25	Isobornyl Methacrylate	5.25
Disperse Blue 3 Methacrylate	2.52	Disperse Red 1 Methacrylate	21.06	Yellow 1 Methacrylate	1.043
AIBN	0.03	AIBN	0.03	AIBN	0.03
Added price per grams = 0.052 £		Added price per grams = 0.175£		Added price per grams = 0.042 £	

Table 2 – Cost of coating P2200 PA-12 particles with an outer shell composed of P(IBMA-dye monomer)

Research was conducted to ascertain why $scCO_2$ is an ideal solvent for the polymerisation and coating reactions which have been performed. $scCO_2$ can swell the amorphous regions of the PA-12 allowing for the shell to slightly penetrate the surface, this results in a more robust outer shell as when the $scCO_2$ is vented part of the shell will also be inside each PA-12 particle. This effect was proven by swelling PA-12 in $scCO_2$, and then measuring the weight of the PA-12 block after exposure, the increase in weight showed that $scCO_2$ penetrated the block and remained thereby increasing the weight, this was also shown visually as PA-12 was impregnated with 4-phenolazophenol via $scCO_2$ (Figure 13)(Table 3).



Figure 13 – Swelling of PA-12 due to $scCO_2$ exposure. A.) PA-12 samples after exposure to $scCO_2$. B.) Colouration of PA-12 with 4-phenolazophenol via exposure to $scCO_2$.

Sample	Pressure (PSI)	Temperature (^{o} C)	Time (Hrs)	Initial weight (g)	Initial Dimensions (mm)	Weight After (g)	Dimensions after (mm)	% Weight gain
1	3000	65	24	0.34378	8.07x11.10x4.57	0.35961	8.08x4.57x11.12	4.62
2	3000	65	24	0.26093	6.39x10.00x4.41	0.27235	6.39x4.45x10.08	4.37
3	3000	65	24	0.25453	5.73x4.69x10.59	0.26504	5.73x4.72x10.65	4.13
4	3000	65	72	0.21646	5.75x4.36x9.25	0.23004	5.76x4.40x9.32	6.27

Table 3 – Results from swelling of PA-12 due to $scCO_2$ exposure.

Supporting information for Developing a Colour Mixing System for SLS:

When a CMYK colour mixing system was being developed for SLS, it was observed that the formulation of target colours was not as easy as envisioned. Largely, due to the unpredictable relationship between the amount of an individual colour used in a formulation vs the colour of a printed part made from that formulation. To try to be able to accurately obtain formulations for target colours two approaches (Chapter 4):

1. The development of a modified genetic algorithm
2. The development of a particle swarm optimization and simplex-lattice/centroid design program.

The genetic algorithm was created using initial colour mixing data, which was used to create equations which modelled the effect of a particular colour on a colour value (table 4-5) (Figures 13-32).

Mix	Red (%)[a]	Blue (%)[a]	Yellow (%)[a]	White (%)[a]	L[b]	A[b]	B[b]	C[b]	H[b]
1	5	5	0	90	25	33	-4	33	354
2	10	10	0	80	19	30	-3	30	355
3	40	10	0	50	35	83	61	103	36
4	15	15	0	70	15	45	-10	47	348
5	25	25	0	50	0	8	-14	16	299
6	33	33	0	33	0	0	0	0	0
7	50	50	0	0	0	0	0	0	0
8	5	0	95	0	74	34	50	61	56
9	0	100	0	0	35	4	-56	56	274
10	0	0	100	0	85	8	43	43	79
11	100	0	0	0	35	83	61	103	36
12	0	15	85	0	60	-25	0	26	179
13	0	87.5	12.5	0	61	-23	2	23	174
14	0	90	10	0	64	-20	4	21	168

Table 4 – Results of initial colour mixing experiments with Nix colour analysis used for the generation of equations for modified Genetic algorithm. [a] Percentage of colour that is used in a formulation. [b] LABCH values given by nix colour analysis.

L	Red
25	5
19	10
35	40
15	15
0	25
0	33
0	50
74	5
35	0
85	0
35	100
60	0
61	0
64	0

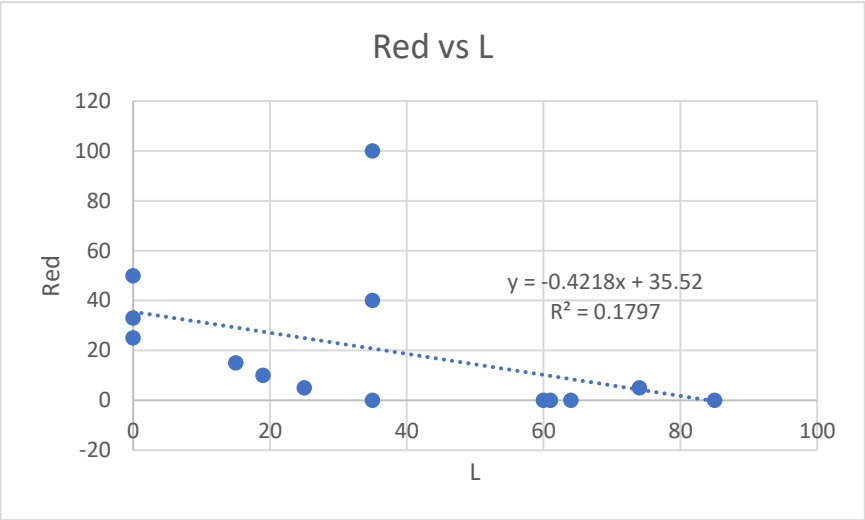


Figure 13 – Modelling the relationship between amount of red PA-12 used in a formulation and the effect on the colour value L.

a	Red
33	5
30	10
83	40
45	15
8	25
0	33
0	50
34	5
4	0
8	0
83	100
-25	0
-23	0
-20	0

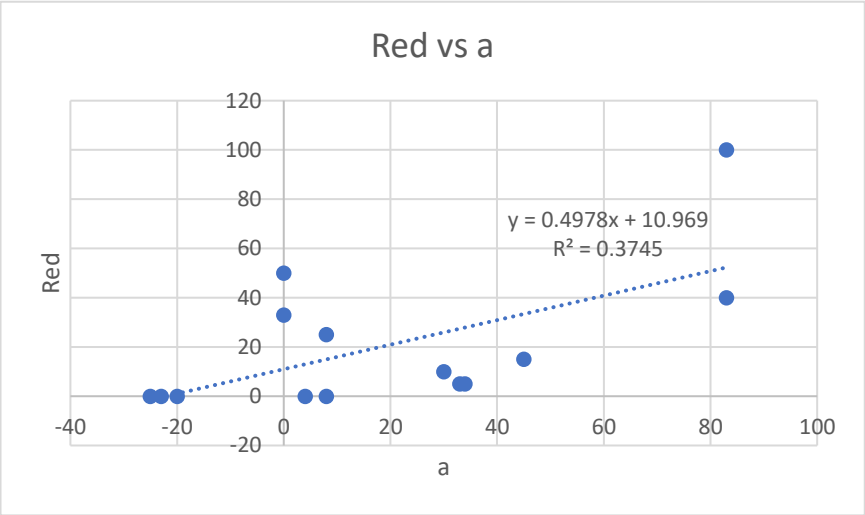


Figure 14 – Modelling the relationship between amount of red PA-12 used in a formulation and the effect on the colour value A.

b	Red
-4	5
-3	10
61	40
-10	15
-14	25
0	33
0	50
50	5
-56	0
43	0
61	100
0	0
2	0
4	0

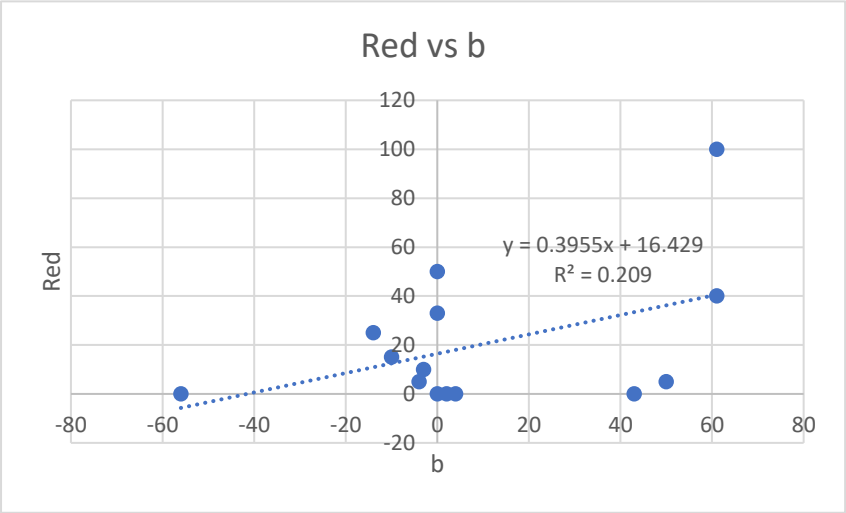


Figure 15 – Modelling the relationship between amount of red PA-12 used in a formulation and the effect on the colour value B.

c	Red
33	5
30	10
103	40
47	15
16	25
0	33
0	50
61	5
56	0
43	0
103	100
26	0
23	0
21	0

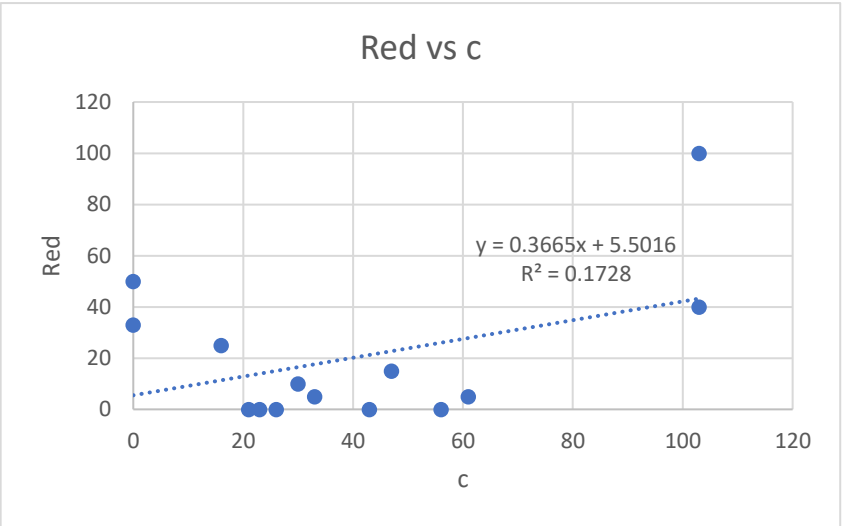


Figure 16 – Modelling the relationship between amount of red PA-12 used in a formulation and the effect on the colour value c.

H	Red
354	5
355	10
36	40
348	15
299	25
0	33
0	50
56	5
274	0
79	0
36	100
179	0
174	0
168	0

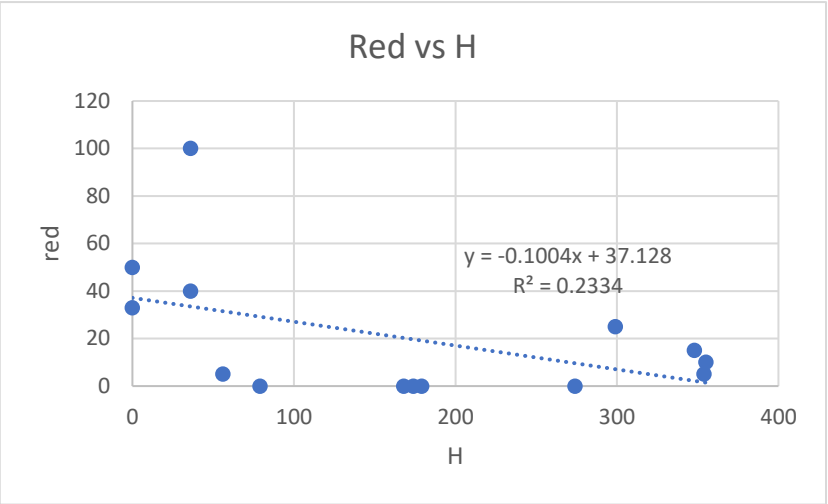


Figure 17 – Modelling the relationship between amount of red PA-12 used in a formulation and the effect on the colour value H.

L	Blue
25	5
19	10
35	10
15	15
0	25
0	33
0	50
74	0
35	100
85	0
35	0
60	15
61	87.5
64	90

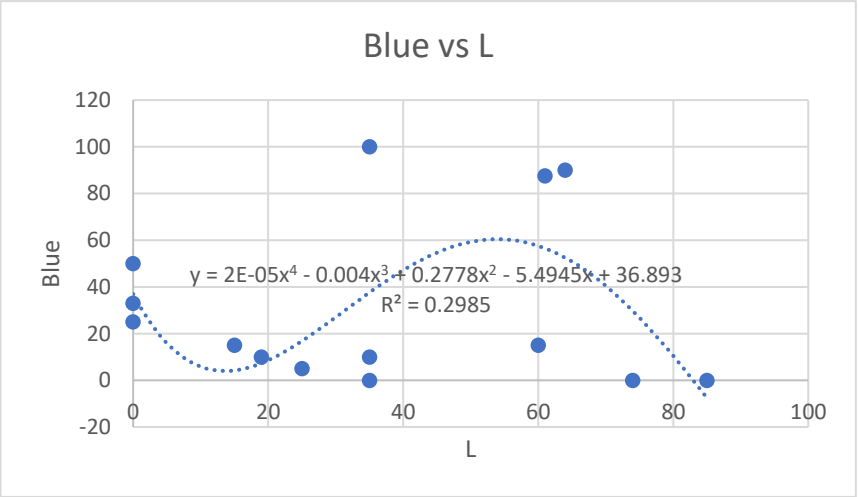


Figure 18 – Modelling the relationship between amount of blue PA-12 used in a formulation and the effect on the colour value L.

a	Blue
33	5
30	10
83	10
45	15
8	25
0	33
0	50
34	0
4	100
8	0
83	0
-25	15
-23	87.5
-20	90

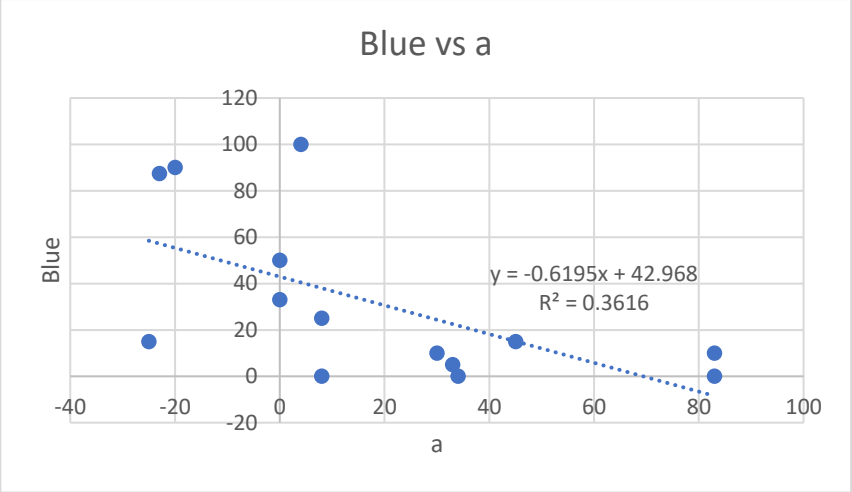


Figure 19 – Modelling the relationship between amount of blue PA-12 used in a formulation and the effect on the colour value a.

b	Blue
-4	5
-3	10
61	10
-10	15
-14	25
0	33
0	50
50	0
-56	100
43	0
61	0
0	15
2	87.5
4	90

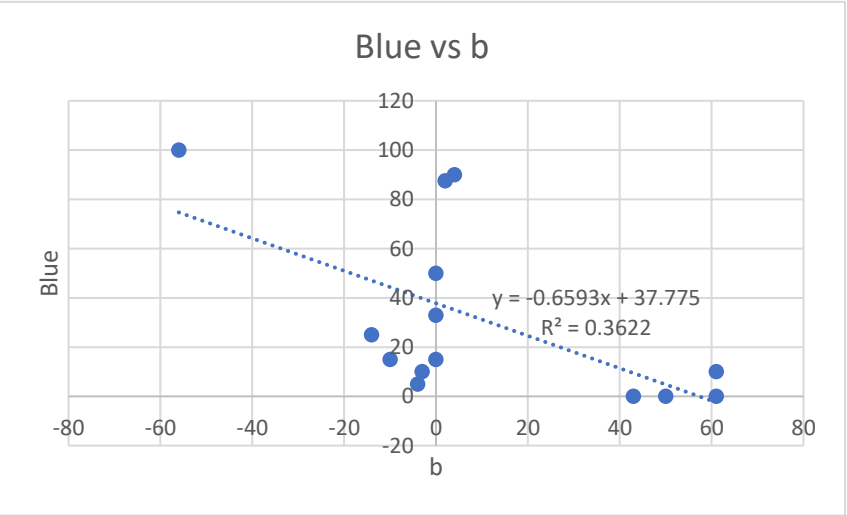


Figure 20 – Modelling the relationship between amount of blue PA-12 used in a formulation and the effect on the colour value b.

c	Blue
33	5
30	10
103	10
47	15
16	25
0	33
0	50
61	0
56	100
43	0
103	0
26	15
23	87.5
21	90

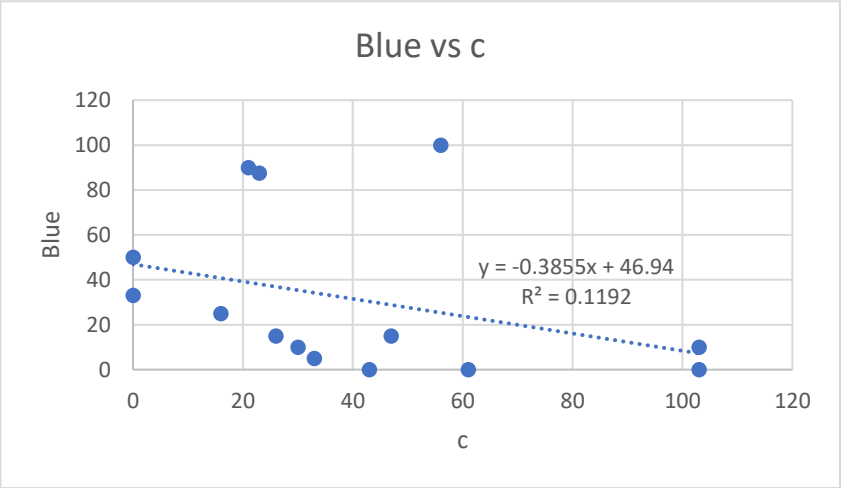


Figure 21 – Modelling the relationship between amount of blue PA-12 used in a formulation and the effect on the colour value c.

H	Blue
354	5
355	10
36	10
348	15
299	25
0	33
0	50
56	0
274	100
79	0
36	0
179	15
174	87.5
168	90

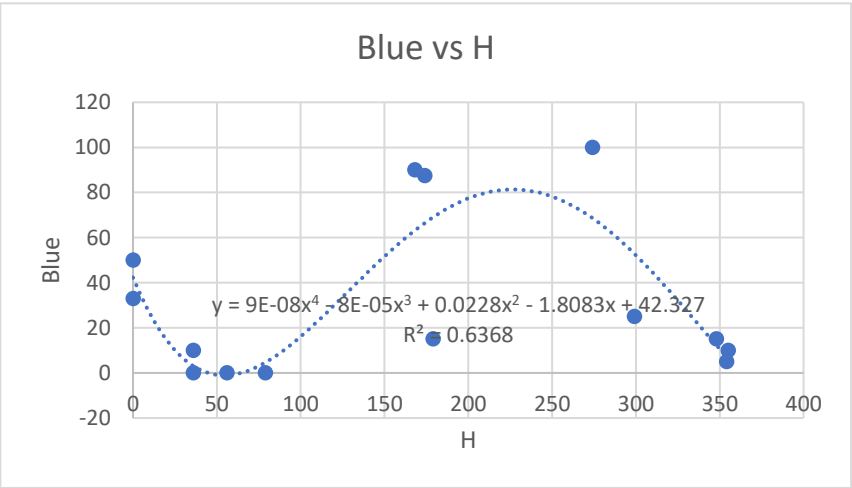


Figure 22 – Modelling the relationship between amount of blue PA-12 used in a formulation and the effect on the colour value H.

L	Yellow
25	0
19	0
35	0
15	0
0	0
0	0
0	0
74	95
35	0
85	100
35	0
60	85
61	12.5
64	10

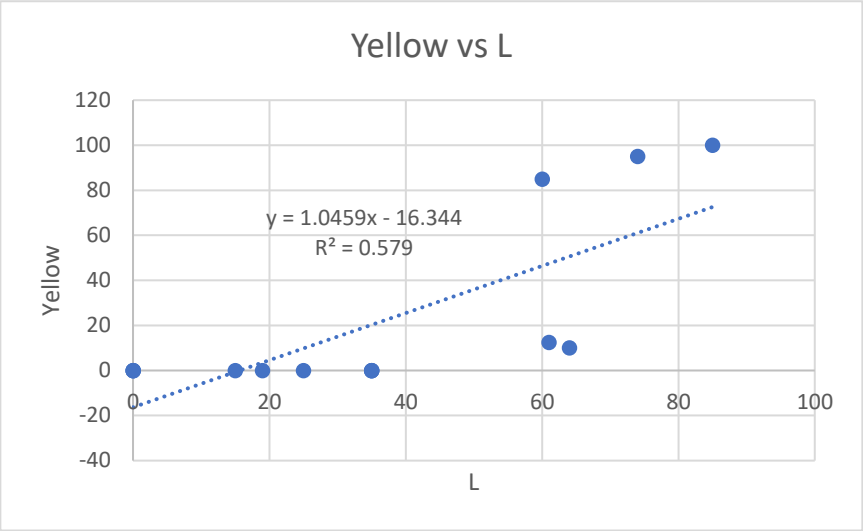


Figure 23 – Modelling the relationship between amount of yellow PA-12 used in a formulation and the effect on the colour value L.

a	Yellow
33	0
30	0
83	0
45	0
8	0
0	0
0	0
34	95
4	0
8	100
83	0
-25	85
-23	12.5
-20	10

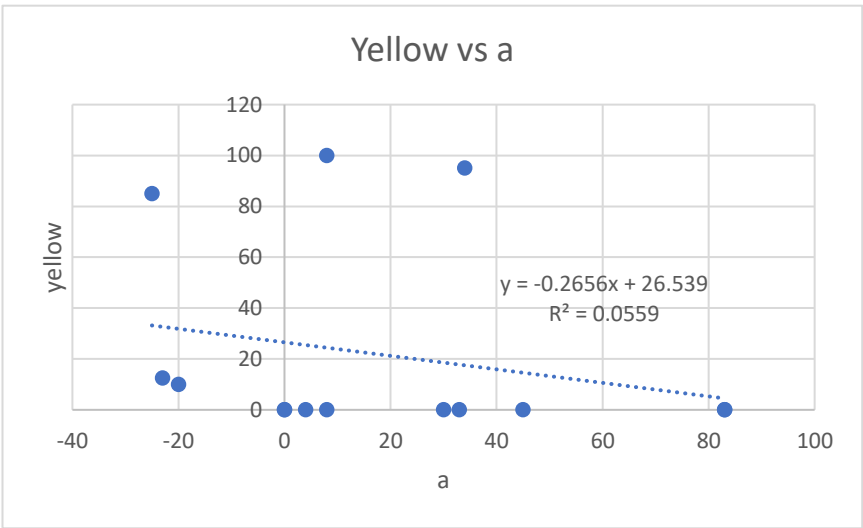


Figure 24 – Modelling the relationship between amount of yellow PA-12 used in a formulation and the effect on the colour value a.

b	Yellow
-4	0
-3	0
61	0
-10	0
-14	0
0	0
0	0
50	95
-56	0
43	100
61	0
0	85
2	12.5
4	10

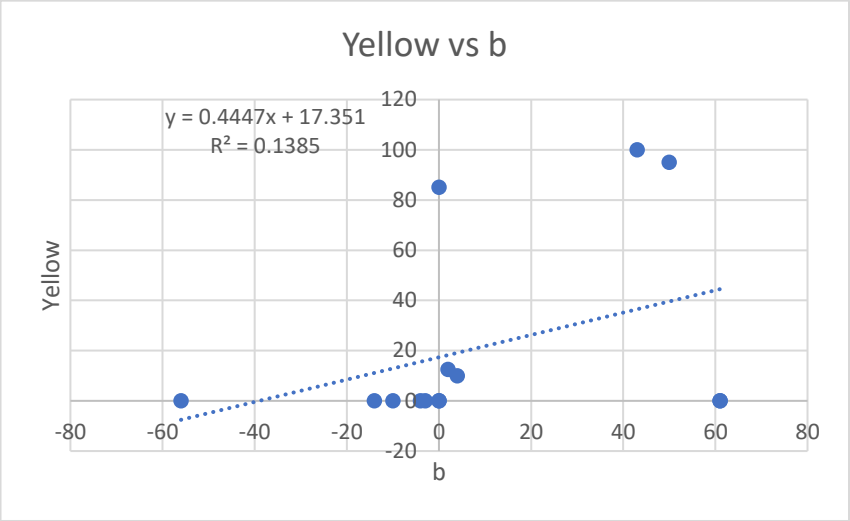


Figure 25 – Modelling the relationship between amount of yellow PA-12 used in a formulation and the effect on the colour value b.

c	Yellow
33	0
30	0
103	0
47	0
16	0
0	0
0	0
61	95
56	0
43	100
103	0
26	85
23	12.5
21	10

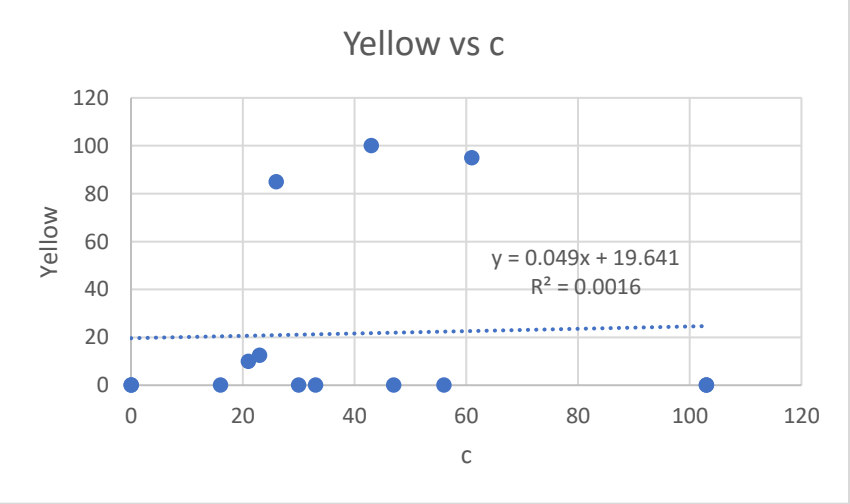


Figure 26 – Modelling the relationship between amount of yellow PA-12 used in a formulation and the effect on the colour value c.

H	Yellow
354	0
355	0
36	0
348	0
299	0
0	0
0	0
56	95
274	0
79	100
36	0
179	85
174	12.5
168	10

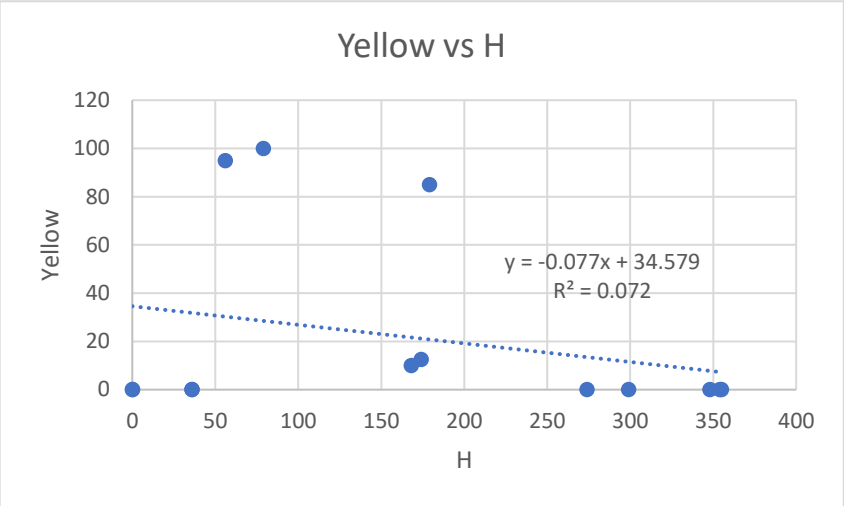


Figure 27 – Modelling the relationship between amount of yellow PA-12 used in a formulation and the effect on the colour value H.

L	White
25	90
19	80
35	50
15	70
0	50
0	33
0	0
74	0
35	0
85	0
35	0
60	0
61	0
64	0

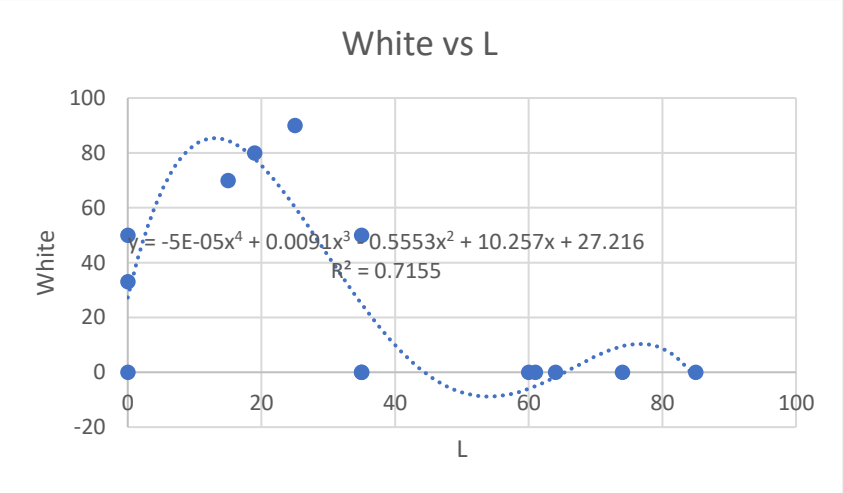


Figure 28 – Modelling the relationship between amount of white PA-12 used in a formulation and the effect on the colour value L.

a	White
33	90
30	80
83	50
45	70
8	50
0	33
0	0
34	0
4	0
8	0
83	0
-25	0
-23	0
-20	0

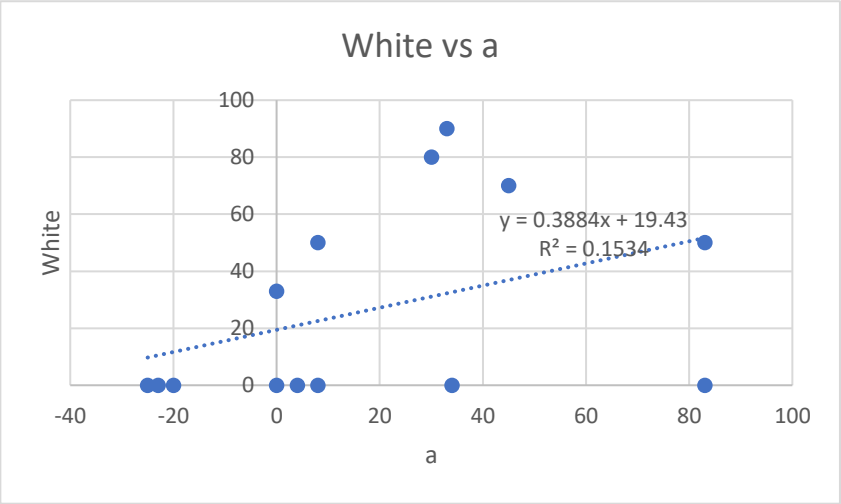


Figure 29 – Modelling the relationship between amount of white PA-12 used in a formulation and the effect on the colour value a.

b	White
-4	90
-3	80
61	50
-10	70
-14	50
0	33
0	0
50	0
-56	0
43	0
61	0
0	0
2	0
4	0

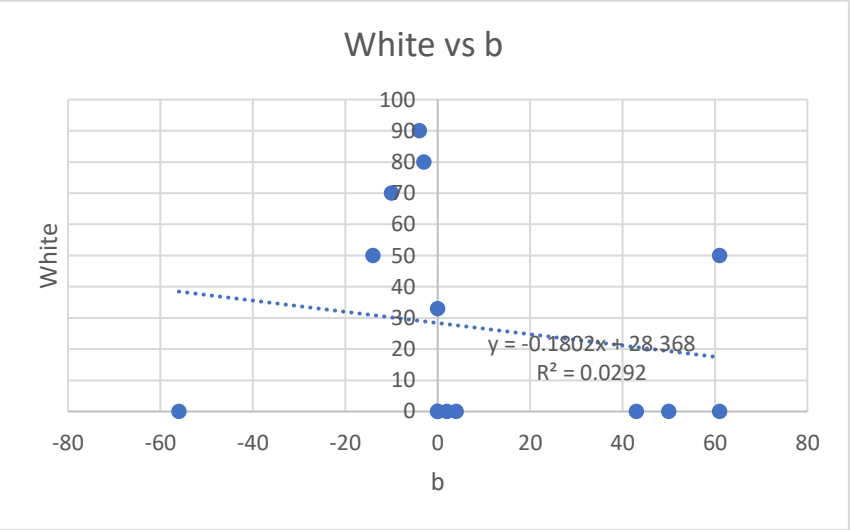


Figure 30 – Modelling the relationship between amount of white PA-12 used in a formulation and the effect on the colour value b.

c	White
33	90
30	80
103	50
47	70
16	50
0	33
0	0
61	0
56	0
43	0
103	0
26	0
23	0
21	0

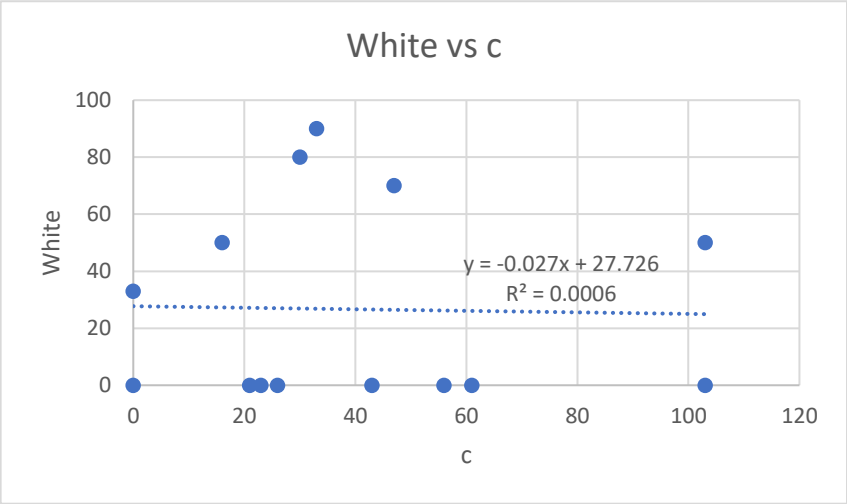


Figure 31 – Modelling the relationship between amount of white PA-12 used in a formulation and the effect on the colour value c.

H	White
354	90
355	80
36	50
348	70
299	50
0	33
0	0
56	0
274	0
79	0
36	0
179	0
174	0
168	0

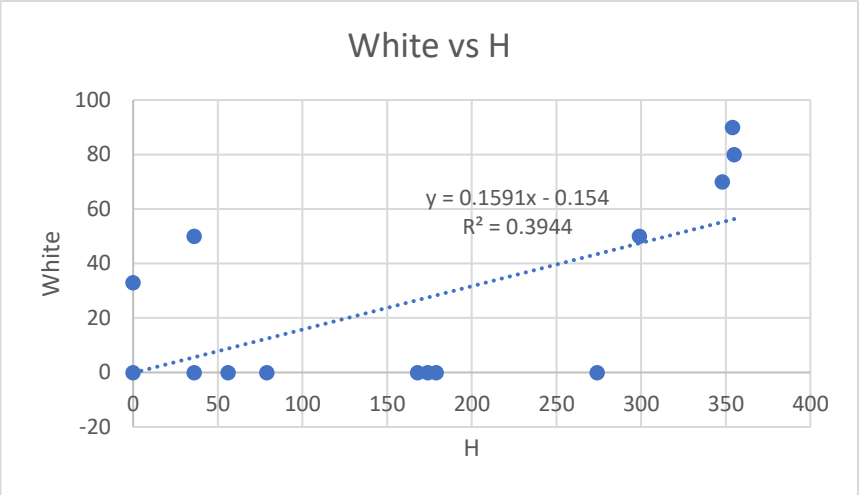


Figure 32 – Modelling the relationship between amount of white PA-12 used in a formulation and the effect on the colour value H.

Equation 17	$y_1 = (-0.4218L2) + 35.52$	Red vs. L	R^2 = 0.1797
Equation 18	$y_2 = (0.4978a2) + 10.969$	Red vs A	R^2 = 0.3745
Equation 19	$y_3 = (0.3955b2) + 16.429$	Red vs B	R^2 = 0.209
Equation 20	$y_4 = (0.3665c2) + 5.5016$	Red vs C	R^2 = 0.1728
Equation 21	$y_5 = (-0.1004H2) + 10.969$	Red vs H	R^2 = 0.2334
Equation 22	$Red_{Amount} = \frac{(y_1 + y_2 + y_3 + y_4 + y_5)}{5}$	Amount of Red PA-12 powder needed for a formulation	
Equation 23	$y_6 = 0.00002L2^4 - 0.004L2^3 + 0.2778L2^2 - 5.4945L2 + 36.843$	Blue vs. L	R^2 = 0.2985
Equation 24	$y_7 = (-0.6195a2) + 42.968$	Blue vs A	R^2 = 0.3616

Equation 25	$y_8 = (-0.6593b2) + 37.775$	Blue vs B	R^2 = 0.3622
Equation 26	$y_9 = (-0.3855c2) + 46.94$	Blue vs C	R^2 = 0.1192
Equation 27	$y_{10} = -0.000000009H2^4 - 0.00008H2^3 + 0.0228H2^2 - 1.8083H2 + 42.327$	Blue vs H	R^2 = 0.6368
Equation 28	$Blue_{Amount} = \frac{(y_6 + y_7 + y_8 + y_9 + y_{10})}{5}$	Amount of Blue PA-12 powder needed for a formulation	
Equation 29	$y_{11} = (1.0495L2) + 16.344$	Yellow vs. L	R^2 = 0.579
Equation 30	$y_{12} = (-.2656a2) - 26.539$	Yellow vs A	R^2 = 0.0559
Equation 31	$y_{13} = (0.4447b2) + 17.351$	Yellow vs B	R^2 = 0.1385
Equation 32	$y_{14} = (0.049c2) + 19.641$	Yellow vs C	R^2 = 0.0016

Equation 33	$y_{15} = (-0.077H2) + 34.579$	Yellow vs H	R^2 = 0.072
Equation 34	$Yellow_{Amount} = \frac{(y_{11} + y_{12} + y_{13} + y_{14} + y_{15})}{5}$	Amount of Yellow PA-12 powder needed for a formulation	
Equation 35	$y_{16} = 0.00005L2^4 + 0.0091L2^3 - 0.5553L2^2 + 10.257L2 + 27.216$	White vs. L	R^2 = 0.7155
Equation 36	$y_{17} = (0.3884a2) - 19.43$	White vs A	R^2 = 0.1534
Equation 37	$y_{18} = (-0.1802b2) + 28.368$	White vs B	R^2 = 0.0292
Equation 38	$y_{19} = (-0.027c2) + 27.726$	White vs C	R^2 = 0.0006
Equation 39	$y_{20} = (0.1591H2) - 0.154$	White vs H	R^2 = 0.3944

Equation 40	$White_{Amount} = \frac{(y_{16} + y_{17} + y_{18} + y_{19} + y_{20})}{5}$	Amount of White PA-12 powder needed for a formulation	

Table 5 – Influence of each colour on each colour value, given by equations 17 – 40, with their corresponding r^2 values.

Supporting information for Further Developments to SLS:

PA-12 was coated with six different copolymeric coatings in an attempt to produce anti-attachment materials for SLS. These materials were produced via an analogous method to the one used to produce coloured PA-12 particles, but instead of the dye monomer, biologically active (meth)acrylates were used resulting in six coatings (Chapter 5):

- P(IBMA-Bornyl methacrylate)
- P(IBMA-Cinnamyl methacrylate)
- P(IBMA-Myrtenol methacrylate)
- P(IBMA-Neryl methacrylate)
- P(IBMA-modified oleic acid acrylate)
- P(IBMA-modified lactic acid acrylate)

These coated materials were analysed via ^{1}H NMR, GPC, and DSC, much like was done for the coloured PA-12 materials (Figures 33-50)(Table 6).

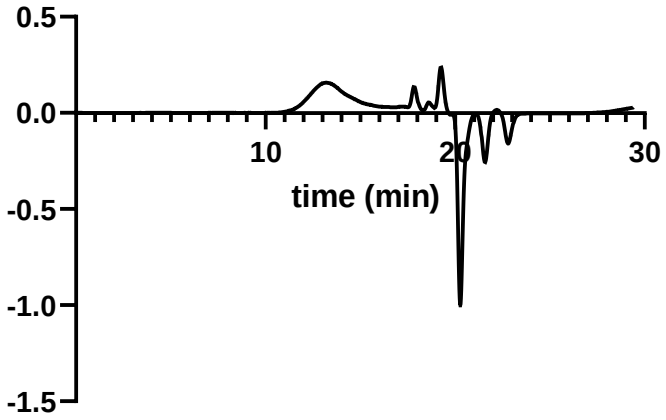


Figure 33 - GPC chromatogram of P(IBMA-Bornyl methacrylate) outer coating extracted from PA-12 particles coated with P(IBMA-Bornyl methacrylate) synthesized in a 60 ml autoclave.

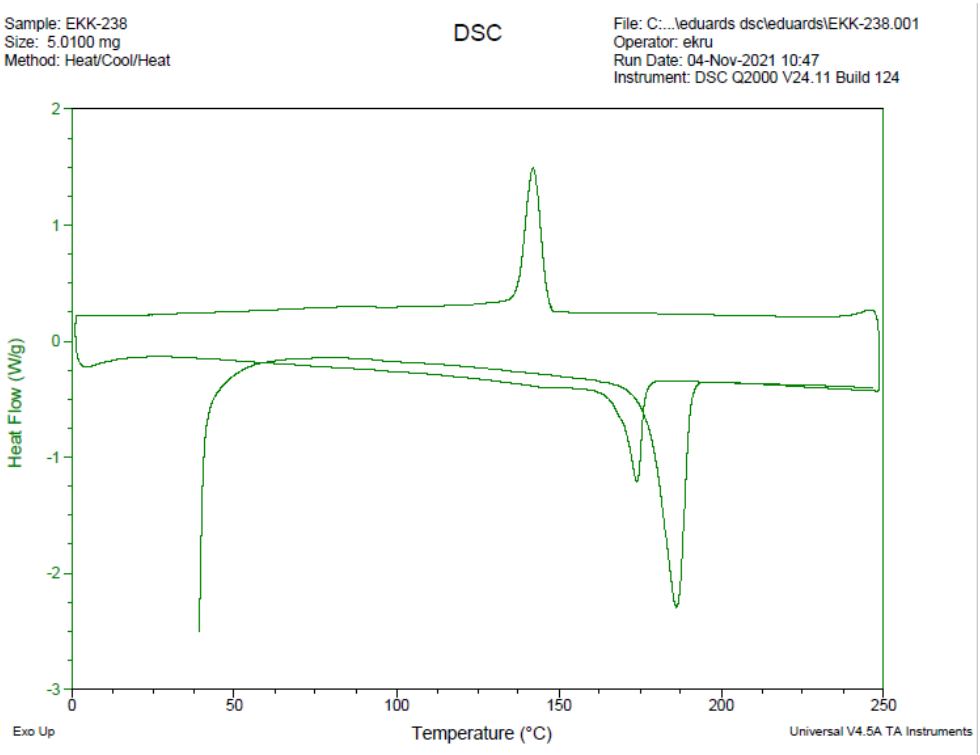


Figure 34 - DSC chromatogram of PA-12 coated with P(IBMA-Cinnamyl methacrylate) synthesized in a 60 ml autoclave

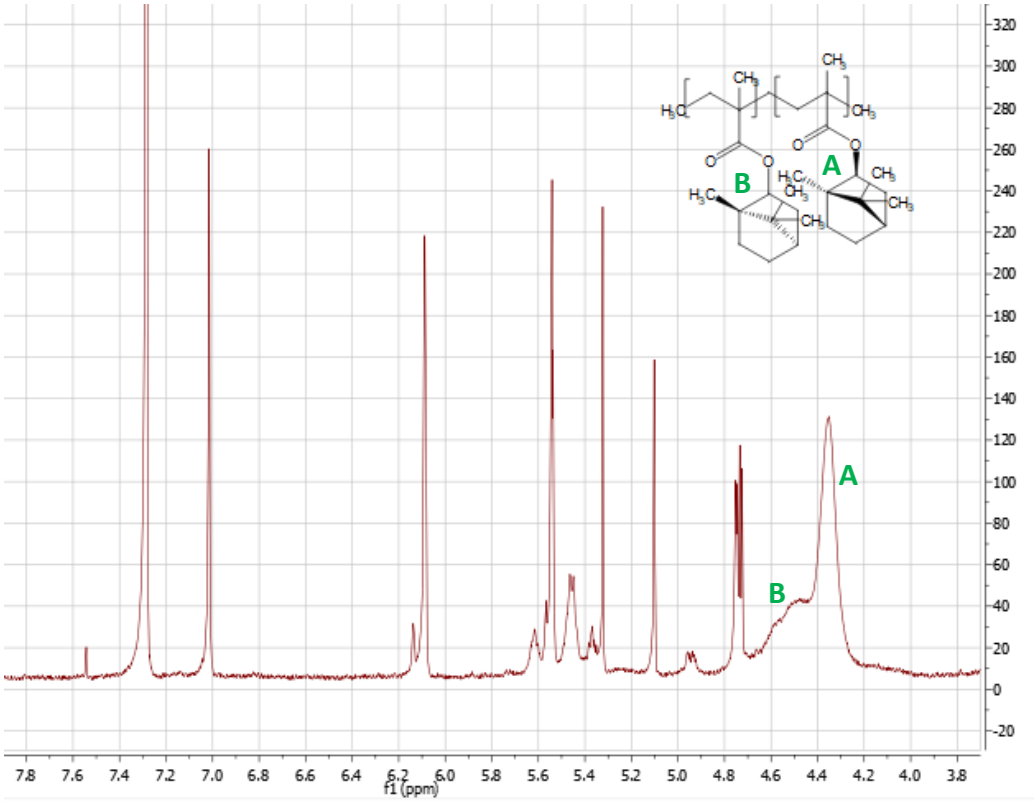


Figure 35 - ^{1}H NMR of P(IBMA-Bornyl methacrylate) outer shell synthesized in 60 mL autoclave ^{1}H NMR (400 MHz, $CHCl_3$-d_3, δ): 4.23-4.69 (mp, 1H, CH), 4.23-4.69 (mp, 1H, CH)

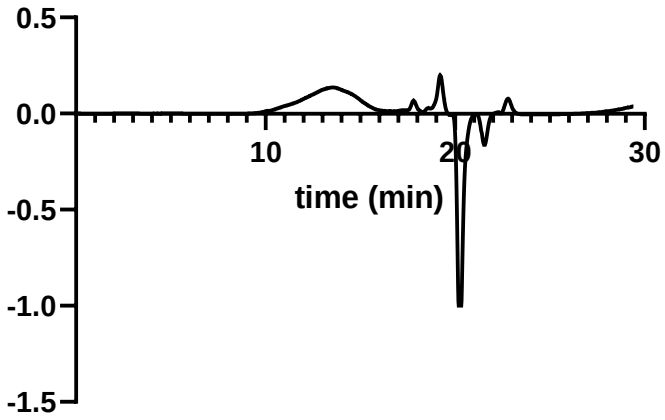


Figure 36 - GPC chromatogram of P(IBMA-Cinnamyl methacrylate) outer coating extracted from PA-12 particles coated with P(IBMA-Cinnamyl methacrylate) synthesized in a 60 ml autoclave.

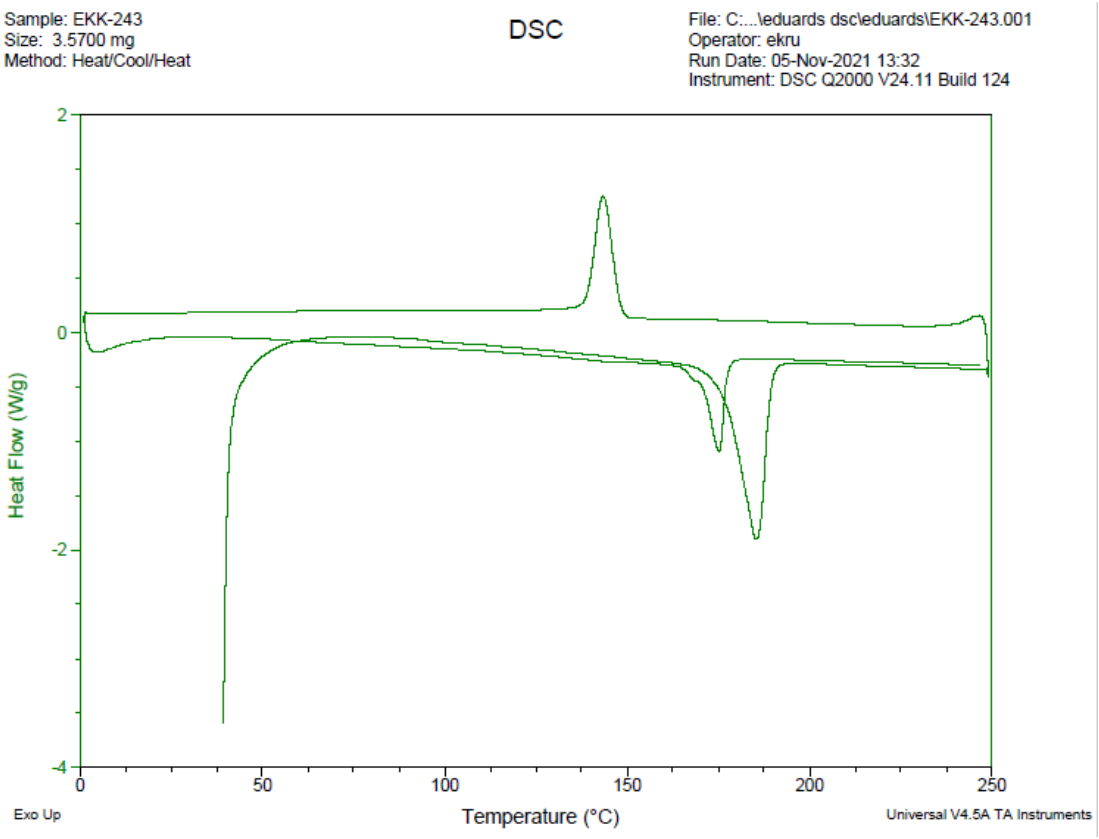


Figure 37 - DSC chromatogram of PA-12 coated with P(IBMA-Cinnamyl methacrylate) synthesized in a 60 ml autoclave

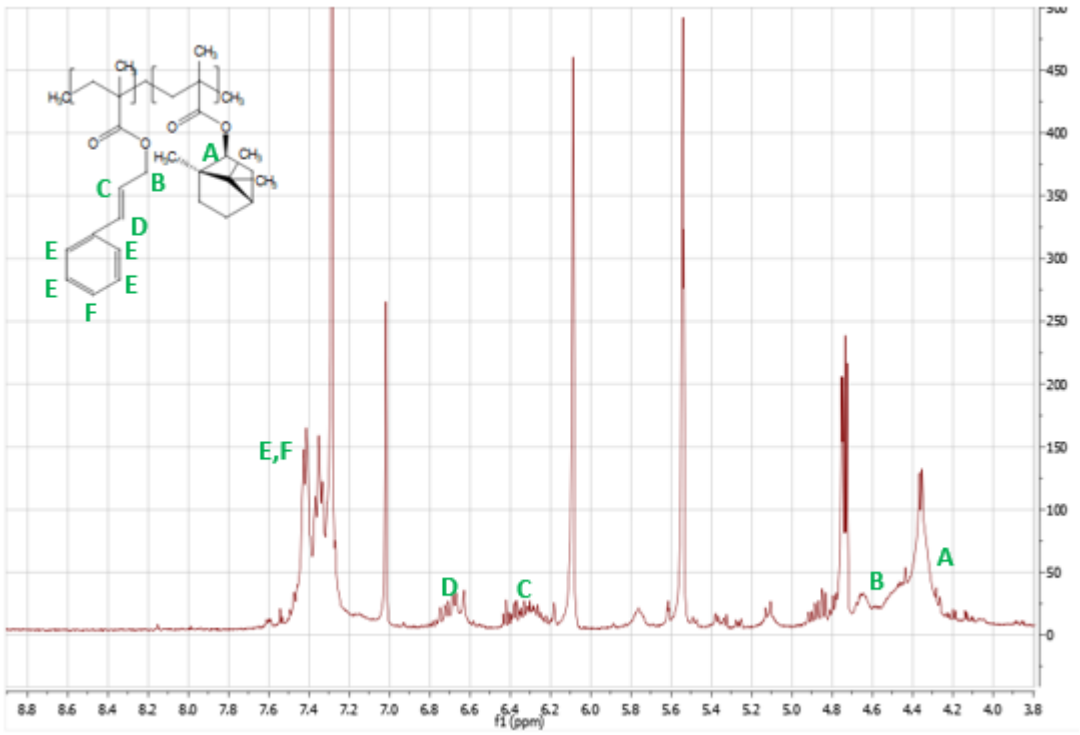


Figure 38 - ^{1}H NMR of P(IBMA-Cinnamyl methacrylate) outer shell synthesized in 60 mL autoclave ^{1}H NMR (400 MHz, $CHCl_3$-d_3, δ): 4.23-4.60 (mp, 1H, CH), 4.59-4.70 (mp, 2H, CH_2), 6.20-6.45 (mp, 1H, CH), 6.54-6.83 (mp, 1H, CH), 7.21-7.54 (mp, 2H, ArH) (mp, 2H, ArH) (mp, 2H, ArH) (mp, 2H, ArH) (mp, 2H, ArH)

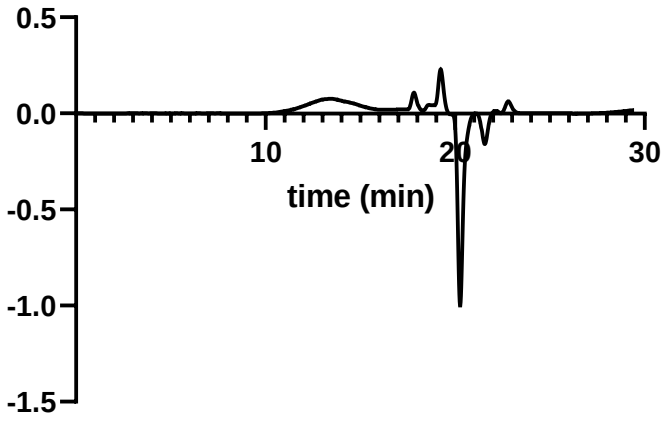


Figure 39 - GPC chromatogram of P(IBMA-Myrtenol methacrylate) outer coating extracted from PA-12 particles coated with P(IBMA-Myrtenol methacrylate) synthesized in a 60 ml autoclave.

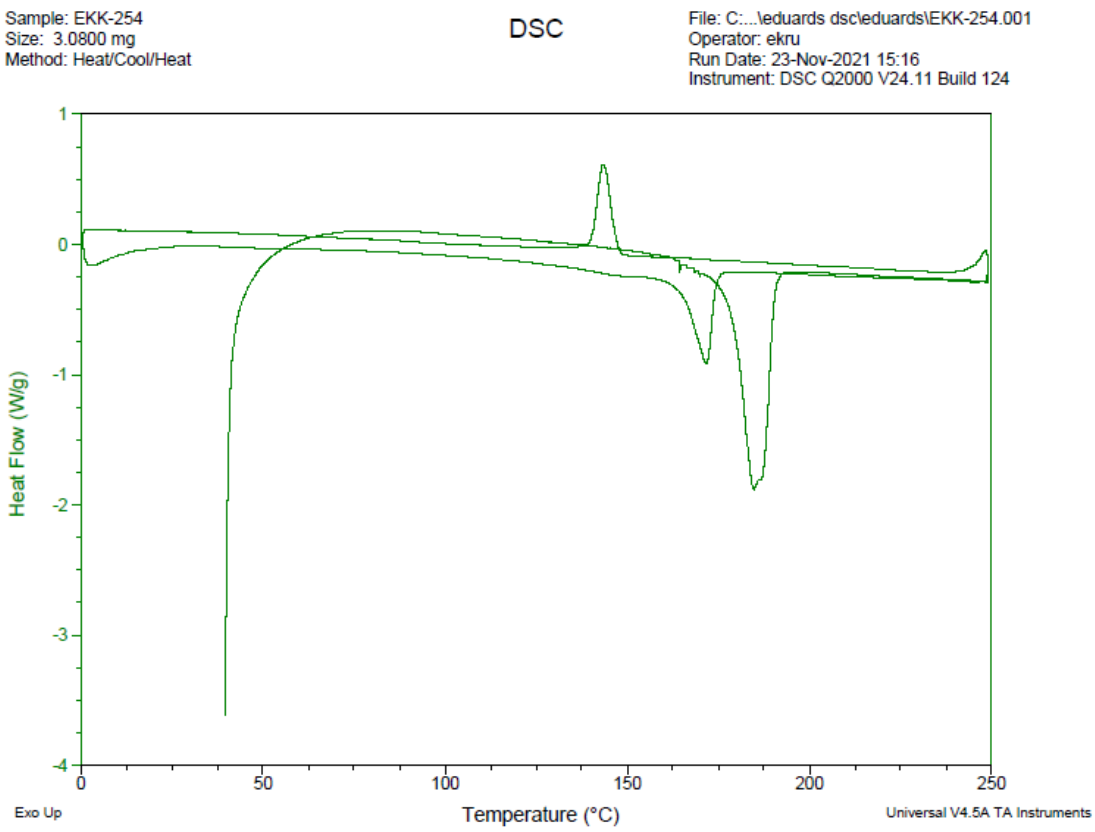


Figure 40 - DSC chromatogram of PA-12 coated with P(IBMA-Myrtenol methacrylate) synthesized in a 60 ml autoclave

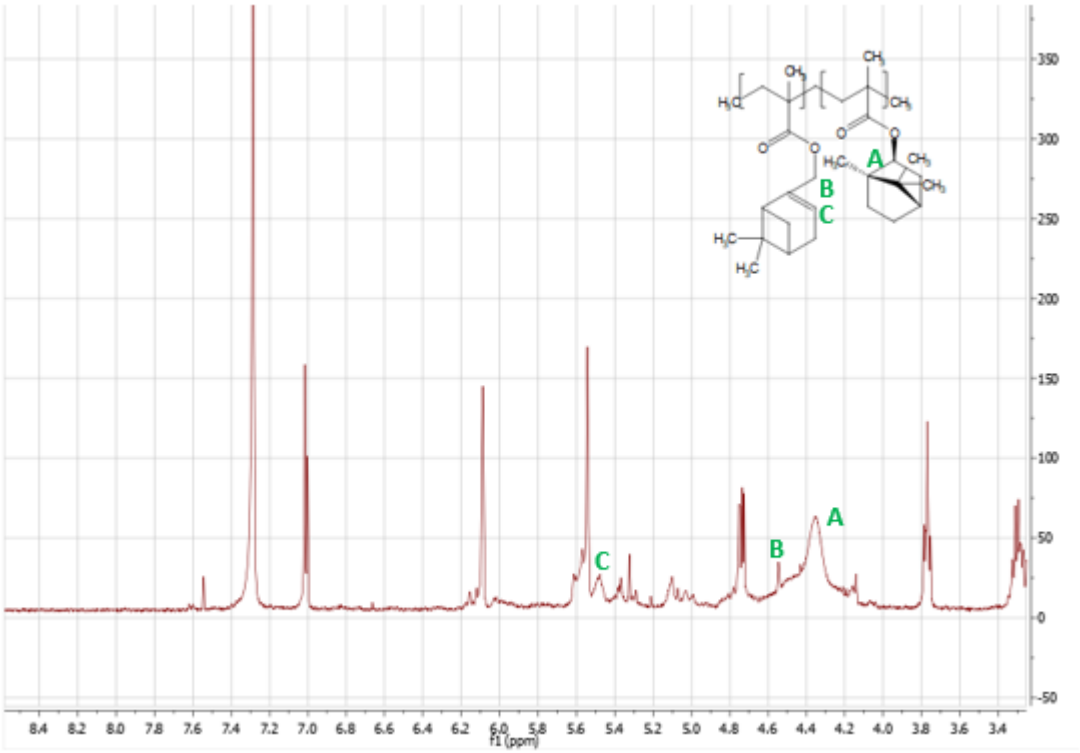


Figure 41 - ^{1}H NMR of P(IBMA-Myrtenol methacrylate) outer shell synthesized in 60 mL autoclave ^{1}H NMR (400 MHz, $CHCl_3$-d_3, δ): 4.21-4.63 (mp, 1H, CH), 4.23-4.62 (mp, 2H, CH_2), 5.43-5.51 (mp, 1H, CH)

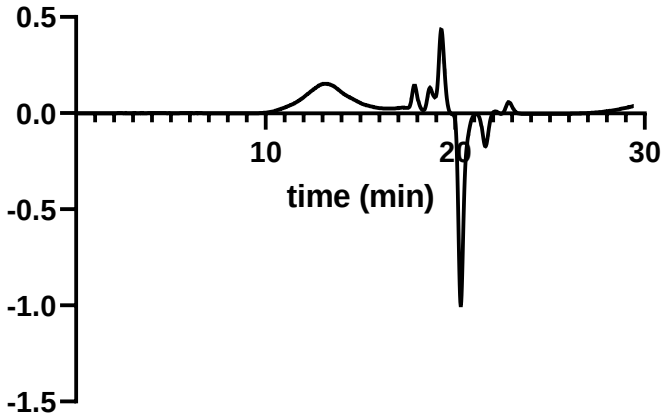


Figure 42 - GPC chromatogram of P(IBMA-Neryl methacrylate) outer coating extracted from PA-12 particles coated with P(IBMA-Neryl methacrylate) synthesized in a 60 ml autoclave.

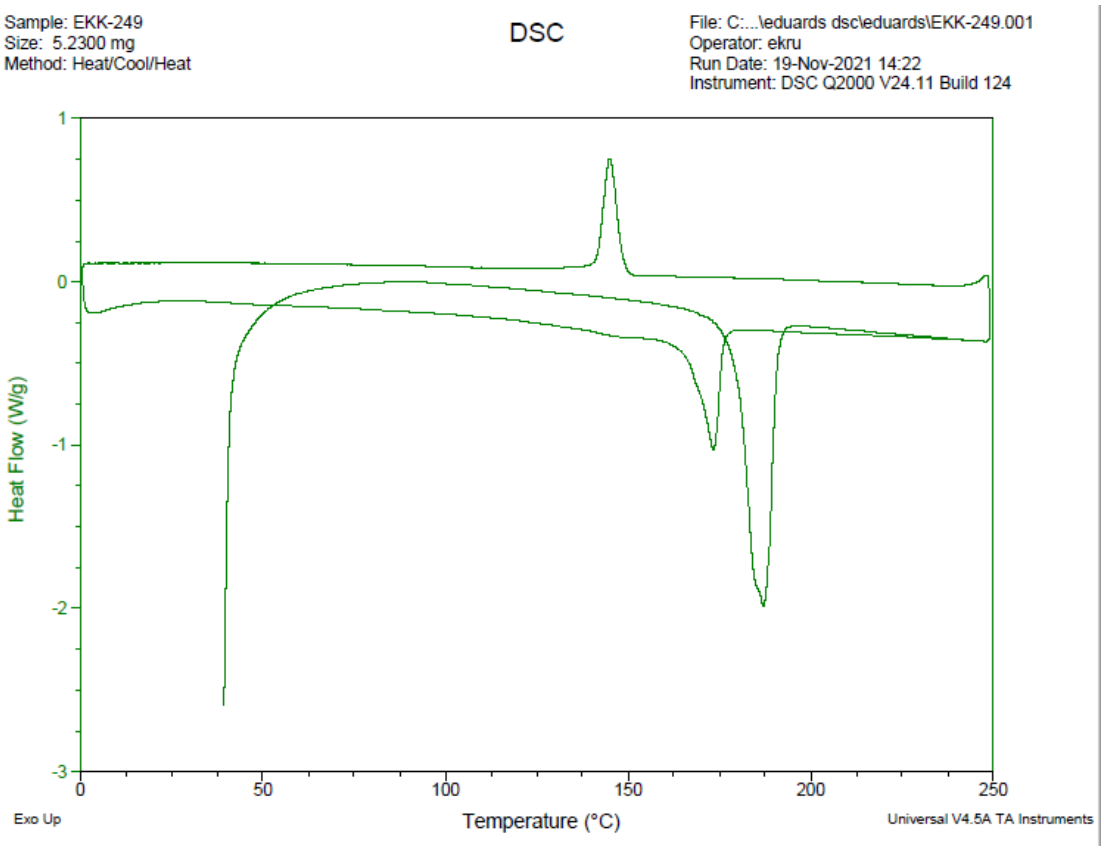


Figure 43 - DSC chromatogram of PA-12 coated with P(IBMA-Neryl methacrylate) synthesized in a 60 ml autoclave

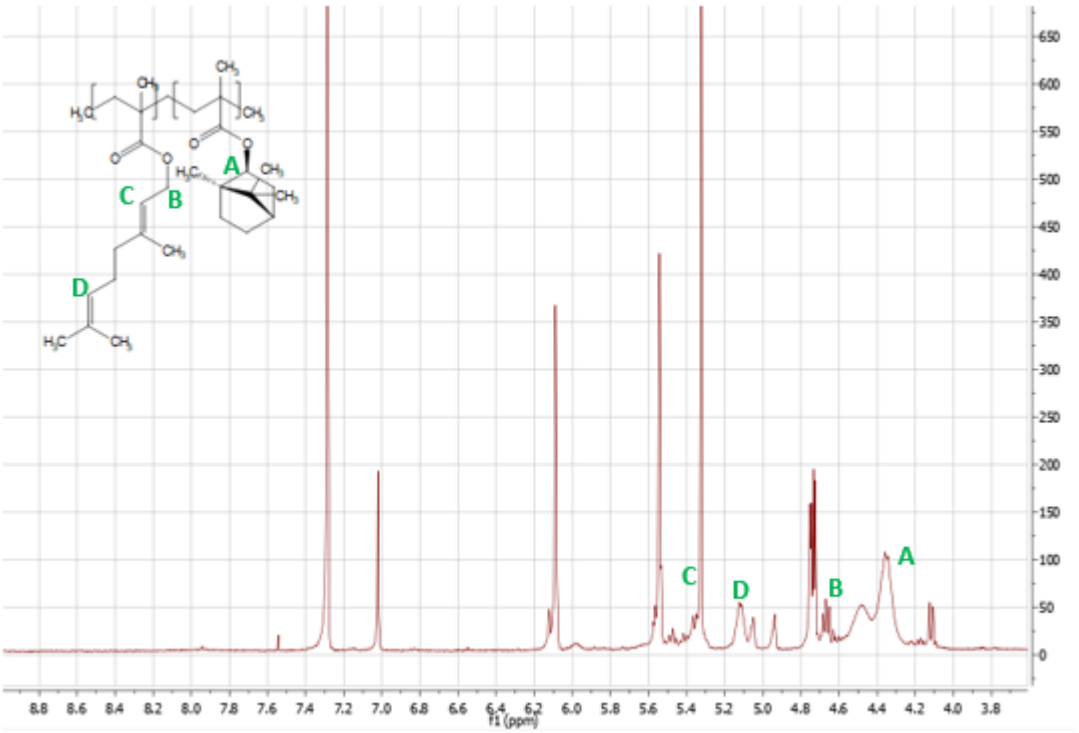


Figure 44 - ^{1}H NMR of P(IBMA-Neryl methacrylate) outer shell synthesized in 60 mL autoclave ^{1}H NMR (400 MHz, $CHCl_3$-d_3, δ): 4.23-4.60 (mp, 1H, CH), 4.59-4.70 (mp, 2H, CH_2), 5.02-5.19 (mp, 1H, CH), 5.25-5.43 (mp, 1H, CH)

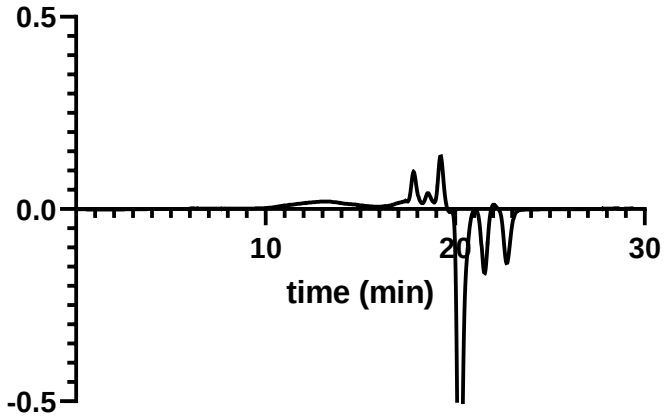


Figure 45 - GPC chromatogram of P(IBMA-modified oleic acid acrylate) outer coating extracted from PA-12 particles coated with P(IBMA-modified oleic acid acrylate) synthesized in a 60 ml autoclave.

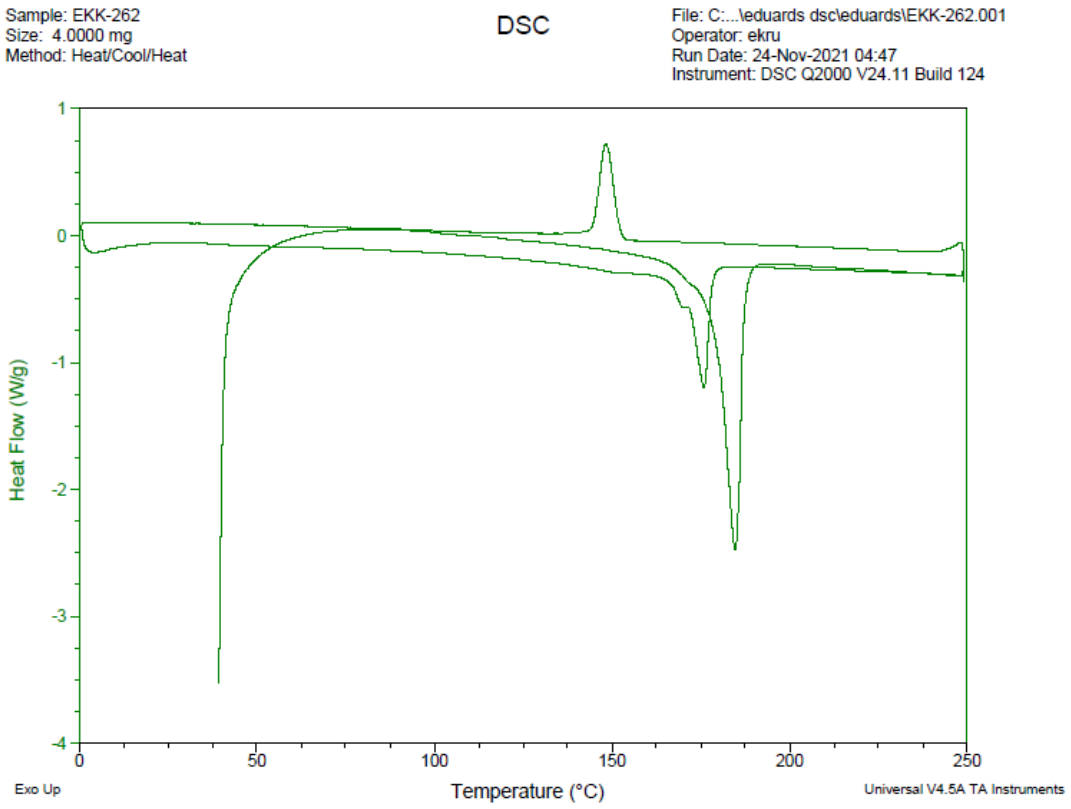


Figure 46 - DSC chromatogram of PA-12 coated with P(IBMA-modified oleic acid acrylate) synthesized in a 60 ml autoclave

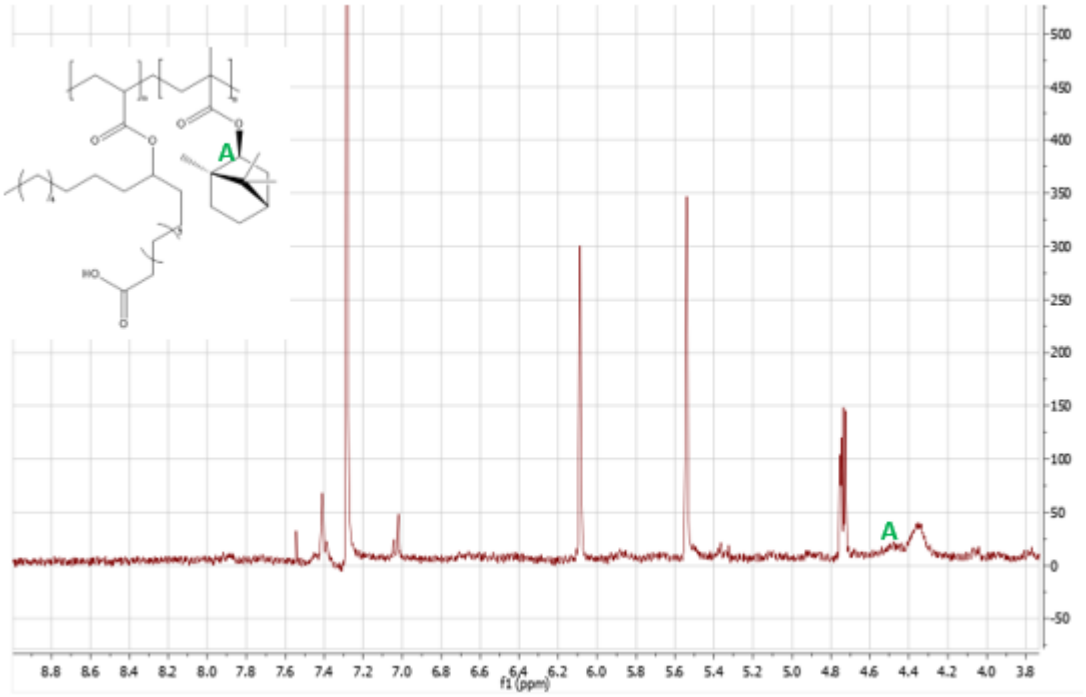


Figure 47 - ^{1}H NMR of P(IBMA- modified oleic acid acrylate) outer shell synthesized in 60 mL autoclave ^{1}H NMR (400 MHz, $CHCl_3$-d_3, δ): 4.23-4.60 (mp, 1H, CH)

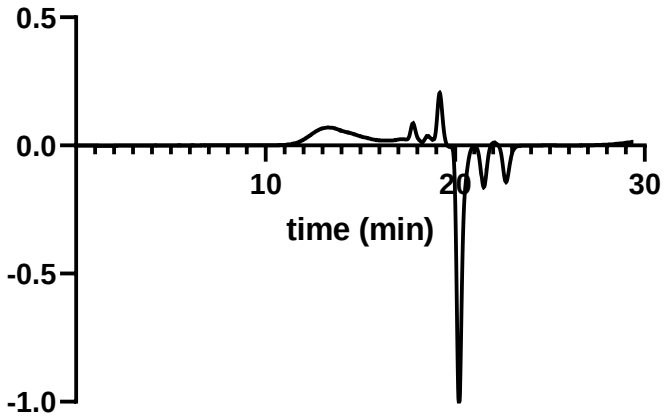


Figure 48 - GPC chromatogram of P(IBMA-modified lactic acid acrylate) outer coating extracted from PA-12 particles coated with P(IBMA-modified lactic acid acrylate) synthesized in a 60 ml autoclave.

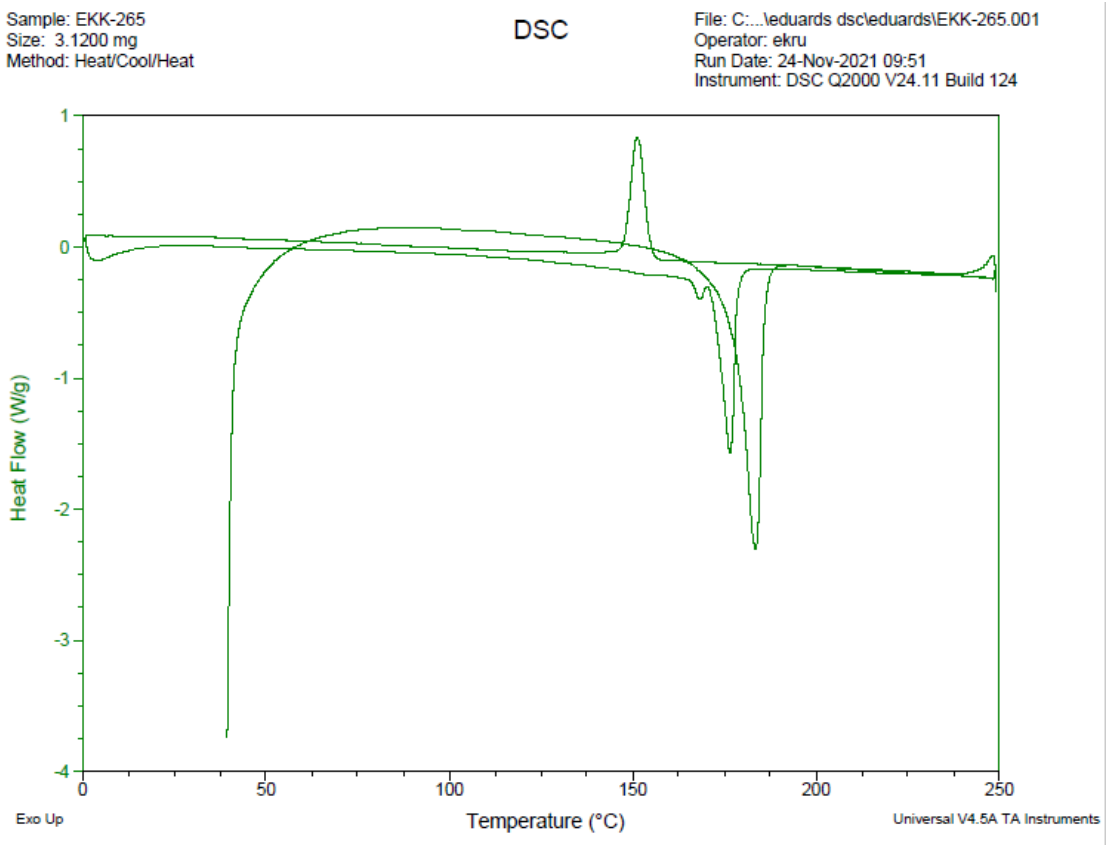


Figure 49 - DSC chromatogram of PA-12 coated with P(IBMA-lactic oleic acid acrylate) synthesized in a 60 ml autoclave

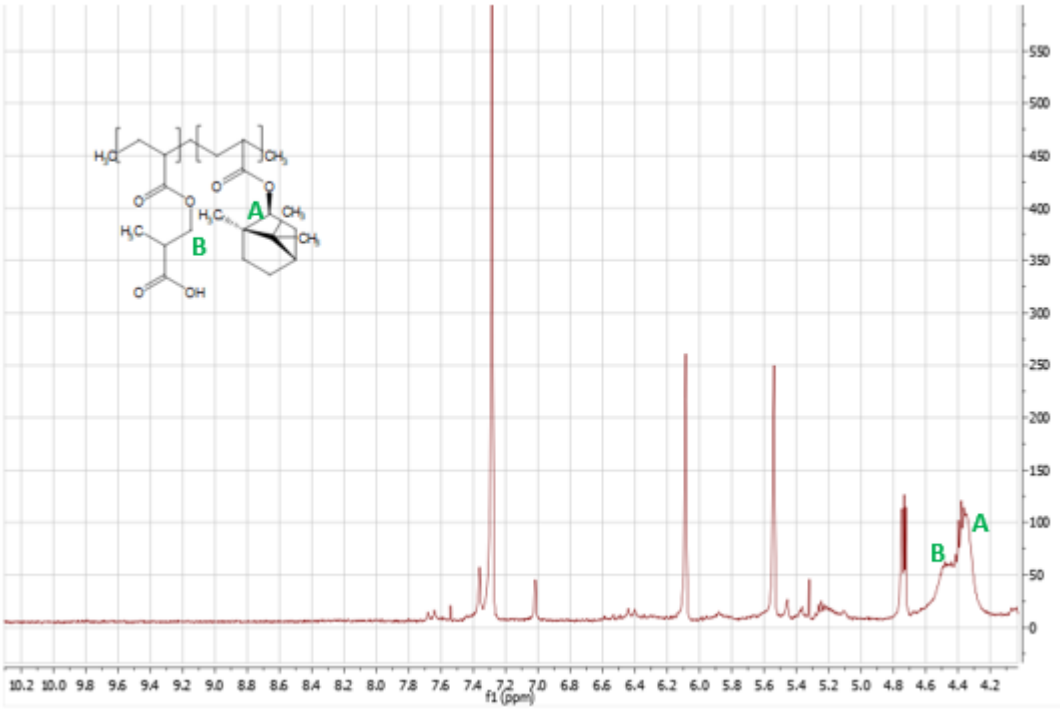


Figure 50 - ^{1}H NMR of P(IBMA- modified lactic acid acrylate) outer shell synthesized in 60 mL autoclave ^{1}H NMR (400 MHz, $CHCl_3$-d_3, δ): 4.23-4.60 (mp, 1H, CH), 4.23-4.60 (mp, 2H, CH_2)

Sample	co-polymer formation [a,b]	Mn (KDa) [a]	Mw (Kda) [a]	Đ [a]	T_g [c]	T_m [c]	T_c [c]
PA-12 coated with P(IBMA-bornyl methacrylate) 10wt%	Yes	22	54	2.4	138.37	172.77	140.37
PA-12 coated with P(IBMA-bornyl methacrylate) 20wt%	Yes	22	132	5.879	139.41	174.06	141.92
PA-12 coated with P(IBMA-bornyl methacrylate) 30wt%	Yes	25	56	2.273	139.21	172.77	140.37

PA-12 coated with P(IBMA-cinnamyl methacrylate) 10wt%	Yes	26	114	4.312	140.39	175.36	143.22
PA-12 coated with P(IBMA-cinnamyl methacrylate) 20wt%	Yes	10	46	4.5	139.62	175.62	143.22
PA-12 coated with P(IBMA-cinnamyl methacrylate) 30wt%	Yes	8	44	5.6	142.04	175.62	144.25
PA-12 coated with P(IBMA-neryl methacrylate) 10wt%	Yes	26	70	2.7	142.97	173.29	145.03
PA-12 coated with P(IBMA-neryl methacrylate) 20wt%	Yes	26	86	3.3	144.76	174.32	146.59
PA-12 coated with P(IBMA-neryl methacrylate) 30wt%	Yes	19	47	2.5	147.28	175.36	147.62
PA-12 coated with P(IBMA-myrtenol methacrylate) 10wt%	Yes	26	72	2.9	143.77	171.47	143.99
PA-12 coated with P(IBMA-myrtenol methacrylate) 20wt%	Yes	21	106	5	142.51	171.99	143.22
PA-12 coated with P(IBMA-myrtenol	Yes	21	112	5.3	142.92	171.99	143.22

methacrylate) 30wt%							
PA-12 coated with P(IBMA- modified oleic acid acrylate) 10wt%	Yes	26	115	4.515	148.28	176.14	148.66
PA-12 coated with P(IBMA-modified oleic acid acrylate) 20wt%	Yes	18	76	4.309	145.62	175.88	148.4
PA-12 coated with P(IBMA-modified oleic acid acrylate) 30wt%	Yes	29	149	5.197	147.97	176.14	149.44
PA-12 coated with P(IBMA- modified lactic acid acrylate) 10wt%	Yes	16	50	3.202	148.52	176.4	149.49
PA-12 coated with P(IBMA-modified lactic acid acrylate) 20wt%	Yes	19	48	2.566	150.36	176.14	151.25
PA-12 coated with P(IBMA-modified lactic acid acrylate) 30wt%	Yes	18	69	3.924	151.22	176.4	151.77

Table 6 – Results from the coating of PA-12 with P(IBMA-terpene monomer) and P(IBMA-modified acid acrylate). [a] Determined through GPC analysis of the outer shell extracted from the coated PA-12 particles. [b] Determined through ^{1}H NMR analysis of the outer shell extracted from the coated PA-12 particles. [c] Determined through DSC analysis of coated PA-12 particles.

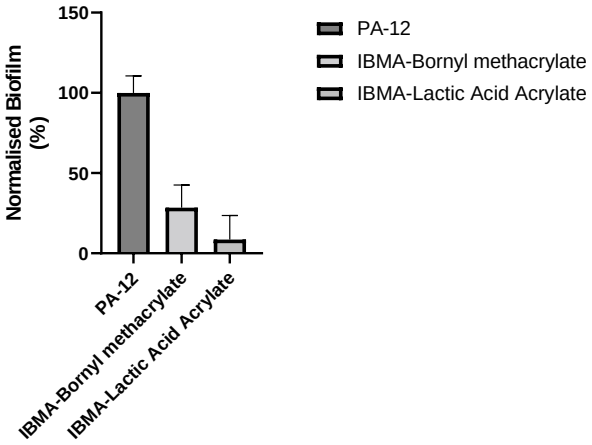


Figure 51 - Bioassay of PBF printed parts testing their activity against the attachment of *C. glabrata*. The control used was a disc made of 100% PA-12, the attachment of the yeast to the coated samples was compared to the attachment of *C. glabrata* on the PA-12 control, so the PA-12 control has a value of 100% attachment.

Materials were made in an effort to synthesise PA-12 based particles with improved mechanical properties for SLS. In an attempt to accomplish this PA-12 was coated with P(IBMA-2-hydroxy ethyl methacrylate(HEMA)) and P(IBMA-Glycidyl methacrylate(GMA)), they were produced via an analogous method to what was used for the production of coloured or anti-attachment materials for SLS.

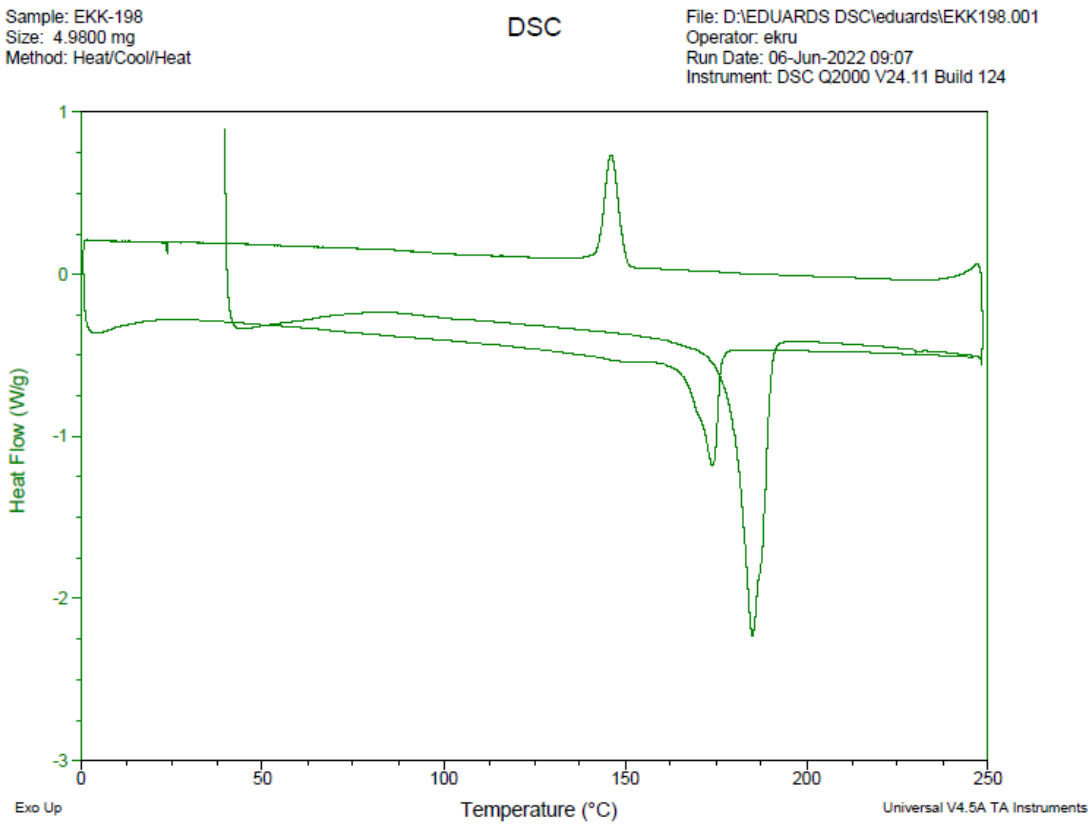


Figure 52 - DSC chromatogram of PA-12 coated with P(IBMA-2-HEMA) synthesized in a 60 ml autoclave

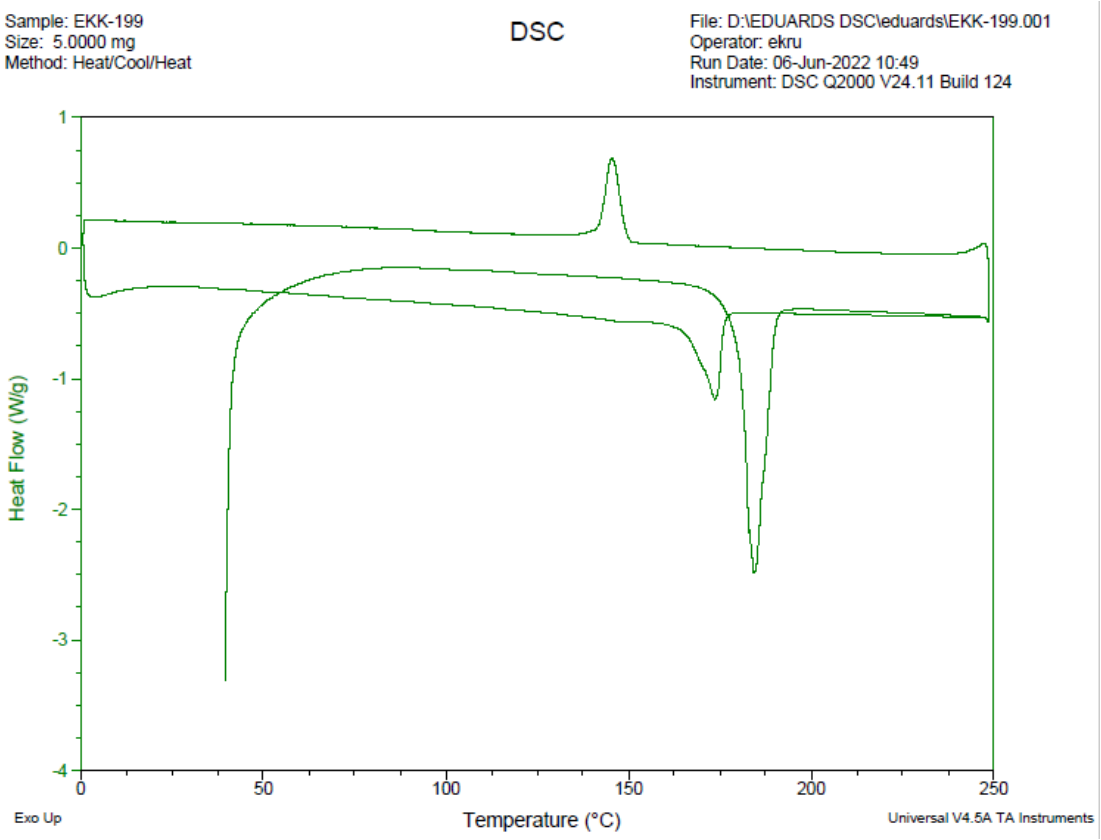


Figure 53 - DSC chromatogram of PA-12 coated with P(IBMA-GMA) synthesized in a 60 ml autoclave.